c.1

INTERACTIONS OF AXIAL LIGANDS AND DIOXYGEN WITH COBALT(II) MACROCYCLE COMPLEXES

by

DAVID W. SMITH

B.Sc., Carleton University, 1974

A THESIS SUBMITTED IN PARTIAL FULFILMENT OF

THE REQUIREMENTS FOR THE DEGREE OF

DOCTOR OF PHILOSOPHY

in

THE FACULTY OF GRADUATE STUDIES

Department of Chemistry

We accept this thesis as conforming

to the required standard

The University of British Columbia

August, 1980

© David W. Smith, 1980

In presenting this thesis in partial fulfilment of the requirements for an advanced degree at the University of British Columbia, I agree that the Library shall make it freely available for reference and study. I further agree that permission for extensive copying of this thesis for scholarly purposes may be granted by the Head of my Department or by his representatives. It is understood that copying or publication of this thesis for financial gain shall not be allowed without my written permission.

Department of CHEMISTRY

The University of British Columbia
2075 Wesbrook Place
Vancouver, Canada
V6T 1W5

Date Sept. 19, 1980

DE-6 BP 75-511E

ABSTRACT

Studies on the interactions of axial ligands and molecular oxygen with Co(II) porphyrin and Schiff base complexes have revealed a number of interesting and significant features regarding the nature of such interactions.

The binding of a first axial ligand to cobalt(II) octamethyltetrabenzoporphyrin (CoOMBP),

$$L + CoOMBP \overset{K_1}{\rightleftharpoons} LCoOMBP, \qquad (I)$$

occurs with greater ligand affinity than is observed for other Co(II) porphyrin (CoP) complexes. Also, LCoOMBP is shown by visible spectroscopy to completely bind a second axial ligand,

$$L + LCoOMBP \overset{K_2}{\rightleftharpoons} L_2CoOMBP, \qquad (II)$$

at high ligand concentrations in several cases, while other LCoP complexes do not under similar conditions. These binding properties are attributed to the very weak σ-basicity of OMBP causing approaching axial ligands to see a metal centre with more positive charge. In contrast, molecular oxygen binds more strongly to LCoOMBP complexes,

$$LCoOMBP + O_2 \overset{K_{O_2}}{\rightleftharpoons} LCoOMBP(O_2), \qquad (III)$$

than would be predicted from the σ-basicity properties of OMBP. This observation is explained in terms of the strong π-donating abilities of OMBP enhancing the affinity of the Co(II) complex for dioxygen; thus good evidence is obtained for coordinated dioxygen being able to accept π-electron density. The π-donating abilities of OMBP are also invoked to

explain the observed similarities in ΔH values associated with K_1 and K_2; it is suggested that the π-interactions inhibit metal centre displacement from the porphyrin plane upon the formation of a five-coordinate adduct. Evidence for π-interactions between porphyrin and axial ligand is provided by an observed enhanced ΔH value for the π-accepting ligand PPh_3.

The formation of dioxygen adducts of LCoOMBP is shown to be enhanced in more polar solvents, and a linear correlation between K_{O_2} and dielectric constant is observed in varying mixtures of the binary toluene-DMF solvent system. Ligand binding is demonstrated to be slightly inhibited in more polar solvent systems. These effects are considered to be due to differences in relative polarity of the products and the reactants of the systems studied.

Studies on ligand binding to a variety of CoP complexes show that the compounds with stronger σ-base porphyrins bind ligands less strongly than those with weaker σ-base porphyrins. This trend does not appear to hold when DMF is the axial ligand being studied; the strong π-donor ability of this ligand is proposed as a possible explanation of the apparent anomalous behavior of DMF. The π-donor effects of DMF are also invoked to explain the enhanced ΔH associated with dioxygen binding to DMFCoOMBP, compared to when predominantly σ-donating-ligand-complexes of CoOMBP are oxygenated. A wide variety of LCoP complexes were monitored for oxygenation, and a good correlation is found between the σ-basicity of the porphyrin and the oxygen affinity of the LCoP complex when L is kept constant; complexes of stronger porphyrin σ-basicity are found to bind dioxygen more strongly than those of weaker σ-basic porphyrins. This is explained in terms of the stronger σ-base putting more electron density on the metal centre, so that transfer of electron density to dioxygen can occur more readily and the cobalt-dioxygen bond ($Co(III)-O_2^-$) can be more easily formed.

Irreversible oxidation of LCoP complexes,

$$2\ LCoP + O_2 \longrightarrow LCoP(O_2)CoPL, \qquad (IV)$$

is also examined. In the course of these experiments, strong evidence is obtained for the formation of aggregates of CoOMBP complexes in non-aqueous media at concentrations as low as 10^{-5} M, the first such CoP aggregates to be observed under these conditions. Oxidation of a variety of LCoP complexes is shown to proceed by a first order process in cobalt, suggestive of an "activated intermediate" in which coordinated dioxygen may more closely resemble the peroxide-like dioxygen in the product than the superoxide-like moiety present in $LCoP(O_2)$. Oxidation of CoOMBP complexes is substantially enhanced when Im is the axial ligand, so much so that formation of the 1:1 Co:dioxygen adduct could not be independently studied, even at lower temperatures where oxidation is normally inhibited. This enhancement is thought to be due to the ability of Im to hydrogen bond to the 1:1 Co:dioxygen adduct, and to thus enhance the formation of the "activated intermediate" and to permit a more facile oxidation of the cobalt porphyrin system. If other non-hydrogen bonding compounds are used as ligands, the LCoOMBP complexes sometimes take days to oxidize in toluene. If a more polar solvent system is used, then the rate of oxidation is increased. This effect is especially manifested when the oxidation of $(CH_3\text{-Im})_2CoOMBP$ is studied in media containing necessarily substantial amounts of polar CH_3-Im; the reaction is now measurable on a stopped-flow kinetics time scale, in spite of the six-coordinate nature of the CoOMBP species present under these conditions.

In the Schiff base system, N,N-bis(salicylaldehyde)ethylenediiminato-cobalt(II) (Co(salen)), ligand adduct formation is found to be much weaker and

dioxygen adduct formation stronger than in the CoP systems, and this is thought to be due to the greater electron density present on the metal centre on the Co(salen) system. The Co(salen) system is shown to be so dioxygen sensitive that four-coordinate Co(salen) is essentially able to completely oxygenate at low temperatures, although the rate of oxygenation of the four-coordinate complex is many orders of magnitude less than that of the five-coordinate LCo(salen) systems.

Compounds with unsaturated carbon-carbon bonds are shown to interact with the cobalt macrocycle complexes. Styrene and 3,4-dichlorobutene under one atmosphere of oxygen cause reversible visible spectral changes to occur with Co(salen) over a period of several days. Maleic anhydride and tetracyanoethylene bind to CoOMBP, but not to other CoP complexes, thus again showing the importance of the π-donating abilities of OMBP.

TABLE OF CONTENTS

	Page
ABSTRACT	ii
TABLE OF CONTENTS	vi
LIST OF TABLES	xxi
LIST OF FIGURES	xxvii
ABBREVIATIONS AND COMMON NAMES	xxxiv
ACKNOWLEDGEMENTS	xlii
CHAPTER I. INTRODUCTION	1
I.1 Biological Oxygen Carrying Systems	1
I.1.1 General	1
I.1.2 Myoglobin and Hemoglobin	5
I.2 Synthetic Oxygen Carriers	8
I.2.1 Rationale for Synthetic Oxygen Carriers	8
I.2.2 General Synthetic Oxygen Carriers	9
I.2.3 Porphyrins	10
I.2.4 Schiff Bases	12
I.2.5 Transition Metal Complexes	18
I.2.5.1 Iron Complexes	18
I.2.5.2 Copper Complexes	20
I.2.5.3 Chromium Complexes	20
I.2.5.4 Manganese Complexes	20
I.2.5.5 Titanium Complexes	21
I.2.5.6 Ruthenium Complexes	21
I.2.5.7 Rhodium Complexes	21

Page

I.3 Cobalt Complexes 22

I.3.1 General 22

I.3.2 Early Cobalt Dioxygen Work 23

I.3.3 Cobalt Schiff Base Compounds 23

I.3.4 Cobalt Porphyrin Compounds 24

I.3.5 Other Cobalt Compounds 27

I.4 Catalytic Properties 27

CHAPTER II. APPARATUS AND EXPERIMENTAL PROCEDURE 29

II.1 Instrumentation 29

II.2 Spectroscopic Cells 31

II.2.1 Ultraviolet-visible Spectroscopic Cells 31

II.2.2 ESR Cells 36

II.3 Constant Temperature Baths 38

II.3.1 Above $0^{\circ}C$ 38

II.3.2 At or Below $0^{\circ}C$ 38

II.4 Equilibrium Constant Measurements 38

II.4.1 Ligand Binding 38

II.4.2 Oxygen Binding 39

II.5 Spectrophotometric Kinetic Measurements 40

II.6 Gas-Uptake Measurements 40

II.6.1 Description 40

II.6.2 Procedure for a Typical Gas-Uptake Experiment 42

II.6.3 Gas Solubility Measurements 45

II.7 Materials 45

II.7.1 Gases 45

Page

II.7.2 Liquids 46

II.7.2.1 General 46

II.7.2.2 Solvents 46

II.7.2.3 Ligands 46

II.7.3 Solids 47

II.7.3.1 Ligands 47

II.7.3.2 Macrocycles and Co(II) Complexes 47

CHAPTER III. THERMODYNAMICS OF REVERSIBLE BINDING OF SELECTED LIGANDS TO CoOMBP 51

III.1 Qualitative Spectral Observations 51

III.1.1 $L + CoOMBP \rightleftharpoons LCoOMBP$, K_1 51

III.1.2 $L + LCoOMBP \rightleftharpoons L_2CoOMBP$, K_2 55

III.2 Treatment of Data 59

III.3 Sources of Error 65

III.4 Ligand Binding Constants 69

III.4.1 $L + CoOMBP \rightleftharpoons LCoOMBP$, K_1 69

III.4.2 $L + LCoOMBP \rightleftharpoons L_2CoOMBP$, K_2 74

III.5 Ligand Binding in 1,2-Dichloroethane 76

CHAPTER IV. THERMODYNAMICS OF REVERSIBLE DIOXYGEN BINDING TO TO CoOMBP COMPLEXES 79

IV.1 Qualitative Spectral Observations 79

IV.1.1 $LCoOMBP + O_2 \rightleftharpoons LCoOMBP(O_2)$, K_{O_2} 79

IV.1.2 $L_2CoOMBP + O_2 \rightleftharpoons LCoOMBP(O_2) + L$, $K_{O_2/L}$ 81

Page

IV.2 Species Present When the CoOMBP-PBu_3 System is Oxygenated 85

IV.3 Treatment of Data 87

IV.4 Sources of Error 91

IV.5 Dioxygen Binding Constants 93

IV.5.1 $LCoOMBP + O_2 \rightleftharpoons LCoOMBP(O_2)$, K_{O_2} 93

IV.5.2 $L_2CoOMBP + O_2 \rightleftharpoons LCoOMBP(O_2) + L$, $K_{O_2/L}$ 97

IV.6 Oxygenation Reaction in Solvent Systems Other Than Neat Toluene 98

CHAPTER V. THERMODYNAMICS OF REVERSIBLE LIGAND BINDING TO CoDADIXDME AND CoDBrDIXDME 105

V.1 Qualitative Spectral Observations 105

V.1.1 $L + CoDADIXDME \rightleftharpoons LCoDADIXDME$, K_{1a} 105

V.1.2 $L + CoDBrDIXDME \rightleftharpoons LCoDBrDIXDME$, K_{1b} .. 108

V.2 Treatment of Data 108

V.3 Sources of Error 110

V.4 Ligand Binding Constants 113

V.5 Comparison of Ligand Binding Among Different Cobalt Porphyrins 113

CHAPTER VI. THERMODYNAMICS OF REVERSIBLE DIOXYGEN BINDING TO LCoDADIXDME AND LCoDBrDIXDME 128

VI.1 Qualitative Spectral Observations 128

VI.2 Treatment of Data 132

VI.3 Sources of Error 132

VI.4 Dioxygen Binding Constants 136

Page

VI.5 Comparison of Dioxygen Binding Among Different Cobalt Porphyrins 139

CHAPTER VII. KINETICS OF THE OXIDATION OF COBALT(II) PORPHYRIN COMPLEXES 154

VII.1 Introduction 154

VII.2 Qualitative Spectral Observations 155

VII.3 Treatment of Data 164

VII.4 Aggregation 165

VII.5 Kinetics of the Oxidation of LCoOMBP 173

VII.5.1 Kinetics of the Oxidation of ImCoOMBP in Toluene ... 173

VII.5.2 Kinetics of the Oxidation of LCoOMBP in Toluene, L = CH_3-Im, Pip, or Py 189

VII.5.3 Kinetics of the Oxidation of LCoOMBP in Solvents Other Than Toluene 195

VII.5.3.1 Kinetics of the Oxidation of CH_3-Im in a Variety of Solvents 195

VII.5.3.2 Kinetics of the Oxidation of LCoOMBP in DCE 197

VII.6 Kinetics of the Oxidation of L_2CoOMBP 200

VII.7 Kinetics of the Oxidation of LCoP, P ≠ OMBP 212

VII.8 Concluding Comments 228

CHAPTER VIII. THERMODYNAMICS AND KINETICS OF REVERSIBLE LIGAND AND DIOXYGEN BINDING TO Co(SALEN) COMPLEXES 232

VIII.1 Qualitative Spectral Observations 232

VIII.2 Treatment of Data 236

VIII.3 Sources of Error 249

Page

VIII.4 Studies in Dichloromethane 249

VIII.4.1 $L + Co(salen) \rightleftharpoons LCo(salen)$, K_1 249

VIII.4.2 $LCo(salen) + O_2 \rightleftharpoons LCo(salen)(O_2)$, K_{O_2} 254

VIII.4.3 $Co(salen) + O_2 \rightleftharpoons Co(salen)(O_2)$ 256

VIII.5 Studies in Other Solvents 265

VIII.5.1 Rationale 265

VIII.5.2 $L + Co(salen) \rightleftharpoons LCo(salen)$ 265

VIII.5.3 $LCo(salen) + O_2 \rightleftharpoons LCo(salen)(O_2)$ 265

CHAPTER IX. THERMODYNAMICS AND KINETICS OF REACTIONS OF COBALT(II) MACROCYCLIC SYSTEMS WITH SUBSTRATES CONTAINING UNSATURATED CARBON-CARBON BONDS 269

IX.1 Reactions of Co(II) Porphyrin Systems with Ethylene and Acetylene 269

IX.2 Reactions of Co(II) Porphyrin Systems with Electron Withdrawing Olefins 276

IX.3 Reactions of Co(salen) Complexes with Unsaturated Substrates 285

CHAPTER X. GENERAL CONCLUSIONS AND SOME RECOMMENDATIONS FOR FUTURE WORK 291

REFERENCES 297

APPENDIX. RAW DATA USED FOR DETERMINING THERMODYNAMIC AND KINETIC PARAMETERS REPORTED IN THIS THESIS 321

APPENDIX I. RAW DATA USED FOR DETERMINING THE THERMODYNAMIC PARAMETERS OF REVERSIBLE LIGAND BINDING TO CoOMBP 322

Page

APPENDIX Ia. Im + CoOMBP $\rightleftharpoons$ ImCoOMBP 323

APPENDIX Ib. CH_3-Im + CoOMBP $\rightleftharpoons$ CH_3-ImCoOMBP 325

APPENDIX Ic. Pip + CoOMBP $\rightleftharpoons$ PipCoOMBP 326

APPENDIX Id. Py + CoOMBP $\rightleftharpoons$ PyCoOMBP 327

APPENDIX Ie. ET_3N + CoOMBP $\rightleftharpoons$ ET_3NCoOMBP 328

APPENDIX If. DMF + CoOMBP $\rightleftharpoons$ DMFCoOMBP 329

APPENDIX Ig. THF + CoOMBP $\rightleftharpoons$ THFCoOMBP 330

APPENDIX Ih. PPh_3 + CoOMBP $\rightleftharpoons$ PPh_3CoOMBP 332

APPENDIX Ii. PBu_3 + CoOMBP $\rightleftharpoons$ PBu_3CoOMBP 333

APPENDIX Ij. CH_3-Im CH_3-ImCoOMBP $\rightleftharpoons$ $(CH_3\text{-Im})_2$CoOMBP 334

APPENDIX Ik. Pip + PipCoOMBP $\rightleftharpoons$ $(Pip)_2$CoOMBP 335

APPENDIX Il. Py + PyCoOMBP $\rightleftharpoons$ $(Py)_2$CoOMBP 337

APPENDIX Im. PBu_3 + PBu_3CoOMBP $\rightleftharpoons$ $(PBu_3)_2$CoOMBP 339

APPENDIX In. CH_3-Im + CoOMBP $\rightleftharpoons$ CH_3-ImCoOMBP in 1,2-dichloroethane 340

APPENDIX Io. Pip + CoOMBP $\rightleftharpoons$ PipCoOMBP in 1,2-dichloroethane 341

APPENDIX Ip. Py + CoOMBP $\rightleftharpoons$ PyCoOMBP in 1,2-dichloroethane 342

APPENDIX Iq. THF + CoOMBP $\rightleftharpoons$ THFCoOMBP in 1,2-dichloroethane 343

APPENDIX II. RAW DATA USED FOR DETERMINING THE THERMODYNAMIC PARAMETERS OF REVERSIBLE DIOXYGEN BINDING TO L_nCoOMBP. (n = 1 or 2) 344

APPENDIX IIa. CH_3-ImCoOMBP + O_2 $\rightleftharpoons$ CH_3-ImCoOMBP(O_2) 345

APPENDIX IIb. PipCoOMBP + O_2 $\rightleftharpoons$ PipCoOMBP(O_2) 346

APPENDIX IIc. PyCoOMBP + O_2 $\rightleftharpoons$ PyCoOMBP(O_2) 347

Page

APPENDIX IId. $Et_3NCoOMBP + O_2 \rightleftharpoons Et_3NCoOMBP(O_2)$ 348

APPENDIX IIe. $DMFCoOMBP + O_2 \rightleftharpoons DMFCoOMBP(O_2)$ 350

APPENDIX IIf. $PPh_3CoOMBP + O_2 \rightleftharpoons PPh_3CoOMBP(O_2)$ 352

APPENDIX IIg. $PBu_3CoOMBP + O_2 \rightleftharpoons PBu_3CoOMBP(O_2)$ 353

APPENDIX IIh. $PBu_3CoOMBP + O_2 \rightleftharpoons PBu_3CoOMBP(O_2)$ as a function of $[PBu_3]$ 354

APPENDIX IIi. $L_2CoOMBP + O_2 \rightleftharpoons LCoOMBP(O_2) + L$ @ $-45^{\circ}C$. 356

APPENDIX IIj. CH_3-ImCoOMBP + $O_2 \rightleftharpoons CH_3$-ImCoOMBP($O_2$) in a solvent system of 4:1 by volume toluene: 1,2-dichloroethane 357

APPENDIX IIk. $L_2CoOMBP + O_2 \rightleftharpoons LCoOMBP(O_2) + L$ @ $-45^{\circ}C$ In a solvent system of 4:1 by volume toluene: 1,2-dichloroethane 359

APPENDIX IIl. CH_3-ImCoOMBP + $O_2 \rightleftharpoons CH_3$-ImCoOMBP In a solvent system of 1:1 by volume toluene:DMF 360

APPENDIX IIm. PipCoOMBP + $O_2 \rightleftharpoons$ PipCoOMBP(O_2) In a solvent system of 1:1 by volume toluene:DMF 362

APPENDIX IIn. PyCoOMBP + $O_2 \rightleftharpoons$ PyCoOMBP(O_2) In a solvent system of 1:1 by volume toluene:DMF 364

APPENDIX IIo. PipCoOMBP + $O_2 \rightleftharpoons$ PipCoOMBP(O_2) With varying amounts of DMF in the solvent system 366

APPENDIX III. RAW DATA USED FOR DETERMINING THE THERMODYNAMIC PARAMETERS OF REVERSIBLE LIGAND BINDING TO CoDADIXDME AND CoDBrDIXDME 368

APPENDIX IIIa. CH_3-Im + CoDADIXDME $\rightleftharpoons CH_3$-ImCoDADIXDME 369

Page

APPENDIX IIIb. Pip + CoDADIXDME $\rightleftharpoons$ PipCoDADIXDME 370

APPENDIX IIIc. Py + CoDADIXDME $\rightleftharpoons$ PyCoDADIXDME 371

APPENDIX IIId. DMF + CoDADIXDME $\rightleftharpoons$ DMFCoDADIXDME 372

APPENDIX IIIe. CH_3-Im + CoDBrDIXDME $\rightleftharpoons$ CH_3-ImCoDBrDIXDME .. 373

APPENDIX IIIf. Pip + CoDBrDIXDME $\rightleftharpoons$ PipCoDBrDIXDME 374

APPENDIX IIIg. Py + CoDBrDIXDME $\rightleftharpoons$ PyCoDBrDIXDME 375

APPENDIX IIIh. DMF + CoDBrDIXDME $\rightleftharpoons$ DMFCoDBrDIXDME 376

APPENDIX IV. RAW DATA USED FOR DETERMINING THE THERMODYNAMIC PARAMETERS OF REVERSIBLE DIOXYGEN BINDING TO LCoDADIXDME AND LCoDBrDIXDME 377

APPENDIX IVa. CH_3-ImCoDADIXDME + O_2 $\rightleftharpoons$ CH_3-ImCoDADIXDME(O_2) . 378

APPENDIX IVb. PipCoDADIXDME + O_2 $\rightleftharpoons$ PipCoDADIXDME(O_2) 380

APPENDIX IVc. PyCoDADIXDME + O_2 $\rightleftharpoons$ PyCoDADIXDME(O_2) 382

APPENDIX IVd. DMFCoDADIXDME + O_2 $\rightleftharpoons$ DMFCoDADIXDME(O_2) 384

APPENDIX IVe. CH_3-ImCoDBrDIXDME + O_2 $\rightleftharpoons$ CH_3-ImCoDBrDIXDME(O_2) 385

APPENDIX IVf. PipCoDBrDIXDME + O_2 $\rightleftharpoons$ PipCoDBrDIXDME(O_2) ... 387

APPENDIX IVg. PyCoDBrDIXDME + O_2 $\rightleftharpoons$ PyCoDBrDIXDME(O_2) 389

APPENDIX IVh. DMFCoDBrDIXDME + O_2 $\rightleftharpoons$ DMFCoDBrDIXDME(O_2) ... 390

APPENDIX V. RAW DATA USED FOR DETERMINING THE KINETICS OF OXIDATION OF COBALT PORPHYRIN COMPLEXES 391

APPENDIX Va. CoOMBP Aggregation Data with Toluene as a Solvent . 392

APPENDIX Vb. CoOMBP Aggregation Data with DCE as a Solvent 394

APPENDIX Vc. ImCoOMBP + O_2 $\longrightarrow$ ImCoOMBP(O_2)CoOMBP·Im

As a function of oxygen pressure 396

Page

APPENDIX Vd. $ImCoOMBP + O_2 \longrightarrow ImCoOMBP(O_2)CoOMBP \cdot Im$

As a function of ligand concentration 398

APPENDIX Ve. $ImCoOMBP + O_2 \longrightarrow ImCoOMBP(O_2)CoOMBP \cdot Im$

As a function of ligand concentration 401

APPENDIX Vf. $ImCoOMBP + O_2 \longrightarrow ImCoOMBP(O_2)CoOMBP \cdot Im$

As a function of ligand concentration 403

APPENDIX Vg. $ImCoOMBP + O_2 \longrightarrow ImCoOMBP(O_2)CoOMBP \cdot Im$

As a function of cobalt concentration 405

APPENDIX Vh. $ImCoOMBP + O_2 \longrightarrow ImCoOMBP(O_2)CoOMBP \cdot Im$

As a function of cobalt concentration 408

APPENDIX Vi. $ImCoOMBP + O_2 \longrightarrow ImCoOMBP(O_2)CoOMBP \cdot Im$

As a function of temperature 409

APPENDIX Vj. $CH_3\text{-}ImCoOMBP + O_2 \longrightarrow CH_3\text{-}ImCoOMBP(O_2)CoOMBP \cdot CH_3\text{-}Im$

As a function of cobalt concentration 411

APPENDIX Vk. $CH_3\text{-}ImCoOMBP + O_2 \longrightarrow CH_3\text{-}ImCoOMBP(O_2)CoOMBP \cdot CH_3\text{-}Im$

As a function of CH_3-Im concentration 414

APPENDIX Vl. $CH_3\text{-}ImCoOMBP + O_2 \longrightarrow CH_3\text{-}ImCoOMBP(O_2)CoOMBP \cdot CH_3\text{-}Im$

As a function of oxygen pressure 416

APPENDIX Vm. $PipCoOMBP + O_2 \longrightarrow PipCoOMBP(O_2)CoOMBP \cdot Pip$ 418

APPENDIX Vn. $PyCoOMBP + O_2 \longrightarrow PyCoOMBP(O_2)CoOMBP \cdot Py$ 419

APPENDIX Vo. $CH_3\text{-}ImCoOMBP + O_2 \longrightarrow CH_3\text{-}ImCoOMBP(O_2)CoOMBP \cdot CH_3\text{-}Im$

As a function of solvent 420

APPENDIX Vp. $CH_3\text{-}ImCoOMBP + O_2 \longrightarrow CH_3\text{-}ImCoOMBP(O_2)CoOMBP \cdot CH_3\text{-}Im$

in DCE 424

APPENDIX Vq. $PyCoOMBP + O_2 \longrightarrow PyCoOMBP(O_2)CoOMBP \cdot Py$ in DCE 426

Page

APPENDIX Vr. $PipCoOMBP + O_2 \longrightarrow PipCoOMBP(O_2)CoOMBP \cdot Pip$ in DCE 428

APPENDIX Vs. $(CH_3\text{-}Im)_2CoOMBP + O_2 \longrightarrow$ $CH_3\text{-}ImCoOMBP(O_2)CoOMBP \cdot CH_3\text{-}Im$ As a function of oxygen pressure 430

APPENDIX Vt. $(CH_3\text{-}Im)_2CoOMBP + O_2 \longrightarrow$ $CH_3\text{-}ImCoOMBP(O_2)CoOMBP \cdot CH_3\text{-}Im$ As a function of temperature 434

APPENDIX Vu. $Py_2CoOMBP + O_2 \longrightarrow PyCoOMBP(O_2)CoOMBP \cdot Py$ In 1:1 v/v toluene:Py 437

APPENDIX Vv. $Py_2CoOMBP + O_2 \longrightarrow PyCoOMBP(O_2)CoOMBP \cdot Py$ In neat Py as a function of temperature 438

APPENDIX Vw. $Py_2CoOMBP + O_2 \longrightarrow PyCoOMBP(O_2)CoOMBP \cdot Py$ In neat Py as a function of cobalt concentration .. 440

APPENDIX Vx. $(CH_3\text{-}Im)_2CoOMBP + O_2 \longrightarrow$ $CH_3\text{-}ImCoOMBP(O_2)CoOMBP \cdot CH_3\text{-}Im$ As a function of solvent 441

APPENDIX Vy. $Py_2CoOMBP + O_2 \longrightarrow PyCoOMBP(O_2)CoOMBP \cdot Py$ In 1:1 v/v DCE:Py as a function of temperature 444

APPENDIX Vz. $Py_2CoOMBP + O_2 \longrightarrow PyCoOMBP(O_2)CoOMBP \cdot Py$ In 1:1 v/v DCE:Py as a function of cobalt concentration .. 446

APPENDIX Vaa. $PipCoOMBP + O_2 \longrightarrow PipCoOMBP(O_2)CoOMBP \cdot Pip$ In 1:1 v/v DCE:Pip 448

APPENDIX Vbb. $CH_3\text{-}ImCoTPP + O_2 \longrightarrow CH_3\text{-}ImCoTPP(O_2)CoTPP \cdot CH_3\text{-}Im$ 449

APPENDIX Vcc. $CH_3\text{-}ImCoTPP + O_2 \longrightarrow CH_3\text{-}ImCoTPP(O_2)CoTPP \cdot CH_3\text{-}Im$ In DCE as a function of cobalt concentration 450

Page

APPENDIX Vdd. CH_3-ImCoEpI + O_2 ⟶ CH_3-ImCoEpI(O_2)CoEpI·CH_3-Im

In DCE asa function of cobalt concentration 451

APPENDIX Vee. CH_3-ImCoEpI + O_2 ⟶ CH_3-ImCoEpI(O_2)CoEpI·CH_3-Im

In DCE as a function of temperature 454

APPENDIX Vff. CH_3-ImCoOEP + O_2 ⟶ CH_3-ImCoOEP(O_2)CoOEP·CH_3-Im

In DCE as a function of cobalt concentration 456

APPENDIX Vgg. CH_3-ImCoOEP + O_2 ⟶ CH_3-ImCoOEP(O_2)CoOEP·CH_3-Im

In DCE as a function of temperature 459

APPENDIX Vhh. CH_3-ImCoOEP + O_2 ⟶ CH_3-ImCoOEP(O_2)CoOEP·CH_3-Im

In DCE as a function of oxygen pressure 461

APPENDIX Vii. CH_3-ImCoOEP + O_2 ⟶ CH_3-ImCoOEP(O_2)CoOEP·CH_3-Im

As a function of solvent 465

APPENDIX Vjj CH_3-ImCoPpIXDME + O_2 ⟶

CH_3-ImCoPpIXDME(O_2)CoPpIXDME·CH_3-Im

As a function of cobalt concentration 467

APPENDIX Vkk CH_3-ImCoOEP + O_2 ⟶ CH_3-ImCoOEP(O_2)CoOEP·CH_3-Im

In DCE as a function of CH_3-Im concentration 469

APPENDIX VI. RAW DATA USED FOR DETERMINING THE THERMODYNAMIC AND KINETIC PARAMETERS OF LIGAND BINDING AND OXYGENATION OF Co(SALEN) COMPLEXES 471

APPENDIX VIa. CH_3-Im + Co(salen) ⇌ CH_3-ImCo(salen)

In dichloromethane 472

APPENDIX VIb. Pip + Co(salen) ⇌ PipCo(salen)

In dichloromethane 474

Page

APPENDIX VIc. Py + Co(salen) $\rightleftharpoons$ PyCo(salen)
In dichloromethane 476

APPENDIX VId. CH_3-ImCo(salen) + O_2 $\rightleftharpoons$ CH_3-ImCo(salen)(O_2)
In dichloromethane 478

APPENDIX VIe. PipCo(salen) + O_2 $\rightleftharpoons$ PipCo(salen)(O_2)
In dichloromethane 480

APPENDIX VIf. PyCo(salen) + O_2 $\rightleftharpoons$ PyCo(salen)(O_2)
In dichloromethane 481

APPENDIX VIg. Co(salen) + O_2 $\rightleftharpoons$ Co(salen)(O_2)
In dichloromethane 483

APPENDIX VIh. Co(salen) + O_2 $\rightleftharpoons$ Co(salen)(O_2)
Kinetics in dichloromethane as a function of
oxygen pressure @ -83.5°C 484

APPENDIX VIi. Co(salen) + O_2 $\rightleftharpoons$ Co(salen)(O_2)
Kinetics of dichloromethane as a function of
oxygen pressure @ -78°C 486

APPENDIX VIj. Co(salen) + O_2 $\rightleftharpoons$ Co(salen)(O_2)
Kinetics in dichloromethane as a function of
temperature 488

APPENDIX VIk. CH_3-Im + Co(salen) $\rightleftharpoons$ CH_3-ImCo(salen) In DMF 490

APPENDIX VIl. Pip + Co(salen) $\rightleftharpoons$ PipCo(salen) In DMF 492

APPENDIX VIm. Py + Co(salen) $\rightleftharpoons$ PyCo(salen) In DMF 494

APPENDIX VIn. CH_3-Im + Co(salen) $\rightleftharpoons$ CH_3-ImCo(salen)
In toluene 496

APPENDIX VIo. Pip + Co(salen) $\rightleftharpoons$ PipCo(salen) In toluene . 499

APPENDIX VIp. Py + Co(salen) $\rightleftharpoons$ PyCo(salen) In toluene ... 500

Page

APPENDIX VIq. CH_3-ImCo(salen) + $O_2 \rightleftharpoons CH_3$-ImCo(salen)($O_2$)
In DMF 504

APPENDIX VIr. PipCo(salen) + $O_2 \rightleftharpoons$ PipCo(salen)(O_2)
In DMF 506

APPENDIX VIs. PyCo(salen) + $O_2 \rightleftharpoons$ PyCo(salen)(O_2)
In DMF 507

APPENDIX VIt. CH_3-ImCo(salen) + $O_2 \rightleftharpoons CH_3$-ImCo(salen)($O_2$)
In toluene 509

APPENDIX VIu. PipCo(salen) + $O_2 \rightleftharpoons$ PipCo(salen)(O_2)
In toluene 510

APPENDIX VIv. PyCo(salen) + $O_2 \rightleftharpoons$ PyCo(salen)(O_2)
In toluene 511

APPENDIX VII. RAW DATA USED FOR DETERMINING THE THERMODYNAMIC AND KINETIC PARAMETERS OF REACTING OLEFINIC SUBSTRATES WITH COBALT MACROCYCLIC SYSTEMS 512

APPENDIX VIIa. MA + CoOMBP $\rightleftharpoons$ MACoOMBP In toluene 513

APPENDIX VIIb. MA + CoOMBP $\rightleftharpoons$ MACoOMBP In DCE 515

APPENDIX VIIc. MA + PipCoOMBP $\rightleftharpoons$ Pip + MACoOMBP
MA + PipCoOMBP $\rightleftharpoons$ PipCoOMBP(MA)
PipCoOMBP(MA) $\longrightarrow$ PipCoOMBP + MA 516

APPENDIX VIId. MA + DMFCoOMBP $\rightleftharpoons$ DMFCoOMBP(MA) In DMF .. 518

APPENDIX VIIe. MACoOMBP + Pip $\longrightarrow$ PipCoOMBP(MA)
MA + CoOMBP $\longrightarrow$ MACoOMBP 520

Page

APPENDIX VIIf. PipCoOMBP + C_2H_4 ⟶ PipCoOMBP(C_2H_4)

In DCE

PipCoOMBP(C_2H_4) ⟶ PipCoOMBP + C_2H_4

In DCE

PipCoOMBP + C_2H_2 ⟶ PipCoOMBP(C_2H_2)

In DCE

PipCoOMBP(C_2H_2) ⟶ PipCoOMBP + C_2H_2

In DCE 521

APPENDIX VIIg. Olefins Reacting with Co(salen) Complexes 523

APPENDIX VIII. DATA USED IN DETERMINING DIELECTRIC CONSTANTS 525

APPENDIX IX. ESR PARAMETERS DETERMINED IN THIS THESIS 529

LIST OF TABLES

Table		Page
I.1	Properties of Oxygen Carriers	4
I.2	Trivial Names and Side Chain Substituents of Porphyrins	11
I.3a	Mnemonic Names and Substituents of Type A Schiff Bases	17
I.3b	Mnemonic Names and Substituents of Type B Schiff Bases	17
III.1	Spectral Data From 350 to 750 nm for the Reaction: $L + CoOMBP \rightleftharpoons LCoOMBP$	54
III.2	Spectral Data From 350 to 750 nm for the Reaction: $L + LCoOMBP \rightleftharpoons L_2CoOMBP$	57
III.3	Thermodynamic Data for the Binding of the First Axial Ligand to CoOMBP in a Toluene Solution	70
III.4	Thermodynamic Data for the Binding of the Second Axial Ligand to LCoOMBP in a Toluene Solution	74
III.5	Thermodynamic Data for the Binding of the First Axial Ligand to CoOMBP in a DCE Solution	77
IV.1a	Spectral Data From 350 to 750 nm for the Reaction: $LCoOMBP + O_2 \rightleftharpoons LCoOMBP(O_2)$	82
IV.1b	Spectral Data From 350 to 750 nm for the Reaction: $L_2CoOMBP + O_2 \rightleftharpoons LCoOMBP(O_2) + L$	85
IV.2	Oxygen Sensitivity as a Function of $[PBu_3]$ at $-63.5^{\circ}C$	86
IV.3	Thermodynamic Data for the Binding of Dioxygen to LCoOMBP in a Toluene Solution	94
IV.4	Expected $P_{\frac{1}{2}}O_2$ Values (Torr) for $L_2CoOMBP$ Complexes at $-45^{\circ}C$	98

Table		Page
IV.5	Thermodynamic Data for the Binding of Dioxygen to LCoOMBP in a 1:1 by Volume Ratio of Toluene to DMF	100
IV.6	Oxygen Affinities at -56.5°C of PipCoOMBP in a Variety of Mixed Toluene-DMF Solvent Systems	102
V.1a	Spectral Data From 350 to 750 nm for the Reaction: L + CoDADIXDME $\rightleftharpoons$ LCoDADIXDME	107
V.1b	Spectral Data From 350 to 750 nm for the Reaction: L + CoDBrDIXDME $\rightleftharpoons$ LCoDBrDIXDME	107
V.2a	Thermodynamic Data for the Binding of an Axial Ligand to CoDADIXDME in a Toluene Solution	114
V.2b	Thermodynamic Data for the Binding of an Axial Ligand to CoDBrDIXDME in a Toluene Solution	114
V.3a	Thermodynamic Data for the Binding of CH_3-Im to Several Cobalt Porphyrin Complexes in Toluene	117
V.3b	Thermodynamic Data for the Binding of Pip to Several Cobalt Porphyrin Complexes in Toluene	118
V.3c	Thermodynamic Data for the Binding of Py to Several Cobalt Porphyrin Complexes in Toluene	119
V.3d	Thermodynamic Data for the Binding of DMF to Several Cobalt Porphyrin Complexes in Toluene	120
VI.1a	Spectral Data From 350 to 750 nm for the Reaction: LCoDADIXDME + O_2 $\rightleftharpoons$ LCoDADIXDME(O_2)	131
VI.1b	Spectral Data From 350 to 750 nm for the Reaction: LCoDBrDIXDME + O_2 $\rightleftharpoons$ LCoDBrDIXDME(O_2)	131
VI.2a	Thermodynamic Data for the Binding of Dioxygen to LCoDADIXDME in a Toluene Solution	137

Table		Page
VI.2b	Thermodynamic Data for the Binding of Dioxygen to LCoDBrDIXDME in a Toluene Solution	138
VI.3a	Thermodynamic Data for the Binding of Dioxygen to CH_3-Im Complexes of Several Cobalt Porphyrins	140
VI.3b	Thermodynamic Data for the Binding of Dioxygen to Pip Complexes of Several Cobalt Porphyrins	141
VI.3c	Thermodynamic Data for the Binding of Dioxygen to Py Complexes of Several Cobalt Porphyrins	142
VI.3d	Thermodynamic Data for the Binding of Dioxygen to DMF Complexes of Several Cobalt Porphyrins	143
VII.1	Spectral Data From 350 to 750 nm for the Reaction: $2L_nCoP + O_2 \longrightarrow LCoP(O_2)CoPL + 2(n-1)L$	162
VII.2a	Kinetic Data for the Oxidation of ImCoOMBP as a Function of Oxygen Pressure	177
VII.2b	Kinetic Data for the Oxidation of ImCoOMBP as a Function of Ligand Concentration; Oxygen Pressure ~ 100 Torr	177
VII.2c	Kinetic Data for the Oxidation of ImCoOMBP as a Function of Ligand Concentration; Oxygen Pressure ~ 400 Torr	178
VII.2d	Kinetic Data for the Oxidation of ImCoOMBP as a Function of Ligand Concentration; Oxygen Pressure ~ 800 Torr	178
VII.2e	Kinetic Data for the Oxidation of ImCoOMBP as a Function of Cobalt Concentration; Oxygen Pressure ~ 160 Torr, Imidazole Concentration ~ 1.8×10^{-3} M	179
VII.2f	Kinetic Data for the Oxidation of ImCoOMBP as a Function of Cobalt Concentration; Oxygen Pressure ~ 100 Torr, Imidazole Concentration ~ 1.8×10^{-3} M	179

Table		Page
VII.2g	Kinetic Data for the Oxidation of ImCoOMBP as a Function of Cobalt Concentration; Oxygen Pressure ~ 100 Torr, Imidazole Concentration ~ 1.5×10^{-3} M	180
VII.2h	Kinetic Data for the Oxidation of ImCoOMBP as a Function of Temperature	180
VII.3	Oxidation Rate as a Function of Solvent Polarity when 1.8×10^{-5} M CH_3-ImCoOMBP is Exposed to 800 Torr O_2 at 20°C	196
VII.4	Kinetic Data for the Oxidation of PipCoOMBP in DCE	199
VII.5a	Kinetic Data for the Oxidation of $(CH_3\text{-Im})_2$CoOMBP in 1:1 v/v toluene:CH_3-Im as a Function of Oxygen Pressure	199
VII.5b	Kinetic Data for the Oxidation of $(CH_3\text{-Im})_2$CoOMBP in 1:1 v/v toluene:CH_3-Im as a Function of Temperature	199
VII.5c	Kinetic Data for the Oxidation of $(CH_3\text{-Im})_2$CoOMBP as a Function of Solvent	206
VII.6a	Kinetic Data for the Oxidation of Py_2CoOMBP as a Function of Cobalt Concentration in 1:1 v/v DCE:py	206
VII.6b	Kinetic Data for the Oxidation of Py_2CoOMBP as a Function of Temperature in 1:1 v/v DCE:Py	206
VII.7	Kinetic Data for the Oxidation of Pip_2CoOMBP as a Function of Cobalt Concentration in 1:1 v/v DCE:Pip	211
VII.8a	Kinetic Data for the Oxidation of CH_3-ImCoOEP in DCE as a Function of Cobalt Concentration	211
VII.8b	Kinetic Data for the Oxidation of CH_3-ImCoOEP in DCE as a Function of Oxygen Pressure	211

Table		Page
VII.8c	Kinetic Data for the Oxidation of CH_3-ImCoOEP in DCE as a Function of CH_3-Im Concentration	217
VII.8d	Kinetic Data for the Oxidation of CH_3-ImCoOEP in DCE as a Function of Temperature	217
VII.8e	Kinetic Data for the Oxidation of CH_3-ImCoOEP as a Function of Solvent	217
VII.9a	Kinetic Data for the Oxidation of CH_3-ImCoEpI in DCE as a Function of Cobalt Concentration	224
VII.9b	Kinetic Data for the Oxidation of CH_3-ImCoEpI in DCE as a Function of Temperature	224
VII.10	Kinetic Data for the Oxidation of CH_3-ImPpIXDME in DCE as a Function of Cobalt Concentration	224
VII.11	Kinetic Data for the Oxidation of CH_3-ImCoTPP in DCE as a Function of Cobalt Concentration	224
VIII.1	Spectral Data From 350 to 750 nm for the Reactions Involving Co(salen)	237
VIII.2	Thermodynamic Data for the Binding of an Axial Ligand to Co(salen) in a Dichloromethane Solution	250
VIII.3	Thermodynamic Data for the Binding of Dioxygen to LCo(salen) in a Dichloromethane Solution	255
VIII.4	Kinetic Data for the Oxygenation of Co(salen)	257
VIII.5	Solubility of Dioxygen in CH_2Cl_2 at Low Temperature	257
VIII.6a	Thermodynamic Data for the Binding of an Axial Ligand to Co(salen) in a DMF Solution	266
VIII.6b	Thermodynamic Data for the Binding of an Axial Ligand to Co(salen) in a Toluene Solution	266

Table		Page
VIII.7a	Thermodynamic Data for the Binding of Dioxygen to LCo(salen) in a DMF Solution	267
VIII.7b	Thermodynamic Data for the Binding of Dioxygen to LCo(salen) in a Toluene Solution	267
IX.1	Spectral Data From 350 to 750 nm for the Reactions of Unsaturated Substrates with Cobalt Macrocycles	271
IX.2	Kinetics of 780 Torr of Ethylene or Acetylene Reacting with PipCoOMBP in DCE at 20°C	274
IX.3	Thermodynamic Data for the Binding of Maleic Anhydride to CoOMBP in a Variety of Solvents	279

LIST OF FIGURES

Figure		Page
I.1	Examples of different porphyrins	2
I.2	The structure of the beta chain of hemoglobin	7
I.3	A variety of cobalt macrocycle complexes	13
I.4	Visible spectra of a variety of cobalt macrocycle complexes	14
I.5	A variety of cobalt Schiff base complexes	16
II.1	Cell used for dielectric constant measurements	30
II.2	Anaerobic spectral cell	32
II.3	10 cm path-length cell	33
II.4	6 cm path-length cell	34
II.5	Short path-length cell used for low temperature work	35
II.6	Anaerobic ESR cell	37
II.7	Gas-Uptake Apparatus	41
II.8	Gas-Uptake Ampoule	43
III.1	$CoOMBP + CH_3\text{-}Im \rightleftharpoons CH_3\text{-}ImCoOMBP$ @ 23°C	52
III.2	$PBu_3 + CoOMBP \rightleftharpoons PBu_3CoOMBP$ @ 22°C	53
III.3	$CH_3\text{-}ImCoOMBP + CH_3\text{-}Im \rightleftharpoons (CH_3\text{-}Im)_2CoOMBP$ @ -23°C ...	56
III.4	$PBu_3 + PBu_3CoOMBP \rightleftharpoons (PBu_3)_2CoOMBP$ @ 22°C	58
III.5	Equilibrium plots for $CH_3\text{-}Im + CoOMBP \rightleftharpoons CH_3\text{-}ImCoOMBP$ ..	61
III.6	Van't Hoff plots for $L + CoOMBP \rightleftharpoons LCoOMBP$ L = Im, CH_3-Im, Pip, and Py	62
III.7	Van't Hoff plots for $L + CoOMBP \rightleftharpoons LCoOMBP$ L = Et_3N, THF, and DMF	63
III.8	Van't Hoff plot for $PPh_3 + CoOMBP \rightleftharpoons PPh_3CoOMBP$	64

Figure		Page
III.9	Equilibrium plots for CH_3-Im + CH_3-Im CoOMBP $\rightleftharpoons$ $(CH_3\text{-Im})_2$CoOMBP	66
III.10	Van't Hoff plots for L + LCoOMBP $\rightleftharpoons$ L_2CoOMBP L = CH_3-Im, Pip, and Py	67
IV.1	Spectra of oxygen binding to CH_3-ImCoOMBP @ -56.5°C	80
IV.2	ESR signal of CH_3-ImCoOMBP in frozen toluene @ 77 K	83
IV.3	Spectra of oxygen binding to $(CH_3\text{-Im})_2$CoOMBP @ -45°C	84
IV.4	Equilibrium plots for CH_3-ImCoOMBP + O_2 $\rightleftharpoons$ CH_3-ImCoOMBP(O_2)	88
IV.5	Van't Hoff plots for LCoOMBP + O_2 $\rightleftharpoons$ LCoOMBP(O_2) L = CH_3-Im, Pip, Py, Et_3N, and DMF	89
IV.6	Equilibrium plot for $(CH_3\text{-Im})_2$CoOMBP + O_2 $\rightleftharpoons$ CH_3-ImCoOMBP(O_2) @ -45°C	92
IV.7	Oxygen Affinity vs. Dielectric Constant for PipCoOMBP in toluene-DMF systems	104
V.1	CH_3-Im + CoDADIXDME $\rightleftharpoons$ CH_3-ImCoDADIXDME @ 22°C	106
V.2	CH_3-Im + CoDBrDIXDME $\rightleftharpoons$ CH_3-ImCoDBrDIXDME @ 22°C	109
V.3	Equilibrium plots for CH_3-Im + CoDADIXDME $\rightleftharpoons$ CH_3-ImDADIXDME	111
V.4	Van't Hoff plots for L + CoDADIXDME $\rightleftharpoons$ LCODADIXDME	112
V.5	Porphyrin band position as a function of porphyrin basicity	116
V.6a	CH_3-Im affinity vs. porphyrin basicity for a variety of cobalt porphyrin complexes	122
V.6b	Pip affinity vs. porphyrin basicity for a variety of cobalt porphyrin complexes	123

Figure		Page
V.6c	Py affinity vs. porphyrin basicity for a variety of cobalt porphyrin complexes	124
V.6d	DMF affinity vs. porphyrin basicity for a variety of cobalt porphyrin complexes	125
VI.1	CH_3-ImCoDADIXDME + $O_2 \rightleftharpoons$ CH_3-ImCoDADIXDME(O_2) ..	129
VI.2	CH_3-ImCoDBrDIXDME + $O_2 \rightleftharpoons$ CH_3-ImCoDBrDIXDME(O_2)	130
VI.3	Equilibrium plots for CH_3-ImCoDADIXDME + $O_2 \rightleftharpoons$ CH_3-ImCoDADIXDME(O_2)	133
VI.4	Van't Hoff plots for LCoDADIXDME + $O_2 \rightleftharpoons$ LCoDADIXDME(O_2); L = CH_3-Im, Pip, Py, and DMF	134
VI.5	Van't Hoff plots for LCoDBrDIXDME + $O_2 \rightleftharpoons$ LCoDBrDIXDME; L = CH_3-Im, Pip, Py, and DMF	135
VI.6a	Dioxygen affinity vs. porphyrin basicity for a variety of CH_3-Im cobalt porphyrin complexes	145
VI.6b	Dioxygen affinity vs. porphyrin basicity for a variety of Pip cobalt porphyrin complexes	147
VI.6c	Dioxygen affinity vs. porphyrin basicity for a variety of Py cobalt porphyrin complexes	148
VI.6d	Dioxygen affinity vs. porphyrin basicity for a variety of DMF cobalt porphyrin complexes	152
VII.1	Spectra showing the oxidation of PipCoOMBP in DCE @ 30°C	156
VII.2	Spectra showing the oxidation of CH_3-ImCoEpI by 800 Torr O_2 in DCE @ 20°C	158
VII.3	Spectra showing the oxidation of CH_3-ImCoOEP by 800 Torr O_2 in DCE @ 30°C	159

Figure		Page
VII.4	Spectra showing the oxidation of CH_3-ImCoTPP by 800 Torr O_2 in DCE @ 20°C	160
VII.5	ESR signals showing the oxidation of CH_3-ImEpI by 800 Torr O_2 in DCE @ 22°C	161
VII.6	Visible spectra of CoOMBP as a function of concentration @ 22°C in toluene	167
VII.7	Aggregation plot of CoOMBP in toluene @ 22°C	170
VII.8	Beer's Law plots of CH_3-ImCoOMBP in toluene @ 22°C	171
VII.9	Beer's Law plots of $(CH_3\text{-Im})_2$CoOMBP in toluene @ 22°C	172
VII.10	ESR spectrum of CH_3-ImCoPpIXDME in toluene @ 77 K	174
VII.11	Spectra showing the oxidation of 2×10^{-5} M ImCoOMBP by 395 Torr O_2 @ 22°C	176
VII.12	Oxidation rate of ImCoOMBP as a function of oxygen pressure	181
VII.13	Oxidation rate of ImCoOMBP as a function of Im concentration	182
VII.14	Analysis of Im dependence on the oxidation of ImCoOMBP	185
VII.15	Arrhenius plot for the oxidation of ImCoOMBP	188
VII.16	Oxidation of CH_3-ImCoOMBP analyzed for first order in cobalt at several cobalt concentrations	191
VII.17	Temperature dependence on the oxidation of 2×10^{-5} M PipCoOMBP in DCE	198
VII.18	First order rate plots for the oxidation of 2×10^{-5} M $(CH_3\text{-Im})_2$CoOMBP in 1:1 toluene:CH_3-Im	202
VII.19	Temperature dependence of the oxidation of 2×10^{-5} M $(CH_3\text{-Im})_2$CoOMBP	203
VII.20	First order rate plots for the oxidation of 2×10^{-5} M $(CH_3\text{-Im})_2$CoOMBP	205

Figure		Page
VII.21	First order rate plots for the oxidation of $Py_2CoOMBP$ in 1:1 DCE:Py as a function of [Co]	207
VII.22	Temperature dependence of the oxidation of 2×10^{-5} M $Py_2CoOMBP$	208
VII.23	First order rate plots for the oxidation of $Pip_2CoOMBP$ in 1:1 DCE:Pip	210
VII.24	First order rate plots for the oxidation of CH_3-ImCoOEP by 800 Torr O_2 in DCE @ 30°C as a function of [Co]	213
VII.25	Oxygen pressure dependence of the oxidation of $\sim 7 \times 10^{-5}$ M CH_3-ImCoOEP @ 30°C in DCE	214
VII.26	First order rate plots for the oxidation of CH_3-ImCoOEP in DCE as a function of CH_3-Im	216
VII.27	Temperature dependence of the oxidation of $\sim 8 \times 10^{-5}$ M CH_3-ImCoOEP in DCE	218
VII.28	Analysis of oxygen dependence on the oxidation of CH_3-ImCoOEP at 30°C	219
VII.29	First order rate plots for the oxidation of 6×10^{-4} M CH_3-ImCoOEP in DCE @ 30°C in a variety of solvents	221
VII.30	First order rate plots for the oxidation of CH_3-ImCoEpI in DCE @ 30°C as a function of [Co]	223
VII.31	Temperature dependence of the oxidation of $\sim 1 \times 10^{-5}$ M CH_3-ImCoEpI in DCE	225
VII.32	First order rate plots for the oxidation of CH_3-ImCoPpIXDME in DCE as a function of [Co]	226
VII.33	First order rate plots for the oxidation of CH_3-ImCoTPP in DCE as a function of [Co]	227

Figure | Page

VIII.1 CH_3-Im + Co(salen) $\rightleftharpoons$ CH_3-ImCo(salen) @ 15°C in dichloromethane 233

VIII.2 CH_3-ImCo(salen) + O_2 $\rightleftharpoons$ CH_3-ImCo(salen) @ -78°C in dichloromethane 234

VIII.3 Spectra showing the oxygenation of Co(salen) by 205 Torr O_2 @ -83.5°C in dichloromethane 235

VIII.4 ESR signal of CH_3-ImCo(salen) @ 77 K in dichloromethane 240

VIII.5 A. ESR signal of CH_3-ImCo(salen)(O_2) @ 77 K in dichloromethane 241

B. ESR signal of Co(salen)(O_2) @ 77 K in dichloromethane 241

VIII.6 Equilibrium plots for CH_3-Im + Co(salen) $\rightleftharpoons$ CH_3-ImCo(salen) 242

VIII.7 Equilibrium plots for CH_3-ImCo(salen) + O_2 $\rightleftharpoons$ CH_3-ImCo(salen)(O_2) 243

VIII.8 Equilibrium plots for Co(salen) + O_2 $\rightleftharpoons$ Co(salen)(O_2) . 244

VIII.9 Van't Hoff plots for L + Co(salen) $\rightleftharpoons$ LCo(salen) L = CH_3-Im, Pip, and Py 246

VIII.10 Van't Hoff plots for LCo(salen) + O_2 $\rightleftharpoons$ LCo(salen)(O_2) L = CH_3-Im, Pip, and Py 247

VIII.11 Van't Hoff plot for Co(salen) + O_2 $\rightleftharpoons$ Co(salen)(O_2) .. 248

VIII.12 Ligand binding constants vs. pK_a for substituted pyridines in dichloromethane @ 25°C 252

VIII.13 Hammett plot for substituted pyrindines binding to Co(salen) in dichloromethane @ 25°C 253

VIII.14 Oxygenation rate constants of Co(salen) as a function of oxygen pressure 258

Figure		Page
VIII.15	Oxygenation rate constants of Co(salen) as a function of oxygen pressure	259
VIII.16	Arrhenius plot of the forward rate constants of the oxygenation of Co(salen) at one atmosphere of oxygen	261
VIII.17	Arrhenius plot for the deoxygenation of Co(salen)(O_2)	262
IX.1	Spectra showing the reaction of PipCoOMBP with 780 Torr acetylene @ 20°C	270
IX.2	Spectra showing PipCoOMBP regeneration @ 20°C after removal of acetylene	273
IX.3	First order rate plots of PipCoOMBP reacting with ethylene and acetylene	275
IX.4	Spectral changes occurring upon the addition of MA to CoOMBP in toluene @ 22°C	277
IX.5	Equilibrium plots for MA + CoOMBP $\rightleftharpoons$ MACoOMBP	278
IX.6	Van't Hoff plots for MA + CoOMBP $\rightleftharpoons$ MACoOMBP in toluene and DMF	280
IX.7	Spectral changes to MACoOMBP upon addition of Pip @ 22°C	281
IX.8	Spectra showing the generation of PipCoOMBP from PipCoOMBP(MA)	283
IX.9	Spectra showing the regeneration of the Co(salen) peak after oxygen is removed from the Co(salen)-3,4-dichlorobutene system	287
IX.10	ESR signal of Co(salen)-3,4-dichlorobutene system at 77 K	289
IX.11	ESR signal of Co(salen)-3,4-dichlorobutene system at 77 K after exposure to O_2 for 42 h at ambient temperature	290

ABBREVIATIONS AND COMMON NAMES

The following list of abbreviations and common names, many of which are commonly adopted in chemical research literature, will be employed in this thesis.

A	absorbance
	acetate, $-CH_2COOH$
	or in ESR, hyperfine coupling
A_o	observed absorbance at the start of an experiment
A_{eq}	observed absorbance when equilibrium has been established
A_∞	observed absorbance when a reaction has been completed
Ac	acetyl, $-COCH_3$
acacen	bis(acetylacetone)ethylenediimine, see Figure I.5a and Table I.3a
atm	atmosphere(s)
B	axial base
	or 2-hyroxyethyl, $-CHOHCH_3$
benacen	bis(benzoylacetylacetone)ethylenediimine, see Figure I.5a and Table I.3a
Br	bromo, -Br
CH_3-Im	N-methylimidazole, $C_4H_6N_2$
cm	centimetre(s)
Co(acacen)	Co(II) bis(acetylacetone)ethylenediimine, see Figure I.5a and Table I.3a
Co(benacen)	Co(II) bis(benzoylacetylacetone)ethylenediimine, see Figure I.5a and Table I.3a

CoDADIXDME	Co(II) diacetyldeuteroporphyrin IX dimethyl ester, see Figure I.1a and Table I.2
CoDBrDIXDME	Co(II) dibromodeuteroporphyrin IX dimethyl ester, see Figure I.1a and Table I.2
CoDpIXDME	Co(II) deuteroporphyrin IX dimethyl ester, see Figure I.1a and Table I.2
CoEpI	Co(II) etioporphyrin I, see Figure I.1a and Table I.2
CoMc	Co(II) complex of a tetradentate macrocycle
CoMpIXDME	Co(II) mesoporphyrin IX dimethyl ester, see Figure I.1a and Table I.2
CoOEP	Co(II) octaethylporphyrin, see Figure I.1d and Table I.2
CoOMBP	Co(II) octamethyltetrabenzoporphyrin, see Figure I.1c and Table I.2
CoP	a Co(II) porphyrin complex
CoPc	a Co(II) phthalocyanine complex, see Figure I.3b
CoPFP	Co(II) picket fence porphyrin
CoPpIXDME	Co(II) protoporphyrin IX dimethyl ester, see Figure I.1b and Table I.2
CoSB	a Co(II) Schiff base complex
CoTPP	Co(II) $\alpha,\beta,\gamma,\delta$-tetraphenylporphyrin, see Figure I.1c and Table I.2
CoT(p-OMe)PP	Co(II) $\alpha,\beta,\gamma,\delta$-(p-methoxy)-tetraphenylporphyrin, see Figure I.1c and Table I.2
CoT(p-X)PP	a Co(II) complex of a para substituted $\alpha,\beta,\gamma,\delta$-tetraphenylporphyrin, see Figure I.c and Table I.2
cot	cyclooctene
DADIXDME	diacetyldeuterporphyrin IX dimethyl ester, see Figure I.1a and Table I.2
DBrDIXDME	dibromodeuteroporphyrin IX dimethyl ester, see Figure I.1a and Table I.2
DCB	3,4-dichlorobutene, CH_2=CHCClCClH_2

DCE	1,2-dichloroethane, CH_2ClCH_2Cl
DCM	dichloromethane, CH_2Cl_2
DEF	diethylfumarate, trans-$C_2H_5O_2CCH{=}CHCO_2C_2H_5$
DEM	diethylmaleate, cis-$C_2H_5O_2CCH{=}CHCO_2C_2H_5$
DMA	N,N-dimethylacetamide, $CH_3CON(CH_3)_2$
DMF	N,N-dimethylformamide, $HCON(CH_3)_2$
DpIXDME	deuteroporphyrin IX dimethyl ester, see Figure I.1a and Table I.2
E or Et	ethyl, $-CH_2CH_3$
EpI	etioporphyrin I, see Figure I.1a and Table I.2
Eq'm	equilibrium
ESR	electron spin resonance
Et_3N	triethylamine, $(C_2H_5)_3N$
e.u.	entropy unit(s), cal $K^{-1}mole^{-1}$
FeTPP	Fe(II) $\alpha,\beta,\gamma,\delta$-tetraphenylporphyrin, see Figure I.1c and Table I.2
g	gram
	or an ESR g value, $g_{\text{free electron}} = 2.0023193$
G	gauss
h	hour(s)
H	ESR applied magnetic field strength
	or hydrogen
Hb	hemoglobin
I	nuclear spin number
Im	imidazole, $C_3H_4N_2$
k	kinetic rate constant
k_{obs}	observed rate constant
k_f	forward rate constant

k_r	reverse rate constant
	or in the case of the ImCoPpIXDME + O_2 system, the anticipated bimolecular rate constant of oxidation
k_d	bimolecular oxidation rate constant in the ImCoOMBP constant
k_t	total rate constant
$k_t obs$	observed total rate constant
k_1	forward rate constant
k_{-1}	reverse rate constant
k^*	rate constant for the formation of the "activated intermediate" species in the oxidation of CoP cmplexes
K	degree(s) Kelvin
	or equilibrium constant
K_{agg}	equilibrium constant of aggregation (4-coordinate species)
K_{ass}	equilibrium constant of association (5-coordinate species)
K_D	equilibrium constant of dissociation
K_{int}	equilibrium constant for Im stabilized intermediate
K_{MA}	equilibrium constant of maleic anhydride binding
K_{O_2}	equilibrium constant of dioxygen binding
$K_{O_{2/L}}$	equilibrium constant of ligand displacement by dioxygen
K_1	equilibrium constant of the binding of one axial ligand
K_2	equilibrium constant of the second axial ligand binding
K^*	equilibrium constant for the Co(salen)* intermediate
L	axial ligand or litre
LCoMc	five-coordinate Co(II) macrocycle complex
L_2CoMc	six-coordinate Co(II) macrocycle complex
LCoMc(O_2)	dioxygen adduct of a five-coordinate macrocycle complex
LCoP	five-coordinate complex of a Co(II) porphyrin

L_2CoP	six-coordinate complex of a Co(II) porphyrin
$LCoP(O_2)$	dioxygen adduct of a five-coordinate Co(II) porphyrin
$LCoP(O_2)^*$	"activated" dioxygen adduct intermediate
LCoSB	five-coordinate adduct of a Co(II) Schiff base
$LCoSB(O_2)$	dioxygen adduct of a five-coordinate Co(II) Schiff base
ln	natural logarithm
log	common logarithm
M	molar
	or metal
MA	maleic anhydride, cis-butenedioic acid anhydride
Mb	myoglobin
Mc	a tetradentate macrocycle
meso	refers to the positions of the bridging methines of a porphyrin ring
mL	millilitre(s)
mm	millimetre(s)
MPh	para-methoxyphenyl $-C_6H_4-OCH_3$, also referred to as p-OMe
MpIXDME	mesoporphyrin IX dimethyl ester, see Figure I.1a and Table I.2
MnTPP	Mn(II) α,β,γ,δ-tetraphenylporphyrin
N	normal
nm	nanometre
NMR	nuclear magnetic resonance
P	porphyrin
	or propionate, $-CH_2CH_2COOH$
PBu_3	tri-n-butylphosphine, $(n-C_4H_9)_3P$
Pc	phthalocyanine
PFP	picket fence porphyrin, meso-tetra-(α,α,α,α-o-pivalamidephenyl)porphyrin
Ph	phenyl, $-C_6H_5$
Pip	piperidine, $C_5H_{11}N$

pK_a	pH at which a base is 50% in the protonated form
PpIXDME	protoporphyrin IX dimethyl ester, see Figure I.1a and Table I.2
PPh_3	triphenylphosphine, $P(C_6H_5)_3$
Py	pyridine, C_5H_5N
$P_{½}$	pressure at which 50% of the substrate is converted
$P_{½}O_2$	pressure at which 50% of the substrate is oxygenated
r	statistical correlation coefficient
RhOEP	Rh(II) octaethylporphyrin, see Figure I.d and Table I.2
RhTPP	Rh(II) α,β,γ,δ-tetraphenylporphyrin, see Figure I.1c and Table I.2
RuOEP	Ru(II) octaethylporphyrin, see Figure I.1d and Table I.2
RuTPP	Ru(II) α,β,γ,δ-tetraphenylporphyrin, see Figure I.1c and Table I.2
s or sec	second(s)
salen	N,N-bis(salicylaldehyde)ethylenediimine, see Figure I.5b and Table I.3b
SB	Schiff base
sty	styrene, $C_6H_5CH=CH_2$
t	time
T	temperature
TCNE	tetracyanoethylene, $(CN)_2C=C(CN)_2$
THF	tetrahydrofuran, C_4H_8O
TiTPP	Ti(II) α,β,γ,δ-tetraphenylporphyrin, see Figure I.1c and Table I.2
$T(p\text{-}OCH_3)PP$	α,β,γ,δ-(p-methoxy)phenylporphyrin, see Figure I.1c and Table I.2
T(p-X)PP	a para-substituted α,β,γ,δ-tetraphenyporphyrin, see Figure I.1c and Table I.2

UV	ultraviolet
V	vinyl, $-CH=CH_2$, or unit displacement on the vertical scale of the oscilloscope used in stopped-flow determinations
Y	fraction of product formed during a particular experiment
α	first meso position on a porphyrin ring
α chain	one of the two types of polypeptide chains present in a Hb tetramer
β	second meso position on a porphyrin ring
β chain	one of the two types of polypeptide chains present in a Hb tetramer
γ	third meso position on a porphyrin ring
δ	fourth meso position on a porphyrin ring
ε	dielectric constant or molar extinction coefficient
ε_o	observed molar extinction coefficient at the start of an experiment
ε_∞	observed molar extinction coefficient when a reaction has been completed
λ	wavelength
μ	micro
ν	frequency
π	bonding where electron density is on either side of internuclear plane
π^*	antibonding π-orbital
σ	bonding where electron density is maximum on an internuclear axis or statistical standard deviation
ΔH	enthalpy of reaction

$\Delta H^{\ddagger}$	enthalpy of activation
ΔS	entropy of reaction
$\Delta S^{\ddagger}$	entropy of activation
1hx	1-hexene, $CH_2=CH_2CH_2CH_2CH_2CH_3$
2ot	2-octene, $CH_3CH=CHCH_2CH_2CH_2CH_2CH_3$
4-CN-Py	4-cyanopyridine
4-NH_2-Py	4-aminopyridine
$[Co]_T$	total cobalt reactant concentration
$[Co_T]$	total cobalt concentration
^oC	degree(s) centigrade
~	approximately
>	greater than
>>	much greater than
<	less than
<<	much less than
dimer	the term dimer is used to apply to the peroxo-bridged binuclear oxidation products formed in this work; this compares to the oxo-bridged products formed in the oxidation of iron systems which are also termed "dimers".
dioxygen	molecular oxygen, O_2, should be referred to as dioxygen, but is commonly referred to as simply oxygen. In this thesis the term dioxygen is used when an O_2 moiety is bound to a substrate; gaseous O_2 or O_2 in solution is referred to as oxygen.
M	the oxidation state of most metals in this thesis is M(II); any other oxidation state is specified in the thesis.

ACKNOWLEDGEMENTS

I wish to thank the help and useful suggestions of the many colleagues I had the privilege of working with at UBC. I would like to especially acknowledge Professor Brian R. James for his guidance and encouragement throughout the course of this work, particularly for his many comments during the preparation of this thesis.

Financial support of this research from the Natural Science and Engineering Research Council of Canada is gratefully appreciated.

Finally, I would like thank my family, especially my wife Joy, whose constant support and encouragement helped to make this thesis possible.

CHAPTER I

INTRODUCTION

I.1 Biological Oxygen Carrying Systems

I.1.1 General

The subject of molecular oxygen (O_2) interacting with metal complexes of macrocyclic ligands has fascinated workers in many scientific disciplines, ever since such a process has been recognized as that which occurs in oxygen storage and oxygen transport in biological systems.

The moiety of major importance in vertebrates is the so-called heme unit, which consists of an iron(II) porphyrin (usually protoporphyrin IX, Figure I.1b) complex. Myoglobin (Mb)[1], which stores oxygen in body tissues, consists of one polypeptide chain of 153 amino acids and one heme group, and has a molecular weight of 17,800. Hemoglobin (Hb)[1], which transports oxygen from the lungs to the body tissues, consists of four Mb type subunits arranged as a tetrahedron, and has a molecular weight of 64,500. Heme units are also the prosthetic group present in several oxygenases[2] (enzymes that incorporate one or two O atoms from O_2 into a substrate) and in cytochrome c oxidase[3], the terminal enzyme in the respiratory redox chain that reduces O_2 to water. The enzymes catalase and peroxidase[4], which utilize H_2O_2, both contain heme centres and are related to the oxygen systems.

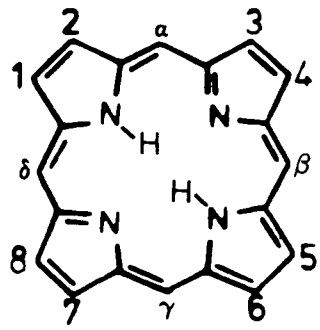

I.1a. Porphine with positions labeled

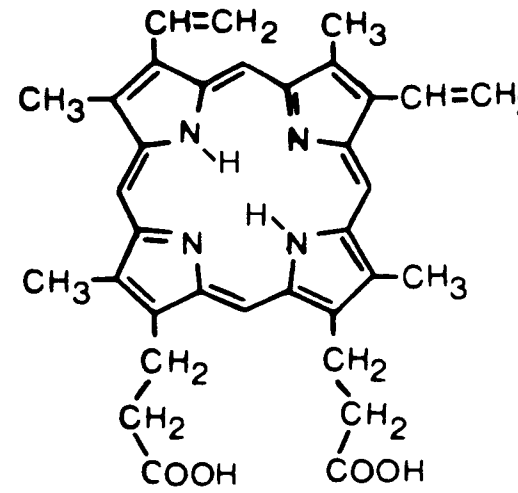

I.1b. Protoporphyrin IX

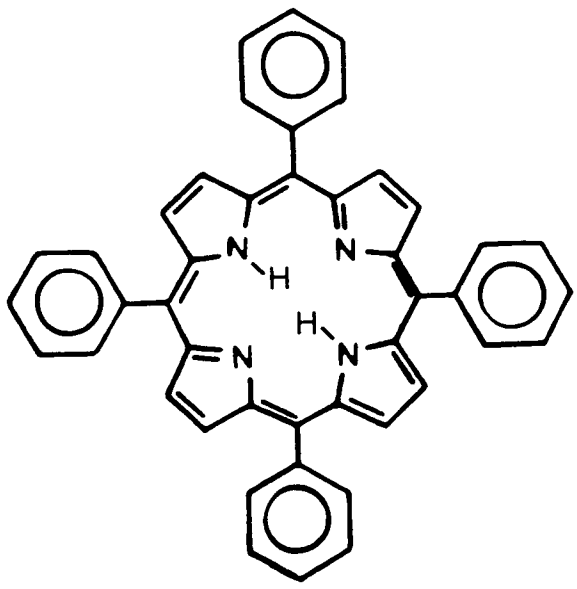

I.1c. Tetraphenylporphyrin

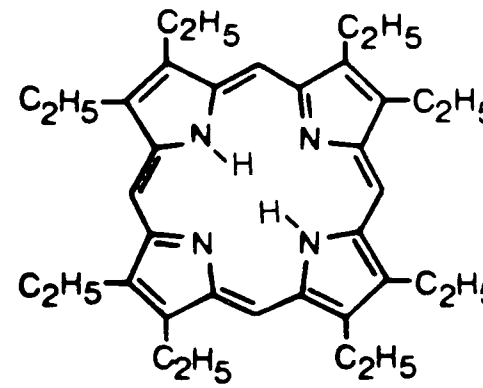

I.1d. Octaethylporphyrin

Figure I.1. Examples of different porphyrins.

Other oxygen-carrying metal complexes in biological systems include the hemerythrins, the hemocyanins, and hemovanadin.

Hemerythrins[5] are iron-containing oxygen carrying proteins found in many invertebrate species. However, the prosthetic group does not contain a porphyrin moiety; rather the iron is bound directly to the protein side chains. In general, hemerythrin occurs as an octamer of a molecular weight of about 108,000, with each subunit containing two iron atoms that bind one molecule of O_2.

Hemocyanins[6] are nonheme copper-containing proteins found in some of the arthropods and mollusks. Hemocyanins consist of a number of subunits which have a molecular weight of from 25,000 per copper atom to 37,000 per copper atom, depending on their source. Like hemerythrins, the manner in which the metal centre is bound to the protein is not clear. Hemocyanins absorb one molecule of O_2 for every two copper atoms in the protein, but the structure of the metal-dioxygen complex has not been well established.

Little is known about the nature of hemovanadin[7]. It is found in the 1.5 to 2.0 N H_2SO_4 solution in the vacuoles of the blood cells of certain tunicates. The partial pressure necessary to oxygenate one half of the available hemovanadin sites, the $P_{\frac{1}{2}}O_2$, for the cells has been found to be about 2 Torr.

A summary of some of the characteristics of these biological oxygen carriers is given in Table I.1.

Table I.1 Properties of Oxygen Carriers. Data taken from Basolo et al, Chem. Rev., 79, 139 (1979).

OXYGEN CARRIER	HEMOCYANIN	HEMERYTHRIN	HEMOGLOBIN	HEMOGLOBIN (α CHAIN)	HEMOGLOBIN (β CHAIN)	MYOGLOBIN	COBOGLOBIN
METAL	Cu	Fe	Fe	Fe	Fe	Fe	Co
OXIDATION STATE OF THE DEOXYGENATED FORM	+1	+2	+2	+2	+2	+2	+2
METAL:DIOXYGEN RATIO	$2Cu:1O_2$	$2Fe:1O_2$	$1Fe:1O_2$	$1Fe:1O_2$	$1Fe:1O_2$	$1Fe:1O_2$	$1Co:1O_2$
MAGNETIC-ELECTRONIC PROPERTIES OF:							
THE DEOXYGENATED FORM	zero spin	zero spin	high spin	high spin	high spin	high spin	low spin
THE OXYGENATED FORM	zero spin	zero spin	zero spin	zero spin	zero spin	zero spin	low spin
$P_{\frac{1}{2}}O_2$ @ 20°C, TORR	4.3[a]	4[b]	2.5[c]	0.46[d]	0.40[d]	0.65[e]	57[f]
BIOLOGICAL FUNCTION	transport	storage	transport	———	———	storage	———
NUMBER OF SUBUNITS	variable	8	4	1	1	1	1
COOPERATIVITY	yes	slight	yes	no	no	no	no*

a. Z. Er-el, N. Shaklai, and E. Daniel, J. Mol. Biol., 64, 341 (1972).
b. G. Bates, M. Brunori, G. Amiconi, E. Antonini, and J. Wyman, Biochem., 7, 3016 (1968).
c. E. Antonini, J. Wyman, M. Brunori, C. Fronticelli, E. Bucci, and A. Rossi-Fanelli, J. Biol. Chem., 240, 1096 (1965).
d. M. Brunori, R. W. Noble, E. Antonini, and J. Wyman, J. Biol. Chem., 241, 5328 (1966).
e. A. Rossi-Fanelli, and E. Antonini, Arch. Biochem. Biophys., 77, 478 (1958).
f. B. M. Hoffman, C. A. Spilburg, and D. H. Petering, J. Biol. Chem., 247, 4219 (1972).
*. The term coboglobin can refer to either apomyoglobin or apohemoglobin reconstituted with cobalt. Hoffman et al studied reconstituted sperm whale and horse myoglobins, and so no cooperativity was observed. Cooperativity is observed for cobalt reconstituted hemoglobin.

I.1.2. Myoglobin and Hemoglobin

The heme group in myoglobin is completely buried within the folded polypeptide chain, except for one edge which contains the two hydrophilic propionic acid groups. The hydrophilic groups of the protein are spread uniformly over the outside surface of the molecule, and the strongly hydrophobic side chains lie inside the molecule. Some of the hydrophobic groups line the inner surfaces of the alpha helices, while the others form a hydrophobic environment for the heme.[8]

The function of myoglobin, to store and release dioxygen, takes place at the iron centre of the heme group. The purpose of the polypeptide chain around the heme is to keep the ferrous iron from being oxidized (metmyoglobin with a ferric iron does not bind dioxygen), and to enhance the dioxygen binding ability of the heme.

The heme group is joined to the polypeptide chain by binding in one of its axial coordination sites to an imidazole nitrogen of a histidine residue. This so-called proximal histidine side chain is locked into position by a hydrogen bond from its other ring nitrogen to the carbonyl oxygen of a nearby leucine. The sixth coordination site, trans to the coordinated imidazole, is vacant in deoxymyoglobin, and is the site for the dioxygen in oxymyoglobin. In metmyoglobin the oxygen site is occupied by a coordinated water molecule.[9]

On the far side of the dioxygen moiety of oxymyoglobin lies a distal histidine, which is too far from the iron atom to coordinate directly with it, but indirect interactions; e.g. hydrogen bonding with a coordinated oxygen or water molecule can possibly occur[8,9].

Upon oxygenation, the iron in myoglobin transforms from a high spin S=2 state to a spin paired S=0 state[10]. The change in spin state upon oxygenation is accompanied by the iron going from out of the plane toward the coordinated imidazole by several tenths of an Angstrom in deoxymyoglobin[11], to occupying the mean plane of the porphyrin ring in oxymyoglobin[11a,12].

As well as being able to bind dioxygen, the sixth coordination site of the protein iron can also coordinate other small molecules or ions, such as CO[10a], NO[13], NO^-[14], OH^-[14], F^-[14], N_3^-[15], CN^-[16], and H_2S[17].

Of the four myoglobin type subunits in hemoglobin, there are two alpha chains and two beta (shown in Figure I.2) chains. They form a compact spheroidal molecule with approximate dimensions of 64 x 55 x 50 A[18]. The four heme groups are arranged in separate pockets on the surface of the molecule, and have environments similar to that of the myoglobin heme. Upon oxygenation, the two alpha hemes are brought closer together by 1 A, while the beta hemes are separated by 6.5 A[12b,19]. This heme-heme interaction upon oxygenation gives rise to the "cooperativity effect," by which the subsequent dioxygen binding is more facile than if no heme-heme interaction were present[8d,12a,20]. The cooperativity effect is of biological use, as it means that hemoglobin can release more of its oxygen to myoglobin in a low oxygen environment, than if there were no cooperativity effect.

Another way in which oxygen transfer from hemoglobin to myoglobin is aided is the Bohr effect[21]. Since oxyhemoglobin behaves as a stronger acid than deoxyhemoglobin, the oxygenated form is favored in the basic lung tissues, and the release of oxygen to myoglobin is aided by the presence

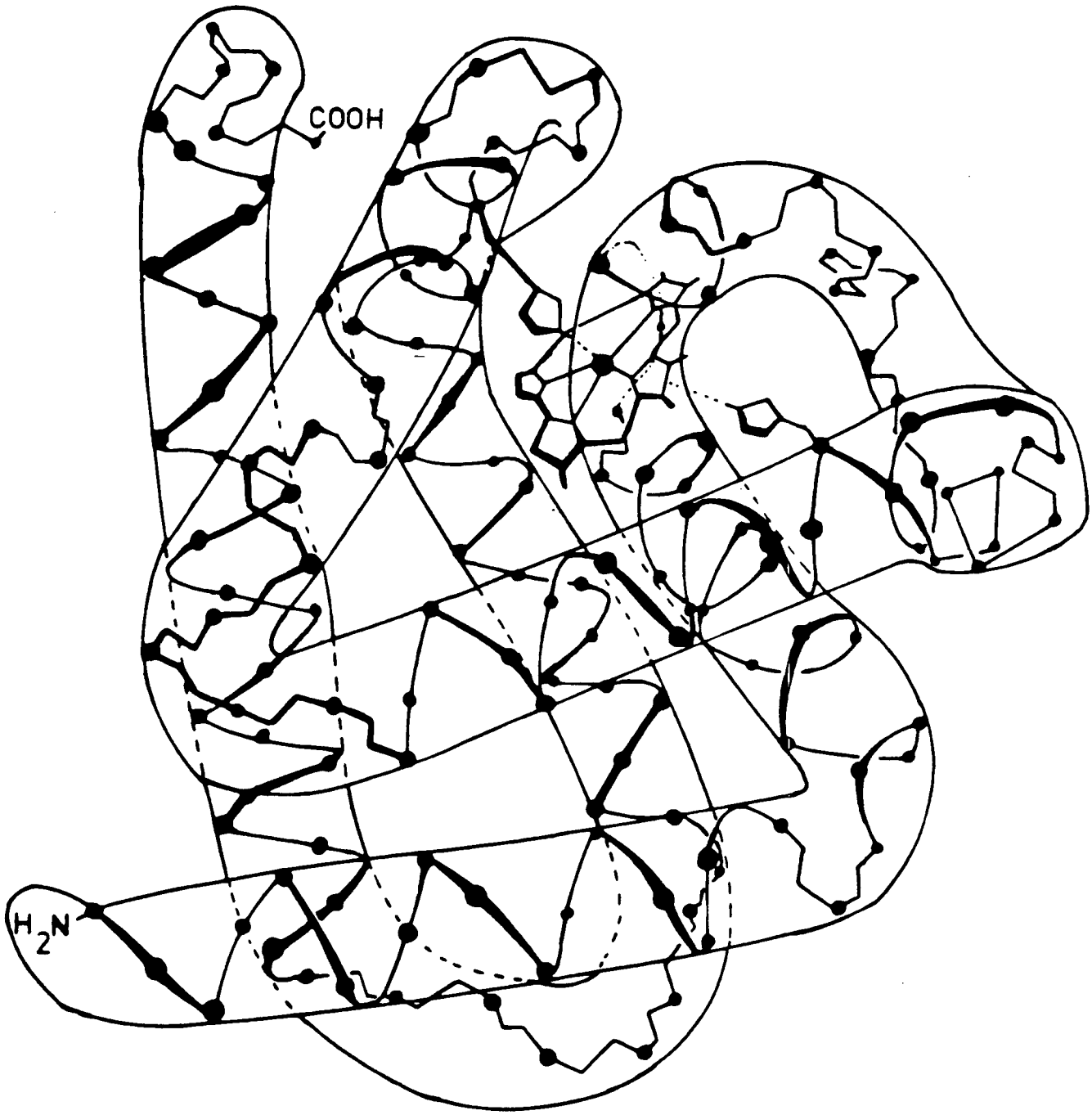

Figure I.2. The structure of the beta chain of hemoglobin. Taken from M. F. Perutz and L. F. TenEyck, Cold Spring Harbor Symp. Quant. Biol., 36, 295 (1971).

of lactic acid and carbonic acid in the body tissues. Like the cooperativity effect, the Bohr effect is not present in myoglobin or in fragmented hemoglobin units.

I.2 Synthetic Oxygen Carriers

I.2.1 Rationale for Synthetic Oxygen Carriers

Kinetic, thermodynamic, and spectroscopic studies, on the reaction of dioxygen with any natural protein systems, whether heme or non-heme systems, are relatively complex, and conclusions regarding the nature of the interaction are sometimes difficult to draw[22].

Since the active site of these proteins often consists of a metal quadridentate macrocyclic complex, it is instructive to study the interactions of such complexes with O_2, both to better appreciate the nature of the metal-dioxygen interactions, and the role of the protein in the natural system.

This model system approach clearly has limitations, and has been reviewed extensively[22,23]. For example, the heme-heme interactions of the hemoglobin protein chains, which generate the cooperativity and the Bohr effects, cannot be elucidated by studies using single metal sites. However, knowledge gained from model systems can be used to help assign the role of the metal in the system, and from that, the role of the protein in the system can be better understood.

Hemes, as well as promoting oxygen storage and transport, are also responsible for several enzymatic oxygenation reactions[2-4]. If similar model complexes can aid similar reactions in vitro, then there may be important implications for industrial catalysis.

I.2.2 General Synthetic Oxygen Carriers

Although the study of transition metal complexes that reversibly bind dioxygen is a relatively new field, many such complexes have been reported. Several of these, such as Vaska's $Ir(PPh_3)_2(CO)(Cl)(O_2)$ complex[24], incorporate a "side-on" π-dioxygen metal linkage. While these compounds have been studied extensively[25], they are probably poor models for biological systems.

These compounds consist of metals in zero or low oxidation states with ligands such as phosphines, which have little or no biological role. The metals of these compounds tend to be "soft", and thus favor binding dioxygen in a soft π-linkage, while metals of biological systems, such as iron, are usually in higher oxidation states and tend to be "hard". Thus a hard σ-bonding mode is favored.

It has been noted[26] that for the biological metals iron(II) and copper(I), a second order Jahn-Teller effect would lead to a bent metal-dioxygen bond, even if a π-bond were initially formed. π-Bonding is also thought to be favored by complexes susceptible to a two electron oxidative addition (e.g. Rh(I) and Ir(I)), while one electron reductants would favor "end-on" binding and result in a one electron reduction of dioxygen to superoxide[25b].

Among the first row transition metals, often those capable of undergoing a one electron oxidation tend to interact with dioxygen[23b]. Thus Mn(II), Fe(II), Co(II), Cu(I), and Cr(II) all complex dioxygen, while Fe(III), Co(III), Cu(II), as well as Ni(II) and Zn(II), which have no readily accessible higher oxidation states, do not.

I.2.3. Porphyrins

Since a porphyrin ligand is present in the prosthetic group of the most important biological oxygen carriers, and such ligands are used in numerous model study systems, it is important to understand the nature of porphyrins.

Porphyrins are macrocyclic compounds that contain four pyrrole or substituted pyrrole rings joined by sp^2 hybridized carbon atoms. Formally, they can be viewed as being derived from the parent compound, porphine (Figure I.1a), by substitution of the hydrogen atoms at the peripheral positions of the macrocyclic ring. Since the porphyrin system is a highly delocalized one, substitution by either electron withdrawing or electron donating groups at the peripheral positions can have profound effects on the molecule's complexing properties with metals, even though the substituents may be separated by many atoms from the metal. Also the fact that many substitutions may be made enhances the versatility of these compounds.

A formal nomenclature system, labeling the eight "pyrrole" positions from 1 to 8 and the four "meso" positions α, β, γ, and δ, has been devised[27]. However, trivial names have been adopted for most porphyrins, and will be used throughout this thesis. Table I.2 lists the substitution patterns and trivial names of the compounds discussed.

Porphyrins can fall into either the "natural" porphyrins, a class of compounds that are derived either from, or by modification of, metallo-porphyrin complexes obtained from nature, or a class of compounds that are obtained from synthesis.

Protoporphyrin IX, mesoporphyrin IX, and the deuteroporphyrin IX compounds are examples of natural porphyrins, as they can be prepared

Table I.2 Trivial Names and Side Chain Substituents of Porphyrins.

See Figure I.1a.

PORPHYRIN	SUBSTITUENTS ON POSITION											
	1	2	3	4	5	6	7	8	α	β	γ	δ
Protoporphyrin IX	M	V	M	V	M	P	P	M	H	H	H	H
Deuteroporphyrin IX	M	H	M	H	M	P	P	M	H	H	H	H
Diacetyldeutero-porphyrin IX	M	Ac	M	Ac	M	P	P	M	H	H	H	H
Dibromodeutero-porphyrin IX	M	Br	M	Br	M	P	P	M	H	H	H	H
Etioporphyrin I	M	E	M	E	M	E	M	E	H	H	H	H
Octaethylporphyrin	E	E	E	E	E	E	E	E	H	H	H	H
Mesoporphyrin IX	M	E	M	E	M	P	P	M	H	H	H	H
Coproporphyrin III	M	P	M	P	M	P	P	M	H	H	H	H
Uroporphyrin III	A	P	A	P	A	P	P	A	H	H	H	H
Hematoporphyrin IX	M	B	M	B	M	P	P	M	H	H	H	H
α,β,γ,δ — tetraphenyl-porphyrin	H	H	H	H	H	H	H	H	Ph	Ph	Ph	Ph
α,β,γ,δ — (p-methoxy)-tetraphenylporphyrin	H	H	H	H	H	H	H	H	MPh	MPh	MPh	MPh

M- $-CH_3$

E- $-CH_2CH_3$

V- $-CH=CH_2$

A- $-CH_2COOH$

Ac- $-COCH_3$

Br- $-Br$

B- $-CHOHCH_3$

P- $-CH_2CH_2COOH$

H- $-H$

Ph- -Phenyl

MPh $-p-OCH_3$-Phenyl, also referred to as p-OMe

from chloroprotoporphyrin IX iron(III), known as hemin, which is obtained from blood hemoglobin. The propionic acid side chains are often converted to dimethyl or diethyl esters in order to prevent side reactions resulting from the proton of the propionic acid side chains, or to aid in solubility.

Of the synthetic porphyrins, $\alpha,\beta,\gamma,\delta$-tetraphenylporphyrin (TPP)[28] and octethylporphyrin (OEP)[29] are the most commonly studied. OEP resembles more closely the natural porphyrins, but TPP is more widely studied because of its relative ease of synthesis, and because substitution into the phenyl rings can be readily achieved[30].

Phthalocyanine[31] is a compound that is similar to porphine except that the porphine methine bridges are replaced by aza bridges, and the pyrrole rings are further delocalized by the presence of benzo groups (Figures I.3a and I.3b). This macrocycle gives rise to spectral properties different from those of porphyrins; for example the relative intensities of the visible and the Soret bands of the cobalt(II) complexes are reversed (Figures I.4a and I.4b).

An especially interesting compound is octamethyltetrabenzoporphyrin (OMBP), since it is structurally intermediate between a porphyrin and a phthalocyanine (Figure I.3c). The intermediate nature of this macrocycle is further suggested by the spectrum of CoOMBP, in which the intensities of the Soret and visible bands are approximately the same (Figure I.4c).

I.2.4 Schiff Bases

Many metal-Schiff base complexes have been found to reversibly bind dioxygen. These complexes generally include tetradentate ligands formed by the Schiff base condensation reaction (Eq. I.1). For example, ethylene-

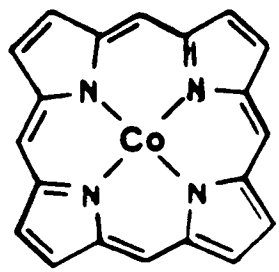

Co PORPHYRIN

Figure I.3a

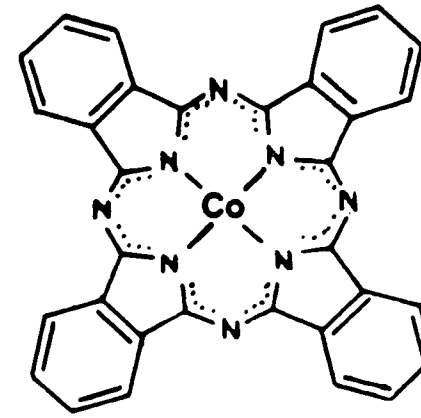

Co PHTHALOCYANINE

Figure I.3b

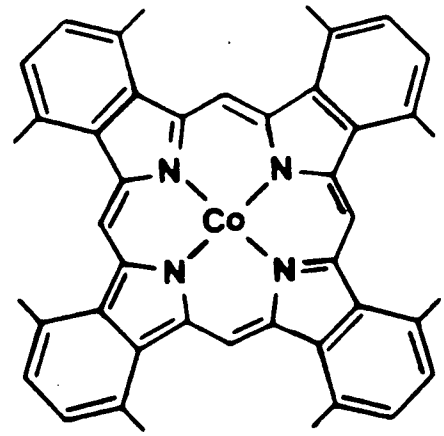

CoOMBP

Figure I.3c

Figure I.3. A variety of cobalt macrocycle complexes.

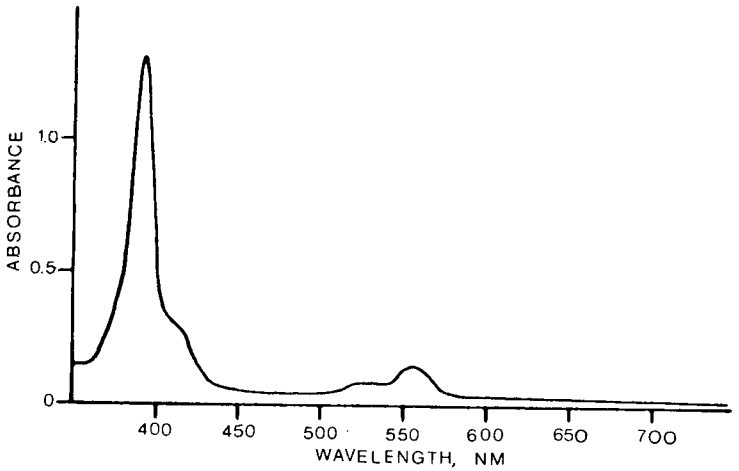

Fig. I.4a. VIS spectrum of cobalt etioporphyrin I. From work in this thesis.

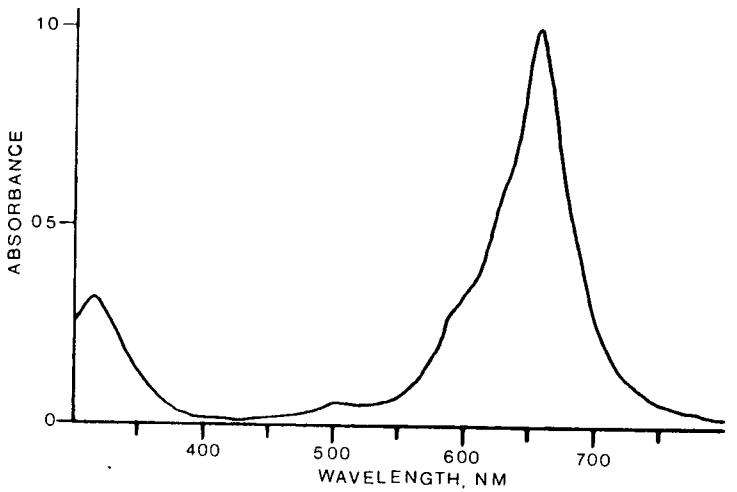

Fig. I.4b. VIS spectrum of cobalt phthalocyanine. From L. Edwards and M. Gouterman, J. Mol. Spectrosc., 33, 292 (1970).

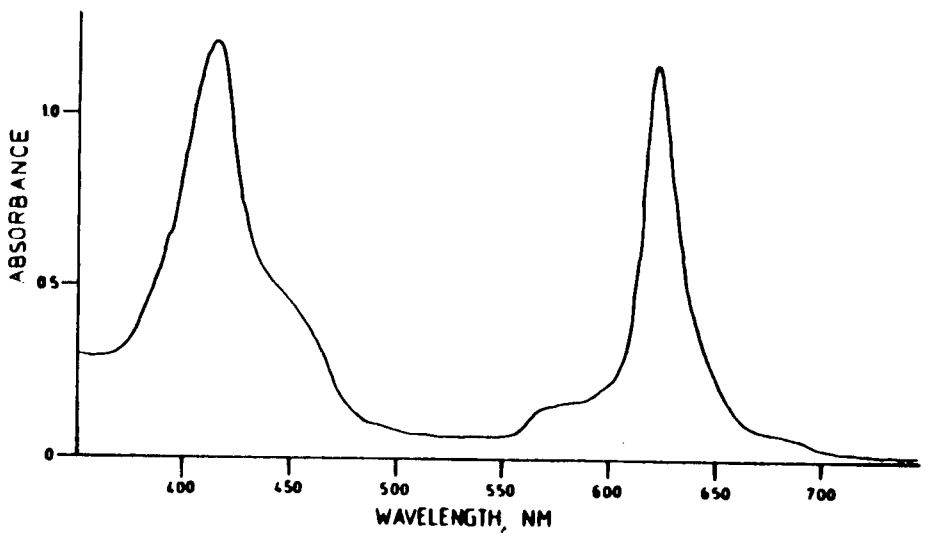

Fig. I.4c. VIS spectrum of CoOMBP, from this thesis.

Figure I.4. Visible spectra of a variety of cobalt macrocycle complexes.

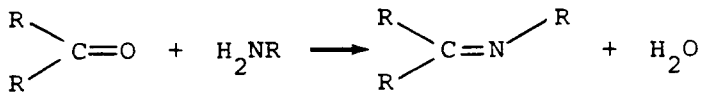

(I.1)

diamine can be reacted with a dicarbonyl compound to give a tetradentate compound with two nitrogen and two oxygen donors (Eq. I.2).

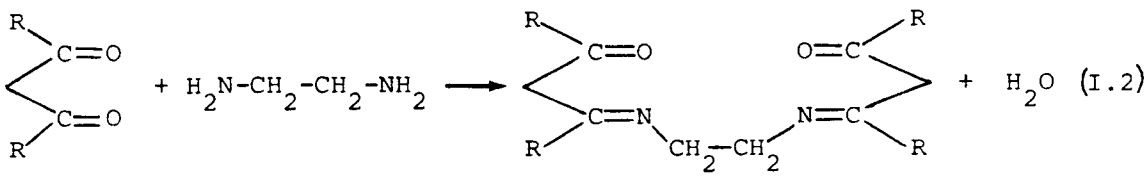

(I.2)

Pentadentate Schiff base compounds can be utilized, and sulfur or nitrogen atoms may replace one or both of the oxygen atoms as donors[32].

Schiff bases are often referred to by their mnemonic abbreviations. For example, bis(acetylacetone)ethylenediimine becomes acacen, and N,N-bis(salicylaldehyde)ethylenediimine becomes salen. If the Schiff base compound has substituents, then the mnemonic simply adds the group symbol; e.g. N,N-bis(3-methoxysalicylaldehyde)ethylenediimine is 3-MeOsalen. Examples of Schiff base compounds are given in Figures I.5a and I.5b, and in Table I.3.

A tetradentate Schiff base ligand is generally arranged in a plane around the chelated metal. Some chelating ligands, such as acacen, allow some distortion from planarity, but the inclusion of an aromatic ring, as in salen, causes the ligand to be more rigid, and adds to its tendency for planarity. If the number of carbon atoms in the alkylene bridge is increased above two, then tetrahedral distortions can occur[33], and if the number of separating carbons exceeds six, the complex can become tetrahedral[34].

Pentadentate complexes can adopt either square pyramidal[35] or trigonal bipyramidal[36] geometries.

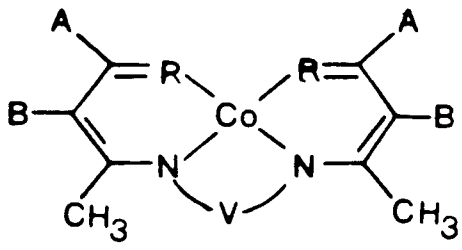

Figure I.5a. Type A Schiff base.

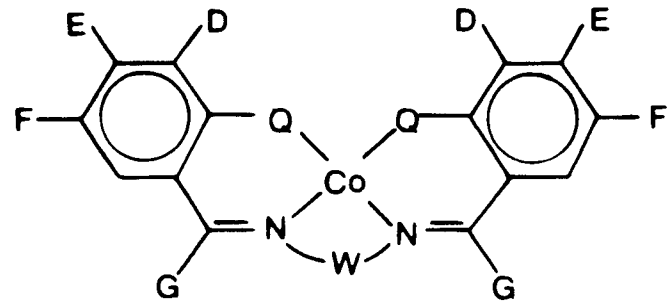

Figure I.5b. Type B Schiff base.

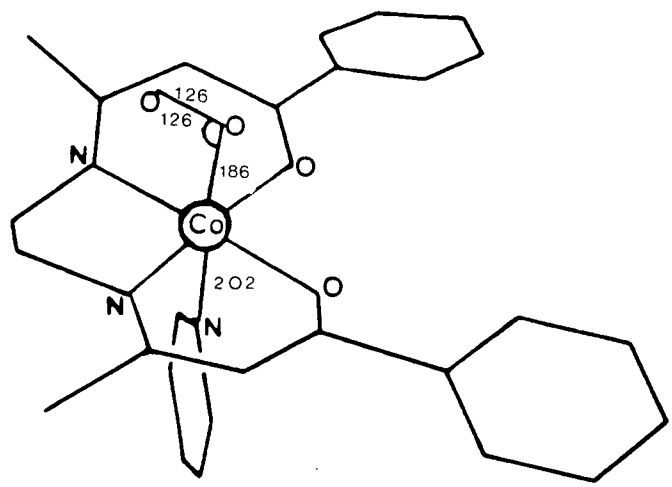

Figure I.5c. Structure of PyCo(benacen)(O_2). From G. A. Rodley and W. T. Robinson, Nature(London), 235, 438 (1972).

Figure I.5. A variety of cobalt Schiff base complexes.

Table I.3a. Mnemonic Names and Substituents of Type A Schiff Bases.

Compound	V	A	B	R
Co(acacen)	$-(CH_2)_2-$	CH_3-	H-	O
Co(Meacacen)	$-(CH_2)_2-$	CH_3-	CH_3-	O
Co(Phacacen)	$-(CH_2)_2-$	CH_3-	C_6H_5-	O
Co(benacacen)	$-(CH_2)_2-$	C_6H_5-	H-	O
Co(Clbenacacen)	$-(CH_2)_2-$	$p\text{-}ClC_6H_4-$	H-	O
Co(sacacen)	$-(CH_2)_2-$	CH_3-	H-	S
Co(acacpn)	$-CH_2-\underset{\displaystyle CH_3}{\overset{\displaystyle |}{CH}}-$	CH_3-	H-	O

Table I.3b. Mnemonic Names and Substituents of Type B Schiff Bases.

Compound	W	D	E	F	G	Q
Co(salen)	$-(CH_2)_2-$	H	H	H	H	O
Co(3-MeOsalen)	$-(CH_2)_2-$	CH_3O	H	H	H	O
Co(4,5-Me_2salen)	$-(CH_2)_2-$	H	CH_3	CH_3	H	O
Co(saloph)	$-C_6H_4-$	H	H	H	H	O
Co(sal(±) or (m)chxn)	$-CH\!\!\!\!\diagup\!\!\!\!\diagdown\!\!\!\!-CH-$ $(CH_2)_4$	H	H	H	H	O
Co(o-Mesalpt)	$-(CH_2)_3-NH-(CH_2)_3-$	H	H	H	CH_3	O
Co(amben)	$-(CH_2)_2-$	H	H	H	H	N
Co(tsalen)	$-(CH_2)_2-$	H	H	H	H	S

As with the porphyrins, a wide variety of substitutions can be made in Schiff base compounds to alter their electronic and solubility properties. Unlike the porphyrins, the Schiff base compounds do not have extensive conjugated systems available for π-bonding to the metal, and it is generally thought that porphyrins are better able to delocalize electron density from the metal centre, causing metalloporphyrin complexes to be less able to bind dioxygen than metal-Schiff bases[32,37].

I.2.5 Transition Metal Complexes

I.2.5.1 Iron Complexes

Since Fe(II) is the metal used in most biological systems, it would be a logical choice for model system studies. Recently, important advances have been made with iron systems, but these have not been accomplished without considerable difficulty. Under ordinary conditions iron complexes tend to rapidly and irreversibly oxidize[38]. Further, ferrous porphyrin species in solution tend to form six-coordinate complexes with any ligand present[39], while in biological systems a five-coordinate moiety may be present; e.g. in deoxymyoglobin.

Iron(II) porphyrins have been designed so that the formation of the bridged μ-oxo-dimer (Fe(III)-O-Fe(III)), the usual oxidation product, is sterically hindered. Such complexes include the picket fence porphyrins[40] and the capped porphyrins[41]. The latter type of compound also prevents the bonding of an axial ligand on one side of the porphyrin ring, while the picket fence type does not. Five-coordinate iron(II) porphyrin complexes can be obtained by using sterically hindered ligands, such as 1,2-dimethylimidazole and 2-methylimidazole[42], and such species are capable of binding dioxygen to form six-coordinate $LFeP\cdot(O_2)$ complexes[43]. Crystal structures

of two such picket fence systems that show the bent geometry of the end-on iron-dioxygen link (Fe-O-O) have been reported[40j-l].

Attaching an oxygen carrying complex to the surface of a solid or to a polymer can prevent the approach of two metal atoms to each other, and thus can impede "dimerization," such as formation of Fe(III)-O-O-Fe(III)[39c], a likely step in irreversible oxidation. This approach was first taken by Wang[44], who showed that dioxygen binds reversibly to 1-(2-phenylethyl)-imidazole heme diethyl ester embedded in a matrix of polystyrene and 1-(2-phenylethyl)imidazole. Attachment of Fe(II) tetraphenylporphyrin to a silica gel support has been shown to produce an efficient oxygen carrier[45]. Fe(II) protoporphyrin attached to several poly-4-vinylpyridine and poly-L-lysine polymers, has also been shown to reversibly bind dioxygen to a ratio of $1Fe:1O_2$ in the solid state[46]. Similar behavior has been observed in solution for iron(II) porphyrin compounds covalently bonded to a highly cross-linked polystyrene[47]. The binding of dioxygen to an iron(II) protoporphyrin poly-L-lysine polymer in solution has exhibited cooperativity, the insertion of dioxygen into the system promoting the reestablishment of the α-helix conformation of the polymer[48]. Recently water soluble poly-aminophosphazenes have been proposed as "carrier" ligands for iron(II) porphyrins[49], but these polymers have not been able to prevent irreversible oxidation.

At low temperatures the oxidation reaction (likely via a bimolecular $Fe(III)(O_2^-)$ + Fe(II) process) is often sufficiently inhibited so that reversible oxygenation can be studied. This was first successfully observed with a five-coordinate pyrroheme-N-(3-(1-imidazoyl)-propylamide system at $-45^{\circ}C$ in dichloromethane[50]. Several workers subsequently examined the

reversible binding to six-coordinate iron(II) porphyrin complexes at low temperatures[51], and detailed kinetic and thermodynamic studies have been accomplished in some cases[52].

I.2.5.2 Copper Complexes

Model systems of copper are of intrinsic interest, as copper can transport oxygen in biological media, although porphyrin complexes are not involved. Two synthetic complexes that bind one mole of dioxygen reversibly per two moles of copper are a copper(I) complex of the pentadentate ligand derived from 2,6-diacetylpyridine and histimine[53], and a binuclear complex of two copper(I) atoms ligated to 1,4-bis(1-oxo-4,10-dithio-7-azacyclododecan-7-ylmethyl)benzene[54].

I.2.5.3 Chromium Complexes

Stomberg[55] has described numerous dioxygen complexes of chromium of the types $(Cr(O_2)_2X_3)$, $(CrO(O_2)_2X)$, or $(Cr(O_2)_4)$ in which the metal centre is formally Cr(IV) or Cr(V) and X is a mono- or bidentate ligand. The dioxygen moieties are bound side-on and are proposed as peroxides that are bound with a π-linkage[26]. However, in the chromium dioxygen adduct, $PyCrTPP(O_2)$, the dioxygen appears to be bound end-on as a superoxide[56]. Redox potentials predict that dioxygen will likely bind more strongly to chromium than to iron, cobalt, or manganese systems[57], and this is consistent with the irreversibility of the formation of the chromium-dioxygen porphyrin complexes.

I.2.5.4 Manganese Complexes

Initial attempts to study the interaction of dioxygen with manganese tetradentate chelates resulted in irreversible oxidation of Mn(II) to Mn(III) or to Mn(IV)[58]. However, reversible oxygenation has been observed with meso-

tetraphenylporphinatopyridine manganese(II), PyMnTPP, in toluene at -78°C[59]. The dioxygen appears to be π-bonded to the metal and the system is formulated as a manganese(IV) peroxide[59b,c]. Similar behavior is reported for para-substituted TPP complexes of Mn[60]. The reversible formation of a manganese phthalocyanine dioxygen adduct, formulated as a superoxide, has been observed at room temperature in dimethylformamide and dimethylacetamide[61].

I.2.5.5 Titanium Complexes

Recent reports[62] describe reversible dioxygen binding to FTi(III)TPP. The FTi(III)TPP was embedded in a matrix of OTi(IV)TPP in order to prevent the irreversible formation of Ti(IV)TPP(O_2), where dioxygen is bound as a peroxide[63]. Reversible oxygenation could be carried for several cycles on this system in the solid state, but when FTi(III)TPP was exposed to dioxygen at -80°C in toluene, irreversible oxidation occurred. ESR evidence suggested that the dioxygen adduct was best formulated as a Ti(IV)-superoxide.

I.2.5.6 Ruthenium Complexes

Solutions of $(CH_3CN)_2$Ru(II)OEP have been shown to reversibly absorb O_2 in a ratio of $1O_2$:1Ru at ambient conditions[64]. At the present time it is uncertain whether Ru binds dioxygen in a σ-end-on or a π-side-on manner. However, THF_2Ru(II)OEP reacts with π-bonding C_2H_4 reversibly[65] which suggests that a side-on Ru(IV)(O_2) configuration is likely.

I.2.5.7 Rhodium Complexes

In 1972 it was reported that an isolated Rh(II)TPP complex was unreactive to O_2[66], but it has recently been suggested that the isolated complex was in a fact a dioxygen adduct[67]. Oxygenation of Rh(II)TPP is thought to be essentially irreversible, as is the oxygenation of $(Rh(II)OEP)_2$. ESR evidence suggests that these adducts are formally Rh(III)-superoxide species.

I.3 Cobalt Complexes

I.3.1 General

The most widely studied transition metal centre for dioxygen binding is Co(II) and much of the current knowledge of metal-dioxygen moieties has come from investigations on such systems.

Because cobalt has one more electron than iron, the eighteen electron rule implies that five-coordinate complexes of Co(II) are likely to be much more stable than those of Fe(II), and so the oxygenation reaction can be studied as a simple addition to a vacant coordination site in Co(II) complexes, rather than as a substitution reaction that occurs with most simple six-coordinate Fe(II) complexes. In this respect, cobalt model systems resemble some natural systems more closely than do iron systems.

The presence of the unpaired electron in cobalt allows the use of ESR as a valuable tool to probe the electron distribution between the metal and the dioxygen, and much information can be obtained on the nature of the metal-dioxygen bond. Indeed, this technique has been dominant in suggesting that dioxygen may be bonded to cobalt as a superoxide in a bent manner, with a formal one electron transfer from the cobalt to dioxygen[68], similar to that initially proposed by Pauling for oxyhemoglobin[69]. It has recently been suggested that the amount of real electron transfer may vary substantially from complex to complex, and in some cases there may be little electron transfer, thus making the formal assignment of oxidation states somewhat misleading[70]. Alternative π-bonded formulations have also been proposed for natural oxygen carriers[71]. Although dioxygen appears to bind to the natural systems and to cobalt primarily as a σ-bonded superoxide, some π-interactions between the cobalt and the dioxygen are possible.

The use of cobalt macrocyclic complexes as models for biological iron

systems has some drawbacks. For example, cobalt does not bind dioxygen as strongly as iron (e.g. in compounds where only the metal is different, the $P_{\frac{1}{2}}O_2$ value for the cobalt complex is generally at least an order of magnitude greater than for the iron complex[72]). To some extent this is an advantage since it results in less tendency of the cobalt to undergo irreversible oxidation[23c]. Also, especially at low temperatures, the dioxygen affinity of Fe(II) complexes is so great that it is often difficult to get solutions sufficiently oxygen-free to observe only the deoxy species.

I.3.2 Early Cobalt Dioxygen Work

In 1852 it was reported that the exposure of ammoniacal solutions of Co(II) salts to the atmosphere resulted in the formation of brown compounds[73]. These were characterized in 1898 as containing the diamagnetic cation[74] $((H_3N)_5Co(O_2)Co(NH_3)_5)^{4+}$. In 1933 it was observed that crystals of the cobalt Schiff base complex Co(salen) darkened when exposed to air[75] and in 1938 Tsumaki[76] showed that this was due to reversible oxygen binding. This work was then followed up by that of Calvin et al[77] and Diehl et al[78]. Interest in this behavior was intense, and for a short period during World War II the US Navy used cobalt Schiff bases as a means of producing pure oxygen[79], and more recently a cobalt Schiff base complex was proposed as a source of pure oxygen for the crew of the B-1 bomber[80].

I.3.3 Cobalt Schiff Base Compounds

By 1969[68a,81] it had been established that under certain conditions, some cobalt Schiff base complexes would reversibly bind dioxygen in non-aqueous solutions. Although four-coordinate cobalt(II) Schiff base chelates bind dioxygen very poorly, the presence of one axial ligand greatly enhances oxygenation[82]. There is no correlation between the dioxygen affinity and the

pK_a of the axial ligand, although a linear correlation has been established between the dioxygen affinity and the ease of oxidation of the cobalt(II) centre, measured as $E_{\frac{1}{2}}$ for Co(II)⟶Co(III)[82,83].

Generally, the greater the electron density on the cobalt centre, the easier it is for that centre to bind dioxygen. This is evidenced by the decreased dioxygen affinity of the cobalt Schiff base complex when the oxygen atoms of the macrocyclic ligand are replaced by π-electron-withdrawing sulfur atoms[84], or when an axial nitrogen-donor is replaced by a phosphorus- or sulfur-donating one[32].

The nature of the bound dioxygen is well established in cobalt(II) Schiff base-dioxygen complexes. As well as the previously mentioned ESR work, there have been infrared[81], resonance Raman spectroscopy[85], and X-ray PES (photoelectron spectroscopy)[86] studies that have all given results consistent with what is essentially a Co(III)-superoxide system. Theoretical calculations also predict $Co(III)(O_2)^-$ [68f,h], and finally numerous crystallographic studies have shown that the dioxygen is bound in the Pauling bent end-on manner[87] with O-O bond lengths comparable to that of superoxide (Figure I.5c).

Cobalt Schiff base work in this thesis will be concerned with Co(II)(salen), its reactivity toward axial ligands and dioxygen, as well as solvent dependencies of the reactions.

I.3.4 Cobalt Porphyrin Compounds

Hoffman and other workers have successfully substituted the iron of hemoglobins and myoglobins with cobalt, and noted the resulting properties of reversible oxygen binding[88]; the cobalt(II) protoporphyrin IX group is thought to be situated in the same place as the original heme group, with

the metal centre slightly displaced from the plane of the porphyrin toward the proximal histidine. Of interest, cobalt-substituted hemoglobin exhibits cooperativity, while cobalt-substituted myoglobin binds dioxygen about 1% as strongly as natural myoglobin[72].

The $P_{\frac{1}{2}}O_2$ value for the 1-methylimidazole complex of CoPpIXDME in toluene at 20°C is ~2.5 x 10^4 Torr[89], while the corresponding value for coboglobin is 57 Torr[88a]. The presence of the protein definitely enhances the oxygen affinity of the cobalt complex centre. Differences in thermodynamic parameters have been discussed in terms of several effects, including transformation of the protein to a more stable conformation upon oxygenation[27c], and the presence of the protein preventing solvation of the metal centre[90].

Extensive thermodynamic work on oxygenation and binding of nitrogen-donor ligands has taken place using various complexes of CoPpIXDME in several solvents. Judging by discrepancies in the data from the work of several groups[89,91], there appear to be difficulties in obtaining good thermodynamic values on these systems. A comparison of the equilibrium constants, the ΔH, and the ΔS values for axial N-donor ligand binding shows that no simple correlation exists between any of these parameters and the pK_a of the protonated ligand[89]. However, for ligands of a structurally similar series, e.g. substituted pyridines, a correlation does exist between the ligand binding constant (K_1) and the pK_a of the protonated ligand[89,92]. Similar observations have been noted for the affinity of dioxygen and the pK_a of the axial ligand[92,93]. Work done on various para substituted PyCo(II)Tp-XPP complexes revealed a Hammett relationship between the σ-value of the para-substituents and log K_1[94]. Limited oxygenation studies on cobalt mesopophyrin, deuterporphyrin[91d,93] and octaethylporphyrin[95] complexes,

together with the work on CoPpIXDME systems[89,91], suggest that oxygen affinity is possibly related to the ease of transfer of electron density to dioxygen, since the more basic axial ligands tended to enhance the cobalt's affinity for dioxygen. Work with the above cobalt porphyrin systems yielded a range of porphyrin basicities too narrow to generate any conclusion about a relationship between oxygen affinity and electron donating abilities of the planar porphyrin ligands[91].

Anomalously high oxygen affinity has been noted for a cobalt picket fence porphyrin system[90a]. Thus, CH_3-ImCo(II)PFP has a $P_{\frac{1}{2}}O_2$ value of 140 Torr at 25°C in toluene[90b], which compares to an estimated value of 15,500 Torr for CH_3-ImCo(II)T(p-OCH_3)PP[92]; the presence of the picket fence is thought to break up adverse solvation effects which hinder oxygenation in the TPP system.

It has also been shown that the presence of a more polar solvent enhances the formation of the more polar Co(III)$\cdot(O_2^-)$ product[91a].

Although a few of the cobalt porphyrin complexes studied form six-coordinate species under certain circumstances[89,92], almost no quantitative work has been done with these species.

Cobalt(II) octamethyltetrabenzoporphyrin (CoOMBP) is unusual in that it was found to readily form six-coordinate species with some axial ligands. Further, OMBP is a very weakly basic porphyrin[96]. Therefore, extensive ligand and dioxygen binding studies on this particular metalloporphyrin were considered likely to give a better insight into the roles that the porphyrin and axial ligands play in dioxygen binding in natural systems.

Since OMBP is also considered to be a relatively strong π-donor[96c], it was also of interest to examine the effect of such a porphyrin on O_2 affinity. More extensive studies in a variety of solvents were also considered likely to lead to a better understanding of the solvent role.

I.3.5 Other Cobalt Compounds

In the late 1940s, it was discovered that cobalt amino acid complexes were capable of binding dioxygen reversibly[97], and recently stable 1:1 dioxygen complexes of Co(II) polyamines have been observed in large zeolite cavities where oxidation via "dimerization" is sterically hindered[68g,98].

The structure of $((CN)_5Co(O_2))^{-3}$ shows a cobalt-dioxygen bond that is in the bent end-on configuration[99], with a Co-O-O bond angle of 153.4°. This angle is somewhat larger than that reported for neutral cobalt-dioxygen complexes, and is thought to arise in part from the repulsive interactions between CN^- anions and the superoxide.

The structure of $(cis\text{-}(C_6H_5)_2\text{-}PCH{=}CHP(C_6H_5)_2)_2Co(O_2)BF_4$ contains a π-bonded dioxygen[100a], but this probably results from the cobalt in the deoxygenated species being in the softer +1 oxidation state, rather than being in the more common +2 oxidation state. However, the dioxygen adduct of the high spin $Co(II)((CF_3)_2C(O)C(O)(CF_3))_2$ complex has been formulated as π-bonded O_2 to Co(II)[100b].

I.4 Catalytic Properties

Cobalt(II) phthalocyanine has been used to catalyze a net insertion of oxygen into cumene or acrolein[101]. The same system has been used to oxidize aldehydes[102], and this behavior has been noted also with Co(II)(T(p-CH_3)PP)[103] and Co(II)TPP[104]. Co(II)(salen)[105] and Co(II)TPP[106] also promote insertion of oxygen into indoles, giving products that are analogous to those resulting from the oxidation of tryptophan by tryptophan 2,3-dioxygenase[107]. These cobalt complexes are thought to initiate the reaction by forming a dioxygen complex with subsequent abstraction of hydrogen from the substrate. Reaction of dioxygen with a substrate radical then leads to peroxy species and oxidation by a free radical process. Cobalt

Schiff base-dioxygen adducts have also been shown to initiate free radical oxidations of various organic substrates, such as flavones, phenols, and ascorbic acid[108], and again initiation is thought to involve abstraction of hydrogen from the substrate. Similarly Co(III) and Fe(III) porphyrins have been found to catalyze the peroxidation of several olefins[109]. Analogous mechanisms have been postulated for enzymic oxygenase systems[25a], but such processes are likely less well understood than the "simple" protein-free model systems.

Although workers have shown that some olefins, such as tetracyanoethylene (TCNE), do interact with cobalt tetradentate macrocycle complexes[110], formation of a cobalt-olefin bond has yet to be established. During the present studies, a report of a π-bonded interaction between TCNE and a Mn(II)TPP complex appeared[111]. If cobalt complexes could form such a bond, then these complexes may be able to act as catalysts for reactions of olefins. This thesis describes some exploratory work in this area.

CHAPTER II

APPARATUS AND EXPERIMENTAL PROCEDURE

II. 1 Instrumentation

Ultraviolet (UV) and visible (VIS) absorption spectra were recorded on a Perkin Elmer 202, a Cary 14 or a Cary 17 spectrophotometer, fitted when necessary with a thermostated cell compartment.

Electron spin resonance (ESR) spectra were recorded on a Varian Associates model E3 spectrometer.

A Wissenschaftlichen und Techniksh Werkstatten model DM01 Diplometer fitted with a DFL1 cell was kindly loaned by N. L. Paddock to measure dielectric constants from $\epsilon = 1.0$ to $\epsilon = 3.6$. For materials with a higher dielectric constant, measurements were obtained with a Bronton Electronics Corporation model 74C-58 Capacitance Bridge which was provided by W. N. Hardy. The material to be studied was placed in a cell designed by W. N. Hardy and built in the chemistry department mechanical shop (Figure II.1).

Stopped-flow kinetics measurements were made on a Durrum-Gibson model D 115 Stopped-Flow Spectrophotometer equipped with a 2 cm path-length cuvette and a thermostated compartment. Absorbance versus time traces were observed on a Tektronix Inc. R5103N oscilloscope fitted with a D11 single beam storage unit, a 5A15N amplifier, and a 5B10N time base.

Flash photolysis measurements were made with a Beckman model 2400 DU spectrophotometer, the photolyzing light being provided by a Braun 2000 F27

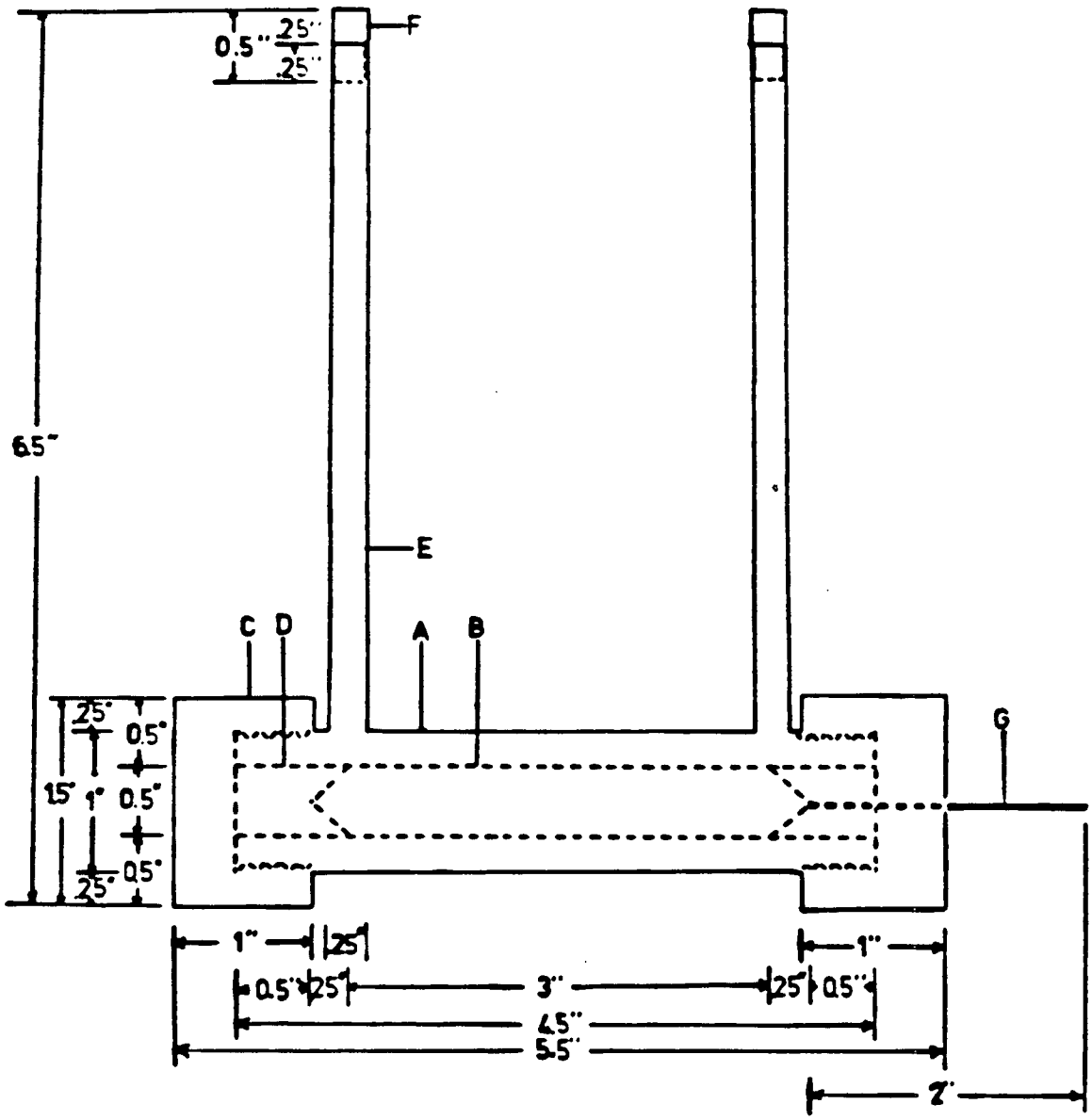

A. Outer Stainless Steel Barrel

B. Inner Stainless Steel Barrel (Separated From Outer By .015 IN.)

C. Nylon Screw Cap

D. Teflon Plug

E. Stainless Steel Tube

F. Teflon Plug

G. Aluminum Electrode

Figure II.1. Cell used for dielectric constant measurements. Sample was placed between the two stainless steel barrels. Electrodes from the capacitance bridge were clipped to G and E.

flasher placed next to the cuvette, perpendicular to the path of the light from the spectrophotometer. The flasher was equipped with a fibre-optic feedback system which cut the pulse time to 100 μsec. By using an appropriate Corion optical filter, light of a selected wavelength could be flashed on the sample without interference from other light wavelengths generated by the flasher.

Temperature readings (when a mercury thermometer was not appropriate to use) were made with a copper-constantan thermocouple. Voltages generated were measured on a Honeywell model 2476 potentiometer.

Weights were measured on a Mettler H20 balance.

II.2 Spectroscopic Cells

II.2.1 Ultraviolet-Visible Spectroscopic Cells

Anaerobic spectral quartz cells with path-lengths of 1,2, or 10 mm (Figure II.2) were used for spectroscopic measurements above $0^{o}C$.

A Kontes-Martin Ltd. 10 cm path-length quartz cell (Figure II.3) was used to study ligand binding in dilute solutions ($\sim 10^{-6}$ M) of cobalt complexes. The cell had a solution capacity of approximately 60 mL and was constructed so that a constant temperature bath surrounded the solution without interfering with the light beam.

A 6 cm path-length quartz cell (Figure II.4) was used for measuring interactions of solutions of cobalt complexes with gases. The cell had a solution capacity of approximately 15 mL and was again constructed so that constant temperature could be maintained.

For low temperature spectroscopic work on solutions in shorter path-length cells, a device (Figure II.5) constructed by the chemistry department mechanical shop was used. Optical cells with a path-length of

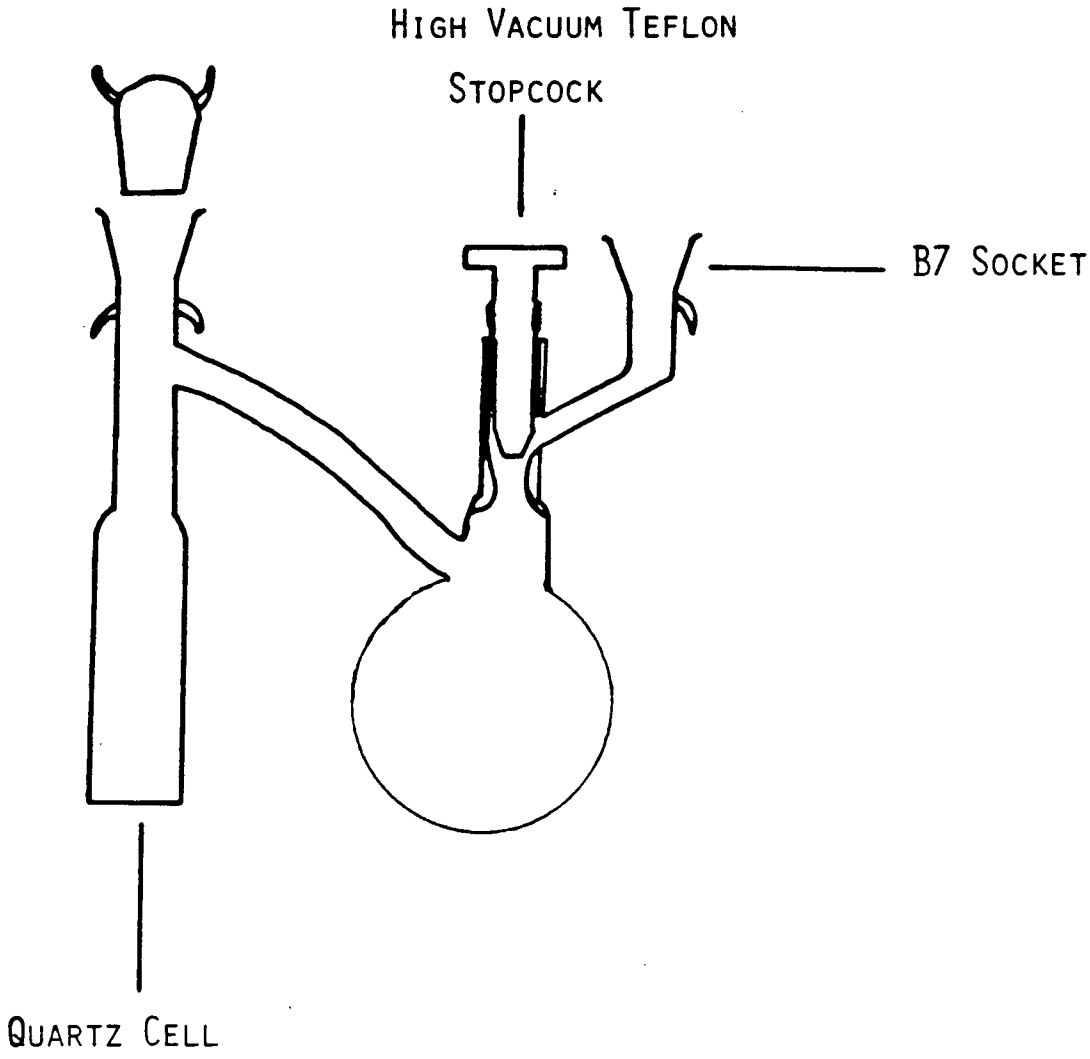

Figure II.2. Anaerobic Spectral Cell.

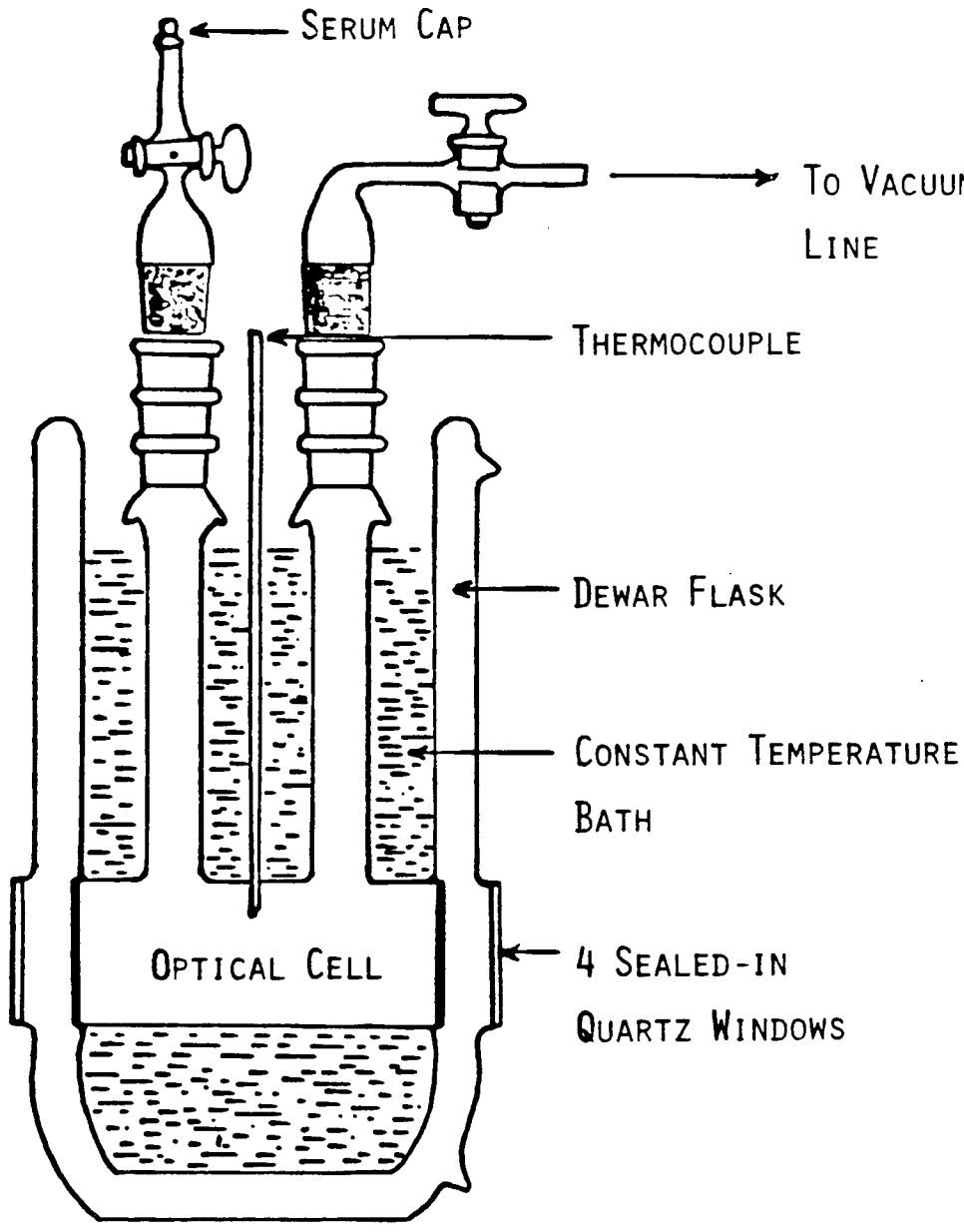

Figure II.3. 10 cm path-length cell.

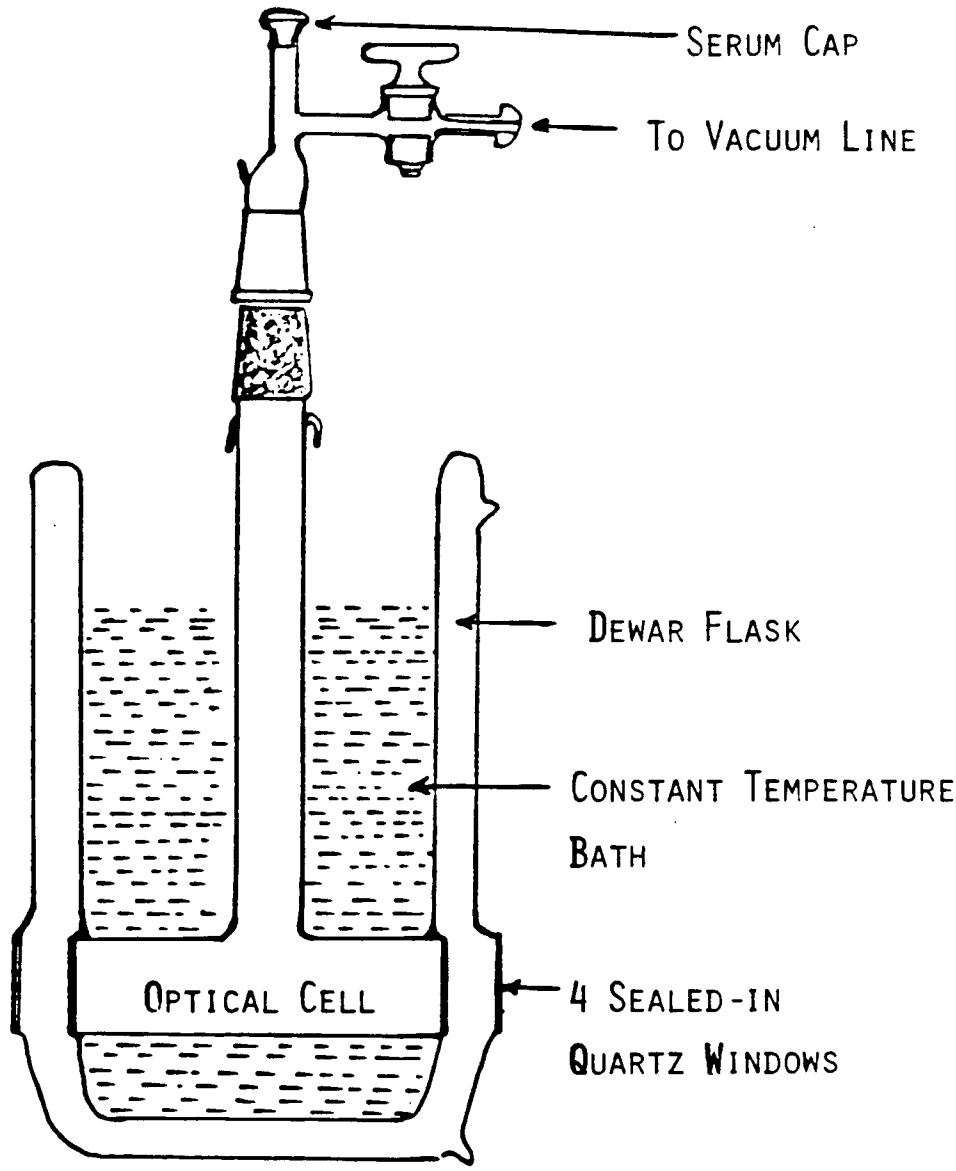

Figure II.4. 6 cm path-length quartz cell.

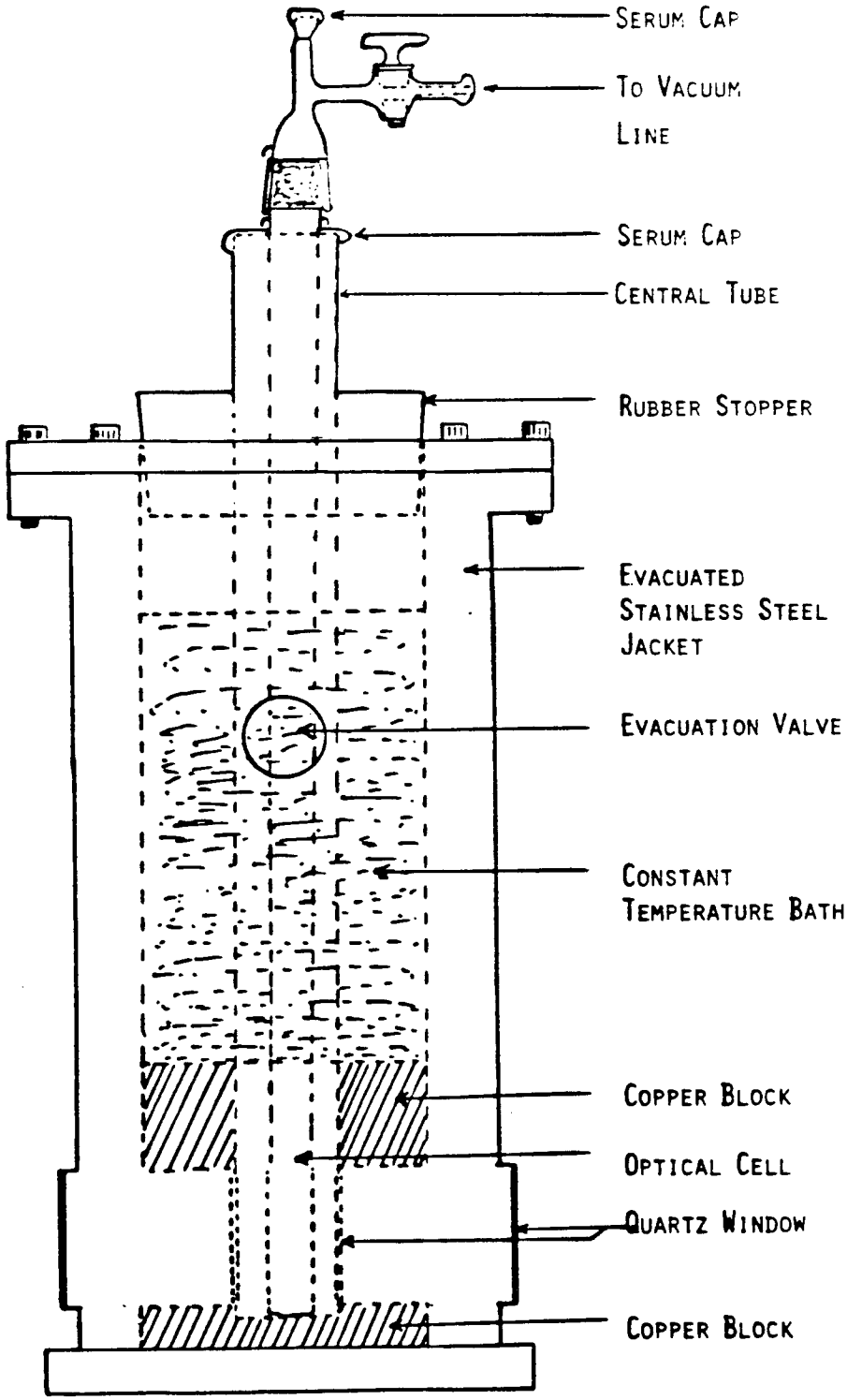

Figure II.5 Short path-length spectroscopic cell for low temperature work.

1 mm or 10 mm were inserted into the central tube of the cell holder. A serum cap sealed the volume between the cell and the central tube to prevent condensation on the cell. The cell holder was then filled with a constant temperature bath which thermally equilibrated with the copper block in the cell holder, and then with the cell. The constant temperature bath was insulated by the evacuated stainless steel jacket and the rubber stopper.

When using the Figure II.2 type cells, the solvent was degassed by repeatedly freezing it in the flask of the cell, pumping off any uncondensed gas, and then thawing the solvent. The degassed solvent could then be added to any solid sample placed in the quartz cell.

For the cells illustrated in Figures II.3, II.4, or II.5 the solvents were degassed in a separate flask, and then transferred through a stainless steel tube under argon to the spectroscopic cell, where the solid sample had already been placed.

II.2.2 ESR Cells

Samples prepared for electron spin resonance measurements were contained in 1 mm inside diameter quartz cells fitted with a high vacuum stopcock and a B7 joint (Figure II.6).

Solvents were initially degassed in a Figure II.2 type cell. The degassed solvent was mixed with the solid sample in the quartz cell, and then the sample was transferred to the ESR cell through the B7 joint.

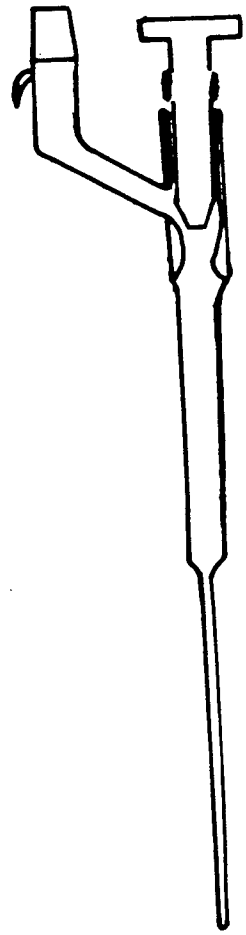

Figure II.6. Anaerobic ESR cell.

II.3 Constant Temperature Baths

II.3.1 Above 0°C

The UV-VIS spectroscopic cells shown in Figures II.3, II.4, and II.5 were maintained at a constant temperature by filling the constant temperature bath container with water and immersing a copper coil in it. The copper coil was attached to a Haake model FK circulating thermostating bath. By appropriately adjusting the thermostating bath, the desired temperature could be held in the spectroscopic cell.

Constant temperature of a Figure II.2 type cell could be maintained by using the thermostated cell compartment of the spectrophotometer.

II.3.2 At or Below 0°C

Low temperatures were attained by surrounding the solution with a cryostatic bath, prepared as described by Shriver[112]. Slushes of the following materials were used: ice-distilled water (0°C); carbon tetrachloride (-23°C); bromobenzene (-30.8°C); anisole (-37.4°C); chlorobenzene (-45°C); octane (-56.5°C); chloroform (-63.5°C); dry ice-acetone (-78°C); and ethyl acetate (-83.5°C).

ESR samples were studied at -196°C (77K) by placing the ESR cell in a finger Dewar filled with liquid nitrogen.

II.4 Equilibrium Constant Measurements

II.4.1 Ligand Binding

Equilibrium constant measurements for the reaction:

$$L + CoMc \underset{}{\overset{K_1}{\rightleftharpoons}} LCoMc \qquad (II.1)$$

where CoMc represents a four-coordinate cobalt macrocycle complex, and L is

any axially coordinating ligand, were made by following VIS and near UV (e.g. the Soret band) spectral changes with changes in added ligand concentration. Aliquots of degassed ligand, or degassed ligand in toluene solution, were added from a calibrated syringe to a solution of cobalt complex under argon. Complete spectra were recorded from 750 to 350 nm. Usually, the total volume of ligand solution added to CoMc to obtain fully formed LCoMc was relatively small, and any dilution corrections were minor. In certain cases, substantial amounts of ligand were needed to completely generate LCoMc, and sometimes LCoMc could not be fully formed. In most cases, however, good analyses for K_1 were achieved by allowing for the dilution effect, and/or by taking into consideration estimated spectral characteristics of the LCoMc species; e.g. by using data from a lower temperature where the complex was completely formed.

Ligand binding equilibrium constants were generally determined at temperatures from -23 to 40°C.

Equilibrium constant measurements for the binding of a second ligand to a cobalt macrocycle complex were carried out in a manner similar to that described above.

II.4.2 Oxygen Binding

Equilibrium constants for the reaction:

$$LCoMc + O_2(g) \overset{K_{O_2}}{\rightleftharpoons} LCoMc(O_2) \qquad (II.2)$$

where $LCoMc(O_2)$ represents the cobalt macrocycle dioxygen adduct, were measured in a manner similar to that used for ligand binding. Known pressures of oxygen were admitted to the evacuated sample solution, the

pressure being measured either with a mercury manometer (for pressures > 10 Torr) or a di-n-butylphthalate manometer (for pressures <40 Torr). Before the spectrum was taken, the cell (as in Figure II.3, II.4, or II.5) containing the sample was carefully shaken in order to ensure complete mixing of the gas in the solution without any spilling of the constant temperature bath.

These measurements were generally determined from -83.5 to -23°C. Sometimes, spectra of the fully formed oxygenated species could not be obtained at a particular temperature, but such spectra could generally be achieved at some lower temperature, and good analyses were effected by making use of the lower temperature spectral data.

II.5 Spectrophotometric Kinetic Measurements

Samples for spectrophotometric kinetic studies were prepared in a manner similar to that described for the equilibrium studies. Since the concentrations of the cobalt macrocycle species were generally very low ($\sim 1 \times 10^{-5}$ M), and the solubilities of the gases were such that their concentrations were of the order of 1×10^{-3} M, the gas concentrations in solution (and the partial pressure of the gas), remained essentially constant throughout the course of any experiment.

II.6 Gas-Uptake Measurements

II.6.1 Description

A constant pressure gas-uptake apparatus (Figure II.7) was used for gas-uptake and gas solubility measurements.

A flexible glass spiral tube connected a capillary manometer (D) at tap (C) to a pyrex two-neck reaction flask (A), which was equipped with

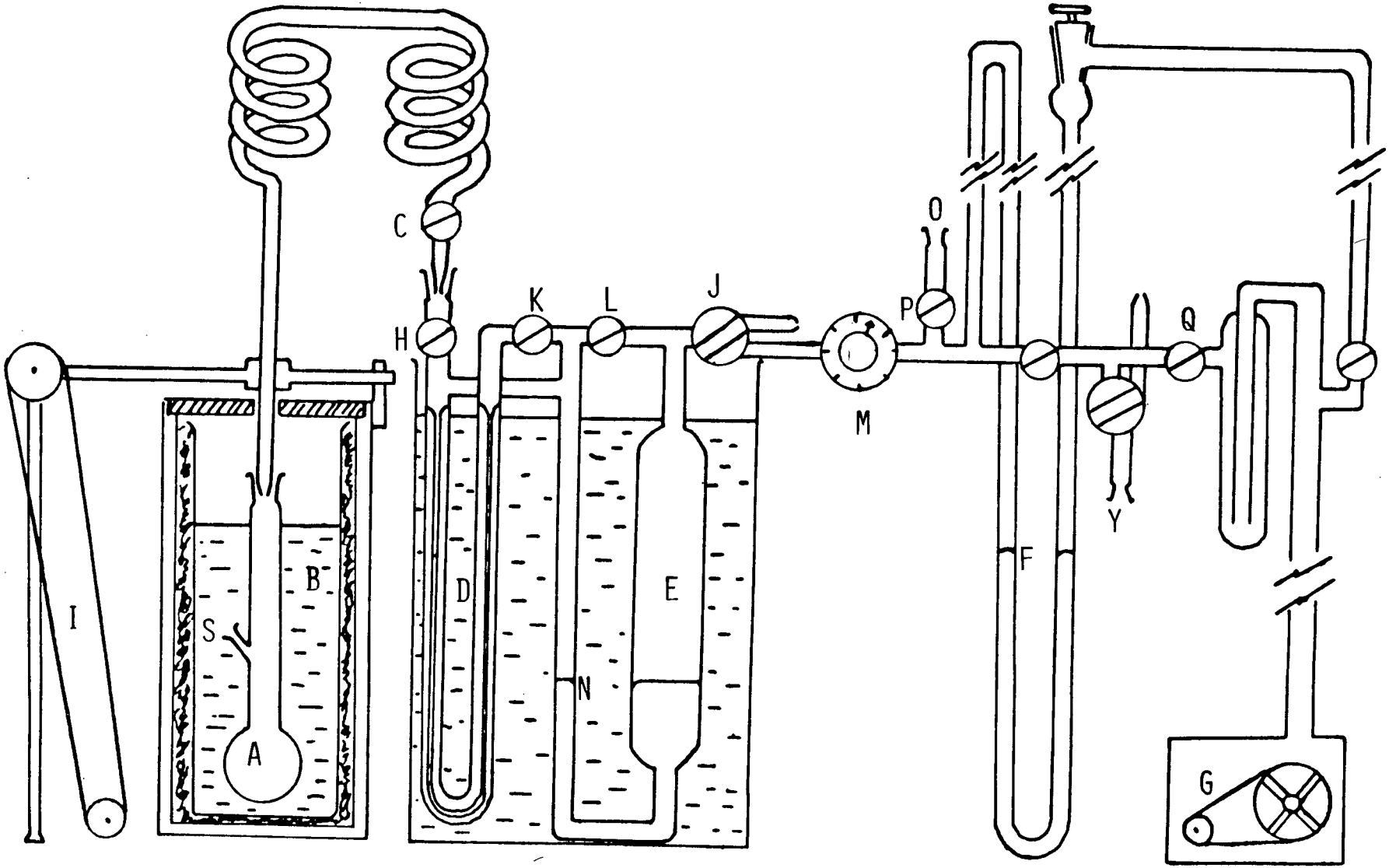

Figure II.7. Gas-Uptake Apparatus.

a dropping side-arm bucket. The reaction flask was clipped to a piston-rod which was driven by an offset wheel connected to a Welch variable speed electric motor (I) for shaking purposes, and the flask was thermostated in a silicone oil bath. The capillary manometer contained di-n-butyl-phthalate (a liquid of negligible vapor pressure at ambient temperatures) and was connected to the gas-measuring burette, which consisted of a mercury resevoir (E) and a precision bored tube (N) of known diameter. The gas burette was in turn connected by an Edwards high vacuum needle valve (M) to the gas handling part of the apparatus. This consisted of a mercury manometer (F), gas inlet (Y), and connections to the Welch Duo-Seal rotary vacuum pump (G). The capillary manometer and gas burette were thermostated at 25°C in a perspex water bath. The silicone oil bath consisted of a four-litre glass beaker insulated by polystyrene foam on all sides and enclosed by a wooden box, with the top also covered by polystyrene. Both thermostat units were controlled by Jumo thermo-regulators and Merc to Merc relay control circuits, with heating provided by a 40 watt elongated light bulb. With mechanical stirring and good insulation, the temperature could be maintained within $\pm$ 0.05°C.

A vertically mounted cathetometer was used to follow the gas-uptake, and time was recorded during kinetic experiments using a Lab-Chron 1400 timer.

II.6.2 Procedure For A Typical Gas-Uptake Experiment

For each experiment, the required amount of solvent (e.g. 5 mL.) was pipetted into the reaction flask.

Generally the cobalt complex could be weighed into a small glass bucket, which was then suspended from the side arm (S). In some cases,

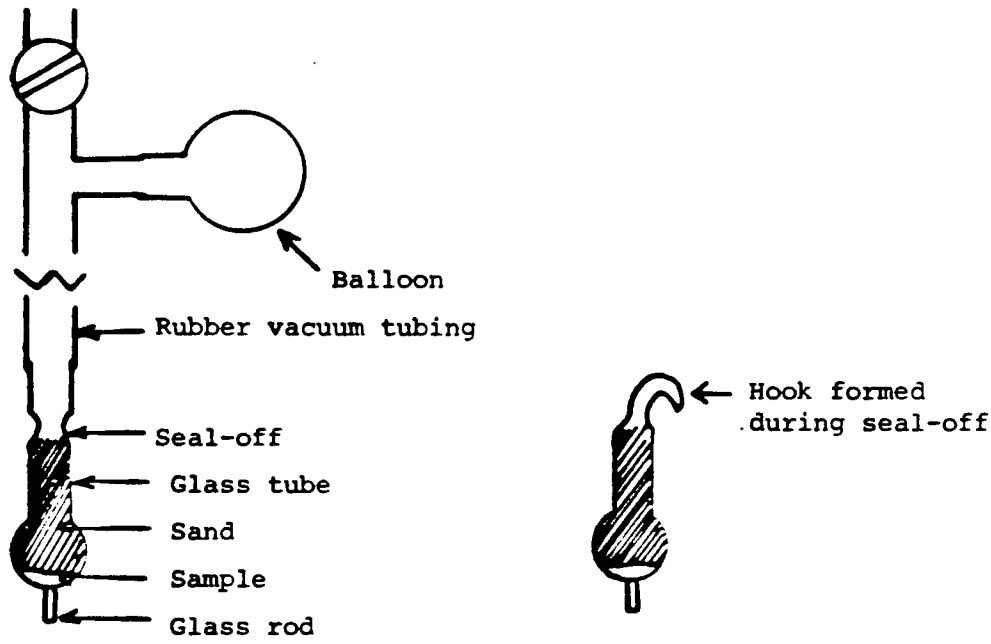

Figure II.8

however, the solvent tended to wet the sample in the bucket, and it was necessary to employ sealed ampoules instead of open buckets in the uptake procedure. A bulb was blown on a glass tube; a constriction was placed in the stem, and a glass rod was welded to the bottom of the bulb so that breakage of the ampoule could be guaranteed when it was dropped into the solvent. After being tested for leaks, the bulb was filled with the sample, then sand, and sealed off under argon, with the pressure being regulated with the aid of a balloon as shown in Figure II.8. These precautions served to minimize gas-uptake when the ampoule was broken. The tube was sealed off in the shape of a hook (Figure II.8) so that the ampoule could be suspended from the side arm.

The solvent was degassed by the freeze-pump-thaw method while the reaction flask was connected by the spiral and tap (C) to the gas handling part of the gas-uptake apparatus at (O).

The reactant gas was admitted at a pressure somewhat less than that required for the experiment, and then taps (C) and (P) were closed. The whole system up to tap (H) was pumped down with taps (K), (L), (J), and (M) open. The flask and spiral arrangement were disconnected from (O) and transferred into the thermostated oil bath with the spiral connected to the di-n-butylphthalate manometer through tap (H). Tap (H) was opened and after the air between tap (H) and (C) was pumped out, tap (Q) was closed. Gas was then admitted to the rest of the gas-uptake apparatus up to tap (C), which was then opened. The solution was shaken to achieve equilibrium at the desired temperature and pressure. Tap (J) and needle valve (M) were closed while the initial reading of the mercury level in (N) was taken. Taps (K) and (L) were closed, the bucket dropped by rotating the side arm, and the timer and the shaker were started simultaneously.

As a result of any gas uptake, the di-n-butylphthalate level on the left hand side of the manometer rose, and to maintain no difference in the heights of the levels, gas was admitted into the gas measuring burette through tap (J) and needle valve (M) to give a resulting rise of mercury in (N). The change in height of mercury was noted as a function of time. Since the diameter of (N) was known, the corresponding volume of gas was determined, and the uptake of gas as a function of time could be followed.

The use of a small volume of solution ($\sim$5 mL.), a relatively large indented vessel ($\sim$30 mL.), and a high shaking rate ensured the absence of diffusion control in the rate of gas consumption.

II.6.3 Gas Solubilty Measurements

Some experiments were carried out to determine gas solubilities in the solvents used. These determinations could be made under specific temperature and pressure conditions using the gas-uptake apparatus and a reaction flask containing a stopcock at its neck. The entire system, including the reaction flask containing a measured amount of solvent, was degassed. The tap at the flask was then closed, and the flask was placed in the bath at the desired temperature. The system was then evacuated to the flask tap and filled with gas to the approximate pressure desired. The flask tap was then opened, and the pressure was adjusted immediately to that required. Taps (K) and (L) were closed, the shaker started, and the immediate uptake measured as described in the previous section. This afforded a means of calculating gas solubility.

For gas solubility measurements at low temperatures, the silicone oil bath was replaced with a large bath containing the appropriate slush.

II.7 Materials

II.7.1 Gases

C.P. grade carbon monoxide was obtained from the Matheson Gas Co. Purified argon, nitrogen, and oxygen were supplied by Canadian Liquid Air Limited. The argon, nitrogen, and oxygen were passed through a column of fresh phosphorus pentoxide and then through molecular sieves (BDH, type 5A) at $-78^{\circ}C$ to remove any traces of water.

Ethylene and acetylene were obtained from the Matheson Gas Co. In order to remove any oxygen present, these gases were frozen in liquid nitrogen and any uncondensed material was pumped off. The frozen gases

were then warmed to room temperature, and this freeze-pump-warm process was repeated for several cycles until all uncondensed materials were eliminated.

II.7.2 Liquids

II.7.2.1 General

Generally all liquids and solutions were handled and stored under an argon atmosphere using Schlenk techniques[112].

II.7.2.2 Solvents

Toluene (Fisher Scientific Co., spectral grade) was refluxed over and distilled from sodium-benzophenone ketyl under nitrogen immediately prior to use. Dichloromethane (DCM) and 1,2-dichloroethane (DCE) (Fisher Scientific Co., spectral grade) were refluxed over and distilled from phosphorus pentoxide immediately prior to use. Chlorobenzene (Mallinckrodt Co., analytical grade) was dried over phosphorus pentoxide and distilled under a reduced pressure of argon. 1-Chlorobutane (Eastman Kodak Co.) and chloroform (Fisher Scientific Co., spectral grade) were dried over phosphorus pentoxide and distilled under vacuum prior to use.

II.7.2.3 Ligands

1-Methylimidazole (CH_3-Im) (Aldrich Chemical Co., analytical grade), piperidine (Pip) (ICN Pharmaceuticals Inc., reagent grade), pyridine (Py) (American Chemical and Scientific Co., reagent grade), and triethylamine (Et_3N) (Eastman Kodak Co., reagent grade) were dried over and distilled from KOH under reduced argon pressure prior to use. N,N-Dimethylformamide (DMF) and N,N-dimethylacetamide (DMA) (Fisher Scientific Co., analytical grade) were dried over and distilled from calcium oxide under reduced argon pressure prior to use. Tetrahydrofuran (THF) (Fisher Scientific Co.,

analytical grade) was dried over sodium-benzophenone ketyl and distilled from lithium aluminum hydride under reduced argon pressure prior to use. Tri-n-butylphosphine (PBu_3) (Aldrich Chemical Co., analytical grade) was purified by vacuum distillation.

The olefins: diethylmaleate (DEM) (Aldrich Chemical Co.), diethylfumarate (DEF) (K & K Laboratories Co.), styrene (sty) (MCB Co.), 1-hexene (1hx) (ICN Pharmaceuticals Inc.), 2-octene (2oc) (K & K Laboratories Co.), cyclooctene (cot) (K & K Laboratories Co.), and 3,4-dichlorobutene (DCB) (Petro-Tex Chemical Corp.) were purified by passage through an activated alumina (Fisher Scientific Co.) column and subsequent vacuum distillation.

2.7.3 Solids

2.7.3.1 Ligands

Imidazole (Im) (Aldrich Chemical Co.), acrylamide (Acr) (K & K Laboratories Co.), and maleic anhydride (MA) (Fisher Scientific Co.) were recrystallized from toluene and dried under vacuo for 24 hours.

Triphenylphosphine (PPh_3) (MCB Co.) was recrystallized from ethanol and dried under vacuo for 24 hours.

Tetracyanoethylene (TCNE) (Eastman Kodak Co.) was purified by sublimation.

2.7.3.2 Macrocycles and Co(II) Complexes

Bis(salicylaldehyde)ethylenediimine (salen) was prepared by the method of Bailes and Calvin[77g]. 28.6 g of salicylaldehyde (Eastman Kodak Co.) and 7g of 98% ethylenediamine (Mallinckrodt Co.) were dissolved in 300 mL of 95% ethanol. The resulting precipitate was filtered and washed with cold water and recrystallized from ethanol.

Analysis: Calculated for $C_{16}N_{16}N_2O_2$: C, 71.6%; H, 6.0%; N, 10.5%. Found: C, 71.4%; H, 6.2%; N, 10.4%.

N,N-bis(salicylaldehyde)ethylenediiminato cobalt(II) (Co(salen)) was prepared by a method similar to that of Bailes and Calvin[77g]. 2.0 g of salen was dissolved in 20 mL of 95% ethanol at 60°C. A 25 mL aqueous solution containing 2.0 g of cobalt acetate, which had been recrystallized from acetic acid, was added dropwise. The resulting mixture was heated at 65°C for two hours, and then left at room temperature for twelve hours before filtration. The solid was dried in vacuo for 48 hours. This preparation was done under nitrogen.

Analysis: Calculated for $C_{16}H_{14}N_2O_2Co$: C, 59.1%; H 4.3%; N, 8.6%. Found: C, 59.0%; H, 4.2%; N, 8.7%.

Cobalt(II) protoporphyrin IX dimethyl ester (CoPpIXDME) and cobalt(II) etioporphyrin I (CoEpI), prepared by the method of Falk[27b], were kindly donated by K. J. Reimer and B. Halko, respectively. Cobalt(II) $\alpha,\beta,\gamma,\delta$-tetraphenylporphyrin (CoTPP), prepared by the method of Adler[113], was also donated by B. Halko.

Diacetyldeuteroporphyrin IX dimethyl ester (DADIXDME) and dibromodeuteroporphyrin IX dimethyl ester (DBrDIXDME) were generously provided by H. C. Welborn.

Cobalt(II) octaethylporphyrin (CoOEP) was prepared by the method of Falk[27b]. 100 mg of octaethylporphyrin (OEP), provided by J. B. Paine III, was added to 15 mL of refluxing $CHCl_3$ under nitrogen. One mL of a boiling solution of cobalt(II) acetate in acetic acid was then added, and refluxing continued until the visible spectrum indicated the disappearance of free porphyrin. The chloroform solution was then washed repeatedly with distilled water until all traces of cobalt acetate and acetic acid were removed. The chloroform was then stripped off, and the product recrystallized from benzene

and dried in vacuo.

Analysis: Calculated for $C_{36}H_{44}N_4Co$: C, 73.1%; H, 7.4%; N, 9.5%. Found: C, 73.3%; H, 7.3%; N, 9.3%.

Cobalt(II) diacetyldeuteroporphyrin IX dimethyl ester (CoDADIXDME) and cobalt(II) dibromodeuteroporphyrin IX dimethyl ester were prepared in a manner similar to that used for CoOEP, but with scaled down proportions due to the very small amount of free porphyrins available. Elemental analyses were not done on the very small amounts of cobalt porphyrin complexes obtained.

Cobalt(II) octamethyltetrabenzoporphyrin (CoOMBP) was prepared by the method of Dolphin and coworkers[114] with some modifications. 5.4 g of 1,3,4,7-tetramethylisoindole was loaded into a 450 mL Carius tube with 27 g of cobalt metal powder (Eastman Kodak Co.). The Carius tube was evacuated, sealed, and then heated at 390°C for four hours. The resulting solid was extracted with pentane for 24 hours, toluene for 8 hours, and then pyridine for 10 hours. The resulting pyridine solution was stripped to about 20 mL, when 100 mL of hexane was then added. The precipitate was filtered and then extracted with hexane for 48 hours. The remaining solid was dried at 80°C in vacuo for 36 hours.

Analysis: Calculated for $C_{44}H_{36}N_4Co$: C, 77.8%; H, 5.3%; N, 8.2%. Found: C, 77.8%; H, 5.4%; N, 8.4%.

The molar extinction coefficients at the absorption maxima for CoOMBP in toluene were determined to be 6.4×10^4 $M^{-1}cm^{-1}$ (412 nm) and 6.2×10^4 $M^{-1}cm^{-1}$ (618 nm) (Chapter VII.4). In pyridine the corresponding values were 8.2×10^{-4} $M^{-1}cm^{-1}$ (428 nm) and 4.3×10^4 $M^{-1}cm^{-1}$ (617 nm) which compare with the reported data of Dolphin et al ($\varepsilon = 7.15 \times 10^4$ $M^{-1}cm^{-1}$ for the Soret band and $\varepsilon = 3.67 \times 10^4$ $M^{-1}cm^{-1}$ for the visible band)[114]. Under these

conditions the bis pyridine adduct would have been formed.

1,3,4,7-Tetramethylisoindole, a precursor of CoOMBP, was prepared by a modified method of Fletcher[115]. 11.5 g of 2,5-hexanedione (Eastman Kodak Co.) was added to a 200 mL aqueous solution of 22 g of ammonium sulfate The resulting solution was refluxed under argon for 20 hours, cooled, and 25 mL of 20% NaOH solution was added. The resulting precipitate was then filtered, dried in vacuo for 18 hours, and then purified by sublimation at 80°C.

Analysis: Calculated for $C_{12}H_{15}N$: C, 83.2%; H, 8.7%; N, 8.1%. Found: C, 83.0%; H, 8.8%; N, 8.0%.

CHAPTER III

THERMODYNAMICS OF REVERSIBLE BINDING OF SELECTED LIGANDS TO CoOMBP

III.1 Qualitative Spectral Observations

III.1.1 $L + CoOMBP \rightleftharpoons LCoOMBP$, K_1.

The visible spectrum of a solution of CoOMBP in toluene (Figure I.3c) had a Soret band at 412 nm ($\varepsilon = 6.4 \times 10^4\ M^{-1}cm^{-1}$) and a visible band at 618 nm ($\varepsilon = 6.2 \times 10^4\ M^{-1}cm^{-1}$) (Chapter VII.4). Addition of a nitrogen-coordinating ligand to the solution, in the absence of air (Figure III.1), resulted in a blue shift of the Soret band to approximately 408 nm, with little change in the peak molar extinction coefficient; the visible band decreased to about two thirds of its original intensity, with little or no change in its peak position. Addition of an oxygen-coordinating ligand to the CoOMBP solution resulted in a red Soret shift of about 5 nm and minor visible changes. While the changes that occurred upon addition of DMF or DMA were very similar, changes upon THF addition were somewhat different, particularly with respect to the Soret intensity. Addition of a phosphorus-coordinating ligand (Figure III.2) caused little change in the peak positions and varying decreases in their intensities. The spectral changes associated with the coordination of one ligand are shown in Table III.1.

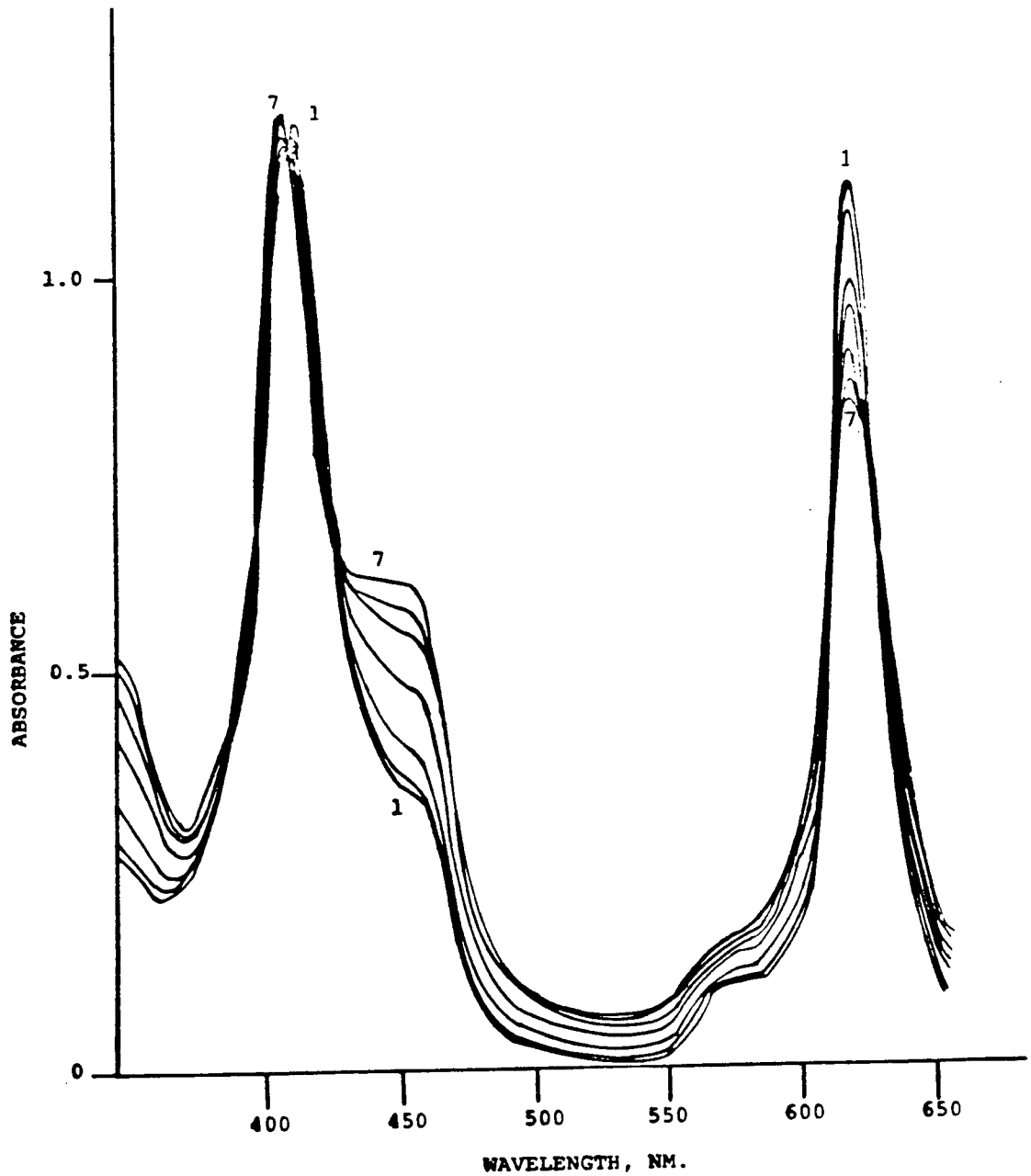

Figure III.1. CoOMBP + CH_3-Im $\rightleftharpoons$ CH_3-ImCoOMBP @ 23°C.

For raw data see Appendix Ib.

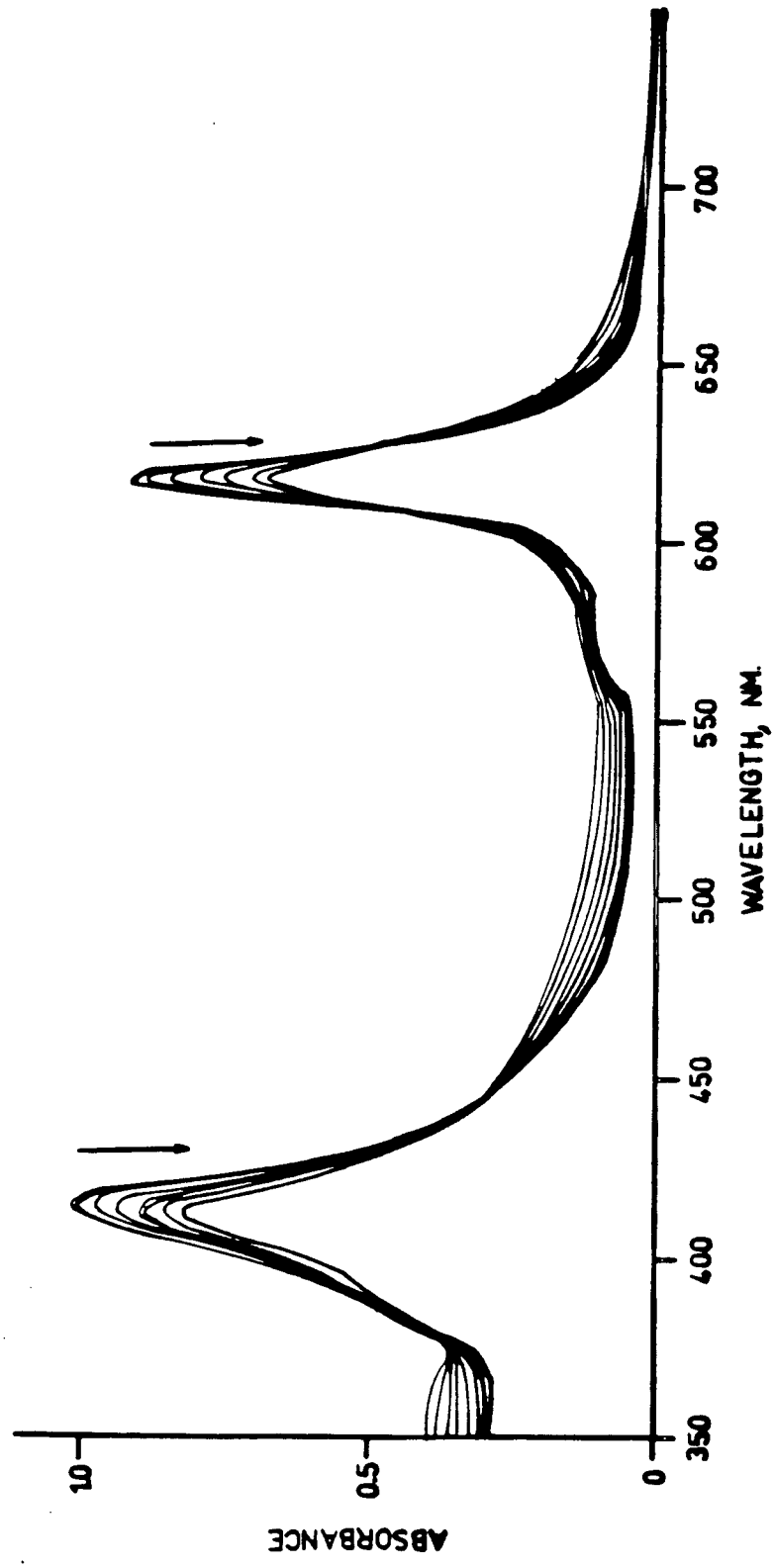

Figure III.2. PBu_3 + CoOMBP $\rightleftharpoons$ PBu_3CoOMBP @ 22°C.

For raw data see Appendix Ii.

Table III.1. Spectral Data From 350 to 750 nm for the Reaction:

$L + CoOMBP \rightleftharpoons LCoOMBP$

Absorbing Species	Absorption Maxima (nm) (Extinction Coefficients, $M^{-1} cm^{-1}$)	Isosbestic Points (nm)
CoOMBP	412 (6.4×10^4) 618 – (6.2×10^4)	
+ Im	407 (6.5×10^4) 618 (4.6×10^4)	385 397 410 428 612 628
+ CH_3-Im	408 (6.5×10^4) 618 (4.7×10^4)	385 398 411 427 610 628
+ Pip	408 (6.5×10^4) 617 (4.1×10^4)	384 398 410 440 610 630
+ Py	407 (5.6×10^4) 618 (4.6×10^4)	382 394 407 432 609 630
+ Et_3N	407 (6.9×10^4) 618 (4.7×10^4)	380 399 410 434 612 628
+ DMF	418 (6.0×10^4) 618 (5.4×10^4)	381 416 610 630
+ THF	417 (8.2×10^4) 616 (4.6×10^4)	382 413 607 634
+ PPh_3	412 (6.3×10^4) 619 (5.3×10^4)	382 438 610 625
+ PBu_3	412 ($\sim 3.5 \times 10^4$) 618 ($\sim 2.8 \times 10^4$)	387 446 608 629

Note: As will be explained in Chapter VII, CoOMBP does not obey Beer's Law as it undergoes aggregation in solution. From considering this, ε_{412nm} and ε_{618nm} are estimated to be 6.4×10^4 $M^{-1}cm^{-1}$ and 6.2×10^4 $M^{-1}cm^{-1}$, respectively.

Spectral changes to some four-coordinate cobalt porphyrin complexes (e.g. CoPpIXDME), occurring after DMF is added, have recently been attributed to small impurities of dimethylamine[116]. In the present work, spectral changes resulting from DMF addition are different from those observed with nitrogen-donors, and are similar to those shown for the binding of THF. Also the spectral changes with Et_3N were found to be very similar to those observed the cyclic amines Im, CH_3-Im, Pip, and Py. Thus, it was concluded that changes resulting from DMF addition were due to the binding of that ligand, and not to the coordination of an amine impurity, such as dimethylamine.

Oxygen-donors generally bound less strongly to CoOMBP than nitrogen-donors. DMA bound so weakly that DMACoOMBP could not be fully formed at ambient temperatures, and so no quantitative equilibrium measurements were made for this ligand.

If the ligand additions were carefully done, distinct isosbestic points could be achieved in all cases, after allowing, if necessary, for changes from solvent dilution. Generally the addition of an axial ligand caused a growth in spectral intensity from 440 to 460 nm, and sometimes the equilibrium analyses were carried out using data in this region.

III.1.2 $L + LCoOMBP \rightleftharpoons L_2CoOMBP, \quad K_2.$

Of the ligands studied, CH_3-Im, Pip, Py, and PBu_3 were found to fully coordinate two molecules to the cobalt centre at ambient temperatures. Solubility reasons prevented the determination of the K_2 values for the Im system, although its K_1 values were similar to those of the above ligands.

The addition of a second nitrogen-coordinating ligand (Figure III.3)

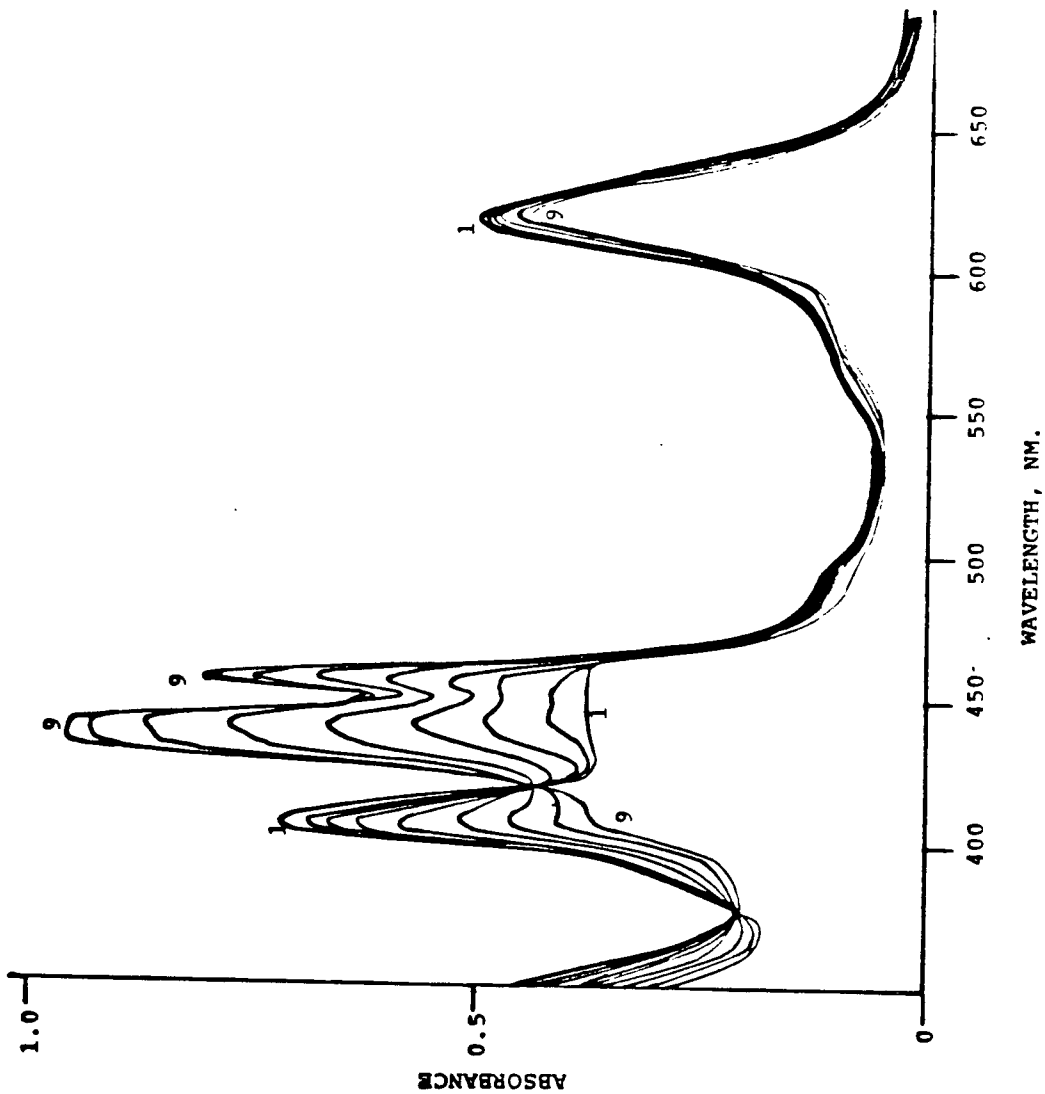

Figure III.3. CH_3-ImCoOMBP + CH_3-Im $\rightleftharpoons$ $(CH_3\text{-Im})_2$CoOMBP @ -23°C

For raw data see Appendix Ij, final trace not shown as isosbestic points are lost due to dilution effects.

caused a Soret band of increased intensity to form in the 430 nm region. There was little change in the size or position of the visible band. The bis CH_3-Im and Pip complexes had sharp side bands at about 455 nm, while there was no such distinct peak for the bis Py system. When the second PBu_3 coordinated to the cobalt (Figure III.4), the decreases in the molar extinction coefficient of the spectral bands resulting from the coordination of the first PBu_3 were reversed, and the Soret intensity became greater than that of the four-coordinate complexes. The spectral changes associated with the coordination of a second ligand are summarized in Table III.2.

Table III.2. Spectral Data From 350 to 750 nm for the Reaction:

$$L + LCoOMBP \rightleftharpoons L_2CoOMBP$$

Ligand	Absorption Maxima (nm) (Extinction Coefficients, $M^{-1}cm^{-1}$)		Isosbestic Points (nm)
CH_3-Im	433	(9.2×10^4)	375 422
	457	(7.6×10^4)	
	618	(4.5×10^4)	
Pip	430	(9.4×10^4)	355 377 419
	456	(4.8×10^4)	602 636
	616	(3.8×10^4)	
Py	428	(8.2×10^4)	372 417
	617	(4.3×10^4)	606 645
PBu_3	412	($\sim 8.0 \times 10^4$)	366 382 403
	614	($\sim 5.5 \times 10^4$)	424 618

For the three amine ligands, there was a distinct interval in the range of added ligand concentration between complete formation of LCoOMBP and the initial formation of L_2CoOMBP, and so accurate determinations of K_1 and K_2 could be achieved. Formation of the bis PBu_3 adduct overlapped

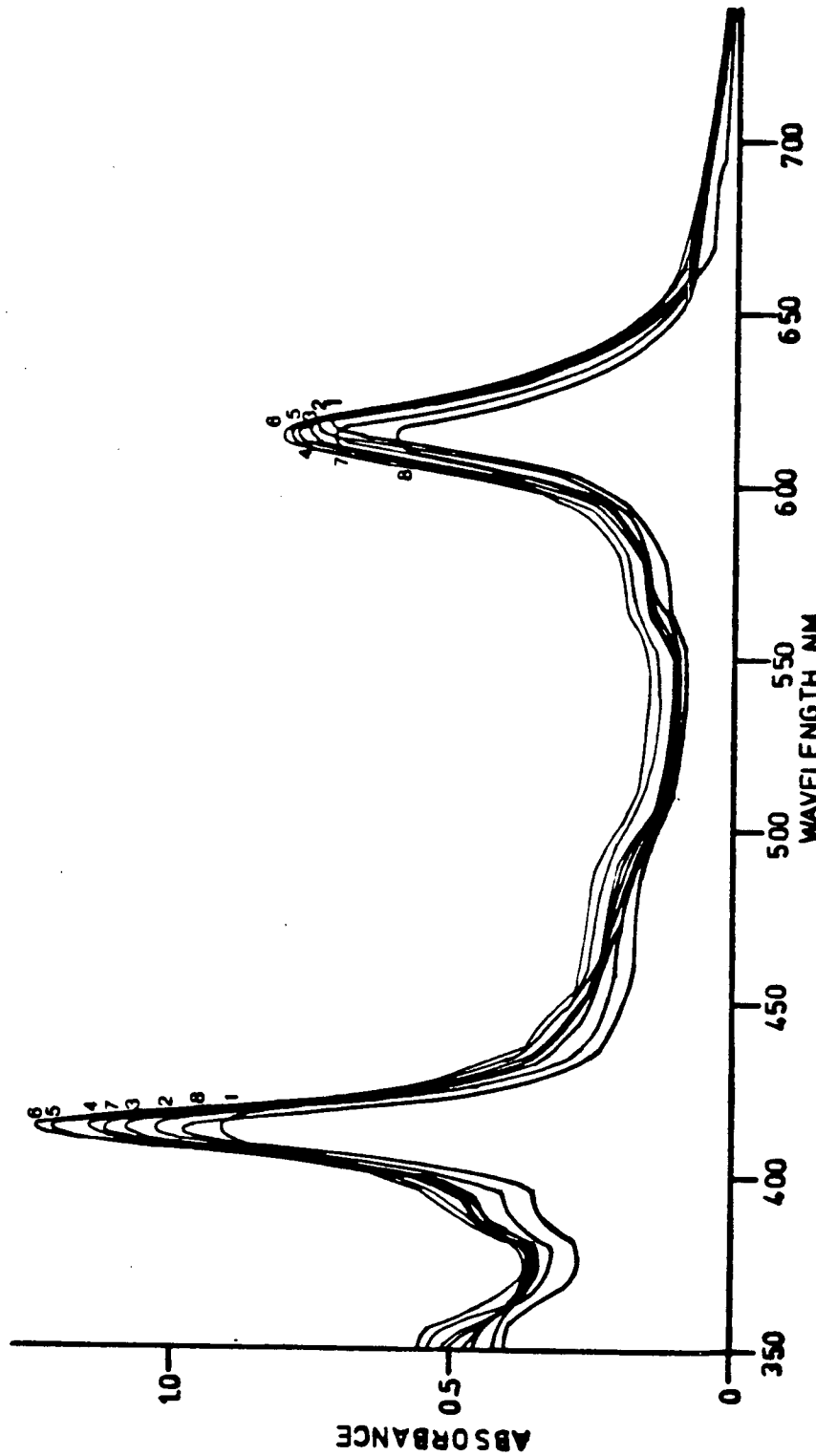

Figure III.4. PBu_3 + $PBu_3CoOMBP \rightleftharpoons (PBu_3)_2CoOMBP$ @ 22°C. For raw data see Appendix Im; apparent loss of isosbestic points is due to dilution effects.

with the formation of $PBu_3CoOMBP$, and thus the determination of K_1 and K_2 was more difficult than when both the initial and final spectral values are known, and the equilibrium values are considered approximate.

The spectral changes for all K_1 and K_2 determinations were instantaneous upon mixing (even on a stopped-flow time scale). In all cases the K_1 and K_2 values were found to decrease with temperature, and since the spectra indicated that less products were present as the solutions were warmed, the reversible nature of these reactions was demonstrated.

III.2 Treatment of Data

The equilibrium constant values were obtained by following either the increase in spectral intensity in the 440 to 460 nm region, or by following the changes in intensity at a peak position, as aliquots of ligand or ligand solution were added. Generally, the absorbances were read where the absorbance changes were the greatest, and where the spectral curves were not too steep. As mentioned, the ligand binding data could sometimes be analyzed over two separate ranges of ligand concentration, corresponding to the binding of the first and second axial ligands.

The formation of a ligand adduct obeys the equation:

$$CoOMBP + nL \underset{}{\overset{K_1}{\rightleftharpoons}} L_nCoOMBP \qquad \text{(III.1)}$$

The fraction, Y, of $L_nCoOMBP$ present at a known ligand concentration was calculated from the following expression:

$$Y = \frac{A - A_o}{A_\infty - A_o} \qquad \text{(III.2)}$$

where A is the absorbance at a known ligand concentration, corrected for any dilution due to ligand addition

A_o is the absorbance observed when no ligand is present

A_∞ is the absorbance of the fully formed coordinated complex, again corrected for any dilutuion.

The equilibrium constant, K_1, was determined from a plot of $\log \frac{A - A_o}{A_\infty - A}$ vs. $\log[L]$.

$$K_1 = \frac{[L_n CoOMBP]}{[CoOMBP][L]^n} = \frac{Y}{(1 - Y)[L]^n} = \frac{(A - A_o)}{(A_\infty - A)[L]^n} \qquad \text{(III.3)}$$

$$\text{and } \log K_1 = \log \frac{A - A_o}{A_\infty - A} - n\log[L] \qquad \text{(III.4)}$$

where $[L]$ is the molar concentration of the free ligand studied.

From such a plot, the slope of the line is n, the number of ligands binding to the complex. The experimental slopes ranged from 0.8 to 1.2, thus showing that only one ligand did coordinate in all cases. Experimental scatter often occurred at either extreme of the plot, and where possible, the range of $\frac{A - A_o}{A_\infty - A}$ values used was kept from 0.2 to 5.0. The plots of $\log \frac{A - A_o}{A_\infty - A}$ vs. $\log[CH_3\text{-Im}]$ are shown in Figure III.5, the intercepts on the abscissa giving $-\log K_1$ values. The ΔH and ΔS values can then be obtained from van't Hoff $\ln K_1$ vs. $1/T$ plots, as shown in Figures III.6-III.8.

The formation of a bis ligand adduct from a mono ligand adduct obeys the equation:

$$LCoOMBP + nL \overset{K_2}{\rightleftharpoons} L_{n+1}CoOMBP \qquad \text{(III.5)}$$

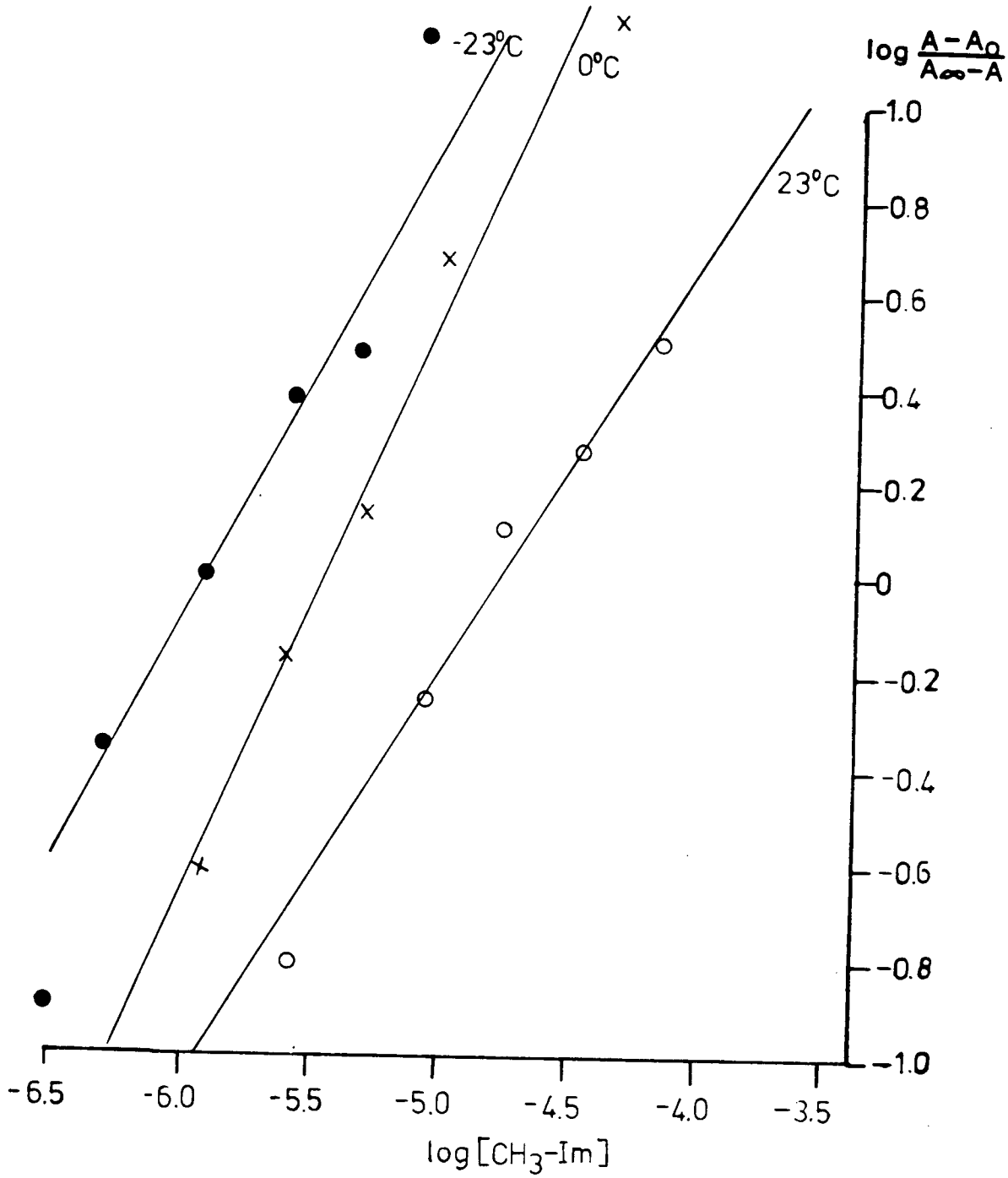

Figure III.5. Equilibrium plots for CH_3-Im + CoOMBP $\rightleftharpoons$ CH_3-ImCoOMBP

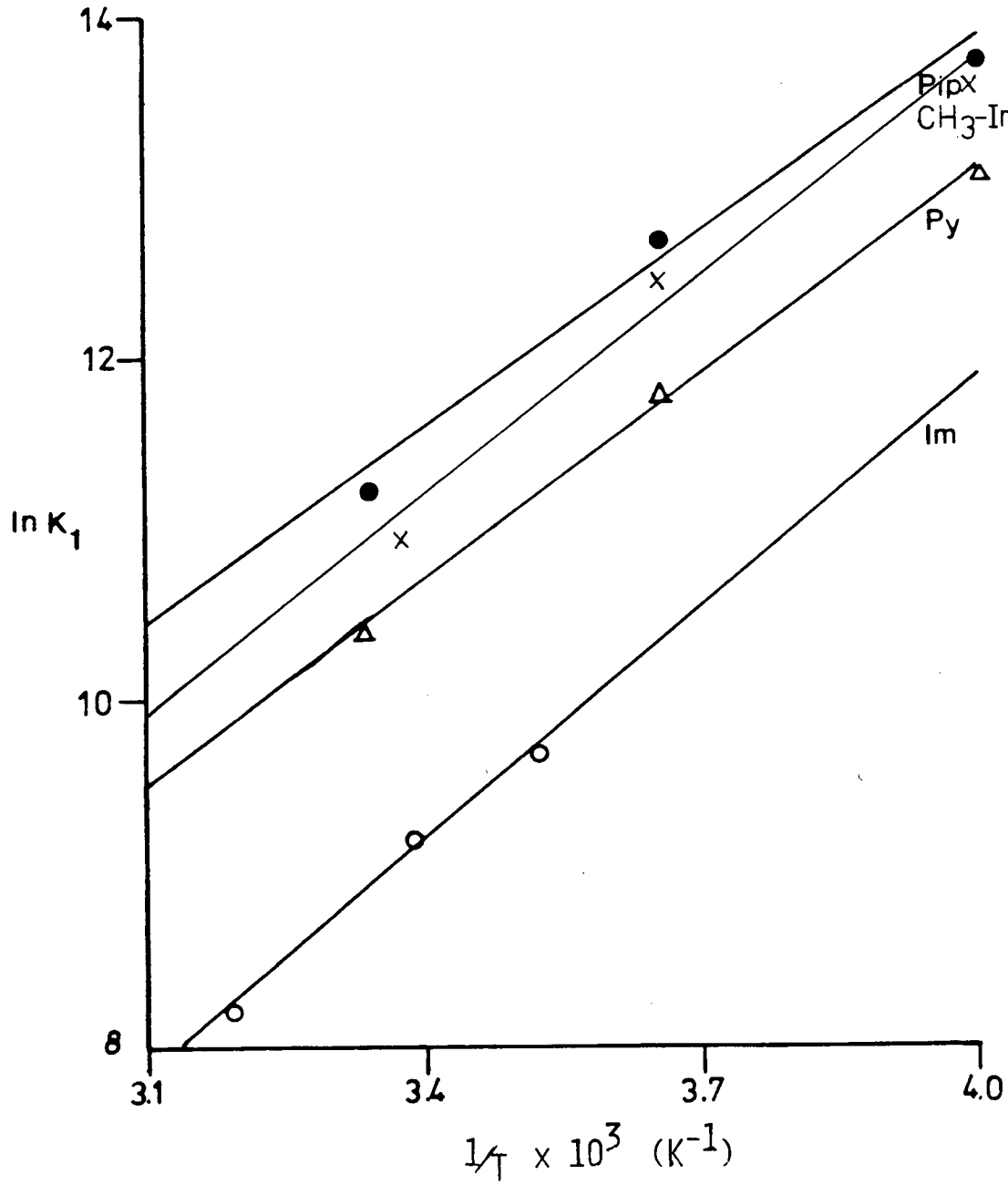

Figure III.6. Van't Hoff plots for L + CoOMBP $\rightleftharpoons$ LCoOMBP

L = Im, CH_3-Im, Pip, and Py

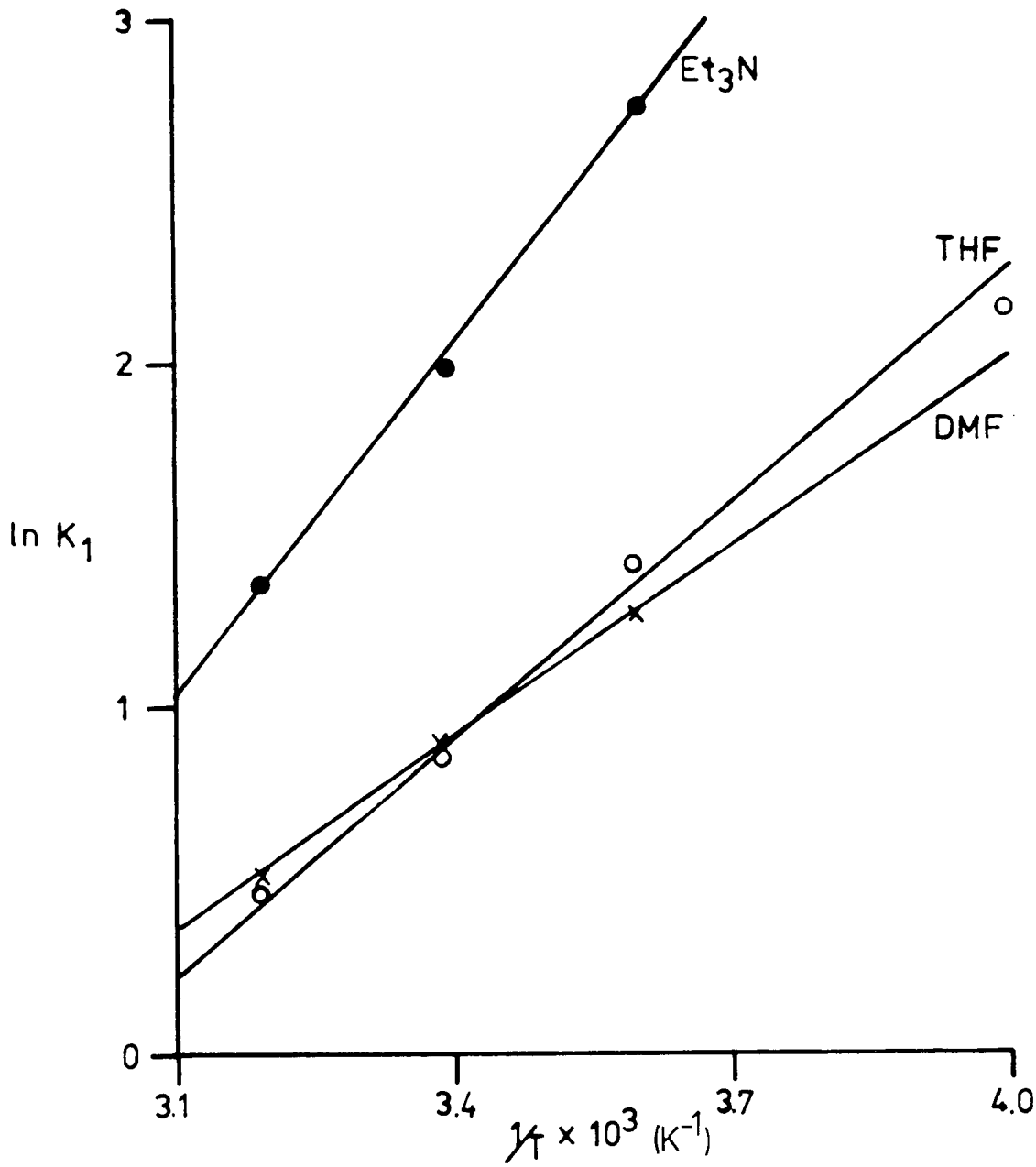

Figure III.7. Van't Hoff plots for L + CoOMBP $\rightleftharpoons$ LCoOMBP

L = Et_3N, THF, and DMF

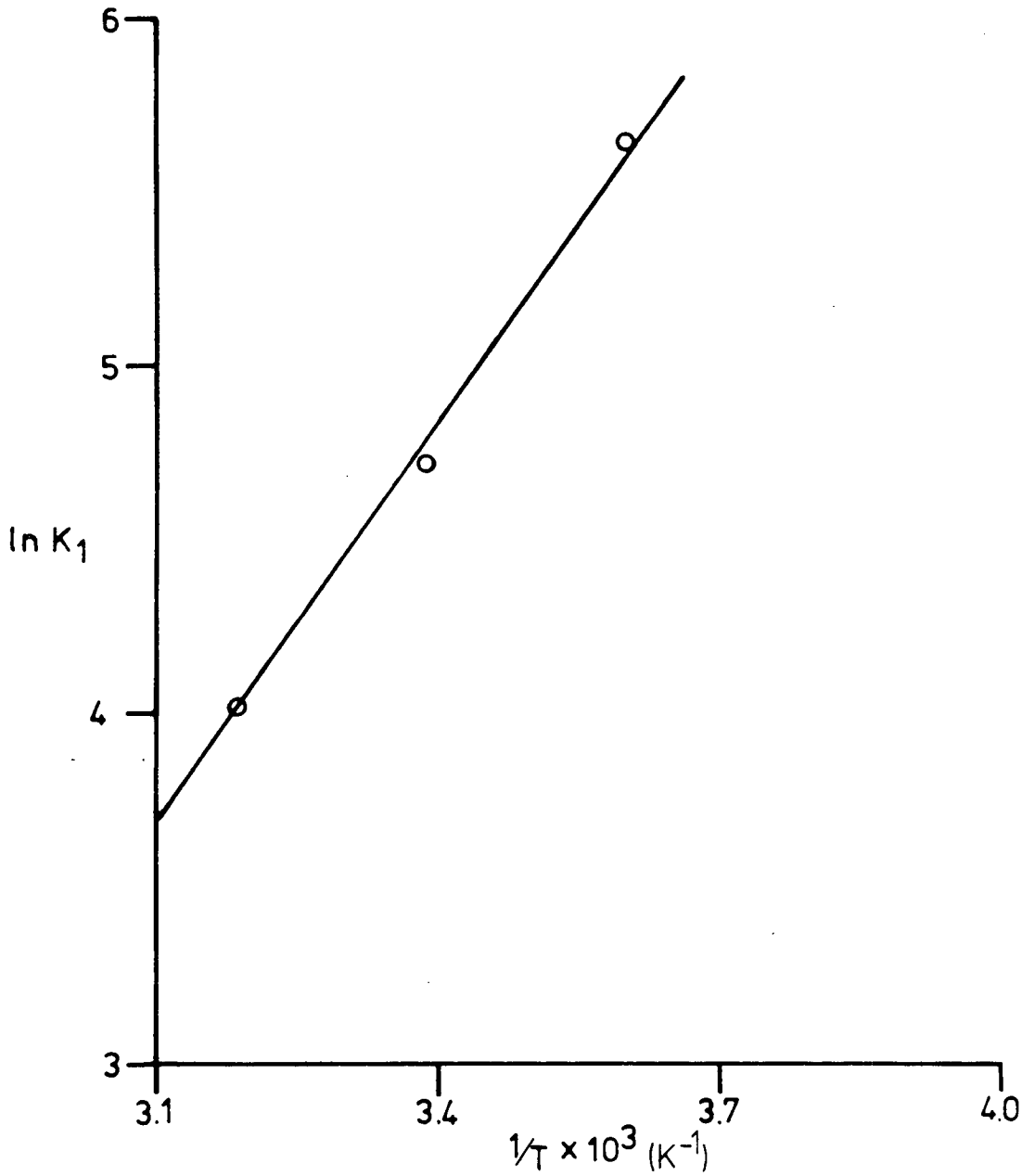

Figure III.8. Van't Hoff plot for PPh_3 + CoOMBP $\rightleftharpoons$ PPh_3CoOMBP.

Thus the analysis of the data for the formation of a six-coordinate complex from LCoOMBP is analogous to that of the formation of a five-coordinate complex from CoOMBP. Again, the experimental slopes of the lines of the appropriate $\log \frac{A - A_o}{A_\infty - A}$ vs. $\log[L]$ plots ranged from 0.8 to 1.2, consistent with the addition of one further ligand . The plots of $\log \frac{A - A_o}{A_\infty - A}$ vs. $\log[CH_3\text{-Im}]$ are shown in Figure III.9, the intercepts on the abscissa giving $-\log K_2$ values. The ΔH and ΔS values then can be obtained from a van't Hoff plot as shown in Figure III.10.

III.3 Sources of Error

When performing ligand binding experiments, care must be taken that trace amounts of oxygen do not enter the system. This requirement was satisfied fairly easily when studying the K_1 equilibrium, although the Im system was very air sensitive. Normally, the binding of the second axial ligand was studied using the same solution that had just been used to measure K_1. However, the CH_3-Im - CoOMBP system became very air sensitve upon coordination of the second of the second CH_3-Im (see Chapter VII), and bis adduct formation had to be studied on freshly made solutions of CoOMBP. Sufficient trace oxygen apparently leaked into the system during studies on the mono adduct formation, such that substantial amounts of oxidized complex were formed if bis adduct formation were studied subsequently.

When ligand binding was investigated in the more polar solvent, 1,2-dichloroethane, all the complexes studied became more oxygen sensitive. Ligand binding sometimes had to be studied using several fresh CoOMBP

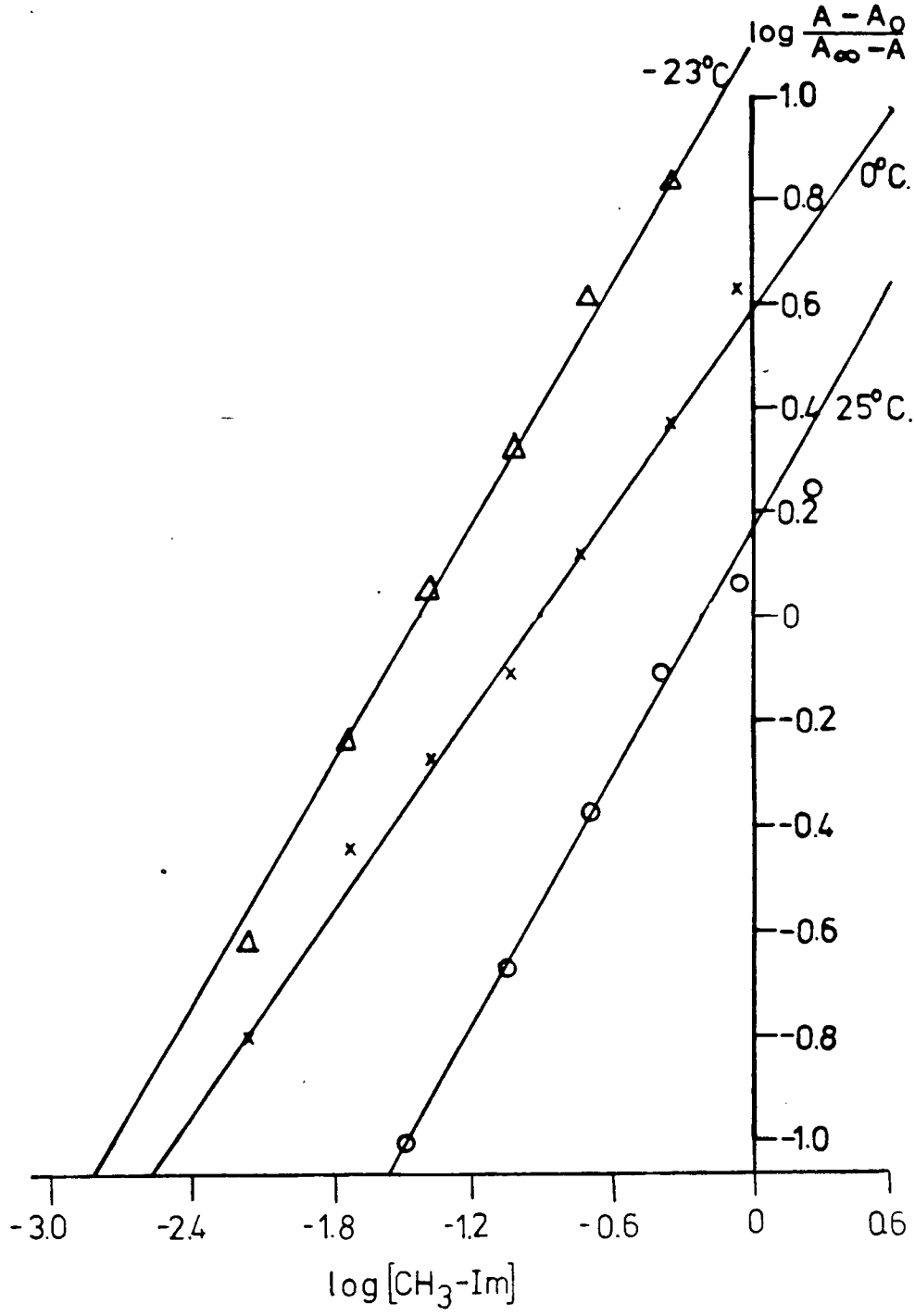

Figure III.9. Equilibrium plots for CH_3-Im + CH_3-ImCoOMBP $\rightleftharpoons$ $(CH_3\text{-Im})_2$CoOMBP

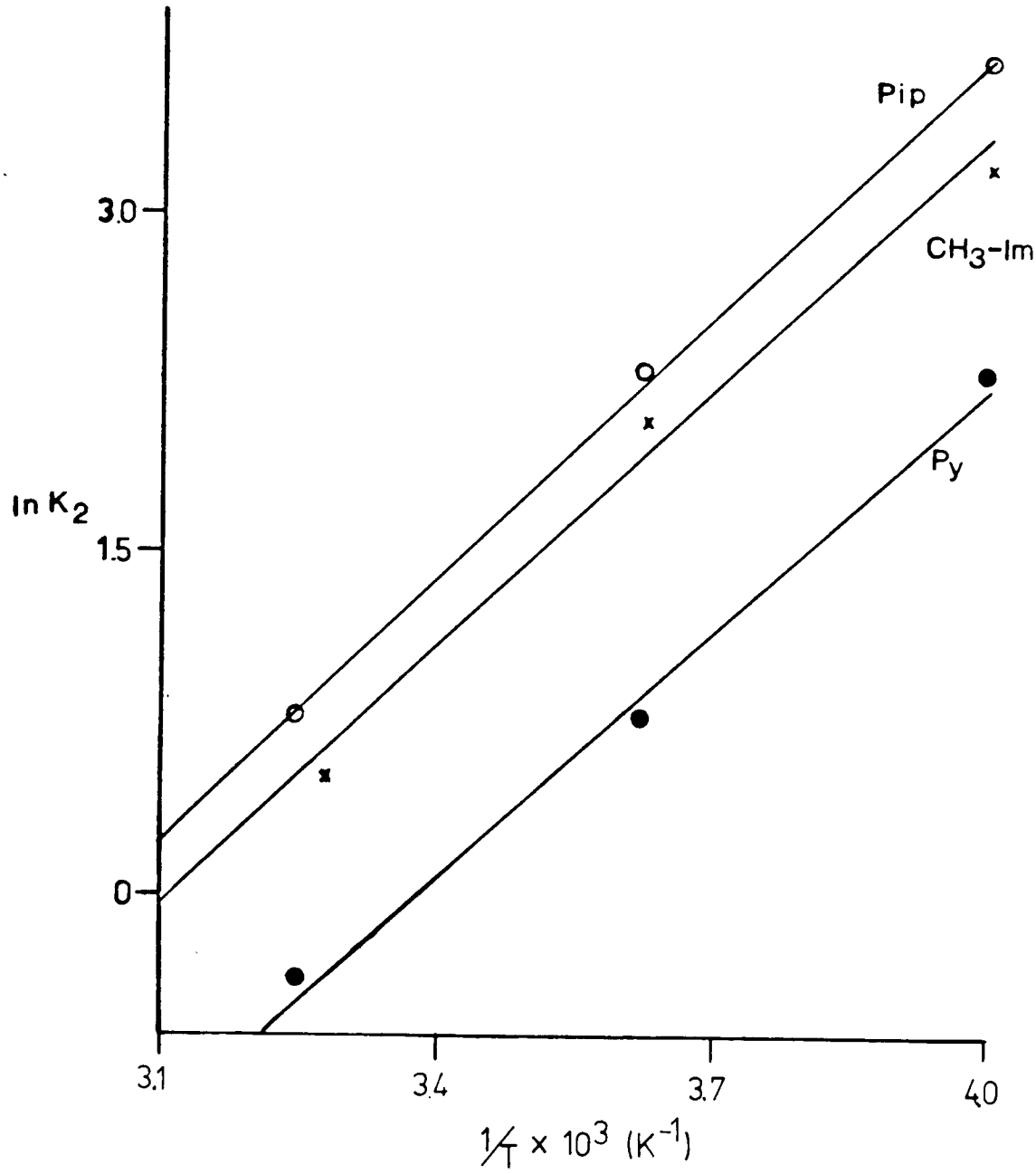

Figure III.10. Van't Hoff plots for L + LCoOMBP $\rightleftharpoons$ L_2CoOMBP

L = CH_3-Im, Pip, and Py

solutions containing fixed concentrations of ligand, in order to avoid complications arising from the oxidation process.

Usually the concentration of adduct formed was insignificant compared to the concentration of added free ligand. However, in a few instances (notably when studying binding of CH_3-Im or Pip at lower temperatures) K_1 values were so high that a substantial fraction of the added ligand coordinated to CoOMBP. In these cases the amount of ligand bound to the metal centre had to be subtracted from the total amount added in order to to calculate the concentration of free ligand.

For some systems studied, substantial amounts of ligand had to be added to fully form the adduct. The resulting high ligand concentration can cause changes in the nature of the solvent with respect to solvation characteristics and dielectric constant. Changes in dielectric constants became important only when ligand concentration became substantial. For example a 0.65 M toluene solution of DMF (the most polar ligand studied) had a dielectric constant of 3.63 compared with $\epsilon = 2.38$ for neat toluene. Generally formation of at least 80% of the ligated species had occurred at lower ligand concentrations. Almost all of the spectral data needed to ascertain equilibrium constants were obtained before sufficient ligand was present in solution to cause significant changes in the dielectric constant, and since a good analysis of the spectral data was generally achieved, any changes in the dielectric constant and solvation properties did not appear to present a problem for the ligand binding studies. Also, as will be shown in Chapter III.5, changing the solvent from toluene ($\epsilon = 2.38$) to 1,2-dichloroethane ($\epsilon = 10.36$) caused only slight differences in CoOMBP-ligand binding constants.

III.4 Ligand Binding Constants

III.4.1 $L + CoOMBP \rightleftharpoons LCoOMBP$, K_1.

The equilibrium constants of ligand binding to CoOMBP are given in Table III.1; the raw data for which are given in Appendices Ia-Ii. Also listed in Table III.3 are the values of ΔH and ΔS obtained, and the pK_a of the protonated ligand studied.

The order in ligand binding abilities observed at 25°C is:

$Pip > CH_3\text{-}Im > Py > PBu_3 > Im >> PPh_3 >> Et_3N > DMF > THF$.

As mentioned in the introduction, no simple correlation between K_1, ΔH and ΔS, and the pK_a of the protonated ligand was observed in some CoPpIXDME or CoTPP systems. In the present work, a wider variety of ligands has been used, and again no overall correlation is observed. For example, Pip, which has a pK_a similar to that of Et_3N, binds more strongly to CoOMBP by a factor of approximately 10^4. Furthermore, Et_3N binds about as strongly as DMF, although the pK_a of the latter ligand is 13 units lower than that of the former.

In general, the nitrogen-donors bound more strongly to CoOMBP, with corresponding higher reaction exothermicities, than the oxygen-and the phosphorus-donors. Within the N-donors, the relatively weak binding of Et_3N is seen to result from a more unfavourable entropy change compared to the cyclic amines; this could result from a greater loss of freedom of motion upon coordination, although differences in solvation in the systems could also be important.

The surprisingly high affinity of PBu_3 compared to Et_3N appears to be reflected in a much less unfavourable entropy change (in fact $\Delta S \sim 0$ for the phosphine system), since the exothermicity is relatively small. This is

Table III.3. Thermodynamic Data for the Binding of the First Axial Ligand to CoOMBP in a Toluene Solution.

LIGAND	TEMP., °C.	K_1, M^{-1}.	ΔH_1^a kcal/mole	ΔS_1^a e.u.	pK_a
Im	5	1.6×10^4	-7.1	-6	6.95[b]
	22	9.1×10^3			
	40	3.7×10^3			
CH_3-Im	-23	8.1×10^5	-8.5	-7	7.25[b]
	0	2.5×10^5			
	23	5.5×10^4			
Pip	-23	1.1×10^6	-7.9	-4	11.30[c]
	0	3.8×10^5			
	26	8.9×10^4			
Py	-23	4.8×10^5	-8.0	-6	5.27[c]
	0	1.3×10^5			
	27	2.1×10^4			
Et_3N	5	15.5	-6.8	-19	11.01[d]
	22	7.4			
	40	3.8			
DMF	5	3.6	-3.7	-11	-2.0[e]
	22	2.5			
	40	1.7			
THF	-23	8.7	-5.0	-16	-2.08[f]
	5	4.2			
	22	2.3			
	40	1.6			
PPh_3	5	2.8×10^2	-7.8	-17	2.73[g]
	22	1.1×10^2			
	40	5.6×10^1			
PBu_3	5	3.5×10^4	$\sim$ -4	$\sim$ 0	8.43[g]
	22	2.3×10^4			
	40	1.5×10^4			

Notes to Table III.3.

a. Since the number of data points on a particular van't Hoff plot is small, error estimates are not very meaningful. Standard deviations were estimated on the basis of least squares analysis for all the above data sets. It was concluded that $\sigma_{\Delta H}$ and $\sigma_{\Delta S}$ were $\pm$ 0.4 kcal/mole and $\pm$ 1.5 e.u., respectively. As the scatter associated with the van't Hoff plots for CH_3-Im and PBu_3 were greater than normal, the $\sigma_{\Delta H}$ and the $\sigma_{\Delta S}$ values for CH_3-Im binding were estimated to be $\pm$ 0.8 kcal/mole and $\pm$ 3 e.u., respectively, while the respective errors associated with PBu_3 binding were set at $\pm$ 1.2 kcal/mole and $\pm$ 6 e.u.

b. K. Hoffman, Chem. Heterocycl. Compounds, 6, 3 (1953).

c. K. Schofield, "Hetero-Aromatic Nitrogen Compounds," Plenum Press, New York, N.Y.,1967, p. 146.

d. A. J. Gordon, R. A. Ford, "The Chemist's Companion, A Handbook of Practical Data, Techniques, and References," J. Wiley, New York, N.Y., 1972, p. 60.

e. J. T. Edwards, H. S. Chang, K. Yates, and R. Stewart, Can. J. Chem., 38, 1518 (1960).

f. E. M. Arnett and C. Y. Wu, J. Amer. Chem. Soc., 84, 1684 (1962).

g. C. A. Streuli, Anal. Chem., 32, 985 (1960).

consistent with a Co-P bond that is weaker and longer than a Co-N bond, which again seems consistent with a lower loss of rotational freedom on coordination of PBu_3 compared with Et_3N, especially in view of the bulkier alkyl groups in the phosphorus donor. In the case of PPh_3, the Co-P bond appears to be as strong as a Co-N bond, but the relatively unfavourable entropy change results in the lower equilibrium constant. This may be due to PPh_3 being a strong π-acceptor[93] which could cause the Co-P bond order to be greater than one. This would result in a greater enthalpy of bond formation and a greater loss of rotational freedom than if no $\pi - \pi$ interactions had been present.

The oxygen-coordinating ligands are the least effective in binding to CoOMBP, and this is mainly reflected in lower exothermicities suggesting, for example, that a Co-O bond is weaker than a Co-N bond. There also appears to be a somewhat greater loss of entropy associated with binding an oxygen donating ligand.

Upon formation of a five-coordinate adduct, the cobalt centre is usually displaced from the centre of the ring[88c,88e,90,117], and this probably results in the full degree of exothermicity of the reaction being realized. Since OMBP is an especially strong π-donating porphyrin[96c], $\pi-\pi$ porphyrin-cobalt interactions could serve to "lock" the cobalt centre more firmly in the porphyrin plane, thus preventing the full release of energy when an axial ligand is bound. Also the ligand, not being so firmly bound to CoOMBP, would be more free to rotate, resulting in less loss of entropy.

Indeed exothermicities for binding a first cyclic amine to CoOMBP are somewhat less than those reported in other cobalt(II) porphyrin systems. For example, ΔH values of -9.7, -9.1,and -9.2 kcal/mole were reported for

Py binding to CoPpIXDME, CoDpIXDME, and CoMpIXDME, respectively[91d]. CoPpIXDME was reported to bind Im, CH_3-Im, Pip, and DMF with respective ΔH vales of -7.9, -10.7, -10.4 and -7.9 kcal/mole[89]. The ΔS values associated with Py binding to CoPpIXDME, CoDpIXDME, and CoMpIXDME have been reported to be -18, -16, and -17 eu, respectively[91d], all of which are more negative than the ΔS value for Py binding to CoOMBP. CoPpIXDME has had respective ΔS values of -10, -19,-17, and -21 eu reported for the binding of Im, CH_3-Im, Pip, and DMF. Again these values indicate a greater loss of entropy than is observed when the corresponding ligands bind to CoOMBP.

In examining the binding of PBu_3 and PPh_3 to CoMpIXDME[93], respective K_1 values at 16°C were found to be 1.8×10^4 M^{-1} and 41.8 M^{-1}, somewhat smaller than in the CoOMBP system, but relative binding strengths of the ligands to the two porphyrin complexes were comparable. However, the ΔH value associated with PBu_3 binding to CoMpIXDME was reported as -13.3 kcal/mole and the corresponding ΔS value at -27 eu, while the respective values associated with PPh_3 binding were reported to be -7.0 kcal/mole and -17 eu. The thermodynamic parameters for PBu_3 binding to CoMpIXDME are substantially more negative than those for CoOMBP, which is consistent with the picture of cobalt being "locked-in" the OMBP plane. However, the reported ΔH value of PPh_3 binding to CoMpIXDME is similar to that observed for binding to CoOMBP. This could be due to PPh_3 being better able to accept π-electron density from CoOMBP, thus strengthening the Co-P bond in PPh_3CoOMBP with respect to PPh_3CoMpIXDME, even though the cobalt centre may remain "locked in" the OMBP plane.

Ligand binding to CoOMBP will be further compared with ligand binding to other cobalt(II) porphyrin complexes in Chapter V.

III.4.2 $L + LCoOMBP \rightleftharpoons L_2CoOMBP, \quad K_2.$

The equilibrium constants for a second axial ligand binding to LCoOMBP are given in Table III.4, together with the ΔH_2 and ΔS_2 values and the pK_a values. The raw data are listed in Appendices Ij-Im.

Table III.4 Thermodynamic Data for the Binding of the Second Axial Ligand to LCoOMBP in a Toluene Solution.

LIGAND	TEMP., °C.	K_2, M^{-1}.	ΔH_2 kcal/mole	ΔS_2 e.u.	pK_a [a]
CH_3-Im	-23	26.3	-8.5	-28	7.25
	0	7.8			
	25	1.7			
Pip	-23	40	-7.4	-25	11.30
	0	10			
	27	3.4			
Py	-23	10	-8.0	-28	5.27
	0	2.2			
	27	0.69			
PBu_3	5	1.4×10^4	~ -2	~ 0	8.43
	22	1.2×10^4			
	40	0.9×10^4			

a. For references see Table III.3.

The formation of a six-coordinate cobalt porphyrin complex at ambient temperatures is of interest as little information on the binding of a ligand in the sixth coordination site is available[89,92b]. Previous work suggests that the formation of the second Co-N bond is less exothermic than the formation of the first. For example, the ΔH_2 value for Pip binding to CoT(p-MeO)PP was reported to be -1.7 kcal/mole[92b], while the ΔH_1 value was -6.8 kcal/mole.

The present work suggests that for the CoOMBP system the ΔH values for the formation of both axial ligand bonds are similar, and that it is a more unfavourable entropy change that leads to the much weaker binding. The entropy differences are much greater than what would result from the usual statistical factor; i.e. the difference resulting from a ligand being able to bind to two equivalent sites rather than one.

It should be noted that Walker[92b] determined thermodynamic parameters of the second ligation by the indirect means of studying the dioxygen binding abilities of LCoT(p-MeO)PP and L_2CoT(p-MeO)PP separately at low temperatures, and assigning the differences in those values to the value of the binding of the second ligand, as the second axial ligand bound so weakly that full formation of the six-coordinate adduct could not be observed at ambient temperatures. Since the K_2 value for the Pip-CoT(p-MeO)PP system was reported to be 4.0 M^{-1} at -65°C[92b], a high concentration of ligand would be required for complete binding, and the toluene solvent would then take on some of the characteristics the more polar ligand. Thus, when dioxygen binding is studied on the six-coordinate species, the oxygen affinity is likely to be increased relative to that of the five-coordinate species[80b], which is maintained using low ligand concentrations ($\sim 10^{-3}$ M), meaning that the solvent is essentially pure toluene. This could mean exothermicities of second ligand binding estimated by the simple Hess' Law treatment are too low.

The observed similarity of the ΔH values for the binding of the fifth and sixth ligands in the present work is interesting. Normally when the first axial ligand coordinates, the metal is lifted out of the plane of the porphyrin ring towards the ligand, while addition of a second identical ligand brings the metal back into the porphyrin plane[118]. Presumably, this

action could weaken, to some extent, the first cobalt-ligand bond, and the observed ΔH_2 would be that of the second ligand binding minus the bond weakening of the first ligand.

Although placing the cobalt into the plane of the porphyrin should increase the bond strength of the porphyrin N-Co bonds, this effect should not be as great as the change in bond strength to the axial ligand, or the metal would not have moved from the plane upon initial ligation. Strong π-donating properties of OMBP could mean that the metal is very near the plane of the porphyrin ring in CoOMBP so that the second ligand binding could release as much enthalpy as the first. However, some displacement from the porphyrin ring is probably necessary to explain the greater loss of entropy upon the second ligation.

III.5 Ligand Binding in 1,2-Dichloroethane

Large solvent effects for dioxygen binding, and, to some extent, ligand binding have been reported for systems involving metal porphyrins[91b,119]. Since it has been established that the nature of the solvent plays a major role in determining the oxygen affinity of a cobalt porphyrin complex[91b], and since on numerous occasions large concentrations of ligand were required to fully form an adduct, a study on ligand binding in an alternate solvent was carried out. A solvent sometimes used in metalloporphyrin studies is dichloromethane[52b]. However, clean spectra of CoOMBP in dichloromethane could not be reliably achieved, regardless of the method used for purification, and so 1,2-dichloroethane (ϵ = 10.36) was used as an alternative to toluene (ϵ = 2.38).

The ligand binding reactions that took place in toluene also occurred in DCE, and the binding of the first ligand results are summarized in Table III.5, with the raw data listed in Appendices I.n-I.q.

Table III.5 Thermodynamic Data for the Binding of the First Axial Ligand to CoOMBP in a DCE Solution.

LIGAND	Temp., °C	K_1, M^{-1}	ΔH_1 kcal/mole	ΔS_1 e.u.	pK_a [a]
CH_3-Im	0*	7.7×10^4	-7.5	-5	7.25
	5	7.4×10^4			
	20	3.4×10^4			
	40	1.5×10^4			
Pip	0*	1.0×10^5	-7.0	-3	11.30
	5	9.8×10^4			
	20	5.3×10^4			
	40	2.7×10^4			
Py	0*	5.3×10^4	-7.5	-6	5.27
	5	3.4×10^4			
	20	1.6×10^3			
	40	7.5×10^3			
THF	5	1.5	-4.7	-16	-2.08
	20	1.2			
	40	0.71			

* Values for 0°C are calculated from the data in the table for ease of comparison with the binding data in toluene.

a. For references see Table III.3. $\sigma_{\Delta H}$ was ±0.8 kcal/mole and $\sigma_{\Delta S}$ was ± 3 e.u.

On the whole, the equilibrium constants in DCE were slightly lower than in toluene. Generally, more polar solvents will tend to stabilize more polar species. In the ligation reaction, CoOMBP could be pictured as an essentially non polar complex that binds with ligands of varying polarity. When the adduct is formed, any ligand polarity is likely to be dispersed over the

whole of the adduct, and thus a polar solvent is more likely to stabilize the free ligand and should tend to destabilize the adduct. Qualitatively such a picture accounts for the above trend.

Although quantitative studies on the reaction, $L + LCoOMBP \rightleftharpoons L_2CoOMBP$ in DCE, could not be carried out due to air sensitivity, the relative binding abilities were observed to be Pip (K_2 @ 20°C ~4 M^{-1}) > CH_3-Im (K_2 @ 20°C ~1.7 M^{-1}) > Py (K_2 @ 20°C ~0.8 M^{-1}), the same as for the mono adduct formation, and the same as observed for K_1 and K_2 in toluene. In all cases, the binding of the second ligand was weaker than measured in toluene, and again this could be rationalized in terms of differences in solvation of the free ligand.

CHAPTER IV

THERMODYNAMICS OF REVERSIBLE DIOXYGEN BINDING TO CoOMBP COMPLEXES

IV.1 Qualitative Spectral Observations

IV.1.1 $LCoOMBP + O_2 \rightleftharpoons LCoOMBP(O_2)$, K_{O_2}

Upon exposure to oxygen gas at low temperatures, solutions of LCoOMBP complexes exhibited a change in visible spectrum which was a function of the oxygen pressure and which was reversible; i.e. pumping off the oxygen gas and/or warming the solution restored the spectrum of LCoOMBP. The spectral changes that occurred when a solution of CH_3-ImCoOMBP was exposed to oxygen are shown in Figure IV.1. This type of spectral change had been previously assigned to the formation of a 1:1 cobalt:dioxygen adduct[89]. Of the complexes studied, only the THF adduct showed no signs of dioxygen binding at low temperature, although the PPh_3 adduct exhibited a very weak tendency to bind dioxygen. No quantitative work was undertaken on the oxygenation of ImCoOMBP, as the complex irreversibly oxidized very readily, even at low temperatures.

In the case of the nitrogen-donating ligands, the Soret band shifted to about 438 nm ($\epsilon \sim 6 \times 10^4$ $M^{-1}cm^{-1}$) and the visible band shifted to 624 nm ($\epsilon \sim 4 \times 10^4$). When the DMF adduct bound dioxygen, a new Soret band was observed at 434 nm ($\epsilon = 5.8 \times 10^4$ $M^{-1}cm^{-1}$), and the visible band shifted to 619 nm ($\epsilon = 4.5 \times 10^4$ $M^{-1}cm^{-1}$). When oxygen was added to the

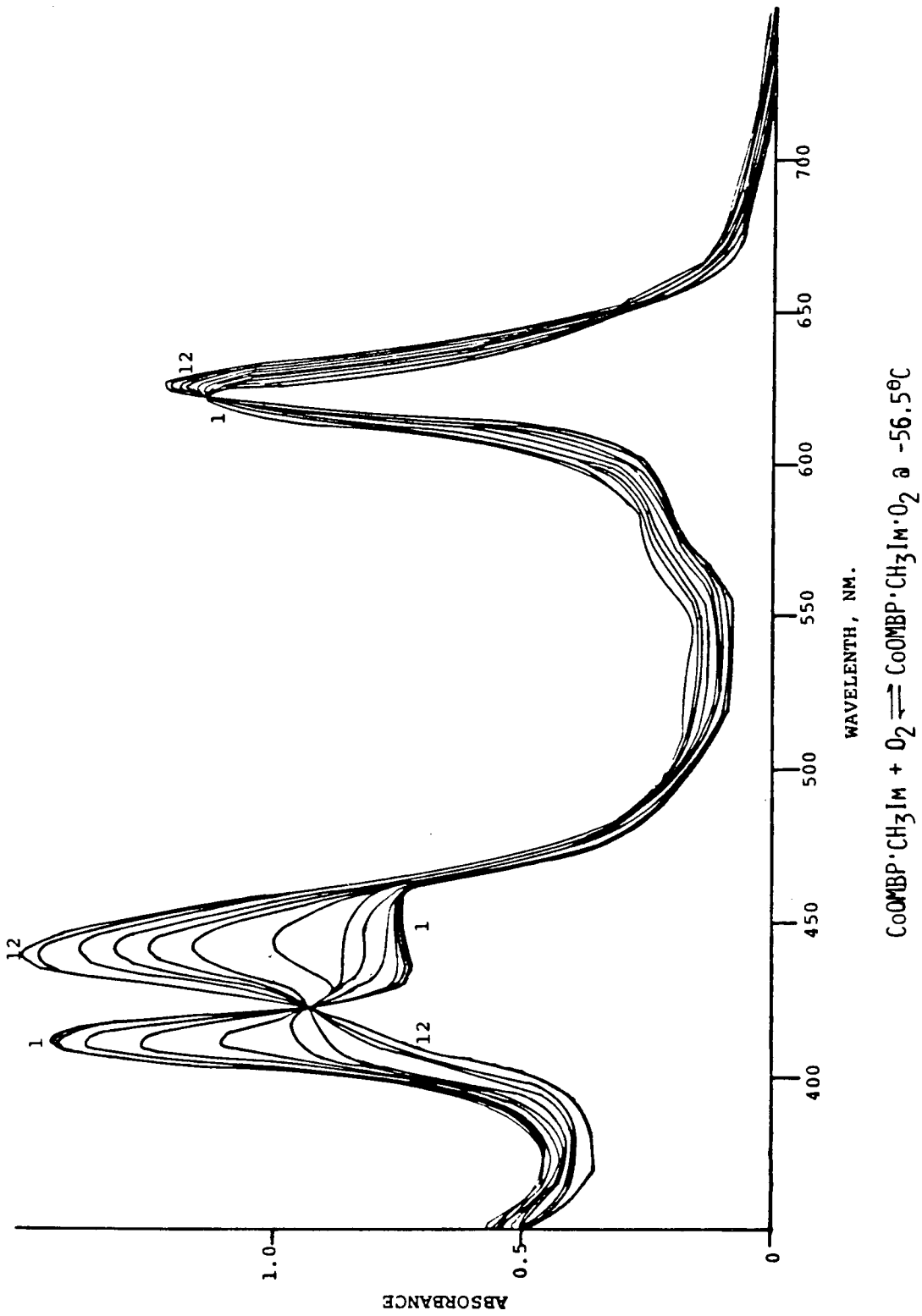

Figure IV.1. Spectra of oxygen binding to CH_3-ImCoOMBP @ -56.5°C

For raw data see Appendix IIa.

CoOMBP-PBu_3 system, the visible band shifted to 632 nm ($\epsilon \sim 3 \times 10^4$ $M^{-1}cm^{-1}$) and the Soret band to 443 nm ($\epsilon \sim 2 \times 10^4$ $M^{-1}cm^{-1}$)*. As the PPh_3 adduct bound dioxygen so weakly, no quantitative work could be undertaken. However, the visible band did diminish and red shift slightly and a decrease in the initial Soret band was accompanied by a spectral growth in the 450 nm region, but peak positions of the dioxygen adduct could not be assigned, since it was estimated that no more than 20% of the adduct was formed under any of the conditions used.

The spectral changes associated with the dioxygen adduct formation are listed in Table IV.1a.

Evidence for formation of the 1:1 cobalt:dioxygen complex was corroborated by ESR measurements in toluene at 77 K (Figure IV.2), which recorded spectra typical of such adducts[92a,120].

Although some 1:1 cobalt:dioxygen complex could be formed at ambient temperatures (e.g. in the cyclic amine systems), the rate of formation was too great to be measured by stopped-flow techniques.

IV.1.2 $L_2CoOMBP + O_2 \rightleftharpoons LCoOMBP(O_2) + L$, $K_{O_{2/L}}$.

The six-coordinate complexes $(CH_3\text{-Im})_2CoOMBP$, $Pip_2CoOMBP$, and $Py_2CoOMBP$ all reacted with dioxygen to some extent under certain conditions. The spectra generated from the bis cyclic amine complexes were those of the $LCoOMBP(O_2)$ complexes, as shown in Fgure IV.3. When oxygen was pumped off the system, the visible spectral changes were reversed in all cases. Upon addition of oxygen to $L_2CoOMBP$, ESR signals of $LCoOMBP(O_2)$ were generated.

*For a discussion of the species present in the CoOMBP-PBu_3 system when oxygenation occurs, see Chapter IV.2.

Table IV.1a. Spectral Data From 350 to 750 nm for the Reaction:

$$LCoOMBP + O_2 \rightleftharpoons LCoOMBP(O_2)$$

Absorbing Species	Absorption Maxima (nm) (Extinction Coefficient, $M^{-1}cm^{-1}$)				Isosbestic Points (nm)	
CH_3-ImCoOMBP	408	(6.5×10^4)	618	(4.7×10^4)	422	620
↓						
CH_3-ImCoOMBP(O_2)	438	(7×10^4)	624	(5×10^4)		
PipCoOMBP	408	(6.5×10^4)	618	(4.1×10^4)	421	619
↓						
PipCoOMBP(O_2)	438	(7×10^4)	624	(5×10^4)		
PyCoOMBP	407	(5.6×10^4)	618	(4.6×10^4)	421	619
↓						
PyCoOMBP(O_2)	438	(7×10^4)	624	(5×10^4)		
Et_3NCoOMBP	407	(6.9×10^4)	618	(4.7×10^4)	419	620
↓						
Et_3NCoOMBP(O_2)	437	(6.5×10^4)	624	(5.4×10^4)		
DMFCoOMBP	418	(6.0×10^4)	618	(5.4×10^4)	425	622
↓						
DMFCoOMBP(O_2)	434	(7.0×10^4)	619	(6.5×10^4)		
PPh_3CoOMBP	412	(6.3×10^4)	619	(5.3×10^4)	422	626
↓						
PPh_3CoOMBP(O_2)	450	(~6×10^4)	620	(~5×10^4)		
PBu_3CoOMBP	412	(3.5×10^4)	618	(2.8×10^4)	424	626
↓						
PBu_3CoOMBP(O_2)	443	(3.5×10^4)	632	(3.5×10^4)		

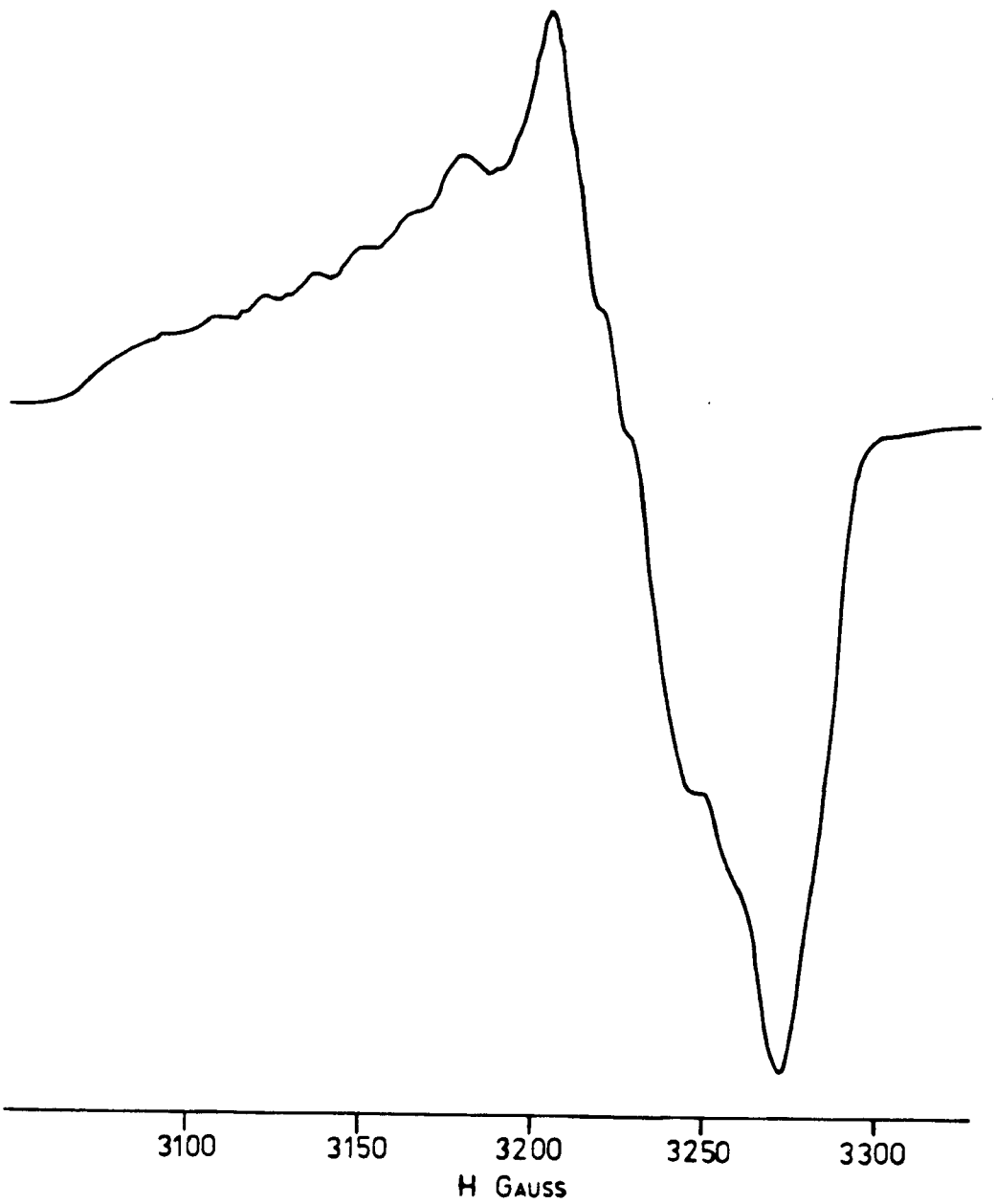

Figure IV.2. ESR signal of CH_3-ImCoOMBP(O_2) in frozen toluene at 77 K.

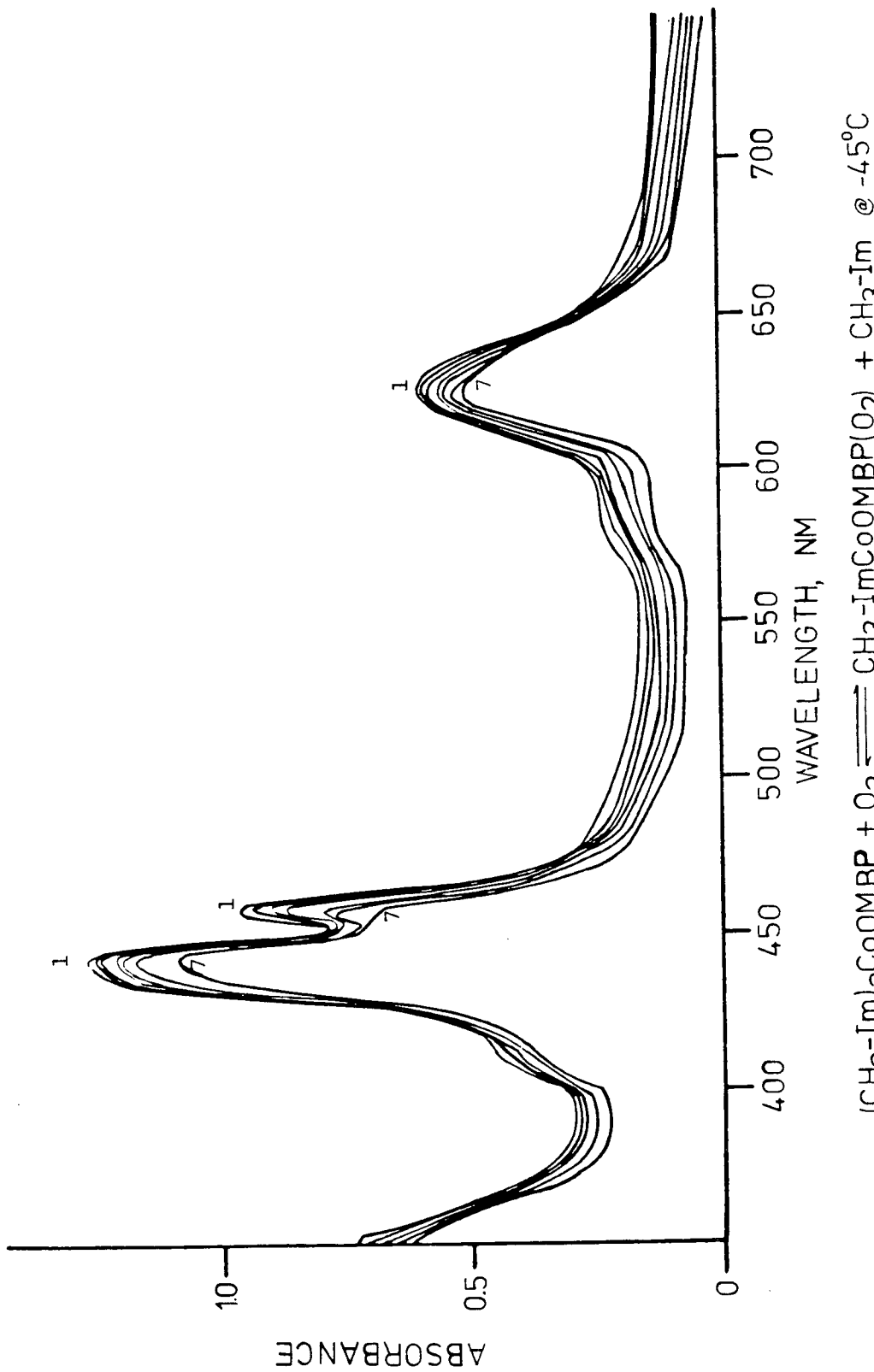

Figure IV.3. Spectra of oxygen binding to $(CH_3\text{-Im})_2CoOMBP$ @ -45°C.
For raw data see Appendix IIi.

Once the $(PBu_3)_2CoOMBP$ complex was fully formed in toluene, no oxygen affinity was observed.

The spectral changes associated with oxygenation of $L_2CoOMBP$ are listed in Table IV.1b.

Table IV.1b. Spectral Data From 350 to 750 nm for the Reaction:

$$L_2CoOMBP + O_2 \rightleftharpoons LCoOMBP(O_2) + L$$

Absorbing Species	Absorption Maxima (nm) (Extinction Coefficient, $M^{-1}cm^{-1}$)	Isosbestic Points (nm)
$(CH_3\text{-Im})_2CoOMBP$	435 (9.2×10^4) 457 (7.6×10^4) 618 (4.5×10^4)	448
$CH_3\text{-ImCoOMBP}(O_2)$	438 (7×10^4) 624 (5×10^4)	
$Pip_2CoOMBP$	430 (9.4×10^4) 456 (4.8×10^4) 616 (3.8×10^4)	—
$PipCoOMBP(O_2)$	— —	
$Py_2CoOMBP$	428 (8.2×10^4) 617 (4.3×10^4)	442
$PyCoOMBP(O_2)$	438 (7×10^4) 624 (5×10^4)	

IV.2 Species Present When the CoOMBP-PBu_3 System is Oxygenated

At ambient temperatures there was a considerable degree of overlap in forming the mono and bis PBu_3 adducts of CoOMBP, and the band positions of the two species were quite similar. In preparation of samples for oxygenation, some of the CoOMBP often did not go into solution since it adhered to the walls of the quartz cell used for low temperature work, so the observed extinction coefficients could not determine which of the two species was present in solution.

Since ΔH for the five-coordinate complex was estimated to be somewhat larger than that for formation of the six-coordinate complex (see Chapter III.4), the increase in the K_1 value, as lower temperatures are used, would be greater than the increase in the K_2 value. Thus essentially full formation of the five-coordinate complex with little formation of the six-coordinate complex should be observed when an appropriate concentration of PBu_3 is used. As shown in Table IV.2, at $-63.5^{\circ}C$ a 2.4×10^{-6} M solution of CoOMBP was observed to be more oxygen sensitive as the concentration of PBu_3 was increased to 1×10^{-5}M. The CoOMBP-PBu_3 system was essentially constant with respect to oxygen sensitivity for $1 \times 10^{-5} < PBu_3 < 10^{-4}$ M, and then the system became less oxygen sensitive after the concentration of PBu_3 exceeded 10^{-4} M.

Table IV.2 Oxygen Sensitivity of CoOMBP as a Function of PBu_3 at $-63.5^{\circ}C$.

PBu_3, M	$P_{\frac{1}{2}}O_2$, Torr
1.01×10^{-6}	589
4.04×10^{-6}	184
1.01×10^{-5}	123
4.04×10^{-5}	111
1.01×10^{-4}	118
4.04×10^{-4}	158
4.04×10^{-3}	"∞"

For raw data see Appendix IIh.

The observed behavior is consistent with full formation of the five-coordinate complex at lower PBu_3 concentrations before a significant amount of the six-coordinate complex occurs. When extra ligand is added, some six-

coordinate complex is formed, and this explains the observed decrease in oxygen affinity at elevated ligand concentrations.

IV.3 Treatment of Data

The equilibrium constants for O_2 binding were obtained by following either the increase in spectral intensity of the Soret band of the 1:1 cobalt:dioxygen complex, or by following the decrease in spectral intensity of the Soret band of the non-oxygenated complex.

The formation of a 1:1 cobalt:dioxygen complex from a mono ligand adduct obeys the equation,

$$LCoOMBP + nO_2 \overset{K_{O_2}}{\rightleftharpoons} LCoOMBP(O_2)_n \qquad (IV.1)$$

and thus occurs by a process of addition that is analogous to the formation of a ligand adduct complex. The data, therefore, can be treated in a manner similar to that described in Chapter III.

The experimental slopes of the lines of the appropriate $\log \frac{A - A_o}{A_\infty - A}$ vs. $\log P_{O_2}$ plots ranged from 0.8 to 1.2 (Figure IV.4), consistent with the addition of one dioxygen molecule to a five-coordinate complex. Also, where possible, $\frac{A - A_o}{A_\infty - A}$ values were kept in the 0.2 to 5.0 range. Van't Hoff plots for the K_{O_2} values obtained from the plots of $\log \frac{A - A_o}{A_\infty - A}$ vs. $\log P_{O_2}$ are shown in Figure IV.5.

The formation of a 1:1 cobalt:dioxygen complex from a six-coordinate complex bis ligand complex obeys the overall substitution reaction,

$$L_2CoOMBP + nO_2 \overset{K_{O_2/L}}{\rightleftharpoons} LCoOMBP(O_2)_n + L \qquad (IV.2)$$

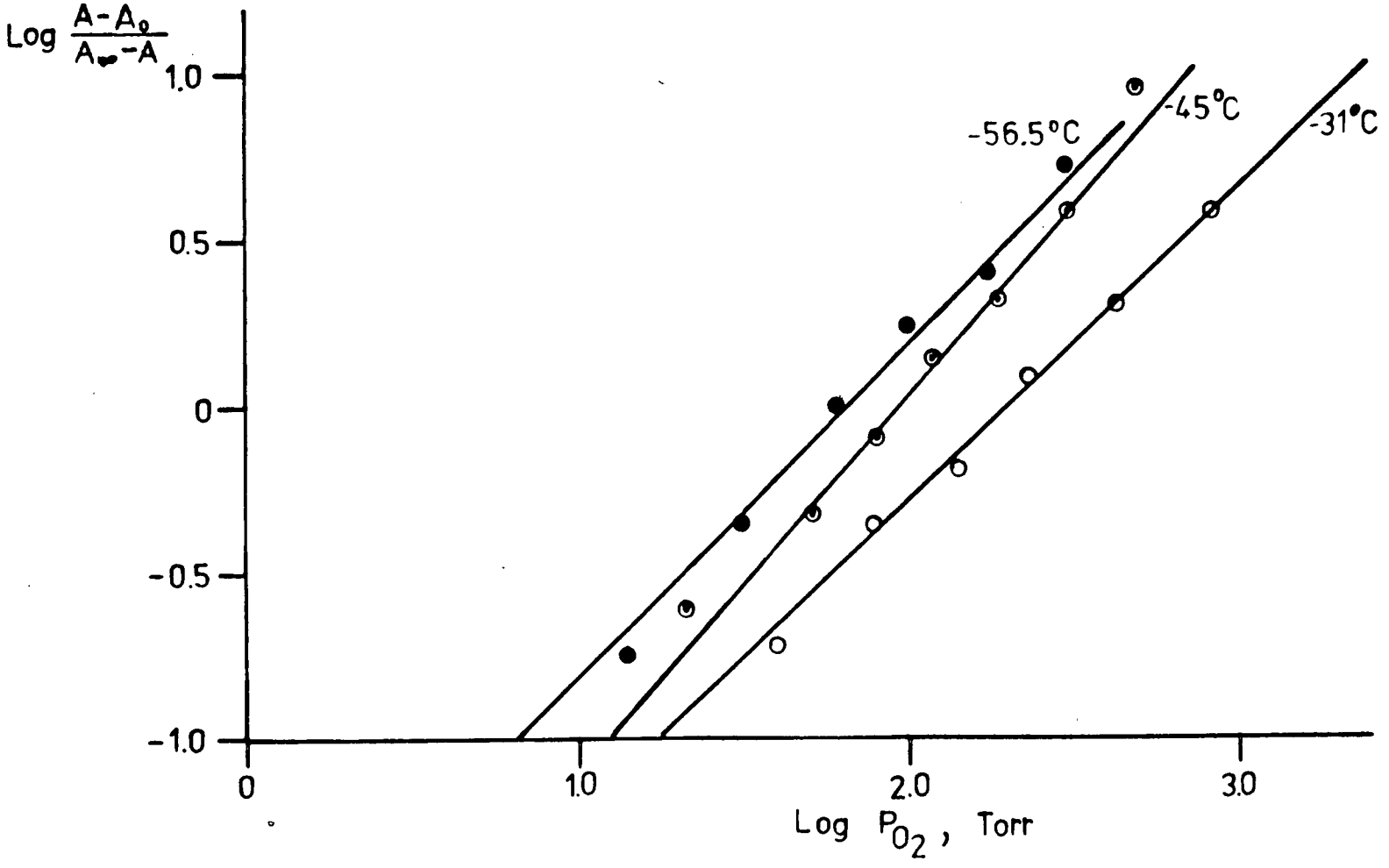

Figure IV.4. Equilibrium plots for CH_3-ImCoOMBP + $O_2 \rightleftharpoons$ CH_3-ImCoOMBP(O_2). For raw data see Appendix IIa.

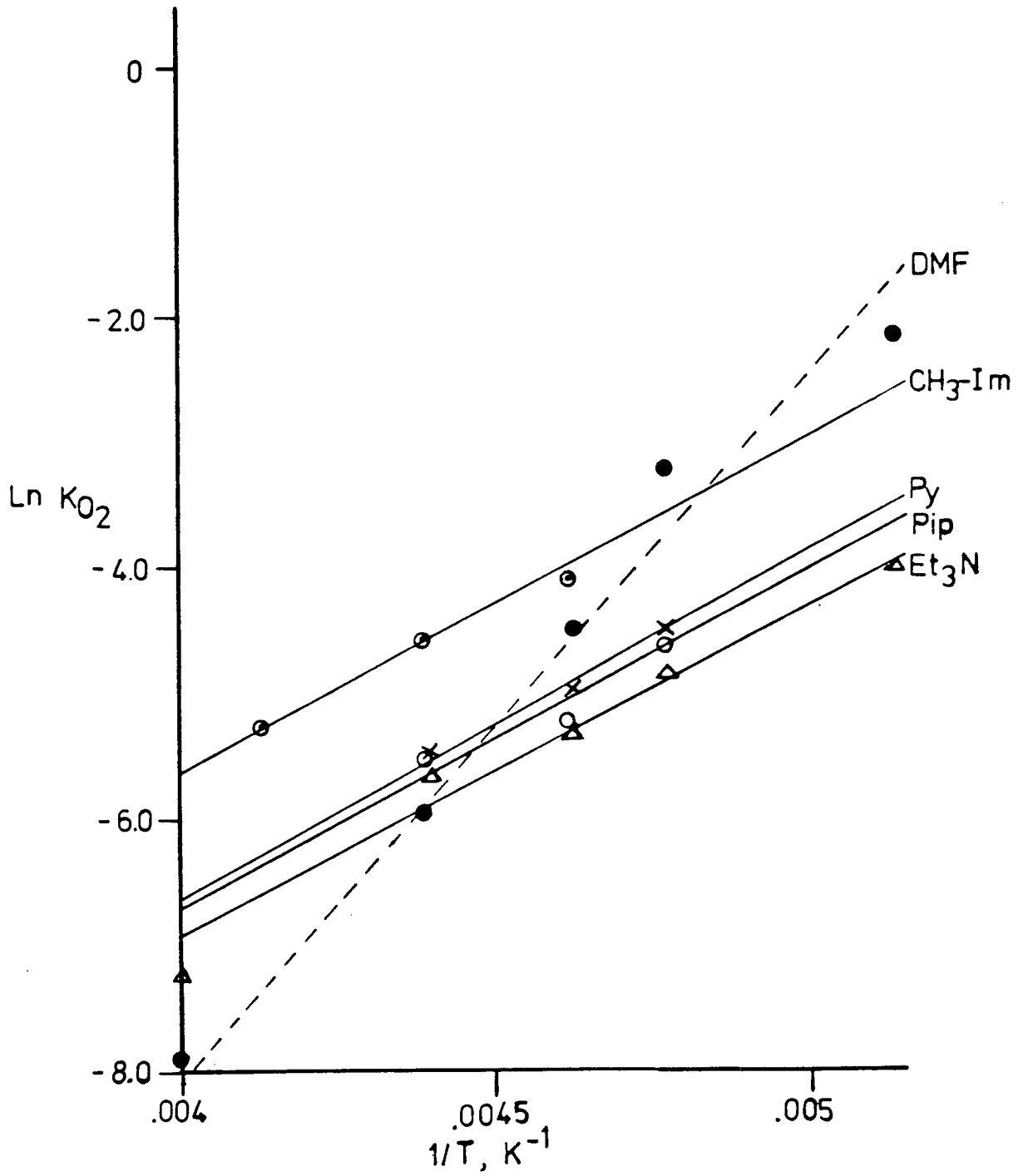

Figure IV.5. Van't Hoff plots for LCoOMBP + $O_2 \rightleftharpoons$ LCoOMBP(O_2)

L = CH_3-Im, Pip, Py, Et_3N, DMF; for raw data see Appendix II.

and, therefore, a different treatment of data is necessary.

The fraction, Y, of $LCoOMBP(O_2)_n$ present at a known partial pressure was calculated from the following expression,

$$Y = \frac{A - A_o}{A_\infty - A_o} \qquad \text{(IV.3a)}$$

while the corresponding fraction, 1-Y, of $L_2CoOMBP$ present was given by

$$1 - Y = \frac{A_\infty - A}{A_\infty - A_o} \qquad \text{(IV.3b)}$$

where A is the absorbance measured at a known partial pressure of oxygen

A_o is the absorbance measured when no oxygen is present

and A_∞ is the absorbance calculated for the fully oxygenated complex, based on data for oxygenation of LCoOMBP.

The equilibrium constant for such a reaction has the expression:

$$K_{O_2/L} = \frac{[LCoOMBP(O_2)_n][L]}{[L_2CoOMBP](P_{O_2})^n} = \frac{Y[Co]_T[L]}{(1-Y)[Co]_T(P_{O_2})^n} \qquad \text{(IV.4)}$$

where $[Co]_T$ is the total concentration of cobalt present.

The value for $[L]$ will be equal to the amount resulting from the dissociation of $L_2CoOMBP$, or $Y[Co]_T$, plus the initial concentration of free L; i.e.,

$$K_{O_2/L} = \frac{Y[Co]_T(Y[Co]_T + [L]_i)}{(1 - Y)[Co]_T (P_{O_2})^n} \qquad \text{(IV.5)}$$

where $[L]_i$ is the initial concentration of free L present in solution.

In the case of the bis cyclic amine complexes, the amount of added ligand present was so great that the $Y[Co]_T$ term was insignificant, and so

$$K_{O_2/L} = \frac{Y[L]_i}{(1-Y)(P_{O_2})^n} \qquad (IV.6)$$

and

$$\log K_{O_2/L}[L]_i = \log \frac{Y}{1-Y} - n\log P_{O_2} = \log \frac{A - A_o}{A_\infty - A} - \log P_{O_2} \qquad (IV.7)$$

As the oxygen affinities of these complexes were relatively low, few quantitative experiments could be done. However, in the case of the $(CH_3\text{-Im})_2$CoOMBP system at -45°C, close to 50% oxygenation was achieved and the plot of $\log \frac{A - A_o}{A_\infty - A}$ vs. $\log P_{O_2}$ had a slope of 1.1 (Figure IV.6).

As the final spectrum of LCoOMBP(O_2) was not achieved in any L_2CoOMBP system, quantitative thermodynamic studies were not undertaken.

IV.4 Sources of Error

When performing oxygenation experiments on LCoOMBP systems, it is important that the starting concentration of LCoOMBP be as high as possible. From the measured thermodynamic parameters listed in Table III.1, it was possible to adjust the concentration of ligand so that at least 95% of the cobalt was initially present as LCoOMBP, with negligible amounts of CoOMBP and L_2CoOMBP. In the case of the cyclic amines, the amount of ligand required to fully form LCoOMBP was so small that solvation effects due to changes in the medium (toluene/ligand) were considered to be negligible.

In the case of ligands, such as DMF and THF, which bind weakly to CoOMBP, the amount of ligand required to fully form the five-coordinate complex is relatively large (ligand concentration several molar in toluene), and solvation effects in these cases must be considered. For these systems,

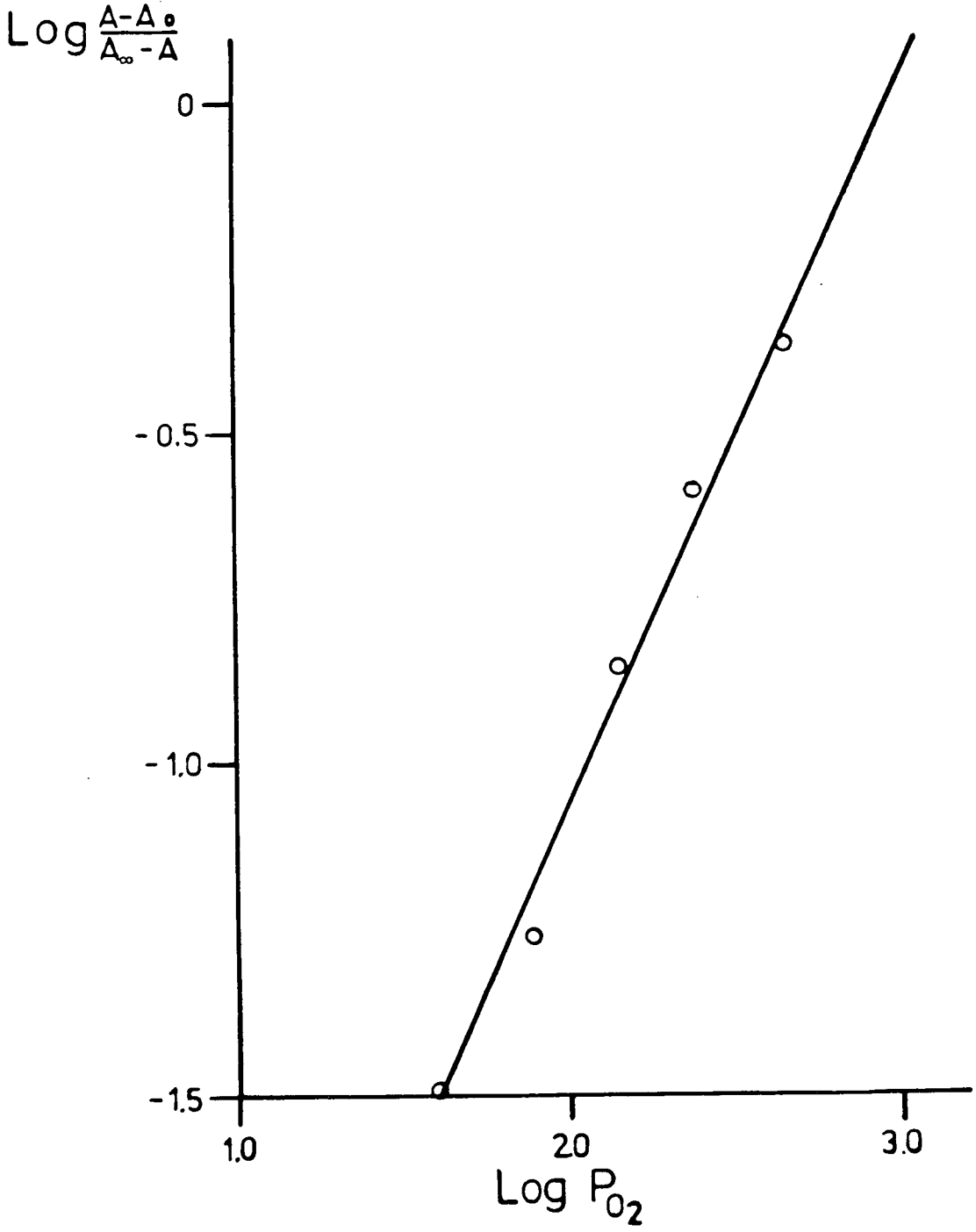

Figure IV.6. Equilibrium plot for $(CH_3\text{-Im})_2CoOMBP + O_2 \rightleftharpoons CH_3\text{-ImCoOMBP}(O_2)$ @ -45°C. For raw data see Appendix IIi.

the concentration of ligand was kept constant for oxygenation experiments at all temperatures, such that the five-coordinate complex was fully formed under all conditions used. There was no evidence of formation of bis ligand adduct in these systems.

Similarly, in studying the L_2CoOMBP complexes, the ligand-solvent composition was kept constant with sufficient ligand present to fully form L_2CoOMBP. A minimum of ligand was added so that solvation effects would be minimized, and to prevent ligand precipitation on lowering the temperature.

Error in oxygenation measurements occurred if any binuclear peroxo-bridged oxidation products were formed. Spectral evidence (an increase of extinction coefficient in the 440 nm region at constant oxygen pressure) indicated that this problem was sufficient in the ImCoOMBP system to prevent oxygenation measurements. Similar observations were made during some of the higher temperature (-23°C) oxygenation experiments, especially if 1,2-dichloroethane were part of the solvent system.

In most cases, however, formation of the oxidation product was not a problem. This was evidenced by: the appropriate plots of $\log \frac{A - A_o}{A_\infty - A}$ vs. $\log P_{O_2}$ which had slopes indicative of 1:1 cobalt:dioxygen; the good isosbestic points that were present when oxygenation was monitored; the totally reversible nature of the spectral changes; and by a strong accompanying ESR signal that was typical of 1:1 cobalt:dioxygen complexes.

IV.5 Dioxygen Binding Constants

IV.5.1 $LCoOMBP + O_2 \rightleftharpoons LCoOMBP(O_2)$, K_{O_2}.

The $P_{\frac{1}{2}O_2}$ values of the five-coordinate LCoOMBP complexes are given in Table IV.3. Also listed are the estimated values of ΔH and ΔS, and the pK_a

Table IV.3. Thermodynamic Data for the Binding of Dioxygen to LCoOMBP in a Toluene Solution.

LIGAND	TEMP., °C.	$P_{\frac{1}{2}O_2}$, Torr	ΔH,[a] kcal/mole	ΔS,[a] e.u.	pK_a[b]
Im		irreversible oxidation			6.95
CH_3-Im	-56.5	62	-5.8	-32	7.25
	-45	98			
	-31	198			
Pip	-63.5	104	-4.9	-32	11.30
	-56.5	184			
	-45	269			
Py	-63.5	91	-5.1	-33	5.27
	-56.5	141			
	-45	240			
Et_3N	-78	54	-5.1	-34	11.01
	-63.5	129			
	-56.5	200			
	-45	295			
	-23	1371			
DMF	-78	8.5	-12.2	-65	-2.0
	-63.5	25			
	-56.5	91			
	-45	389			
	-23	2700			
THF		no reaction			-2.08
PPh_3	-63.5	4000			2.73
PBu_3	-63.5	123	-3.0	-24	8.43
	-45	204			
	-23	398			

a. $\sigma_{\Delta H}$ and $\sigma_{\Delta S}$ values were estimated to be ± 0.5 kcal/mole and ± 2 e.u., respectively.

b. For references see Table III.3.

c. For raw data see Appendix IIa - Appendix IIg.

of the ligand studied.

The order of the oxygen affinities for the LCoOMBP complexes as a function of axial ligand at -63.5°C with toluene as a solvent is: DMF~ CH_3-Im>Py~Pip>Et_3N>PBu_3 ≫ PPh_3 ≫ THF. No simple correlation exists between K_{O_2}, ΔH_{O_2}, ΔS_{O_2}, and the pK_a of the protonated ligand. Indeed the ΔH_{O_2} and ΔS_{O_2} values associated with all of the nitrogen-donor systems are very similar, while the DMF complex binds dioxygen more exothermically and with a less favourable entropy change.

DMF and THF, which have similar pK_a and K_1 values (Table III.3), behave very differently with respect to promoting oxygen affinity of CoOMBP. The THF complex does not bind dioxygen at all, while the DMF complex binds dioxygen the most exothermically of all the systems studied, including the much more basic cyclic amine complexes, which also have K_1 values several orders of magnitude greater than the DMF complex (Table III.3).

If oxygenation enhancement of LCoOMBP occurred strictly by σ-electron donation from the axial ligand to the metal centre, which in turn could more readily transfer electron density to dioxygen, and stabilize a Co(III)-O_2^- species, then the DMF complex, with its low K_1 and pK_a values, would be expected to have a very low oxygen affinity. Possibly oxygenation enhancement can also occur through π-electron density transfer from the ligand. (The possibility of oxygenation enhancement from increased solvent polarity is discussed in Section 6.)

An infrared study of $LMo(CO)_5$ complexes has suggested that, compared to Py and Pip, DMF is a very strong π-donating ligand[121]. Since OMBP is also a strong π-donor[96c], it is possible that the π-donating properties of DMF, coupled with those of OMBP, could be responsible for the observed

oxygen binding results. Based on the above considerations, similar behavior was noted in the LCoPpIXDME systems, as the DMF adduct bound dioxygen better than the Py adduct, but not as well as the CH_3-Im adduct. However, the observed thermodynamic parameters in the DMF system were similar to the other ligand adducts of CoPpIXDME[89]. In contrast to this evidence of π-electron effects, other work[70,91b] suggests that ligand π-donor ability is not important in dioxygen binding, and that other ligand characteristics, such as hydrogen bonding ability or stereochemistry are factors affecting oxygen affinity.

From work in this thesis, in a manner also observed in the LCoPpIXDME systems[89], the CH_3-Im complex is seen to bind dioxygen more strongly than the Pip (or Py) complex, although CH_3-Im is a weaker base than Pip. Mossbauer studies on iron porphyrins indicate that CH_3-Im is a stronger π-donor than either Pip or Py[122], and so again the importance of the π-donating effects is evident.

That the PPh_3 complex binds dioxygen very weakly is consistent with its low basicity. Since PPh_3 is a π-acceptor, oxygenation could be substantially inhibited, even though the ΔH_1 value in the PPh_3 system approached those of the nitrogen-donor systems (Table III.3). THF is the weakest base of any of the systems studied, with a very low K_1 value, and the inability of this complex to bind dioxygen can be explained by this property. Similarly, π-bonding effects do not need to be invoked to understand the oxygen affinity of the PBu_3 system. Studies with other phosphine ligand systems should probably be undertaken before more precise assignments of the importance of π-donor and σ-donor properties of these ligands are made.

IV.5.2 $L_2CoOMBP + O_2 \rightleftharpoons LCoOMBP(O_2) + L$, $K_{O_{2/L}}$.

The $P_{\frac{1}{2}}O_2$ values for $L_2CoOMBP$ at $-45^{\circ}C$, in a solution of 95% by volume of toluene and 5% by volume of ligand, were as follows; 950 Torr for L = CH_3-Im and about 4000 Torr for L = Py. No oxygen affinity was detected for $Pip_2CoOMBP$ under these conditions.

The reaction being studied, $L_2CoOMBP + O_2 \overset{K_{O_{2/L}}}{\rightleftharpoons} LCoOMBP(O_2) + L$, can be thought of as a combination of two other reactions that have been studied separately, $LCoOMBP + L \overset{K_2}{\rightleftharpoons} L_2CoOMBP$ and $LCoOMBP + O_2 \overset{K_{O_2}}{\rightleftharpoons} LCoOMBP(O_2)$.

The equilibrium constants can be combined to give:

$$K_{O_2} = K_2 K_{O_{2/L}} \qquad (IV.8)$$

Since $P_{\frac{1}{2}}O_2$ values for the five- and six-coordinate complexes are given by $1/K_{O_2}$ and $L/K_{O_{2/L}}$, respectively, Equation IV.8 yields

$$P_{\frac{1}{2}}O_2(\text{six-coordinate complex}) = P_{\frac{1}{2}}O_2(\text{five-coordinate complex}) \cdot K_2 \cdot L \qquad (IV.9)$$

The $P_{\frac{1}{2}}O_2$ values for the oxygenation of the six-coordinate complexes, as calculated from Eq. IV.9, are listed in Table IV.4.

From these considerations, the six-coordinate complexes are expected to exhibit a very weak oxygen affinity in the order Py>CH_3-Im>Pip.

The experimental data agree well for the Py and Pip systems, but with the CH_3-Im complex the oxygen affinity is an order of magnitude greater than expected, and the observed oxygen affinities are in the order CH_3-Im>Py>Pip. Solvent effects may play a role. In order to ensure full

Table IV.4. Expected $P_{\frac{1}{2}}O_2$ Values (Torr) for $L_2CoOMBP$ Complexes at -45°C.

LIGAND (conc., M^{-1})	$P_{\frac{1}{2}}O_2$(five-coord)	K_2, M^{-1}	Expected $P_{\frac{1}{2}}O_2$(six-coord)
CH_3-Im (0.628)	98	150	11,000
Pip (0.505)	270	170	24,000
Py (0.671)	141	48	4,200

formation of the six-coordinate adduct for oxygenation studies, the ligand constituted 5% of the total solution volume. Under these circumstances the solvent takes on some of the characteristics of the ligand used. For example, dielectric constants at 22°C were measured to be 2.54, 2.89, and 3.71 for the Pip, Py, and CH_3-Im systems, respectively, while for neat toluene the value was 2.38. The CH_3-Im system is the most polar, and it is possible that the enhanced oxygenation results from stabilization of the Co(III)-O_2^- species. Enhanced oxygen affinity has been previously reported as the medium becomes more polar[91a,c].

These observations suggest that the nature of the solvent might play a major role in determining oxygen affinity, and care must be taken in the interpretation of data from studies where large concentrations of ligand are required.

IV.6 Oxygenation Reaction in Solvent Systems Other Than Neat Toluene.

Initial studies in more polar solvent systems were done using a 4:1 by volume ratio of toluene (ϵ = 2.38) and 1,2-dichloroethane (ϵ = 10.36). Studies in neat DCE were not feasible, as this solvent freezes at -35°C. The 4:1 toluene:DCE solvent system has a dielectric constant of 3.41.

Although the observed thermodynamic parameters in the mixed solvent system were not substantially different from those observed in neat toluene (i.e. for the CH_3-ImCoOMBP + $O_2 \rightleftharpoons$ CH_3-ImCoOMBP(O_2) reaction in the mixed solvent system the ΔH and ΔS values were -5.3 kcal/mole and -31 e.u., respectively, cf. Table IV.3), the $P_{\frac{1}{2}}O_2$ values were reduced by a factor of about three (e.g. the $P_{\frac{1}{2}}O_2$ of CH_3-ImCoOMBP at -45°C was 98 Torr in neat toluene and was 36 Torr in the mixed solvent system; see Appendix IIj).

Although an increase in dielectric constant upon DCE addition caused a noticeable increase in oxygen affinity in these fairly non polar media, quantitative work was not done with higher concentrations of DCE, as DCE tended to "freeze out" and irreversible oxidation was judged to be occurring, based on observed increasing spectral intensity at 440 nm under constant oxygen pressure.

In the case of the six-coordinate CoOMBP-cyclic amine complexes, when the solvent system was changed from 5% ligand and 95% toluene by volume to 5% ligand, 20% DCE, and 75% toluene by volume, some changes in oxygen affinity were observed. The $P_{\frac{1}{2}}O_2$ value at -45°C for the CH_3-Im system (ϵ = 4.68) was reduced from 950 Torr to 500 Torr; for the Py system (ϵ = 3.86) the oxygen affinity was increased ($P_{\frac{1}{2}}O_2$ ~ 2500 Torr), but still no accurate quantitative results could be achieved; for the Pip system (ϵ = 3.53) there was still no oxygenation evident. However, when the solvent system was changed to a ratio of 1:1 by volume of DCE:Pip (ϵ = 7.4), then the six coordinate Pip_2CoOMBP exhibited some oxygen affinity. Again, due to the low degree of oxygen affinity, and a tendency for irreversible oxidation to occur, no quantitative measurements were made at higher DCE concentrations. Raw data are presented in Appendix IIk.

In studying the oxygenation reaction of DMFCoOMBP, it was necessary to use substantial amounts of DMF to obtain the fully formed DMFCoOMBP adduct. The 1:1 volume to volume ratio of toluene to DMF used had a measured dielectric constant of about 18.

To check how much of the enhanced oxygen affinity, reflected in the greater exothermicity (Table IV.3) of the DMFCoOMBP system, was due to a solvent effect, and how much was due to the effect of DMF as a ligand, studies were carried out on the cyclic amine complexes in the 1:1 toluene:DMF system. The predominant species in solution was the CoOMBP-cyclic amine complex, as verified by the Soret peak position of the visible spectrum. The results of these studies are shown in Table IV.5.

Table IV.5. Thermodynamic Data for the Binding of Dioxygen to LCoOMBP in a 1:1 by Volume Ratio of Toluene to DMF.

LIGAND	TEMP., °C.	$P_{\frac{1}{2}}O_2$, Torr	ΔH, kcal/mole	ΔS, e.u.
CH_3-Im	-56.5	6.8	-7.1	-37
	-45	12		
	-31	44		
	-23	63		
Pip	-56.5	15	-6.9	-37
	-45	29		
	-31	93		
	-23	145		
Py	-56.5	42	-6.7	-38
	-45	66		
	-31	151		
	-23	457		

For raw data see Appendix III - Appendix IIn.

In comparison to neat toluene as solvent (Table IV.3), the mixed toluene-DMF system enhances the oxygen affinity of the CoOMBP-cyclic amine complexes by about an order of magnitude and this is seen to be due to a more favourable ΔH term, which seems reasonable if the polar $LCo(III)-O_2^-$ species is being stabilized. The ΔS values in the two media are not very different, suggesting any greater solvation of the $Co(III)-O_2^-$ product is balanced by a similar increased solvation of the reactants. The above trend in observed thermodynamic parameters is similar to that reported for oxygenation of CoPpIXDME, CoDpIXDME, and CoMpIXDME systems[91c].

From these results it can be seen that the oxygen sensitivity of the DMFCoOMBP complex was in part due to the effect of DMF as ligand and also due to the solvent properties of DMF. In the mixed solvent system, all the cyclic amine complexes became more oxygen sensitive than the DMF adduct, at the temperatures studied. However, oxygenation enhancement due to DMF as ligand was shown by the observation that the DMF system had the highest degree of exothermicity of all the complexes studied, even in the mixed solvent system.

Oxygenation studies were then carried out at $-56.6^{\circ}C$ on the PipCoOMBP system containing varying amounts of toluene and DMF as the solvent system (Table IV.6). The results show that the oxygenation enhancement is not as great as observed in the mixed toluene-DCE solvent system, for a corresponding change in dielectric constant. Also, all the reactions in the toluene-DMF solvent systems were completely reversible. Thus, the dielectric constant is not the only solvent characteristic to play a role in adjusting oxygen sensitivity of the various CoOMBP complexes. It should be noted that DMF is a weak base, while DCE could, to some small extent, yield acidic protons[52b]. This was confirmed when PipHCl crystals were observed

Table IV.6. Oxygen Affinities at -56.6°C of PipCoOMBP in a Variety of Mixed Toluene-DMF Solvent Systems.

% BY VOLUME OF DMF AS SOLVENT	DIELECTRIC CONSTANT	$P_{\frac{1}{2}}O_2$, TORR
0	2.38	184
5	3.63	136
10	4.92	79
20	7.80	54
33	11.2	20
50	~18	14

For raw data see Appendix IIo.

precipitating from a 1:1 Pip:DCE system after some time at ambient temperature (Chapter VII.7). The presence of an acidic proton in the ImCoPpIXDME system has been invoked to explain the enhanced irreversible oxygenation rate of that system[123]. In the present studies the ImCoOMBP system was similarly irreversibly oxidized (Chapter VII.5). Clearly similar oxidation effects would be observed if protons from the solvent are available to the system.

Many attempts have been made to correlate the reactivity of a system with the dielectric constant of a solvent[124]. However, since a solvent cannot be merely regarded as a dielectric continuum and specific solute-solvent interactions must be accounted for, few of these correlations have been successful[125]. Such correlations have succeeded when reactions have been studied in very similar solvents[126] or in varying concentrations of binary solvent systems[127], presumably because the solute-solvent interaction changes parallel those of the dielectric constant.

Several relationships between the observed reaction rate constant, k, and solvent dielectric constant have been proposed. Among the more notable are ones predicting an inverse relationship between k and ϵ[128], a direct relationship between log k and $\frac{\epsilon - 1}{2\epsilon + 1}$[129], or a direct relationship between log k and Y, an empirical measurement of solvent ionizing power related to ϵ[130]. Since K can be related to k ($K = k_f/k_r$), such relationships between ε and K should also hold. However, for the PipCoOMBP + O_2 reaction in toluene-DMF systems, the best correlation obtained was a direct one between ϵ and K ($P_{\frac{1}{2}O_2}^{-1}$) with a correlation coefficient, r, of 0.980 (Figure IV.7).

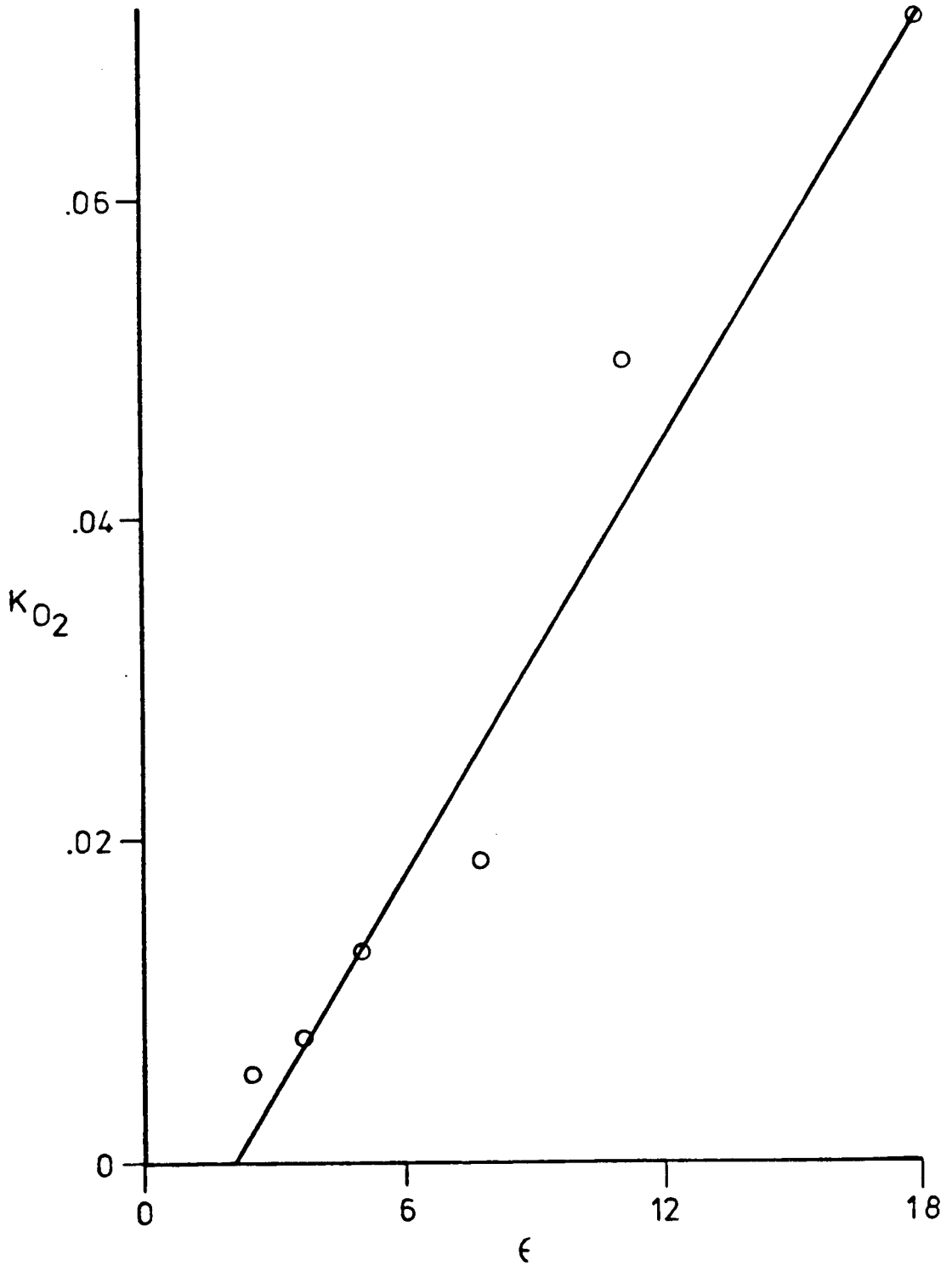

Figure IV.7. Oxygen Affinity vs. Dielectric Constant for PipCoOMBP in toluene-DMF systems.

CHAPTER V

THERMODYNAMICS OF REVERSIBLE LIGAND BINDING TO CoDADIXDME AND CoDBrDIXDME.

V.1 Qualitative Spectral Observations

V.1.1 L + CoDADIXDME $\rightleftharpoons$ LCoDADIXDME, K_{1a}.

The visible spectrum of solutions of CoDADIXDME in toluene had a 412 nm Soret band (ϵ = 8 x 10^4 $M^{-1}cm^{-1}$) and a visible band at 574 nm (ϵ = 1 x 10^4 $M^{-1}cm^{-1}$) with a shoulder at 546 nm (ϵ = 7 x 10^3 $M^{-1}cm^{-1}$). Addition of a nitrogen-coordinating ligand caused the position of the Soret band to shift to 420 nm ($\epsilon \sim 6$ x 10^4 $M^{-1}cm^{-1}$), while the visible band and shoulder coalesced to a broad band at 562 nm ($\epsilon \sim 8$ x 10^3 $M^{-1}cm^{-1}$) (Figure V.1. The lack of good isosbestic points is due to dilution effects from the addition of the ligand solution; correcting for this shows that isosbestic points occurred at approximately 422 nm, 568 nm, and 602 nm). Addition of DMF caused the position of the Soret band to red shift by about 7 nm (ϵ = 7 x 10^4 $M^{-1}cm^{-1}$) and the visible absorption to coalesce to a very broad band with a maximum intensity at 568 nm (ϵ = 8 x 10^3 $M^{-1}cm^{-1}$). The spectral changes associated with the formation of ligand adducts of CoDADIXDME are listed in Table V.1a.

There was no evidence for formation of any six-coordinate complex, since further addition of substantial amounts of ligand caused no changes in the spectra of the five-coordinate complexes.

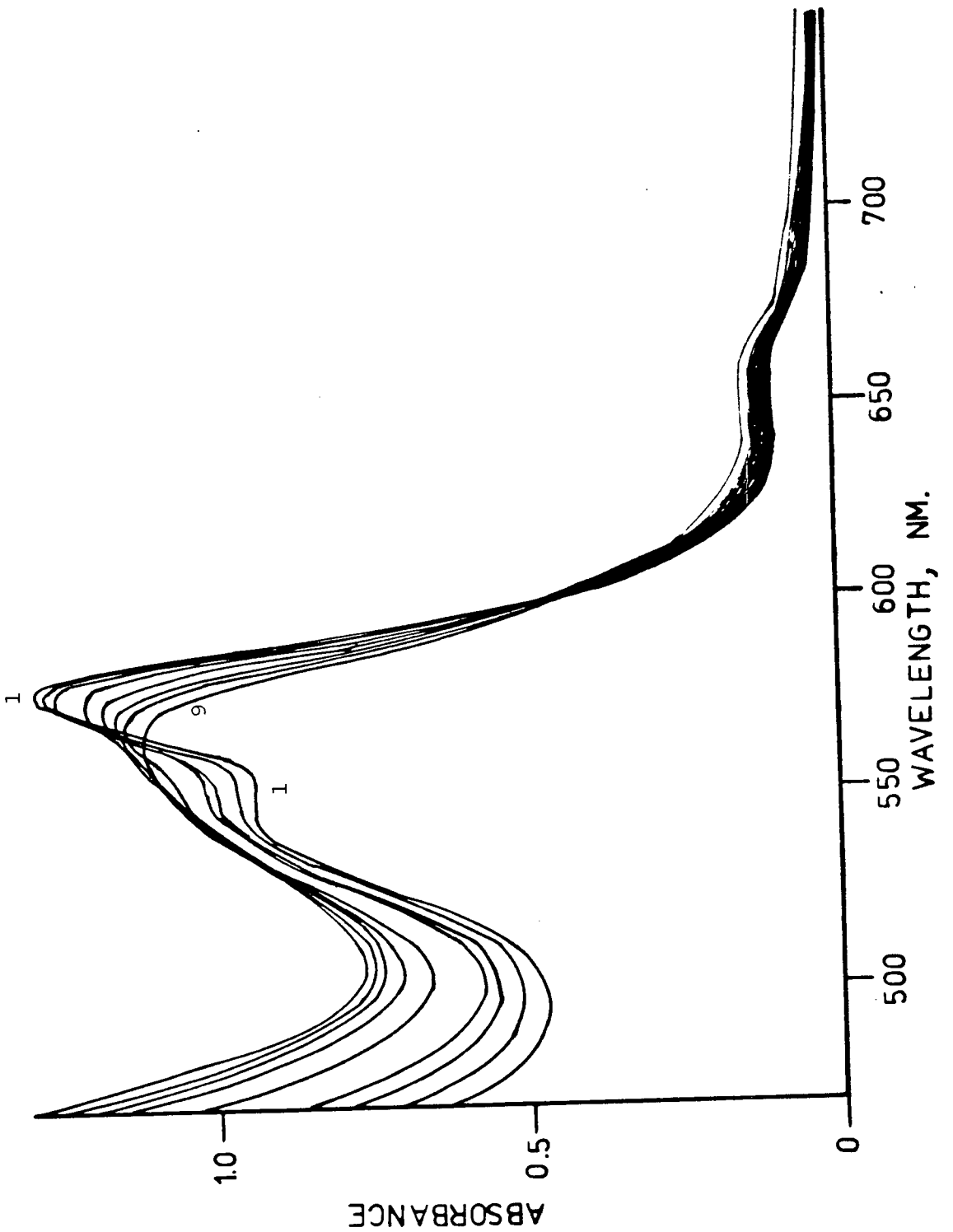

Figure V.1. CH_3-Im + CoDADIXDME $\rightleftharpoons$ CH_3-ImCoDADIXDME @ 22°C

Apparent loss of isosbestic points due to dilution effect from ligand solution addition. For raw data see Appendix IIIa.

Table V.1a. Spectral Data From 350 to 750 nm for the Reaction:

$$L + CoDADIXDME \rightleftharpoons LCoDADIXDME$$

Absorbing Species	Absorption Maxima (nm) (Extinction Coefficients, $M^{-1}cm^{-1}$)		Isosbestic Points (nm)		
CoDADIXDME	412	(8×10^4)			
	546	(7×10^3)			
	574	(1×10^4)			
+ CH_3-Im	420	(6×10^4)	422	570	596
	562	(8×10^3)			
+ Pip	420	(6×10^4)	422	568	602
	562	(8×10^4)			
+ Py	420	(6×10^4)	422	570	598
	562	(8×10^3)			
+DMF	419	(7×10^4)	425	568	612
	568	(8×10^3)			

Table V.1b. Spectral Data From 350 to 750 nm for the Reaction:

$$L + CoDBrDIXDME \rightleftharpoons LCoDBrDIXDME$$

Absobing Species	Absorption Maxima (nm) (Extinction Coefficient, $M^{-1}cm^{-1}$)		Isosbestic Points (nm)			
CoDBrDIXDME	398	(9×10^4)				
	522	(7×10^3)				
	555	(1×10^4)				
+ CH_3-Im	400	(8×10^4)	368	402	548	574
	549	(9×10^3)				
+ Pip	400	(8×10^4)	370	402	550	576
	547	(9×10^3)				
+ Py	400	(8×10^4)	368	402	548	574
	548	(9×10^3)				
+ DMF	402	(8×10^4)	372	447	542	
	552	(9×10^3)				

V.1.2 $L + CoDBrDIXDME \rightleftharpoons LCoDBrDIXDME$, K_{1b}.

The visible spectrum of solutions of CoDBrDIXDME in toluene had a 398 nm Soret band ($\epsilon = 9 \times 10^4\ M^{-1}cm^{-1}$) and a visible band at 555 nm ($\epsilon = 1 \times 10^4\ M^{-1}cm^{-1}$) with a shoulder at 522 nm ($\epsilon = 7 \times 10^3\ M^{-1}cm^{-1}$). Addition of a nitrogen-coordinating ligand caused the position of the Soret band to shift to 400 nm ($\epsilon \sim 8 \times 10^4\ M^{-1}cm^{-1}$), while the visible band broadened and the peak position became 547 nm ($\epsilon \sim 9 \times 10^4\ M^{-1}cm^{-1}$). The 522 nm shoulder became less intense and less pronounced (Figure V.2). Once ligand solution dilution effects had been corrected for, isosbestic points were found at approximately 378 nm, 549 nm, and 574 nm.

When the concentration of a cyclic amine ligand was increased to several molar, there was a 10% decrease in the molar extinction coefficient of the Soret band of the five-coordinate adduct, accompanied by the formation of a shoulder at 413 nm, while the visible band shifted to 550 nm with a 10% decrease in extinction coefficient. Also a band began to appear in the 525 nm region. These spectral changes were probably due to the formation of some six-coordinate adduct, but a limiting spectrum was not reached.

Addition of DMF to CoDBrDIXDME caused the Soret band to shift to 402 nm with ϵ decreasing by about 5%. The visible band shifted to 552 nm and decreased by about 10% in intensity. The shoulder at 522 nm shifted to 525 nm and became less distinct.

V.2 Treatment of Data

The equilibrium constants, K_{1a} and K_{1b} were obtained by following the decrease in the intensity of the visible band. The spectral changes of the Soret bands were not analyzed because the curve of those bands (in the case

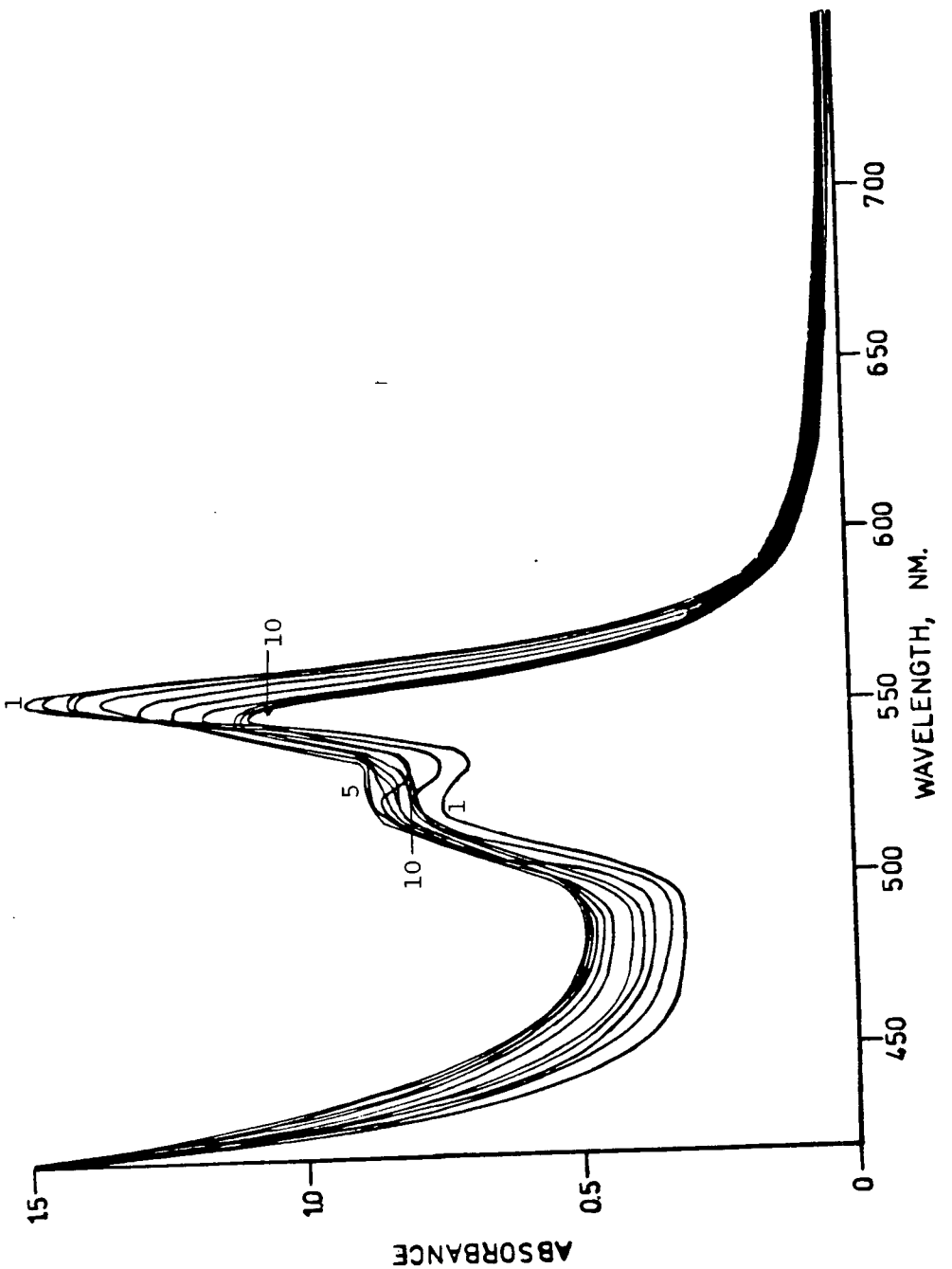

Figure V.2. CH_3-Im + CoDBrDIXDME $\rightleftharpoons$ CH_3-ImCoDBrDIXDME @ 22°C

Apparent loss of isosbestic points due to dilution effects from ligand solution addition. For raw data see Appendix IIIe.

of CoDADIXDME), or because there was little change in the peak position (in the case of CoDBrDIXDME).

The formation of the ligand adduct obeys the equation:

$$CoP + nL \overset{K_1}{\rightleftharpoons} L_nCoP \qquad (V.1)$$

where CoP represents a cobalt porphyrin complex.

The analysis presented in Chapter III for ligand binding to CoOMBP was used. The experimental data analyzed satisfactorily, and Figure V.3 shows the $\log \frac{A - A_o}{A_\infty - A}$ vs. log[L] plots for the CH_3-Im - CoDADIXDME system, while Figure V.4 shows the van't Hoff plots that are derived from the various $\log \frac{A - A_o}{A_\infty - A}$ vs. log[L] plots.

V.3 Sources of Error

In studying ligand binding to CoDADIXDME and CoDBrDIXDME, the sources of error are similar to those considered for studying ligand binding to CoOMBP (Chapter III.3).

The problem of oxygen entering the system did not appear to be important, as there was no evidence of irreversible oxidation. For the three nitrogen-donors examined, the concentrations of the ligands used were always sufficiently small that changes in the solvent were negligible. It was necessary to add substantial volumes of dilute ($\sim 10^{-2}$ M) ligand solution to achieve complete spectral changes. Presumably if more concentrated stock solutions were used, then lesser volumes would be required, and good isosbestic points would be achieved.

In monitoring cyclic amine ligand binding to CoDADIXDME and CoDBrDIXDME, the spectral changes were somewhat less marked than those observed with the

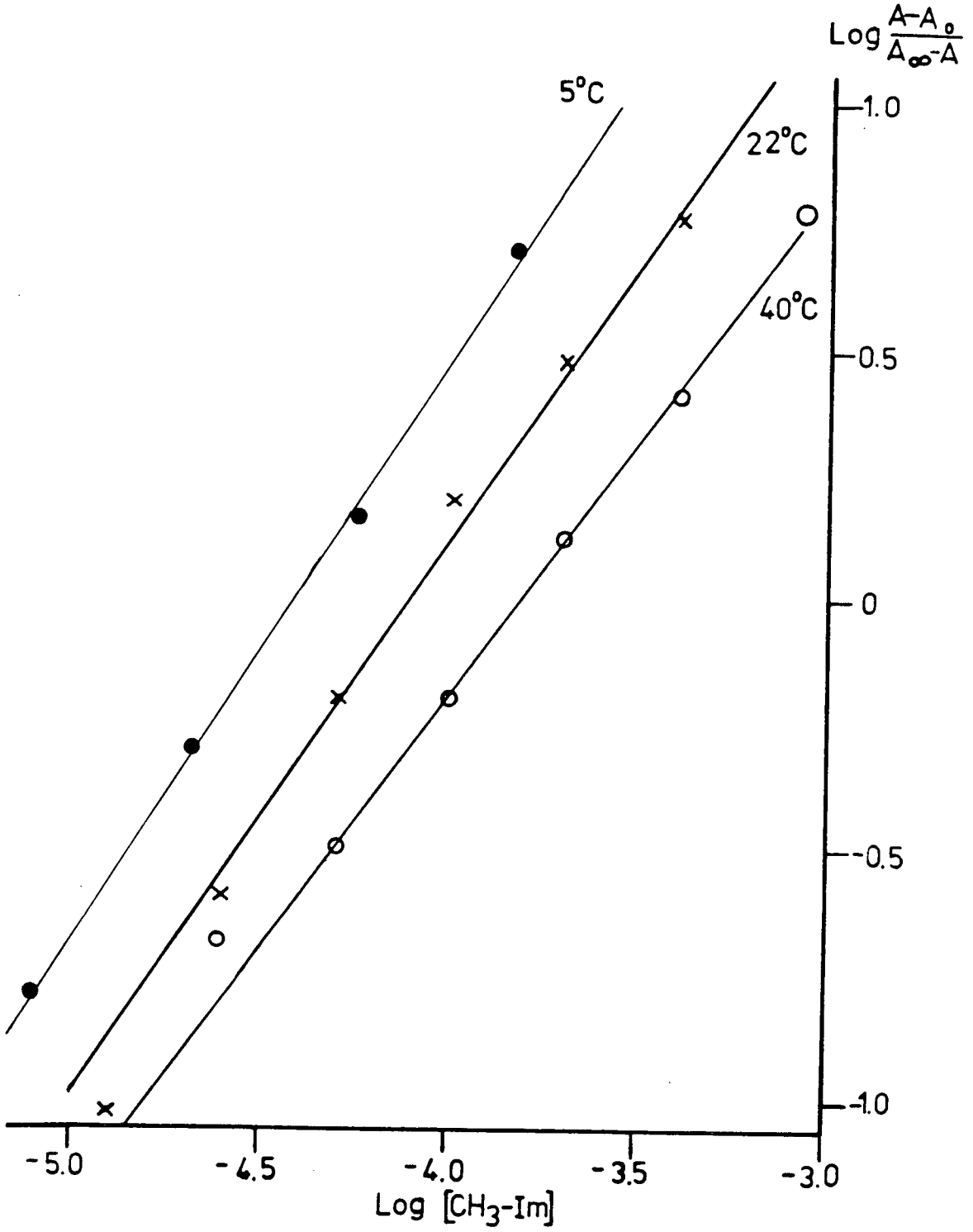

Figure V.3. Equilibrium plots for CH_3-Im + CoDADIXDME $\rightleftharpoons$ CH_3-ImCoDADIXDME

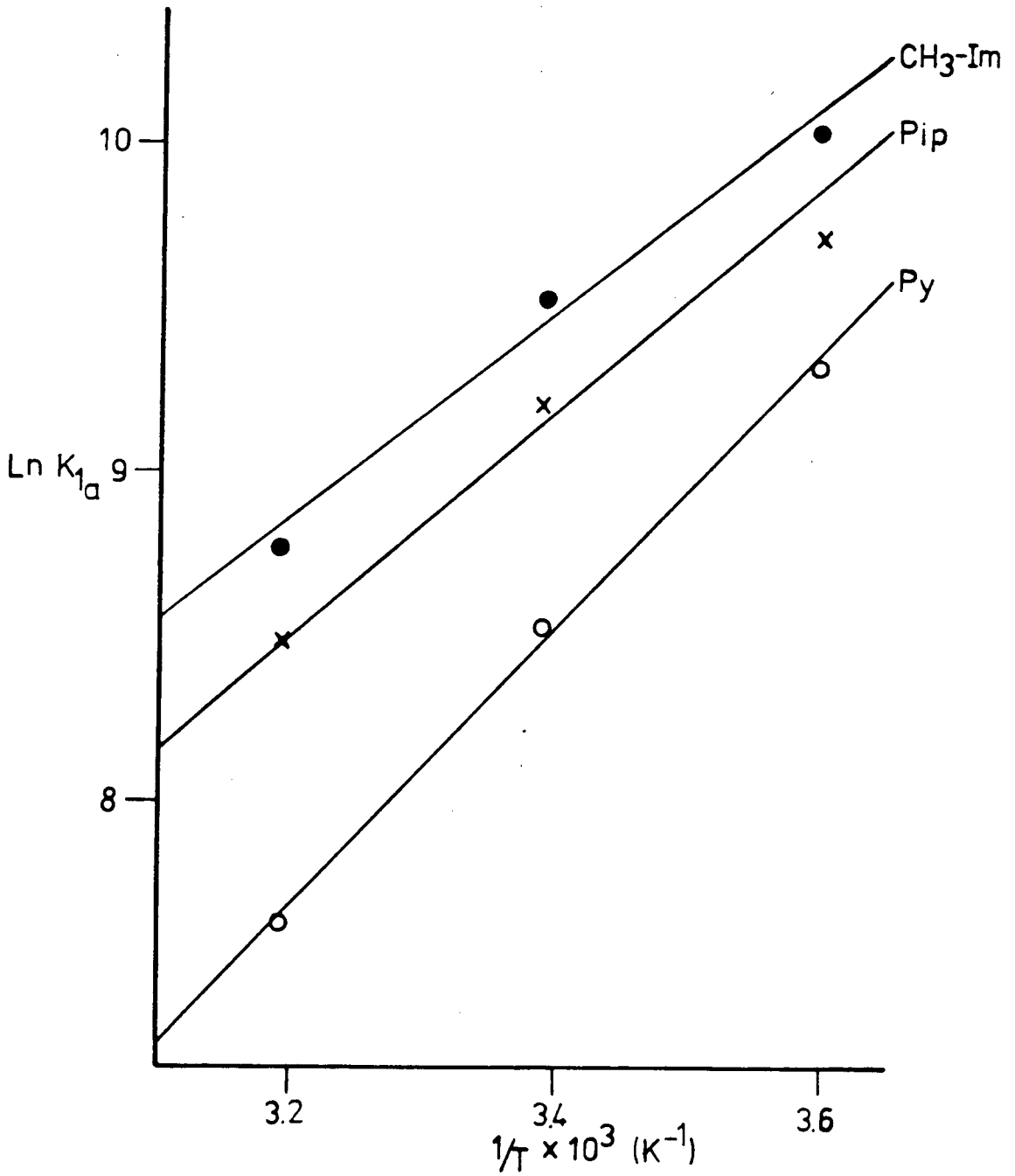

Figure V.4. Van't Hoff plots for L + CoDADIXDME $\rightleftharpoons$ LCoDADIXDME

L = CH_3-Im, Pip, and Py

CoOMBP system, but satisfactory analysis of the results was still readily achieved.

Substantial amounts of DMF were necessary to approach full formation of the five-coordinate adducts, and therefore some solvent effects probably occurred. Further, the dilution effects were such that any determination of equilibrium constants was rendered approximate. Also, full formation of the CoDADIXDME adduct was not realized, and this made K_{1a} determinations even more difficult.

V.4 Ligand Binding Constants

The equilibrium constants for ligand binding to CoDADIXDME and CoDBrDIXDME, together with the values of ΔH and ΔS obtained, and the pK_a of the protonated ligand studied, are given in Tables V.2a and V.2b. The order in ligand binding ability for both cobalt porphyrin complexes at the temperatures studied is CH_3-Im>Pip>Py >> DMF. There are no obvious correlations between the K_1, ΔH, or ΔS_1 values and the pKa of the protonated ligand.

V.5 Comparison of Ligand Binding Among Different Cobalt Porphyrins

If the binding ability of an axial ligand to a metal porphyrin complex were solely dependent on simple electrostatic considerations, then the donor electrons of the ligand would be most strongly attracted to the metal centre with the highest positive charge. Thus, in a series of cobalt porphyrin complexes, the poorest porphyrin donor (i.e. the weakest base) should form complexes with the most strongly bound axial ligand(s). Such considerations have been invoked to account for trends in axial ligand binding in both the six-coordinate iron porphyrin[131] and five-coordinate cobalt porphyrin[22] systems.

Table V.2a. Thermodynamic Data for the Binding of an Axial Ligand to CoDADIXDME in a Toluene Solution.

LIGAND	TEMP., °C.	K_{1a}, M^{-1}.	ΔH,[a] kcal/mole	ΔS,[a] e.u.	pK_a[b]
CH_3-Im	5	2.6×10^4	-7.0	-5	7.25
	22	1.4×10^4			
	40	6.3×10^3			
Pip	5	2.0×10^4	-7.6	-8	11.30
	22	1.0×10^4			
	40	4.8×10^3			
Py	5	1.1×10^4	-8.5	-12	5.27
	22	5.0×10^3			
	40	2.0×10^3			
DMF	5	~.4	~-3	~-7	-2.0
	22	~.3			
	40	~.2			

Table V.2b. Thermodynamic Data for the Binding of an Axial Ligand to CoDBrDIXDME in a Toluene Solution.

LIGAND	TEMP., °C.	K_{1b}, M^{-1}.	ΔH,[a] kcal/mole	ΔS,[a] e.u.	pK_a[b]
CH_3-Im	5	2.5×10^4	-7.1	-6	7.25
	22	8.9×10^3			
	40	6.0×10^3			
Pip	5	1.6×10^4	-6.9	-6	11.30
	22	7.8×10^3			
	40	4.5×10^3			
Py	5	7.1×10^3	-8.2	-10	5.27
	22	3.7×10^3			
	40	1.4×10^3			
DMF	5	1.4	-5	-16	-2.0
	22	1.1			
	40	.7			

a. $\sigma_{\Delta H}$ for cyclic amine binding was estimated to be $\pm$ 0.7 kcal/mole and $\sigma_{\Delta S}$ was estimated to be $\pm$ 3 e.u.

b. For references see Table III.1.

c. For raw data see Appendix IIIa - Appendix IIIh.

The method most commonly used to determine the basicity of a porphyrin is to measure the pK_a value of the third nitrogen of the porphyrin ring ($H_3P^+ \rightleftharpoons H^+ + H_2P$, pK_3)[27b,c]. When the above basicity measurements were initially carried out, an increase in absorption band peak wavelength was noted as the pK_3 value decreased[27b]. However, subsequent studies on an extensive series of 2,4-substituted deuteroporphyrins indicated that while a qualitative trend between band position and pK_3 may exist, other properties such as resonance and steric effects and molecular symmetry are also important, and an estimate of porphyrin basicity based solely on spectroscopic data is probably unreliable (Figure V.5)[132]. For example, the approximately 20 nm difference in peak positions of DAD and DBrD, in spite of their similar basicities has been explained in terms of DAD having larger resonance effects than DBrD[133].

Tables V.3a-3d list series of cobalt porphyrin complexes, in decreasing order of porphyrin basicity, on which ligand binding studies have been done. The Tables summarize the ligand binding constants, the observed ΔH and ΔS values, and the basicity of the porphyrins. Tables V3a, V3b, V3c, and V3d deal with binding of a single CH_3-Im, Pip, Py, and DMF ligand, respectively.

Previous work[91c] on pyridine binding to a series of 2,4-substituted deuteroporphyrins has shown that the binding ability of the amine does increase as the porphyrin basicity decreases. The present work extends the range of porphyrin basicities used. Figures V.6a-6d show that there is a reasonable correlation between ligand affinity at 23°C and porphyrin basicity for the binding of CH_3-Im, Pip, and Py. Discrepencies, considered to be within experimental error, between the data of different groups[89,91c] for Py binding to CoPpIXDME at 23°C are included in Table V.3c and

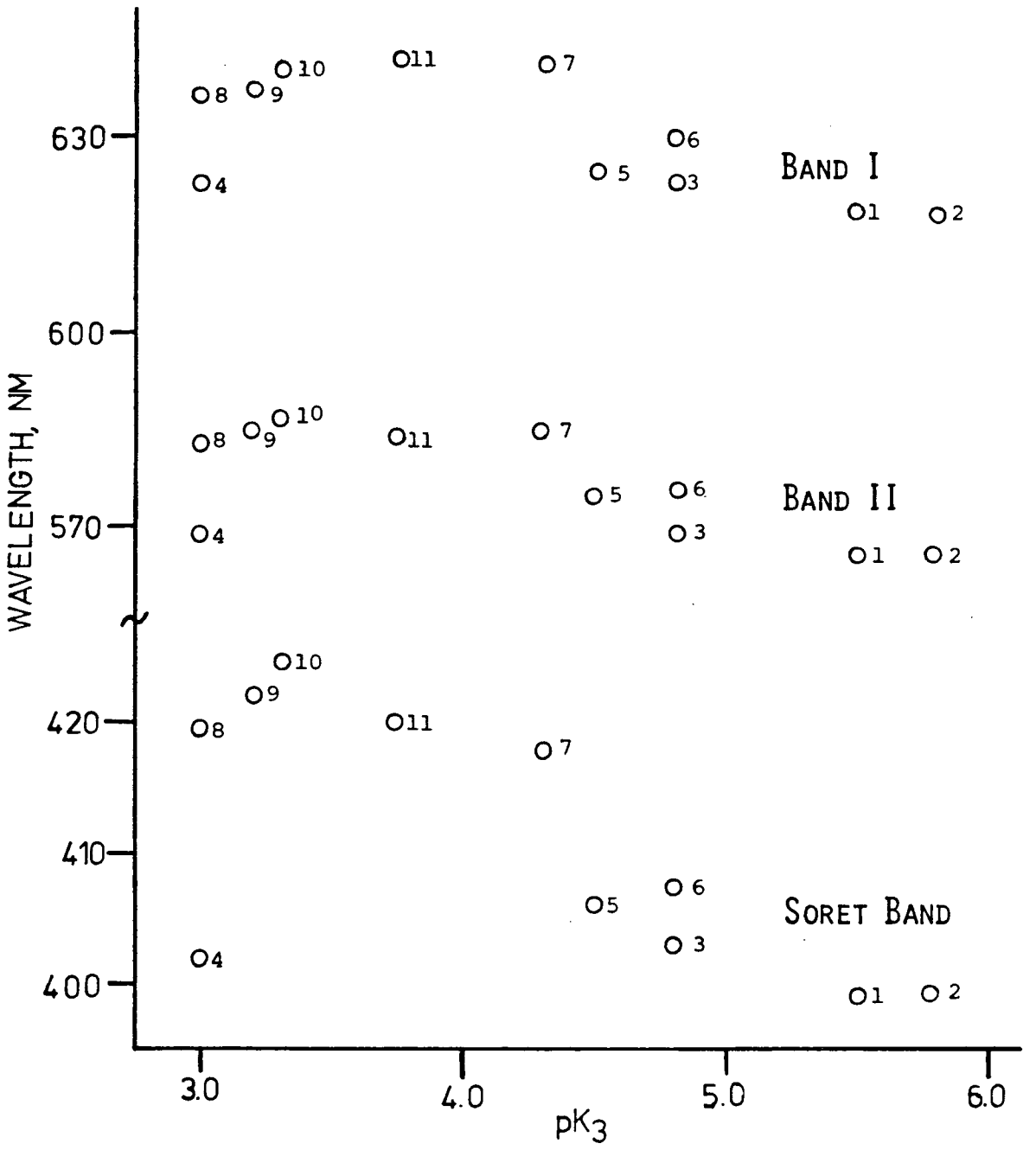

Nature of the 2,4-substituents:

1. Hydrogen
2. Ethyl
3. 2'Ethoxycarbonylcyclopropyl
4. Bromo
5. Acetyloxime
6. Vinyl
7. Oximino
8. Methoxycarbonyl
9. Propionyl
10. Acetyl
11. Formyl

Figure V.5. Porphyrin band position as a function of porphyrin basicity, taken from ref. 132.

Table V.3a. Thermodynamic Data for the Binding of CH_3-Im to Several Cobalt Porphyrin Complexes in Toluene.

PORPHYRIN	TEMP., °C	K, M^{-1}.	ΔH kcal/mole	ΔS e.u.	pK_3	REFERENCE
OEP	-45	1.7×10^5	-10	-20	6[a]	95
	-31	2.8×10^4				
	23	9.1×10^2				
PpIXDME	-23	1.4×10^5	-10.7	-19	4.8[b]	89
	0	2.5×10^4				
	23	5.0×10^3				
T(p-OMe)PP	25	2.4×10^3	-11.4	-23	>3[c]	92
DADIXDME	5	2.6×10^4	-7.0	-5	3.3[b]	Table V.2a
	22	1.4×10^4				
	40	6.3×10^3				
DBrDIXDME	5	2.5×10^4	-7.1	-6	3.0[b]	Table V.2b
	22	8.9×10^3				
	40	6.0×10^3				
OMBP	-23	5.2×10^5	-9.2	-10	~2.0[d]	Table III.3
	0	2.3×10^5				
	23	3.2×10^4				

For an explanation of the footnotes see p. 121.

Table V.3b. Thermodynamic Data for the Binding of Pip to Several Cobalt Porphyrin Complexes in Toluene.

PORPHYRIN	TEMP., °C	K, M^{-1}.	ΔH kcal/mole	ΔS e.u.	pK_3	REFERENCE
OEP	23	1.9×10^3	———	———	6[a]	95
PpIXDME	-23	1.8×10^5	-10.4	-17	4.8[b]	89
	0	4.1×10^4				
	23	6.8×10^3				
T(p-OMe)PP	25	2.4×10^3	-6.8	-7	>3[c]	92
DADIXDME	5	2.0×10^4	-7.6	-8	3.3[b]	Table V.2a
	22	1.0×10^4				
	40	4.8×10^3				
DBrDIXDME	5	1.6×10^4	-6.9	-6	3.0[b]	Table V.2b
	22	7.8×10^3				
	40	4.5×10^3				
OMBP	-23	9.4×10^5	-7.3	-4	~2.0[d]	Table III.3
	0	3.4×10^5				
	23	8.9×10^4				

For an explanation of the footnotes see p. 121.

Table V.3c. Thermodynamic Data for the Binding of Py to Several Cobalt Porphyrin Complexes in Toluene.

PORPHYRIN	TEMP., °C	K, M^{-1}.	ΔH kcal/mole	ΔS e.u.	pK_3	REFERENCE
OEP	23	7.0×10^2	———	———	6[a]	95
MpIXDME	22.9	1.1×10^3	-9.2	-17	5.8[b]	91c
	27.5	8.9×10^2				
	33.7	5.9×10^2				
	38.3	5.0×10^2				
DpIXDME	22.7	1.6×10^3	-9.1	-16	5.5[b]	91c
	28.0	1.2×10^3				
	31.8	1.0×10^3				
	36.9	7.6×10^2				
PpIXDME	23.0	2.0×10^3	-9.7	-18	4.8[b]	91c
	27.6	1.7×10^3				
	33.6	1.1×10^3				
	37.8	9.9×10^2				
PpIXDME	-23	5.0×10^4	-6.9	-6	4.8[b]	89
	0	1.0×10^4				
	23	6.0×10^3				
T(p-OMe)PP	25	7.0×10^2	-8.5	-16	>3[c]	92
DADIXDME	5	1.1×10^4	-8.5	-12	3.3[b]	Table V.2a
	22	5.0×10^3				
	40	2.0×10^3				
DBrDIXDME	5	7.1×10^3	-8.2	-10	3.0	Table V.2b
	22	3.7×10^3				
	40	1.4×10^3				
OMBP	-23	4.8×10^5	-8.0	-6	2.0[d]	Table III.3
	0	1.3×10^5				
	23	2.1×10^4				

For an explanation of the footnotes see p.121.

Table V.3d. Thermodynamic Data for the Binding of DMF to Several Cobalt Porphyrin Complexes in Toluene.

PORPHYRIN	TEMP., ^{o}C	K, M^{-1}.	ΔH kcal/mole	ΔS e.u.	pK_3	REFEERENCES
PpIXDME	-23	1.8×10^{2}	-7.9	-21	4.8[b]	89
	0	4.3×10^{1}				
	23	1.5×10^{1}				
DADIXDME	5	.4	~-3	~-7	3.3[b]	Table V.2a
	22	.3				
	40	.2				
DBrDIXDME	5	1.4	-4.5	-16	3.0[b]	Table V.2b
	22	1.1				
	40	.7				
OMBP	-23	3.6	-3.7	-11	2.0[d]	Table III.3
	0	2.5				
	23	1.7				

For an explanation of the footnotes see p.121.

Notes to Tables V.3a - V.3d.

a. D. J. Kent, BSc. Thesis, UBC, Vancouver, B.C., (1973).

The method of determining the pK_3 value was to note the positions of the visible bands of the porphyrin complex and to compare them with the spectroscopic data for other porphyrins of known basicity. For reasons mentioned in the text of this chapter, this method should probably not be relied upon for a precise determination.

b. W. S. Caughey, W. J. Fujimoto, and B. P. Johnson, Biochem., 5, 3830 (1966).

c. B. R. James, in "The Porphyrins," Vol. 5, D. Dolphin, Ed., Academic Press, New York, N.Y., 1978, p. 265.

d. No determination of the pK_3 value of OMBP has been reported. Since the method of measuring pK_3 values is not an absolute one, and a series of several porphyrins should be used (ref 27b), no determination of the pK_3 value of OMBP was attempted in this work. However, work with FeOMBP complexes (ref 89), and with ZnOMBP complexes (K. J. Reimer, M. Reimer, and C. Spindle-Sprague, 62nd Canadian Chemical Conference, Vancouver, B.C. (1979)), indicates that the basicity of OMBP is much less than the other porphyrins examined. For purposes of placing CoOMBP on Figures V.6a-6d, OMBP was arbitrarily assigned a pK_3 value of 2.0 ± 0.5, which seems reasonable, from the plots of amine binding.

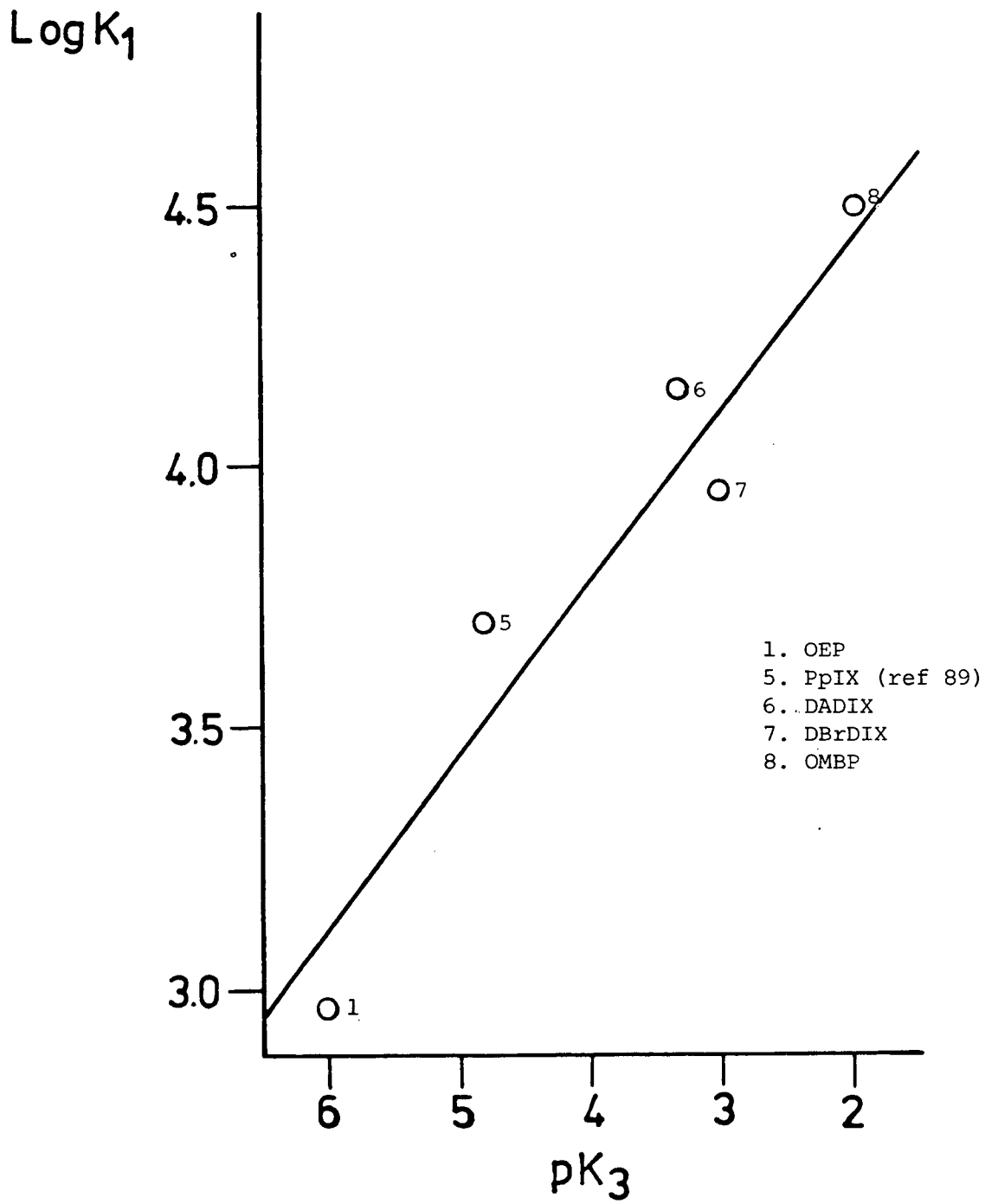

Figure V.6a. CH_3-Im Affinity vs. Porphyrin Basicity for a Variety of Cobalt Porphyrin Complexes.

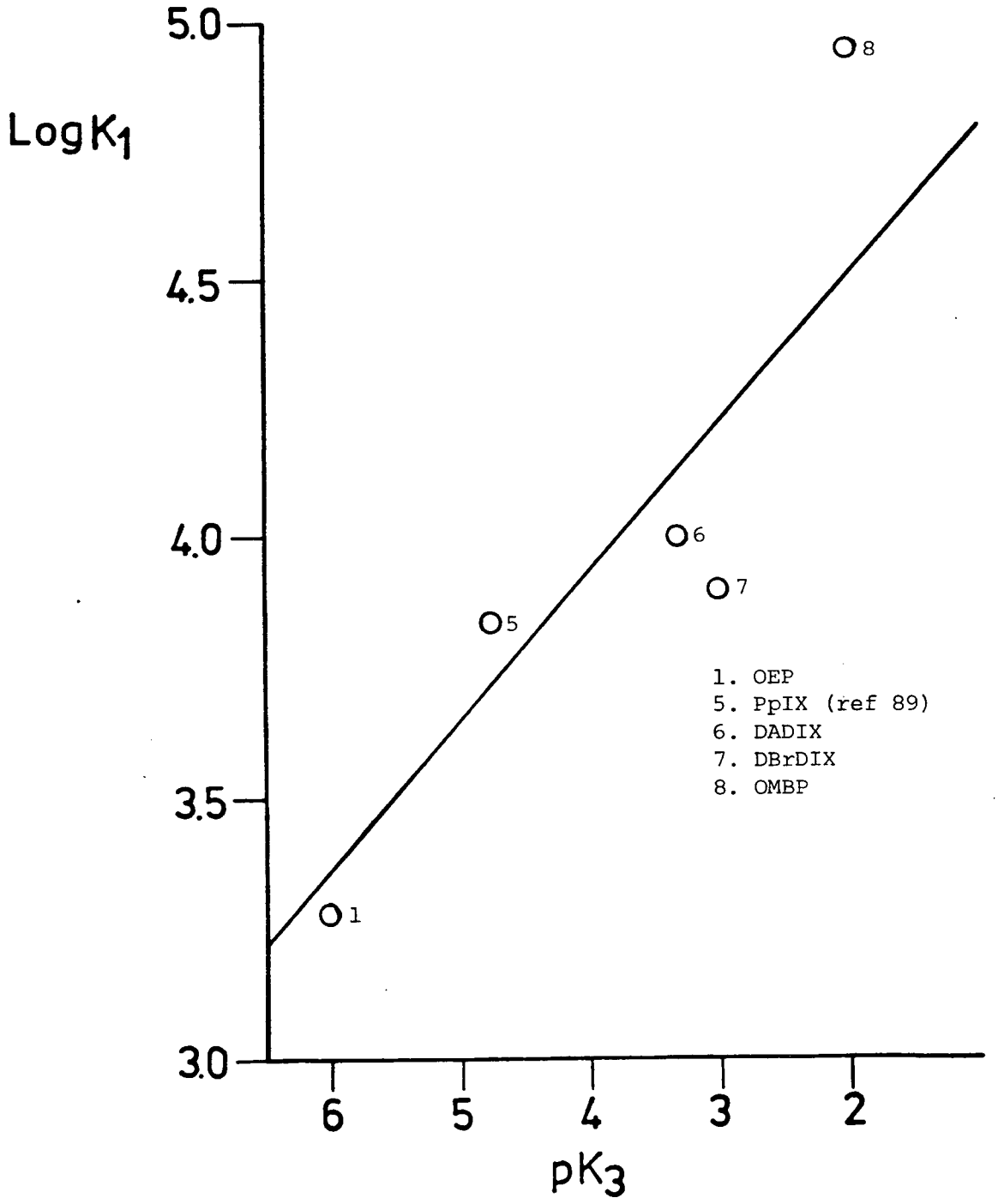

Figure V.6b. Pip Affinity vs. Porphyrin Basicity for a Variety of Cobalt Porphyrin Complexes.

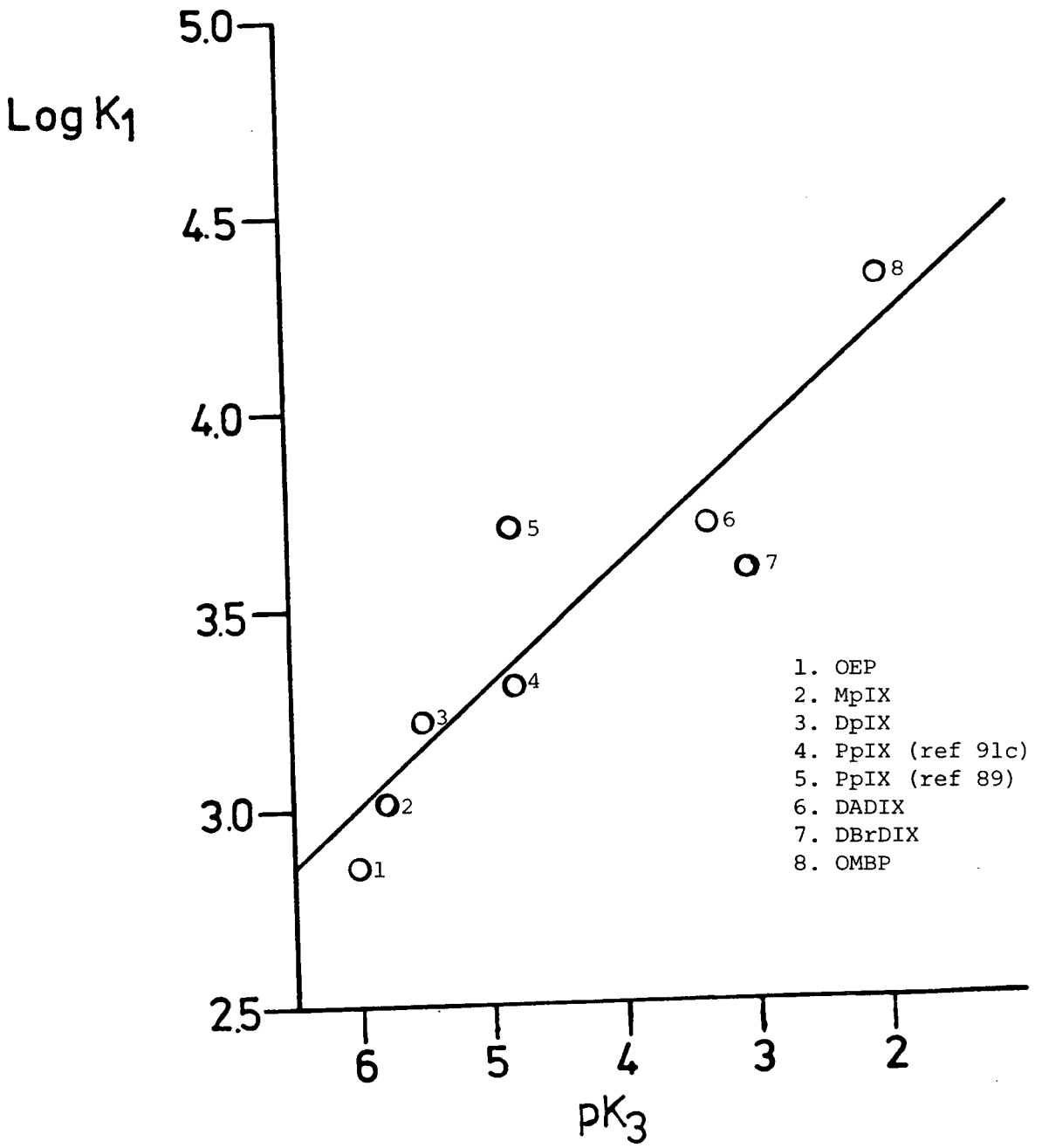

Figure V.6c. Py Affinity vs. Porphyrin Bascity for a Variety of Cobalt Porphyrin Complexes.

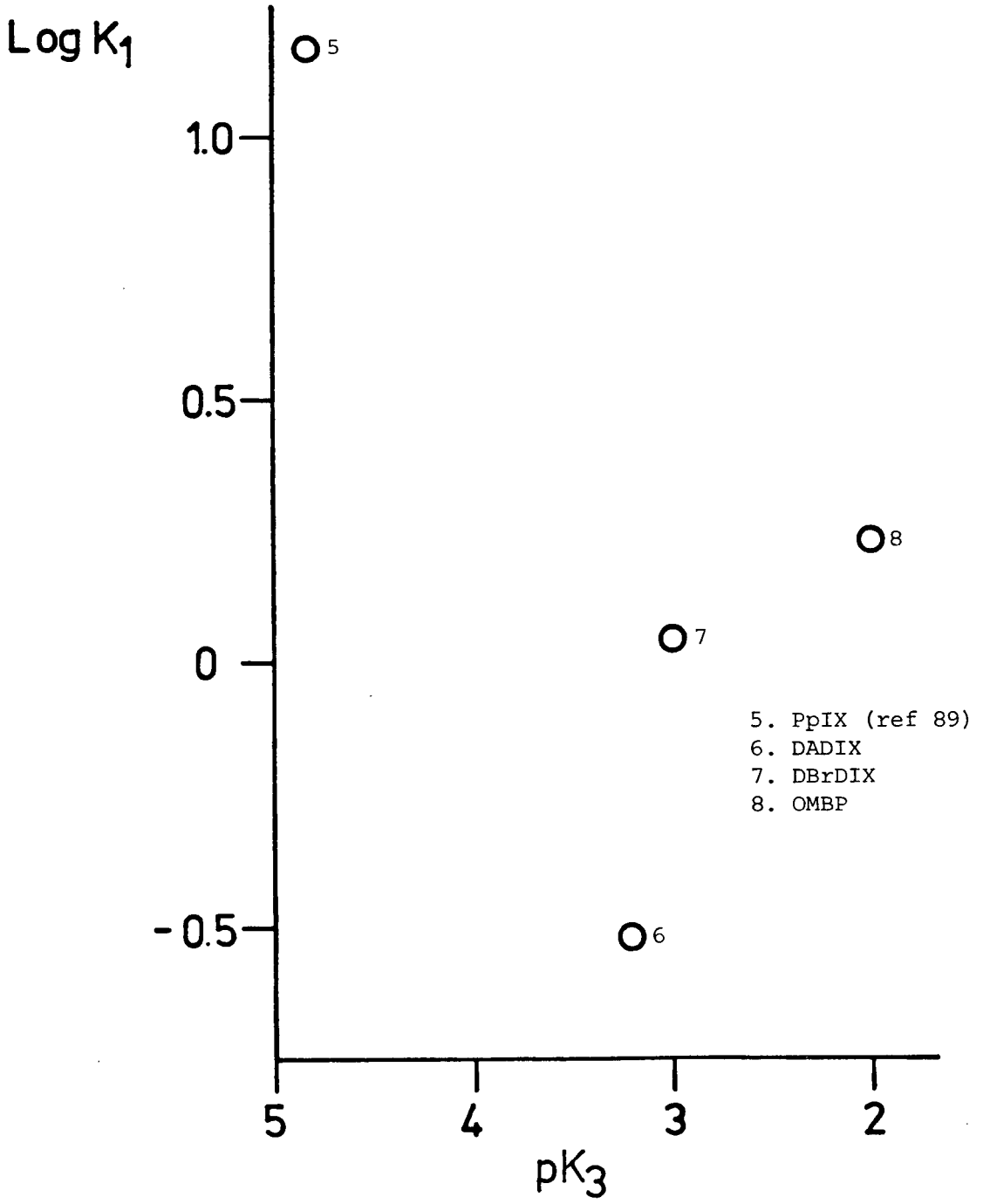

Figure V.6d. DMF Affinity vs. Porphyrin Basicity for a Variety of Cobalt Porphyrin Complexes.

Figure V.6c.

The amine ligand binding constants of CoDBrDIXDME are consistently slightly lower than those measured for CoDADIXDME, although the reported pK_3 value for DBrDIXDME is slightly lower than that of DADIXDME. When the pK_3 values were measured[132], some difficulty in determining the value of DBrDIXDME was noted as that particular porphyrin was only sparingly soluble. Also the pK_3 measurements were carried out in 2.5% aqueous sodium dodecylsulfate at 25°C. Since the ligand binding studies were carried out in toluene, it is possible that the relative basicities of the porphyrins could be changed somewhat as the solvent is changed.

CH_3-Im binds more strongly to CoDADIXDME and to CoDBrDIXDME than does Pip; however, Pip binds more strongly than CH_3-Im to CoOMBP and to CoPpIXDME[89]. This latter behavior is reasonable in view of the stronger basicity of Pip than CH_3-Im. Also, since CH_3-Im is a stronger π-donor than is Pip[122], the strongly π-donating OMBP may be expected to hinder the coordination of CH_3-Im, relative to Pip, to the metal centre of CoOMBP. Since other porphyrins, such as DADIXDME and DBrDIXDME, are generally not as strongly π-donating as OMBP[96c], any repulsive π-effects on CH_3-Im are probably not so important in the other porphyrin systems. For all the cobalt porphyrin systems studied, Py was the weakest binding cyclic amine, consistent with Py being the weakest σ-base of these compounds.

Figure V.6d shows the binding constants of DMF to the different cobalt porphyrins; no obvious correlation with porphyrin basicity is apparent. As mentioned in Chapter III, problems with impurities of dimethylamine in DMF have been proposed[116], and such impurities could explain the apparent high DMF affinity of CoPpIXDME. Dimethylamine-free DMF would thus result in the lower DMF affinities observed in the other cobalt porphyrins. Ignoring the

DMF binding to CoPpIXDME, increased DMF affinity is noted as the porphyrin basicity is decreased. Alternatively, the scattered DMF affinities could result from its strong π-donor nature[121] if π-effects dominate over σ-effects (i.e. basicity).

CHAPTER VI

THERMODYNAMICS OF REVERSIBLE DIOXYGEN BINDING TO LCoDADIXDME AND LCoDBrDIXDME

VI.1 Qualitative Spectral Observations

Addition of dioxygen to 2×10^{-5} M toluene solutions of five-coordinate CoDADIXDME-amine adduct (Figure VI.1) caused the visible band at 562 nm to split into two bands at about 555 nm ($\varepsilon \sim 8 \times 10^{3}$ $M^{-1}cm^{-1}$) and 590 nm ($\varepsilon \sim 7 \times 10^{3}$ $M^{-1}cm^{-1}$). The Soret band shifted from 420 nm ($\varepsilon \sim 6 \times 10^{4}$ $M^{-1}cm^{-1}$) to about 438 nm ($\varepsilon \sim 7 \times 10^{4}$ $M^{-1}cm^{-1}$). Numerous isosbestic points occurred around both the Soret and visible bands. Spectral changes of a similar pattern were observed for oxygenation of 2×10^{-5} M toluene solutions of five-coordinate CoDBrDIXDME-amine adducts (Figure VI.2). These changes were reversed when oxygen was pumped off the system.

Bands at 552 nm ($\varepsilon = 8 \times 10^{3}$ $M^{-1}cm^{-1}$) and 588 nm ($\varepsilon = 6 \times 10^{3}$ $M^{-1}cm^{-1}$) appeared when dioxygen was reacted with toluene solutions of DMFCoDADIXDME; the Soret band shifted to 436 nm ($\varepsilon = 8 \times 10^{4}$ $M^{-1}cm^{-1}$) with isosbestic points occurring at 422, 495, 543, 561, and 578 nm. Similar spectral changes were observed when oxygen was added to the DMFCoDBrDIXDME system. As with the amine systems, the spectral changes were reversible.

The spectral changes associated with oxygenation of the CoDADIXDME and CoDBrDIXDME are listed in Table VI.1.

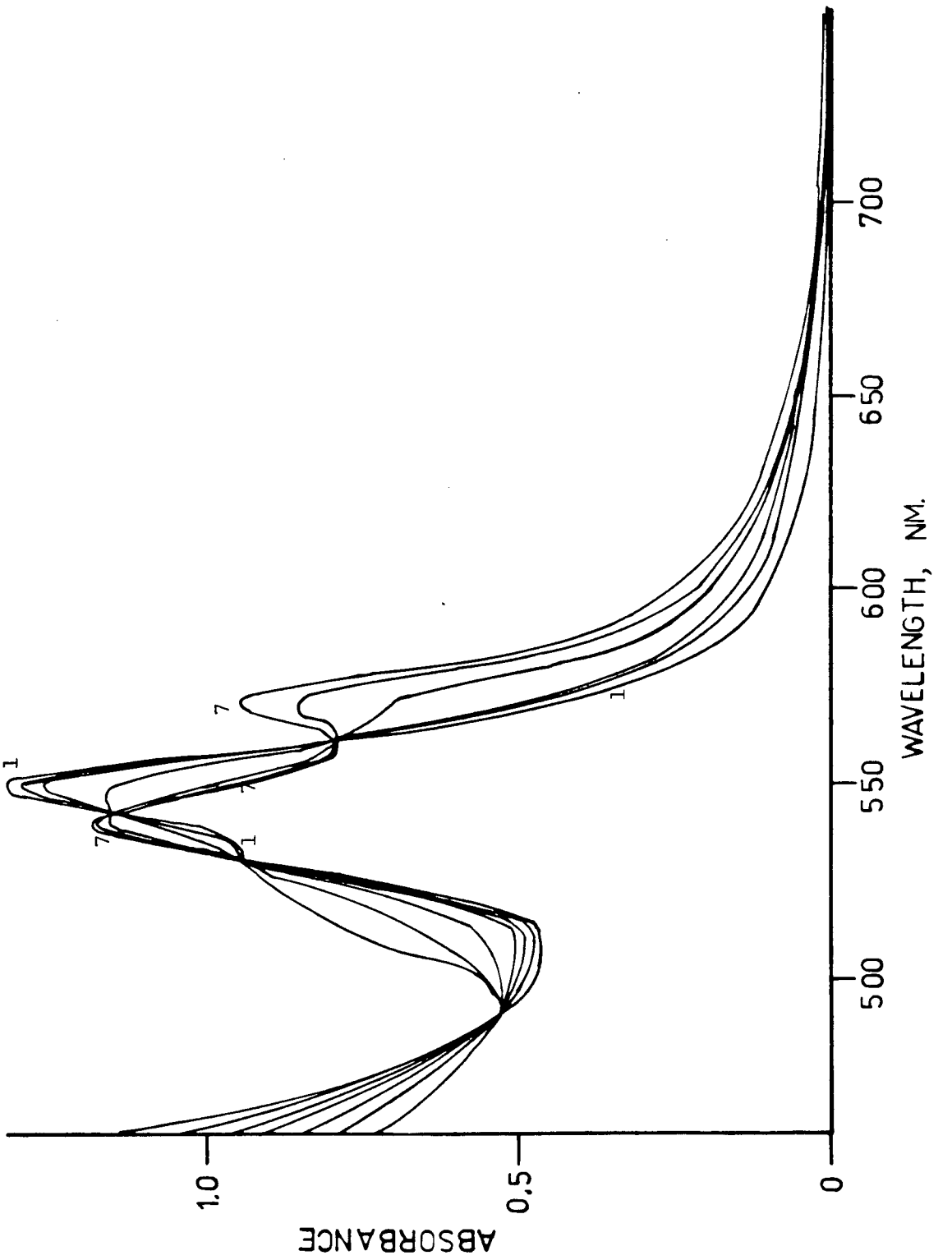

Figure VI.1. CH_3-ImCoDADIXDME + $O_2 \rightleftharpoons$ CH_3-ImCoDADIXDME(O_2) @ -56.5°C

For raw data see Appendix IVa.

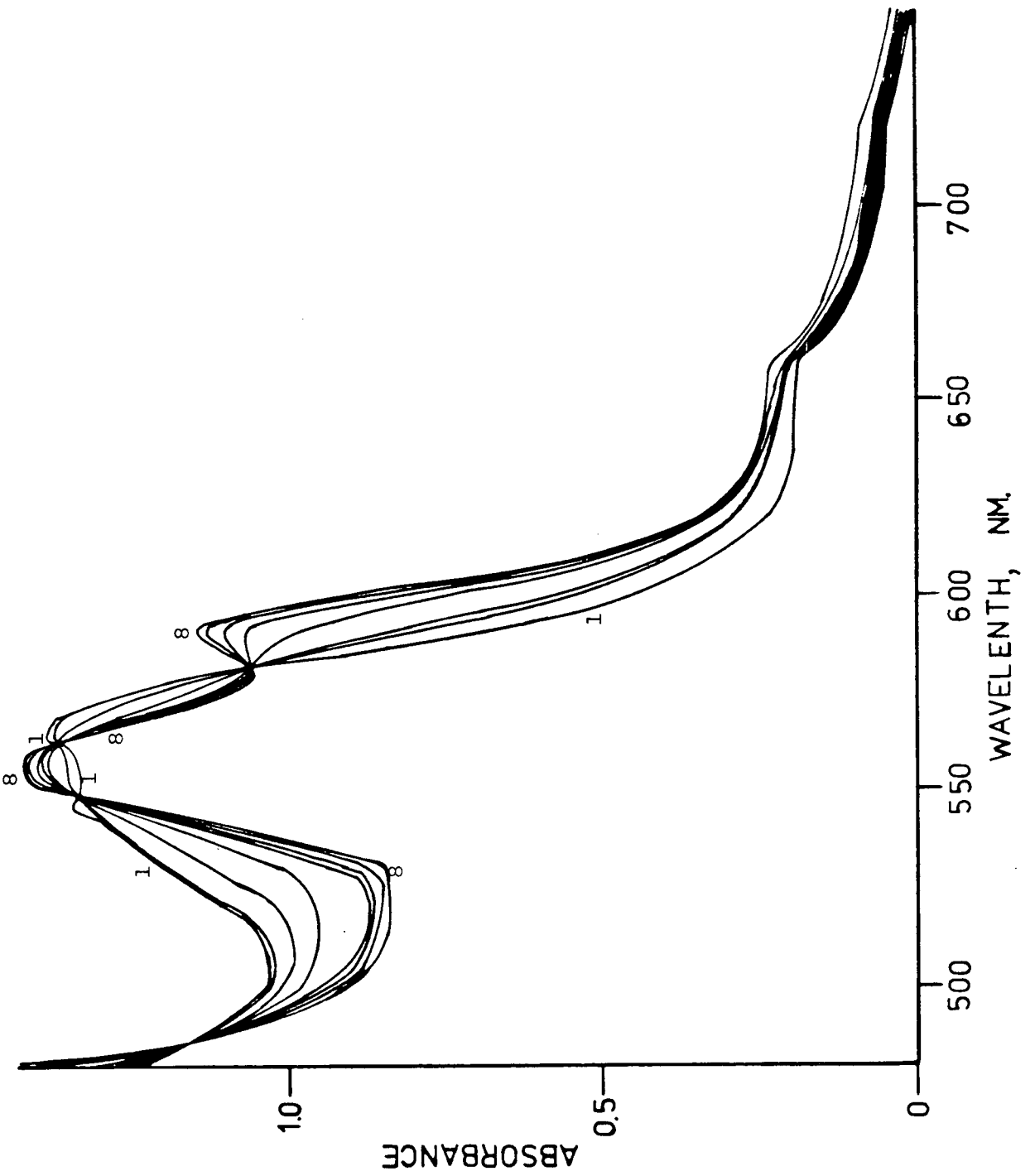

Figure VI.2. CH_3-ImCoDBrDIXDME + $O_2 \rightleftharpoons$ CH_3-ImCoDBrDIXDME @ -56.5°C

For raw data see Appendix IVe.

Table VI.1a. Spectral Data From 350 to 750 nm for the Reaction:

$$LCoDADIXDME + O_2 \rightleftharpoons LCoDADIXDME(O_2)$$

Absorbing Species	Absorption Maxima (nm) (Extinction Coefficients, $M^{-1}cm^{-1}$)		Isosbestic Points (nm)
CH_3-ImCoDADIXDME	438	(7×10^4)	426 486 548 561 581
↓	555	(8×10^3)	
CH_3-ImCoDADIXDME(O_2)	591	(7×10^3)	
PipCoDADIXDME	438	(7×10^4)	426 494 548 558 579
↓	555	(8×10^3)	
PipCoDADIXDME(O_2)	589	(7×10^3)	
PyCoDADIXDME	437	(7×10^4)	426 494 548 562 580
↓	555	(8×10^3)	
PyCoDADIXDME(O_2)	590	(7×10^3)	
DMFCoDADIXDME	436	(8×10^4)	422 495 543 561 578
↓	552	(8×10^3)	
DMFCoDADIXDME(O_2)	588	(6×10^3)	

Table VI.1b. Spectral Data From 350 to 750 nm for the Reaction:

$$LCoDBrDIXDME + O_2 \rightleftharpoons LCoDADIXDME(O_2)$$

Absorbing Species	Absorption Maxima (nm) (Extinction Coefficients, $M^{-1}cm^{-1}$)		Isosbestic Points (nm)
CH_3-ImCoDBrDIXDME	412	(8×10^4)	363 410 484 529 542 560
↓	536	(8×10^3)	
CH_3-ImCoDBrDIXDME(O_2)	569	(6×10^3)	
PipCoDBrDIXDME	412	(8×10^4)	363 410 494 530 540 559
↓	536	(7×10^3)	
PipCoDBrDIXDME(O_2)	568	(6×10^3)	
PyCoDBrDIXDME	412	(8×10^4)	363 410 490 528 540 559
↓	537	(7×10^3)	
PyCoDBrDIXDME(O_2)	569	(6×10^3)	
DMFCoDBrDIXDME	415	(9×10^4)	407 496 529 544 562
↓	541	(8×10^3)	
DMFCoDBrDIXDME(O_2)	571	(6×10^3)	

VI.2 Treatment of Data

The equilibrium constants were obtained by following the decrease in the spectral intensity of the visible band of the five-coordinate complex, or the increase in the spectral intensity of the higher wavelength visible band of the oxygenated complex. In addition to the reasons mentioned in Chapter V, the Soret band was not monitored because of difficulties arising from working with the necessarily dilute solutions.

The formation of the oxygenated complex obeys the equation:

$$LCoP + nO_2 \underset{}{\overset{K_{O_2}}{\rightleftharpoons}} LCoP(O_2)_n \qquad (VI.1)$$

and the data were analyzed by the same method described for dioxygen binding to LCoOMBP (Chapter IV). Figure VI.3 shows the $\log \frac{A - A_o}{A_\infty - A}$ vs. $\log P_{O_2}$ plots obtained from data on the oxygenation of CH_3-ImCoDADIXDME, and Figures VI.4 and VI.5 show the van't Hoff plots that are derived from the various plots of $\log \frac{A - A_o}{A_\infty - A}$ vs. $\log P_{O_2}$.

VI.3 Sources of Error

From the thermodynamic parameters listed in Table V.1, it was possible to adjust the ligand concentration so that at least 95% of the cobalt complex was initially present in the form of LCoP for the oxygenation measurements.

Although there was some evidence for six-coordinate cyclic amine complexes of LCoDBrDIXDME at high ligand concentrations (Chapter V), the formation of such complexes did not occur to any great extent at ligand concentrations used in the oxygenation measurements. There was never sufficient formation of the six-coordinate complexes, even at low

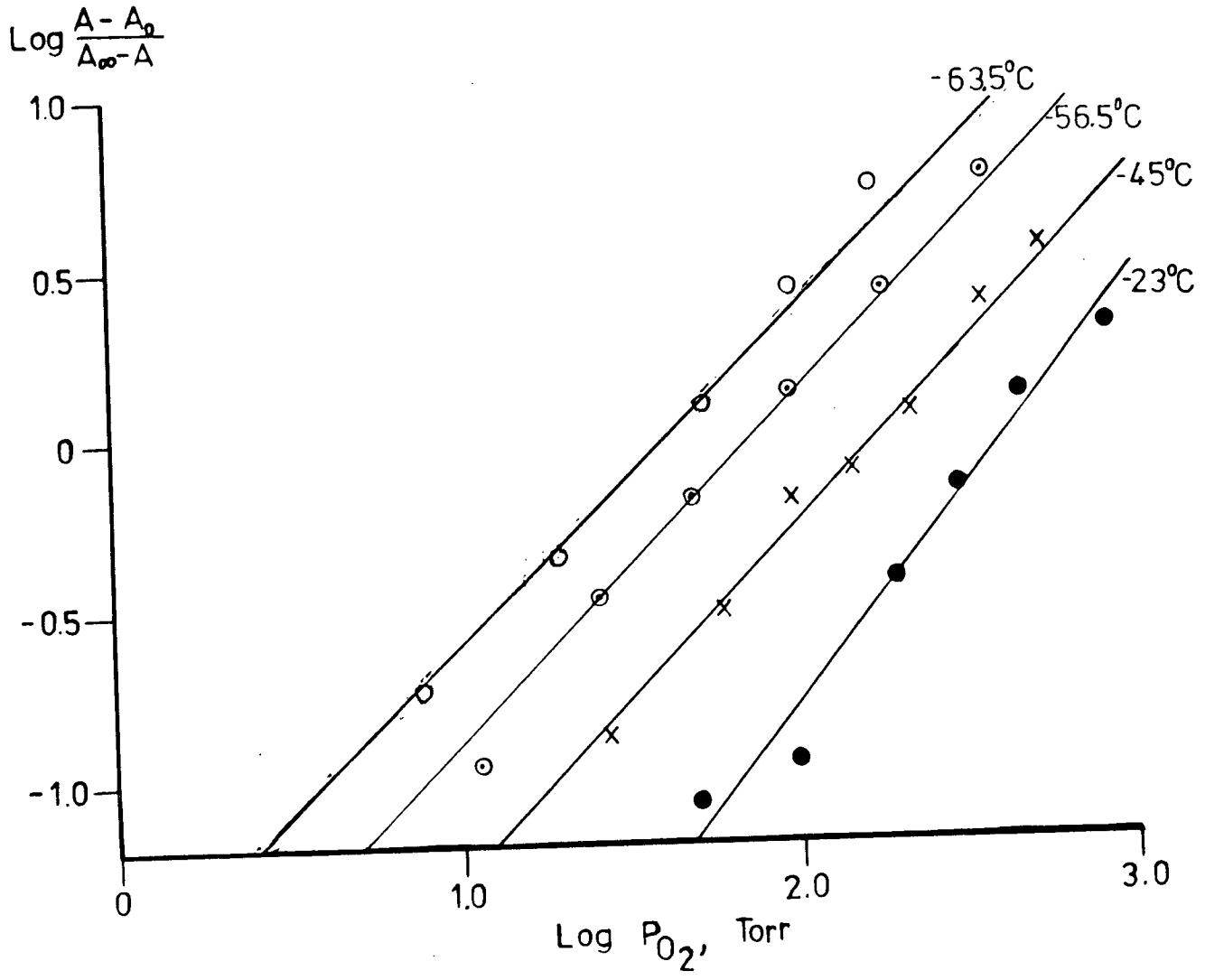

Figure VI.3 Equilibrium plots for CH_3-ImCoDADIXDME $\rightleftharpoons$ CH_3-ImCoDADIXDME(O_2). For raw data see Appendix IVa.

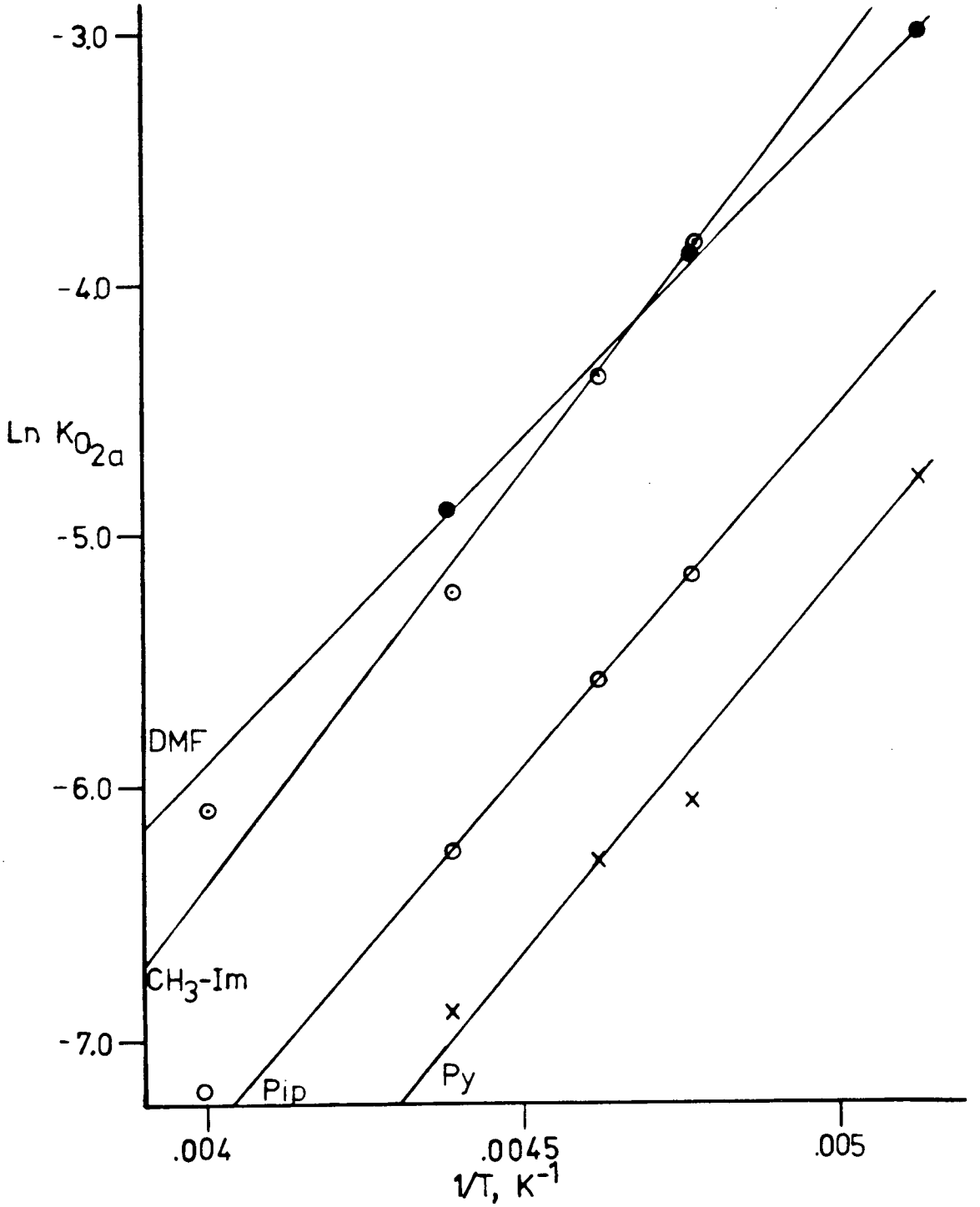

Figure VI.4. Van't Hoff plots for LCoDADIXDME + $O_2 \rightleftharpoons$ LCoDADIXDME(O_2). For raw data see Appendices IVa-d.

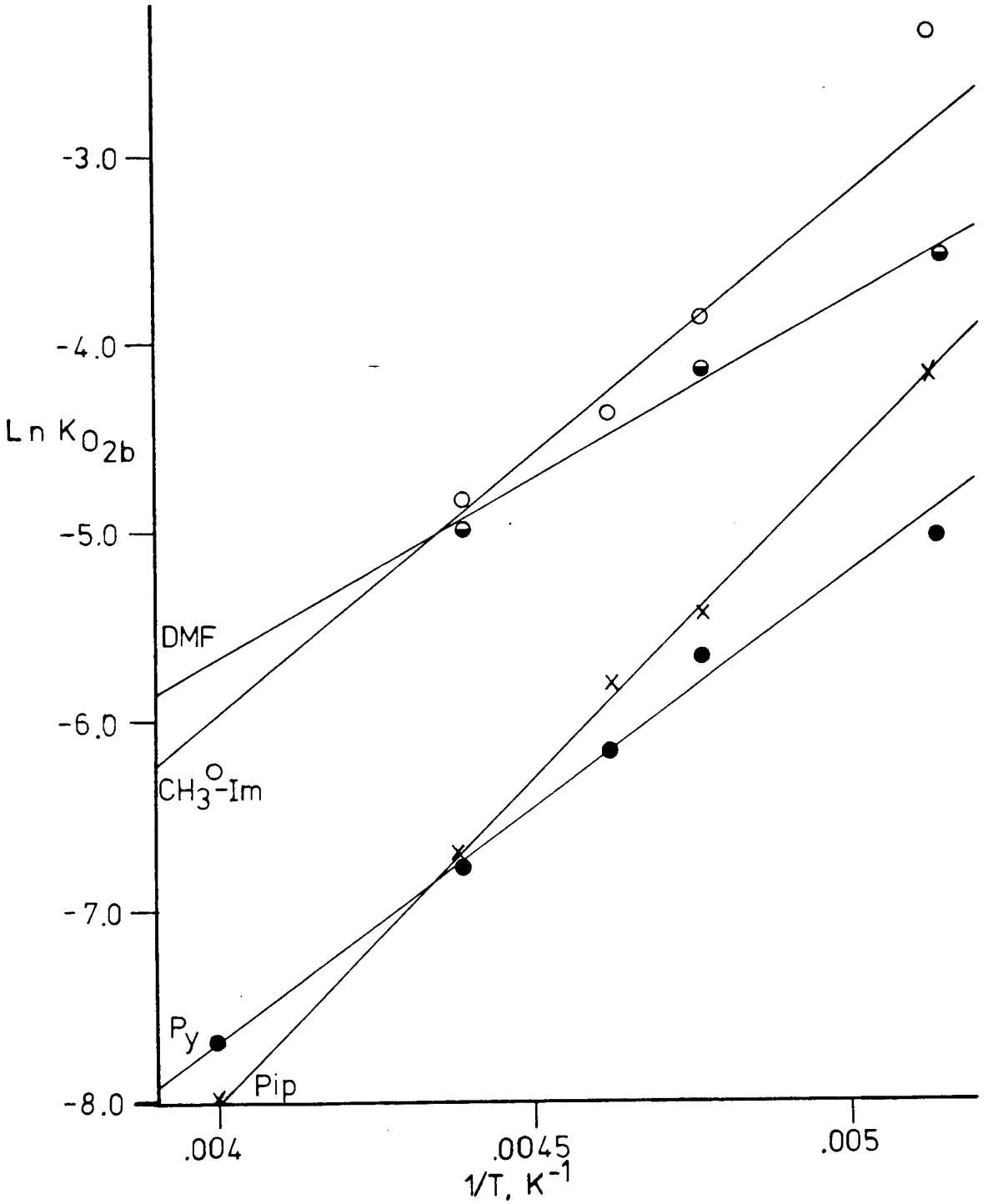

Figure VI.5. Van't Hoff plots for LCoDBrDIXDME + $O_2 \rightleftharpoons$ LCoDBrDIXDME(O_2). For raw data see Appendices IVe-h.

temperatures, to do oxygenation studies on such species.

The concentrations of the amine ligands were very small during oxygenation of the LCoP systems, and the solvent could be considered as "pure" toluene. In the case of the DMF adduct, it was necessary to study dioxygen binding in a 1:1 volume to volume ratio of toluene to DMF, so that the DMF adduct would be fully formed and a constant solvent would be maintained.

The formation of an irreversibly oxidized species was not a problem, as judged by the completely reversible and clean spectral changes, and by the consistent analysis of the spectral data for formation of a 1:1 cobalt:dioxygen adduct.

VI.4 Dioxygen Binding Constants

The $P_{\frac{1}{2}}O_2$ values of the five-coordinate LCoDADIXDME complexes in toluene are given in Table VI.2a, together with the ΔH and ΔS values, and the pK_a of the ligand studied. Table VI.2b lists the comparable values of the five-coordinate LCoDBrDIXDME systems. The order of the oxygen affinities for both porphyrin systems as a function of axial ligand over the temperature range studied is CH_3-Im~DMF>Pip>Py.

Although the order of dioxygen affinity of the five-coordinate cyclic amine systems is the same as that of the amine binding to the four-coordinate complex, there is again no obvious correlation between K_{O_2}, ΔH_{O_2}, ΔS_{O_2}, and the pK_a of the protonated amine ligand. The π-donor properties of CH_3-Im[122] within the amine series is thought to enhance the oxygenation of cobalt porphyrin complexes, as suggested for the CoPpIXDME system[89] and observed in the CoOMBP system (Chapter IV). The cyclic amines bind to CoDADIXDME and CoDBrDIXDME more strongly than does

Table VI.2a. Thermodynamic Data for the Binding of Dioxygen to LCoDADIXDME in a Toluene Solution.

LIGAND	TEMP., °C.	$P_{\frac{1}{2}O_2}$, Torr.	ΔH kcal/mole	ΔS e.u.	pK_a^a
CH_3-Im	-63.5	45	-6.7	-40	7.25
	-56.5	74			
	-45	186			
	-23	447			
Pip	-63.5	172	-5.7	-37	11.30
	-56.5	263			
	-45	513			
	-23	1288			
Py	-78	120	-6.0	-40	5.27
	-63.5	422			
	-56.5	537			
	-45	962			
DMF	-78	20	-5.2	-33	-2.0
	-63.5	48			
	-45	135			

$\sigma_{\Delta H}$ for dioxygen binding was estimated to be ± 0.6 kcal/mole.

$\sigma_{\Delta S}$ for dioxygen binding was estimated to be ± 2 e.u.

a. For references see Table III.1.

Table VI.2b. Thermodynamic Data for the Binding of Dioxygen to LCoDBrDIXDME in a Toluene Solution.

LIGAND	TEMP., °C.	$P_{\frac{1}{2}}O_2$, Torr	ΔH kcal/mole	ΔS e.u.	pK_a^a
CH_3-Im	-78	10	-6.1	-37	7.25
	-63.5	48			
	-56.5	78			
	-45	127			
	-23	537			
Pip	-78	61	-6.9	-43	11.30
	-63.5	219			
	-56.5	359			
	-45	813			
	-23	~3000			
Py	-78	151	-5.7	-39	5.27
	-63.5	288			
	-56.5	479			
	-45	851			
	-23	~2200			
DMF	-78	36	-3.7	-26	-2.0
	-63.5	63			
	-45	145			

$\sigma_{\Delta H}$ for dioxygen binding was estimated to be ± 0.6 kcal/mole.

$\sigma_{\Delta S}$ for dioxygen binding was estimated to be ± 2 e.u.

a. For references see Table III.1.

DMF by a factor of 10^4, while the DMF adduct binds dioxygen as well as the CH_3-Im adduct. Even after consideration of enhanced dioxygen binding in 1:1 toluene:DMF mixtures due to solvent effects (Chapter IV), the dioxygen affinity of the DMF adduct is much greater than expected from any σ-ligand basicity correlation, and again the strong π-donor ability of DMF[121] is thought to be responsible.

VI.5 Comparison of Dioxygen Binding Among Different Cobalt Porphyrins

Considerations from Chapter V indicate that the tendency of the first axial ligand to bind with a cobalt porphyrin complex is enhanced as the basicity of the porphyrin is decreased.

Since the cobalt-dioxygen bond is generally thought to be formed by the transfer of some electron density from the cobalt to the dioxygen, the dioxygen binding ability of a cobalt porphyrin complex should increase as electron density at the cobalt centre is increased. Therefore, the complexes with the most basic porphyrins should bind dioxygen to the greatest degree. Tables VI.3a-d list, in decreasing order of porphyrin basicity, a series of cobalt porphyrin complexes on which binding studies have been done. Values listed in these tables include dioxygen binding constants (as $P_{\frac{1}{2}O_2}$), the corresponding ΔH and ΔS values, and the basicity of the porphyrin. Tables VI.3a, VI.3b, VI.3c, and VI.3d deal with dioxygen binding to the CH_3-Im, Pip, Py, and DMF cobalt porphyrin complexes, respectively.

Some work has been done previously on binding of dioxygen to a series of amine-coordinated cobalt 2,4-substituted deuteroporphyrins[89,91c]. No definite conclusions concerning a correlation between dioxygen binding and porphyrin basicity could be drawn, since an insufficient range of porphyrin basicities were used within one particular amine system. Experiments

Table VI.3a. Thermodynamic Data for the Binding of Dioxygen to CH_3-Im Complexes of Several Cobalt Porphyrins.

PORPHYRIN	TEMP., °C	$P_{\frac{1}{2}}O_2$, Torr	ΔH kcal/mole	ΔS e.u.	pK_3 [a]	REFERENCE
OEP	-63.5	5	-11.0	-56	6[b]	95
	-45	43				
	-31	200				
MpIXDME*	-45	31			5.8[b]	95
PpIXDME	-45	50	-11.8	-59	4.8[b]	89
	-37.4	110				
	-31	229				
T(p-OMe)PP	-65	29	-8.9	-49	~3[c]	92b
	-45	154†				
TPP*	-45	633			~3[b]	95
DADIXDME	-63.5	46	-6.7	-40	3.3[b]	Table VI.2a
	-56.5	74				
	-45	186				
	-23	447				
DBrDIXDME	-78	10	-6.1	-37	3.0[b]	Table VI.2b
	-63.5	48				
	-56.5	78				
	-45	127				
	-23	537				
OMBP	-56.5	62	-5.8	-32	"2.0"[d]	Table IV.4
	-45	98				
	-31	198				

Table VI.3b. Thermodynamic Data for the Binding of Dioxygen to Pip Complexes of Several Cobalt Porphyrins.

PORPHYRIN	TEMP., °C	$P_{\frac{1}{2}}O_2$, Torr	ΔH kcal/mole	ΔS e.u.	pK_3[a]	REFERENCE
OEP	-45	562			6[b]	95
PpIXDME	-63.5	45	-9.0	-50	4.8[b]	89
	-45	224				
	-31	832				
T(p-OMe)PP	-65	147	-8.2	-49	~3[c]	92b
	-45	714[†]				
DADIXDME	-63.5	112	-5.7	-37	3.3	Table VI.2a
	-56.5	263				
	-45	513				
	-23	1288				
DBrDIXDME	-78	61	-6.9	-43	3.0	Table VI.2b
	-63.5	219				
	-56.5	359				
	-45	813				
	-23	3000				
OMBP	-63.5	104	-4.9	-32	"2.0"[d]	Table IV.4
	-56.5	184				
	-45	269				

Table VI.3c. Thermodynamic Data for the Binding of Dioxygen to Py Complexes of Several Cobalt Porphyrins.

PORPHYRIN	TEMP., °C	$P_{\frac{1}{2}}O_2$, Torr	ΔH kcal/mole	ΔS e.u.	pK_3[a]	REFERENCE
OEP	-45	708			6[b]	95
MpIXDME	-58.0	50	-9.0	-50	5.8[b]	91c
	-54.5	78				
	-49.5	141				
	-44.5	192				
DpIXDME	-57.5	104	-9.9	-55	5.5[b]	91c
	-51.0	189				
	-49.0	250				
	-46	313				
PpIXDME	-59.0	78	-10.3	-57	4.8	91c
	-53.5	125				
	-49.0	208				
	-43.5	400				
PpIXDME	-63.5	123	-9.2	-53	4.8[b]	89
	-57.5	178				
	-45	691				
PpIXDME	-52.7	1009	-7.8	-48.7	4.8	91b
	-45	1595†				
	-41.6	1958				
	-29.5	5507				
	-5.9	22700				
T(p-OMe)PP	-65	157†	-9.3	-55	~3[c]	92b
	-45	1168†				
DADIXDME	-78	120	-6.0	-40	3.3[b]	Table VI.2a
	-63.5	432				
	-56.5	537				
	-45	962				
DBrDIXDME	-78	151	-5.7	-39	3.0[b]	Table VI.2b
	-63.5	288				
	-56.5	479				
	-45	851				
	-23	2200				
OMBP	-63.5	91	-5.1	-33	"2.0"[d]	Table IV.4
	-56.5	141				
	-45	240				

Table VI.3d. Thermodynamic Data for the Binding of Dioxygen to DMF Complexes of Several Cobalt Porphyrins.

PORPHYRIN	TEMP., °C	$P_{\frac{1}{2}}O_2$, Torr	ΔH kcal/mole	ΔS e.u.	pK_3 [a]	REFERENCE
PpIXDME	-63.5	22	-11.0	-59	4.8[b]	89
	-45	186				
	-31	759				
DADIXDME	-78	20	-5.2	-33	3.3[b]	Table VI.2a
	-63.5	48				
	-45	135				*
DBrDIXDME	-78	36	-3.7	-26	3.0[b]	Table VI.2b
	-63.5	63				
	-45	145				
OMBP	-78	8.5	-12.2	-65	"2.0"[d]	Table IV.4
	-63.5	25				
	-56.5	91				
	-45	389				
	-23	2700				

Notes for Tables VI.3a-d.

For references a-d, see Table V.3.

* Values taken from data where Im is the axial ligand.

† $P_{\frac{1}{2}}O_2$ values at -45°C calculated from thermodynamic data presented.

described in this thesis on CoDADIXDME, CoDBrDIXDME and CoOMBP systems extend the range of porphyrin basicities studied.

Figure VI.6a indicates that a reasonable dioxygen binding-porphyrin basicity correlation (log $P_{\frac{1}{2}}O_2$ at -45°C vs. pK_3) exists for the three CH_3-Im coordinated 2,4-substituted deuteroporphyrins studied. Oxygen binding to ImCoMpIXDME appears to fall within the CH_3-Im cobalt porphyrin binding correlation. The assumption that ImCoMpIXDME binds dioxygen in a similar manner to CH_3-ImCoMpIXDME is supported by observations in the CoPpIXDME system[89] that ImCoPpIXDME has a $P_{\frac{1}{2}}O_2$ value of 69 Torr while CH_3-ImCoPpIXDME has a $P_{\frac{1}{2}}O_2$ value of 50 Torr. Also the two ligands have similar basicities (Table III.3). CH_3-ImCoOEP appears to fall within this correlation, but CH_3-ImCoOMBP, although it binds dioxygen less strongly than CH_3-ImCoOEP and CH_3-ImCoPpIXDME, binds dioxygen more strongly than the corresponding DADIXDME and DBrDIXDME complexes, despite these being more basic porphyrins than OMBP (Chapter V). The CH_3-ImCoT(p-OMe)PP system binds dioxygen in line with the correlation of Figure VI.6a. On the other hand, ImCoTPP binds dioxygen much less strongly than the above relationship would predict. However, the pK_3 value reported for TPP can only be considered approximate, since it was determined from spectroscopic peak positions (Chapter V.5).

Other work on 2-methylimidazole complexes of cobalt porphyrins in DMF found that at -10°C the order of oxygen affinity was MpIXDME>DpIXDME~PpIXDME[91c]; in a series of coboglobins where the axial ligand is the imidazole moiety of a histidine residue, ambient temperature studies revealed an oxygen affinity sequence of DpIXDME>MpIXDME~PpIXDME for

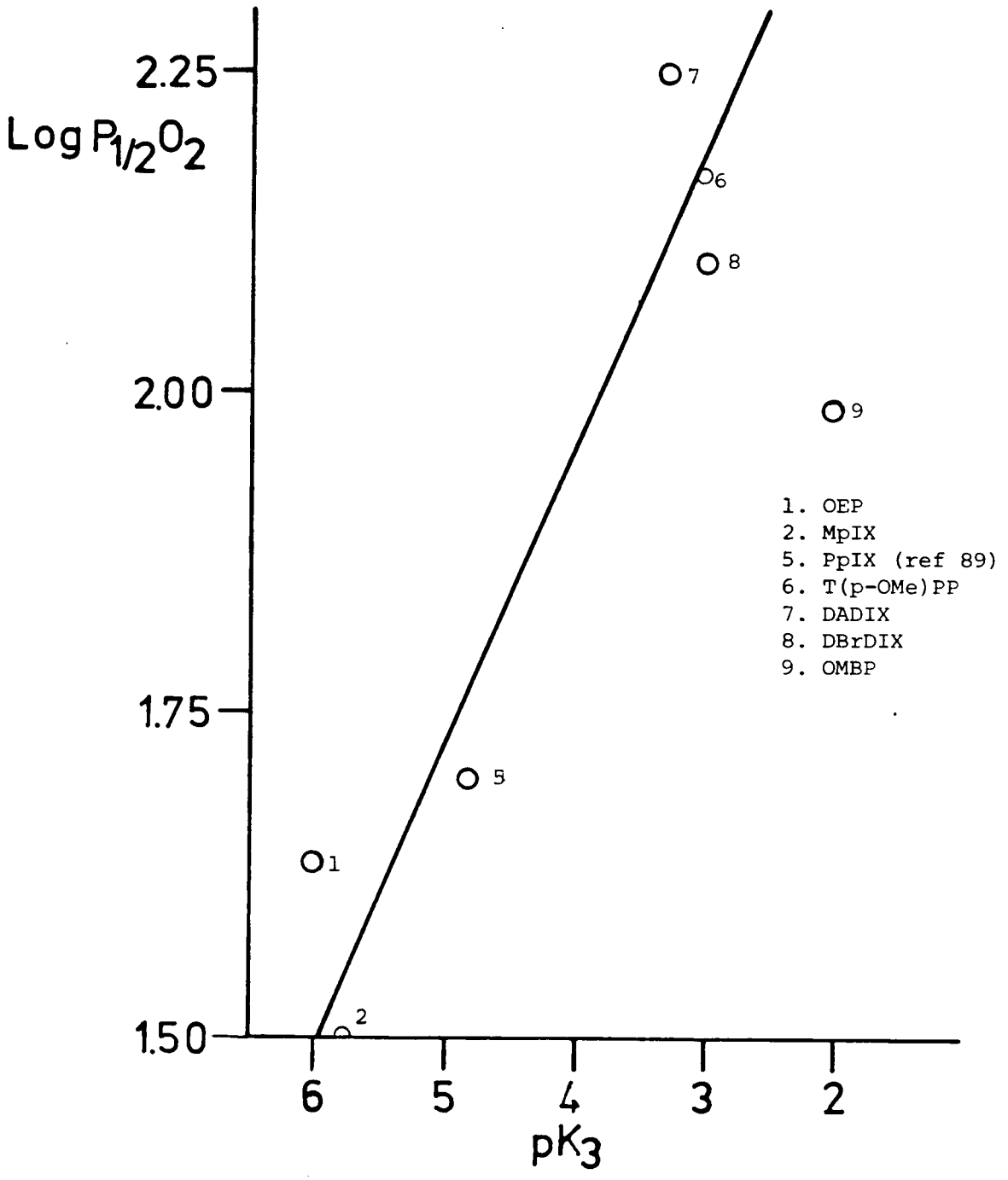

Figure VI.6a. Dioxygen Affinity vs. Porphyrin Basicity for a Variety of CH_3-Im Cobalt Porphyrin Complexes.

sperm whale myoglobin, and MpIXDME>DpIXDME>PpIXDME for substituted human hemoglobin[134]. Since the nature of these systems is different from the ones plotted on Figure VI.6a (e.g. different solvent, presence of protein), the precise dioxygen binding constants do not fall on that plot, but in each case the least basic CoPpIX system bound dioxygen the least strongly in the series. That the CoDpIX system sometimes bound dioxygen more strongly than the CoMpIX system and sometimes the relative binding abilities were reversed, is not surprising as the basicities of the two systems are so similar.

Figure VI.6b shows that a good dioxygen binding-porphyrin basicity correlation exists for the Pip coordinated 2,4-deuteroporphyrins. Although the dioxygen affinity of PipCoT(p-OMe)PP falls within this correlation, the dioxygen binding by PipCoOEP is much weaker, and that by PipCoOMBP much stronger, than those anticipated by the σ-basicity correlation.

Figure VI.6c shows dioxygen binding data to the Py cobalt porphyrin systems. There appears to be a reasonably good dioxygen binding-porphyrin basicity correlation for the Py coordinated 2,4-substituted deuteroporphyrins, and oxygenation of PyCoT(p-OMe)PP falls reasonably within this relationship. As with the Pip cobalt porphyrin complexes, PyCoOEP binds dioxygen less strongly than would be expected, while PyCoOMBP again binds dioxygen more strongly.

In Chapter V it was noted that the Py binding data to CoPpIXDME varied somewhat between those of two different groups[89,91c]. Again there is a similar discrepency for the oxygenation data of PyCoPpIXDME. In addition to the values reported by Yamamoto et al[91c] ($P_{\frac{1}{2}O_2}$ @ -45°C = 300 Torr) and Stynes et al[89] ($P_{\frac{1}{2}O_2}$ @ -45°C = 691 Torr), there are the data of Drago et al[91b] which state that PyCoPpIXDME binds dioxygen more weakly ($P_{\frac{1}{2}O_2}$ @ -45°C

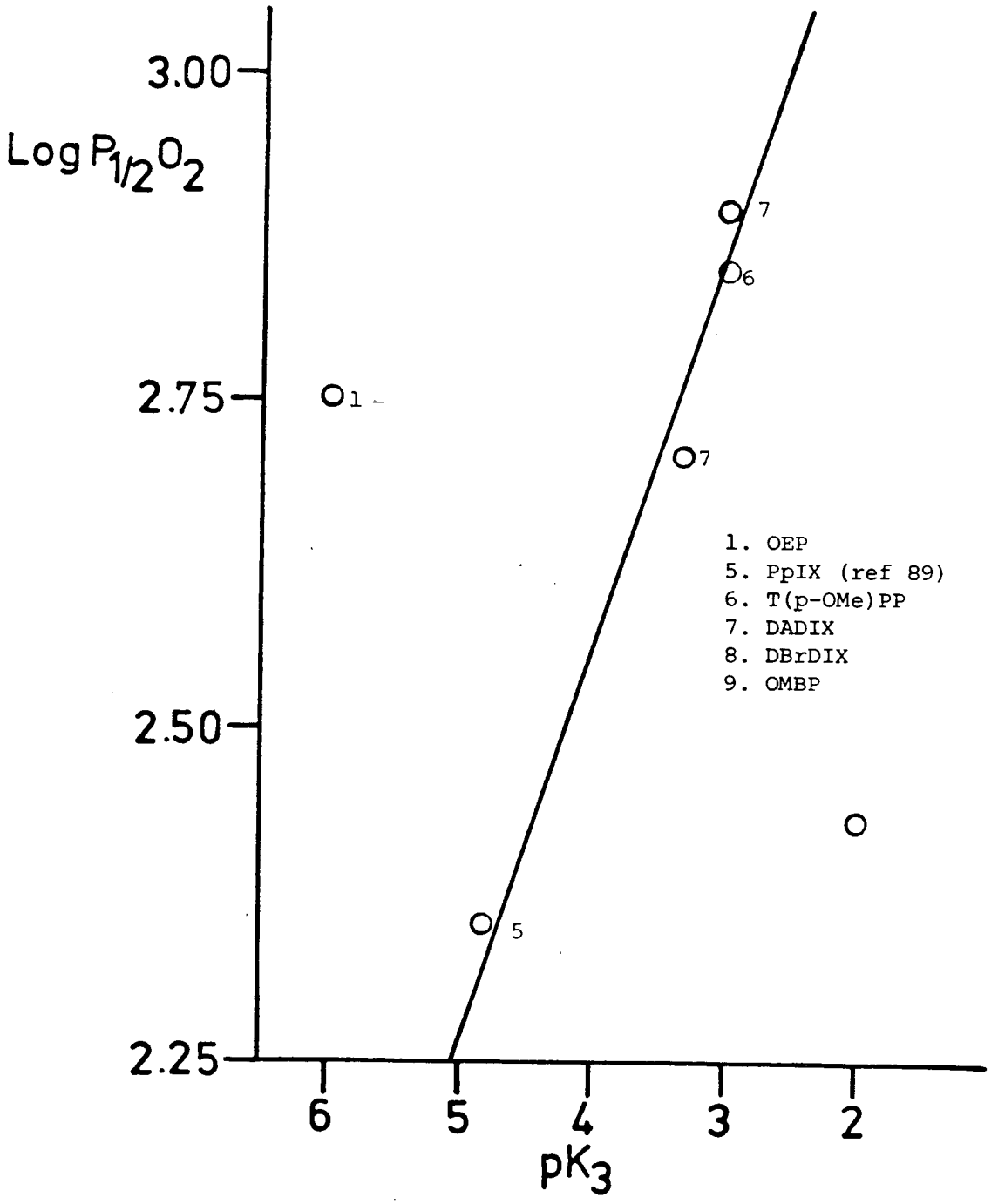

Figure VI.6b. Dioxygen Affinity vs. Porphyrin Basicity for a Variety of Pip Cobalt Porphyrin Complexes.

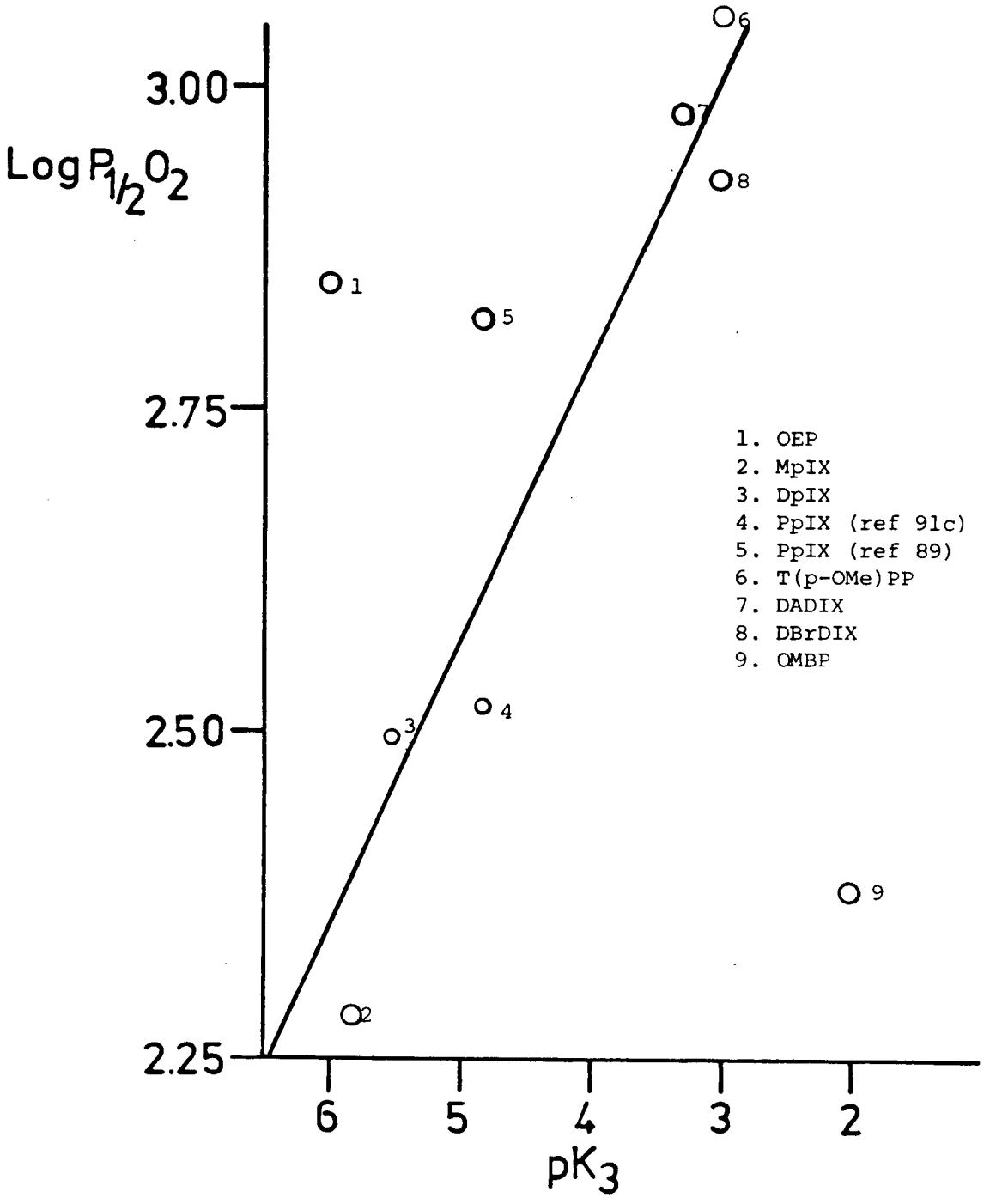

Figure VI.6c. Dioxygen Affinity vs. Porphyrin Basicity for a Variety of Py Cobalt Porphyrin Complexes.

= 1595 Torr). The data of the first two groups are considered to agree reasonably well since the experiments were indeed performed by different groups and the spectrophotometric titration data were analyzed somewhat differently. Stynes et al treated their data by a method similar to the one outlined in Chapter III, while Yamamoto et al examined theirs by the Ketalaar[135] method where

$$\frac{1}{A - A_o} = \frac{1}{P_{O_2} K_{O_2} (\varepsilon_\infty - \varepsilon_o)[Co_T]} + \frac{1}{(\varepsilon_\infty - \varepsilon_o)[Co_T]} \qquad \text{(VI.2)}$$

where A_o is the absorbance when no oxygen is present

A is the absorbance at a set oxygen pressure

ε_o is the molar extinction coefficient of LCoP

ε_∞ is the molar extinction coefficient of LCoP(O_2)

and $[Co_T]$ is the total molar concentration of cobalt present.

Drago's group also chose a different method of analyzing their spectrophotometric data. For each $A - A_o$ and P_{O_2} data point of an individual run, plots were calculated based on the equation:

$$\frac{dK_{O_2}^{-1}}{d(\varepsilon_\infty - \varepsilon_o)} = \frac{A - A_o}{(\varepsilon_\infty - \varepsilon_o)^2} + \frac{P_{O_2}[LCoP]}{A - A_o} . \qquad \text{(VI.3)}$$

Where the lines resulting from those data points intersected, the "true" K^{-1} and $\varepsilon_\infty - \varepsilon_o$ could be determined. However, Drago's group worked with a 0.13 cm path-length cell which required cobalt porphyrin concentrations of ~4×10^{-4} M. Under these conditions of relatively high concentration and low temperature, the possibility of porphyrin aggregation (see Chapter VII)

cannot be ignored, and if any aggregate were present, this would result in an observed lower oxygen affinity. Also the authors appeared to have relied on oxygen gas diffusing into the solution for equilibration, and it is possible that full equilibration did not take place, which would again result in a lower observed oxygen affinity.

The observed $P_{\frac{1}{2}}O_2$ values at $-45^{\circ}C$ for the CH_3-Im and Py adducts of CoDADIXDME are slightly higher than those for the corresponding CoDBrDIXDME complexes, in spite of the higher basicity of the diacetyl porphyrin, although the $P_{\frac{1}{2}}O_2$ values of the Pip complexes follow the basicity correlation. However, $P_{\frac{1}{2}}O_2$ values of a LCoDADIXDME complex are similar (within 50%) to the corresponding value of a LCoDBrDIXDME complex, consistent with the similarity in porphyrin basicity. Since the experimental error associated with a measured $P_{\frac{1}{2}}O_2$ value is ~±10%, and the measurement of the pK_3 value of DBrDIXDME was complicated by solubility problems[132], the oxygen binding values of LCoDADIXDME and LCoDBrDIXDME are probably not inconsistent with the oxygen affinity-porphyrin basicity correlation.

In all cases, the oxygen affinity of LCoOMBP complexes were substantially greater than anticipated from any σ-basicity correlation, and it seems reasonable to attribute this to the extra π-electron density on the cobalt centre, resulting from the unusually strong π-donating properties of OMBP. This extra π-electron density could then enhance dioxygen binding by donating to the empty π^*-orbitals of dioxygen.

The dioxygen affinity of CH_3-ImCoOEP falls within the range expected from consideration of the reported σ-basicity of OEP, but the dioxygen affinities of PipCoOEP and PyCoOEP are much less than would have been expected.

In all cases the dioxygen affinity of a CH_3-Im adduct of a particular cobalt porphyrin complex was the strongest of all the nitrogen donor ligands studied, and this could again be due to the ability of CH_3-Im to donate π-electron density to the cobalt centre[122]. With the exception of CoOMBP, where the Pip and Py adducts bind dioxygen similarly, the Py adduct of a given cobalt porphyrin binds dioxygen less strongly than a Pip adduct. This could be rationalized by Py being a π-acceptor and Pip not π-interacting[122], but the trend is also consistent with the σ-basicity of Py and Pip.

Figure VI.6d shows dioxygen binding constants at $-45^{o}C$ for DMF adducts of different cobalt porphryins. There is no obvious correlation with porphyrin basicity. The strong π-donor effects of DMF complexes[121] could possibly override simple porphyrin σ-basicity effects in determining the order of dioxygen binding ability. For example, the exothermicity associated with oxygenation of DMFCoOMBP is much greater than those associated with oxygenation of other CoOMBP ligand adducts, presumably because the π-effects from both OMBP and DMF markedly enhance oxygenation. However, the DMF adducts of CoDADIXDME, CoDBrDIXDME, and CoPpIXDME bind dioxygen with exothermicities similar to those of other adducts of these systems, so oxygenation enhancement from π-interactions for these three porphyrins does not appear to be as important as in the CoOMBP system.

Ligand binding constants (K_1) of the cobalt porphyrins increase by a factor of about 6 as the range of porphyrin basicities goes from MpIXDME to DBrDIXDME. A similar decrease in K_{O_2} is noted for the same porphyrins.

Presumably as axial ligand binding (K_1) is enhanced with the more weakly basic porphyrin complexes, there should be more electron transfer from the ligand to the metal centre in the case of the weakly basic

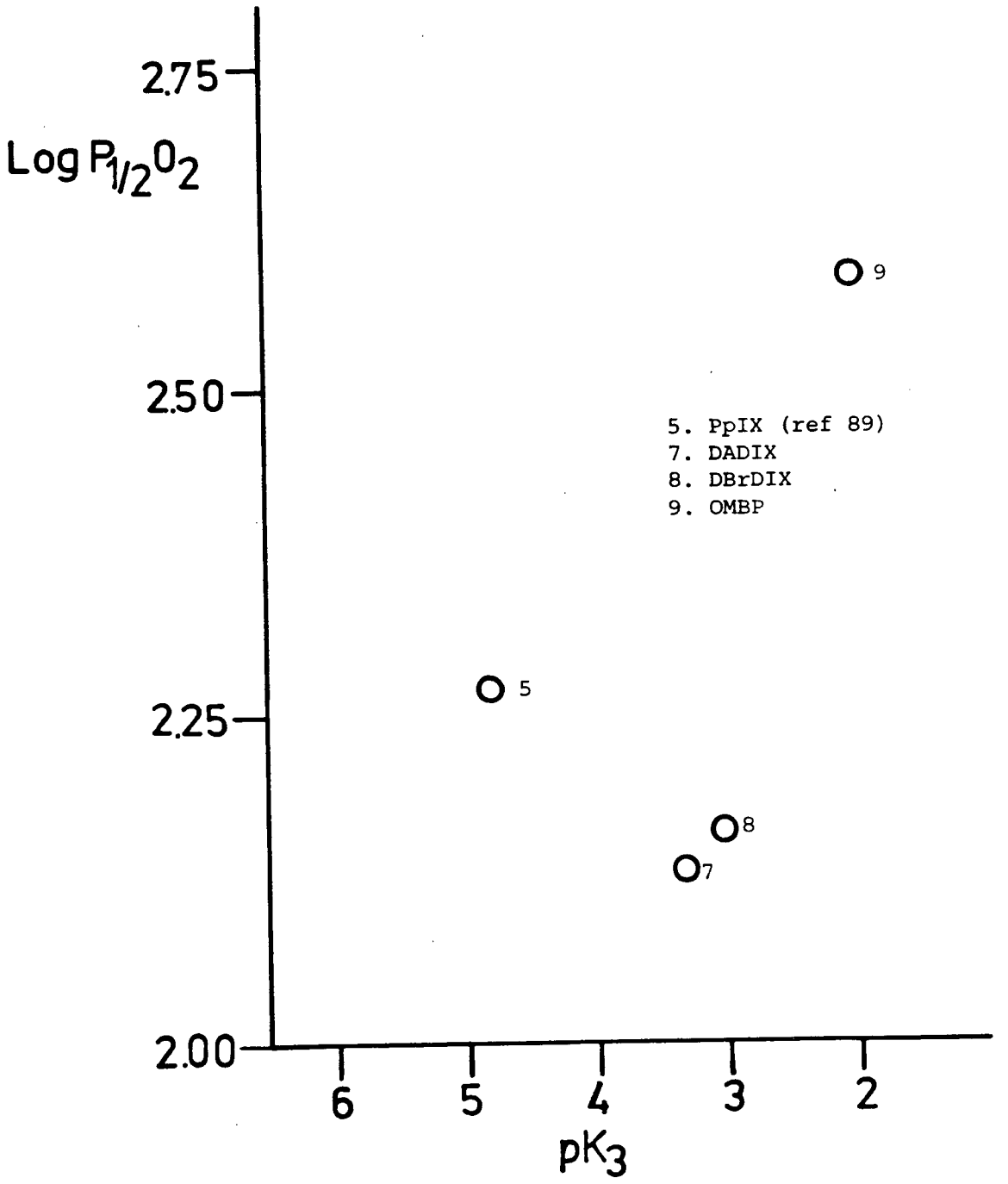

Figure VI.6d Dioxygen Affinity vs. Porphyrin Basicity for a Variety of DMF Cobalt Porphyrin Complexes.

porphyrins. This extra electron density from the axial ligand would then be expected to compensate for the decreased electron density of the weakly basic porphyrins, and temper the relationship between dioxygen binding and porphyrin basicity, especially since the σ-electron density from the ligand goes to the cobalt d_{z^2} orbital, which is thought to be the cobalt orbital which transfers σ-electron density to dioxygen. However, porphyrin basicity seems to affect both ligand and dioxygen affinities by similar magnitudes.

CHAPTER VII

KINETICS OF THE OXIDATION OF COBALT(II) PORPHYRIN COMPLEXES

VII.1 Introduction

Work in the preceding chapters has dealt with the formation of five-or six-coordinate cobalt porphyrin complexes and their dioxygen adducts, which are all formed reversibly at rates too great to measure on a stopped-flow scale. Observations in this work have suggested that at higher temperatures (e.g. ambient) an irreversible oxidation reaction of a cobalt(II) porphyrin complex can occur with dioxygen. The loss of the familiar ESR signals of the 1:1 $Co:O_2$ systems at the completion of the oxidation reaction is consistent with the formation of a bridged peroxo dimer, for example, $LCoOMBP(O_2)CoOMBP$, similar to a corresponding reaction proposed for the CoPpIXDME system[123]. In contrast to an expected second order dependence on cobalt (resulting from a likely mechanism involving a bimolecular rate determining step:

$$LCoP(O_2) + LCoP \xrightarrow{k_r} LCoP(O_2)CoPL \qquad \text{(VII.1)}$$

where P represents porphyrin), a first order dependence was observed[123] over a cobalt concentration range from 5×10^{-6} to 5×10^{-5} M, and it was proposed that the reaction proceeded by a rate determining rearrangement or distortion of $LCoP(O_2)$:

$$LCoP(O_2) \xrightarrow{k^*} LCoP(O_2)^* \qquad \text{(VII.2)}$$

A change in geometry resulting in the O_2 moiety being bound more as a peroxide than a superoxide was suggested, the $LCoP(O_2)^*$ intermediate then rapidly reacting with LCoP to give the final product. The more obvious alternate explanation for the observed cobalt dependence invokes formation of $LCoP(O_2)$ as the rate determining step followed by rapid reaction with LCoP; however, this picture is not consistent with the observed rapid formation of $LCoP(O_2)$ at lower temperatures[89].

In the above studies[123], the reaction rate was greatly enhanced when using the ligands imidazole and benzimidazole, both of which have acidic protons, and hydrogen bonding was thus considered to help form the intermediate, and accelerate the overall reaction.

The maximum concentration of CoPpIXDME used was 10^{-5}M, and it was confirmed that cobalt porphyrin aggregation was not a factor at these concentrations[123].

With the above results in mind, a similar kinetic investigation was undertaken on complexes of CoOMBP. Unexpected observations caused work to be done on other porphyrin systems including CoEpI, CoOEP, CoPpIXDME, and CoTPP.

VII.2 Qualitative Spectral Observations

Upon oxidation of $L_nCoOMBP$ complexes (L = Im, CH_3-Im, Pip, and Py; n = 1 or 2) a new Soret band occurred in the 440 nm region (Figure VII.1) with molar extinction coefficients similar to those of the $LCoOMBP(O_2)$ dioxygen adducts (Table IV.I). The visible band red shifted to about 630 nm with an approximate increase of 10% in extinction coefficient. Often,

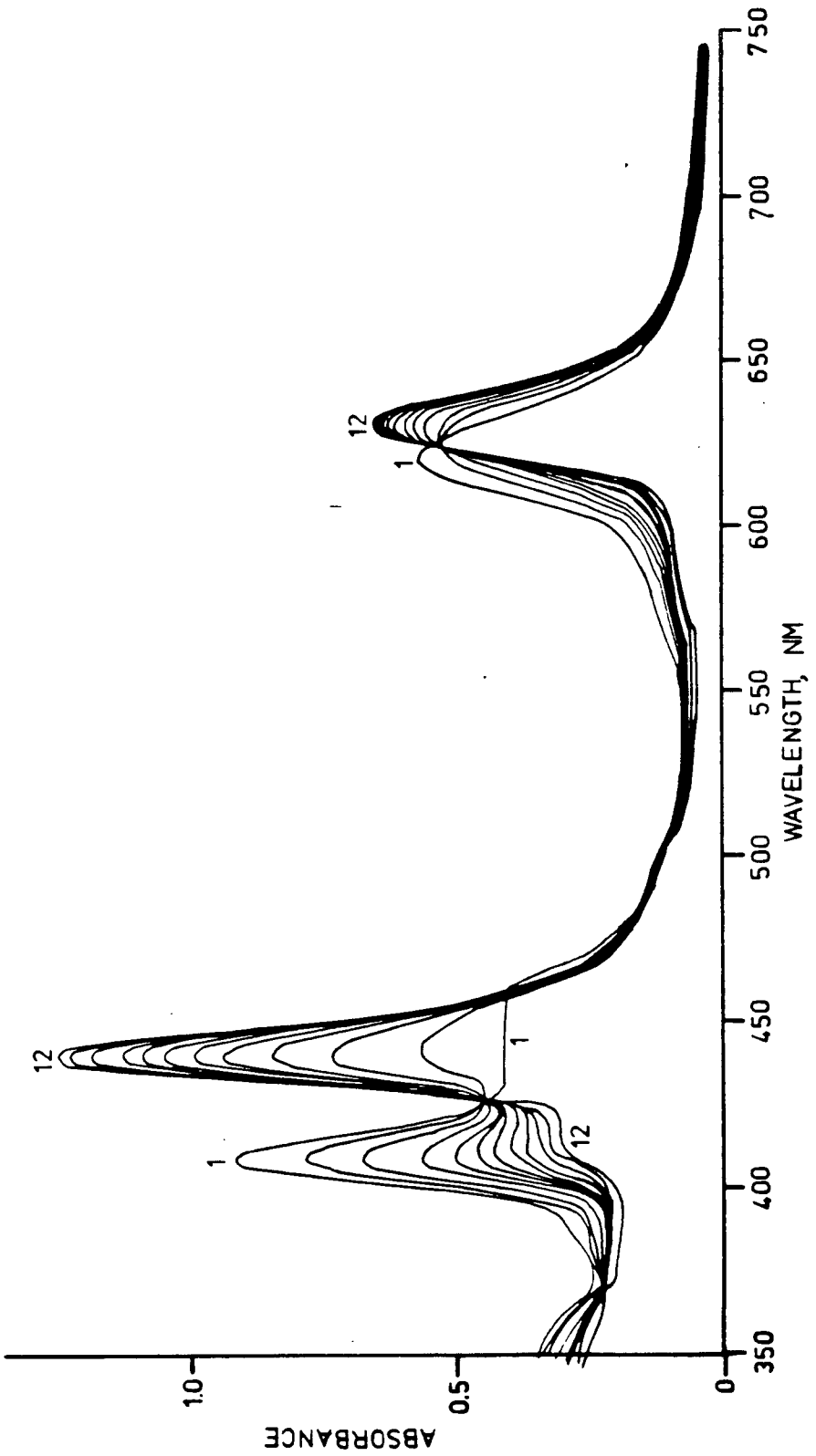

Figure VII.1. Spectra showing the oxidation of PipCoOMBP in DCE @ 30°C. For raw data see Appendix Vr.

especially for the relatively fast reactions, good isosbestic points were achieved. On some of the reactions which took days to complete the isosbestic points were lost.

Oxidation of the CoEpI, CoOEP, CoPpIXDME, and CoTPP complexes was accompanied by a red Soret shift of about 20 nm and an increase in molar extinction coefficient (Figure VII.2). In the CoEpI, CoOEP, and CoPpIXDME systems the visible band around 550 nm split into two somewhat smaller bands on either side of the original band (Figure VII.3). In the CoTPP system the visible band at 540 nm shifted to 556 nm with a 20% increase in molar extinction coefficient (Figure VII.4). Generally good isosbestic points were achieved in these reactions, after sometimes allowing for initial rapid formation of some 1:1 $Co:O_2$ adducts which could occur under the conditions used.

Although the CoPpIXDME systems in toluene were reported not to form a dioxygen adduct at ambient temperatures[123], many of the other porphyrin systems described in this thesis exhibited a substantial rapid initial spectral change when oxygen was added, especially when the solvent was DCE. This change, the magnitude of which was dependent on the pressure of O_2 in the system, was at least partially reversible if oxygen were immediately removed. As a result of these observations, and from the fact that a room temperature ESR signal was detected upon admission to the CoEpI and CoOEP systems (Figure VII.5), it was concluded that the initial spectral changes were due to the formation of a 1:1 $Co:O_2$ adduct at ambient temperatures. The final "irreversible" spectrum in each case is attributed to the bridged peroxide species[123].

A summary of the visible spectral changes is presented in Table VII.1.

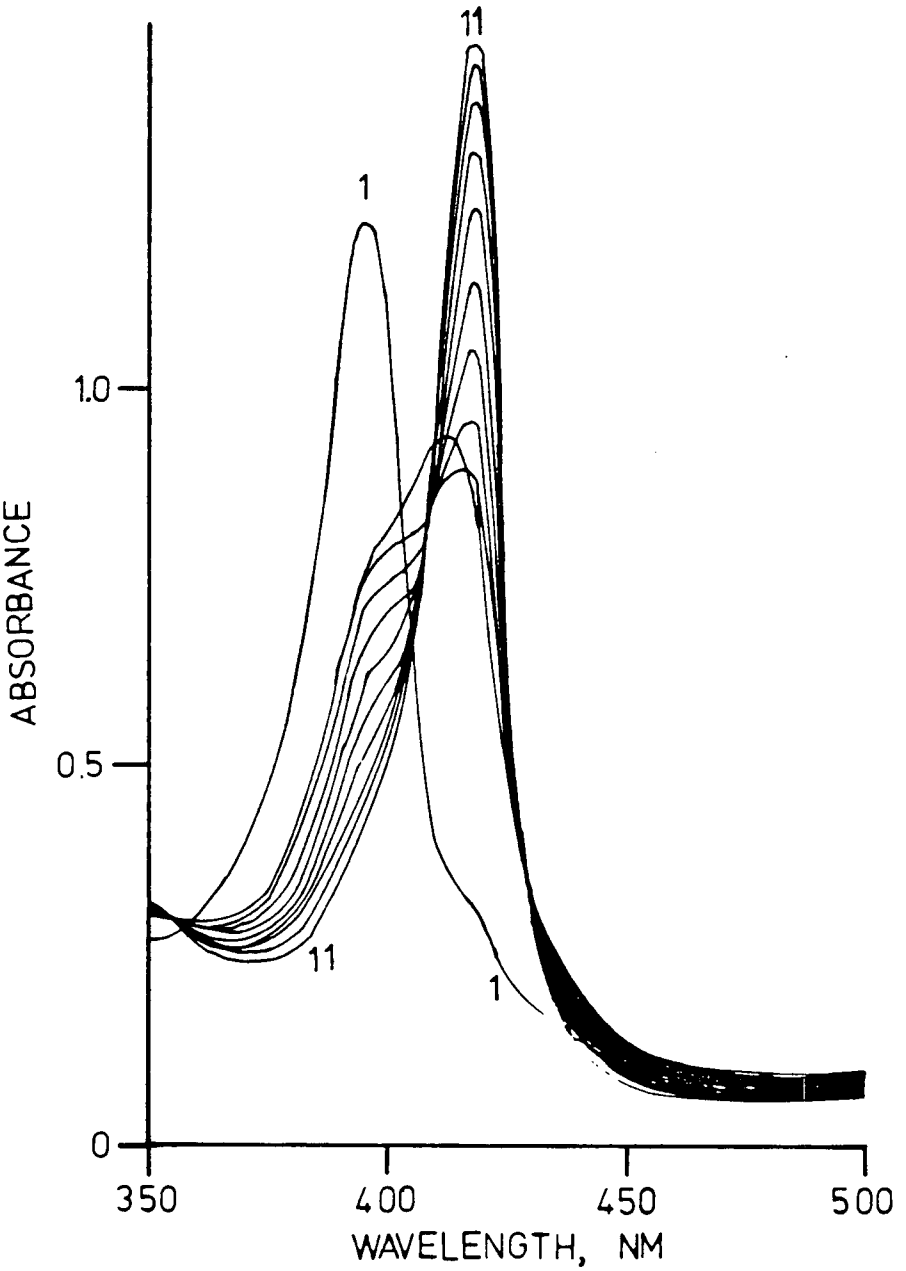

Figure VII.2. Spectra showing the oxidation of CH_3-ImCoEpI by 800 Torr O_2 in DCE @ 20°C.

For raw data see Appendix Vee.

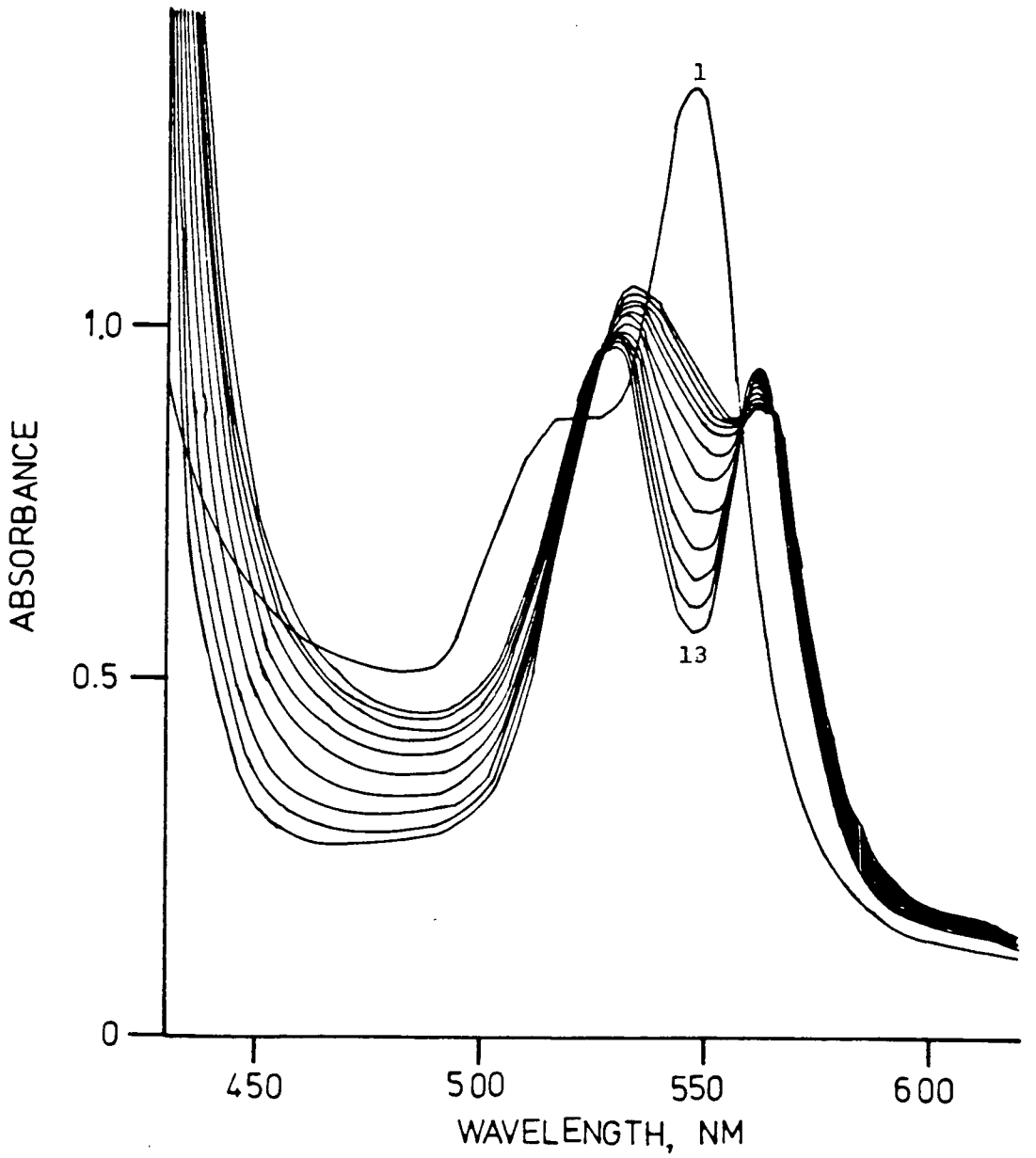

Figure VII.3. Spectra showing the oxidation of CH_3-ImCoOEP by 800 Torr O_2 in DCE @ 30°C.

For raw data see Appendix Vff.

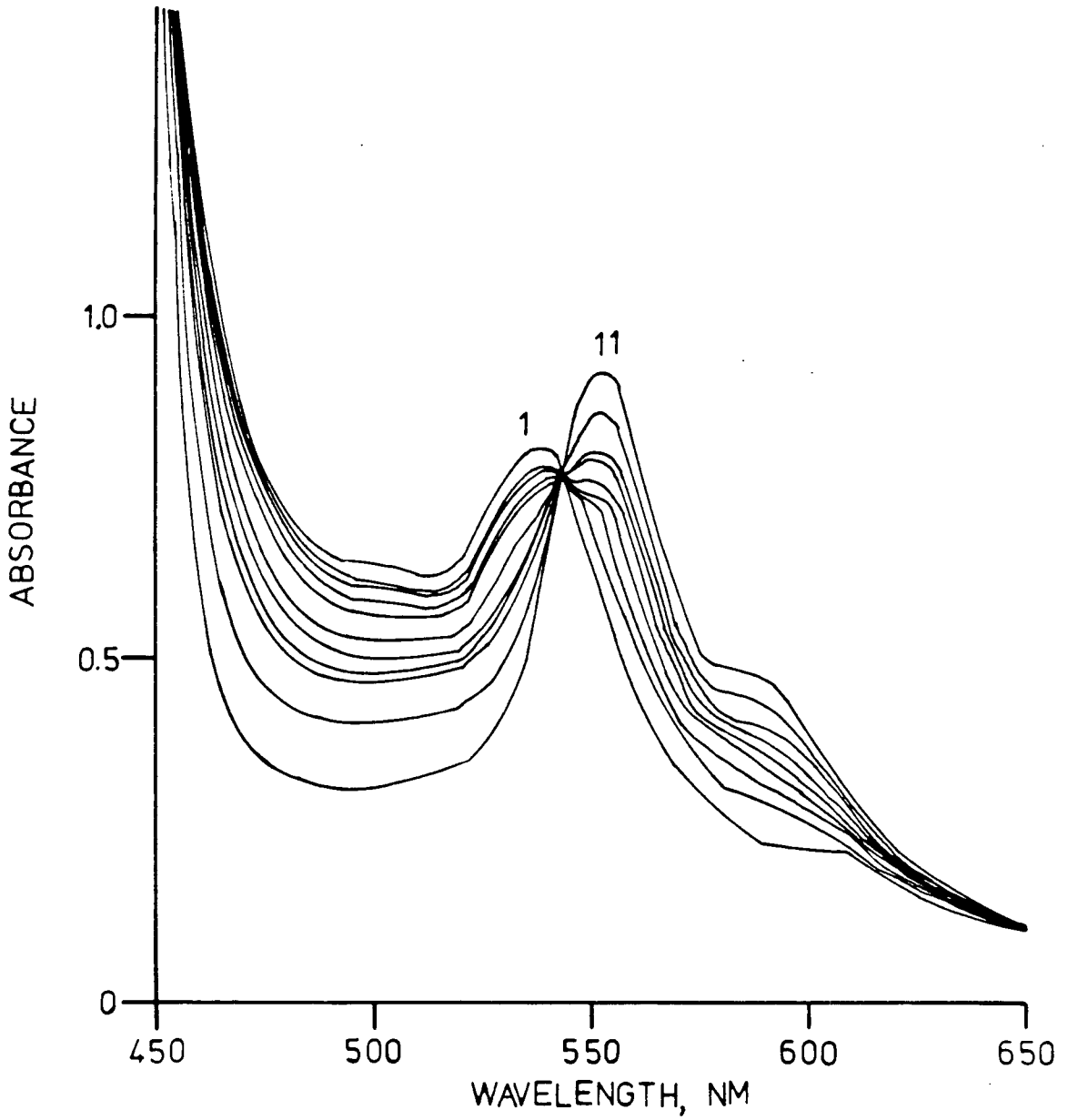

Figure VII.4. Spectra showing the oxidation of CH_3-ImCoTPP by 800 Torr O_2 in DCE @ 20°C.

For raw data see Appendix Vcc.

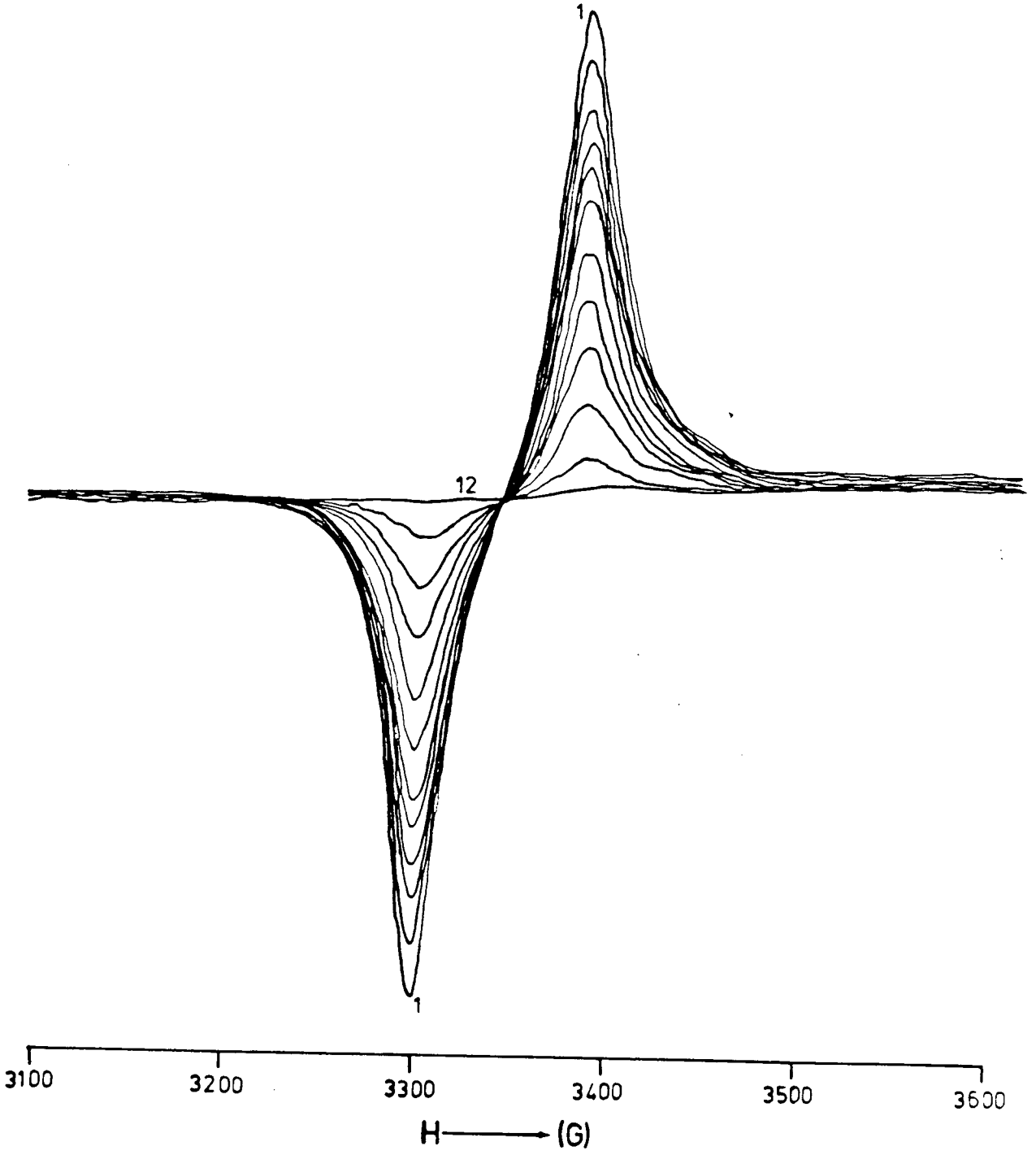

Figure VII.5. ESR signals showing the oxidation of CH_3-ImEpI by 800 Torr O_2 in DCE @ 22°C.

For raw data see Appendix Vdd.

Table VII.1 Spectral Data From 350 to 750 nm for the Reaction:

$2L_nCoP + O_2 \longrightarrow LCoP(O_2)CoPL + 2(n-1)L$ (P represents a porphyrin)

Absorbing Specicies	Absorption Maxima (nm) (Extinction Coefficient, $M^{-1}cm^{-1}$)						Isosbestic Points (nm)				
ImCoOMBP	407	(6.5×10^4)	618	(4.6×10^4)							
↓							425	510	630		
$(ImCoOMBP)_2(O_2)$	442	(7×10^4)	628	(4.2×10^4)							
CH_3-ImCoOMBP	408	(6.5×10^4)	618	(4.7×10^4)							
↓							428		630		
$(CH_3\text{-}ImCoOMBP)_2(O_2)$	444	(9.2×10^4)	629	(4.7×10^4)							
PipCoOMBP	408	(6.5×10^4)	618	(4.7×10^4)							
↓							396	427	624		
$(PipCoOMBP)_2(O_2)$	440	(8.5×10^4)	629	(4.7×10^4)							
PyCoOMBP	407	(5.6×10^4)	618	(4.6×10^4)							
↓											
$(PyCoOMBP)_2(O_2)$	443	(9.3×10^4)	634	(4.8×10^4)							
CH_3-ImCoEpI	395	(1.0×10^5)	546	(1.6×10^4)							
↓							361	408	438	558	568
$(CH_3\text{-}ImCoEp)_2(O_2)$	418	(1.3×10^5)	539	(1.2×10^4)	562	(1.1×10^4)					
CH_3-ImCoOEP	395	(1.1×10^5)	547	(1.8×10^4)							
↓							358	408	428	544	557 565
$(CH_3\text{-}ImCoOEP)_2(O_2)$	418	(1.8×10^5)	539	(1.4×10^4)	562	(1.3×10^4)					

Table VII.1 contd. Spectral Data From 350 to 750 nm for the Reaction:

$2L_nCoP + O_2 \longrightarrow LCoP(O_2)CoPL + 2(n-1)L$ (P represents porphyrin)

Absorbing Species	Absorption Maxima (nm) (Extinction Coefficient, $M^{-1}cm^{-1}$)						Isosbestic Points (nm)			
CH_3-ImCoPpIXDME	404	(1.0×10^5)	556	(7.2×10^3)			365	416	440	572
$(CH_3\text{-ImCoPpIXDME})_2(O_2)$	426	(1.1×10^5)	540	(5.5×10^3)	574	(5.3×10^3)				
CH_3-ImCoTPP	412	(2.4×10^5)	540	(1.5×10^4)			372	424	454	547
$(CH_3\text{-ImCoTPP})_2(O_2)$	434	(3.0×10^5)	556	(1.8×10^4)						
$(CH_3\text{-Im})_2$CoOMBP	435	(9.2×10^5)	457	(7.6×10^4)	618	(4.5×10^4)	360	430	454	623
$(CH_3\text{-ImCoOMBP})_2(O_2)$	442	(9.7×10^4)	632	(5.0×10^4)						
$(Pip)_2$CoOMBP	430	(9.4×10^4)	456	(4.8×10^4)	618	(3.8×10^4)	418	435	458	
$(PipCoOMBP)_2(O_2)$	440	($\sim 9 \times 10^4$)	630	($\sim 5 \times 10^4$)						
Py_2CoOMBP	428	(8.2×10^4)	618	(4.3×10^4)			436	458	629	
$(PyCoOMBP)_2(O_2)$	442	(9.7×10^4)	635	(4.8×10^4)						

All the above spectral characteristics were measured in DCE except for the ImCoOMBP and $(CH_3\text{-Im})_2$CoOMBP systems, which were studied in toluene.

VII.3 Treatment of Data

The oxidation reactions were followed by observing the decrease in the intensity of the Soret band of the non oxidized species or the increase in the Soret band of the oxidized species for the CoOMBP systems. In the other cobalt porphyrin systems, the Soret band was usually so sharp that accurate absorbance readings were often difficult to achieve at the various stages of oxidation, and so Soret changes were usually monitored only when cobalt dependence studies were done at low concentration. On the other hand, changes in the visible band could be readily followed.

The observed reaction rate was often first order in cobalt and the observed rate constant could readily be determined under pseudo first order conditions by the standard relationship:

$$\ln \frac{A - A_\infty}{A_o - A_\infty} = -k_{obs} t \qquad \text{(VII.3)}$$

where A is the absorbance at time, t

A_∞ is the absorbance at the completion of the reaction

A_o is the absorbance at the start of the reaction

and k_{obs} is the observed rate constant.

Dependence on other parameters, such as oxygen pressure and ligand concentration, was obtained by noting how the pseudo first order rate constant changed as a particular parameter was varied.

The reaction rate was sometimes not first order in cobalt, and attempts to analyze for other reaction orders (e.g. second order, three halves order, and half order) were not generally successful. In such cases the reaction rate is usually reported in terms of the first half life at a particular cobalt concentration.

VII.4 Aggregation

For the LCoPpIXDME + O_2 system in toluene, a first order reaction rate dependence had been established for cobalt[123]. However, the dependence on cobalt in the LCoOMBP system in toluene, when the ligand was CH_3-Im, Pip or Py, was found in this work to be less than first order. Because of this, the possibility of CoOMBP complexes forming aggregates at higher cobalt concentrations was investigated.

Porphyrins have been long known to aggregate, and the subject has been recently reviewed[136]. As early as 1937[137] a variety of free porphrins was shown to form films on water surfaces, in which the polar side chains were in the water, while the more hydrophobic parts of the molecule were stacked face to face. The ability of these porphyrins to form face to face stacks diminishes as the solvent is changed from water to ones of lower dielectric constant[138]. Porphyrin aggregates tend to break up as temperature increases[139], or in the case of metalloporphyrins, if a coordinating solvent is added[136a], although this may only change the form of aggregation[140].

In metalloporphyrins the nature of the metal is important in determining to what extent the complex will aggregate. Weaker solvation of the metal will result in a greater tendency of the metalloporphyrin complexes to aggregate. In non aqueous solutions, Cu(II), Ni(II), Zn(II), and Pd(II) porphyrin complexes aggregate more readily than the corresponding free porphyrins[141], although there is little Zn(II) porphyrin aggregation in aqueous solutions[142]. The higher oxidation state of the metal, the less a metalloporphyrin will tend to aggregate. For example Mn(II) hematoporphyrin in 0.1 M KOH was shown to be aggregated, while the Mn(IV) complex did not aggregate under the same conditions[143].

ESR and NMR have been used to study aggregation in 10^{-3} to 10^{-4} M porphyrin and metalloporphyrin systems where spin pairing[144] is monitored in the former, and chemical shift in the latter[145]. Porphyrin concentrations in UV-VIS observations are usually a couple of orders of magnitude lower than in resonance studies. If the porphyrin complex does not obey Beer's Law and an isosbestic point is found in dilution studies where the amount of porphyrin in the light path is kept constant, this is taken as strong evidence for porphyrin dimerization or further aggregation[139,142,146]. To further corroborate evidence of aggregation, temperature jump kinetic behavior of the porphyrin system may be noted[147]. In the case of Mn(III) hematoporphyrin aggregation has been demonstrated by polarographic[148] and kinetic studies[149], while Beer's Law for this system was observed[143,149].

An observed aggregation of CoOMBP in toluene at spectroscopic concentrations (10^{-6} - 10^{-4} M) during the present studies is especially interesting as neither free nor metallo-porphyrins have been reported to aggregate in non aqueous solvents under these conditions[136a,150], although they have been shown to aggregate at concentrations used in ESR[144] and NMR[151] studies. OMBP, with its rigid planar structure and highly aromatic nature, might be expected to be especially prone to aggregation in non aqueous solvents. In fact NiOMBP, when partially oxidized by I_2[152], has been shown to exhibit unidirectional conduction properties as NiOMBP is able to form "infinite" closely packed stacks.

The change in extinction coefficient of CoOMBP as a function of concentration is shown in Figure VII.6. A gradual decrease in extinction coefficient of the CoOMBP in solution of both the Soret and the visible band was observed with increasing concentration in both toluene and DCE, with the Soret band blue shifting by about 10 nm.

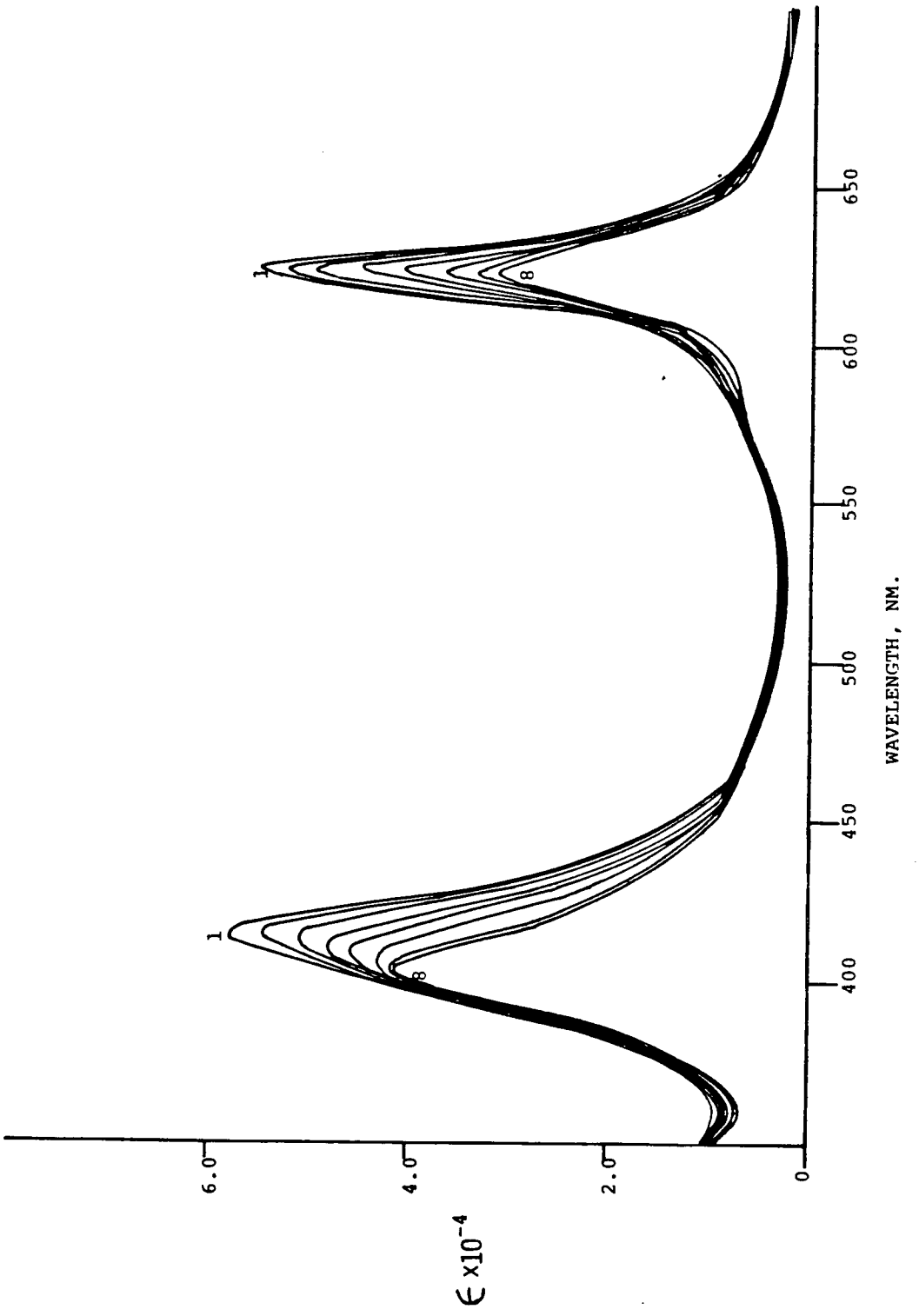

Figure VII.6. Visible spectra of CoOMBP as a function of concentration @ 22°C in toluene.

For raw data see Appendix Va.

The aggregation reaction is:

$$n\text{CoOMBP} \rightleftharpoons (\text{CoOMBP})_n \qquad \text{(VII.4)}$$

From considerations in Chapter III.2 it can be shown that

$$[\text{CoOMBP}] = \frac{\varepsilon - \varepsilon_\infty}{\varepsilon_o - \varepsilon_\infty}[\text{Co}_T] \qquad \text{(VII.5)}$$

$$\text{and } [(\text{CoOMBP})_n] = \frac{1}{n} \cdot \frac{\varepsilon_o - \varepsilon}{\varepsilon_o - \varepsilon_\infty}[\text{Co}_T] \qquad \text{(VII.6)}$$

where $[\text{Co}_T]$ is the concentration of total cobalt present

ε_o is the molar extinction coefficient of CoOMBP

and ε_∞ is the cobalt molar extinction coefficient of $(\text{CoOMBP})_n$.

$$\text{Therefore } K_{agg} = \frac{[(\text{CoOMBP})_n]}{[\text{CoOMBP}]^n} = \frac{\frac{1}{n}\cdot\frac{\varepsilon_o - \varepsilon}{\varepsilon_o - \varepsilon_\infty}[\text{Co}_T]}{\left(\frac{\varepsilon - \varepsilon_\infty}{\varepsilon_o - \varepsilon_\infty}[\text{Co}_T]\right)^n} \qquad \text{(VII.7)}$$

$$\text{and } \log n + \log K_{agg} + n\log\frac{\varepsilon - \varepsilon_\infty}{\varepsilon_o - \varepsilon_\infty}[\text{Co}_T] = \log\frac{\varepsilon_o - \varepsilon}{\varepsilon_o - \varepsilon_\infty}[\text{Co}_T] \qquad \text{(VII.8a)}$$

$$\text{or } \log n + \log K_{agg} + n\log[\text{CoOMBP}] = \log n[(\text{CoOMBP})_n] \qquad \text{(VII.8b)}$$

where K_{agg} is the aggregation equilibrium constant.

Therefore, a plot of $\log n[(\text{CoOMBP})_n]$ vs. $\log[\text{CoOMBP}]$, values which are readily determined from the spectroscopic data, should give a line with the slope n and the intercept $\log n + \log K_{agg}$.

A difficulty in analyzing these data arose in not being able to experimentally find limiting extinction coefficients. At low cobalt concentration ($\sim 10^{-6}$ M) the observed absorbance of solutions with the same measured cobalt concentration fluctuated by 10 - 15%, compared with

absorbance variance at ~10^{-5} M of about 3%. At the higher cobalt concentrations the spectral peaks moved off scale, and so extinction coefficient determinations could not be made. However, by assigning to the visible band an ε_o value of 6.2 x 10^4 $M^{-1}cm^{-1}$ and an ε_∞ value of 2.4 x 10^4 $M^{-1}cm^{-1}$, a straight line with a slope of 1.98 was obtained (Figure VII.7). K_{agg} was determined to be 1.3 x 10^4 M^{-1} in toluene and ~1.5 x 10^4 M^{-1} in DCE. Although these results could not be checked by temperature jump kinetics due to the nature of the solvent, they are indicative of the presence of a dimer of CoOMBP in the above solvents. In $CHCl_3$ solutions, aggregates formed from the π-π interactions of the porphyrin tend to be dimers at concentrations where NMR can be used[148].

The presence of a CoOMBP dimer could have effects on measuring ligand binding constants. However, in these studies the CoOMBP concentrations were of the order of 2 x 10^{-6} M, and under these conditions the monomer constitutes more than 95% of the cobalt concentration (~1.92 x 10^{-6} M). Even at the concentrations where most of the oxidation kinetics were carried out (~2 x 10^{-5} M), the amount of CoOMBP monomer present in the absence of ligand would be ~1.7 x 10^{-5} M. When oxidation is studied, at least 95% of the CoOMBP is initially converted to LCoOMBP, and this would further reduce the concentration of any dimer (~3 x 10^{-7} M).

Beer's Law studies were also carried out on five-and six-coordinate CoOMBP complexes in both toluene and DCE. However, no deviations were detected (Figures VII.8,9).

From these studies, formation of a CoOMBP dimer is clearly important, although the concentration of that dimer is not significant under the conditions used to measure the ligand binding constants. No visible spectral evidence is found for aggregation of the five-and six-coordinate complexes,

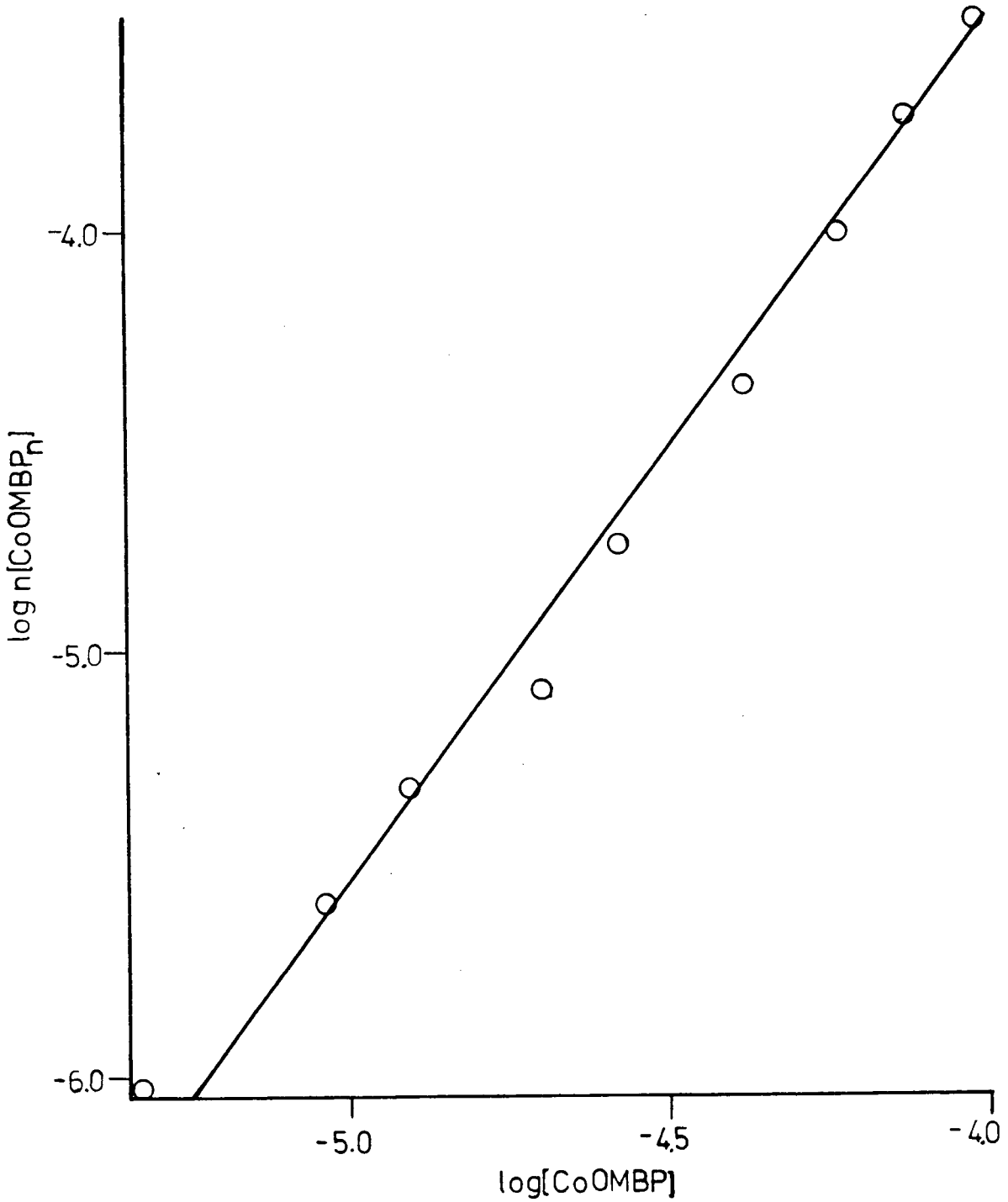

Figure VII.7 Aggregation plot of CoOMBP in toluene @ 22°C.

For raw data see Appendix Va.

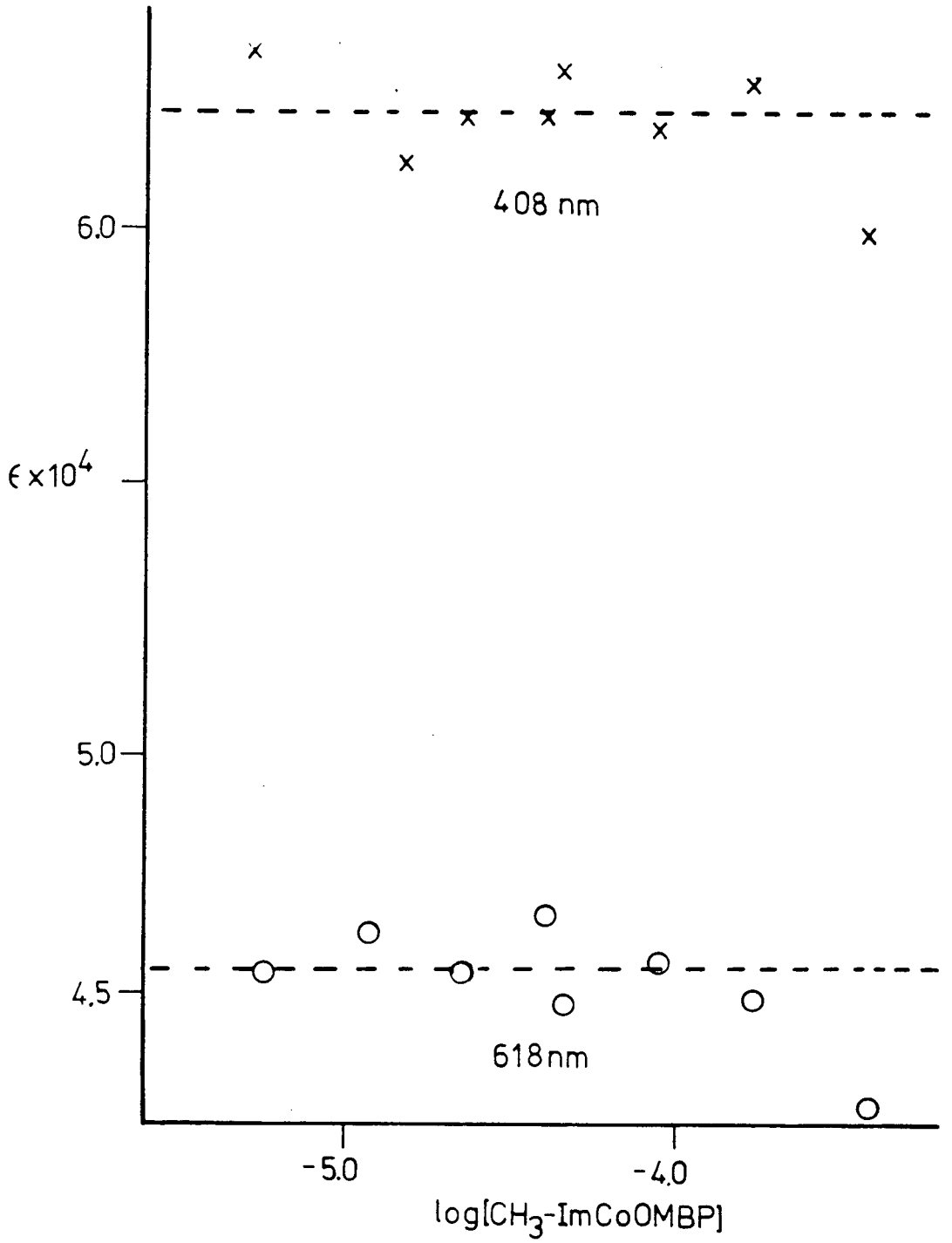

Figure VII.8 Beer's Law plots of CH_3-ImCoOMBP in toluene @ 22°C.

For raw data see Appendix Va.

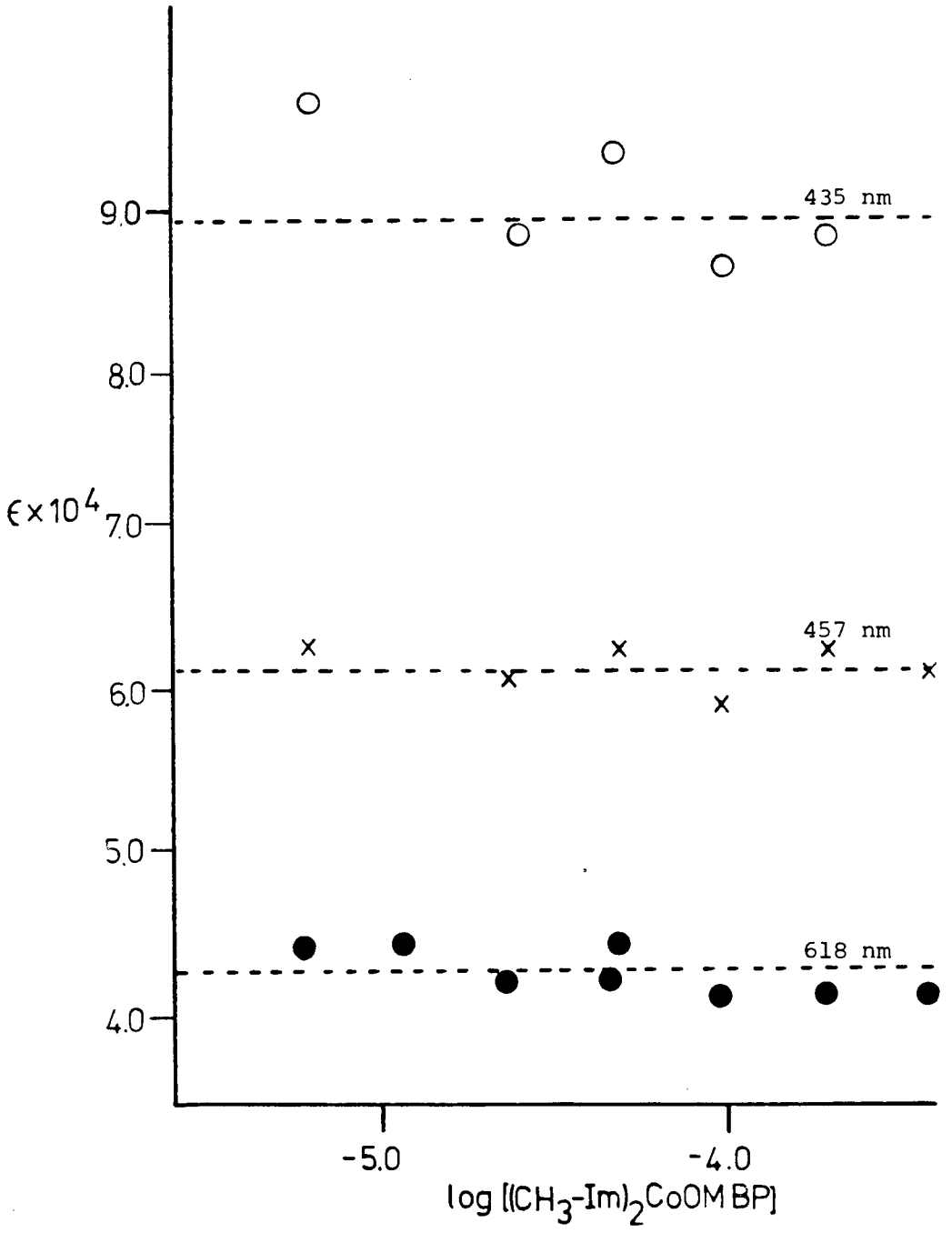

Figure VII.9 Beer's Law plots of $(CH_3\text{-Im})_2$CoOMBP in toluene @ 22°C

For raw data see Appendix Va.

although this cannot be entirely ruled out, as aggregation has been noted in six-coordinate Mn(III) hematoporphyrin systems[148,149], although Beer's Law appeared to be obeyed[143,149].

ESR studies have been extensively used to investigate cobalt(II) porphyrin systems[136a,153]. While a signal is readily detected for CH_3-ImCoPpIXDME at concentrations of 10^{-3} M in toluene (Figure VII.10), signals for CH_3-ImCoOMBP solutions under similar conditions are weak and ill defined, as are signals for comparable solutions of $(CH_3\text{-Im})_2$CoOMBP. This suggests that some spin pairing mechanism likely exists in CoOMBP systems that does not exist in CoPpIXDME systems. One possible way is for the CoOMBP moieties, even in five-or six-coordinate systems, to dimerize.

NMR studies on dicyanohemin[140] have shown that that six-coordinate complex in methanol exists as a dimer, which is formed by a π-π linkage of a pyrrole ring of each of the component molecules. A similar mechanism of aggregation could operate for the five-and six-coordinate CoOMBP systems.

VII.5 Kinetics of the Oxidation of LCoOMBP

VII.5.1 Kinetics of the Oxidation of ImCoOMBP in Toluene

When a solution of ImCoOMBP in toluene was exposed to one atmosphere of oxygen, rapid oxidation of the system was observed and the reaction rates were thus monitored primarily at lower oxygen pressures where more readily measurable rates prevailed. Although there was no detectable amount of the ImCoPpIXDME(O_2) complex in the previously reported ambient temperature kinetic studies[123], observation of a rapid initial spectral change in the present work led to the conclusion that there was some initial ImCoOMBP(O_2) formation during the kinetic studies. Calculations based on the thermodynamic

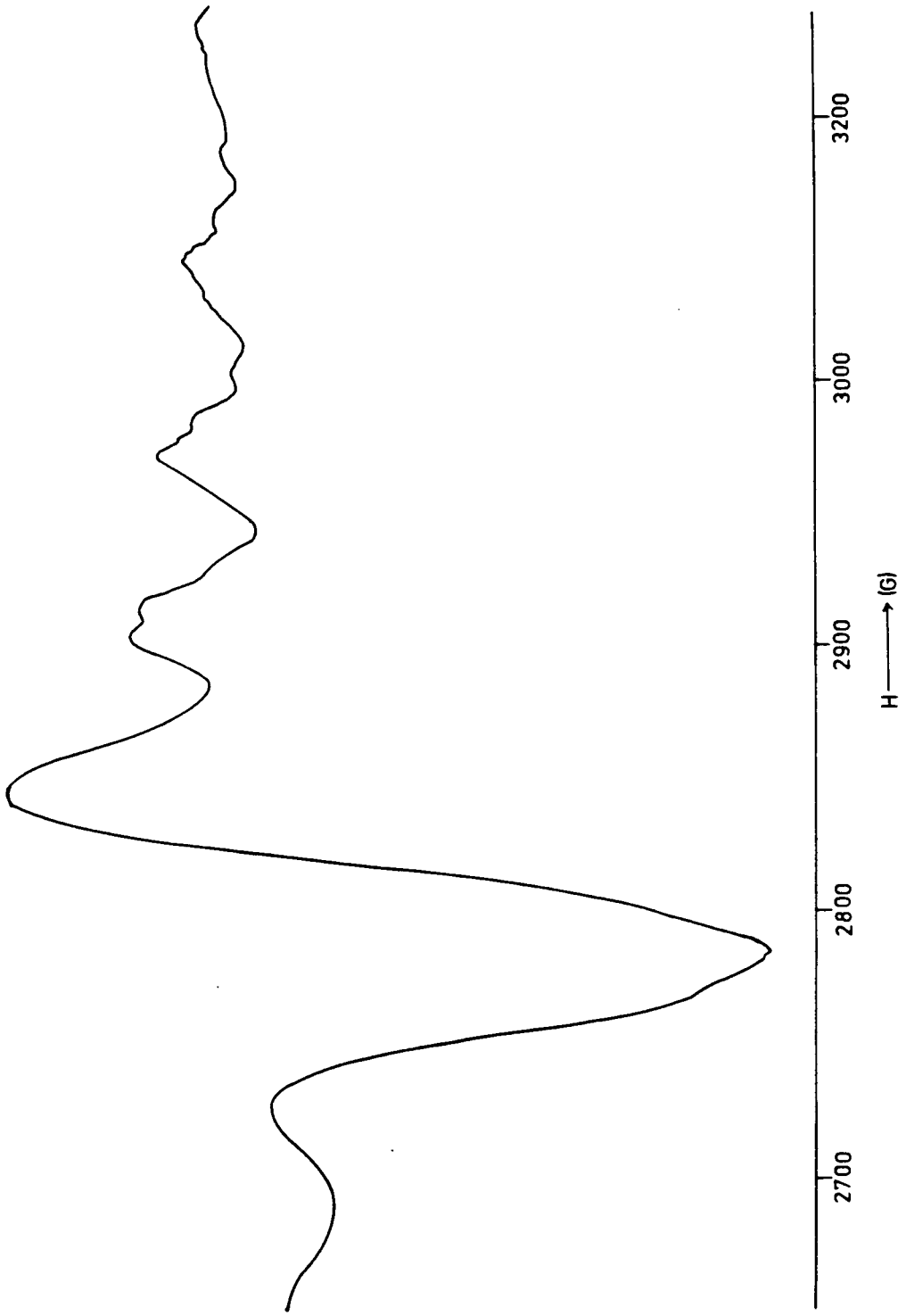

Figure VII.10 ESR spectrum of CH_3-ImCoPpIXDME in toluene @ 77 K.

data of oxygen binding to CoOMBP-amine systems (Chapter IV) also predict about 10 to 20% formation of the 1:1 cobalt:dioxygen adduct at 20°C under one atmosphere of oxygen pressure, and the spectral evidence was compatible with this.

A set of spectra resulting from the oxidation of ImCoOMBP is shown in Figure VII.11, and a summary of the kinetic data is presented in Tables VII.2a-h. At lower concentrations of ImCoOMBP (up to ~10^{-5} M) the pseudo first order rate constants remained effectively constant (Tables VII.2e,f), but at higher cobalt concentrations (up to ~2.5 x 10^{-4} M), k_{obs} values increased with increasing cobalt concentration (Tables VII.2f,g). The oxygen concentrations in solution (~10^{-3} M atm^{-1}[123]) were such that they remained effectively constant during a kinetic run, and a plot of k_{obs} vs. oxygen pressure (Figure VII.12) indicates a reasonable first order dependence on oxygen pressure (but the order may be decreasing at higher pressures). The dependence on ligand concentration (Figure VII.13) approached first order at low concentrations, but decreased toward zero order at higher concentrations. These dependences are similar to those observed for the oxidation of the ImPpIXDME system[123]. (However, no decrease in oxygen dependence was observed in that system).

There is some question about the exact nature of the final product (e.g. ImCo(III)OMBP$(OH)^-$ could be formed by abstraction of a ligand or even a solvent hydrogen). The presence of isosbestic points probably rules out slow formation of the hydroxide product through a possible slowly formed peroxide bridged intermediate. Also the spectrum of the final product is similar to that of the 1:1 cobalt:dioxygen adduct, and other related systems have been shown to give a bridged dimer[23c]. Therefore, the product is thought to be the bridged dimer ImCoOMBP(O_2)CoOMBP·Im.

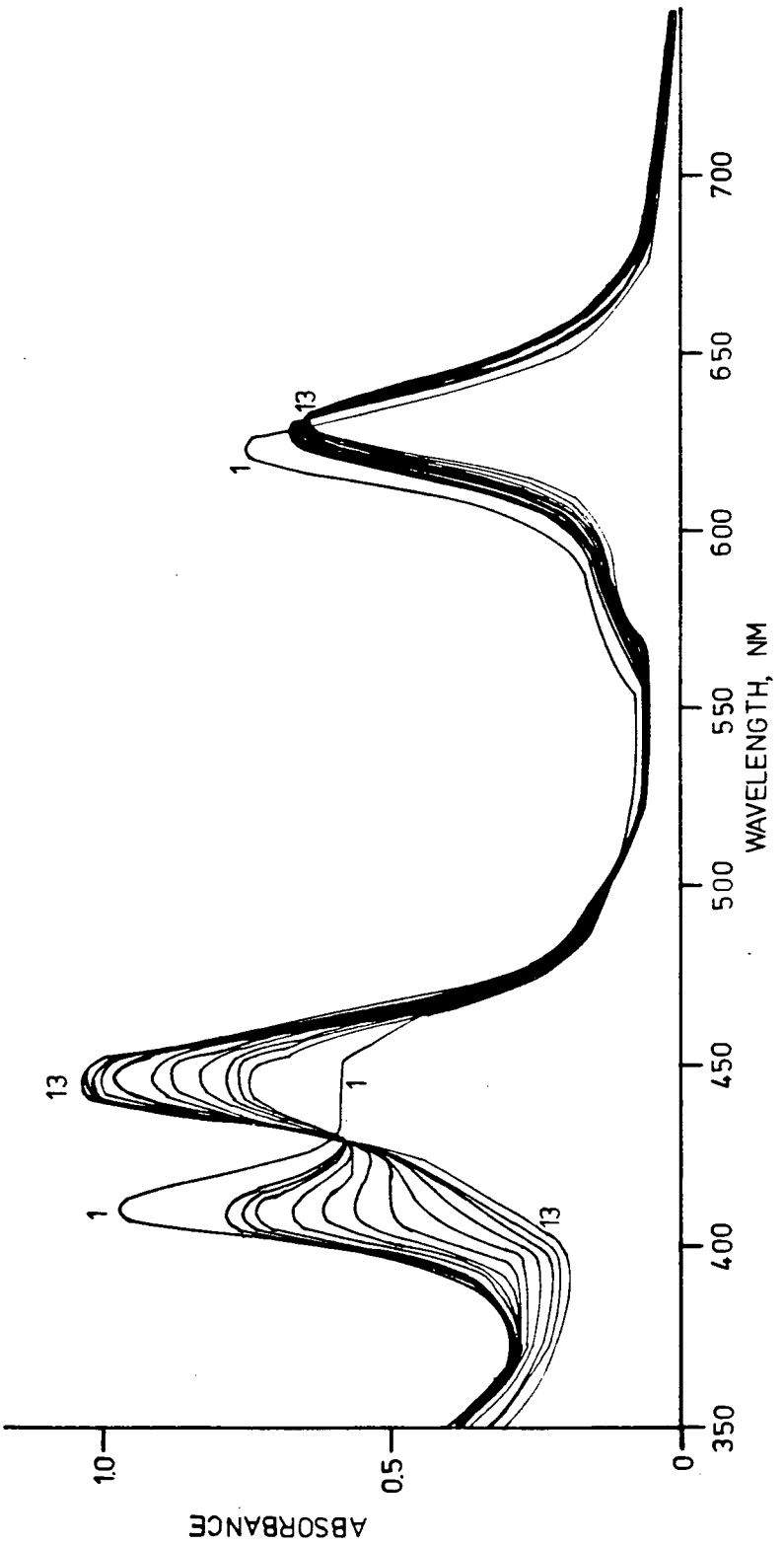

Figure VII.11 Spectra showing the oxidation of 2×10^{-5} M ImCoOMBP by 395 Torr O_2 @ 22°C; for raw data see Appendix Ve. ([Im] = 0.55×10^{-4} M)

Table VII.2a. Kinetic Data for the Oxidation of ImCoOMBP as a Function of Oxygen Pressure.

[Co], M	P_{O_2}, Torr	Temperature, °C	[Im], M	k_{obs}, sec^{-1}
1.9×10^{-5}	54	22	14.6×10^{-4}	1.66×10^{-3}
1.8×10^{-5}	97	22	14.6×10^{-4}	2.92×10^{-3}
1.8×10^{-5}	147	22	14.6×10^{-4}	4.03×10^{-3}
1.7×10^{-5}	190	22	14.6×10^{-4}	4.75×10^{-3}
1.8×10^{-5}	278	22	14.6×10^{-4}	7.15×10^{-3}

Table VII.2b. Kinetic Data for the Oxidation of ImCoOMBP as a Function of Ligand Concentration; Oxygen Pressure ~100 Torr.

[Co], M	P_{O_2}, Torr	Temperature, °C	[Im], M	k_{obs}, sec^{-1}
1.6×10^{-5}	95	22	2.2×10^{-4}	0.82×10^{-3}
1.7×10^{-5}	95	22	4.4×10^{-4}	1.39×10^{-3}
1.8×10^{-5}	96	22	7.3×10^{-4}	2.03×10^{-3}
1.7×10^{-5}	95	22	9.2×10^{-4}	2.08×10^{-3}
1.8×10^{-5}	97	22	14.6×10^{-4}	2.92×10^{-3}
1.6×10^{-5}	95	22	18.4×10^{-4}	3.59×10^{-3}
1.7×10^{-5}	95	22	29.2×10^{-4}	4.77×10^{-3}

Table VII.2c. Kinetic Data for the Oxidation of ImCoOMBP as a Function of Ligand Concentration; Oxygen Pressure ~ 400 Torr.

[Co], M	P_{O_2}, Torr	Temperature, °C	[Im], M	k_{obs}, sec^{-1}
2.0×10^{-5}	395	22	0.55×10^{-4}	0.80×10^{-3}
1.7×10^{-5}	405	22	1.1×10^{-4}	1.26×10^{-3}
1.9×10^{-5}	395	22	2.2×10^{-4}	2.43×10^{-3}
1.7×10^{-5}	397	22	4.4×10^{-4}	3.73×10^{-3}

Table VII.2d. Kinetic Data for the Oxidation of ImCoOMBP as a Function of Ligand Concentration; Oxygen Pressure ~ 800 Torr.

[Co], M	P_{O_2}, Torr	Temperature, °C	[Im], M	k_{obs}, sec^{-1}
1.8×10^{-5}	825	22	0.15×10^{-4}	0.20×10^{-3}
1.9×10^{-5}	825	22	0.23×10^{-4}	0.51×10^{-3}
1.7×10^{-5}	825	22	0.30×10^{-4}	1.00×10^{-3}
1.6×10^{-5}	825	22	0.60×10^{-4}	1.49×10^{-3}
1.7×10^{-5}	825	22	1.2×10^{-4}	2.11×10^{-3}

Table VII.2e. Kinetic Data for the Oxidation of ImCoOMBP as a Function of Cobalt Concentration; Oxygen Pressure ~160 Torr, Imidazole Concentration ~1.8×10^{-3} M.

[Co], M	P_{O_2}, Torr	Temperature, °C	[Im], M	k_{obs}, sec^{-1}
0.06×10^{-5}	160	22	18.4×10^{-4}	4.6×10^{-3}
0.1×10^{-5}	160	22	18.4×10^{-4}	4.4×10^{-3}
0.2×10^{-5}	160	22	18.4×10^{-4}	4.5×10^{-3}

Table VII.2f. Kinetic Data for the Oxidation of ImCoOMBP as a Function of Cobalt Concentration; Oxygen Pressure ~100 Torr, Imidazole Concentration ~1.8×10^{-3} M.

[Co], M	P_{O_2}, Torr	Temperature, °C	[Im], M	k_{obs}, sec^{-1}
0.8×10^{-5}	100	22	18.4×10^{-4}	2.56×10^{-3}
1.6×10^{-5}	95	22	18.4×10^{-4}	3.48×10^{-3}†
2.4×10^{-5}	100	22	18.4×10^{-4}	3.52×10^{-3}†
4.5×10^{-5}	100	22	18.4×10^{-4}	4.18×10^{-3}†
7.0×10^{-5}	100	22	18.4×10^{-4}	5.68×10^{-3}†
8.0×10^{-5}	100	22	18.4×10^{-4}	5.92×10^{-3}†

† "k_{obs}" in these cases determined from initial linear regions obtained from first order in cobalt analyses. In these experiments reasonable first order plots could be achieved over 75% of the reaction before the deviations became marked.

Table VII.2g. Kinetic Data for the Oxidation of ImCoOMBP as a Function of Cobalt Concentration; Oxygen Pressure ~100 Torr, Imidazole Concentration ~1.5×10^{-3} M.

[Co], M	P_{O_2}, Torr	Temperature, °C	[Im], M	k_{obs}, sec^{-1}
1.8×10^{-5}	97	22	14.6×10^{-4}	2.96×10^{-3} ≠
13×10^{-5}	100	22	14.6×10^{-4}	4.34×10^{-3} ≠
23×10^{-5}	95	22	14.6×10^{-4}	7.02×10^{-3} ≠

Table VII. 2h. Kinetic Data for the Oxidation of ImCoOMBP as a Function of Temperature.

[Co], M	P_{O_2}, Torr	Temperature, °C	[Im], M	k_{obs}, sec^{-1}
2.3×10^{-5}	97	10	14.6×10^{-4}	3.78×10^{-3}
1.8×10^{-5}	97	22	14.6×10^{-4}	2.92×10^{-3}
2.6×10^{-5}	98	30	14.6×10^{-4}	2.46×10^{-3}
1.6×10^{-5}	100	35	14.6×10^{-4}	1.87×10^{-3}

≠ "k_{obs}" in these cases determined from initial regions obtained from first order in cobalt analyses. In these experiments deviation from first order occurred very quickly (e.g. at less than 25% of extent of reaction). The reactions could not be analyzed for second order in cobalt, and attempts to graphically determine the reaction order did not produce linear plots, presumably because the reaction order in cobalt changes as the cobalt concentration changes. Better first order approximations occurred at lower cobalt concentrations.

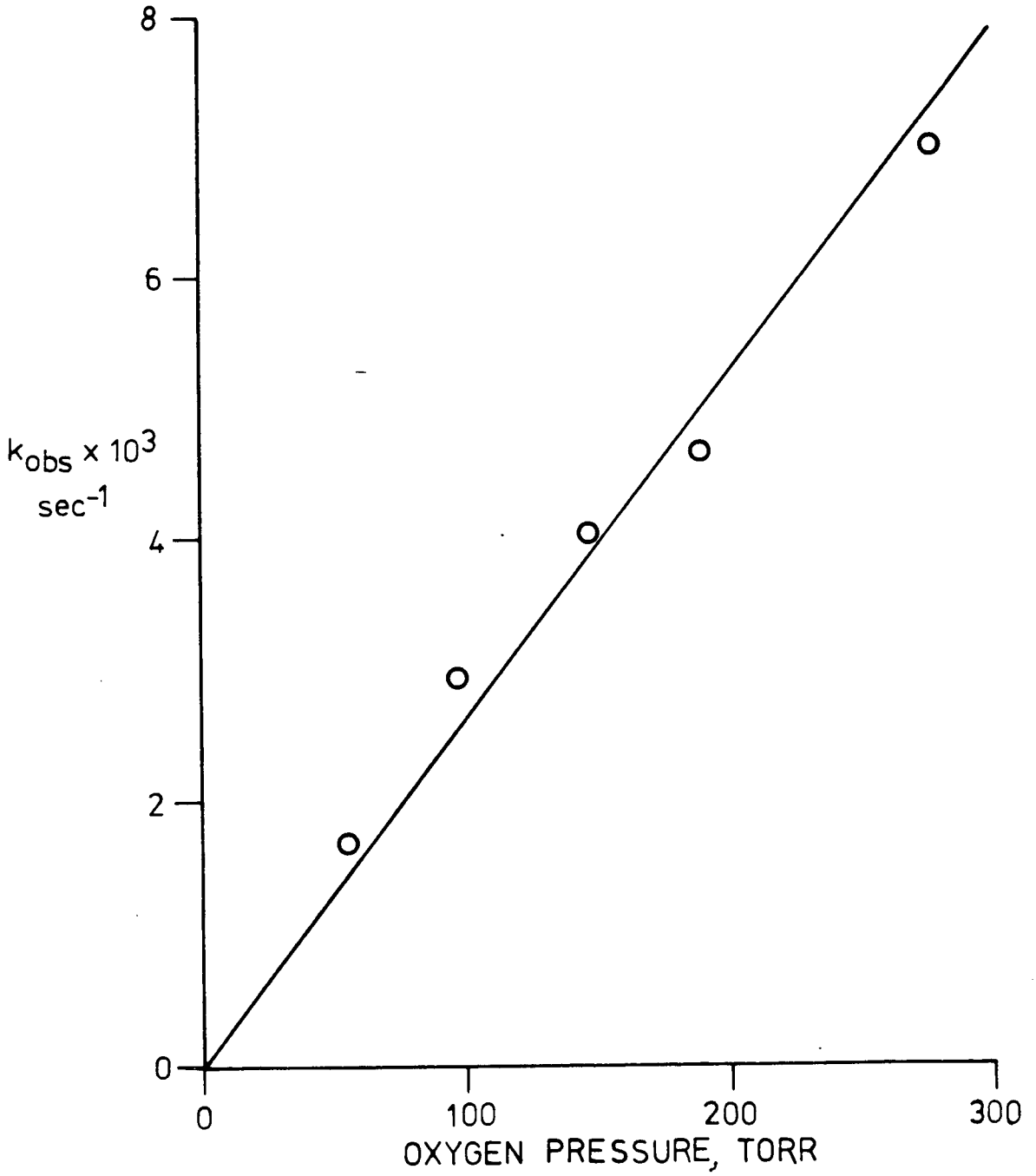

Figure VII.12 Oxidation rate of ImCoOMBP as a function of oxygen pressure.

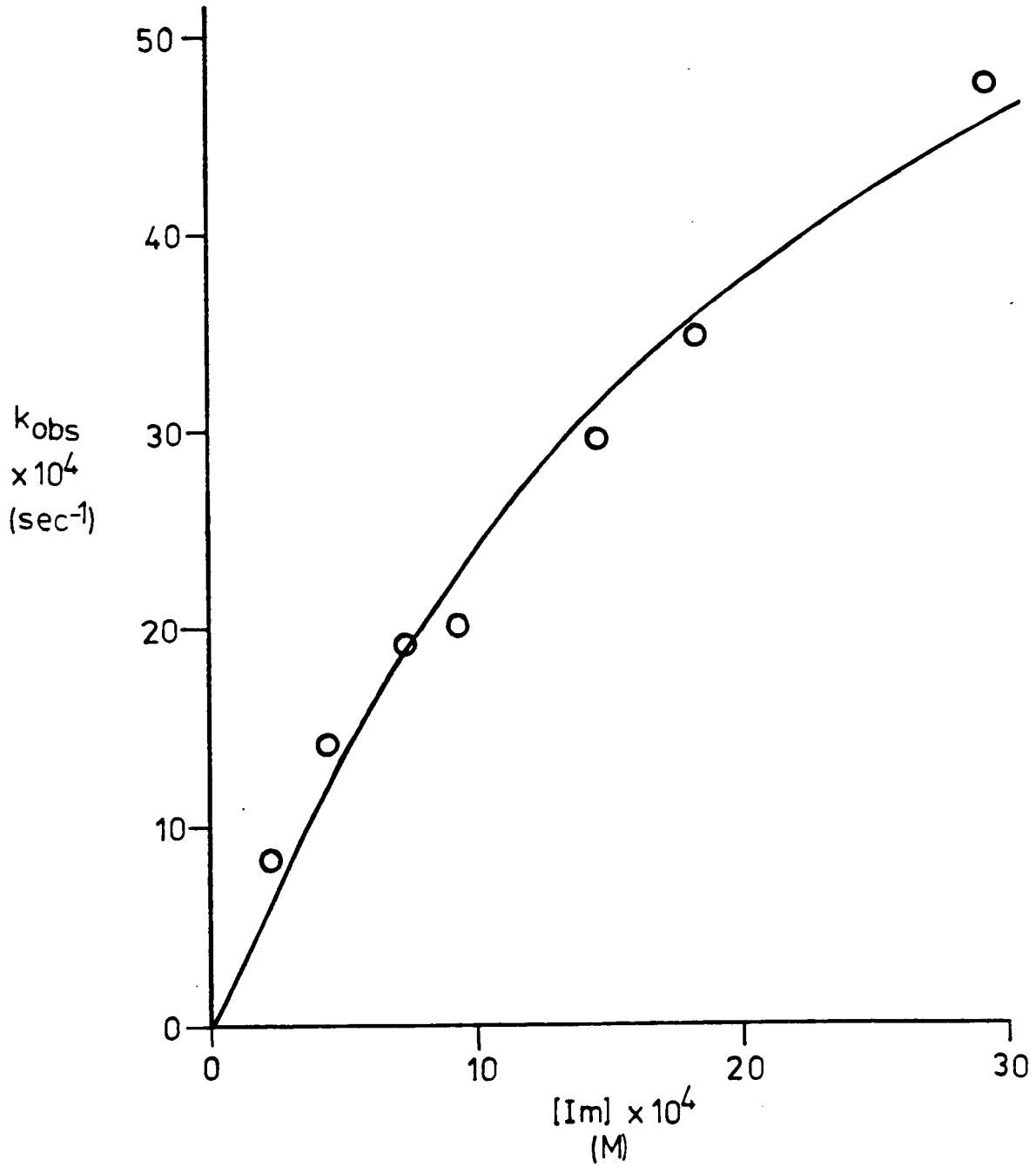

Figure VII.13 Oxidation rate of ImCoOMBP as a function of Im concentration.

Since a rapid initial equilibrium is observed for the reaction

$$\text{ImCoOMBP} + O_2 \rightleftharpoons \text{ImCoOMBP}(O_2) \qquad \text{(VII.9)}$$

this cannot be the rate determining step although it would be consistent with first order rate dependence on both Co and O_2.

The mechanism proposed previously for the oxidation of the ImCoPpIXDME[123] system was:

$$\text{Im} + \text{CoPpIXDME} \overset{K_1}{\rightleftharpoons} \text{ImCoPpIXDME} \qquad \text{(VII.10)}$$

$$\text{ImCoPpIXDME} + O_2 \overset{K_{O_2}}{\rightleftharpoons} \text{ImCoPpIXDME}(O_2) \qquad \text{(VII.11)}$$

$$\text{ImCoPpIXDME}(O_2) \xrightarrow{k^*} \text{ImCoPpIXDME}(O_2)^* \qquad \text{(VII.12)}$$

$$\text{ImCoPpIXDME}(O_2)^* + \text{ImCoPpIXDME} \xrightarrow{\text{fast}} \text{ImCoPpIXDME}(O_2)\text{CoPpIXDME}\cdot\text{Im} \qquad \text{(VII.13)}$$

This led to the rate law:

$$\frac{d}{dt}[\text{product}] = \frac{k^* K_1 K_{O_2} [O_2][L][Co]_T}{1 + K_1[L]} \qquad \text{(VII.14)}$$

where $[Co]_T$ is the total concentration of reactant cobalt.

In the CoPpIXDME systems[123] the Im complex was found to oxidize faster than other five-coordinate amine complexes, and this was rationalized in terms of Im forming a hydrogen bond with the O_2 moiety of both species in reaction VII.12, particularly in the transition state where charge separation would be more important.

In the CoPpIXDME system[123] the first to zero order dependence in Im was explained in terms of formation of ImCoPpIXDME under the conditions of oxidation. This was supported by plotting k_{obs}^{-1} vs. $[L]^{-1}$; from the intercept/slope a K_1 value similar to that obtained spectrophotometrically was obtained. However, in the studies on the CoOMBP system, the Im

concentration was such that the ImCoOMBP species was fully formed (Chapter III), and the plot of k_{obs}^{-1} vs $[Im]^{-1}$ (Figure VII.14) yielded an intercept/slope value of $7 \times 10^2\ M^{-1}$, substantially lower than the spectrophotometrically determined K_1 value of $9 \times 10^3\ M^{-1}$. Therefore, an explanation of the observed Im dependence in terms of formation of a hydrogen bonded Im to the O_2 moiety of ImCoOMBP(O_2) seems reasonable.

Although the oxidation of the CoPpIXDME system[123] was first order in cobalt at all concentrations studied, the cobalt dependence of the CoOMBP system became greater than first order at higher cobalt concentrations. Oxidation through a bimolecular pathway at higher cobalt concentrations would explain this observation.

Considering that CoOMBP dimerizes, the overall mechanism becomes:

$$\tfrac{1}{2}(\text{CoOMBP})_2 \underset{}{\overset{K_D}{\rightleftharpoons}} \text{CoOMBP} \qquad \text{(VII.15)}$$

$$\text{Im} + \text{CoOMBP} \overset{K_1}{\rightleftharpoons} \text{ImCoOMBP} \qquad \text{(VII.16)}$$

$$\text{ImCoOMBP} + O_2 \overset{K_{O_2}}{\rightleftharpoons} \text{ImCoOMBP}(O_2) \qquad \text{(VII.17)}$$

$$\text{ImCoOMBP}(O_2) + \text{ImCoOMBP} \xrightarrow{k_d} \text{ImCoOMBP}(O_2)\text{CoOMBP}\cdot\text{Im} \qquad \text{(VII.18)}$$

$$\text{ImCoOMBP}(O_2) + \text{Im} \overset{K_{int}}{\rightleftharpoons} \text{ImCoOMBP}(O_2)\cdots\text{Im} \qquad \text{(VII.19)}$$

$$\text{ImCoOMBP}(O_2)\cdots\text{Im} \xrightarrow{k^*} \text{ImCoOMBP}(O_2)^*\cdots\text{Im} \qquad \text{(VII.20)}$$

$$\text{ImCoOMBP}(O_2)^*\cdots\text{Im} + \text{ImCoOMBP} \xrightarrow{k_{fast}} \text{ImCoOMBP}(O_2)\text{CoOMBP}\cdot\text{Im} + \text{Im} \qquad \text{(VII.21)}$$

The overall rate law would then be:

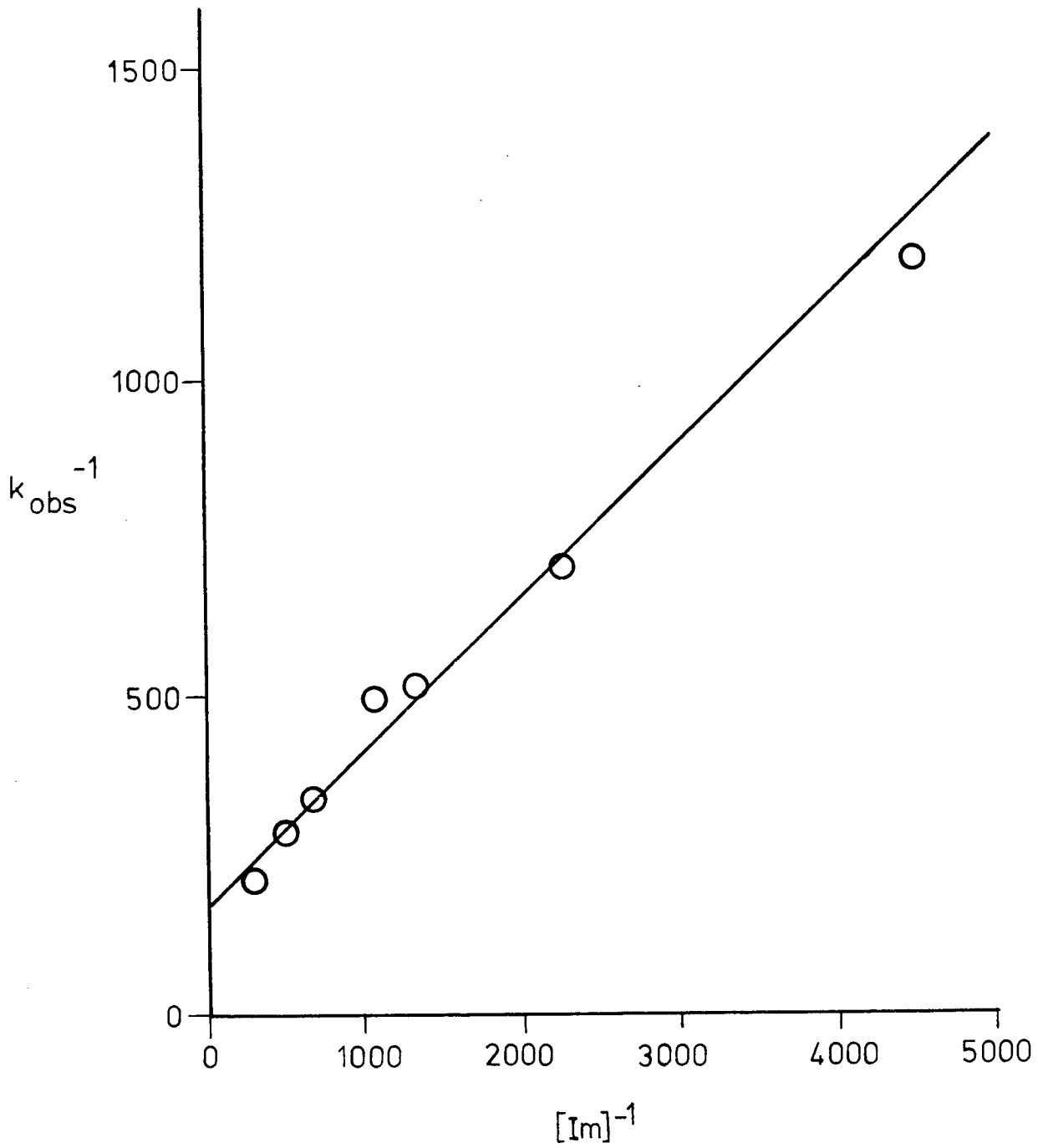

Figure VII.14 Analysis of Im dependence on the oxidation of ImCoOMBP

$$\frac{d}{dt}[\text{product}] = \frac{K_1K_{O_2}[Im][O_2][Co]_T}{((1 + K_1[Im] + K_1K_{O_2}[Im][O_2] + K_1K_{O_2}K_{int}[Im]^2[O_2])^2 + \frac{2[Co]_T}{K_D^2}\Big)^{\frac{1}{2}}}$$

$$\times \left(K_{int}k^*[Im] + \frac{k_dK_1[Im][Co]_T}{((1 + K_1[Im] + K_1K_{O_2}[Im][O_2] + K_1K_{O_2}K_{int}[Im]^2[O_2])^2 + \frac{2[Co]_T}{K_D^2}\Big)^{\frac{1}{2}}}\right) \quad \text{(VII.22)}$$

Under the experimental conditions used, the amount of $(CoOMBP)_2$ present was negligible and the ImCoOMBP species was essentially fully formed. When this is taken into consideration the overall rate law simplifies to:

$$\frac{d}{dt}[\text{product}] = \frac{K_{O_2}[O_2][Co]_T}{(1 + K_{O_2}[O_2] + K_{int}K_{O_2}[Im][O_2])}$$

$$\times \left(K_{int}k^*[Im] + \frac{k_d[Co]_T}{(1 + K_{O_2}[O_2] + K_{int}K_{O_2}[Im][O_2])}\right) \quad \text{(VII.23)}$$

From this rate law it can be seen that second order dependence on cobalt is only observed if $k_d[Co]_T$ is large. If $k_d[Co]_T$ is negligible and [Im] is relatively small, the reaction is first order in Im. At higher Im concentrations the reaction would become zero order in Im. Experiments were not carried out at higher Im concentrations since Im aggregation becomes important[154]. First order dependence in oxygen is observed if very little of the 1:1 cobalt: dioxygen adduct is initially formed.

At sufficiently low concentrations of cobalt, where most of the studies were carried out, the reaction becomes first order in cobalt and obeys the rate law:

$$\frac{d}{dt}[\text{product}] = \frac{K_{O_2} K_{int} k^{*} [O_2][Im][Co_T]}{(1 + K_{O_2}[O_2] + K_{int} K_{O_2}[Im][O_2])} \qquad \text{(VII.24)}$$

According to Equation VII.24, under conditions where the reaction is predominantly first order in cobalt, a intercept/slope value obtained from a plot of k_{obs}^{-1} vs $[Im]^{-1}$ (as in Figure VII.14) represents $\frac{K_{int} K_{O_2}[O_2]}{1 + K_{O_2}[O_2]}$. Since the amount of dioxygen adduct formed under the conditions of this work has been estimated to be on the order of 10% (see p 175), an estimate of K_{int} being about 10^4 M^{-1} can be made. The ability of ImCoOMBP(O_2) to form a hydrogen bonded adduct Im must be less than that of ImCoPpIXDME(O_2), where the corresponding species was thought to be completely formed when any dioxygen adduct was available to interact with any hydrogen bonding Im[123]. This appears consistent with the weaker basicity of OMBP[96], since the weakly basic porphyrin would be less able to transfer electron density to the dioxygen moiety, and thus make it less susceptible to hydrogen bonding.

The intercept value in Figure VII.14 is equivalent to k^{*-1} and gives a k^{*} value of approximately 6×10^{-3} sec^{-1}. This compares to a k^{*} value of 1.0×10^{-1} sec^{-1} in the ImCoPpIXDME system[123]; the difference between the two systems can possibly be accounted for by the relative basicities of the porphyrins used in the two systems.

The pseudo first order rate constant increased as the temperature was lowered (Figure VII.15, Table VII.2h, $\Delta H^{\ddagger}$ = -4.2 kcal/mole, and $\Delta S^{\ddagger}$ = -84 eu). This observation is consistent with an increase in K_{O_2} and K_{int} at low

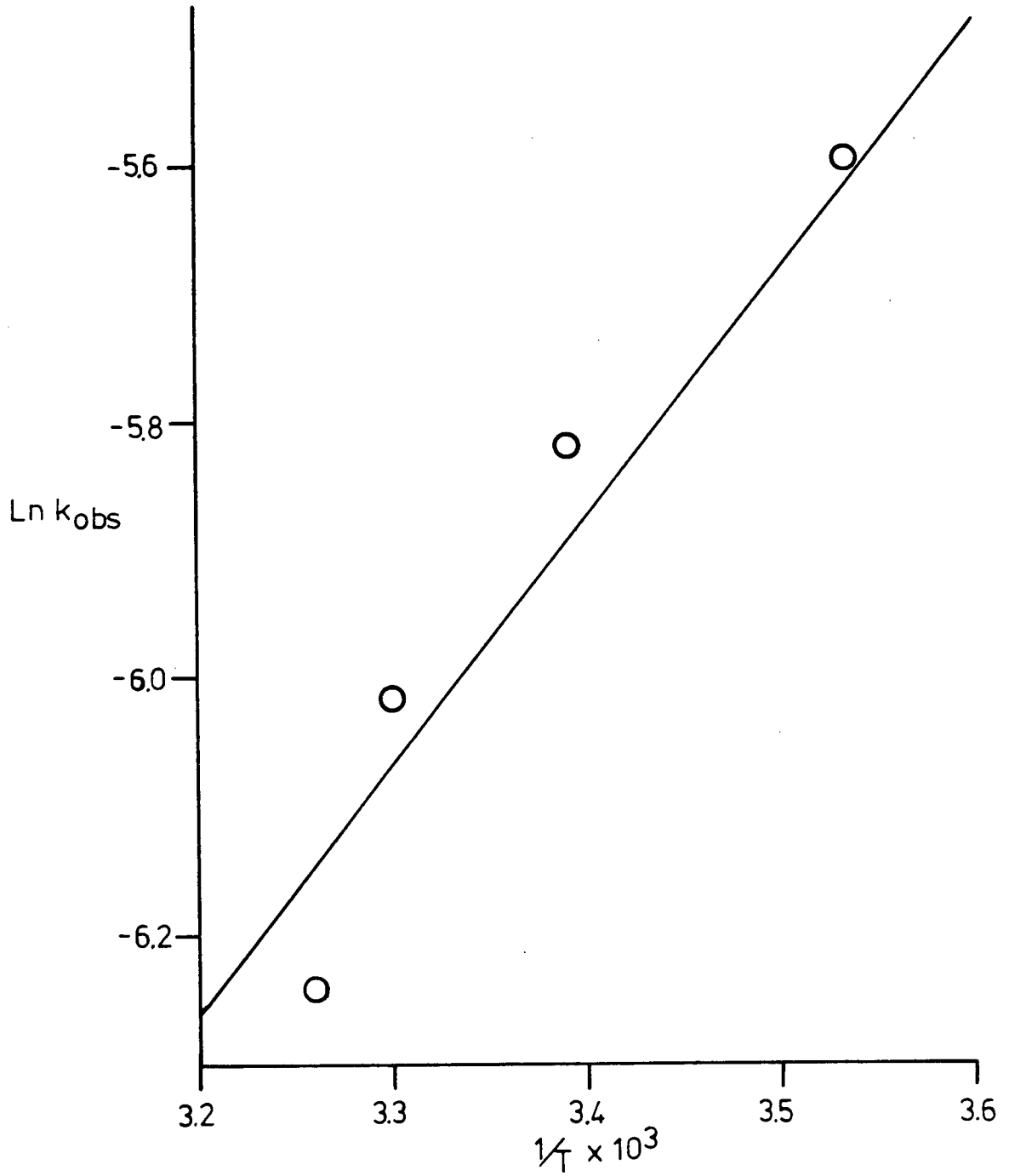

Figure VII.15 Arrhenius plot for the oxidation of ImCoOMBP.

temperatures; both of theses values would be expected to be associated with exothermic processes. Although a decrease in the rate constant k^* must occur, this is not sufficient to counteract the above enhancements to the pseudo first order constant.

VII.5.2 Kinetics of the Oxidation of LCoOMBP in Toluene, L = CH_3-Im, Pip, or Py

When toluene solutions of five-coordinate LCoOMBP (L = CH_3-Im, Pip, or Py) were exposed to about an atmosphere of oxygen at 20°C, an initial rapid decrease in Soret intensity was noted. This was followed by a slow further decrease in Soret intensity with an absorbance increase in the 440 nm region. Isosbestic points were maintained for several hours, but then lost as the reaction proceeded. The reaction approached 95% completion after times up to one week. The reaction was monitored by visible spectroscopy, ESR, and gas-uptake. As the concentration of LCoOMBP was increased, the time required to complete the reaction increased until at some of the highest concentrations used (~2×10^{-2} M), no oxygen-uptake was observed. ESR signals of the 1:1 cobalt:dioxygen adduct (@ ~10^{-3} M Co) were detected throughout the course of the reaction.

The observation of the initial decrease in Soret intensity is consistent with the formation of a 1:1 cobalt:dioxygen adduct at room temperature in toluene. This conclusion is supported by the observation that the amount of initial Soret change is dependent on the oxygen pressure (Appendix V.j) and by calculations based on the thermodynamic data of CoOMBP-amine oxygenation (Chapter IV) which predict that about 20% of the dioxygen adduct would be present at 20°C. This ambient temperature detection of the oxygenation adduct contrasts with observations for the

CoPpIXDME[89.91c], CoMpIXDME[91c], and CoDpIXDME[91c] systems in which no observable amount of reversible oxygenation occurred in toluene.

In experiments with varying ligand concentrations, essentially the same oxidation rates were observed. The ligand concentrations (3×10^{-4} - 10^{-2} M) were such that full formation of the five-coordinate adduct was accomplished. This implies that, in contrast to the ImCoOMBP system, the ligand plays no role in the oxidation of the complex other than forming the oxygen-sensitive five-coordinate adduct. Figure VII.16 shows oxidation vs. time curves for CH_3-ImCoOMBP as a function of cobalt concentration. If the oxidation mechanism present in the ImCoOMBP system (Eq. VII.15-VII.21) were applicable in the CH_3-ImCoOMBP system, then a first order dependence in cobalt should be observed. Although a reasonable first order dependence was observed at lower concentrations (~10^{-6} M), the reaction took longer to complete at higher cobalt concentrations, contrary to expectation if "dimerization" occurred by a rate determining direct reaction of CH_3-ImCoOMBP(O_2) and CH_3-ImCoOMBP. Similar kinetic dependences were observed for the PipCoOMBP and PyCoOMBP systems. The oxidation rates for the latter two systems were somewhat less than for the CH_3-ImCoOMBP system and were not extensively investigated. The faster rate for the CH_3-ImCoOMBP system is consistent with larger initial oxygenation, as observed and calculated from the low temperature binding data, if the reaction occurs by a mechanism including steps similar to Eq. VII.15-VII.21.

ESR experiments were carried out on the LCoOMBP systems at 77 K. When these solutions (~10^{-3} M) were initially exposed to oxygen an intense 1:1 cobalt:dioxygen adduct signal was detected.If the solution were left for 12 h at ambient temperature, the intense cobalt:dioxygen signal at 77 K remained. Over a period of ten days at ambient temperature the dioxygen

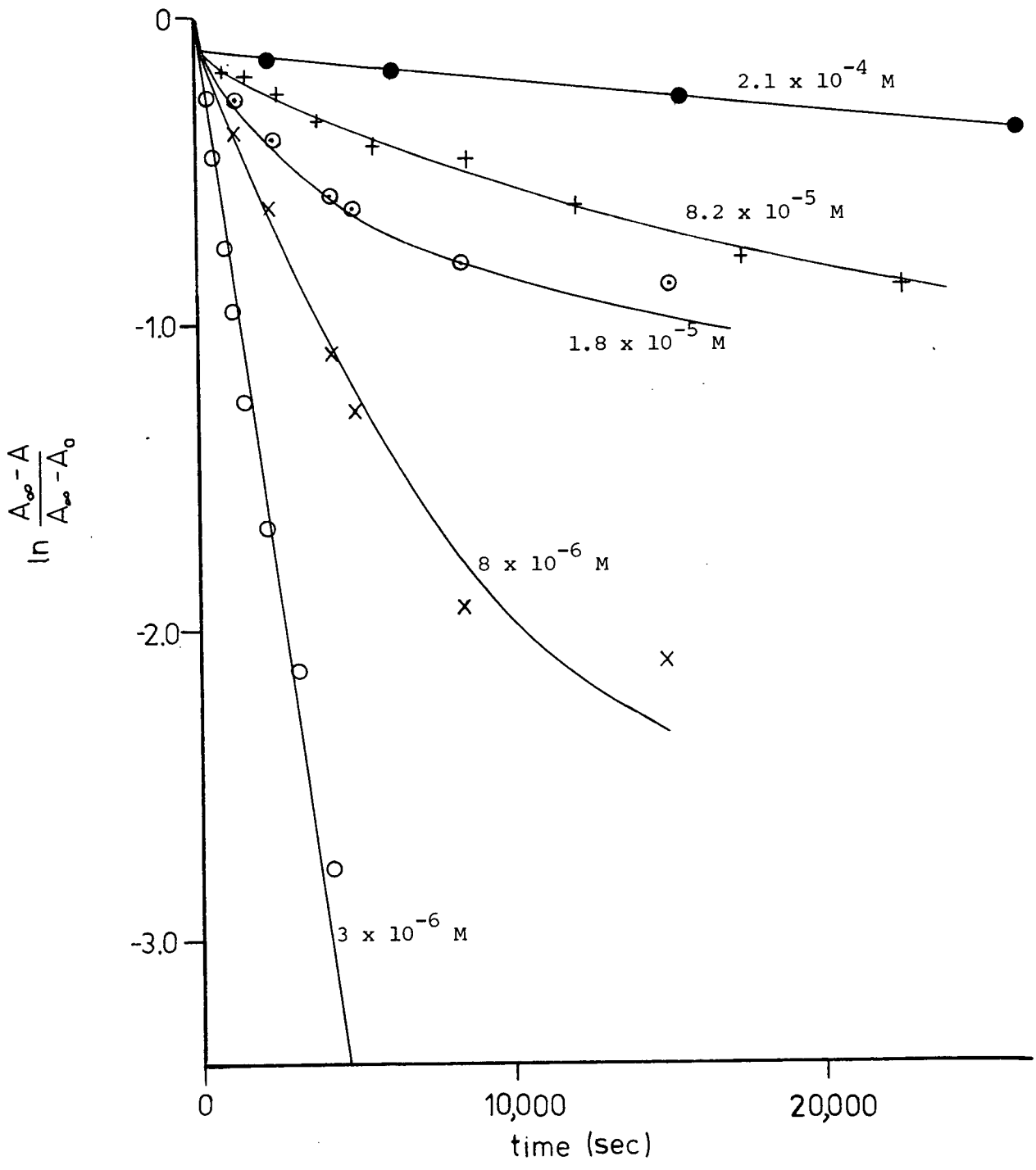

Figure VII.16 Oxidation of CH_3-ImCoOMBP analyzed for first order in cobalt at several cobalt concentrations.

adduct signal at 77 K was seen to decrease to about one tenth of its original intensity.

While the visible spectroscopy experiments were done on LCoOMBP solutions of 10^{-6} - 10^{-4} M, and the ESR measurements were carried out at LCoOMBP concentrations of 10^{-3} M, the gas-uptake determinations were made when the LCoOMBP concentrations approached 10^{-2} M. An experiment carried out on a 2×10^{-2} M LCoOMBP solution indicated no reaction whatsoever. At a concentration of 5×10^{-3} M the reaction approached only 10% completion after two days. When the solutions from the gas-uptake experiments were appropriately diluted, the visible spectra verified that very little oxidation had taken place. If a gas-uptake solution were taken to 77 K under oxygen, then a sharp ESR signal formed, indicating the presence of dioxygen adduct.

The above observations are consistent with the slow formation of oxidation products after an initial formation of a 1:1 cobalt:dioxygen adduct. That the reaction time is increased so markedly at higher cobalt concentrations implies that aggregation of the five-coordinate LCoOMBP probably plays a major role. As the dioxygen adduct is formed at low temperatures at a cobalt concentration where the oxidation reaction is effectively stopped at ambient temperature, it is concluded that oxygenation is more exothermic than the proposed aggregation process.

In spite of the above kinetic observations suggesting aggregation, no significant visible spectroscopic changes were detected as the concentrations of five-and six-coordinate CoOMBP adducts were varied from 5×10^{-6} - 5×10^{-4} M (Ch. VII.4). Therefore, the nature and degree of the aggregation could not be determined. A possible mode of aggregation could be similar to that which occurs in the dicyanohemin system[140], where a pyrrole ring of one porphyrin is weakly π-bonded to a pyrrole ring of another porphyrin. Since

the four-coordinate CoOMBP system, which could be expected to more readily form higher order aggregates[136a], tended to dimerize at concentrations where visible spectroscopic studies were carried out, dimerization of the five-coordinate CoOMBP systems appears to be the most likely extent of aggregation at concentrations used in visible spectroscopic determinations. Assuming that the five-coordinate complex does dimerize, the overall mechanism could be:

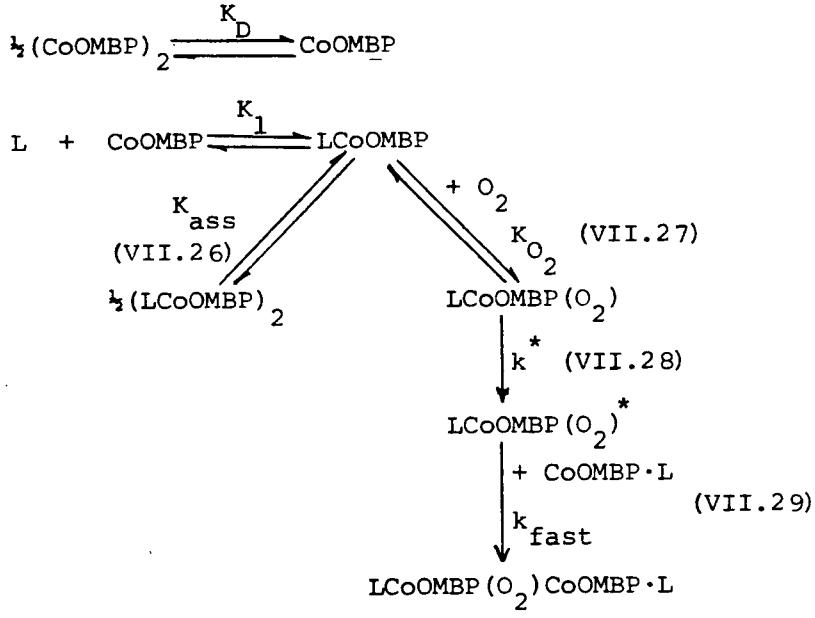

and the resulting rate law would be:

$$\frac{d}{dt}[\text{product}] = \frac{k^* K_{O_2} [O_2][Co]_T}{\sqrt{(1 + K_1^{-1}[L]^{-1} + K_{O_2}[O_2])^2 + 2[Co]_T(K_{ass}^2 + K_1^{-2}[L]^{-2} K_D^{-2})}} \quad \text{(VII.30)}$$

From this rate law it can be seen that as the concentration of cobalt increases, the dependence on cobalt decreases from first order to half order. This is consistent with the observed increase in oxidation time, although the order of the reaction could not be determined at higher concentrations, presumably because the order is increasing as the concentration

of reacting cobalt is decreasing during the course of a particular reaction. At higher cobalt concentrations aggregates greater than dimeric of the four- or five-coordinate species could be possible, and if such a higher order aggregate becomes the dominant form of cobalt, then the order in cobalt consumption would further decrease with increasing cobalt concentration. The oxygen dependence would decrease from first to zero order with increasing oxygen pressure as the 1:1 cobalt:dioxygen adduct becomes fully formed. Similarly the ligand dependence decreases from first to zero order as the five-coordinate adduct becomes fully formed. However, if the four-coordinate dimer is dominant the ligand dependence would be first order; if the five-coordinate dimer is dominant the reaction rate is independent of ligand concentration.

Under the experimental conditions used in these studies, there is almost no four-coordinate dimer present and the five-coordinate LCoOMBP species is essentially fully formed. The overall rate law then simplifies to

$$\frac{d}{dt}[\text{product}] = \frac{k^{*}K_{O_2}[O_2][Co]_T}{\sqrt{(1 + K_{O_2}[O_2])^2 + 2[Co]_T K_{ass}}^2} \qquad \text{(VII.31)}$$

The main contrast in the oxidation rates of the CH_3-Im, Pip, and Py CoOMBP systems to the ImCoOMBP system is the marked relative slowness of the former systems. As has been noted when Im is present, the reaction rate is dependent on the concentration of Im, even when the five-coordinate adduct is fully formed, presumably because the Im helps form the intermediate oxygenation species, possibly by a hydrogen bond from the acidic proton of Im. CH_3-Im, Pip, and Py have no acidic protons and no ligand concentration enhancement of oxidation is observed. Also in the ImCoOMBP system there is no kinetic evidence for the role of ImCoOMBP aggregates. Perhaps the acidic

proton of Im hinders aggregate formation; pseudo first order reactions can be observed when $[Co]_T$ is monitored. Support of this supposition is obtained from studies on the oxidation of the ImCoPpIXDME system where the kinetics of that system were explained by proposing that Im is associated with the porphyrin complex before oxygenation occurs[123]. Similar association of Im with CoOMBP could reasonably be expected to hinder aggregation. Although CH_3-Im, Pip, and Py do not enhance the oxidation rate the same way Im does, oxidation of LCoOMBP still appears to take place through an analogous $LCoOMBP(O_2)^*$ activated intermediate, since the oxidation reaction approaches first order in cobalt at lower concentrations of CoOMBP.

VII.5.3 Kinetics of the Oxidation of LCoOMBP in Solvents Other Than Toluene

VII.5.3.1 Kinetics of the Oxidation of CH_3-ImCoOMBP in a Variety of Solvents

Upon the observation that the CH_3-Im, Pip, and Py CoOMBP systems oxidized so slowly, with resulting difficulties in performing kinetic analyses, the oxidation rate was monitored in a series of somewhat more polar solvents. In order to avoid complicating side reactions, the solvent had to be essentially non coordinating and non protic. It was also desirable that the solvents have low freezing points so that oxygenation studies could be attempted. With the above requirements in mind, a series of chlorinated hydrocarbons; chlorobenzene (ε = 5.6), 1-chlorobutane (ε = 7.39), dichloromethane (ε = 8.93), and DCE (ε = 10.36)[155]; and a series of mixed toluene-DCE solvents; toluene:DCE 5:1 v/v (ε = 3.22), toluene:DCE 4:1 v/v (ε = 3.43), and toluene:DCE 1:1 (ε = 5.32) were used. Since the CH_3-ImCoOMBP system was found to have the highest and most convenient oxidation rates for study, this species was studied in the above solvents.

Trends observed in the more polar solvents were similar to those observed

in toluene. Although good isosbestic points occurred throughout the course of the reaction, the reactions usually did not analyze for first order in cobalt. When the cobalt concentration in dichloromethane was increased, the reaction took longer to proceed to completion. A more substantial spectral change was observed as the solvent became more polar, consistent with greater oxygenation in more polar media (Chapter IV). The reaction rate tended to increase with solvent polarity, although there was no general correlation between the reaction half life and ε (Table VII.3). However, a reasonable correlation existed within the toluene-DCE mixtures.

Table VII.3 Oxidation Rate as a Function of Solvent Polarity when 1.8×10^{-5} M CH_3-ImCoOMBP is Exposed to 800 Torr O_2 at 20°C.

Solvent	ε	$t_{1/2}$ [a] (sec)
Toluene	2.38	8400
5:1 toluene:DCE	3.22	7200
4:1 toluene:DCE	3.43	1900
1:1 toluene:DCE	5.32	250
Chlorobenzene	5.6	5200
1-Chlorobutane	7.39	8500
Dichloromethane	8.93	450
1,2-Dichloroethane	10.36	130

[a] $t_{1/2}$ is used since linear first order rate plots could not always be obtained. $t_{1/2}$ in these measurements does not include the initial spectral change due to oxygenation.

VII.5.3.2 Kinetics of the Oxidation of LCoOMBP in DCE

As the oxidation of CH_3-ImCoOMBP in DCE proceeded fairly rapidly and yielded good isosbestic points, further studies were carried out in DCE with the ligands CH_3-Im, Pip, and Py.

In the CH_3-ImCoOMBP system, the observed reaction rates were rather large for conventional kinetic studies. The reaction times remained essentially the same as the cobalt concentration was increased from 1.6×10^{-6} to 1.4×10^{-4} M; the initial spectral change, along with the oxidation rate, increased somewhat as the oxygen pressure was changed from 200 to 800 Torr (Appendix Vp). This behavior is similar to that of CH_3-ImCoOMBP in toluene, but the consistent first order dependence on cobalt suggests that aggregation of porphyrin complexes is unimportant.

In the Py system, clean spectra were obtained but the reaction time increased as the cobalt concentration was increased from 1.8×10^{-5} to 1.6×10^{-4} M (Appendix Vq). Therefore, some aggregate could be present in this system.

For the Pip system, reasonable first order dependence on cobalt was observed, the rates being very similar at cobalt concentrations of 1.9×10^{-5} M and 1.9×10^{-4} M (Table VII.4), indicating that aggregation was not important at these concentrations. A linear Arrhenius plot of pseudo first order rate constants was obtained from 20°C to 40°C ($\Delta H^{\ddagger}$ = 9.7 kcal/mole, $\Delta S^{\ddagger}$ = -39 eu, Figure VII.17, Table VII.4), The increase of the rate constant with temperature in this system contrasts with the oxidation of ImCoOMBP in toluene. When Pip is the axial ligand, there is presumably no stabilization of LCoOMBP(O_2) by ligand hydrogen bonding, and so there is no exothermic K_{int} step which could lower the observed $\Delta H^{\ddagger}$ value.

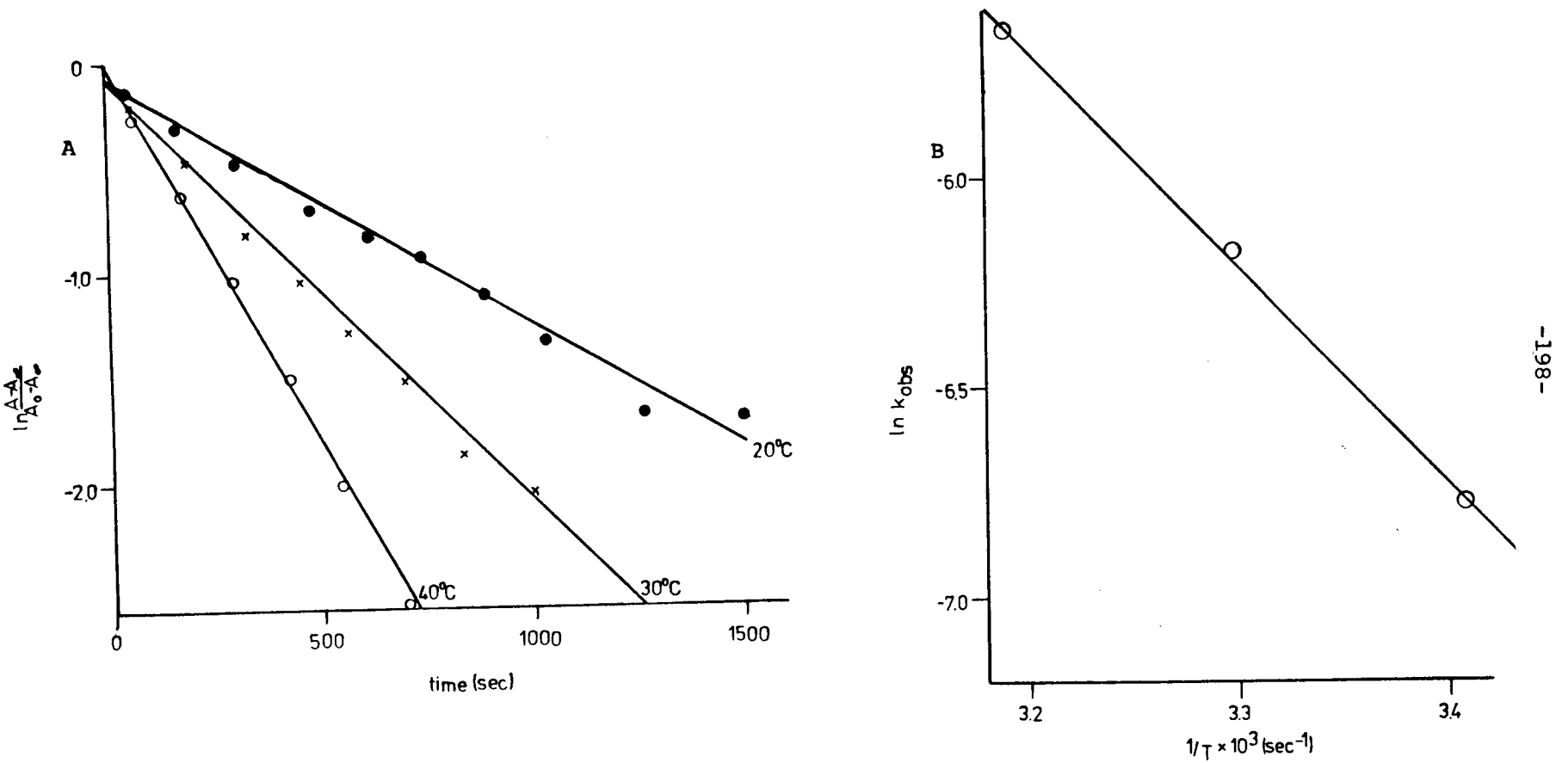

Figure VII.17 Temperature dependence on the oxidation of 2 x 10^{-5} M PipCoOMBP in DCE

A. Pseudo first order rate plots

B. Arrhenius plot

For raw data see Appendix Vr.

Table VII.4 Kinetic Data for the Oxidation of PipCoOMBP in DCE

Cobalt concentration, M	P_{O_2}, Torr	T, °C	[Pip], M	k_{obs} sec^{-1}
1.8×10^{-5}	800	20	7.6×10^{-4}	1.12×10^{-3}
1.9×10^{-5}	800	30	7.6×10^{-4}	2.05×10^{-3}
1.9×10^{-5}	800	40	7.6×10^{-4}	3.66×10^{-3}
1.9×10^{-4}	800	40	7.6×10^{-4}	3.35×10^{-3}

Table VII.5a Kinetic Data for the Oxidation of $(CH_3\text{-Im})_2$CoOMBP in 1:1 v/v toluene:CH_3-Im as a Function of Oxygen Pressure

Cobalt concentration, M	P_{O_2}, Torr	T, °C	[CH_3-Im], M	k_{obs}, sec^{-1}
2×10^{-5}	100	20	6.28	1.7×10^{-3}
2×10^{-5}	200	20	6.28	3.7×10^{-3}
2×10^{-5}	300	20	6.28	6.4×10^{-3}
2×10^{-5}	400	20	6.28	1.1×10^{-2}

Table VII.5b Kinetic Data for the Oxidation of $(CH_3\text{-Im})_2$CoOMBP in 1:1 v/v toluene:CH_3-Im as a Function of Temperature

Cobalt concentration, M	P_{O_2}, Torr	T, °C	[CH_3-Im], M	k_{obs}, sec^{-1}
2×10^{-5}	400	10	6.28	6.0×10^{-3}
2×10^{-5}	400	20	6.28	1.1×10^{-2}
2×10^{-5}	400	30	6.28	2.0×10^{-2}

Although the reaction did proceed faster and aggregation appeared to be less important in DCE than in toluene at concentrations up to 10^{-4} M, ESR experiments indicated the persistence of the LCoOMBP species (detected as the dioxygen adduct) for 48 h at [Co] ~ 10^{-3} M, and the expected amount of gas-uptake (O_2:Co = 1:2) still had not taken place after 96 h at [Co] ~ 10^{-2} M. Therefore, aggregation probably occurs at higher concentrations, even in the more polar solvents.

VII.6 Kinetics of the Oxidation of L_2CoOMBP

The presence of a second axial ligand on CoOMBP should block the path to oxygenation and any subsequent oxidation via an inner sphere mechanism. Oxygenation studies (Chapter IV) showed that all L_2CoOMBP complexes were less oxygen sensitive than the corresponding LCoOMBP complexes. However, the bis CH_3-Im complex was more oxygen sensitive than expected and solvent polarity contributions from CH_3-Im were thought to be a factor. In studying ambient temperature oxidation, the solvent system consisted of 50% by volume of the coordinating amine, and so again contributions of the ligand to solvent polarity were considered.

In studying Pip_2CoOMBP (~2 x 10^{-5} M) in the least polar of the solvent systems used, 1:1 v/v toluene:Pip (ε = 3.22), there was no evidence of any reaction after the system was exposed to 800 Torr of O_2 at 20°C. For Py_2CoOMBP (~2 x 10^{-5} M) in 1:1 v/v toluene:Py (ε = 7.37) under similar conditions a pseudo first order rate constant (k ~ 1.4 x 10^{-5} sec^{-1}) was measured and the reaction proceeded somewhat more quickly to completion than did 2 x 10^{-5} M PyCoOMBP under 800 Torr O_2 in toluene (Ch. VII.5.2), suggesting a possible role of solvent polarity in enhancing oxidation.

The oxidation of $(CH_3\text{-Im})_2$CoOMBP in 1:1 v/v toluene:CH_3-Im (ε = 18.5)

proceeded so quickly that stopped-flow kinetic techniques had to be used to monitor the reaction at cobalt concentrations of 2×10^{-5} M. As well as the reaction being first order in oxygen (Figure VII.18, Table VII.5a), a good first order dependence on cobalt was obtained at concentrations of 2×10^{-5} M, but the reaction time increased somewhat as the concentration was increased to 2×10^{-4} M. A 5.6×10^{-3} M solution of $(CH_3\text{-Im})_2$CoOMBP in the mixed toluene-CH_3-Im solvent showed a Co:O_2 uptake in the ratio of 1:0.7 after 42 h of monitoring (see p 204). No uptake was observed in a 1.2×10^{-2} M $(CH_3\text{-Im})_2$CoOMBP solution. If the oxidation reaction of 2×10^{-5} M solutions of $(CH_3\text{-Im})_2$CoOMBP were monitored as a function of temperature, a reasonably linear Arrhenius plot of the pseudo first order rate constants was obtained ($\Delta H^{\ddagger}$ = 12.8 kcal/mole, $\Delta S^{\ddagger}$ = -24 eu, Figure VII.19, Table VII.5b). Compared to the LCoOMBP systems that were studied (Ch. VII.5), the $\Delta H^{\ddagger}$ value of the $(CH_3\text{-Im})_2$CoOMBP system is large, probably as a result of an endothermic dissociation of $(CH_3\text{-Im})_2$CoOMBP being a necessary step for the oxidation of this system.

The three bis amine complexes of CoOMBP were further studied in solutions of neat ligand.

Pip_2CoOMBP in neat Pip (ε = 5.8) showed no signs of oxidation after 4h under 800 Torr of oxygen at 40°C, nor at 20°C after 1 day.

Py_2CoOMBP in neat Py (ε = 12.4) oxidized very slowly ($t_{\frac{1}{2}}$ @ 40°C ~ 15 h) via a non first order in cobalt process. During the course of some of these reactions exposure to light was seen to cause an increase in reaction rate, possibly due to photolysis of a coordinated Py. However, in attempts to study this by flash photolysis, the recombination of the Py could not be observed, possibly because it was so fast or only a small amount of

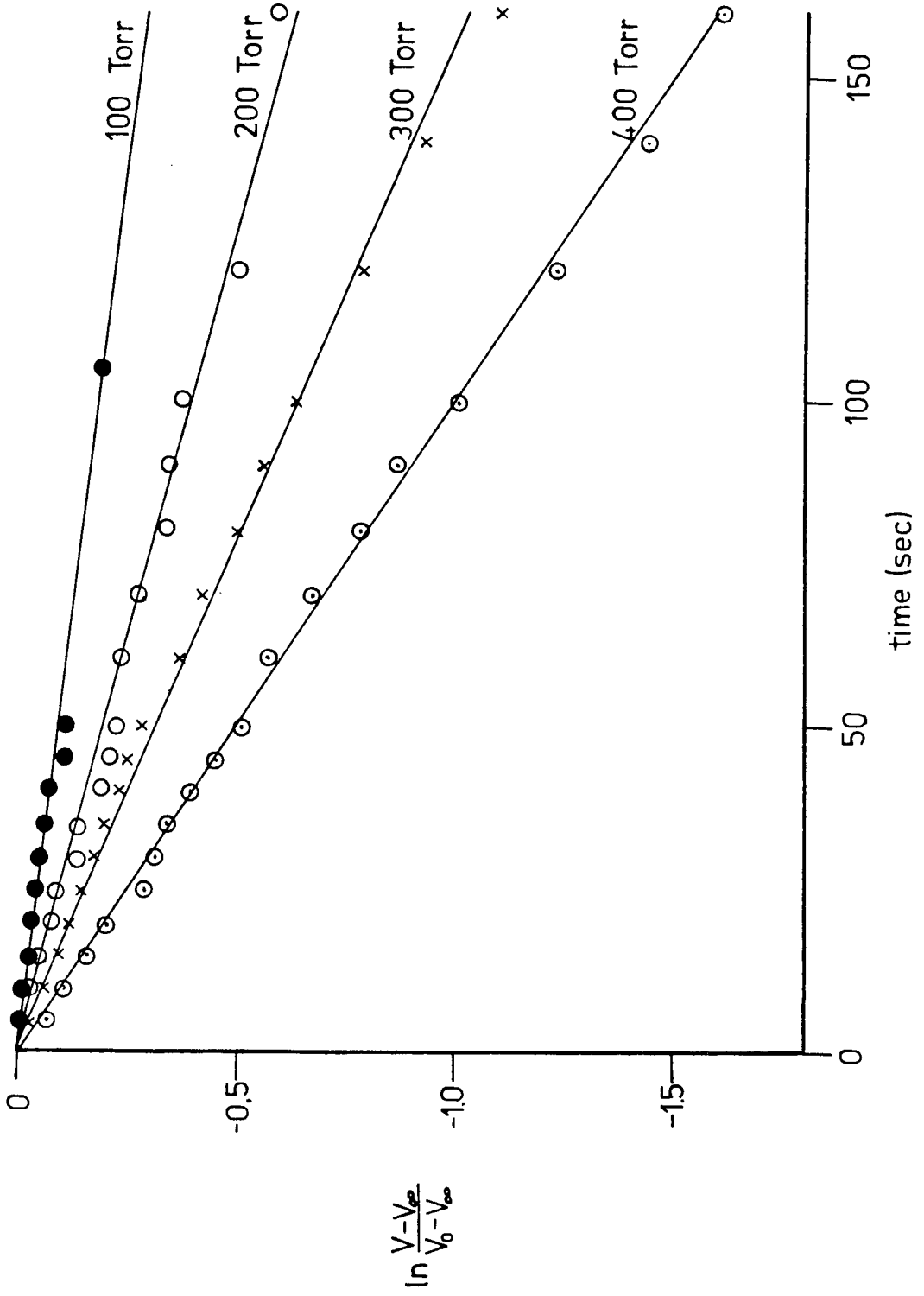

Figure VII.18 First order rate plots for the oxidation of 2×10^{-5} M $(CH_3\text{-Im})_2$CoOMBP in 1:1 toluene:CH_3-Im. For raw data see Appenix Vs.

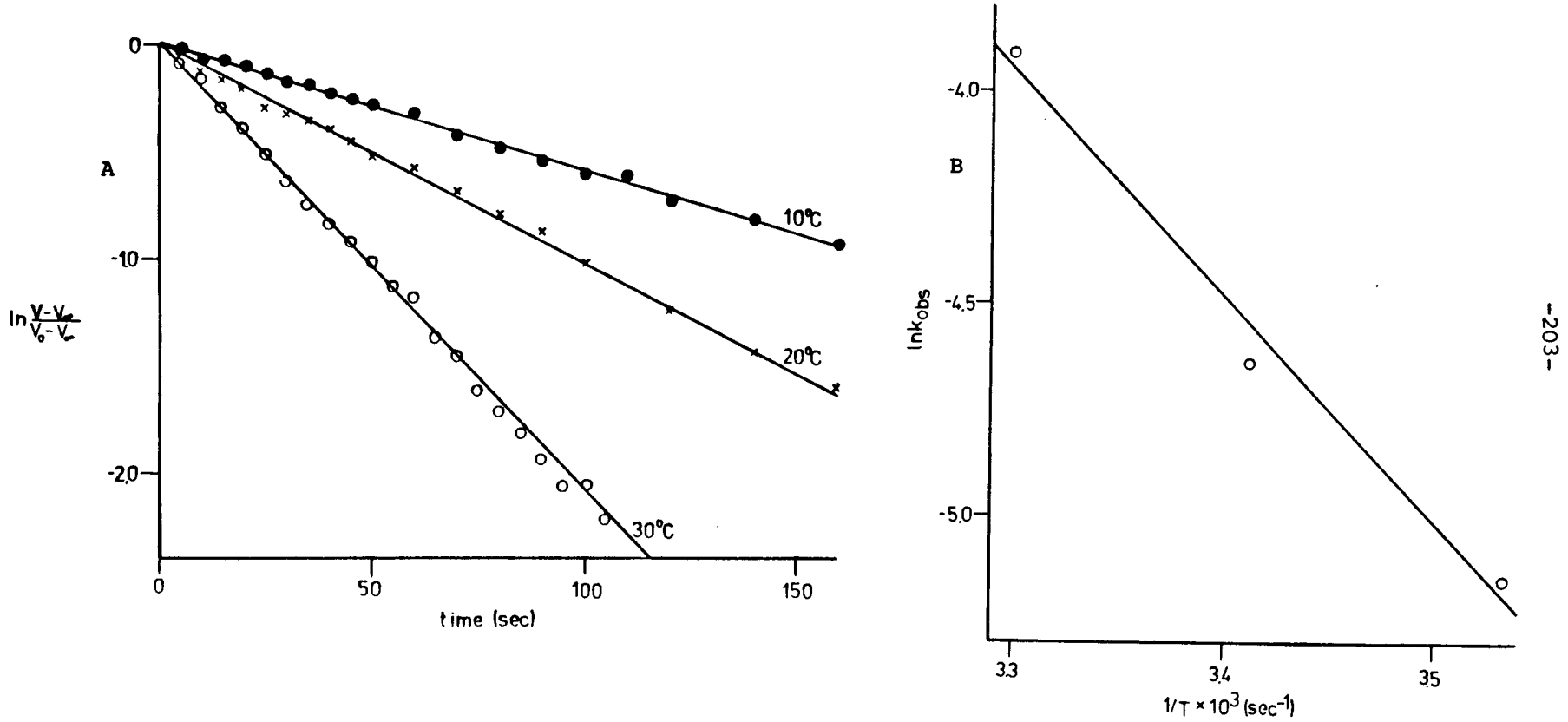

Figure VII.19 Temperature dependence of the oxidation of 2×10^{-5} M $(CH_3\text{-Im})_2$CoOMBP.

A. Pseudo first order rate plots.

B. Arrhenius plot.

For raw data see Appendix Vt.

dissociation was required to cause the observed enhancement of reaction.

In neat CH_3-Im (ε ~ 35)[156], $(CH_3\text{-Im})_2$CoOMBP was observed to oxidize at a rapid first order rate (Figure VII.20, Table VII.5c). Gas-uptake results also showed an immediate uptake of oxygen to a 0.5:1 O_2:Co ratio for the oxidation reaction. This was followed by a very slow steady uptake over the course of days which is not related to the oxidation $(CH_3\text{-Im})_2$CoOMBP. The data suggest that in neat CH_3-Im there is insufficient aggregation occurring to impede the oxidation reaction. The very slow O_2 uptake likely refers to oxidation of the amine solvent (this may or may not be catalyzed by the complex). The previous uptakes of 0.7:1 O_2:Co measured in the toluene solutions (see p 201) could similarly refer to amine oxidation. Comparable behavior has been noted for the oxidation of phosphines to phosphine oxide in the presence of metal complexes[157].

In solvent systems consisting of 1:1 v/v ligand:DCE the oxidation rates were even greater than those in the neat ligand solutions.

$(CH_3\text{-Im})_2$CoOMBP was oxidized with an observed pseudo first order rate constant of 2.3 x 10^{-1} sec^{-1} at 30°C under 400 Torr in 1:1 CH_3-Im:DCE (ε ~ 25, Figure VII.20, Table VII.5c). This system also produced an immediate gas uptake in a 0.5:1 O_2:Co ratio.

The oxidation of Py_2CoOMBP in 1:1 Py:DCE (ε = 12.7), (Figures VII.21,22, Tables VII.6a,6b) gave linear first order in cobalt plots and yielded a linear Arrhenius plot ($\Delta H^{\ddagger}$ = 3.6 kcal/mole, $\Delta S^{\ddagger}$ = -64 eu). The low $\Delta H^{\ddagger}$ value, compared to that of the $(CH_3\text{-Im})_2$CoOMBP system, is consistent with DCE enhancing the formation of the LCoOMPB$(O_2)^*$ intermediate compared to the toluene-CH_3-Im solvent used in the $(CH_3\text{-Im})_2$CoOMBP system; enhanced formation of LCoOMBP$(O_2)^*$ could occur from any protons present in DCE hydrogen bonding

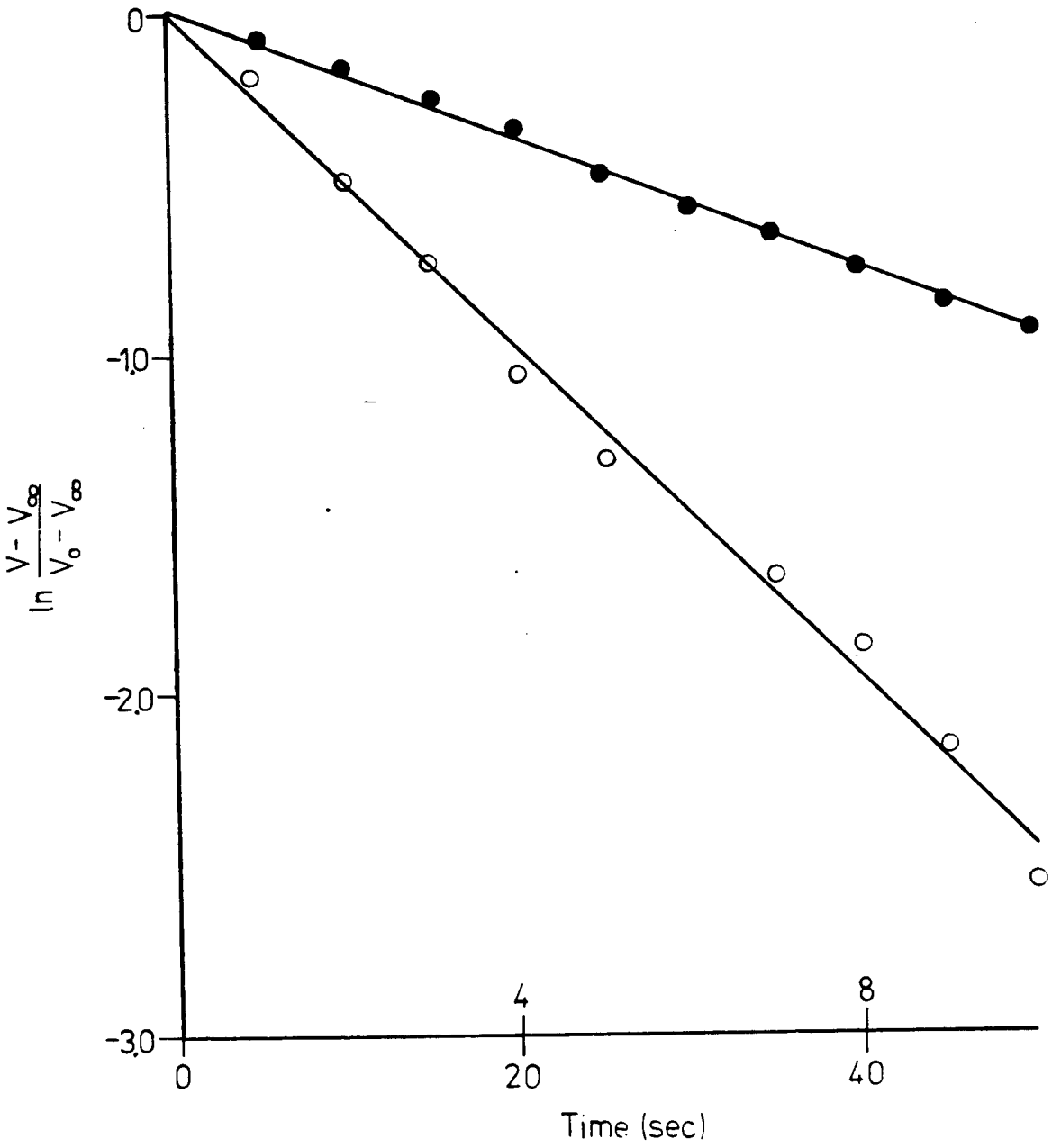

Figure VII.20 First order rate plots for the oxidation of 2×10^{-5} M $(CH_3\text{-Im})_2CoOMBP$. For raw data see Appendix Vx.

● In neat CH_3-Im (lower time axis)

○ In 1:1 DCE:CH_3-Im (upper time axis)

Table VII.5c Kinetic Data for the Oxidation of $(CH_3\text{-Im})_2CoOMBP$ as a Function of Solvent

Cobalt concentration, M	P_{O_2}, Torr	T, °C	Solvent	k_{obs}, sec^{-1}
2×10^{-5}	400	20	1:1 tol:CH_3-Im	1.1×10^{-2}
2×10^{-5}	400	20	neat CH_3-Im	1.5×10^{-2}
2×10^{-5}	400	30	1:1 tol:CH_3-Im	2.0×10^{-3}
2×10^{-5}	400	30	1:1 DCE:CH_3-Im	2.4×10^{-1}

Table VII.6a Kinetic Data for the Oxidation of $Py_2CoOMBP$ as a Function of Cobalt Concentration in 1:1 v/v DCE:Py

Cobalt concentration, M	P_{O_2}, Torr	T, °C	[Py], M	k_{obs}, sec^{-1}
2×10^{-6}	800	20	6.21	1.55×10^{-4}
1.8×10^{-5}	800	20	6.21	1.43×10^{-4}
1.9×10^{-4}	800	20	6.21	1.74×10^{-4}

Table VII.6b Kinetic Data for the Oxidation of $Py_2CoOMBP$ as a Function of Temperature in 1:1 v/v DCE:Py

Cobalt concentration, M	P_{O_2}, Torr	T, °C	[Py], M	k_{obs}, sec^{-1}
1.8×10^{-5}	800	20	6.21	1.43×10^{-4}
1.8×10^{-5}	800	30	6.21	1.88×10^{-4}
1.9×10^{-5}	800	40	6.21	2.32×10^{-4}

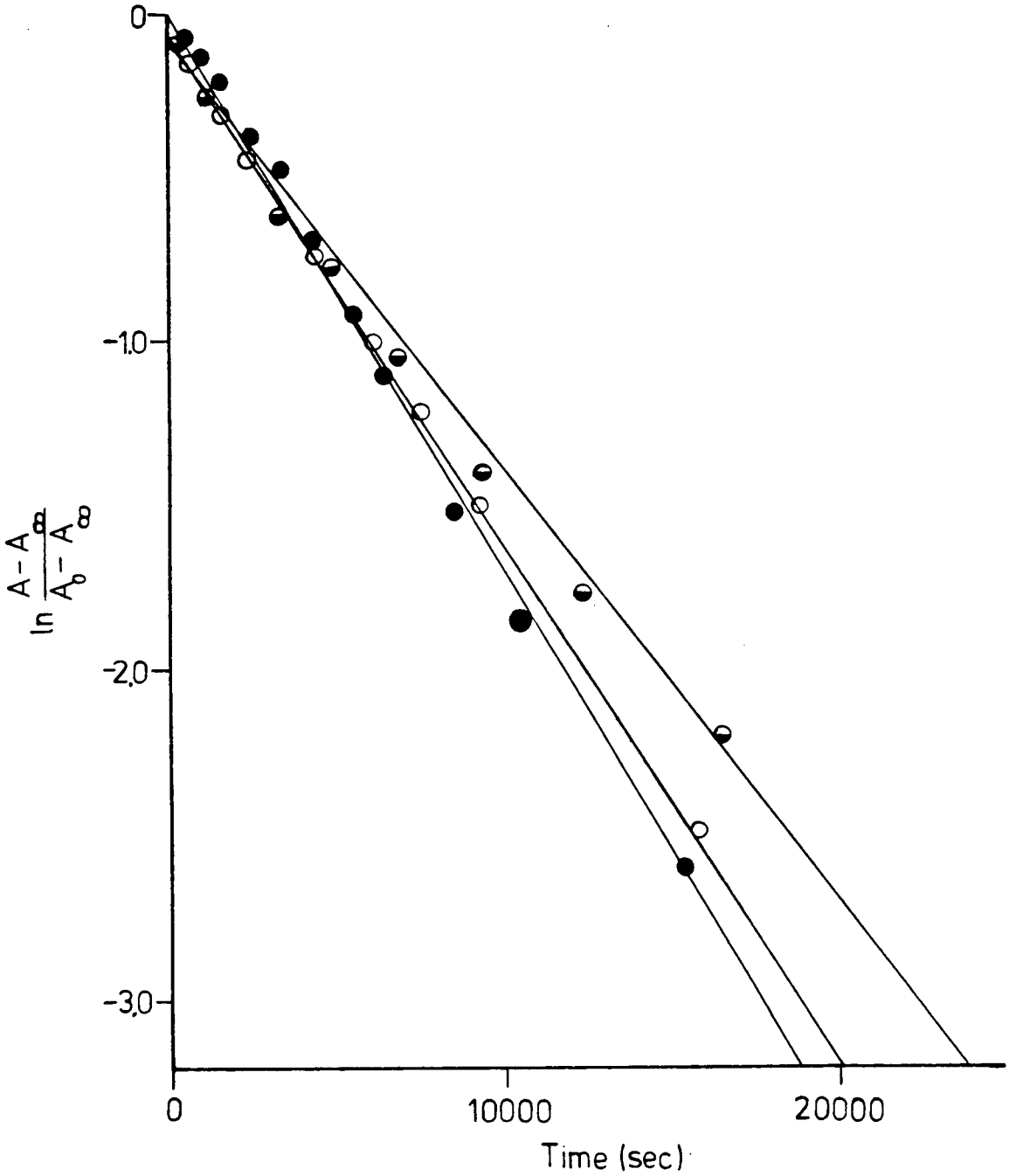

Figure VII.21 First order rate plots for the oxidation of $Py_2CoOMBP$ in 1:1 DCE:Py as a function of [Co]. For raw data see Appendix Vz.

○ [Co] = 2×10^{-6} M

◒ [Co] = 1.8×10^{-5} M

● [Co] = 1.9×10^{-4} M

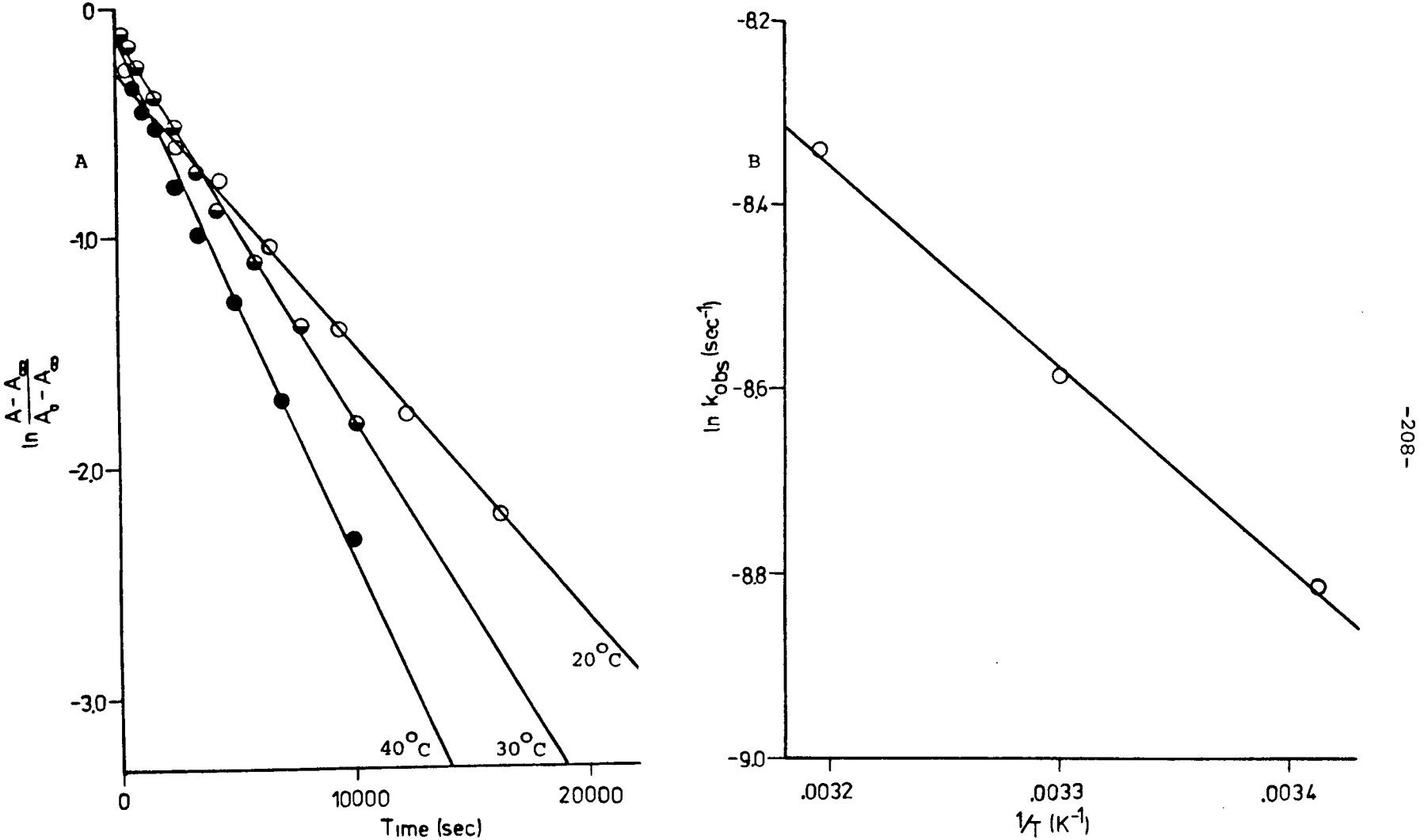

Figure VII.22 Temperature dependence of the oxidation of 2 x 10^{-5} M $Py_2CoOMBP$.

A. Pseudo first order rate plots.

B. Arrhenius plot.

For raw data see Appendix Vy.

to LCoOMBP(O_2). In contrast to the studies in toluene, first order in cobalt behavior persisted as the cobalt concentration was increased from 2×10^{-6} to 1.9×10^{-4} M, again showing that the nature of the solvent is important in determining the degree of aggregation of porphyrin systems.

The oxidation of Pip_2CoOMBP solutions in 1:1 Pip:DCE ($\varepsilon = 7.4$) proceeded in a first order manner when the cobalt concentration was 2×10^{-5} M, but at 2×10^{-4} M the observed rate was much less and non first order (Figure VII.23, Table VII.7). However, after about an hour, crystals of Pip·HCl precipitated. This also occurred in the absence of complex. The mixed Pip-DCE solvent system was the only one where the ligand hydrochloride was observed, probably in part due to Pip being the strongest base of all the ligands studied, so that there is sufficient formation of the salt to cause precipitation. Formation of amine hydrochloride has been noted previously in chlorinated hydrocarbon solvents[51e]. Oxidation of Pip_2CoOMBP is enhanced in the more polar DCE solvent system; protons are present in this system, and the presence of protons has been shown to enhance oxidation rates[123] and has been suggested to prevent porphyrin aggregation (Ch. VII.5.2). Since there is a large concentration of basic Pip required to fully form Pip_2CoOMBP, and since amine hydrochlorides were not observed when similar concentrations of the other strongly basic ligands, CH_3-Im and Py, were used, the concentration of free protons present must be very small. However, the formation constant of the hydrogen bonded Im adduct of the ImCoOMBP system ($K_{int} \sim 10^4$ M^{-1}) suggests that any available protons could form hydrogen bonded adducts of LCoOMBP(O_2) complexes. The presence of even trace amounts of such complexes could account for the observed enhanced oxidation, if the oxidation rate of these complexes were sufficiently high.

The mechanism of oxidation of L_2CoOMBP systems appears to be similar

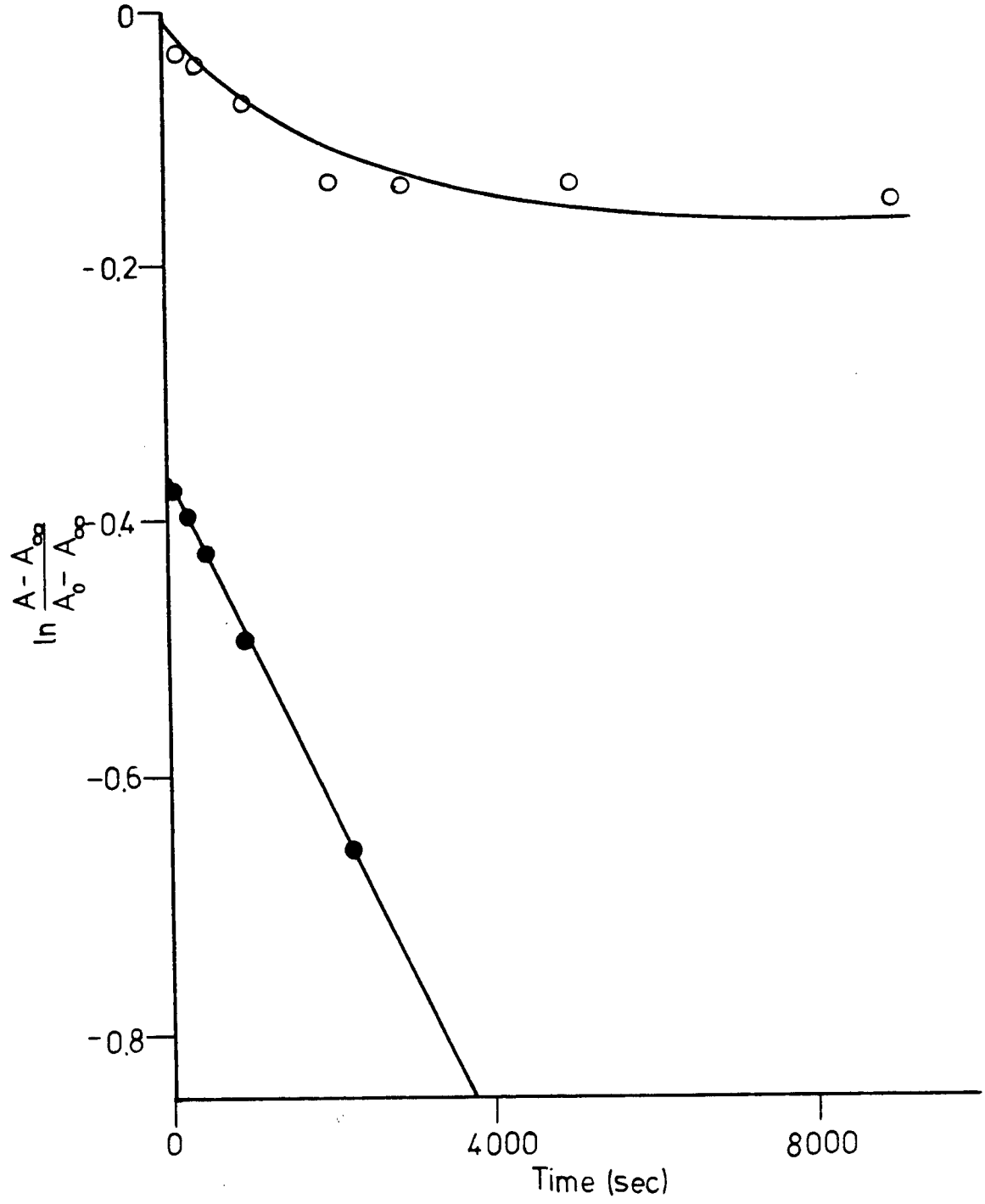

Figure VII.23 First order rate plots for the oxidation of $Pip_2CoOMBP$ in 1:1 DCE:Pip. For raw data see Appendix Vaa

● [Co] = 2.0×10^{-5} M

○ [Co] = 2.1×10^{-4} M

Table VII.7 Kinetic Data for the Oxidation of $Pip_2CoOMBP$ as a Function of Cobalt Concentration in 1:1 v/v DCE:Pip

Cobalt concentration, M	P_{O_2}, Torr	T, °C	[Pip], M	k_{obs}, sec^{-1}
2.0×10^{-5}	800	20	5.05	1.37×10^{-4}
2.1×10^{-4}	800	20	5.05	slower, non first order

Table VII.8a Kinetic Data for the Oxidation of CH_3-ImCoOEP in DCE as a Function of Cobalt Concentration

Cobalt concentration, M	P_{O_2}, Torr	T, °C	[CH_3-Im], M	k_{obs}, sec^{-1}
7.5×10^{-6}	800	30	0.0625	1.32×10^{-3}
3.1×10^{-5}	800	30	0.0625	1.53×10^{-3}
7.9×10^{-5}	800	30	0.0625	1.60×10^{-3}
6.6×10^{-4}	800	30	0.0625	1.22×10^{-3}
2×10^{-3}	800	23	0.0625	$\sim 3.2 \times 10^{-4}$ non first order

Table VII.8b Kinetic Data for the Oxidation of CH_3-ImCoOEP in DCE as a Function of Oxygen Pressure

Cobalt concentration, M	P_{O_2}, Torr	T, °C	[CH_3-Im], M	k_{obs}, sec^{-1}
6.7×10^{-5}	100	30	0.0625	2.62×10^{-4}
7.9×10^{-5}	150	30	0.0625	3.55×10^{-4}
7.2×10^{-5}	200	30	0.0625	5.72×10^{-4}
8.2×10^{-5}	300	30	0.0625	7.60×10^{-4}
7.9×10^{-5}	400	30	0.0625	1.00×10^{-3}
5.6×10^{-5}	530	30	0.0625	1.29×10^{-3}
6.5×10^{-5}	670	30	0.0625	1.49×10^{-3}
7.9×10^{-5}	800	30	0.0625	1.60×10^{-3}

to that outlined in equations VII.15, 25-29 with the additional formation of $L_2CoOMBP$ and possibly $(L_2CoOMBP)_2$.

VII.7 Kinetics of the Oxidation of LCoP, P ≠ OMBP

In order to determine whether the observed aggregation phenomena were peculiar to CoOMBP, oxidation of several other cobalt(II) porphyrin complexes was investigated. Previous equilibrium studies have shown that CoPpIXDME[89], CoMpIXDME[89], and CoOEP[95] and the five-coordinate analogues do not form aggregates at concentrations from 10^{-6} to 10^{-5} M, although studies were not carried out at higher concentrations.

When 8×10^{-5} M solutions of CH_3-ImCoOEP in DCE were exposed to oxygen, a large, rapid, initial spectral change was observed. This was followed by spectral changes with good isosbestic points. The reaction rates analyzed for first order in cobalt and the pseudo first order constants were essentially independent of cobalt concentration from 7.5×10^{-6} to 6.6×10^{-4} M (Figure VII.24, Table VII.8a). A strong ESR signal of the cobalt-dioxygen adduct, observed in a 2×10^{-3} M CH_3-ImCoOEP solution under 800 Torr O_2 at 22°C, gradually disappeared, but in a non first order manner and over a period of time longer than observed in the more dilute systems. The amount of initial spectral change was dependent on oxygen pressure (Figure VII.25), but was too fast to be followed, even by using stopped-flow techniques. Gas-uptake studies at 15°C under 800 Torr of O_2 on a 6×10^{-3} M CH_3-ImCoOEP solution showed an initial 1:3 O_2:Co rapid uptake, followed by uptake over the next five hours to the 1:2 O_2:Co ratio expected for formation of CH_3-ImCoOEP(O_2)CoOEP·CH_3-Im. Oxygen dependence studies (Figure VII.25, Table VII.8b) on 8×10^{-5} M CH_3-ImCoOEP at 30°C showed that the reaction was first order in oxygen to 400 Torr, but decreased towards a zero order

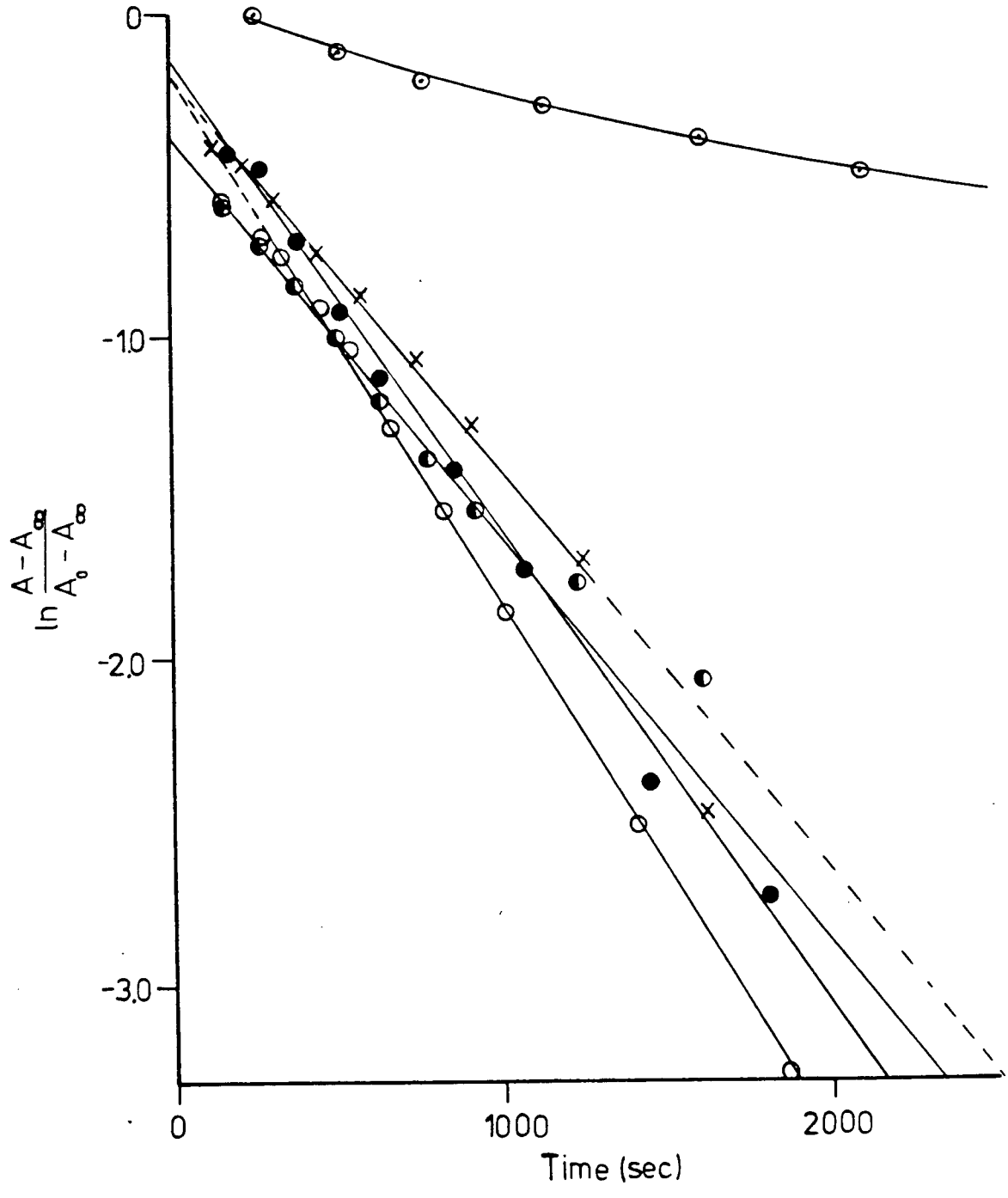

Figure VII.24 First order rate plots for the oxidation of CH_3-ImCoOEP by 800 Torr O_2 in DCE @ 30°C as a function of [Co]. See Appendix Vff.

× [Co] = 7.5×10^{-6} M
● [Co] = 3.1×10^{-5} M
○ [Co] = 7.9×10^{-5} M
◐ [Co] = 6.6×10^{-4} M
⊙ [Co] = 2×10^{-3} M

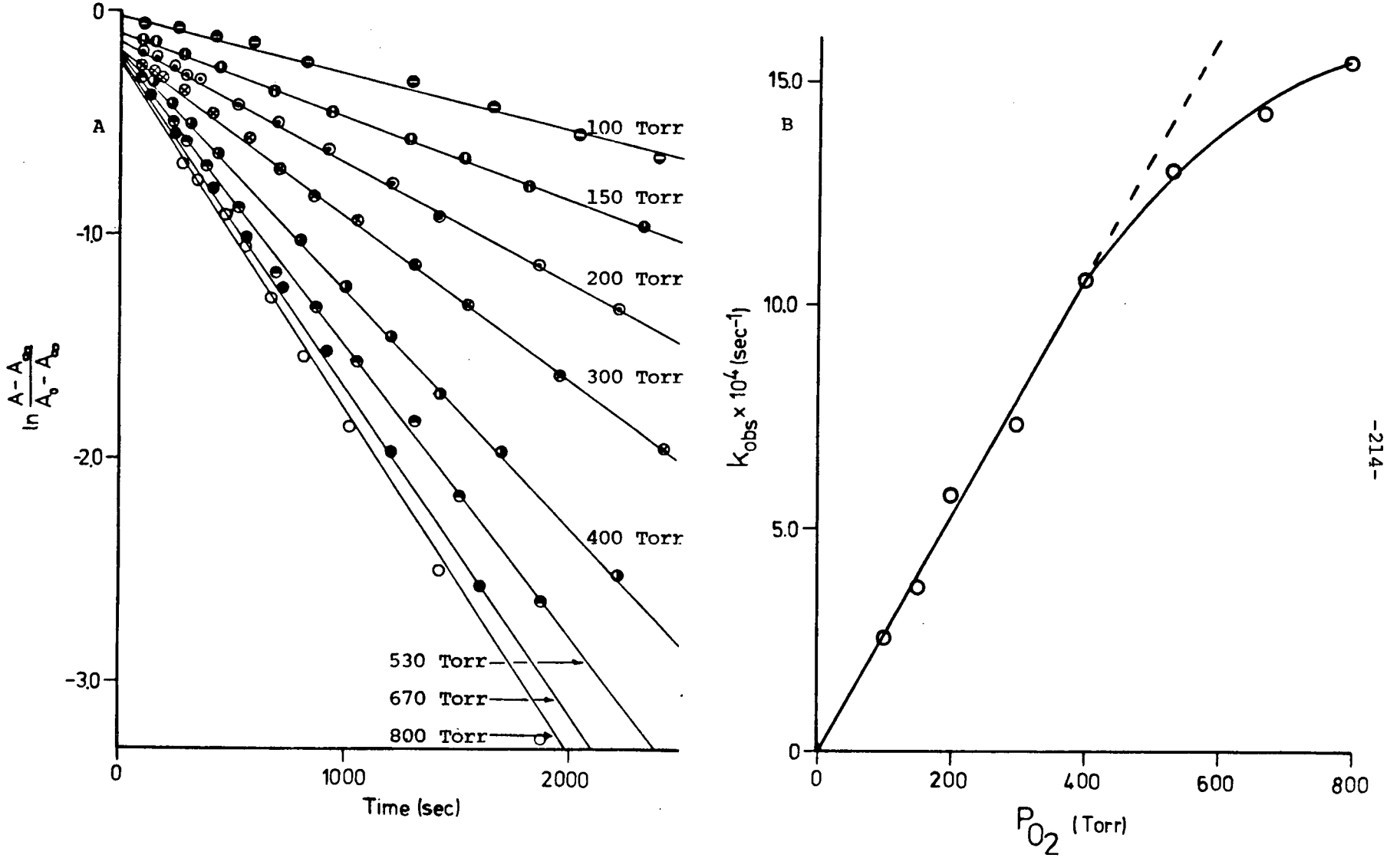

Figure VII.25 Oxygen pressure dependence of the oxidation of ~7 x 10^{-5} M CH_3-ImCoOEP @ 30°C in DCE.

A. Pseudo first order rate plots.

B. Pressure dependence plot.

For raw data see Appendix Vhh.

dependence at higher pressures. The pseudo first order rate constant was essentially invariant as the CH_3-Im concentration was changed from 0.0251 to 0.248 M (Figure VII.26, Table VII.8c). The amount of initial spectral change upon exposure to 800 Torr O_2 increased as the temperature at which the reaction was studied was lowered from 30°C to 10°C (Figure VII.27). A linear Arrhenius relationship was found for the pseudo first order rate constants ($\Delta H^{\ddagger}$ = 18.5 kcal/mole, $\Delta S^{\ddagger}$ = -10 eu, Figure VII.27, Table VII.8d). The fairly large observed $\Delta H^{\ddagger}$ value is consistent with much of the reacting system being present as enthalpically favored CH_3-ImCoOEP(O_2).

The observed first order dependence in cobalt at concentrations less than 10^{-3} M is consistent with the mechanism involving a rate determining formation of CH_3-ImCoOEP(O_2)* postulated for the CoOMBP systems (Chapter VII.5) and for the ImCoPpIXDME system in toluene[123]. Aggregation of CH_3-ImCoOEP does not appear to be important at these concentrations. Although the increase in reaction time at a CH_3-ImCoOEP concentration of 2×10^{-3} M in the ESR experiment is consistent with aggregation, the oxygen concentration is not greatly in excess (O_2 solubility 7.2×10^{-3} $Matm^{-1}$), and this could also contribute to the apparent "slow down" in reaction. However, the further extended reaction time in the 6×10^{-3} M CH_3-ImCoOEP system used in the gas-uptake experiment is indicative of aggregation as the oxygen concentration is kept constant throughout the experiment.

The observed oxygen dependence is consistent with increasing formation of CH_3-ImCoOEP(O_2) as the pressure is increased. That the oxygen dependence decreases at higher pressures lends support to this picture and is interesting as studies on other systems[123] showed strictly first order dependence, because little dioxygen adduct had been formed. The intercept/slope value of the plot of k_{obs}^{-1} vs $P_{O_2}^{-1}$ (Figure VII.28) yields a $P_{\frac{1}{2}}O_2$ value of

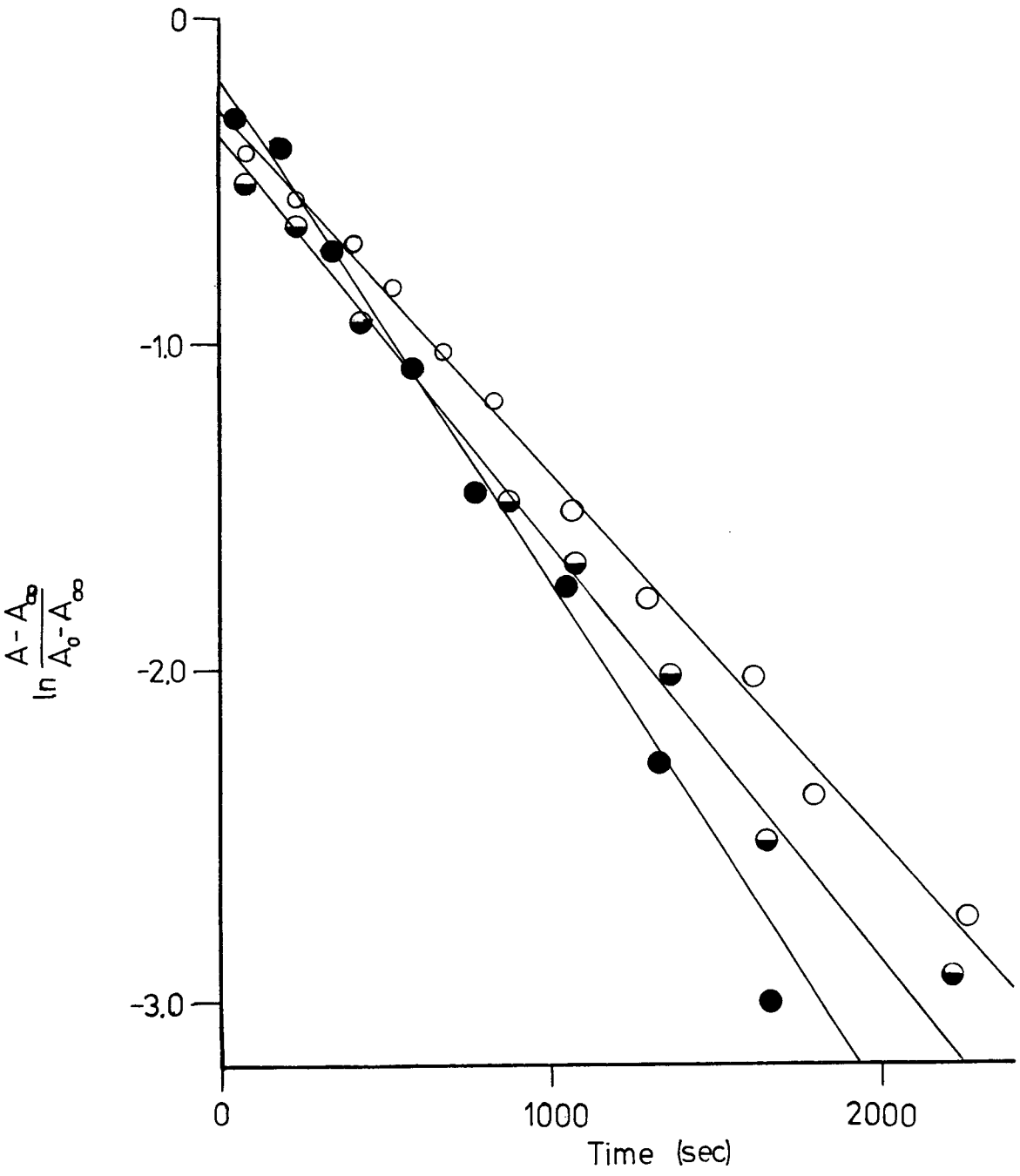

Figure VII.26 First order rate plots for the oxidation of CH_3-ImCoOEP in DCE as a function of [CH_3-Im]. For raw data see Appendix Vk.

○ [CH_3-Im] = 0.0251 M

◒ [CH_3-Im] = 0.0827 M

● [CH_3-Im] = 0.248 M

Table VII.8c Kinetic Data for the Oxidation of CH_3-ImCoOEP in DCE as a Function of CH_3-Im Concentration

Cobalt concentration, M	P_{O_2}, Torr	T, °C	[CH_3-Im], M	k_{obs}, sec^{-1}
7.8×10^{-5}	800	24	0.0251	1.12×10^{-3}
8.2×10^{-5}	800	24	0.0827	1.25×10^{-3}
7.6×10^{-5}	800	24	0.248	1.60×10^{-3}

Table VII.8d Kinetic Data for the Oxidation of CH_3-ImCoOEP in DCE as a Function of Temperature

Cobalt concentration, M	P_{O_2}, Torr	T, °C	[CH_3-Im], M	k_{obs}, sec^{-1}
7.0×10^{-5}	800	10	0.0625	1.8×10^{-4}
7.9×10^{-5}	800	20	0.0625	6.4×10^{-4}
7.9×10^{-5}	800	30	0.0625	1.60×10^{-3}

Table VII.8e Kinetic Data for the Oxidation of CH_3-ImCoOEP as a Function of Solvent

Cobalt concentration, M	P_{O_2}, Torr	T, °C	Solvent	k_{obs}, sec^{-1}
6.6×10^{-4}	800	30	DCE	1.22×10^{-3}
6.0×10^{-4}	800	30	CH_3-Im	1.09×10^{-3}
6.1×10^{-4}	800	30	DMA	1.03×10^{-4}

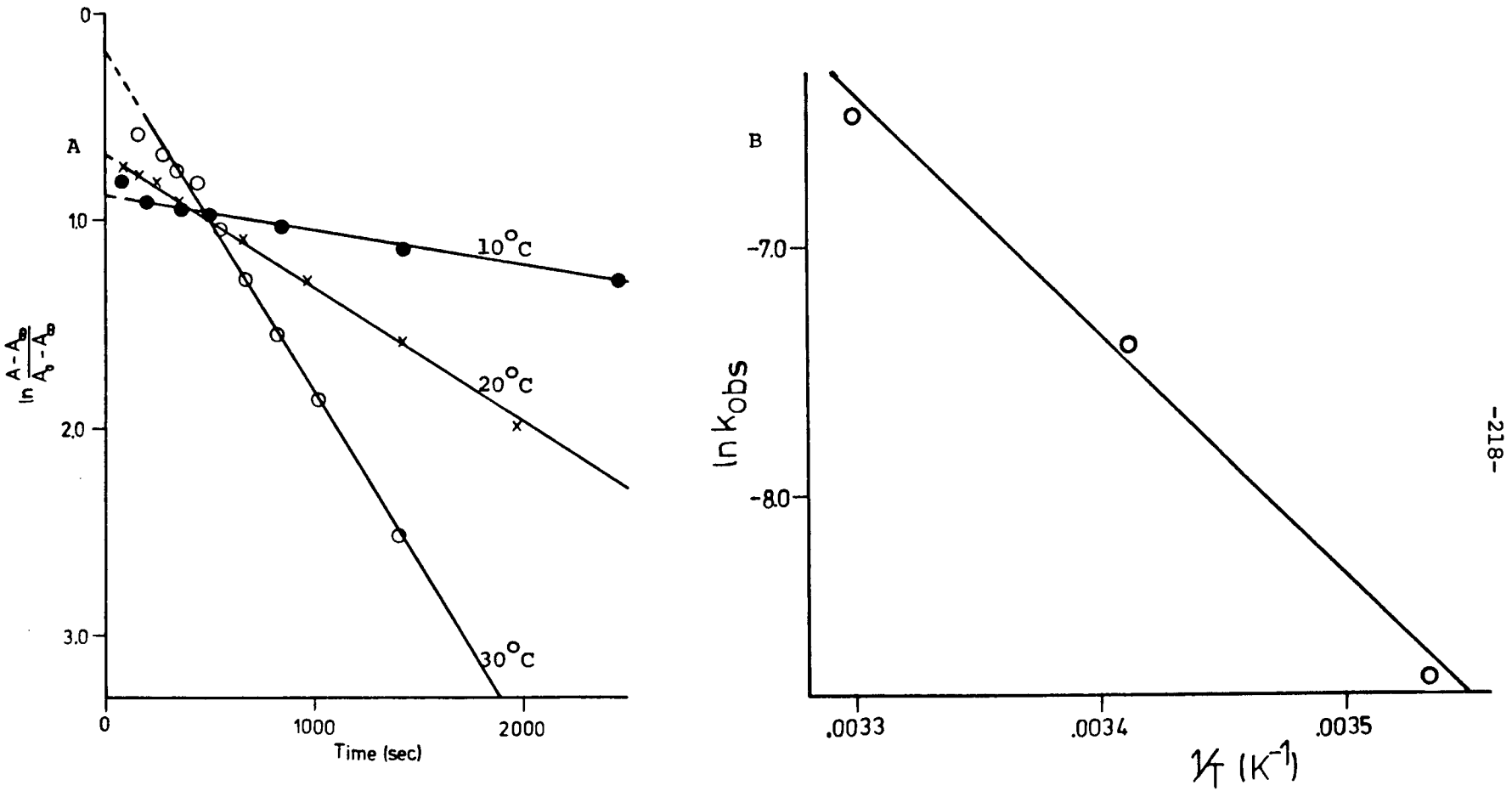

Figure VII.27 Temperature dependence of the oxidation of ~8 x 10^{-5} M CH_3-ImCoOEP in DCE.

A. Pseudo first order rate plots.

B. Arrhenius plot.

For raw data see Appendix Vgg.

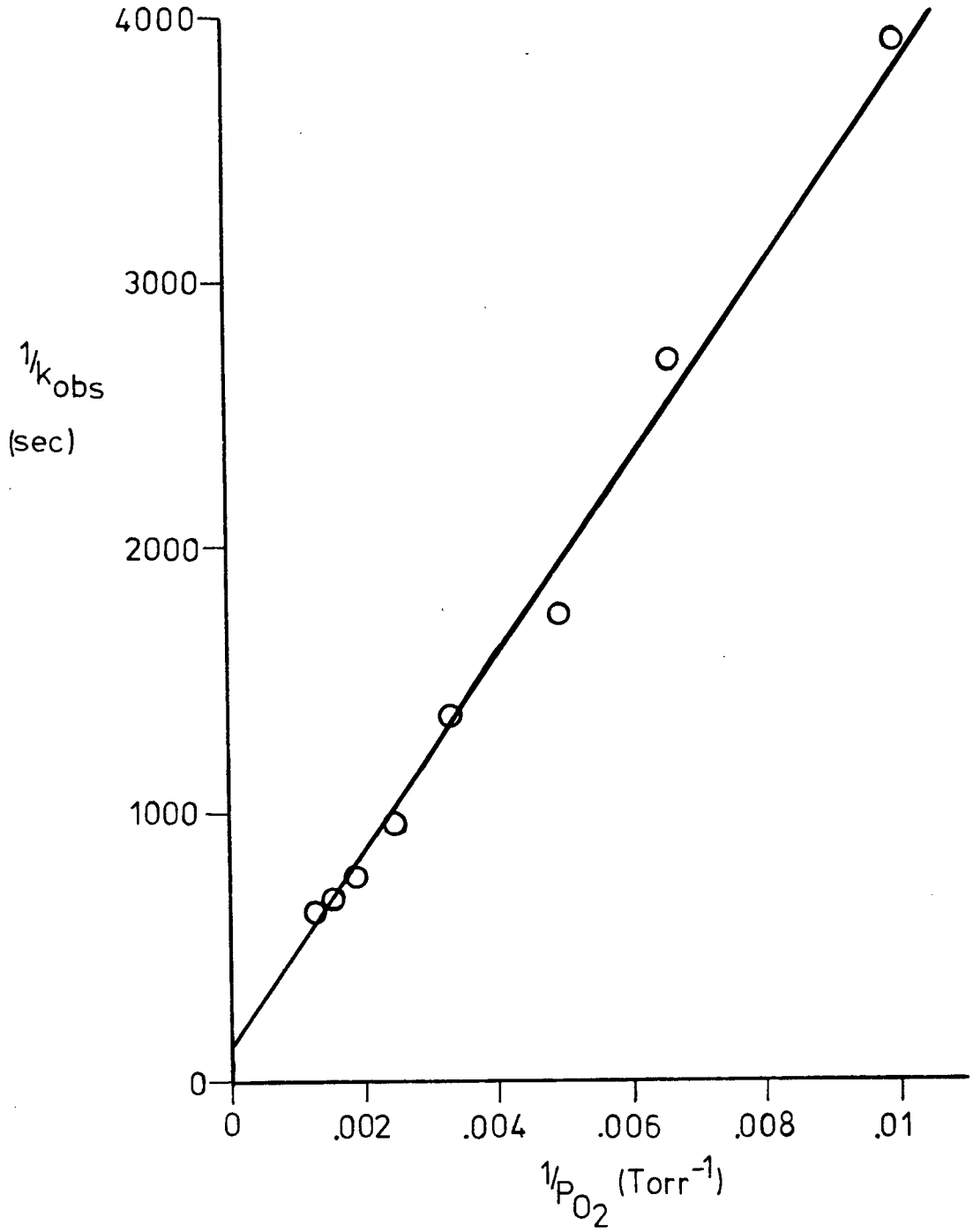

Figure VII.28 Analysis of oxygen dependence on the oxidation of CH_3-ImCoOEP at 30°C.

2.9×10^3 Torr at 30°C. Although the experimental error involved in this determination must be considered large as the intercept occurs very close to the origin, the $P_{\frac{1}{2}}O_2$ does agree reasonably with the value of 2.4×10^3 Torr estimated from the initial spectral change observed when 800 Torr of O_2 is added to CH_3-ImCoOEP. The gas-uptake results imply a $P_{\frac{1}{2}}O_2$ value of $\sim 1.6 \times 10^3$ Torr at 15°C, and the initial spectral changes suggest a $P_{\frac{1}{2}}O_2$ value of ~700 Torr at this temperature. While the discrepency between these two values is not unreasonable, it is also consistent with aggregated CH_3-Im at the higher concentration. Direct P_{O_2} measurements of the CH_3-ImCoOEP system in DCE are not feasible as oxidation proceeds rapidly at ambient temperature and the solvent freezes at lower temperatures.

The independence of the rate on CH_3-Im is consistent with the five-coordinate CH_3-Im species being fully formed at all concentrations studied, with the CH_3-Im taking no further part in the reaction mechanism. This view is supported by independent CH_3-Im binding studies where K_1 was found to be 9.1×10^2 M^{-1} at 23°C in toluene[95]. Solvent variation studies suggest that K_1 values do not vary much from solvent to solvent (Chapter III).

The linear Arrhenius plot and observed pseudo first order nature of the reaction throughout the temperature range studied are more indications that no aggregation occurs at CH_3-ImCoOEP concentrations of 8×10^{-5} M.

In DMA the oxidation rate of 6×10^{-4} M CH_3-ImCoOEP was an order of magnitude slower than in the less polar DCE (Figure VII.29, Table VII.8e). However, DMA binding to CoOEP was not measured, so it cannot be certain that the reacting species is CH_3-ImCoOEP, although the CH_3-Im adducts of CoPpIXDME[89] and CoOMBP (Chapter IV) appear to remain as such in the similar DMF solvent system. In neat CH_3-Im the oxidation rate was comparable to that observed in DCE (Figure VII.29, Table VII.8e).

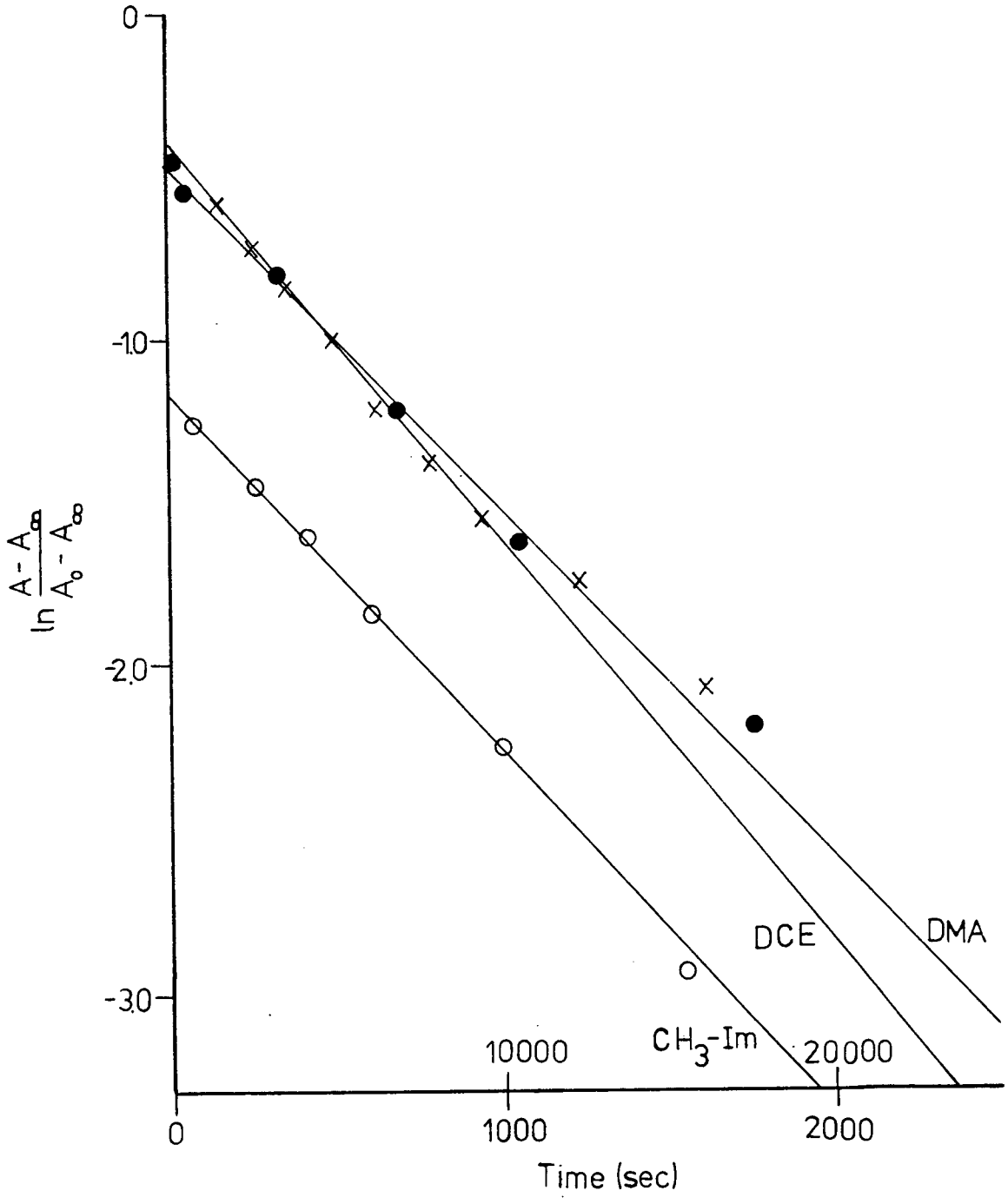

Figure VII. 29 First order rate plots for the oxidation of 6 x 10^{-4} M CH_3-ImCoOEP in DCE @ 30°C in a variety of solvents. Upper time axis refers to DMA, lower to DCE and CH_3-Im. For raw data see Appendix Vii.

Similar observations were also noted in the other porphyrin systems.

With CH_3-ImCoEpI in DCE a first order dependence in cobalt was observed at concentrations used in visible spectroscopy (Figure VII.30, Table VII.9a). Large initial spectral changes were observed and an ambient temperature ESR signal of CH_3-ImCoEpI(O_2) was detected which took longer to go to products than was the case when visible studies were done at lower concentrations. Also a linear Arrhenius relationship for the pseudo first order rate constants was observed ($\Delta H^{\ddagger}$ = 11.8 kcal/mole, $\Delta S^{\ddagger}$ = -32 eu, Figure VII.31, Table VII.9b). Again the $\Delta H^{\ddagger}$ value is fairly high and this is consistent with much of the reacting system being present as LCoP(O_2).

For CH_3-ImCoPpIXDME in concentrations from 7.6×10^{-6} to 7.9×10^{-4} M in DCE pseudo first order behavior was observed at 20°C (Figure VII.32, Table VII.10).

In DCE reasonable pseudo first order plots were achieved for the oxidation of CH_3-ImCoTPP (Figure VII.33, Table VII.11), and the rate constants remained reasonably constant over a 200 fold change in cobalt concentration from 4.0×10^{-6} to 7.6×10^{-4} M. In contrast to the other porphyrin systems studied in DCE, there was very little initial oxygenation in this system. Oxidation of CH_3-ImCoTPP in toluene proceeded very slowly ($t_{\frac{1}{2}}$ - 4 d at 30°C under 800 Torr O_2). The observed behavior was similar at cobalt concentrations of 3.6×10^{-6} and 5.1×10^{-5} M (Appendix Vbb).

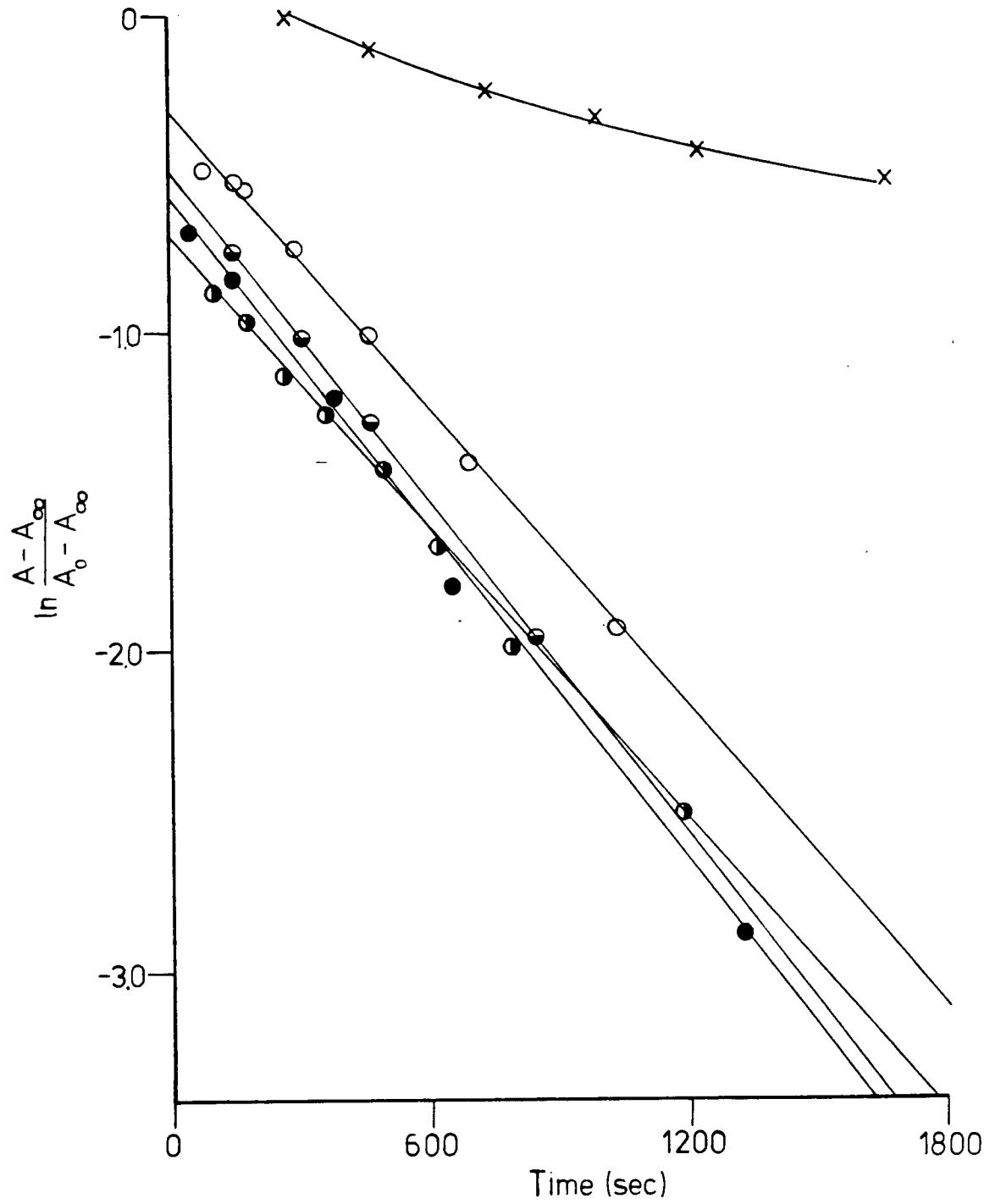

Figure VII.30 First order rate plots for the oxidation of CH_3-ImCoEpI in DCE @ 30°C as a function of [Co]. See Appendix Vdd.

● [Co] = 6.0 x 10^{-6} M

◑ [Co] = 1.1 x 10^{-5} M

◒ [Co] = 5.2 x 10^{-5} M

○ [Co] = 4.7 x 10^{-4} M

X [Co] = 2 x 10^{-3} M

Table VII.9a Kinetic Data for the Oxidation of CH_3-ImCoEpI in DCE as a Function of Cobalt Concentration

Cobalt concentration, M	P_{O_2}, Torr	T, °C	$[CH_3\text{-Im}]$, M	k_{obs}, sec^{-1}
6.0×10^{-6}	800	30	0.0625	1.75×10^{-3}
1.1×10^{-5}	800	30	0.0625	1.51×10^{-3}
5.2×10^{-5}	800	30	0.0625	1.60×10^{-3}
4.7×10^{-4}	800	30	0.0625	1.54×10^{-3}
2×10^{-3}	800	22	0.0625	$\sim 3.7 \times 10^{-4}$ non first order

Table VII.9b Kinetic Data for the Oxidation of CH_3-ImCoEpI in DCE as a Function of Temperature

Cobalt cocentration, M	P_{O_2}, Torr	T, °C	$[CH_3\text{-Im}]$, M	k_{obs}, sec^{-1}
1.2×10^{-5}	800	10	0.0625	3.6×10^{-4}
1.2×10^{-5}	800	20	0.0625	8.1×10^{-4}
1.1×10^{-5}	800	30	0.0625	1.51×10^{-3}

Table VII.10 Kinetic Data for the Oxidation of CH_3-ImPpIXDME in DCE as a Function of Cobalt Concentration

Cobalt concentration, M	P_{O_2}, Torr	T, °C	$[CH_3\text{-Im}]$, M	k_{obs}, sec^{-1}
7.6×10^{-6}	800	20	0.0625	7.7×10^{-4}
6.0×10^{-5}	800	20	0.0625	8.0×10^{-4}
7.9×10^{-4}	800	20	0.0625	6.2×10^{-4}

Table VII.11 Kinetic Data for the Oxidation of CH_3-ImCoTPP in DCE as a Function of Cobalt Concentration

Cobalt concentration, M	P_{O_2}, Torr	T, °C	$[CH_3\text{-Im}]$, M	k_{obs}, sec^{-1}
4.0×10^{-6}	800	30	0.0625	6.36×10^{-4}
5.2×10^{-5}	800	30	0.0625	7.04×10^{-4}
7.6×10^{-4}	800	30	0.0625	7.23×10^{-4}

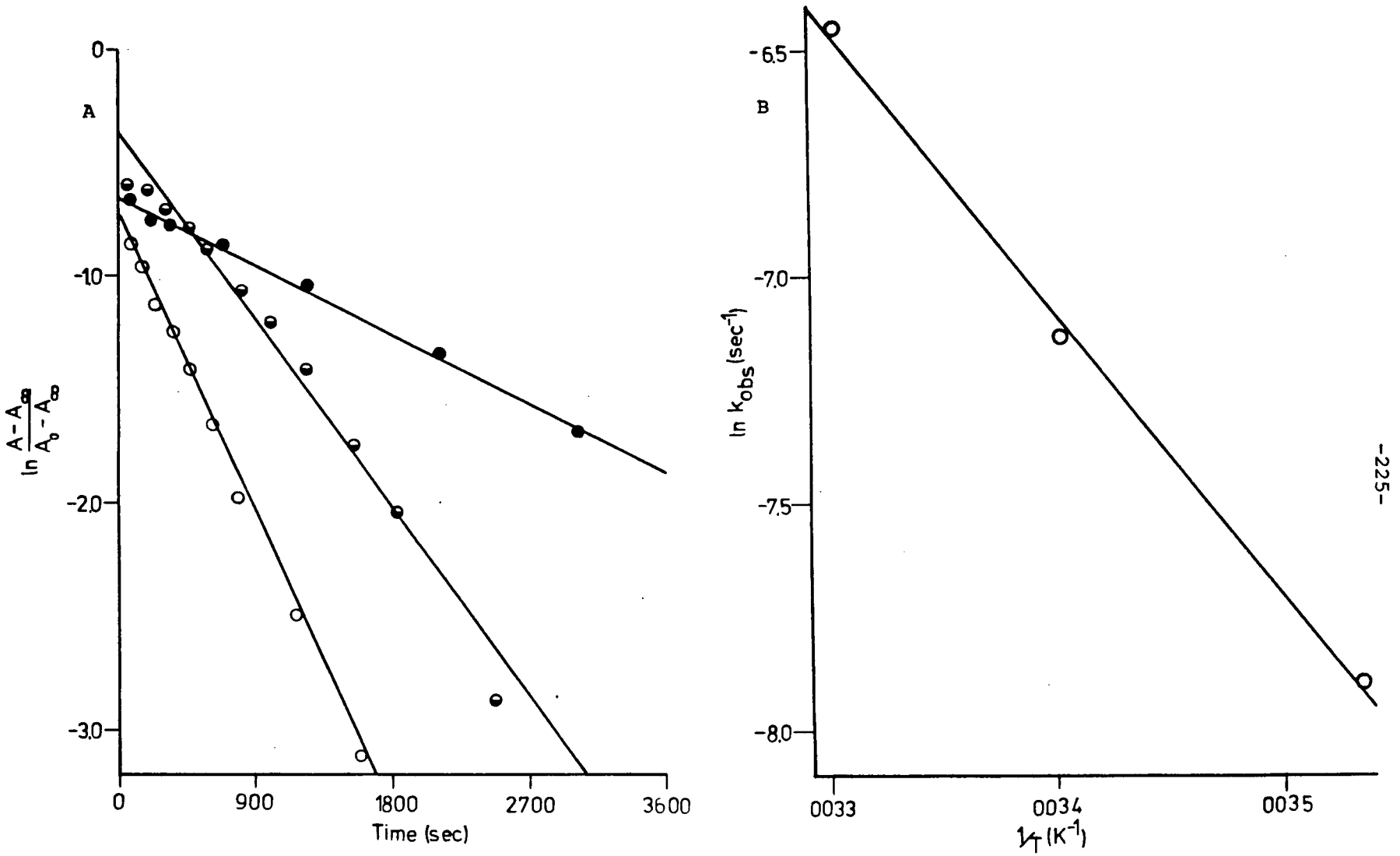

Figure VII.31 Temperature dependence of the oxidation of ~1 x 10^{-5} M CH_3-ImCoEpI in DCE.

A. Pseudo first order rate plots.

B. Arrhenius plot.

For raw data see Appendix Vee.

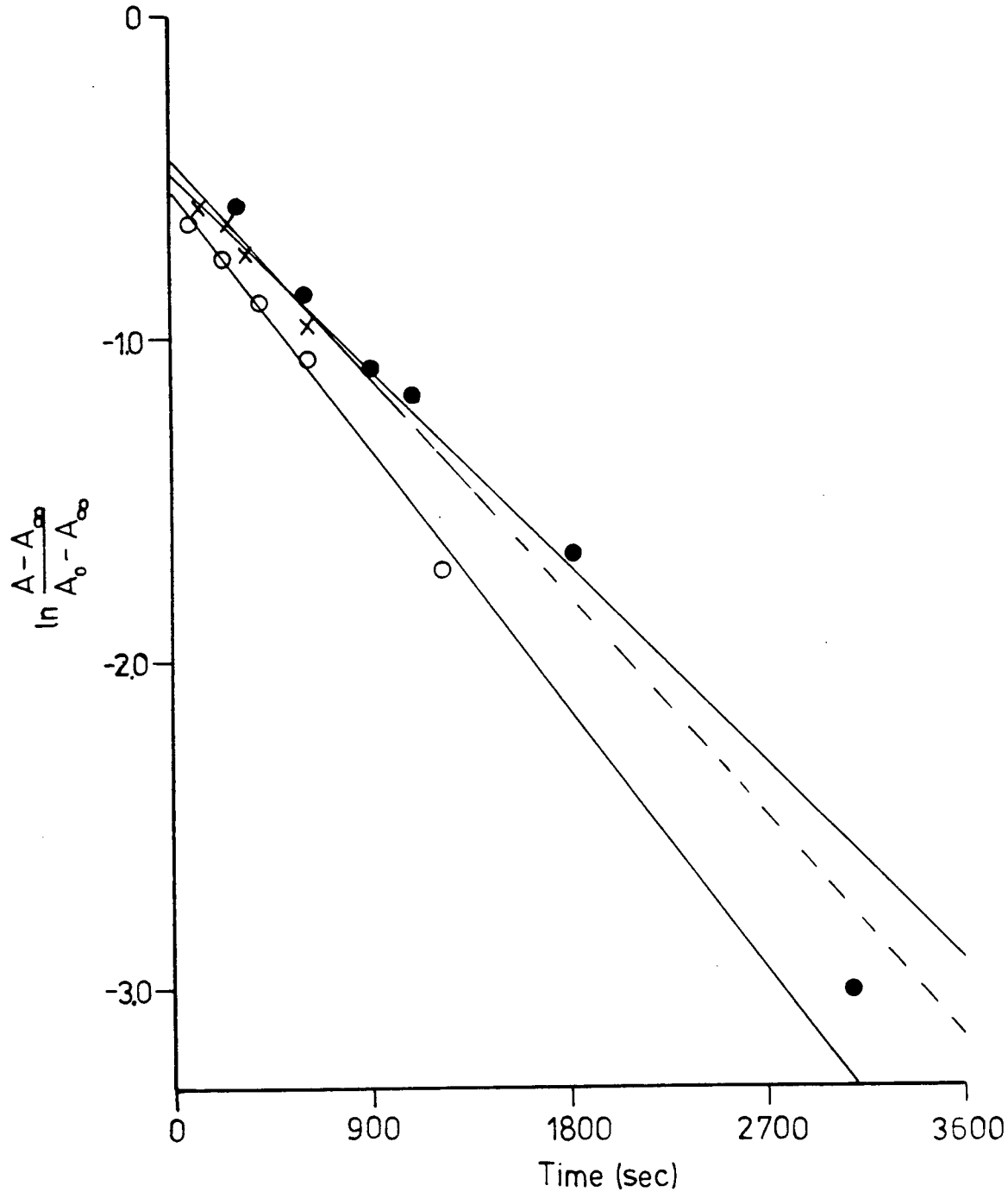

Figure VII.32 First order rate plots for the oxidation of CH_3-ImCoPpIXDME in DCE as a function of [Co]. See Appendix Vjj.

O $[Co] = 7.6 \times 10^{-6}$ M

● $[Co] = 6.0 \times 10^{-5}$ M

X $[Co] = 7.9 \times 10^{-4}$ M

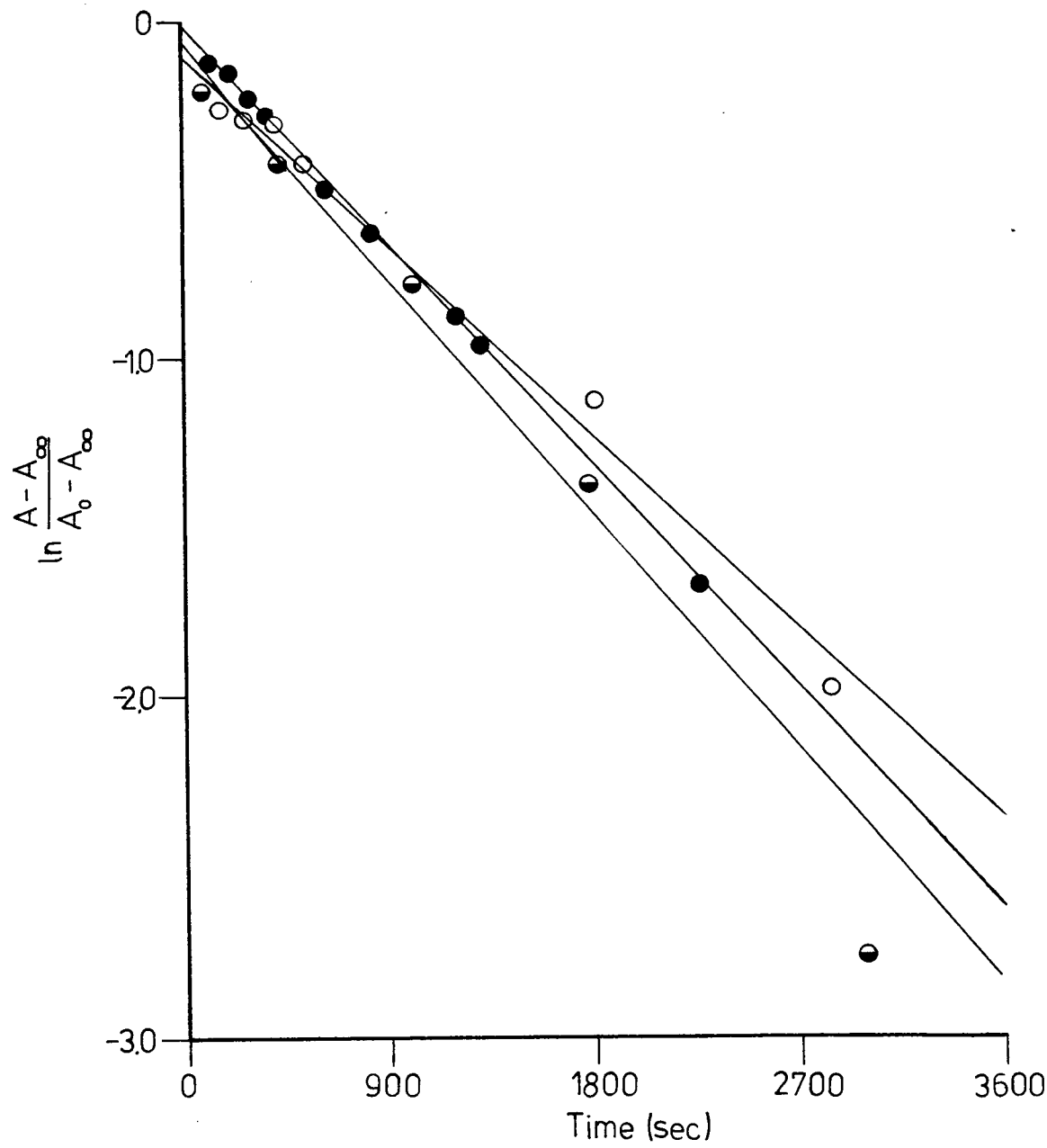

Figure VII.33 First order rate plots for the oxidation of CH_3-ImCoTPP in DCE as a function of [Co]. See Appendix Vcc

○ [Co] = 4.0×10^{-6} M

◒ [Co] = 5.2×10^{-5} M

● [Co] = 7.6×10^{-4} M

VII.8 Concluding Comments

From these studies it can be seen that numerous species may be involved in the irreversible oxidation of cobalt porphyrin systems. An overall scheme for this process could be:

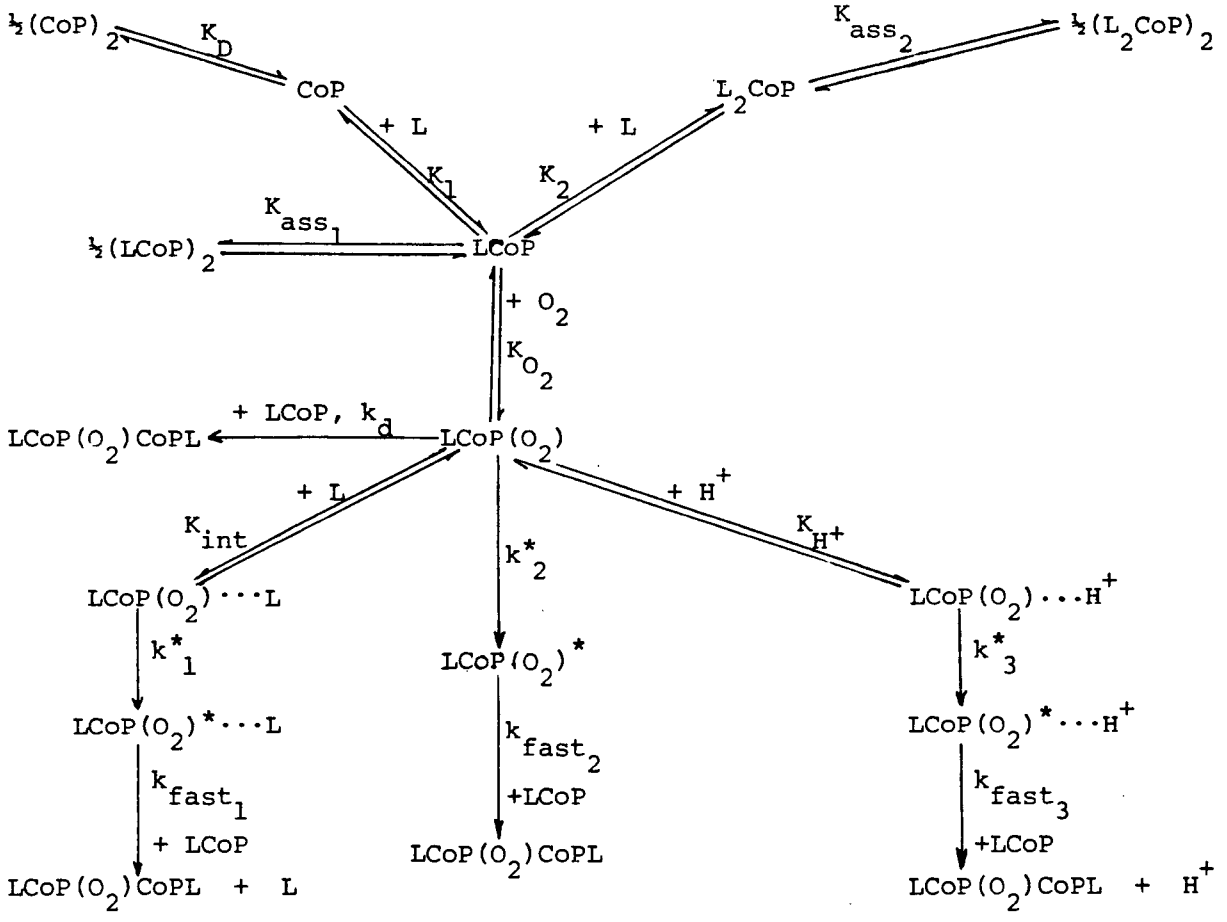

This scheme could be further complicated by the presence of higher order aggregates of cobalt porphyrins, especially at higher concentrations. Although studies in DCE suggest the reaction is enhanced by free protons, the precise pathway has not been elucidated, and evidence has been presented in other studies[158] for outer sphere O_2 oxidation of metalloporphyrins with protons being involved.

Deriving an overall rate law for the above scheme, entailing all the steps indicated, yields the following somewhat intractable expression:

$$\frac{d}{dt}[\text{product}] = \frac{K_{O_2}[O_2][Co]_T}{\left((1 + K_1^{-1}[L]^{-1} + K_2[L] + (1 + K_{int}[L] + K_{H^+}[H^+])K_{O_2}[O_2]\right)^2 + 2[Co]_T(K_{ass_1}^2 + K_{ass_2}^2 K_2^2[L]^2 + K_1^{-2}[L]^{-2}K_D^{-2})\Big)^{\frac{1}{2}}}$$

$$\times \left[\frac{k_d[Co]_T}{\left((1 + K_1^{-1}[L]^{-1} + K_2[L] + (1 + K_{int}[L] + K_{H^+}[H^+])K_{O_2}[O_2]\right)^2 + 2[Co]_T(K_{ass_1}^2 + K_{ass}^2 K_2^2[L]^2 + K_1^{-2}[L]^{-2}K_D^{-2})\Big)^{\frac{1}{2}}} + k^*_1 K_{int}[L] + k^*_2 + k^*_3 K_{H^+}[H^+]\right] \quad \text{(VII.32)}$$

In spite of the very complex overall nature of the oxidation of cobalt porphyrins, several of the parameters involved in these systems are sometimes eliminated by selecting appropriate reaction conditions, and simplified treatments can be used (e.g. Eq. VII.24). From detailed studies of the cobalt porphyrins, the relative energy levels of the species involved in oxidation can be estimated, and are represented in the energy level diagram below:

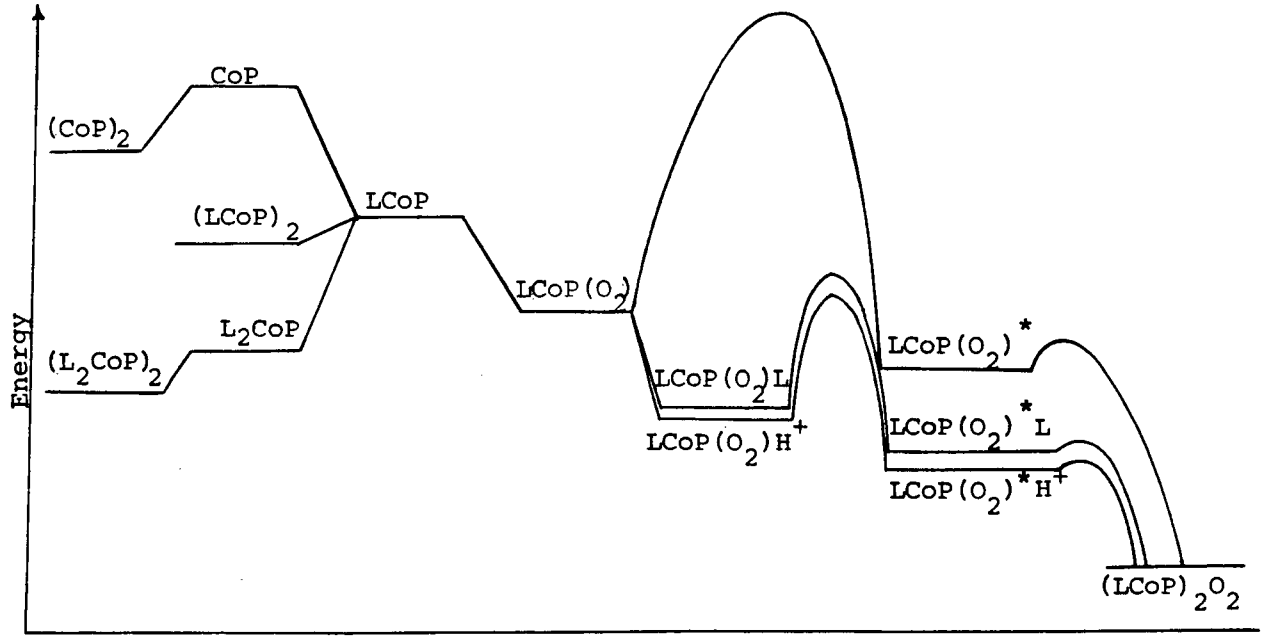

The relative energy levels of CoP, LCoP, L_2CoP, and LCoP(O_2) are determined by independent thermodynamic studies on one species being converted to another (Ch. III - Ch. VI). The energy levels of the dimeric species are estimated from reports that aggregation is an exothermic process[139] and an observation that oxygenation of LCoOMBP is more exothermic than aggregation of that species (Ch. VII.5). Ligand-stabilized or proton-stabilized dioxygen adducts should lie at lower energy than non-stabilized adducts. The slowness in formation of any "activated intermediate" demonstrates a substantial energy barrier to the formation of these species. The energy level of the "activated intermediate" could lie anywhere between that of the transition state of its formation and that of the final unreactive product. For a negative $\Delta H^{\ddagger}$ value to be observed in the oxidation of the ImCoOMBP system, the energy level of ImCoOMBP must be higher than that of the transition state in that process. The above diagram shows that this seems reasonable. As mentioned previously, the pathway involved in proton-enhanced oxidation is not yet clear, and what is represented on the energy level diagram results from a plausible process.

One striking aspect of the foregoing work is the observation of a first order dependence on cobalt at 10^{-6} - 10^{-5} M for oxidation, throughout all the cobalt porphyrin complexes studied. Some form of activated intermediate (LCoP(O_2)*) has already been postulated for these systems[123]. As the oxidation reaction is enhanced in more polar media, this suggests that the activated intermediate could be even more polar than the superoxide-like Co(III)-$O-O^-$ moiety generally accepted to be present in the 1:1 Co:O_2 adduct[22,23]. A recent report[159] suggests that an essential step for the reaction of $Pt(PPh_3)_2O_2$ (where the dioxygen is present as a peroxide) with HX (X = NO_3^-, Cl^-, of BF_4^-) or RCOR' is the rearrangement of the peroxide to a superoxide-like intermediate:

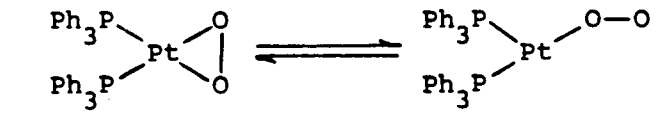

(VII.33)

$((PPh_3)_2Pt(II)O_2^{2-})$ $((PPh_3)_2Pt(I)O_2^{-})$

An observation of the above study was a decrease in reaction rate with an increase in solvent polarity. In the LCoP-dioxygen systems considerable change in geometry and bonding characteristics ($sp^2 \longrightarrow sp^3$) of coordinated dioxygen is required for formation of the bridged dimer species. Kinetic findings in this chapter suggest that a large amount of this change to the more peroxide-like dioxygen occurs before a rapid attack by another cobalt complex. A peroxide-like species, having more charge density than a superoxide-like species, would be expected to be formed more readily in more polar media, thus accounting for the enhanced oxidation rate in the more polar solvents.

From these studies it can be seen that the nature of the solvent plays a major role in aiding the oxygenation or oxidation of a cobalt(II) porphyrin complex. As would be anticipated, the solvent polarity is important in stabilizing the polar 1:1 cobalt:dioxygen adduct. However, solvents such as DCE appear to facilitate oxidation by another important process, that is by preventing aggregation of porphyrin complexes, which appears to occur generally for cobalt porphyrins if their concentration becomes sufficiently high. Of the cobalt porphyrins studied, the OMBP systems appear to aggregate the most readily in non aqueous solvents. At visible spectroscopic concentrations (10^{-6}-10^{-5}M) the other cobalt porphyrins do not appear to aggregate, as deduced from the kinetic results presented in this chapter and observations that CoPpIXDME[89], CoMpIXDME[89], and CoOEP[95] have constant K_1 and K_{O_2} values throughout this range. Similar observations for CoDADIXDME and CoDBrDIXDME systems indicate that aggregation of these porphyrins is not important in this concentration range where K_1 and K_{O_2} are determined.

CHAPTER VIII

THERMODYNAMICS AND KINETICS OF REVERSIBLE LIGAND AND DIOXYGEN BINDING TO Co(SALEN) COMPLEXES

VIII.1 Qualitative Spectral Observations

The visible spectrum of a solution of Co(salen) in dichloromethane has a prominent band at 410 nm ($\varepsilon = 1.15 \times 10^4\ M^{-1}cm^{-1}$) which is somewhat broader than cobalt porphyrin Soret bands. A similar visible spectrum is observed in DMF or toluene, with the band position shifted to 408 nm in the former solvent and 418 nm in the latter.

Addition of a nitrogen-coordinating ligand (L) caused a general decrease of absorption in the band region with an isosbestic point occurring between 530 and 555 nm (Figure VIII.1).

Exposure of a five-coordinate LCo(salen) adduct to dioxygen at low temperature caused a broad band to develop in the 390 nm region with isosbestic points occurring at either side of the band (Figure VIII.2).

Addition of dioxygen at low temperature to Co(salen) resulted in spectral changes somewhat similar to those occurring when amine ligands were added (Figure VIII.3); at higher concentrations, the orange Co(salen) solution became very dark (black) upon oxygenation.

All of the above reactions were reversed when the solution was warmed and/or when dioxygen was pumped off. Amine ligation, and oxygenation of an amine adduct, were too fast to be measured on a stopped-flow time scale;

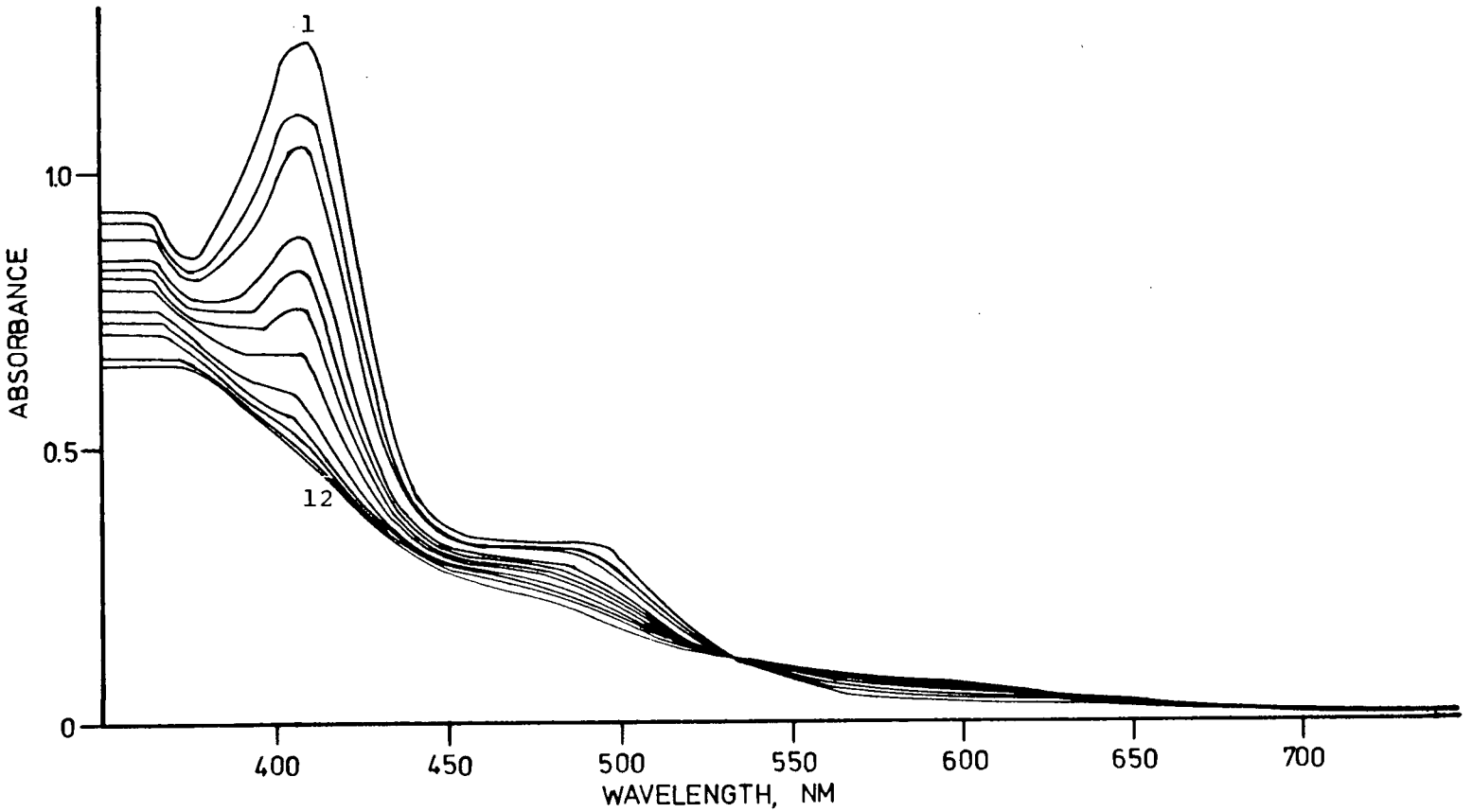

Figure VIII.1 CH_3-Im + Co(salen) $\rightleftharpoons$ CH_3-ImCo(salen) @ 15°C in dichloromethane.

For raw data see Appendix VIa.

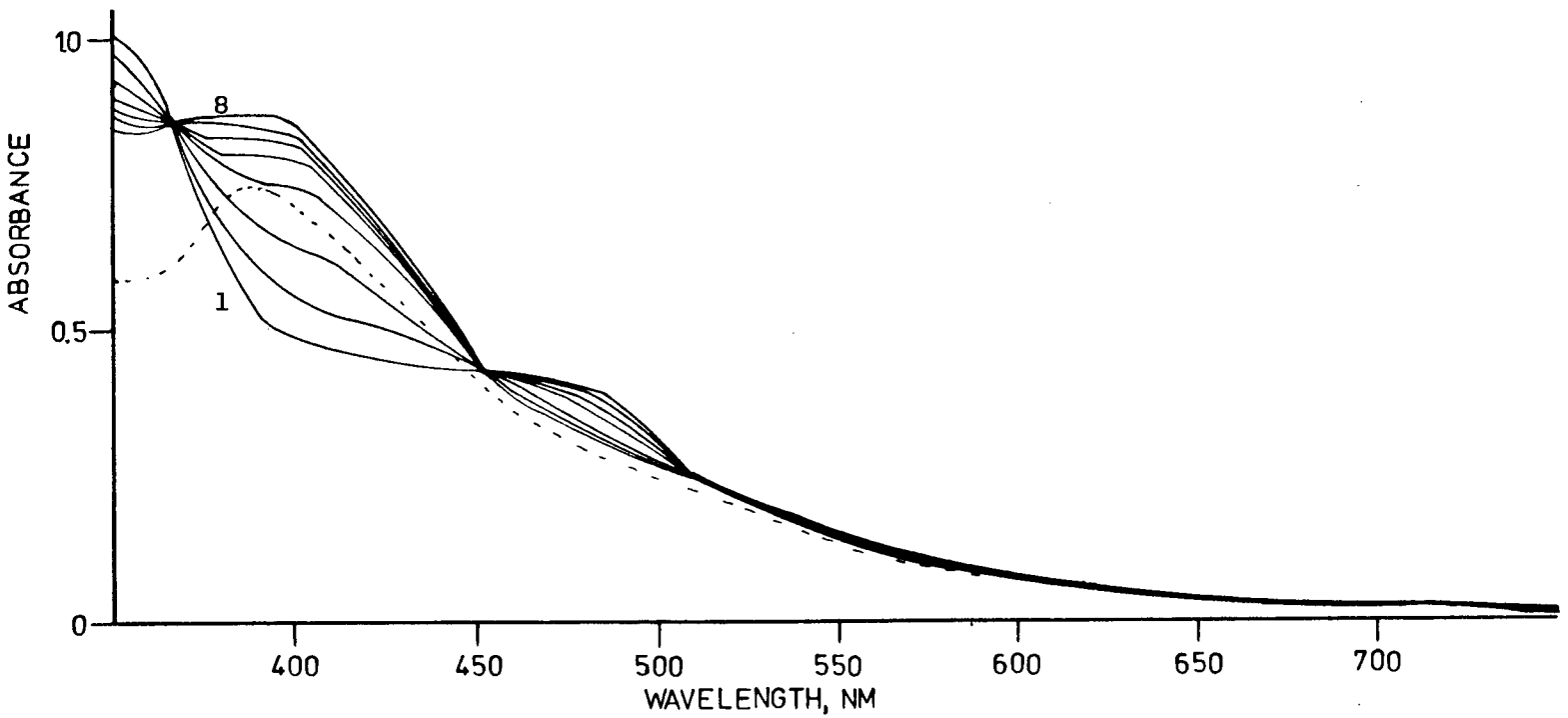

Figure VIII.2 CH_3-ImCo(salen) + $O_2 \rightleftharpoons$ CH_3-ImCo(salen)(O_2) @ -78°C in dichloromethane.

Dotted trace shows the spectrum of CH_3-ImCo(salen)(O_2)Co(salen)CH_3-Im.

For raw data see Appendix VId.

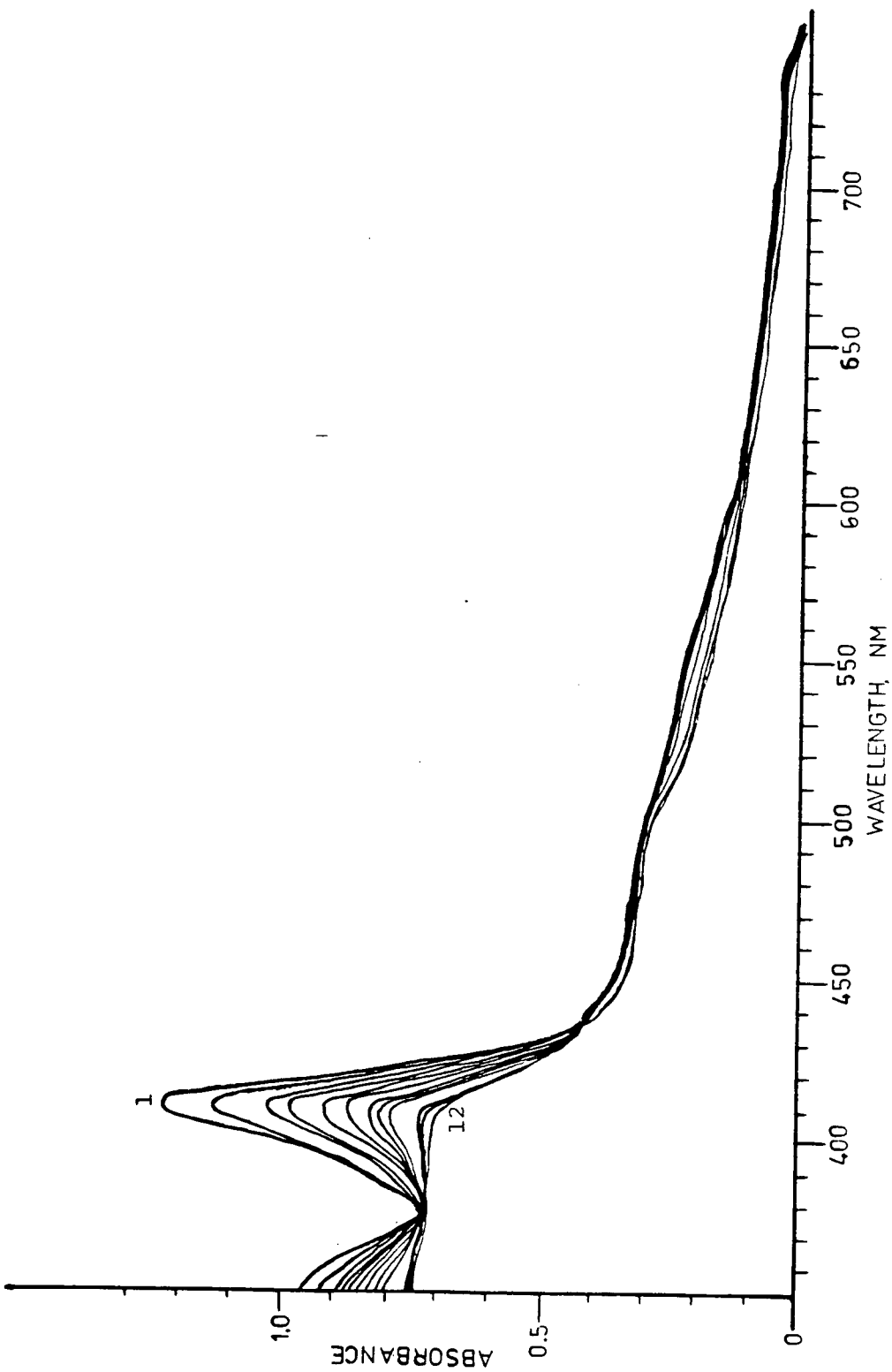

Figure VIII.3 Spectra showing the oxygenation of Co(salen) by 205 Torr O_2 @ -83.5°C in dichloromethane. See Appendix VIh.

oxygenation of Co(salen) proceeded at a rate readily measured by conventional methods.

A band more distinct than that of the 1:1 dioxygen adducts frequently occurred in the 390 nm region (Figure VIII.2), especially in the later stages of an experiment and at higher temperatures; this spectrum was attributed to a bridged dioxygen LCo(salen)(O_2)Co(salen)L species.

A summary of the spectral observations is presented in Table VIII.1.

VIII.2 Treatment of Data

The ligand and dioxygen binding reactions of Co(salen) are analogous to the corresponding reactions of CoOMBP, and are treated in a manner similar to that discussed for those systems (Chapters III, IV). A 1:1 binding behavior was consistently observed in these systems. In the case of CH_3-Im and Pip reacting with Co(salen), the 1:1 observed binding behavior was corroborated by a three line superhyperfine splitting in ESR signals at 77 K in dichloromethane (Figure VIII.4) resulting from the coordinated nitrogen (I = 1). However, in the case of the Co(salen)-Py system a five line superhyperfine ESR splitting was observed at 77 K in frozen dichloromethane-Py, indicative of a bis Py adduct under these conditions. Confirmation that 1:1 Co:O_2 adduct occurred upon low temperature addition of dioxygen to four-and five-coordinate Co(salen) systems was obtained from the presence of a sharp ESR signal (Figure VIII.5), indicative of some unpaired electron density on the oxygen atoms (I = 0).

Figure VIII.6 shows the $\log \frac{A_o - A}{A - A_\infty}$ vs $\log [CH_3\text{-Im}]$ plots resulting from the addition of CH_3-Im to Co(salen) in dichloromethane. Figures VIII.7 and 8 show the $\log \frac{A_o - A}{A - A_\infty}$ vs $\log P_{O_2}$ plots for the addition of dioxygen to

Table VIII.1 Spectral Data From 350 to 750 nm for the Reactions Involving Co(salen).

a. $L + Co(salen) \rightleftharpoons LCo(salen)$

Absorbing Species	Solvent	Absorption Maximum, nm (Extinction Coefficient, $M^{-1}cm^{-1}$)	Isosbestic Points (nm)
Co(salen)	CH_2Cl_2	410 (1.15×10^4)	
+ CH_3-Im	CH_2Cl_2	— —	544
+ Pip	CH_2Cl_2	— —	530
+ Py	CH_2Cl_2	— —	479 475 519
+ O_2	CH_2Cl_2	— —	434
Co(salen)	DMF	408 (1.13×10^4)	
+ CH_3-Im	DMF	— —	554
+ Pip	DMF	— —	552
+ Py	DMF	— —	446 456 534
Co(salen)	Toluene	418 (1.18×10^4)	
+ CH_3-Im	Toluene	— —	449
+ Pip	Toluene	— —	445
+ Py	Toluene	— —	450 464 532

Table VIII.1 cont. Spectral Data From 350 to 750 nm for the Reactions Involving Co(salen).

b. $LCo(salen) + O_2 \rightleftharpoons LCo(salen)(O_2)$

Oxygenated Species (Axial Ligand)	Solvent	Absorption Maximum, nm (Extinction Coefficient, $M^{-1}cm^{-1}$)	Isosbestic Points (nm)
CH_3-Im	CH_2Cl_2	385 (9×10^3)	362 444
Pip	CH_2Cl_2	386 (9×10^3)	443 489
Py	CH_2Cl_2	384 (9×10^3)	445
CH_3-Im	DMF	385 (9×10^3)	364 456
Pip	DMF	389 (9×10^3)	452
Py	DMF	386 (9×10^3)	447 515
CH_3-Im	Toluene	382 (8×10^3)	366 446
Pip	Toluene	382 (8×10^3)	372 457
Py	Toluene	382 (8×10^3)	368

Table VIII.1 conc. Spectral Data From 350 to 750 nm for the Reactions Involving Co(salen).

c. $LCo(salen)(O_2)Co(salen)L$

Absorbing Species (Axial Ligand)	Solvent	Absorption Maximum (Extinction Coefficient, $M^{-1}cm^{-1}$)
CH_3-Im	CH_2Cl_2	387 (7×10^3)
Pip	CH_2Cl_2	392 (7×10^3)
Py	CH_2Cl_2	390 (7×10^3)
CH_3-Im	DMF	390 (7×10^3)
Pip	DMF	392 (7×10^3)
Py	DMF	390 (7×10^3)
CH_3-Im	Toluene	390 (7×10^3)

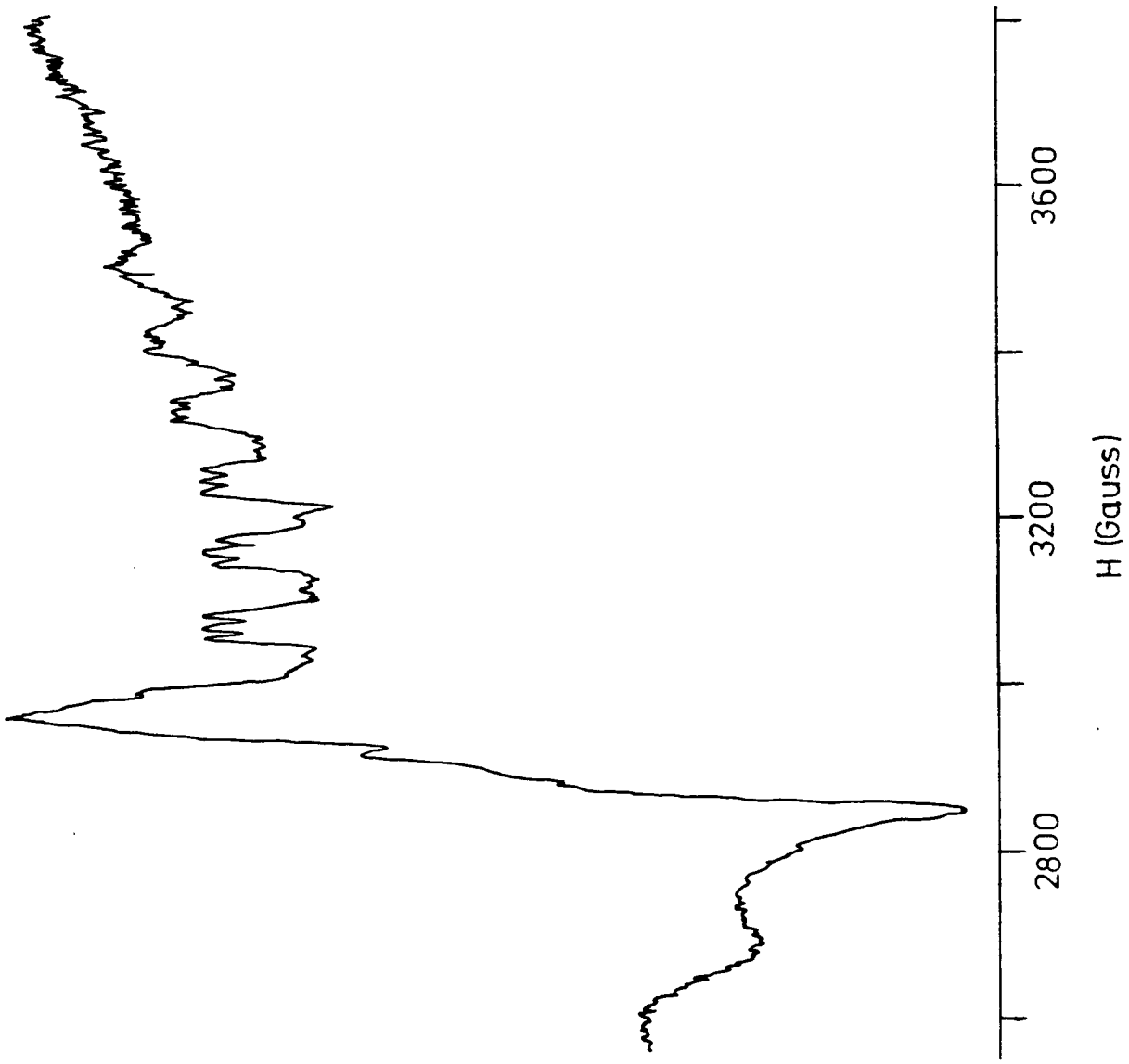

Figure VIII.4 ESR signal of CH_3-ImCo(salen) @ 77 K in dichloromethane.

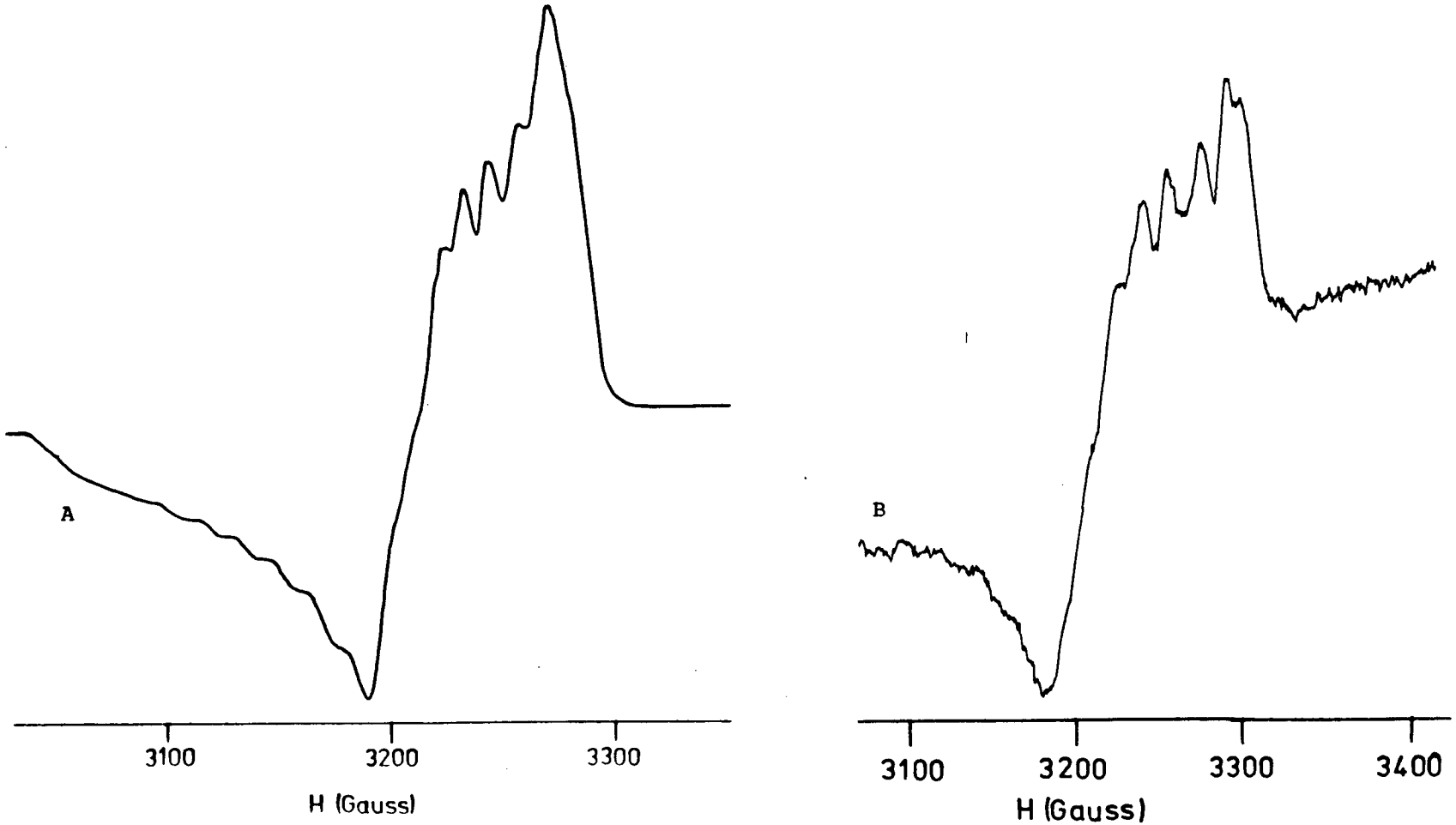

Figure VIII.5 A. ESR signal of CH_3-ImCo(salen)(O_2) @ 77 K in dichloromethane.

B. ESR signal of Co(salen)(O_2) @ 77 K in dichloromethane.

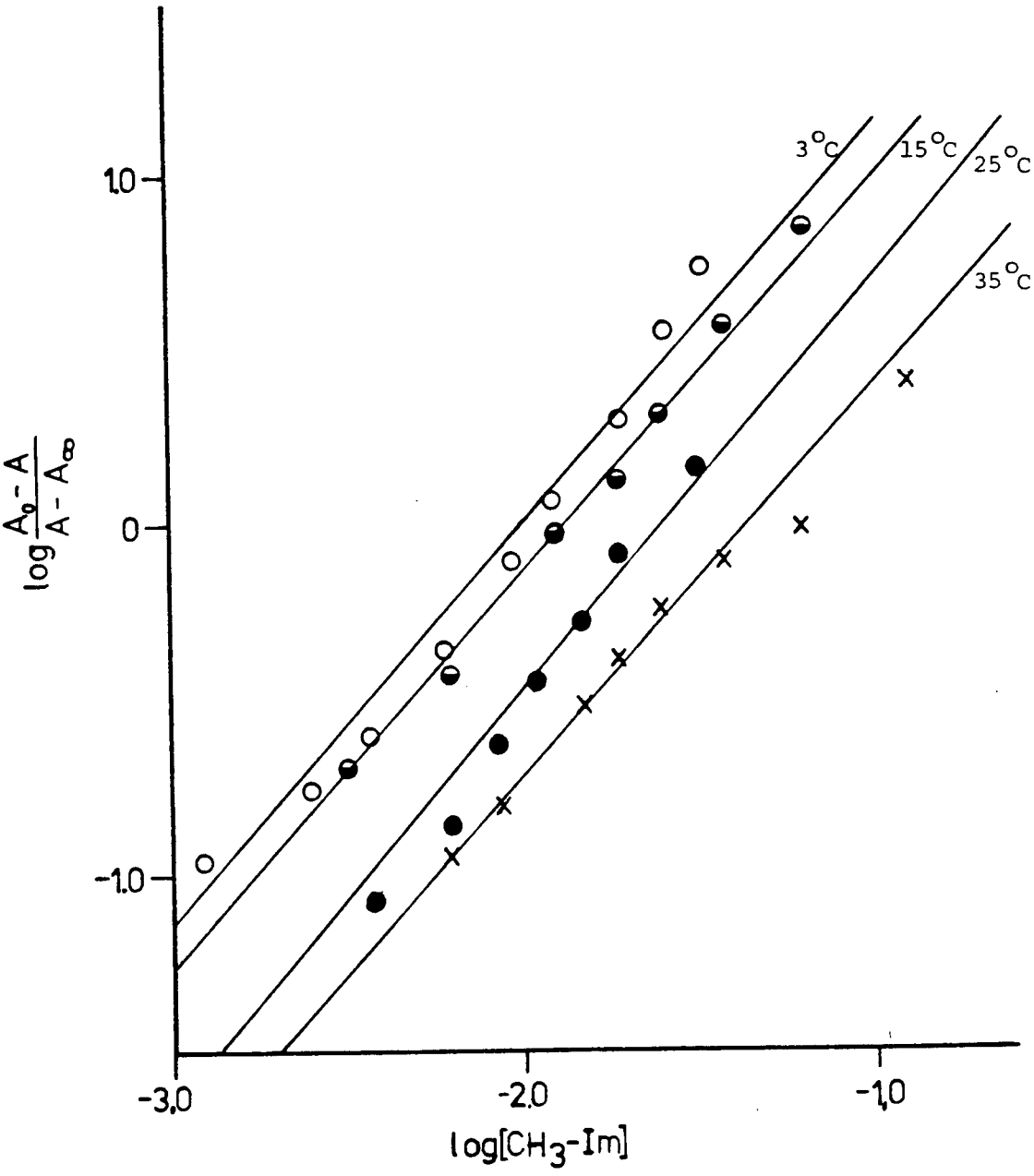

Figure VIII.6 Equilibrium plots for CH_3-Im + Co(salen) $\rightleftharpoons$ CH_3-ImCo(salen)

For raw data see Appendix VIa.

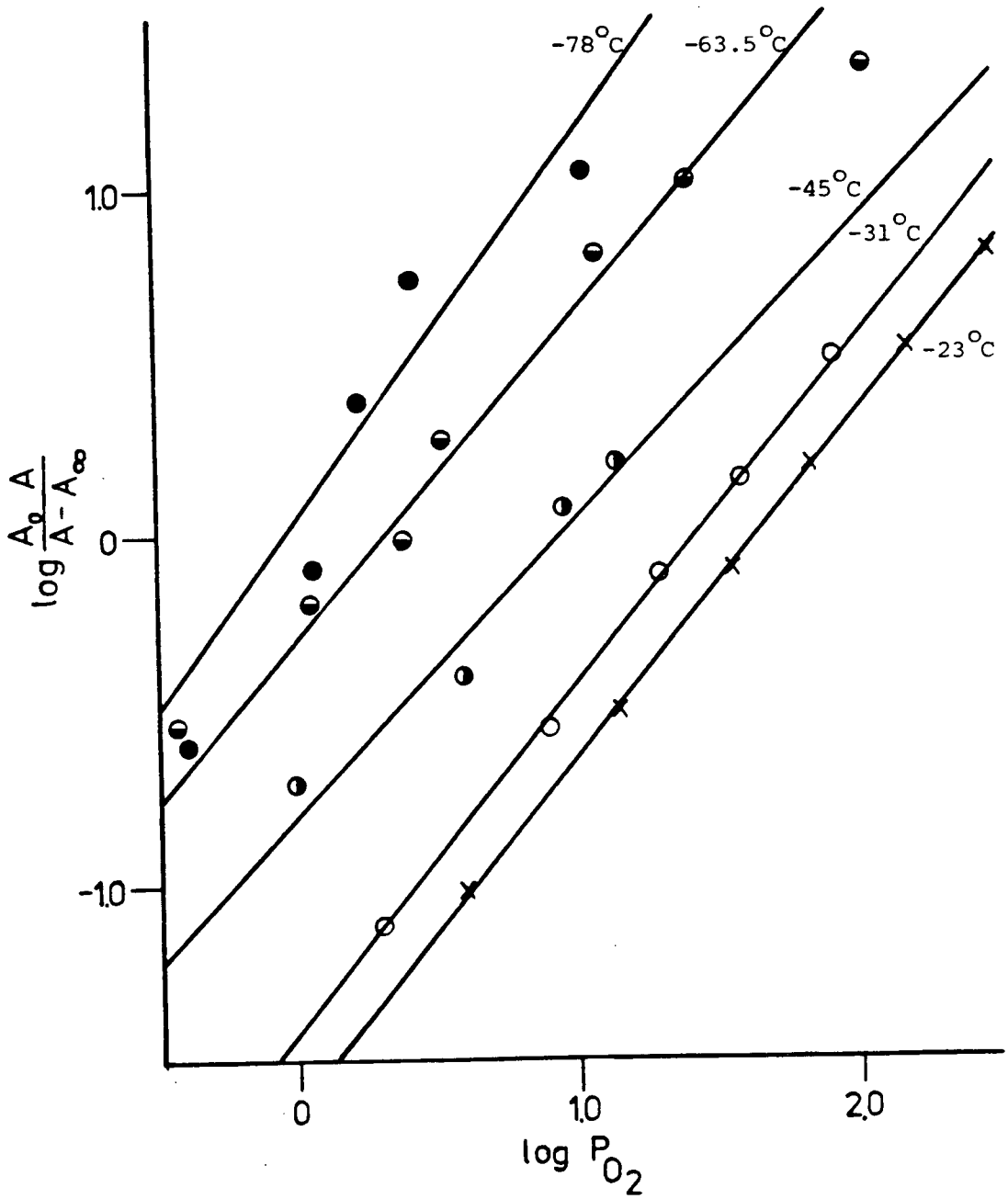

Figure VIII.7 Equlibrium plots for CH_3-ImCo(salen) + $O_2 \rightleftharpoons$ CH_3-ImCo(salen)(O_2)

For raw data see Appendix VId.

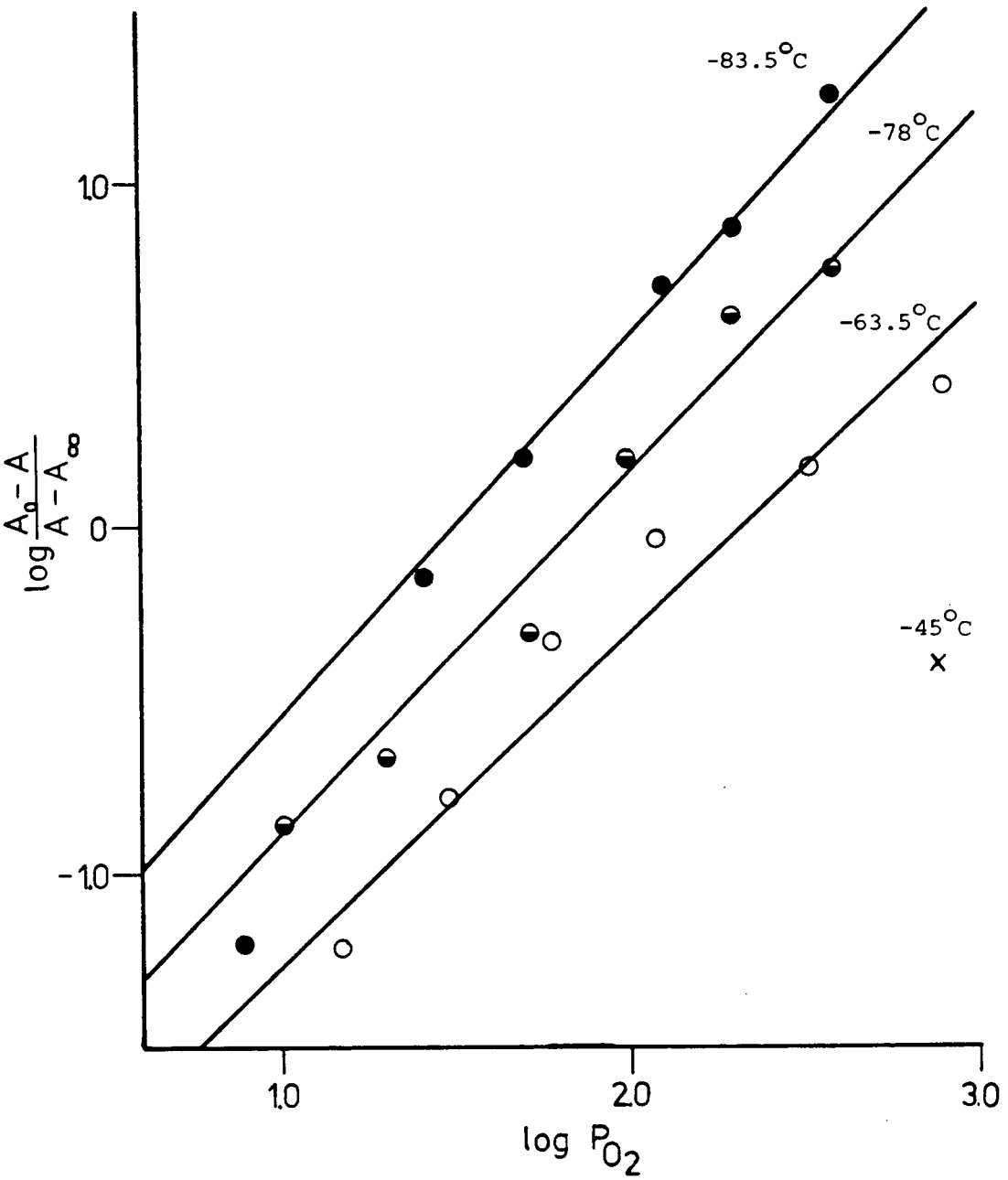

Figure VIII.8 Equilibrium plots for Co(salen) + $O_2 \rightleftharpoons$ Co(salen)(O_2)

For raw data see Appendix VIg.

CH_3-ImCo(salen) in dichloromethane and Co(salen) in dichloromethane, respectively. Figure VIII.9 shows the van't Hoff plots arising from ligand addition to Co(salen) in dichloromethane. Figures VIII.10 and 11 show the van't Hoff plots resulting from dioxygen addition to Co(salen) amine adducts and to Co(salen) in dichloromethane, respectively.

Since the oxygenation of Co(salen) approached an equilibrium position at lower oxygen pressures or higher temperatures, the kinetics of that reaction were analyzed by the following expression:

$$\ln \frac{A - A_{eq}}{A_o - A_{eq}} = -k_t^{'}obs \cdot t = -(k_1 obs + k_{-1} obs)t \qquad \text{(VIII.1)}$$

where A_o is the absorbance of Co(salen) in the absence of oxygen

A is the absorbance reading at time = t

A_{eq} is the absorbance reading at equilibrium

$k_t obs$ is the total observed pseudo first order rate constant

$k_1 obs$ is the pseudo first order forward rate constant

and $k_{-1} obs$ is the first order reverse rate constant

Since the equilibrium constant, K, could also be determined, and K is related to the rate constants by the expression:

$$K = k_1/k_{-1} \qquad \text{(VIII.2)}$$

the forward and back rate constants could be determined.

Direct determination of the off rate was hampered by slow diffusion of oxygen from the dichloromethane solution on pumping. If the temperature were raised to cause the equilibrium to shift sufficiently to the left so that the residual oxygen in the dichloromethane did not oxygenate the complex, the reaction was completed before thermal equilibrium was reached.

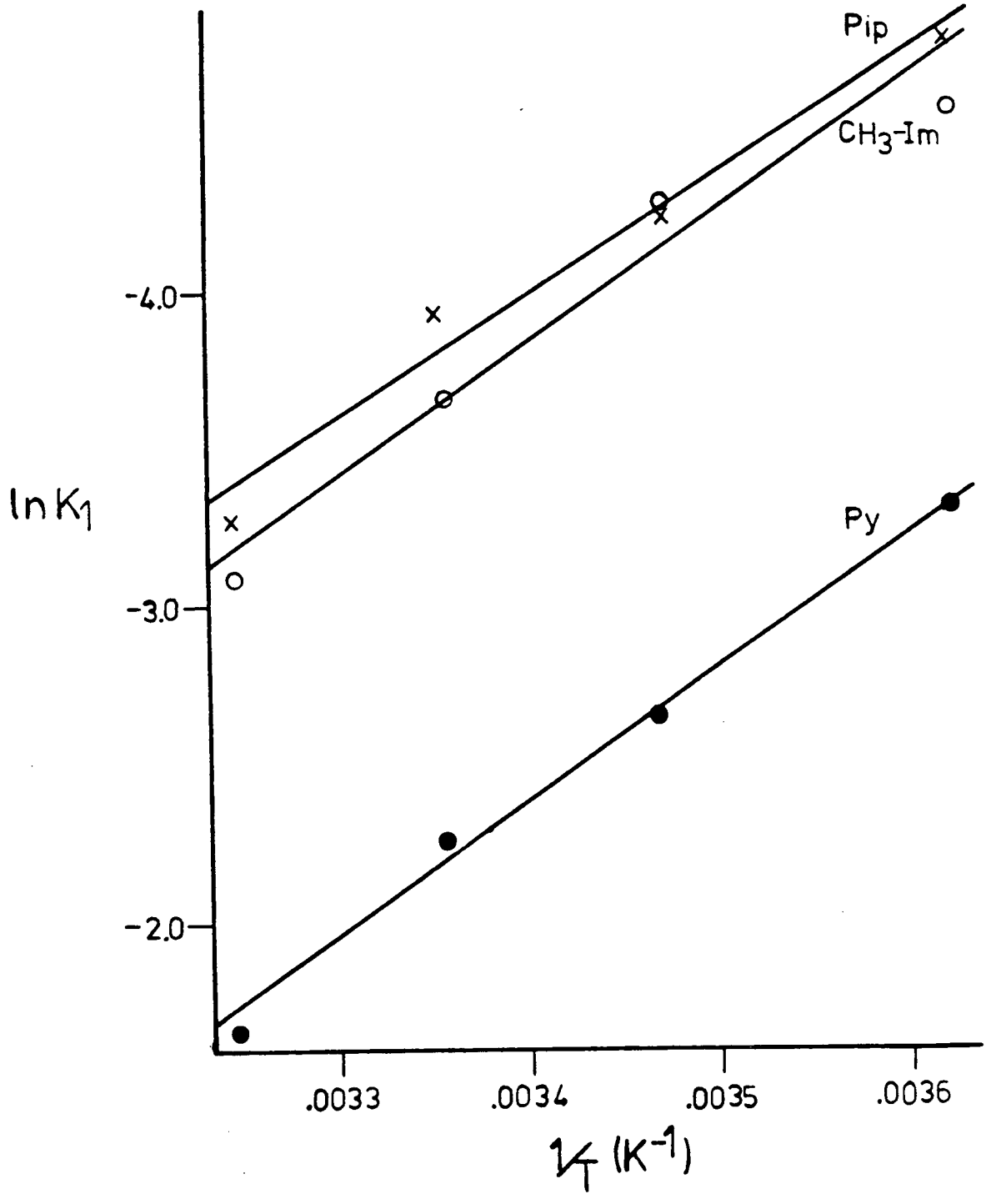

Figure VIII.9 Van't Hoff plots for L + Co(salen) $\rightleftharpoons$ LCo(salen)

L = CH_3-Im, Pip, and Py

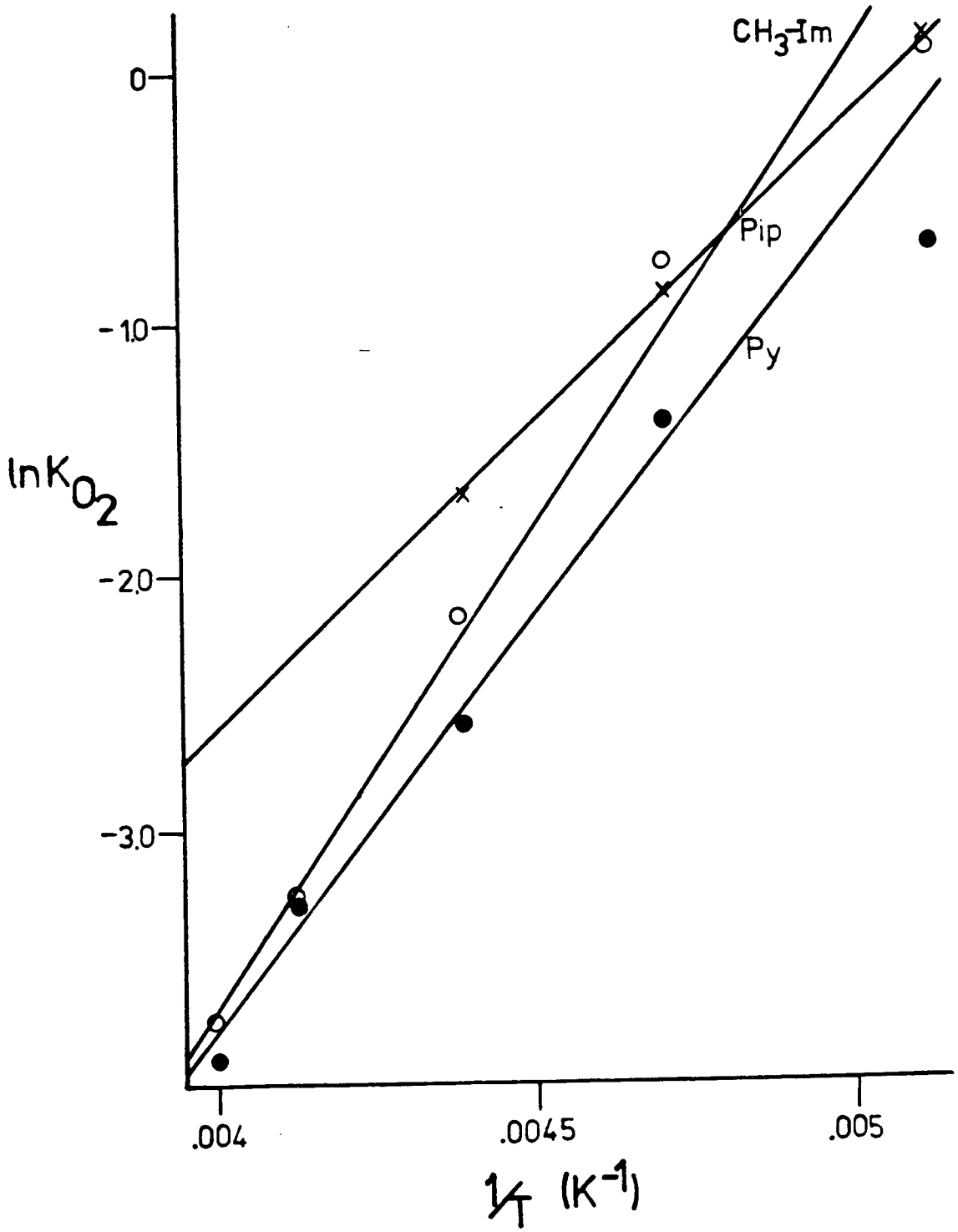

Figure VIII.10 Van't Hoff plots for LCo(salen) + $O_2 \rightleftharpoons$ LCo(salen)(O_2)

L = CH_3-Im, Pip, and Py

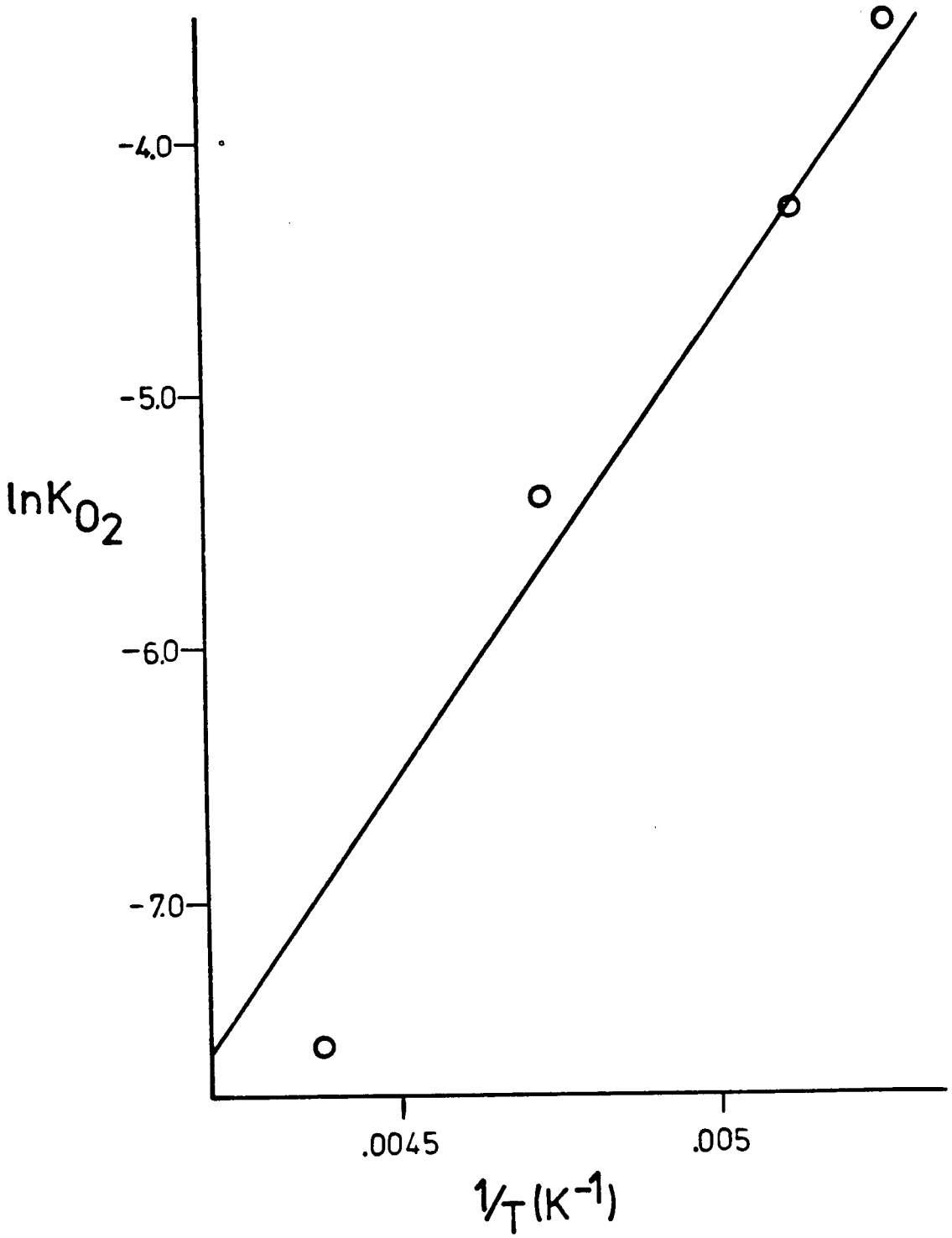

Figure VIII.11 Van't Hoff plot for Co(salen) + $O_2 \rightleftharpoons$ Co(salen)(O_2)

VIII.3 Sources of Error

Errors similar to those noted in the cobalt porphyrin studies are also present during the studies on ligand and dioxygen binding to Co(salen) complexes. These complexes, especially in the more polar dichloromethane and DMF solvent systems, bound dioxygen more readily than corresponding cobalt porphyrin complexes, and the problem of irreversible oxidation was more important; the presence of the bridged peroxide species was frequently noted in ligand and dioxygen binding experiments. Ligand binding studies could still be carried out, although several attempts were sometimes necessary to complete a particular experiment successfully. Lowering the temperature for dioxygen binding studies usually prevented irreversible oxidation, but oxygenation studies could not be completed on the PipCo(salen) system in dichloromethane at -23°C and -31°C due to oxidation. Compared to the formation of cobalt porphyrin adducts, addition of higher concentrations of ligand were necessary to complete the formation of LCo(salen) adducts. However, from considerations similar to those for binding a second ligand to CoOMBP (Chapter III), solvent variation effects were not thought to be important. The concentration of ligand (up to ~0.5 M) required to perform oxygenation studies was not considered to substantially affect the nature of the solvent under the conditions used.

VIII.4 Studies in Dichloromethane

VIII.4.1 $L + Co(salen) \rightleftharpoons LCo(salen)$, K_1

The equilibrium constants of CH_3-Im, Pip, and Py binding to Co(salen) are given in Table VIII.2, the raw data being given in Appendices VIa - VIc. Table VIII.2 also gives the values obtained for ΔH and ΔS, and the pK_a of the protonated ligands.

Table VIII.2 Thermodynamic Data for the Binding of an Axial Ligand to Co(salen) in a Dichloromethane Solution.

LIGAND	TEMP., °C	K_1, M^{-1}	ΔH_1 kcal/mole	ΔS_1 e.u.	pK_a [a]
CH_3-Im	3	99	-8.5	-21	7.25
	15	73			
	25	39			
	35	22			
Pip	3	123	-7.8	-18	11.30
	15	69			
	25	51			
	35	26			
Py	3	27.5	-8.3	-24	5.27
	15	14.1			
	25	9.5			
	35*	5.2			
4-CN-Py†	15	4.57	-8.7	-27	1.86
	25	2.14			
	35	1.62			
4-NH_2-Py†	3	275	-11.8	-31	9.30
	15	105			
	25	82			
	35	46			
PPh_3†	15	0.16			2.73
	25	0.10			

a. For references see Table III.3; see Py ref for values of substituted Py's.

†. D. Hegedic, B. R. James, unpublished results.

*. Data obtained from †; K_1 values for CH_3-Im, Pip, and Py binding from † very similar to those presented above; thermodynamic parameters analyze for: ΔH = -9.2 kcal/mole, ΔS = -24 e.u. (CH_3-Im); ΔH = -9.5 kcal/mole, ΔS = -24 e.u. (Pip); and ΔH = -8.9 kcal/mole, ΔS = -25 e.u. (Py). These parameters are considered to agree with those presented above.

4-CN-Py = 4-cyanopyridine, 4-NH_2-Py = 4-aminopyridine

The order for ligand binding abilities observed at 25°C is: 4-NH_2-Py> Pip>CH_3-Im>Py>4-CN-Py>PPh_3. As with the cobalt porphyrin complexes studied, no general correlation exists between K_1, ΔH_1, ΔS_1 and the pK_a of the protonated ligand, although the three pyridine ligands exhibit a reasonable correlation between log K_1 and pK_a (Figure VIII.12), similar to that observed in the CoPpIXDME systems[89], and a good Hammett relationship is also obtained (Figure VIII.13, ρ = +1.17). The above general ligand binding order is similar to that observed in the CoPpIXDME[89], CoDADIXDME (Chapter V), CoDBrDIXDME (Chapter V), and the CoOMBP (Chapter III) systems, although the relative positions of two adjacent ligands are sometimes reversed.

The affinity of a particular ligand for Co(salen) is two to three orders of magnitude less than for cobalt porphyrin systems. In contrast to the cobalt porphyrin studies in toluene, Co(salen) complexes were initially examined in dichloromethane. However, studies on CoOMBP (Chapter III), and subsequent studies on Co(salen) (Chapter VIII.5), show that the solvent has some effect on ligand binding ability, but not sufficient to account for the large observed differences between Co(salen) and cobalt porphyrin complexes. Attempts to study quantitative ligand binding to cobalt complexes of substituted acacen Schiff bases were frustrated by very small visible spectral changes, but the approximate ligand affinity for a series of these complexes[82] has been reported to be about one to two orders of magnitude less than for cobalt porphyrins. The weaker ligand binding to the Schiff base complexes compared to the porphyrins is attributed to the more electron rich metal centre in Schiff base systems[32,37].

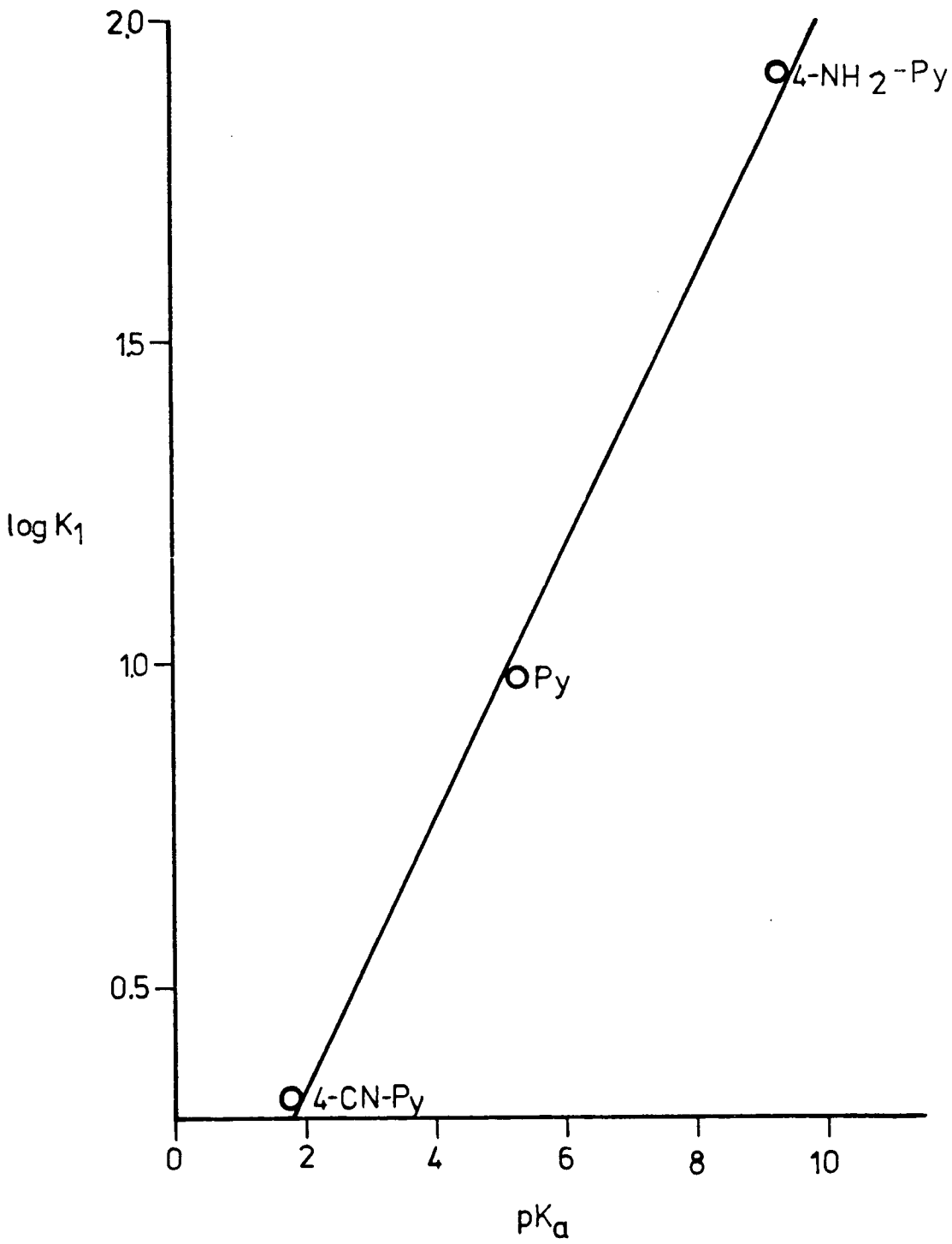

Figure VIII.12 Ligand binding constants vs. pK_a for substituted pyridines in dichloromethane @ 25°C.

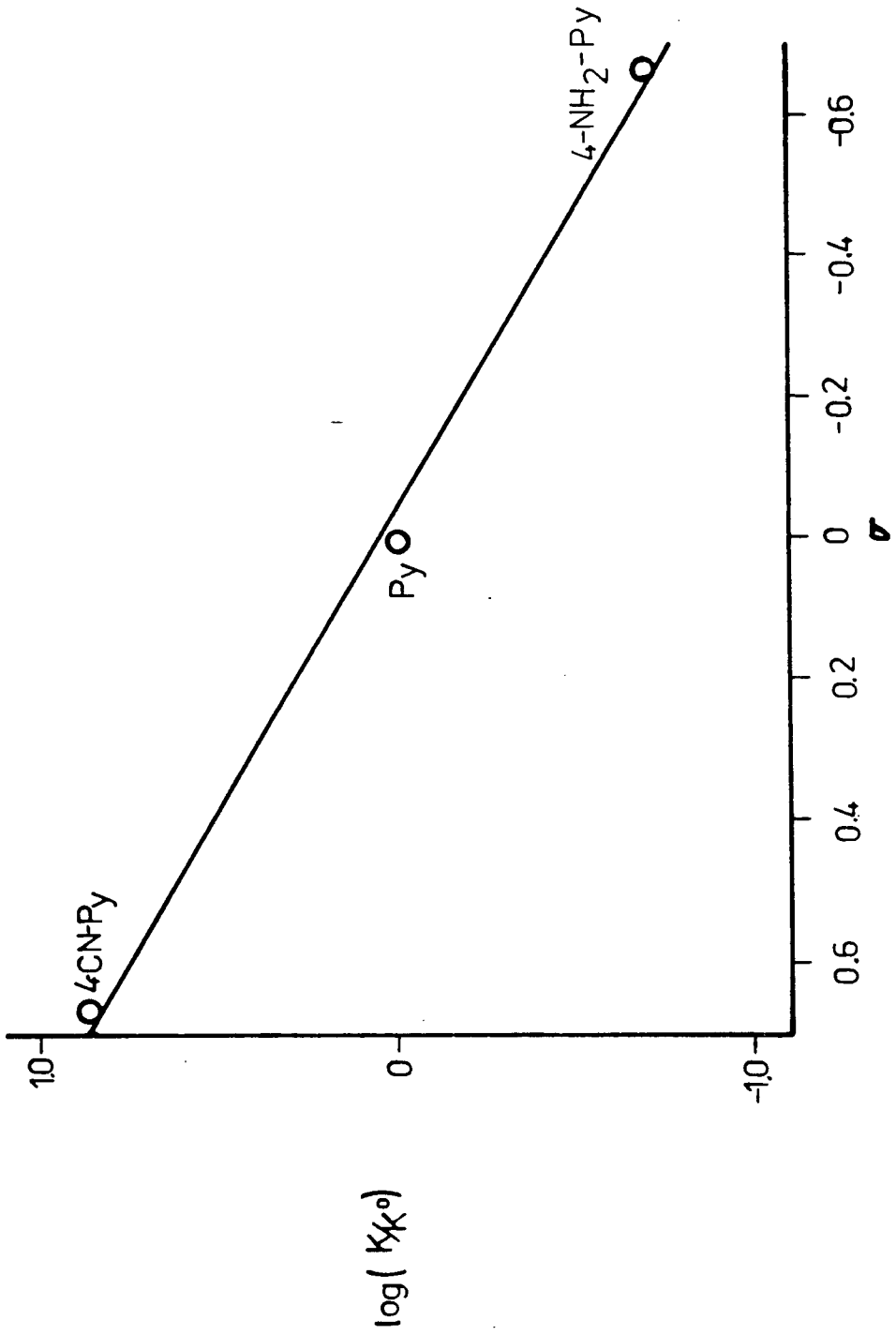

Figure VIII.13 Hammett plot for substituted pyridines binding to Co(salen) in dichloromethane @ 25°C.

VIII.4.2 $LCo(salen) + O_2 \rightleftharpoons LCo(salen)(O_2)$, K_{O_2}.

The $P_{\frac{1}{2}}O_2$ values of the five-coordinate LCo(salen) complexes are given in Table VIII.3, the raw data being given in Appendices VId- VIg. Also listed are the estimated ΔH and ΔS values and the pK_a of the protonated ligand studied. The order of oxygen affinities for the LCo(salen) complexes as a function of axial ligand at -45°C is Pip>CH_3-Im >Py, which is generally the same as the order of ligand binding to Co(salen) and of dioxygen binding to LCoPpIXDME[89], LCoDADIXDME (Chapter VI), LCoDBrDIXDME (Chapter VI), and to LCoOMBP (Chapter IV). Sometimes within the porphyrins the CH_3-Im adduct binds dioxygen more strongly than the Pip adduct and this trend is apparent in the LCo(salen) systems at -63.5°C. A similar dioxygen binding sequence has also been reported for LCo(benacen)[82] with the CH_3-Im adduct binding dioxygen more strongly than the Pip adduct. LCo(salen) complexes bind dioxygen by one or two orders of magnitude more strongly than the corresponding LCoP complexes, again consistent with the more electron rich nature of the Schiff base complex[32,37]. LCo(benacen)[82] complexes bind dioxygen somewhat more strongly than the corresponding LCo(salen) complexes (e.g. $P_{\frac{1}{2}}O_2$ @ -23°C for CH_3-ImCo(benacen) ~8 Torr vs. 43 Torr for CH_3-ImCo(salen), implying that salen withdraws more electron density from the metal centre than benacen. Despite the Co(benacen) studies being carried out in toluene and Co(Salen) being examined in dichloromethane, this conclusion seems reasonable since Co(salen) has a more extensive network of π-electrons around the metal centre than does Co(benacen). The more polar dichloromethane would be expected to enhance oxygenation (Chapter IV), but the oxygen affinity of the Co(salen) system is still less than that of the Co(benacen) system.

Table VIII.3 Thermodynamic Data for the Binding of Dioxygen to LCo(salen) in a Dichloromethane Solution.

LIGAND	TEMP., °C	$P_{\frac{1}{2}}O_2$, Torr	ΔH kcal/mole	ΔS e.u.	pK_a [a]
CH_3-Im	-78	0.89	-7.5	-37	7.25
	-63.5	2.1			
	-45	8.6			
	-31	25.6			
	-23	42.9			
CH_3-Im*	-45	10.2	-7.5	-37	7.25
	-31	26.3			
	-23	44.7			
Pip	-78	0.87	-4.8	-25	11.30
	-63.5	2.3			
	-45	5.4			
Py	-78	2.0	-6.5‡	-33‡	5.27
	-63.5	4.0			
	-45	13.2			
	-31	27.5			
Py*	-45	12.6	-6.7	-35	5.27
	-31	26.3			
	-23	50.1			
no ligand	-83.5	34.7	-8.2	-51	——
	-78	71			
	-63.5	224			
	-45	1900			

a. For references see Table III.3.

*. D. Hegedic, B. R. James, unpublished results

‡. -23°C data from other source (*) considered in calculating thermodynamic parameters

Inspite of LCo(salen) complexes having higher dioxygen affinities than the cobalt porphyrins, the enthalpy of oxygenation of the Co(salen) systems is similar to that of the CoOMBP (Chapter IV) and the CoDADIXDME and CoDBrDIXDME (Chapter VI) systems, and is somewhat less than the CoPpIXDME[89] systems. As the relatively favorable entropy term in the Co(salen) system appears to be important in oxygenation, perhaps the amount of internal rearrangement of the Co(salen) complexes is different from the cobalt porphyrins upon oxygenation. In the more strongly dioxygen binding substituted acacen complexes of cobalt[82], the enthalpy of oxygenation is much greater than in the Co(salen) systems (ΔH_{O_2} of PyCo(benacen) = -16.6 kcal/mole).

VIII.4.3 $\underline{\text{Co(salen)} + O_2 \rightleftharpoons \text{Co(salen)}(O_2),\ K_{O_2}}$

The four-coordinate Co(benacen) system was found to oxygenate in toluene only very slightly at -83.5°C and not at all at -63.5°C[82], and this system was considered air stable. In contrast, exposure of four-coordinate Co(salen) to dioxygen in dichloromethane resulted in visible spectroscopic changes which were reversible in nature. The thermodynamic parameters for the oxygenation are presented in Table VIII.3. The dioxygen affinity of the four-coordinate species is substantially less than those of the five-coordinate complexes; the ΔH value is close to that for O_2 binding to CH_3-ImCo(salen), but the ΔS value is much less favorable, and the weaker binding is generally reflected in the unfavourable entropy.

Kinetic studies were carried out on this system (Table VIII.4), and the overall reaction to equilibrium analyzed for first order in cobalt (Figure VIII.14). However, the observed forward rate constant, which increased with oxygen pressure (Figure VIII.15), decreased with temperature

Table VIII.4. Kinetic Data for the Oxygenation of Co(salen).

TEMP °C	P_{O_2} Torr	Eq'm % Oxygenated	$k_t$obs, sec^{-1}	$k_1$obs, sec^{-1}	k_{-1}obs, sec^{-1}
-83.5	205	85.5	0.88×10^{-3}	0.75×10^{-3}	0.13×10^{-3}
-83.5	415	92.3	1.58×10^{-3}	1.46×10^{-3}	0.12×10^{-3}
-83.5	795	95.8	3.2×10^{-3}	3.1×10^{-3}	0.1×10^{-3}
-78	197	73.5	0.62×10^{-3}	0.46×10^{-3}	0.16×10^{-3}
-78	407	85.1	1.19×10^{-3}	1.01×10^{-3}	0.18×10^{-3}
-78	790	91.7	1.88×10^{-3}	1.72×10^{-3}	0.16×10^{-3}
-63.5	743	77.6	1.33×10^{-3}	1.03×10^{-3}	0.30×10^{-3}
-45	750	28.1	1.65×10^{-3}	0.47×10^{-3}	1.18×10^{-3}

Table VIII.5. Solubility of Dioxygen in CH_2Cl_2 at Low Temperature.

TEMP., °C	P_{O_2}, Torr	O_2 Solubility (M)	O_2 Solubility/atm ($M\ atm^{-1}$)
-78	190	1.55×10^{-3}	6.20×10^{-3}
-78	380	3.15×10^{-3}	6.30×10^{-3}
-78	670	4.45×10^{-3}	5.93×10^{-3}
-78	760	6.25×10^{-3}	6.25×10^{-3}
-63.5	190	1.45×10^{-3}	5.80×10^{-3}
-63.5	380	2.90×10^{-3}	5.80×10^{-3}
-63.5	670	4.60×10^{-3}	6.13×10^{-3}
-63.5	760	5.63×10^{-3}	5.63×10^{-3}
-45	380	2.98×10^{-3}	5.96×10^{-3}
-45	760	6.33×10^{-3}	6.33×10^{-3}

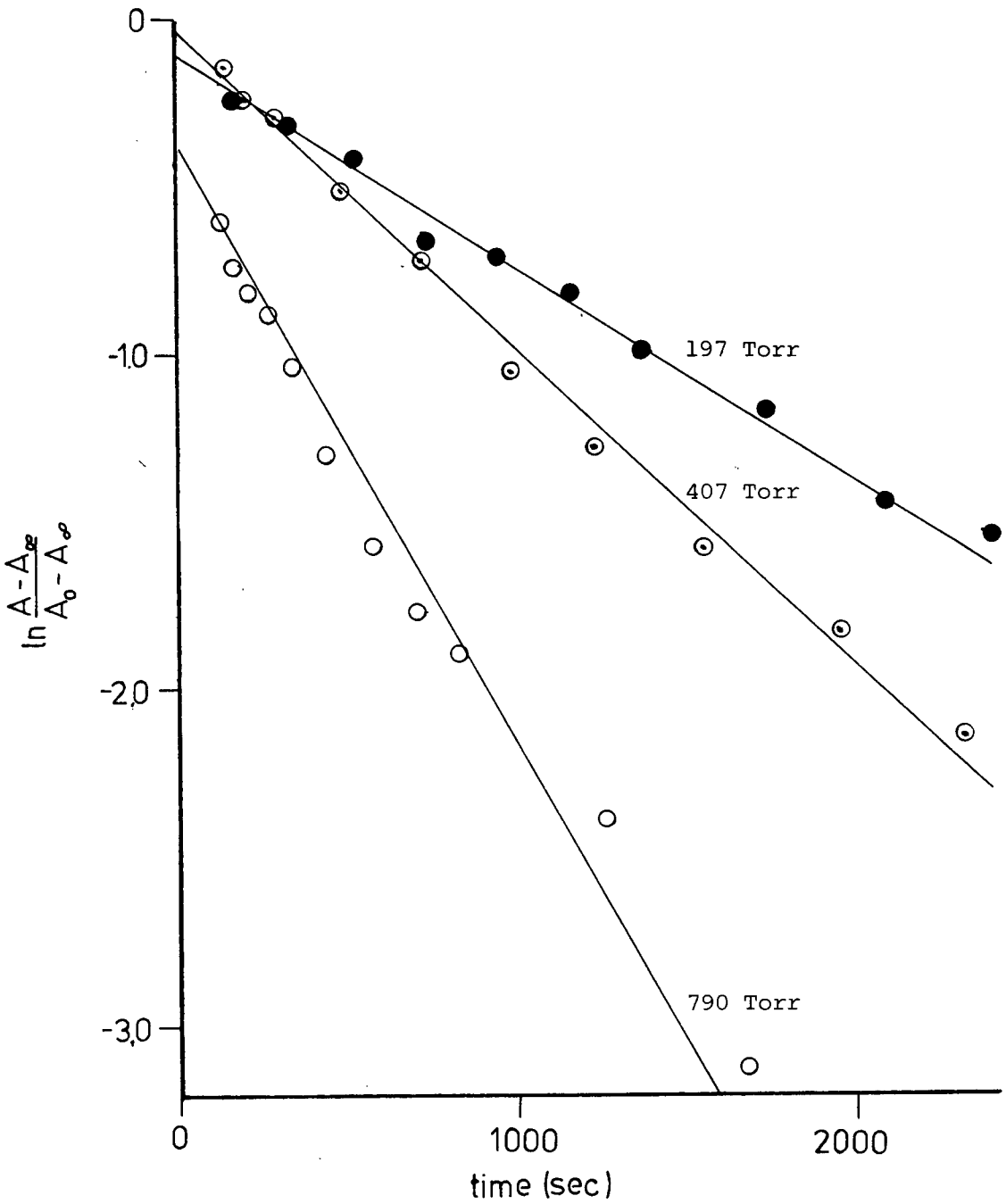

Figure VIII.14 First order plots of Co(salen) oxygenation in CH_2Cl_2 @ -78°C as a function of oxygen pressure.

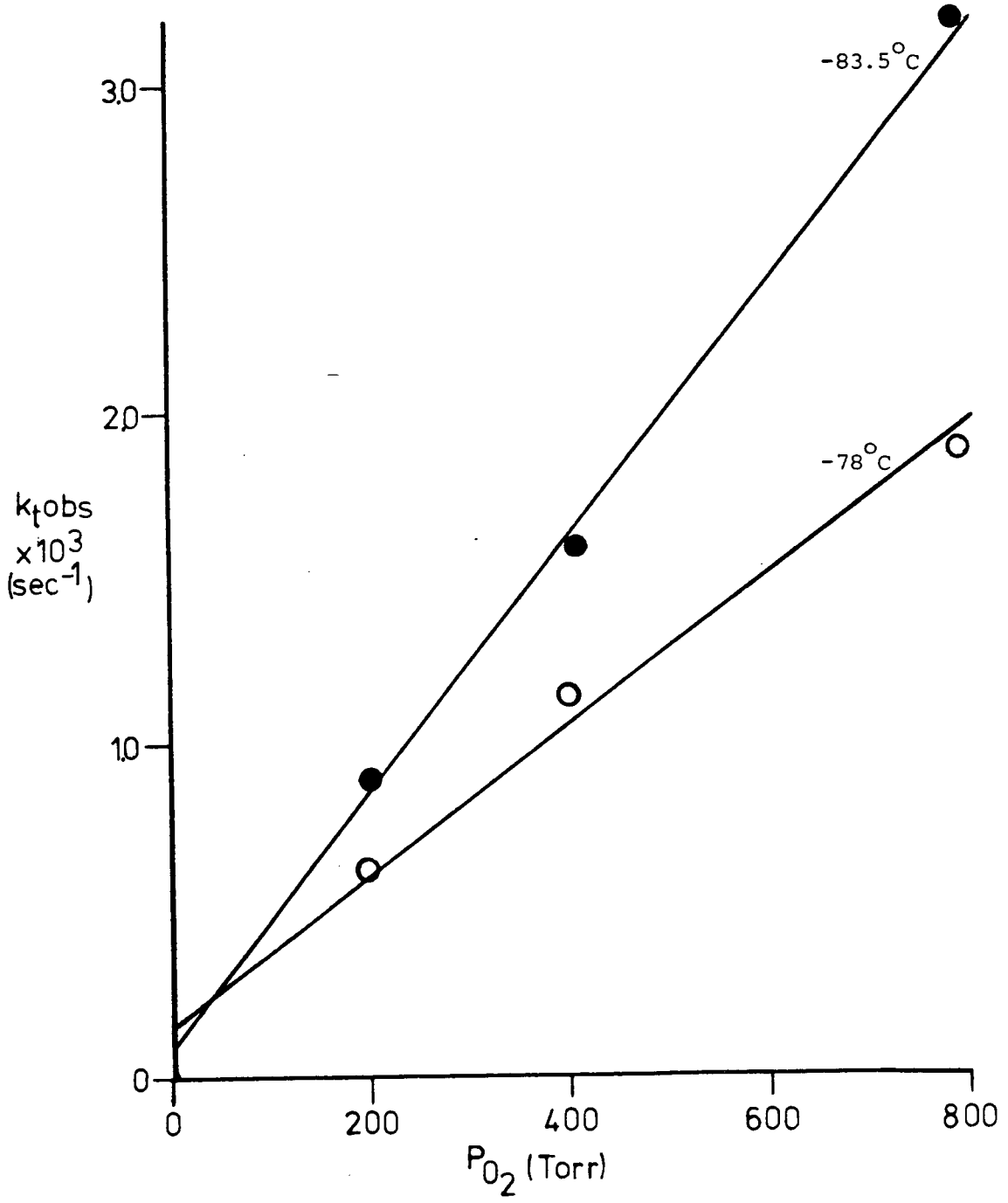

Figure VIII.15 Oxygenation rate constants of Co(salen) as a function of oxygen pressure.

(Figure VIII.16, $\Delta H^{\ddagger}$ = -4.7 kcal/mole and $\Delta S^{\ddagger}$ = -94 e.u.), while the observed reverse rate constant increased with temperature, as is usual (Figure VIII.17, $\Delta H^{\ddagger}$ = 3.9 kcal/mole and $\Delta S^{\ddagger}$ = -55 e.u.).

Generally, gas solubility decreases as temperature increases, and this effect could explain enhanced oxygenation rates at lower temperatures. However, measured oxygen solubilities showed little variation from (6.0 ± 0.4) x 10^{-3} M atm^{-1} on going from -78°C to -45°C (Table VIII.5). The data agree reasonably well with a literature value of (4.9 ± 0.3) x 10^{-3} M atm^{-1} at -78°C[52b].

The increasing forward rate constant at lower temperatures could possibly result from an exothermic coordination process in which Co(salen) obtains the preferred, but only partially formed, five-coordinate geometry for dioxygen binding. One possibility is a dimerization of Co(salen), possibly by linkage of a Co of one complex to a salen-N of another, which could then react with dioxygen. However, this is inconsistent with analysis of thermodynamic data that indicates a 1:1 stoichiometry, and the kinetic data which shows a first order dependence on cobalt. Trace water could also coordinate to Co(salen) at lower temperatures to give a five-coordinate dioxygen-binding geometry. However, no change from the characteristic four-coordinate Co(salen) ESR signals[68] was observed after addition of water (~10^{-2} M) to dichloromethane solutions of Co(salen), and water-saturated dichloromethane solutions of Co(salen) yielded visible spectra no different from that of the four-coordinate species. Co(salen) similarly gives a four-coordinate visible spectrum in neat acetone, and in acetone with water added. Also oxygenation proceeds at similar rates with and without the presence of added water in the system. Therefore, water coordination does not appear to be important. A third source of coordination could be from

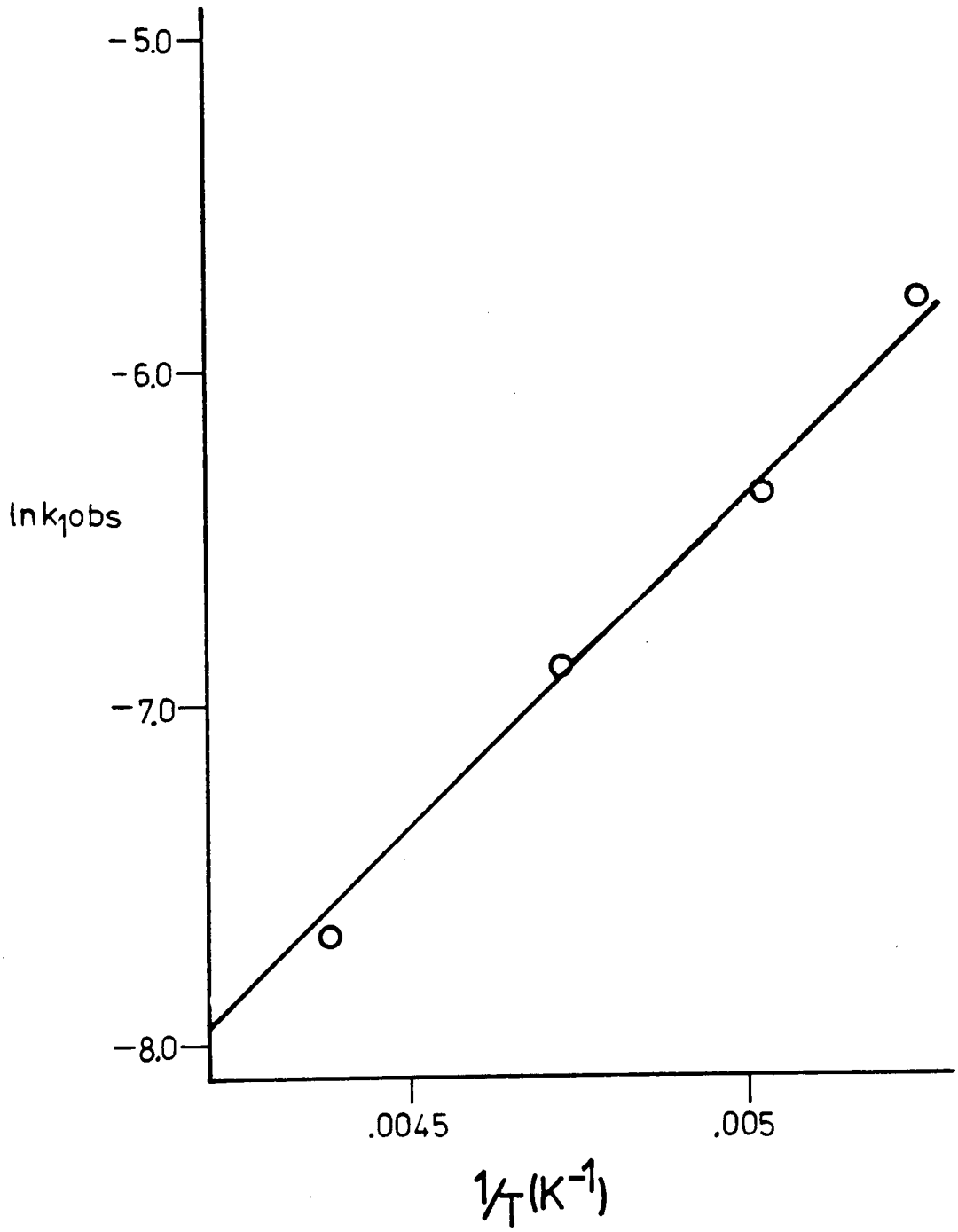

Figure VIII.16 Arrhenius plot of the forward rate constants of the oxygenation of Co(salen) at one atmosphere of oxygen.

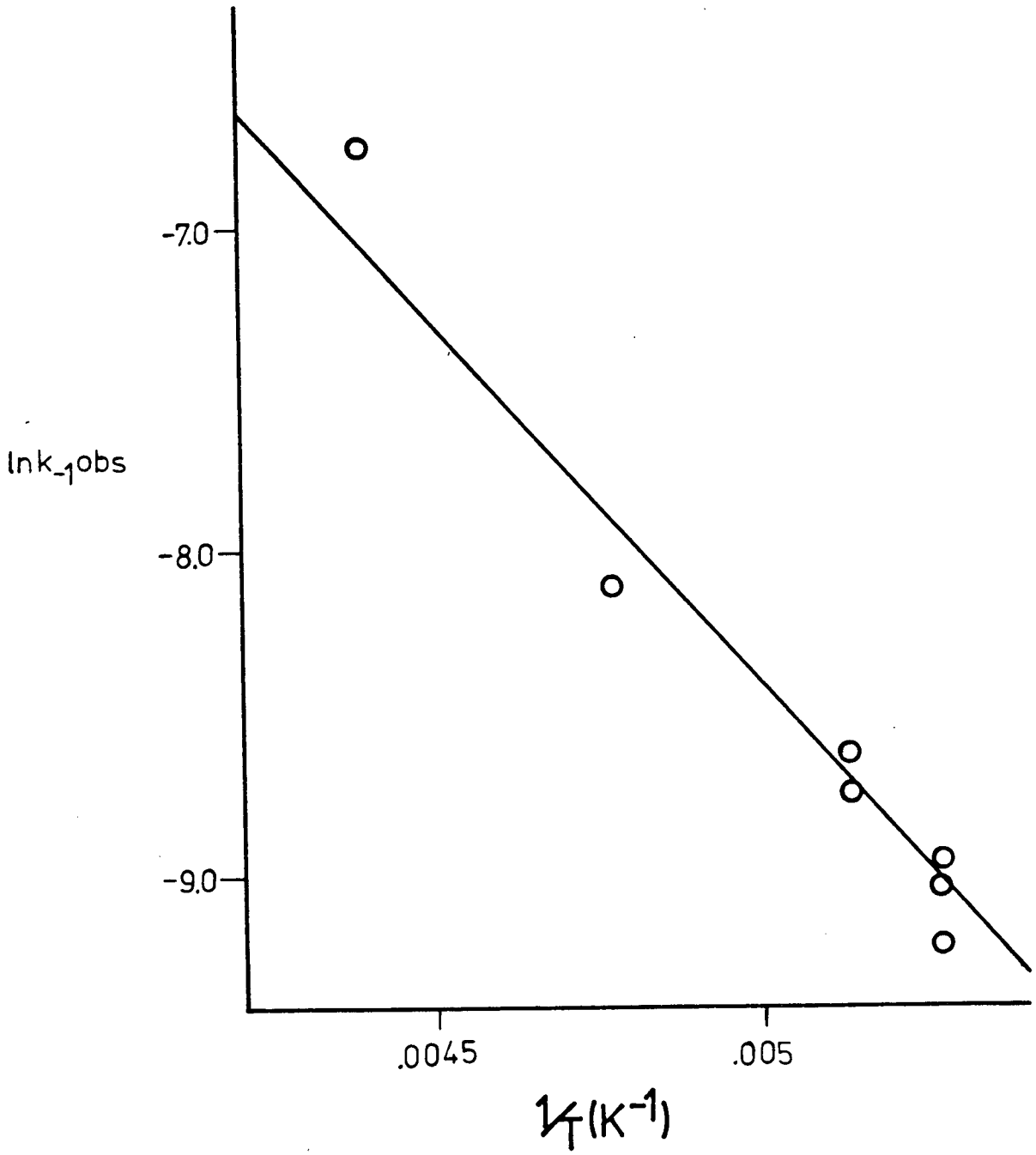

Figure VIII.17 Arrhenius plot for the deoxygenation of Co(salen)(O_2).

the dichloromethane solvent. Although ESR spectra of Co(salen) in dichloromethane at 77 K indicate that no such coordination takes place, it is very difficult to completely rule out the possibility of some trace solvent adduct being responsible for oxygenation of Co(salen) with no added ligand present.

ESR studies[23c] indicate that, in four-coordinate cobalt Schiff base or porphyrin complexes, the unpaired electron is in an orbital oriented in the plane of the macrocycle, the axial d_{z^2} orbital being fully occupied. The presence of an axial ligand usually serves to raise the energy level of the d_{z^2} orbital above that of the planar orbital, and under these conditions the axial d_{z^2} orbital is now half-filled, and it is thought that these conditions are necessary for oxygenation to proceed[23c]. Thus the presence of an exothermic process that places the unpaired electron in the d_{z^2} orbital can explain the observed greater oxygenation rate at lower temperatures.

A possible mechanism would thus be:

$$\text{Co(salen)} \underset{k_r}{\overset{k_f}{\rightleftharpoons}} \text{Co(salen)}^*, \ K^* \qquad \text{(VIII.3)}$$

$$\text{Co(salen)}^* + O_2 \underset{k_{-1}}{\overset{k_1}{\rightleftharpoons}} \text{Co(salen)}(O_2) \qquad \text{(VIII.4)}$$

where Co(salen) is "inactive" Co(salen) with paired d_{z^2} electrons and Co(salen)^* is active Co(salen) with an unpaired d_{z^2} electron.

Assuming that Co(salen)^* exists in a steady state yields the following rate law:

$$\frac{d[\text{Co(salen)}(O_2)]}{dt} = k_1 \left(\frac{k_f[\text{Co(salen)}] + k_{-1}[\text{Co(salen)}(O_2)]}{k_r + k_1[O_2]} \right) [O_2] - k_{-1}[\text{Co(salen)}(O_2)] \qquad \text{(VIII.5)}$$

If k_f and k_r are very large, compared to k_1 and k_{-1}, the rate law becomes:

$$\frac{d[Co(salen)(O_2)]}{dt} = k_1K^*[Co(salen)][O_2] - k_{-1}[Co(salen)(O_2)] \quad \text{(VIII.6)}$$

and the kinetic treatment is that described earlier (Chapter VIII.2) with $k_1obs = k_1K^*$.

The spectroscopic data require that K^* be very small, as no intermediate is detected; this is consistent with the steady state treatment.

The $\Delta H^{\neq}$ of -4.7 kcal/mole associated with k_1obs suggests that the ΔH value associated with K^* is exothermic to at least that amount. This degree of exothermicity is about half that associated with the binding of nitrogen-donating ligands. The exothermicity of coordinating water is expected to be less than that of a nitrogen-donating ligand (Chapter III), and that of an essentially non-coordinating dichloromethane solvent molecule would be even less. Oxygenation and deoxygenation rates of cobalt Schiff base or porphyrin complexes that have an axial amine coordinated are too great to be measured by conventional means. For the Co(salen) in dichloromethane system, the deoxygenation rate constant is relatively small, being of the order of 10^{-3} sec^{-1}. This suggests that the nature of the reacting complex is quite different from the usual six-coordinate $LCoP(O_2)$ or $LCo(salen)(O_2)$ species. However, in the above observations there is nothing that rules out the possibility of weakly coordinating dichloromethane being responsible for the K^* step, rather than some internal rearrangement of the four-coordinate Co(salen) complex leading to the activation of the complex to oxygenation.

VIII.5 Studies in Other Solvents

VIII.5.1 Rationale

Since the above work with Co(salen) systems was done in dichloromethane and other systems, such as the substituted acacen complexes of cobalt and the cobalt porphyrin complexes, were done in toluene, and solvent effects, especially with dioxygen binding, can play a major role, Co(salen) studies were also carried out in toluene and in DMF.

VIII.5.2 $L + Co(salen) \rightleftharpoons LCo(salen)$

The equilibrium constants of CH_3-Im, Pip, and Py binding to Co(salen) in DMF and in toluene are given in Tables VIII.6a and VIII.6b, respectively, the raw data for which are given in Appendices VIk - VIp. Also listed are ΔH and ΔS values obtained, and the pK_a of the protonated ligand studied.

In DMF, the order of ligand binding abilities at 25°C (Pip>CH_3-Im>Py) is the same as in dichloromethane, while in toluene CH_3-Im binds more strongly than Pip. Py always binds to Co(salen) less strongly than CH_3-Im or Pip. The general trend for ligand affinity as a function of solvent is toluene>CH_2Cl_2>DMF, consistent with slightly greater affinity in less polar solvent systems, as observed in the CoOMBP systems, and presumably similar reasoning applies (Chapter III).

VIII.5.3 $LCo(salen) + O_2 \rightleftharpoons LCo(salen)(O_2)$

The $P_{\frac{1}{2}}O_2$ values of five-coordinate Co(salen) complexes in DMF and in toluene are given in Tables VIII.7a and VIII.7b, respectively, the raw data being given in Appendices VIq - VIv. In DMF, determinations of ΔH and ΔS values were difficult, as the solvent freezes at -60°C, and irreversible oxidation tended to occur above -45°C. Since dioxygen tended to bind so

Table VIII.6a. Thermodynamic Data for the Binding of an Axial Ligand to Co(salen) in a DMF Solution.

LIGAND	TEMP., °C	K_1, M^{-1}	ΔH_1 kcal/mole	ΔS_1 e.u.	pK_a
CH_3-Im	5	47.2	-3.6	-6	7.25
	15	31.1			
	25	27.1			
	35	23.4			
	45	18.8			
Pip	5	88	-5.0	-9	11.30
	25	48.2			
	35	38.9			
	55	21.9			
Py	5	23.7	-6.9	-19	5.27
	15	14.1			
	25	7.9			
	35	5.9			
	65	2.4			

Table VIII.6b. Thermodynamic Data for the Binding of an Axial Ligand to Co(salen) in a Toluene Solution.

LIGAND	TEMP., °C	K_1, M^{-1}	ΔH_1 kcal/mole	ΔS_1 e.u.	pK_a
CH_3-Im	5	305	-5.2	-7	7.25
	15	236			
	25	171			
	35	130			
	45	99			
	55	88			
Pip	5	531	-9.8	-23	11.30
	15	291			
	25	81.3			
	35	47.9			
	45	37.6			
	65	16.2			
Py	5	56.2	-7.8	-20	5.27
	15	26.9			
	25	20.4			
	35	12.4			
	45	7.4			

Table VIII.7a. Thermodynamic Data for the Binding of Dioxygen to LCo(salen) in a DMF Solution.

LIGAND	TEMP., °C	$P_{\frac{1}{2}}O_2$, Torr	ΔH_{O_2} kcal/mole	ΔS_{O_2} e.u.	pK_a [a]
CH_3-Im	-45	1.1	~ -6.2	~ -27	7.25
	-23	3.0			
	0	10, oxidation a problem			
Pip	-45	2.5	~ -5.4	~ -26	11.30
	-23	7, oxidation a problem			
Py	-45	4.7	~ -5.0	~ -25	5.27
	-23	7.0			
	0	25			

Table VIII.7b. Thermodynamic Data for the Binding of Dioxygen to LCo(salen) in a Toluene Solution.

LIGAND	TEMP., °C	$P_{\frac{1}{2}}O_2$, Torr	ΔH_{O_2} kcal/mole	ΔS_{O_2} e.u.	pK_a [a]
CH_3-Im	-45	24	———	———	7.25
	-45	30			
Pip	-78	132	———	———	11.30
Py	-45	154	———	———	5.27

a. For references see Table III.3.

weakly to Co(salen) complexes in toluene, ΔH and ΔS values were not determined in this solvent either.

LCo(salen) complexes are seen to have considerably higher dioxygen affinities in the more polar solvents, consistent with observations in the CoPpIXDME[91a] and CoOMBP (Chapter IV) systems.

For CH_3-ImPpIXDME[91a] the $P_{\frac{1}{2}}O_2$ value decreased from 388 to 12.6 Torr (a factor of ~30) on going from toluene to DMF. The change for CH_3-ImCo(salen) was by a similar factor ($P_{\frac{1}{2}}O_2$ ~ 27 Torr in toluene; $P_{\frac{1}{2}}O_2$ ~ 1.1 Torr in DMF).

With PipCo(salen) strong dioxygen binding was observed in DMF ($P_{\frac{1}{2}}O_2$ @ $-45^{\circ}C$ = 2.5 Torr), but the dioxygen affinity in toluene was very weak, and the binding studies had to be carried out at $-78^{\circ}C$ to observe a $P_{\frac{1}{2}}O_2$ of 132 Torr, which was even higher than that of most cobalt porphyrin complexes (Chapter VI).

For both PyCo(salen) and CH_3-ImCo(salen) the $P_{\frac{1}{2}}O_2$ values at $-45^{\circ}C$ were less than those for the corresponding complexes of all the porphyrins studied under similar conditions (Chapter VI).

The enhanced oxygen affinity of Co(salen) complexes in more polar solvents can also be shown by gas-uptake experiments which indicate an immediate 1:1 Co:O_2 uptake for CH_3-ImCo(salen) in neat CH_3-Im or DMF at $15^{\circ}C$. The immediate uptake in CH_2Cl_2 was 1:0.6 Co:O_2, which compares to an expected 74% oxygenation calculated from the thermodynamic data in Table VIII.3. No oxygen-uptake was seen in toluene, but since Co(salen) has a very limited solubility in this solvent, no conclusion could be made about CH_3-ImCo(salen) oxygen affinity, based on gas-uptake data alone.

CHAPTER IX

THERMODYNAMICS AND KINETICS OF REACTIONS OF COBALT(II) MACROCYCLIC SYSTEMS WITH SUBSTRATES CONTAINING UNSATURATED CARBON-CARBON BONDS

IX.1 Reactions of Co(II) Porphyrin Systems with Ethylene and Acetylene

Evidence that unsaturated hydrocarbon substrates react with CoOMBP systems was obtained when a DCE solution of PipCoOMBP was exposed to an atmosphere of ethylene or acetylene (Figure IX.1) at 20°C; spectral changes (Table IX.1), similar to those resulting from oxidation (Table VII.1), occurred over a period of several hours (Appendix VIIf). The spectral changes, which suggested that the reaction had proceeded almost to completion, were reversed substantially when the system was evacuated (Figure IX.2).

In spite of the resemblance of the spectral changes to those of irreversible oxidation, their reversible nature discounts the possibilty that they are due to irreversible oxidation rather than a reaction with the substrate. The rate of the forward reaction with the substrates (Table IX.2) is about one fourth of that of irreversible oxidation (Table VII.4); it is highly unlikely that sufficient oxygen could enter the system to cause an oxidation reaction at that rate. Oxidation did appear to play a role, however, as an increase in spectral intensity in the 440 nm region, indicative of increasing $(PipCoOMBP)_2O_2$, occurred before complete reversal of the reaction with either substrate could be achieved.

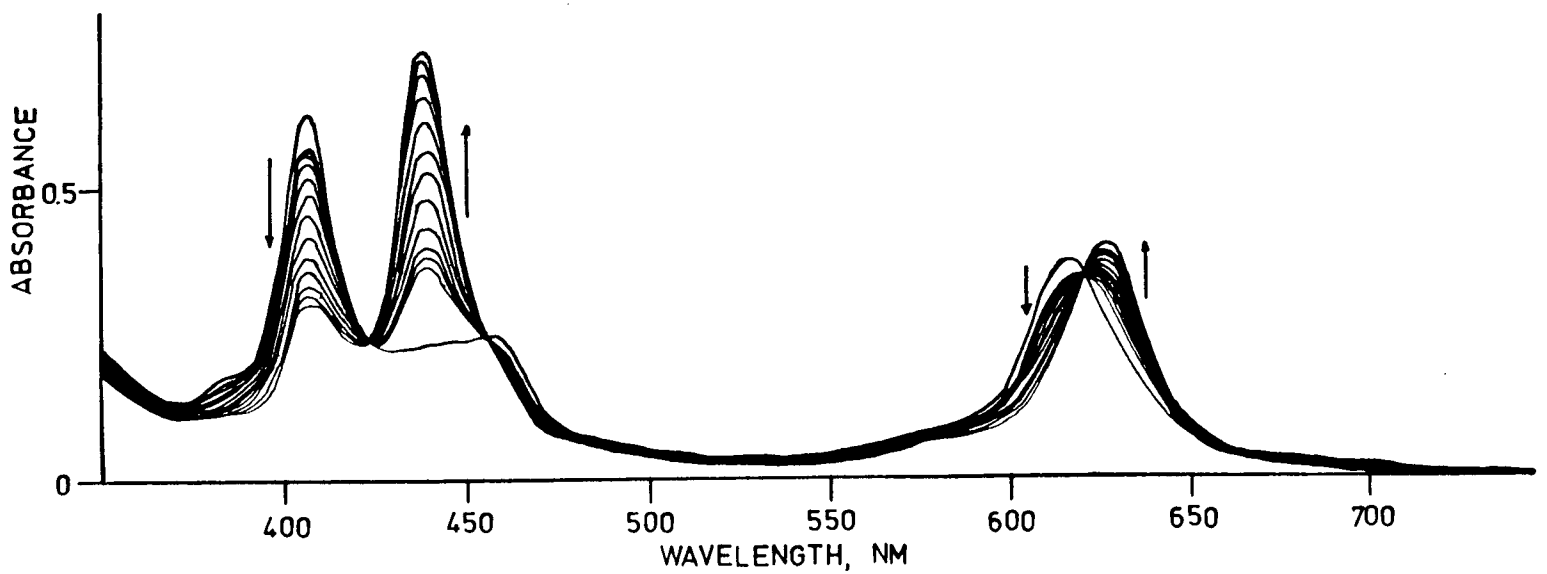

Figure IX.1 Spectra showing the reaction of PipCoOMBP with 780 Torr acetylene @ 20°C.

For raw data see Appendix VIIf.

Table IX.1 Spectral Data From 350 to 750 nm for the Reactions of Unsaturated Substrates with Cobalt Macrocycles

Absorbing Species	Absorption Maxima (nm) (Extinction Coefficient, $M^{-1}cm^{-1}$)		Isosbestic Points (nm)			
PipCoOMBP	408 (6.3×10^4)	618 (3.9×10^4)				
+ C_2H_4*	439 (7.7×10^4)	629 (4.3×10^4)	427	457	624	
+ C_2H_2*	439 (8.8×10^4)	633 (4.6×10^4)	426	457	623	
CoOMBP	412 (6.4×10^4)	618 (6.2×10^4)				
+ acrylamide	415 (6.1×10^4)	618 (5.9×10^4)	435	606	634	
+ MA	356 (6.2×10^4)	444 (1.0×10^4) 629 (5×10^3)		374		
MACoOMBP	as above					
+ Pip	444 (6.2×10^4)	631 (3.0×10^4)	405	472	595	
DMFCoOMBP	418 (5.9×10^4)	618 (5.3×10^4)				
+ MA	444 (7.3×10^4)	632 (4.3×10^4)	362	429	457	629
CoOMBP	412 (6.4×10^4)	618 (6.2×10^4)				
+ TCNE	440 (~1×10^4)	630 (~5×10^3)				

* Extinction coefficients based on estimated spectral characteristics of fully formed species.

Table IX.1 cont. Spectral Data From 350 to 750 nm for the Reactions of Unsaturated Substrates with Cobalt Macrocycles

Absorbing Species	Absorption Maxima (nm) (Extinction Coefficients, $M^{-1}cm^{-1}$)	Isosbestic Points (nm)
Co(salen)	410 (1.15×10^4)	
+ cot, O_2	410 (1.12×10^4), i.e. no evidence of any reaction	
+ 1-hx, O_2	410 (1.11×10^4), i.e. no evidence of any reaction	
+ sty, O_2	410 (6.6×10^3), Co(salen) peak substantially reduced	
+ DCB, O_2	410 (8.0×10^3), Co(salen) peak somewhat reduced	
+ DEF, O_2	—— ———— , Co(salen peak completely eliminated	

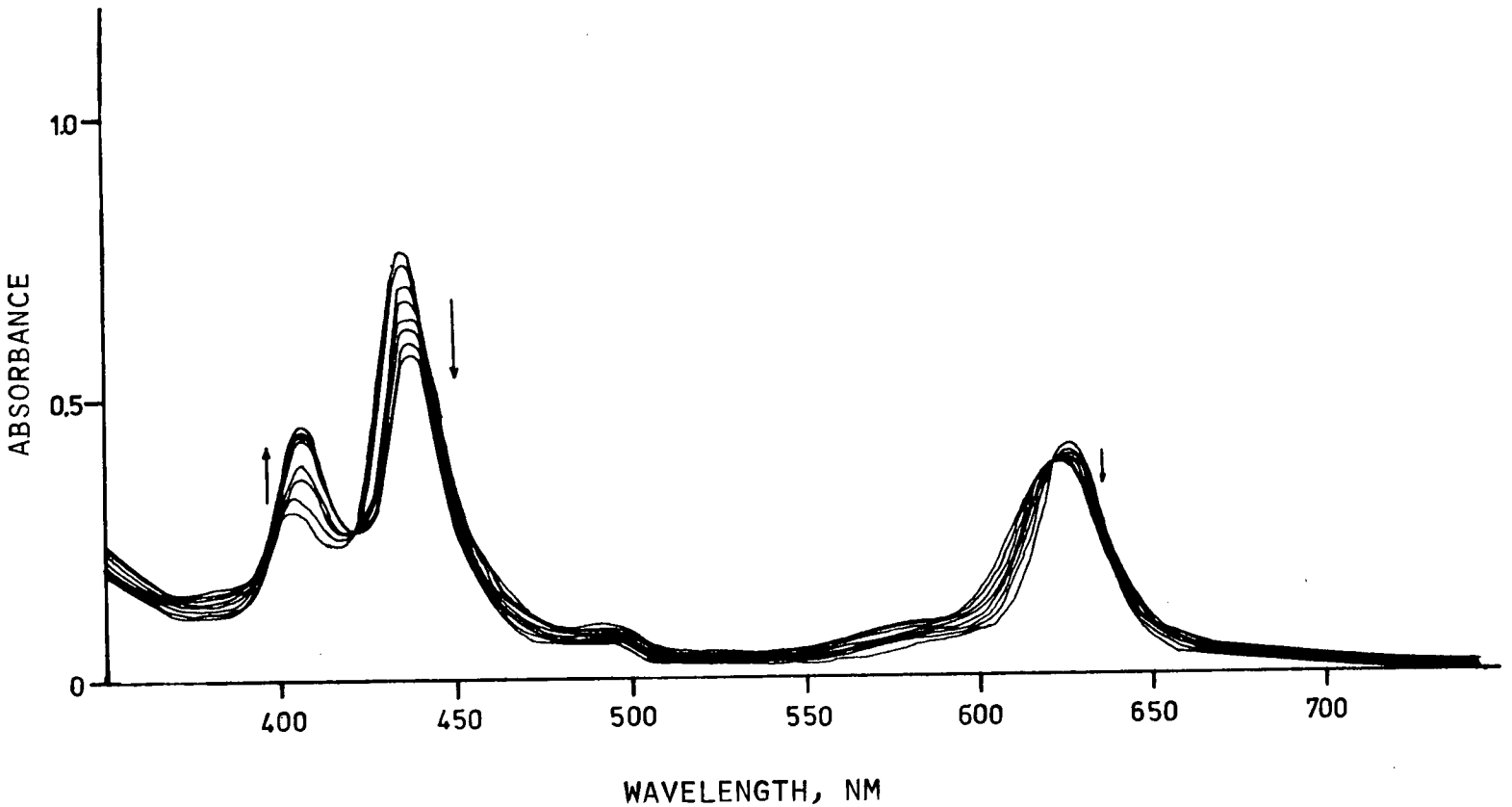

Figure IX.2 Spectra showing PipCoOMBP regeneration @ 20°C after removal of acetylene.

For raw data see Appendix VIIf.

Table IX.2 Kinetics of 780 Torr of Ethylene or Acetylene Reacting with PipCoOMBP in DCE at 20°C.

Co , M	Reaction	k_{obs}, sec^{-1}
1.5×10^{-5}	PipCoOMBP + $C_2H_4 \rightleftharpoons$ PipCoOMBP(C_2H_4)	2.25×10^{-4}
1.3×10^{-5}	PipCoOMBP + $C_2H_2 \rightleftharpoons$ PipCoOMBP(C_2H_2)	2.75×10^{-4}
1.3×10^{-5}	PipCoOMBP(C_2H_2) $\rightleftharpoons$ PipCoOMBP + C_2H_2	4.6×10^{-5}

Although the reversal of the acetylene reaction analyzed for first order in cobalt (Figure IX.3), the reversal of the ethylene reaction was slower and sufficient data could not be obtained before substantial formation of the oxidation product occurred, presumably as a result of air leakage into the evacuated system. PipCoOMBP reacted at ambient temperature with ethylene and acetylene in a manner that approximated first order in cobalt (Figure IX.3, Table IX.2).

When other axial ligands, CH_3-Im and Py, were added and the reactions of LCoOMBP with ethylene or acetylene were studied, spectral changes similar to those described above were observed. However, no reversal was observed, and as these systems tended to be more oxygen sensitive than the PipCoOMBP systems; the possibility of irreversible oxidation due to trace O_2 cannot be completely ruled out in these systems.

All the above systems were studied at lower temperatures (-78°C, -63.5°C, and -45°C) in toluene and in the 4:1 toluene:DCE by volume mixed solvent system, but there was little evidence for the reaction with ethylene or acetylene under these conditions.

Other cobalt(II) porphyrin systems (LCoPpIXDME, LCoOEP; L = CH_3-Im, Pip, or Py) and four-or six-coordinate CoOMBP complexes did not appear to

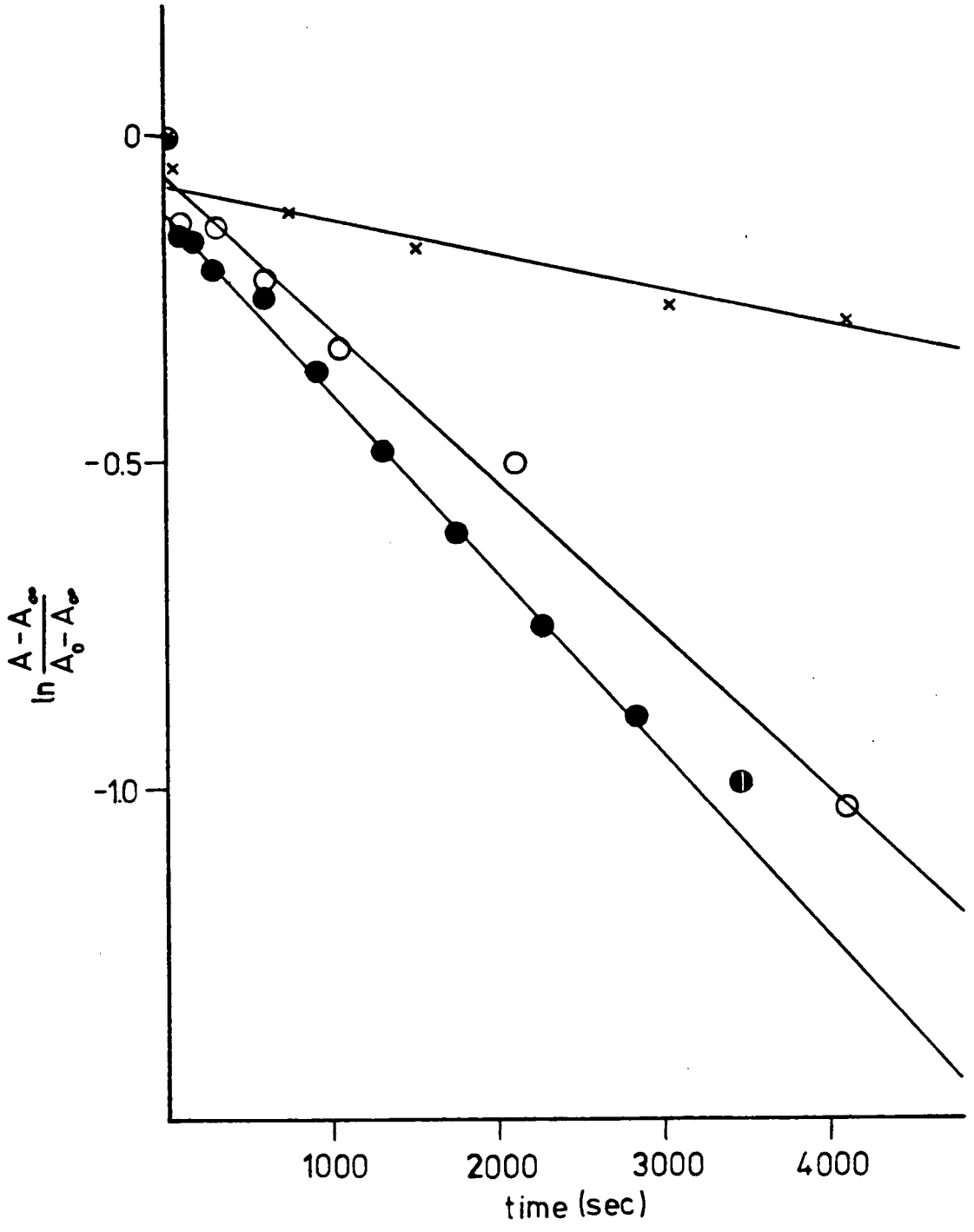

Figure IX.3 First order rate plots of PipCoOMBP reacting with ethylene and acetylene.

○ PipCoOMBP + $C_2H_4 \rightleftharpoons$ PipCoOMBP(C_2H_4)

● PipCoOMBP + $C_2H_2 \rightleftharpoons$ PipCoOMBP(C_2H_2)

× PipCoOMBP(C_2H_2) $\rightleftharpoons$ PipCoOMBP + C_2H_2

react with either of the substrates in DCE at ambient temperatures.

LCoOMBP did not react with ethylene or acetylene at ambient temperatures in toluene.

Presumably, any reaction between a cobalt(II) porphyrin and an unsaturated substrate would involve the transfer of some electron density between the cobalt(II) porphyrin and the π^*-orbital of the substrate. Because of this, studies were carried out on activated olefins containing electron-withdrawing groups.

IX.2 Reactions of Co(II) Porphyrin Systems with Electron Withdrawing Olefins

Initial studies with CoOMBP and acrylamide resulted in spectral changes (Table IX.1) similar to those observed upon addition of DMA or DMF to CoOMBP (Table III.1). Therefore, it was concluded that the binding of this ligand occurred through the amide group; the binding to CoOMBP of acrylamide, like DMA, was so weak that equilibrium constants could not be determined.

Dramatic spectral changes occurred when maleic anhydride (MA) was added to CoOMBP (Table IX.1, Figure IX.4), as the Soret band underwent a marked blue shift and the intensity of the visible band was greatly diminished.

The binding of MA to CoOMBP in toluene was such that equilibrium constants could be readily determined (Table IX.3). The addition of MA to CoOMBP was treated as a reaction similar to the addition of other ligands, and the binding data were analyzed in a like manner (Chapter III), the analysis being consistent with the formation of a 1:1 adduct (Figure IX.5). Unlike the binding of predominantly σ-donating ligands (Chapter III), the reaction with MA was not virtually instantaneous. Several minutes were required to establish equilibrium at a particular concentration of MA, but the kinetics of the reaction could not be studied conveniently since

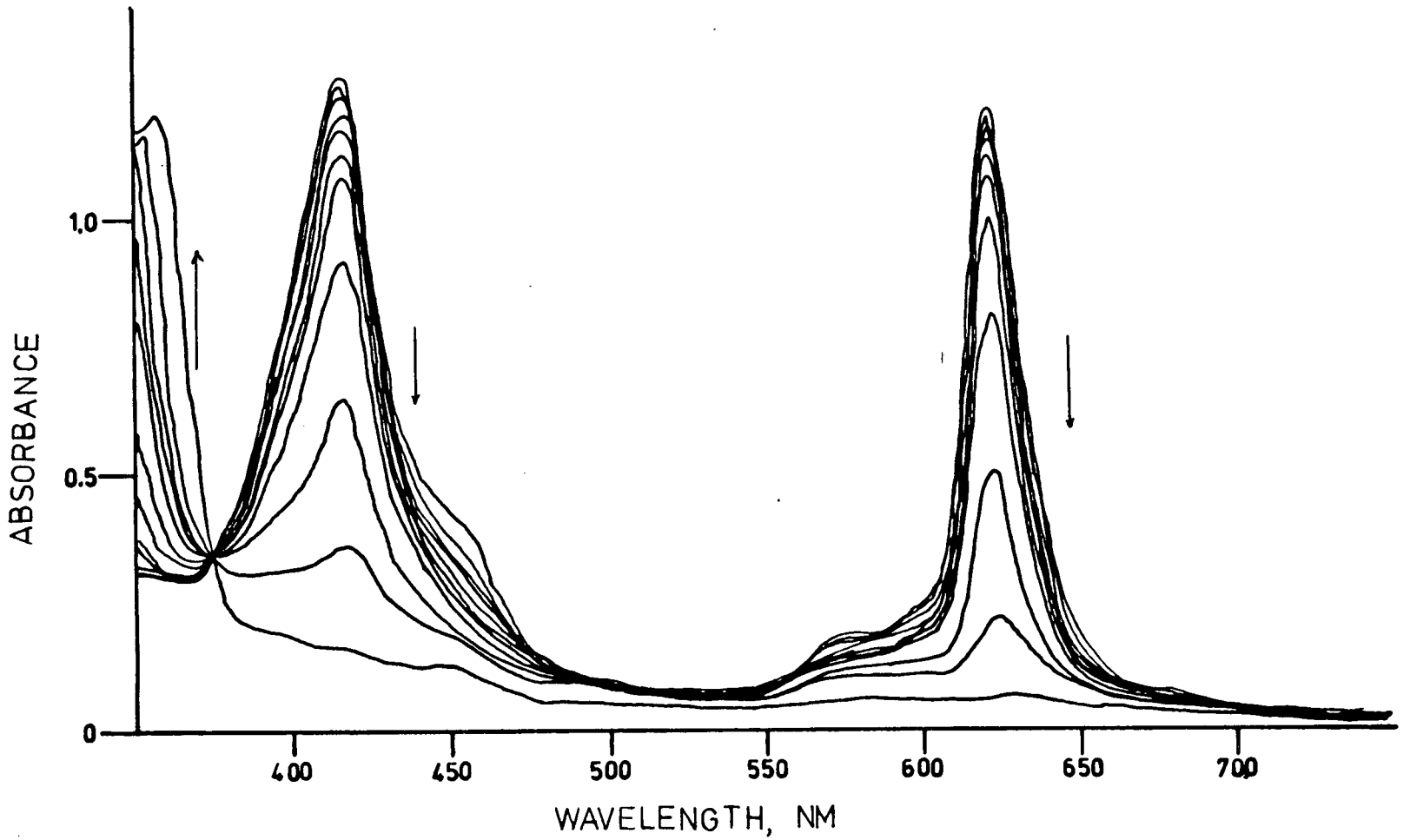

Figure IX.4 Spectral changes occurring upon the addition of MA to CoOMBP in toluene @ 22°C.

For raw data see Appendix VIIa.

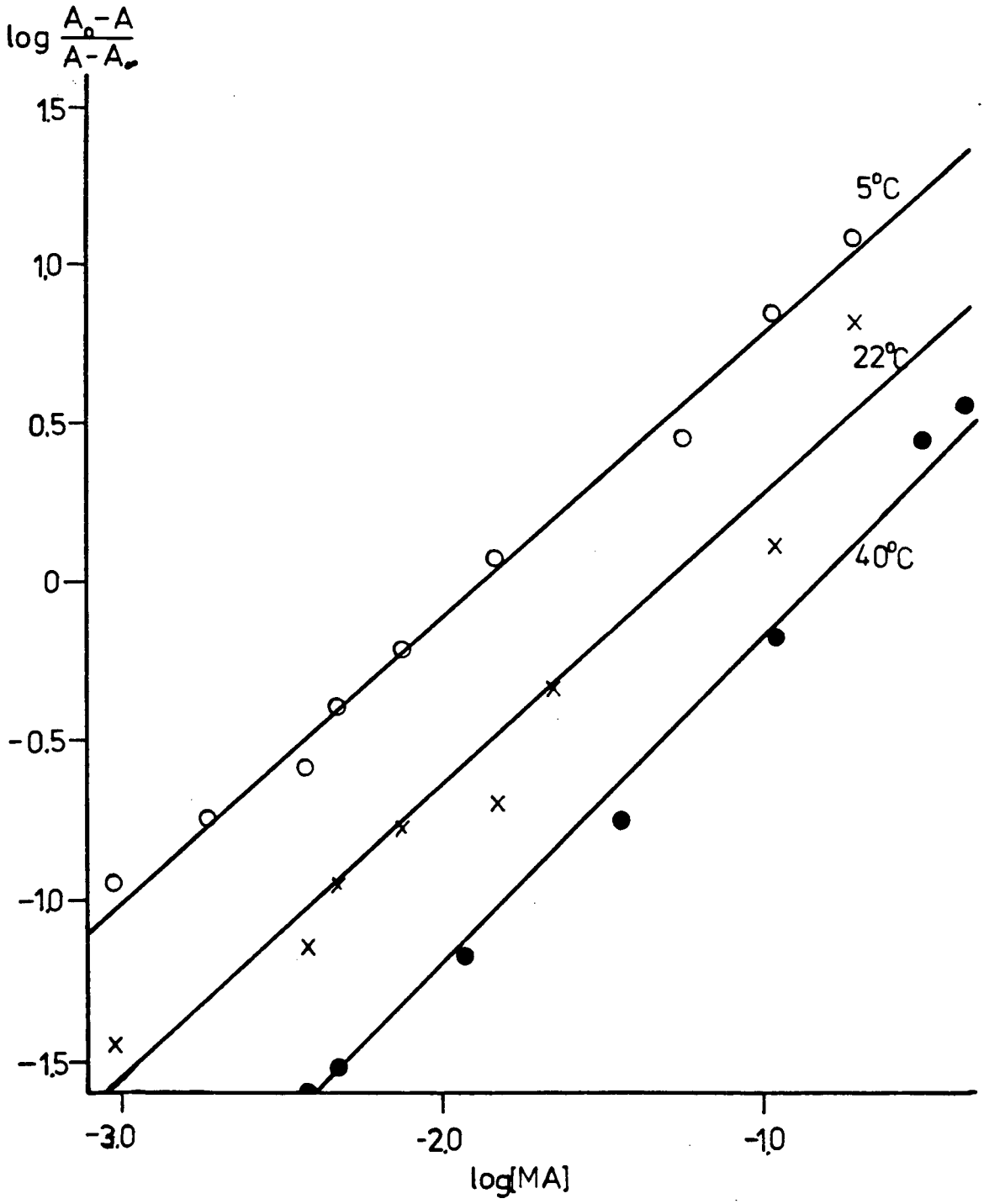

Figure IX.5 Equilibrium plots for MA + CoOMBP $\rightleftharpoons$ MACoOMBP

For raw data see Appendix VIIa.

Table IX.3. Thermodynamic Data for the Binding of Maleic Anhydride to CoOMBP in a Variety of Solvents.

SOLVENT	TEMP., °C	K_{MA}, M^{-1}	ΔH_{MA} kcal/mole	ΔS_{MA} e.u.
Toluene	5	82.2	-12.2	-35
	22	20.9		
	40	6.6		
DCE	20	~5		
DMF	5	31.7	-9.7	-28
	22	11.7		
	40	3.8		

by the time a particular addition was made and the system was properly mixed, the reaction was almost complete.

By studying the MA system at several temperatures in toluene (Table IX.3, Figure IX.6), CoOMBP is seen to bind MA with a somewhat more favourable ΔH and less favorable ΔS than the primarily σ-bonding N-and O-donor ligands considered in Chapter III.

The above observations suggest substantial rearrangement of the electronic structure of CoOMBP upon formation of the MA-CoOMBP adduct, possibly by the transfer of some π-electron density from OMBP to MA through the Co centre, upon formation of the metal-olefin π-bond, $Co^{\delta+}—\|^{\delta-}$.

Reversibilty of the formation of MACoOMBP is demonstrated by a partial regeneration of the spectrum of CoOMBP as the temperature of the system is raised. Also, when Pip is added to the MA-CoOMBP system, a general growth in spectral intensity is noted (Figure IX.7), and a new species with

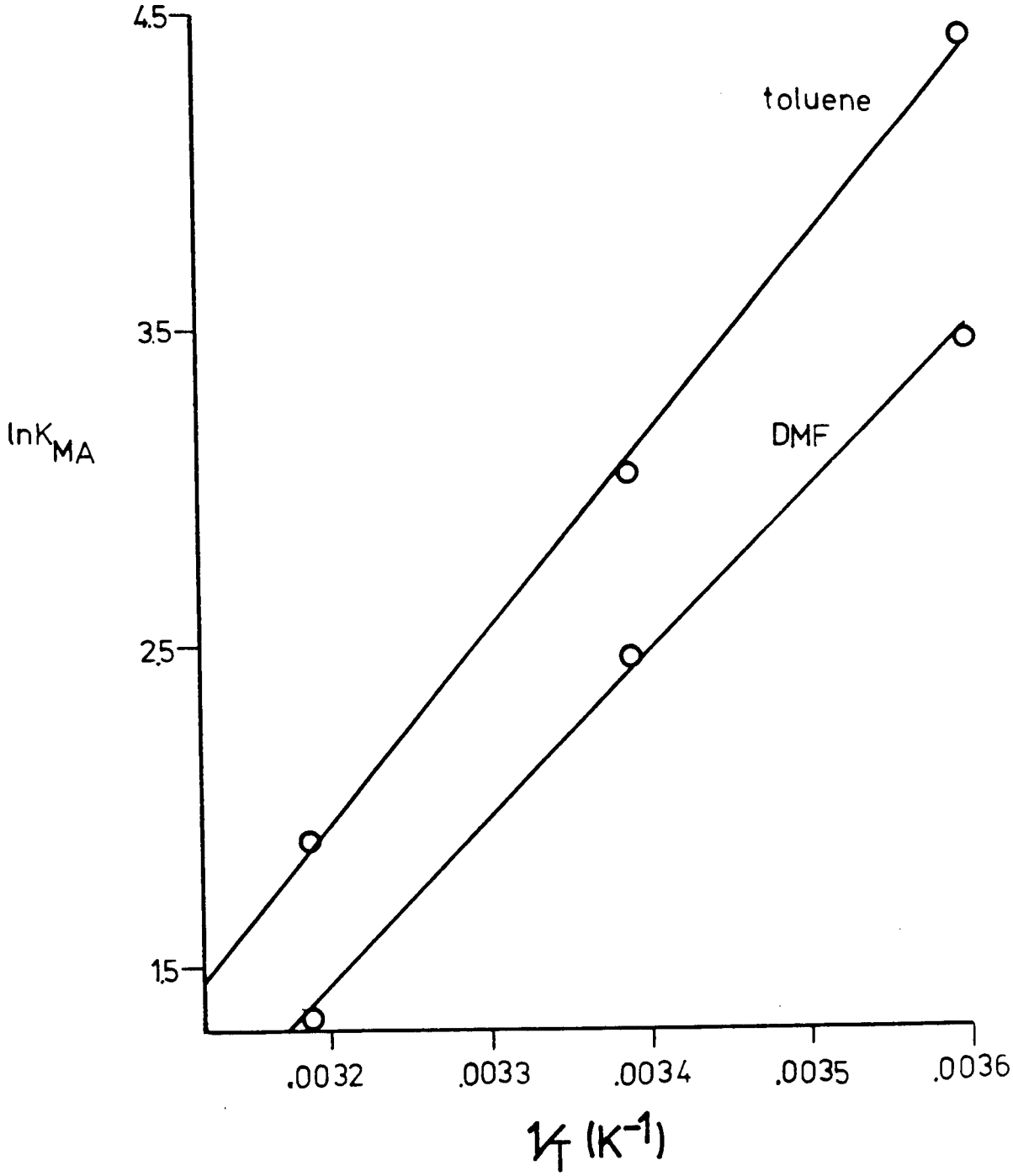

Figure IX.6 Van't Hoff plots for MA + CoOMBP $\rightleftharpoons$ MACoOMBP in toluene and DMF.

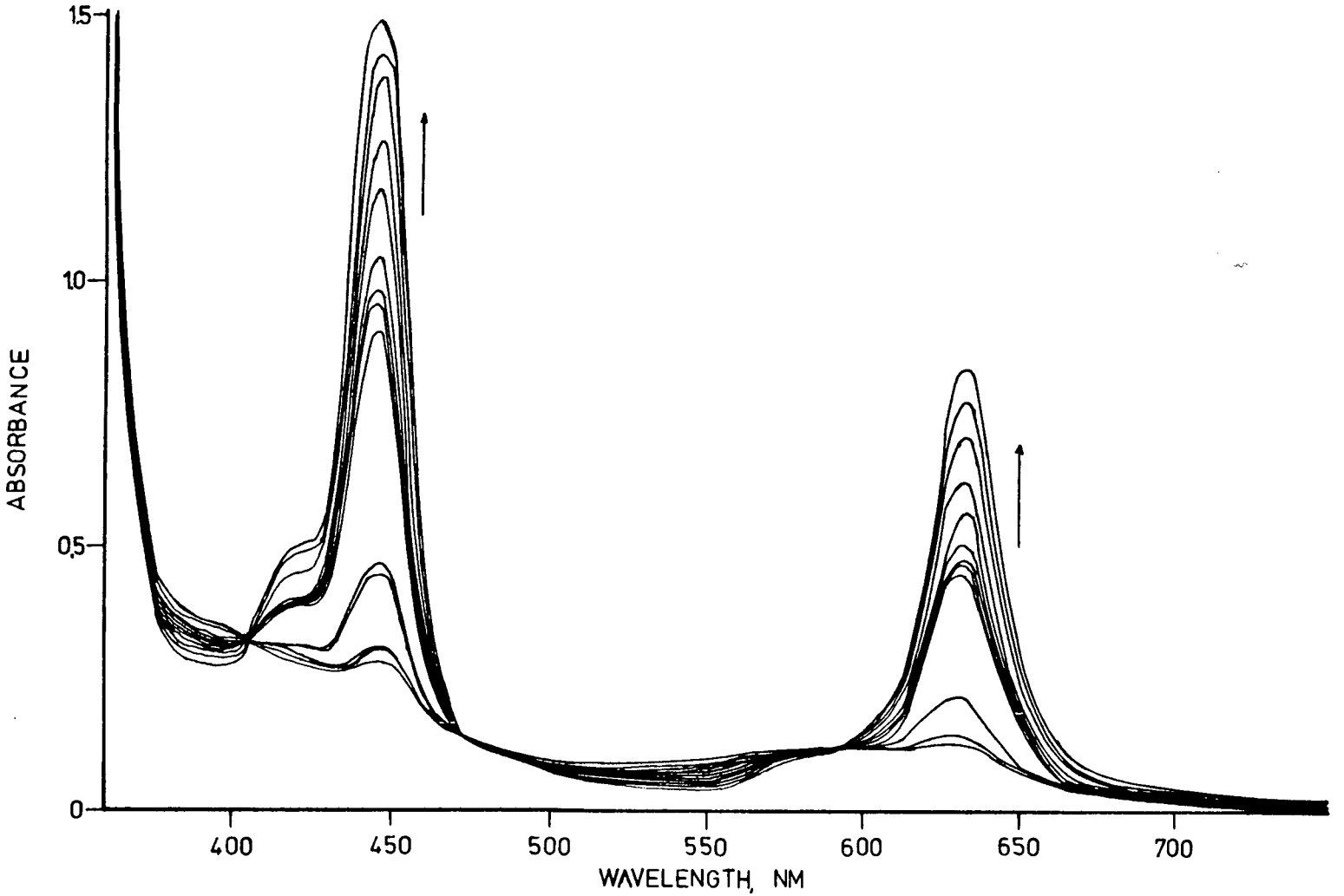

Figure IX.7 Spectral changes to MACoOMBP upon addition of Pip @ 22°C.

For raw data see Appendix VIIe.

an intense band at 444 nm is formed. This suggests that PipCoOMBP(MA) results from this addition, as CoOMBP complexes with two axial lgands so far studied generally have a strong band in the 440 nm region. The visible band position at 631 nm confirms that this adduct is not Pip_2CoOMBP as the position of the visible band of that complex is at 616 nm; also insufficient Pip is present to form Pip_2CoOMBP. At lower MA concentrations (<0.1 M), addition of Pip (~5 x 10^{-3} M) results in initial formation of PipCoOMBP(MA) followed by the gradual generation of the five-coordinate PipCoOMBP complex (Figure IX.8). Addition of MA to a 2 x 10^{-3} M Pip in toluene solution of PipCoOMBP results in initial formation of some PipCoOMBP(MA) followed by formation of MACoOMBP, although this adduct is not fully formed at concentrations of MA where MACoOMBP is fully formed in the absence of Pip. Addition of MA to a 4 x 10^{-2} M Pip in toluene solution of PipCoOMBP (~85%) and Pip_2CoOMBP (~15%) resulted in the spectrum of PipCoOMBP(MA). Analysis of the equilibria is made difficult due to the occurrence of more than one reaction at a particular time.

Upon addition of MA to CoOMBP in DCE (Table IX.3), the observed K_{MA} value was less than that observed in toluene, consistent with observations for the binding of other ligands (Chapter III). That ethylene and acetylene bind to LCoOMBP in DCE and not in the less polar toluene could be rationalized in terms of stabilization of a polar adduct in the more polar DCE, analogous to stabilization of dioxygen adducts as Co(III)-O_2^- species. The larger and already polar olefin, MA, is likely to delocalize any transferred electron density, thus solvent polarity would be expected to stabilize the reactants rather than the products.

Enhanced formation of ethylene and acetylene adducts of CoOMBP with the presence of an axial Pip is consistent with the axial ligand contributing greater electron density to the metal centre, and thus enhancing transfer of

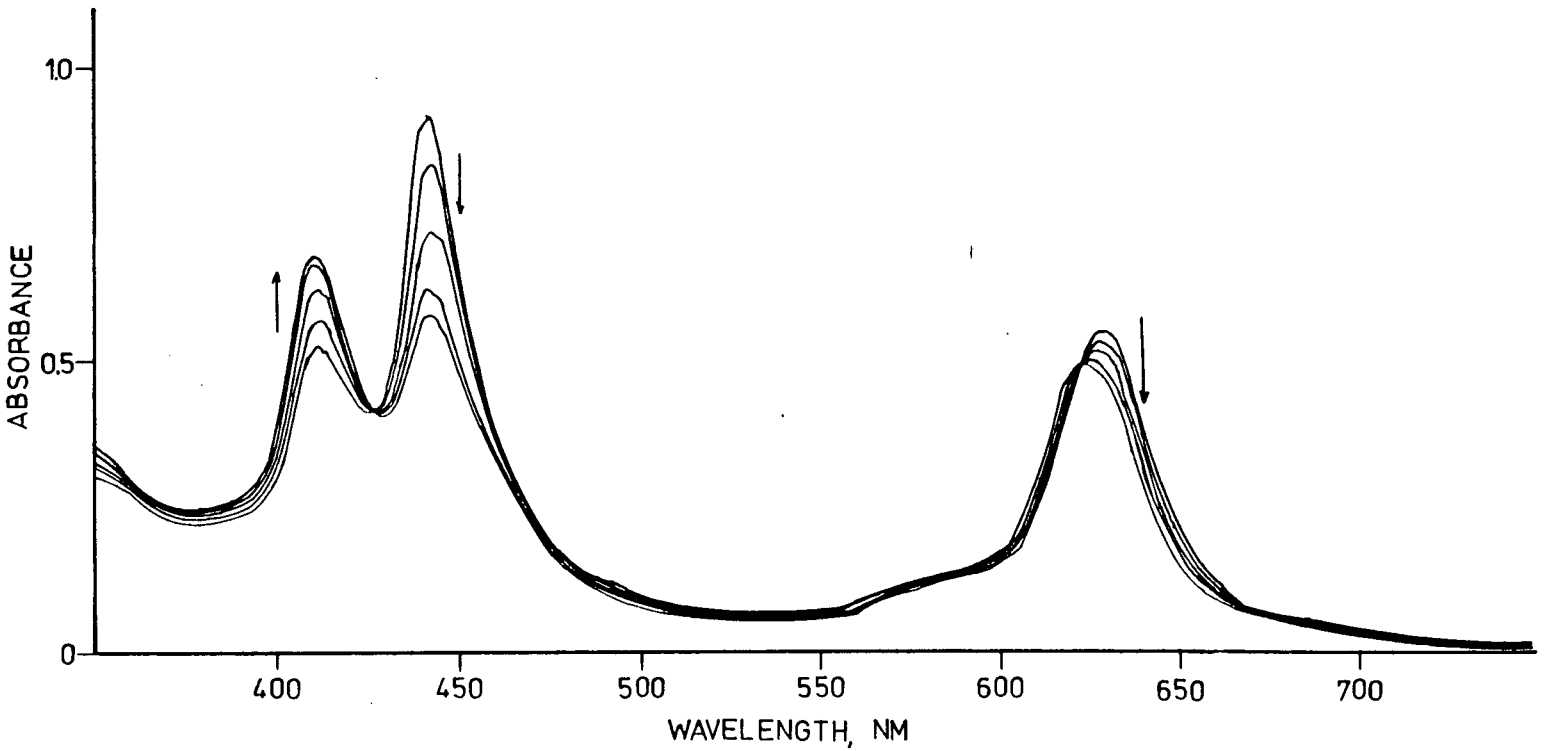

Figure IX.8 Spectra showing the generation of PipCoOMBP from PipCoOMBP(MA).

For raw data see Appendix VIIc.

electron density to the substrate. The electron withdrawing MA is able to form an adduct with CoOMBP without the aid of an axial ligand, but it appears that substantial changes occur in the electronic structure of OMBP. Appearance of a PipCoOMBP spectrum upon the addition of Pip to MACoOMBP in a dilute MA in toluene solution suggests that axial Pip weakens the Co-MA bond. The formation of a spectrum similar to that of other six coordinate species, upon addition of Pip to MACoOMBP in stronger MA solutions, suggests that electronic changes to OMBP upon MA coordination are somewhat reversed upon coordination of a second axial ligand.

When the MA addition to CoOMBP is carried out in DMF, the reacting species is DMFCoOMBP (Chapter III). DMF, a strong π-donor[121], might be expected to stabilize the formation of the MA adduct. However, the K_{MA} values in DMF and the ΔH_{MA} value in DMF (Table IX.3) are somewhat less in magnitude than in toluene, although MA binds more strongly to DMFCoOMBP in DMF than to CoOMBP in DCE. Weaker binding in DMF than in toluene would be consistent with destabilizing the product in a more polar solvent. Stronger MA binding in DMF than in DCE could be due to π-stabilization from the DMF ligand. The spectrum of DMFCoOMBP(MA) is similar to that of other six-coordinate OMBP systems which suggests that a bond weakening similar to that occurring when Pip is the axial ligand; this would also explain the weakened binding in DMF compared to toluene. However, this effect appears to be discounted by the stronger binding in DMF than in DCE; perhaps the π-electron density helps compensate for the electronic changes occurring to OMBP upon the binding of MA to CoOMBP. The formation of the DMFCoOMBP adduct with MA appears to be complete, while when MA is added to PipCoOMBP incomplete product formation is apparent at a comparable concentration of MA. This also suggests that the π-donor nature of DMF is important in maintaining a MA adduct of CoOMBP.

Studies similar to those for MA binding were carried out with tetracyanoethylene (TCNE). This reaction was hampered by the formation of TCNE charge transfer complexes with toluene and the previously studied amine ligands[160]. However, when DCE was the solvent, there were spectral changes similar to those observed for the MA reaction with CoOMBP in DCE (Table IX.1). TCNE concentrations required to complete the reaction were similar to those of MA to fully form the adduct with CoOMBP. This is evidence that the ligand binding takes place through the olefinic bond, since this is the only functional group that MA and TCNE have in common.

Attempts to detect a well resolved ESR signal for the olefin complexes of CoOMBP were unsuccessful; weak and ill defined spectra similar to those for LCoOMBP (L = CH_3-Im, Pip, or Py, Chapter VII) were observed. Presumably similar spin coupling phenomena that likely occur for the LCoOMBP systems also occur for the MA complex.

No reaction with MA or TCNE was observed when other cobalt(II) porphyrin complexes (LCoPpIXDME, LCoDADIXDME, or LCoDBrDIXDME; L = CH_3-Im, Pip, Py, or no ligand) were involved. Presumably this results from the strong π-donor ability of OMBP[96c], allowing greater stability of a cobalt-olefin interaction by greater π-back donation to the olefin π^*-orbitals.

IX.3 Reactions of Co(salen) Complexes with Unsaturated Substrates

Four-coordinate Co(salen) showed no sign of reaction when exposed to ethylene, acetylene, or TCNE. Five-coordinate CH_3-ImCo(salen), upon exposure to ethylene or acetylene, showed some slight spectral changes at -63.5°C (an absorbance increase from 0.95 to 0.99 at 400 nm under one atmosphere of gas). The spectral changes, which were reversible upon evacuation, resembled those which would be expected from the presence of a small amount of oxygen (Figure VIII.2), but an ESR investigation of the ethylene or acetylene systems at 77 K revealed a decrease (by 40%) of the CH_3-ImCo(salen) signal, with no new

signal apparent. The formation of an adduct of LCo(salen) with an unsaturated substrate appears to involve the loss of unpaired electron density, which could occur by the coupling of spins, possibly in a manner similar to that which is present in the CoOMBP complexes with unsaturated substrates.

Attempts to study interactions of LCo(salen) with the activated, electron-withdrawing olefin, TCNE, were frustrated by the formation of TCNE-amine charge transfer complexes[160].

Ambient temperature visible spectroscopic studies were carried out with a variety of liquid olefins. The presence of peroxides, which reacted very readily with Co(salen), was a problem for all these olefins and the peroxides had to be thoroughly removed (Chapter II). Neither five-coordinate LCo(salen), nor four-coordinate Co(salen), complexes would react with 1-hexene, cyclooctene, styrene, 3,4-dichlorobutene, diethylmaleate, or diethylfumarate in dichloromethane at room tempreature. Also there was no visible spectroscopic evidence for binding of the above olefins at lower temperatures (-78°C, -63.5°C, -45°C, -31°C, or -23°C).

Upon exposure to 800 Torr oxygen at 22°C, the visible spectra of the Co(salen)-cyclooctene and Co(salen)-1-hexene systems did not change over a period of 10 h; this is the same behavior as when no olefin is present in the system. The 410 nm Co(salen) band diminished quite considerably over 12 h when styrene or 3,4-dichlorobutene were present, while the same band disappeared completely when diethylfumarate was present. After the systems were evacuated, the 410 nm peak in both the styrene and 3,4-dichlorobutene systems (Figure IX.9) were largely regenerated after 40 h, although there was no peak regeneration in the diethylfumarate system.

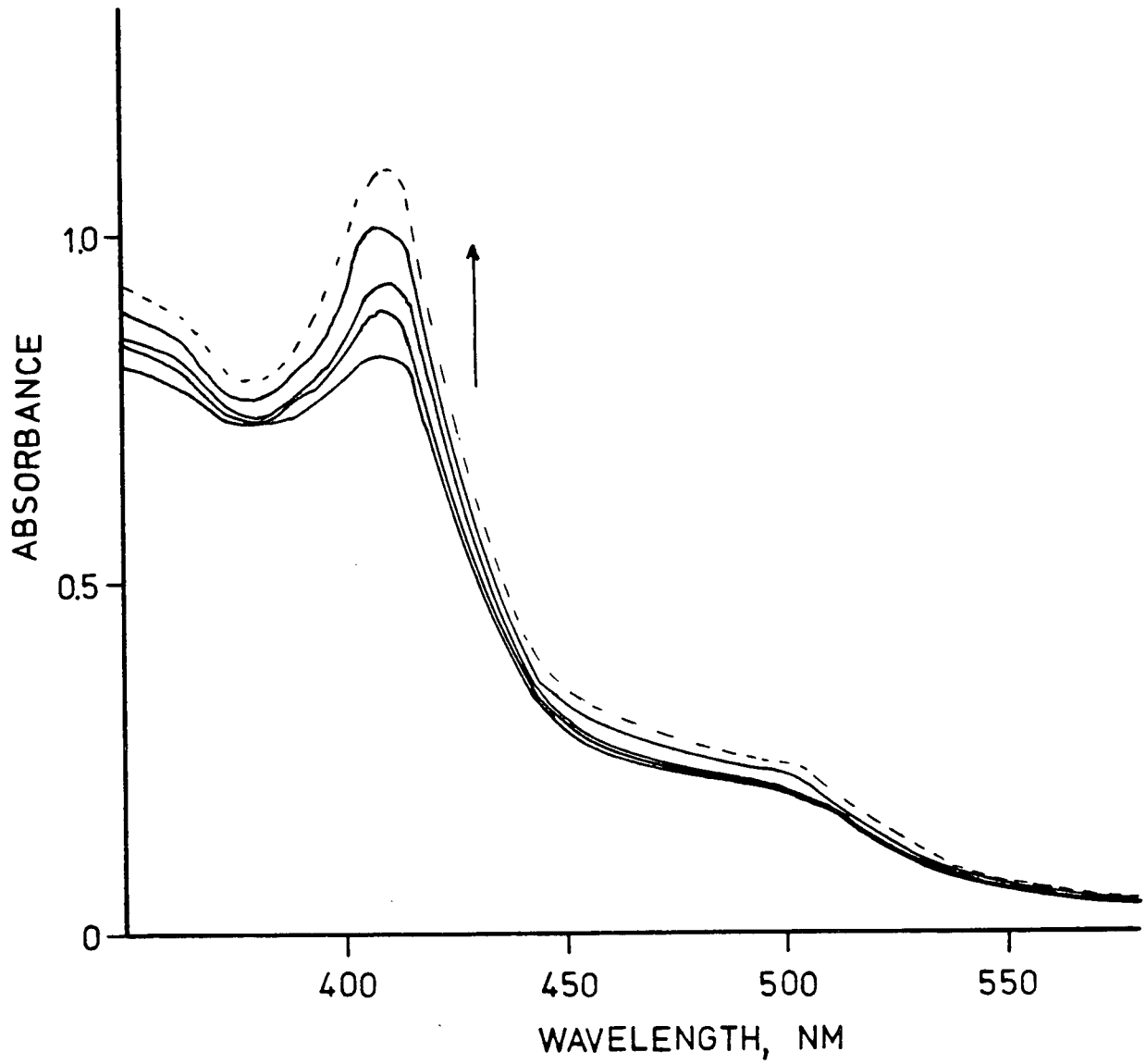

Figure IX.9 Spectra showing the regeneration of the Co(salen) peak after oxygen is removed from the Co(salen)-3,4-dichlorobutene system. For raw data see Appendix VIIg.

--- Spectrum before oxygen is admitted to the system

ESR spectra at 77K of Co(salen) in the presence of styrene or 3,4-dichlorobutene exhibited a very broad signal with no fine structure (Figure IX.10); this contrasts markedly with the characteristic, well-defined signal obtained from the amine complexes of Co(salen) (Figure VIII.4). If an atmosphere of oxygen were added to the above systems at ambient temperature, and the system then taken to 77 K, the same signal results. If the Co(salen)-olefin (styrene or 3,4-dichlorobutene) system were exposed to oxygen for 42 h at ambient temperature, a sharp, well-resolved ESR signal (Figure IX.11) could be obtained. This signal is similar to that observed for dioxygen adducts of Co(salen)-amine systems (Figure VIII.5), but the A_z values associated with the olefin systems were substantially greater than those associated with the amine systems (Appendix IX).

These preliminary results suggest that olefinic compounds can bind, albeit very weakly, with Co(salen), which can then activate Co(salen) to bind dioxygen. Initial attempts to isolate a product from some of these systems yielded a dark brown powder after dichloromethane was evaporated from the Co(salen)-styrene system under a stream of oxygen. However, the product has yet to be characterized. Further studies of these systems should complement work that has already been performed in studying the use of metallomacrocycles in selectively oxidizing unsaturated substrates, such as 3-substituted indoles and flavonols[161].

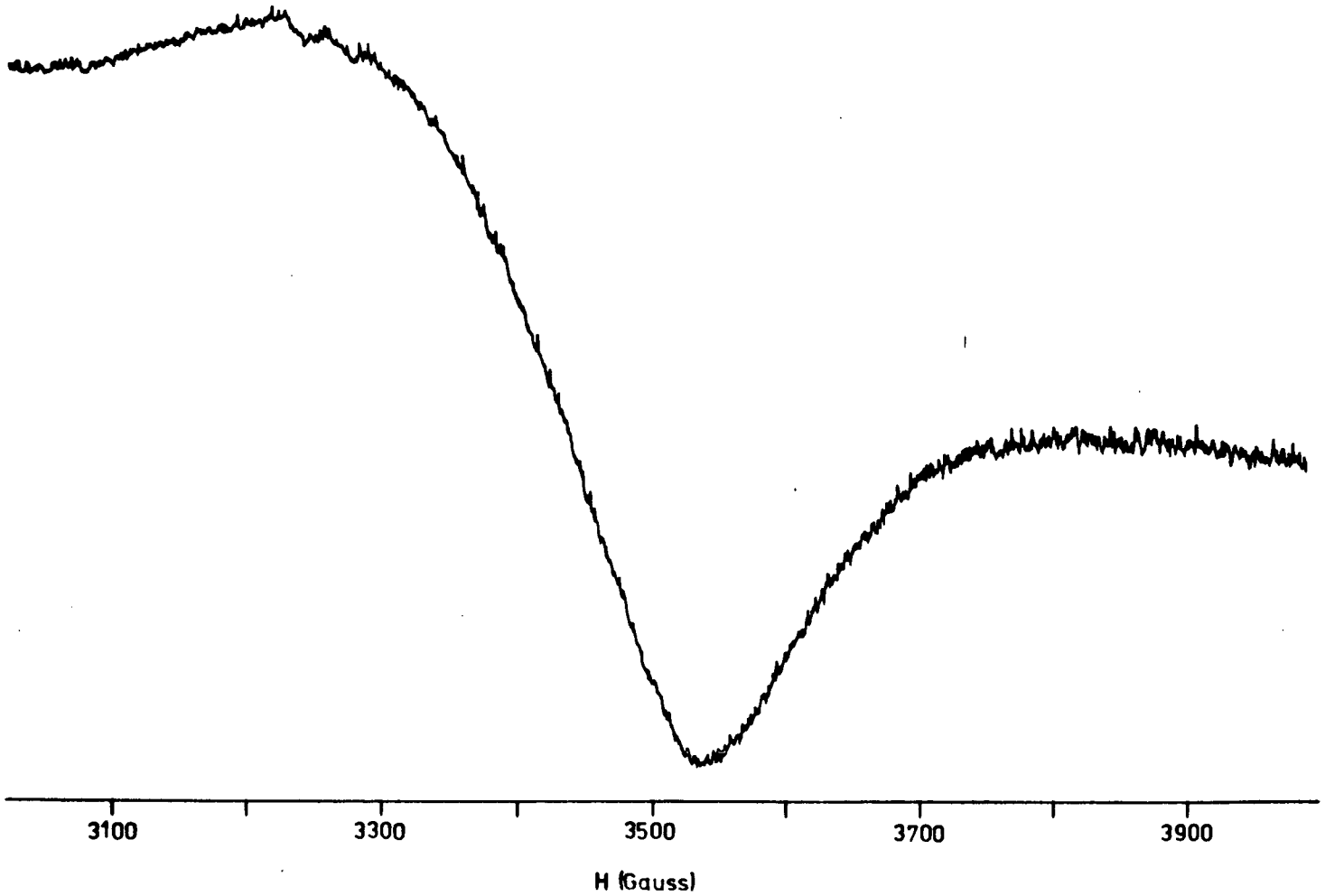

Figure IX.10 ESR signal of Co(salen)-3,4-dichlorobutene system at 77 K.

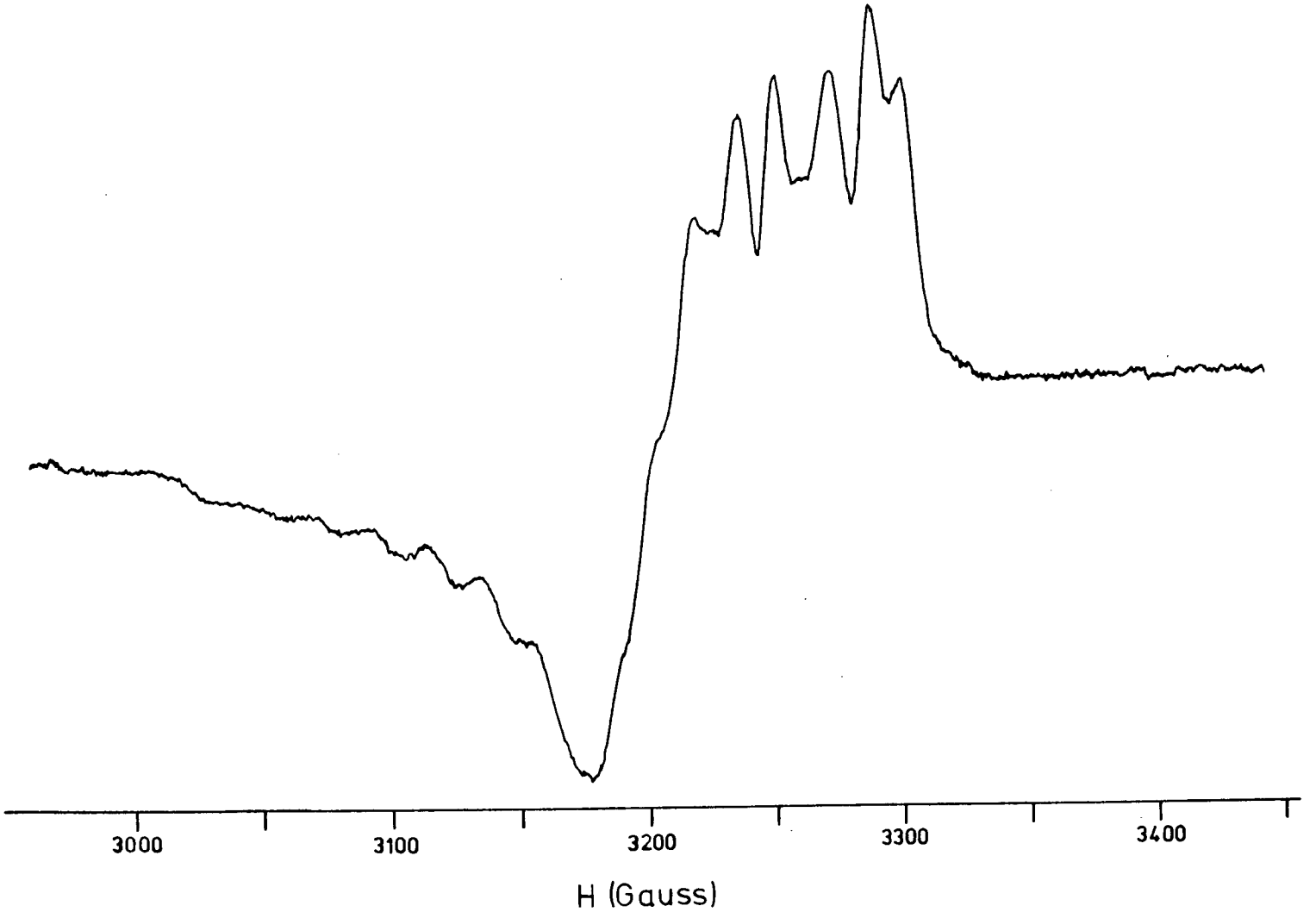

Figure IX. 11 ESR signal of Co(salen)-3,4-dichlorobutene system at 77K after exposure to O_2 for 42 h at ambient temperature.

CHAPTER X

GENERAL CONCLUSIONS AND SOME RECOMMENDATIONS FOR FUTURE WORK

Work in this thesis is an important extension of previous work done on ligand and dioxygen binding to cobalt(II) porphyrin complexes[22,23]. Work was done primarily on CoOMBP, CoDADIXDME, and CoDBrDIXDME complexes in which the porphyrin σ-basicity is weaker than in the cobalt(II) porphyrin complexes previously studied. It was definitely established that axial ligands bind to cobalt(II) more strongly with decreasing basicity of the porphyrin.

One of the porphyrins, OMBP, was sufficiently weakly basic that direct quantitative studies of binding both a first and second axial ligand to a cobalt(II) porphyrin were accomplished for the first time:

$$L + CoOMBP \overset{K_1}{\rightleftharpoons} LCoOMBP \qquad (X.1)$$

$$L + LCoOMBP \overset{K_2}{\rightleftharpoons} L_2CoOMBP \qquad (X.2)$$

The ΔH of the second ligand binding was found to be very similar to that of the first ligand binding, and the order of affinity for the first axial ligand binding (Pip>CH_3-Im>Py) was the same as for the second ligand binding.

Trends previously reported[22,23] for ligand affinity with the more strongly basic porphyrin complexes of cobalt(II) were similar to those observed in the present work with the weakly basic porphyrin complexes. For

all cobalt(II) complexes studied there is no overall correlation between pK_a of the protonated binding axial ligand and the thermodynamics of the ligand binding, although a Hammett relationship has been noted for substituted pyridines on binding to CoPpIXDME[89].

As a result of CoOMBP binding ligands so strongly, the quantitative thermodynamic parameters for binding the weakly basic ligand THF could be determined at ambient temperature. This ligand could not be studied with the more strongly basic porphyrin complexes of cobalt(II).

For dioxygen binding to LCoP complexes it was established that dioxygen tends to bind more strongly with complexes of more strongly basic porphyrins. Trends in dioxygen binding to cobalt(II) complexes of weakly basic porphyrin complexes as a function of axial ligand are similar to those reported previously for strongly basic porphyrin complexes. No overall correlation between the thermodynamic parameters of dioxygen binding and the pK_a of protonated axial ligands was apparent for the cobalt(II) porphyrin complexes, except for a limited Hammett relationship found earlier for dioxygen binding with CoPpIXDME complexes of substituted pyridines[89].

Evidence was also obtained for the ability of a cobalt(II) porphyrin complex to stabilize a dioxygen adduct with π-interactions, as well as σ-interactions. Thus, CoOMBP complexes bind dioxygen more strongly than would be expected from the σ-basicity of OMBP, and this is rationalized in terms of the exceptional π-donor ability of OMBP. Also, compared with other ligand adducts, the DMF complex of CoOMBP binds dioxygen with a greatly enhanced exothermicity. Dioxygen binds more strongly to DMF complexes of cobalt(II) porphyrins than would be expected from the pK_a value of DMF, and this is attributed to DMF being a strong π-donor compared with the other axial

ligands investigated.

A more polar solvent has been found to play a major role in stabilizing the Co(III)-O_2^- adduct, and a linear correlation between solvent polarity and dioxygen binding to PipCoOMBP in the binary toluene-DMF solvent mixtures has been found.

Evidence for solvent polarity playing a role in stabilizing Co(III)-O_2^- complexes was also obtained from studying the reaction:

$$L_2CoOMBP + O_2 \underset{}{\overset{K_{O_2/L}}{\rightleftharpoons}} LCoOMBP(O_2) + L \qquad (X.3)$$

When CH_3-Im was the axial ligand, dioxygen bound more strongly than was expected from considerations of the K_2 and K_{O_2} values of that system. This arises since such a high concentration of CH_3-Im is required for full formation of the bis amine adduct that the polarity of the solvent is substantially greater than that of the toluene in which K_2 and K_{O_2} were measured. In contrast, no evidence for oxygenation of $Pip_2CoOMBP$ was obtained; Pip is essentially non polar compared with CH_3-Im, and thus the dioxygen adduct of this system is presumably not sufficiently stabilized.

With a solvent system of 4:1 by volume toluene:DCE, the oxygen affinity of LCoOMBP was found to be increased to a greater extent than occurred in a toluene-DMF mixture of similar polarity; the tendency to irreversibly oxidize was also greater than in the toluene-DMF solvent mixture. This can be explained by the possible presence of more protons in DCE than in basic DMF enhancing the formation of the Co(III)-O_2^- adduct and the presumed peroxide-like intermediate present during oxidation.

Binding of the ligands CH_3-Im, Pip, Py, and THF was found to be somewhat weaker in a more polar solvent. However, the decrease in ligand affinity was not as great as the amount of enhancement observed in dioxygen binding,

presumably because ligand adduct formation does not involve as much change in overall polarity as does dioxygen adduct formation.

In the course of this work, the first evidence of metalloporphyrin aggregation in non polar solvents at concentrations as low as 10^{-5} M was obtained for some CoOMBP systems. This phenomenon has recently been observed in systems involving another metal (ZnOMBP[150]). Aggregation of CoOMBP complexes is thought to hinder oxygenation and subsequent oxidation of CoOMBP complexes, since the reaction time becomes progressively larger at higher CoOMBP concentrations to the point where CoOMBP complexes become essentially inert to oxidation at concentrations where gas-uptake determinations are made (10^{-2} M).

As in CoPpIXDME complexes[123], it was found that having a protic axial ligand, such as Im, enhanced oxidation rates, and hydrogen bonding from the free ligand is thought to stabilize an activated oxygenated intermediate and lower a kinetic barrier for the oxidation process. When Im was the axial ligand on CoOMBP, no evidence of aggregation was noted, and so it is concluded that the availabilty of protons can help break up aggregates.

If porphyrin aggregation could be avoided, the cobalt(II) complexes studied in this thesis were oxidized via a process that was first order in cobalt, as was observed in the CoPpIXDME complexes[89]. This is explained by invoking a slow rearrangement of the superoxide-like Co(III)-O_2^- to an activated intermediate in which the coordinated dioxygen is more peroxide-like in character.

Oxidation rates of the LCoP and L_2CoOMBP systems studied in this thesis were somewhat greater in DCE than in toluene. Two factors could help account for this: the more polar solvent could enhance the formation of the intermediate Co(III)-O_2^{-*} species that according to the oxidation mechanism

reacts subsequently with the remaining LCoP complex; and any protons present could also aid in formation of the dioxygen adduct intermediate, as well as break up any relatively unreactive porphyrin aggregates present. The importance of solvent polarity in the oxidation process was shown further by the very fast oxidation of CoOMBP in substantial concentrations of polar CH_3-Im, even though in these solvent systems there are two axial CH_3-Im ligands coordinated to the CoOMBP. The more CH_3-Im present, the faster the reaction proceeded, and the less evidence there was of porphyrin aggregation, even at concentrations as high as 10^{-2} M (where gas-uptake determinations were made).

Studies with Co(salen) show that although ligands bind substantially less strongly to Co(salen) than to cobalt(II) porphyrin complexes, which is rationalized in terms of greater electron density on the metal centre in the Schiff base complex, similar trends in ligand binding exist for the Schiff base and porphyrin system. Also, a Hammett relationship occurs for the binding of substituted pyridines to Co(salen).

When dioxygen binding to LCo(salen) systems was studied, the dioxygen affinity as a function of axial ligand was found to be similar to that found for the cobalt(II) porphyrins.

Variation of solvent plays a similar role in ligand and dioxygen binding to Co(salen) as it does in cobalt(II) porphyrin systems.

Enhanced oxygen affinity for the more electron-rich metal centre in Schiff base systems was further demonstrated when dioxygen was found to bind reversibly to four-coordinate Co(salen) at low temperatures (e.g. $-78^{\circ}C$). This behavior is unusual since four-coordinate cobalt porphyrins[22,23] and four-coordinate cobalt(II) complexes of other Schiff base systems[81,82] are essentially inert to oxygenation at comparable temperatures.

Some preliminary studies strongly indicate that CoOMBP forms complexes with electron withdrawing olefins. Visible spectroscopic data reveal interactions of MA and TCNE with CoOMBP which seem amenable to detailed kinetic and mechanistic studies, and these should be carried out before firm conclusions are made. While initial ESR studies on these systems are somewhat thwarted by some spin coupling mechanism, possibly through aggregation, further attempts should probably be made since the potential for information on the interaction of hydrocarbon substrates with metalloporphyrin systems is considerable.

While studies on Co(salen) reactions with unsaturated substrates must be considered preliminary, these too appear to be potentially very interesting, and studies on the Co(salen)-olefin systems that interact with dioxygen would also appear to be worthwhile.

REFERENCES

1 (a). E. Antonini and M. Brunori, "Hemoglobin and Myoglobin in Their Reactions with Ligands," American Elsevier, New York, N.Y., 1971.

(b). J. M. Rifkind, in "Inorganic Biochemistry," G. L. Eichhorn, Ed., American Elsevier, New York, N.Y., 1973, p. 832.

(c). N. W. Makinen, in "Techniques and Topics in Bioinorganic Chemistry," Part 1, C. A. McAuliffe, Ed., Wiley, New York, N.Y., 1975, p. 3.

(d). M. J. Bennett and P. B. Donaldson, J. Amer. Chem. Soc., 93 , 3307 (1971).

(e). M. F. Perutz, Brit. Med. Bull., 32, 195 (1976).

(f). J. M. Baldwin, Brit. Med. Bull., 32, 213 (1976).

2. M. N. Hughes, "The Inorganic Chemistry of Biological Processes," Wiley, New York, N.Y., 1972, p. 146.

3 (a). E. J. Land and A. J. Swallow, Arch. Biochem. Biophys., 145, 365 (1971).

(b). C. Creutz and N. Sutin, Proc. Natl. Acad. Sci. USA, 70, 1701 (1973).

(c). W. G. Miller and M. A. Cusanovitch, Biophys. Struct. Mech., 1, 97 (1975).

(d). C. E. Castro, in "The Porphyrins," Vol. 5, D. Dolphin, Ed., Academic Press, 1978, p. 1.

4 (a). B. C. Saunders, A. G. Holmes-Siedle, and B. P. Stark, "Peroxidase," Butterworth, London, 1964.

(b). A. S. Brill, Compr. Biochem., 14, 447, (1976).

(c). B. C. Saunders, in "Inorganic Biochemistry," G. L. Eichhorn, Ed., American Elsevier, New York, N.Y., 1973, p. 988.

(d). I. Yamazaki, in "Molecular Mechanisms of Oxygen Activation," O. Hayaishi, Ed., Academic Press, New York, N.Y. 1974, p. 535.

4 (e). "The Enzymes," Vol. 8, P. D. Boyer, Ed., 3rd. ed., Academic Press, New York, N.Y., 1973, p. 345, p.363.

(f). R. H. Felton, in "The Porphyrins," Vol. 5, D. Dolphin, Ed., Academic Press, 1978, p. 53.

5 (a). C. Manwell, Annu. Rev. Physiol., 22, 191 (1960).

(b). D. M. Kurtz, Jr., D. F. Shriver, and I. M. Klotz, Coord. Chem. Rev., 24, 145 (1977).

(c). M. Y. Okamura and I. M. Klotz, in "Inorganic Biochemistry," G. L. Eichhorn, Ed., American Elsevier, New York, N.Y., 1973, p. 320.

(d). J. L. York and A. J. Beardon, Biochemistry, 9, 4549 (1970).

(e). K. Garbett, C. E. Johnson, I. M. Klotz, M. Y. Okamura, and R. J. P. Williams, Arch. Biochem. Biophys., 142, 574 (1971).

(f). J. W. Dawson, H. B. Gray, H. E. Hoenig, G. R. Rossman, J. M. Shredder, and R. H. Wang, Biochemistry, 11, 461 (1972).

(g). J. B. Dunn, D. F. Shriver, and I. M. Klotz, Biochemistry, 14, 2689 (1975).

(h). R. E. Stenkamp, L. C. Sieker, and L. H. Jensen, Proc. Natl. Acad. Sci. USA, 73, 349 (1976).

(i). K. B. Ward, W. A. Hendrickson, and G. L. Klippenstein, Nature (London), 257, 818 (1975).

(j) R. E. Stenkamp, L. C. Sieker, and L. H. Jensen, J. Mol. Biol., 126, 457 (1978).

(k). R. E. Stenkamp, L. C. Sieker, L. H. Jensen, and J. E. McQueen, Jr., Biochem., 17, 2499 (1978).

(l). S. E. Clarke, L. C. Sieker, R. E. Stenkamp, and J. S. Loehr, Biochem., 18, 684 (1979).

5 (m). R. H. Stenkamp and L. H. Jensen, Adv. Inorg. Biochem., 1, 219 (1979).

6 (a). R. Lontie and R. Witters, in "The Biochemistry of Copper," J. Peisach, D Aisen, and W. E. Blumberg, Eds., Academic Press, New York, N.Y., 1966, p. 455.

(b). R. Lontie and R. Witters, in "Inorganic Biochemistry," G. L. Eichhorn, Ed., American Elsevier, New York, N.Y., 1973, p.344.

(c). T. H. Moss, D. C. Gould, A. Ehrenberg, J. S. Loehr, and H. S. Mason, Biochem., 12, 2444 (1973).

(d). T. B. Freedman, J. S. Loehr, and T. M. Loehr, J. Amer. Chem. Soc., 98, 2809 (1976).

(e). E. I. Solomon, D. M. Dooley, R. H. Wang, H. B. Gray, M. Cerdonio, F. Mongo, and R. L. Romani, J. Amer. Chem. Soc., 98, 1029 (1976).

(f). T. J. Thamann, J. S. Loehr, and T. M. Loehr, J. Amer. Chem. Soc., 99, 4187 (1977).

(g). R. Lontie and C. Gielens, Metalloproteins, Autumn Meet. Ger. Biochem. Soc., 62 (1979).

(h). J. M. Brown, L. Powers, B. Kincaid, J. A. Larrabee, and T. G. Spiro, J. Amer. Chem. Soc., 102, 4210 (1980).

(i). J. A. Larrabee and T. G. Spiro, J. Amer. Chem. Soc., 102, 4217 (1980).

7 (a). D. B. Carlisle, Proc. R. Soc., London, Ser. B, 171, 31 (1968).

(b). R. M. K. Carlson, Proc. Natl. Acad. Sci. USA, 72, 2217 (1975).

8 (a). R. E. Dickerson and I. Geis, "The Structure and Action of Proteins," Harper and Row, New York, N.Y., 1969, p. 50.

(b). J. C. Kendrew, Science, 139, 1259 (1963).

(c). J. C. Kendrew, R. E. Dickerson, B. E. Strandberg, R. G. Hart, D. R. Davies, D. C. Phillips, and V. C. Shore, Nature (London), 185, 422 (1960).

8 (d). J. C. Kendrew, H. C. Watson, B. E. Strandberg, R. E. Dickerson, D. C. Phillips, and V. C. Shore, Nature (London), 190, 666 (1961).

9. J. C. Kendrew, Brookhaven Symp. Biol. 15, 216 (1962).

10 (a). C. D. Coryell, F. Stitt, and L. Pauling, J. Amer. Chem. Soc., 59, 633 (1937).

(b). C. D. Coryell, J. Phys. Chem., 43, 841 (1939).

(c). A. S. Brill and R. J. P. Williams, Biochem. J., 78, 246 (1961).

11 (a). J. P. Collman, R. R. Gagne, C. A. Reed, W. T. Robinson, and G. A. Rodley, Proc. Natl. Acad. Sci. USA, 71, 1326 (1974).

(b). J. L. Hoard, in "Porphyrins and Metalloporphyrins," K. M. Smith, Ed., American Elsevier, New York, N.Y., 1975, p.317.

12 (a). M. F. Perutz, Nature (London), 228, 726 (1970).

(b). M. F. Perutz, Nature (London), 237, 495 (1972).

13. C. D. Coryell, L. Pauling, and R. W. Dodson, J. Phys. Chem., 43, 825 (1939).

14 (a). H. Theorell and A. Ehrenberg, Acta. Chem. Scand., 5, 823 (1951).

(b). D. Keilin and E. F. Hartree, Biochem. J., 49, 88 (1951).

15. L. Stryer, J. C. Kendrew, and H. C. Watson, J. Mol. Biol., 8, 96 (1964).

16. C. F. Mulks, C. P. Scholes, L. C. Dickinson, and A. Lapidot, J. Amer. Chem. Soc., 101, 1645 (1979).

17. H. A. O. Hill, A. Roder, and R. J. P. Williams, Struct. Bondg., 8, 123 (1970).

18. M. F. Perutz, H. Muirhead, J. M. Cox, and L. C. G. Goaman, Nature, (London), 219, 131 (1968).

19. H. Muirhead, J. M. Cox, L. Mazzerella, and M. F. Perutz, J. Mol. Biol., 28, 117 (1967).

20 (a). J. Monod, J. Wyman, and J. P. Changeux, J. Mol. Biol., 12, 88, (1965).

(b). S. Ogawa, H. M. McConnell, and A. Horwitz, Proc. Natl. Acad. Sci. USA, 61, 401 (1968).

21. M. F. Perutz, Nature (London), 228, 734 (1970).

22. B. R. James, in "The Porphyrins," Vol. 5, D. Dolphin, Ed., Academic Press, New York, N.Y., 1978, p.207.

23 (a). E. I. Ochiai, "Bioinorganic Chemistry, an Introduction," Allen and Bacon Inc., Boston, Mass., 1976, Ch. 6.

(b). G. McLendon and A. E. Martell, Coord. Chem. Rev., 19, 1 (1976).

(c). R. D. Jones, D. A. Summerville, and F. Basolo, Chem. Rev., 79, 139, (1979).

24. L. Vaska, Science, 140, 809 (1963).

25 (a). M. M. Taqui Khan and A. E. Martell, "Homogeneous Catalysis by Metal Complexes," Vol. 1, Academic Press, New York, N.Y., 1974.

(b). L. Vaska, Acc. Chem. Res., 1, 335 (1968).

(c). J. Valentine, Chem. Rev., 73, 235 (1973).

(d). L. Vaska, Acc. Chem. Res., 9, 175 (1976).

26. D. M. P. Mingos, Nature, Phys. Sci. (London), 230, 154 (1970).

27 (a). L. Wittenberg and D. Shemin, J. Biol. Chem. 185, 103 (1950).

(b). J. E. Falk, "Porphyrins and Metalloporphyrins," American Elsevier, New York, N.Y., 1964.

(c). K. M. Smith, Ed., "Porphyrins and Metalloporphyrins," American Elsevier, New York, N.Y., 1975.

28 (a). A. D. Adler, F. R. Longo, J. D. Finarelli, J. Goldmacher, J. Assour, and L. Korsakoff, J. Org. Chem., 32, 476 (1967).

(b). G. H. Barnett, M. F. Hudson, and K. M. Smith, Tet. Lett., 2887 (1973).

29 (a). H. W. Whitlock and R. Hanauer, J. Org. Chem., 33, 2169 (1968).

(b). H. H. Inhoffen, J.-H. Fuhrhop, H. Voight, and H. Brockmann, Jr., Just. Lieb. Ann. Chem., 695, 133 (1966).

30. P. M. Hambright, in "Porphyrins and Metalloporphyrins", K. M. Smith, Ed., American Elsevier, New York, N.Y., 1975, p. 233.

31. F. H. Maser and A. L. Thomas, "Phthalocyanine Compounds," Reinhold Pub. Co., New York, N.Y., 1963.

32 (a). M. J. Carter, D. P. Rillema, and F. Basolo, J. Amer. Chem. Soc., 96, 392 (1974).

(b). R. H. Niswander and L. T. Taylor, J. Amer. Chem. Soc., 99, 5935 (1977).

(c). A van den Bergen, M. F. Corrigan, K. S. Murray, R. M. Slade, and B. O. West, Inorg. Nucl. Chem. Lett., 10, 859 (1974).

(d). R. H. Niswander and A. E. Martell, Inorg. Chem., 17, 1511 (1978).

33. N. Bresciani, M. Calligaris, G. Nardin, and L. Randaccio, J. Chem. Soc. Dalton, 498 (1974).

34. V. V. Zelentsov, A. P. Bogdanov, E. G. Rukhadze, and G. P. Talyzenkova, Russ. J. Inorg. Chem., 18, 1784 (1973).

35 (a). L. Sacconi and I. Bertini, J. Amer. Chem. Soc., 88, 5180 (1966).

(b). D. P. Freyberg, G. M. Mockler, and E. Sinn, J. Chem. Soc. Dalton, 447 (1976).

36. E. M. Boge, D. P. Freyberg, E. Kokot, G. M. Mockler, and E. Sinn, Inorg. Chem., 16, 1655 (1977).

37. H. C. Stynes and J. A. Ibers, J. Amer. Chem. Soc., 94, 1559 (1972).

38 (a). A. H. Corwin and Z. Reyes, J. Amer. Chem. Soc., 78, 2437 (1956).

(b). I. A. Cohen, J. Amer. Chem. Soc., 91, 1980 (1969).

(c). E. B. Fleischer and T. S. Srivastava, J. Amer. Chem. Soc., 91, 2403 (1969).

(d). N. Sadisvan, H. I. Eberspaecher, W. H. Fuchsman, and W. S. Caughey, Biochemistry, 8, 534 (1969).

(e). A. B. Hoffman, D. M. Collins, V. W. Day, E. B. Fleischer, T. S. Srivastava, and J. L. Hoard, J. Amer. Chem. Soc., 94, 3620 (1972).

39 (a). R. Hill, Biochem. J., 19, 341 (1925).

(b). A. H. Corwin and J. G. Erdman, J. Amer. Chem. Soc., 68, 2473 (1946).

(c). D. H. Chin, G. N. La Mar, and A. L. Balch, J. Amer. Chem. Soc., 102, 4344 (1980).

40 (a). L. K. Gottwald and E. F. Ullman, Tet. Lett., 3071 (1969).

(b). J. P. Collman, R. R. Gagne, T. R. Halbert, J. C. Marchon, and C. A. Reed, J. Amer. Chem. Soc., 95, 7868 (1973).

(c). J. P. Collman, R. R. Gagne, H. B. Gray, and J. W. Hare, J. Amer. Chem. Soc., 96, 6522 (1974).

(d). J. P. Collman, R. R. Gagne, C. A. Reed, W. T. Robinson, and G. A. Rodley, Proc. Natl. Acad. Sci. USA, 71, 1326 (1974).

(e). J. P. Collman, R. R. Gagne, and C. A. Reed, J. Amer. Chem. Soc., 96, 2629 (1974).

(f). J. P. Collman, R. R. Gagne, C. A. Reed, T. R. Halbert, G. Lang, and W. T. Robinson, J. Amer. Chem. Soc., 97, 1427 (1975).

(g). J. P. Collman, J. I. Brauman, and K. S. Suslick, J. Amer. Chem. Soc., 97, 7185 (1975).

(h). K. Spartalian, G. Lang, J. P. Collman, R. R. Gagne, and C. A. Reed, J. Chem. Phys., 63, 5375 (1975).

(i). J. P. Collman, J. I. Brauman, E. Rose, and K. S. Suslick, Proc. Natl. Acad. Sci. USA, 75, 1052 (1978).

(j). G. B. Jameson, G. A. Rodley, W. T. Robinson, R. R. Gagne, C. A. Reed, and J. P. Collman, Inorg. Chem., 17, 850 (1978).

(k). G. B. Jameson, F. S. Molinaro, J. A. Ibers, J. P. Collman, J. I. Brauman, E. Rose, and K. S. Suslick, J. Amer. Chem. Soc., 100, 6769 (1978).

(l). G. B. Jameson, F. S. Molinaro, J. A. Ibers, J. P. Collman, J. I. Brauman, E. Rose, and K. S. Suslick, J. Amer. Chem. Soc., 102, 3224 (1980).

(m). J. P. Collman, J. I. Brauman, K. M. Doxsee, T. R. Halbert, E. Bunnenberg, R. E. Linder, G. N. LaMar, J. Del Gaudio, G. Lang, and K. Spartalian, J. Amer. Chem. Soc., 102, 4182 (1980).

41 (a). J. Almog, J. E. Baldwin, and J. Huff, J. Amer. Chem. Soc., 97, 227, (1975).

(b). J. Almog, J. E. Baldwin, R. L. Dyer, and M. Peters, J. Amer. Chem. Soc., 97, 226 (1975).

(c). J. R. Budge, P. E. Ellis Jr., R. D. Jones, J. E. Linard, F. Basolo, J. E. Baldwin, and R. L. Dyer, J. Amer. Chem. Soc., 101, 4760 (1979).

(d). J. R. Budge, P. E. Ellis Jr., R. D. Jones, J. E. Linard, T. Szymanski, F. Basolo, J. E. Baldwin, and R. L. Dyer, J. Amer. Chem. Soc., 101, 4762 (1979).

(e). P. E. Ellis, Jr., J. E. Linard, T. Szymanski, R. D. Jones, J. R. Budge, and F. Basolo, J. Amer. Chem. Soc., 102, 1889 (1980).

41 (f). J. E. Linard, P. E. Ellis, Jr., J. R. Budge, R. D. Jones, and F. Basolo, J. Amer. Chem. Soc., 102, 1896 (1980).

(g). G. B. Jameson and J. A. Ibers, J. Amer. Chem. Soc., 102, 2823 (1980).

42 (a). J. P. Collman and C. A. Reed, J. Amer. Chem. Soc., 95, 2048 (1973).

(b). D. Brault and M. Rougee, Biochem. Biophys. Res. Commun., 57, 654 (1974).

(c). G. C. Wagner and R. J. Kassner, Biochem. Biophys. Acta., 392, 319 (1975).

43. J. P. Collman, J. I. Brauman, K. M. Doxsee, T. R. Halbert, S. E. Hayes, and K. S. Suslick, J. Amer. Chem. Soc., 100, 2761 (1978).

44 (a). J. H. Wang, J.Amer. Chem. Soc., 80, 3168 (1958).

(b). J. H. Wang, Acc. Chem. Res., 3, 90 (1970).

45. O. Leal, D. L. Anderson, R. G. Bowman, F. Basolo, and R. L. Burwell, Jr., J. Amer. Chem. Soc., 97, 5125 (1975).

46 (a). E. Tsuchida, K. Honda, and H. Sata, Biopolymers, 13, 2147 (1974).

(b). H. A. O. Hill, D. R. Turner, and G. Pellizer, Biochem. Biophys. Res. Comm., 56, 739 (1974).

(c). E. Tsuchida, K. Honda, S. Hata, H. Suwa, and K. Kohn, Chem. Lett., 761 (1975).

(d). E. Tsuchida and K. Honda, Chem. Lett., 119 (1975).

(e). E. Tsuchida, K. Honda, and H. Sata, Makromol. Chem., 176, 2251 (1975).

(f). E. Tsuchida and K. Honda, Polymer J., 7, 498 (1975).

(g). E. Tsuchida, K. Honda, and H. Sata, Inorg. Chem., 15, 352 (1976).

(h). K. Honda, H. Sata, and E. Tsuchida, Bull. Chem. Soc. Jpn., 49, 868 (1976).

47. H. Ledon and Y. Brigandat, J. Organomet. Chem., 165, C25 (1979).

48. E. Tsuchida, E. Hasegawa, and K. Honda, Biochim. Biophys. Acta., 427, 520 (1976).

49. H. R. Allcock, P. P. Greigger, J. E. Gardner, and J. L. Schmutz, J. Amer. Chem. Soc., 101, 606 (1979).

50. C. K. Chang, and T. G. Traylor, Proc. Natl. Acad. Sci. USA, 70, 2647 (1973).

51 (a). G. C. Wagner and R. J. Kassner, J. Amer. Chem. Soc., 96, 5593 (1974).

(b). W. S. Brinigar and C. K. Chang, J. Amer. Chem. Soc., 96, 5595 (1974).

(c). W. S. Brinigar, C. K. Chang, J. Geibel, and T. G. Traylor, J. Amer. Chem. Soc., 96, 5597 (1974).

(d). D. L. Anderson, C. J. Weschler, and F. Basolo, J. Amer. Chem. Soc., 96, 5599 (1974).

(e). J. Almog, J. E. Baldwin, R. L. Dyer, J. Huff, and C. J. Wilkerson, J. Amer. Chem. Soc., 96, 5600 (1974).

52 (a). C. J. Weschler, D. L. Anderson, and F. Basolo, J. Chem. Soc. Chem. Comm., 757 (1974).

(b). C. J. Weschler, D. L. Anderson, and F. Basolo, J. Amer. Chem. Soc., 97, 6707 (1975).

53. M. G. Simmons and L. J. Wilson, J. Chem. Soc. Chem. Comm., 634 (1978).

54. J. E. Bulkowski, P. L. Burke, M.-F. Ludmann, and J. A. Osborn, J. Chem. Soc. Chem. Comm., 498 (1977).

55. R. Stomberg, Arkiv. Kemi, 24, 283 (1965).

56. S. K. Cheung, C. J. Grimes, J. Wong, and C. A. Reed, J. Amer. Chem. Soc., 98, 5028 (1976).

57. J. H. Fuhrhop, K. M. Kadish, and D. G. Davis, J. Amer. Chem. Soc., 95, 5140 (1973).

58 (a). J. A. Elvidge and A. B. P. Lever, Proc. Chem. Soc., 195 (1959).

(b). S. Engelsma, A. Yamamoto, E. Markham, and M. Calvin, J. Phys. Chem., 66, 2517 (1962).

(c). M. Calvin, Rev. Pure Appl. Chem., 15, 1, (1965).

(d). L. H. Vogt, Jr., A. Zalkin, and D. H. Templeton, Science, 151, 569 (1966).

(e). L. H. Vogt, Jr., A. Zalkin, and D. H. Templeton, Inorg. Chem., 6, 1725 (1967).

(f). G. L. Johnson and W. D. Beveridge, Inorg. Nucl. Chem. Lett., 3, 323 (1967).

(g). A. Yamamoto, L. K. Phillips, and M. Calvin, Inorg. Chem., 7, 847 (1968).

(h). T. Yarino, T. Matsushita, I. Masuda, and K. Shinra, J. Chem. Soc. Chem. Comm., 1317 (1970).

(i). J. D. Miller and F. D. Oliver, J. Inorg. Nucl. Chem., 34, 1873 (1972).

(j). T. Matsushita, T. Yarino, I. Masuda, T. Shono, and K. Shinra, Bull. Chem. Soc. Jpn., 46, 1712 (1973).

(k). H. S. Maslen and T. N. Waters, J. Chem. Soc. Chem. Comm., 760 (1973).

(l). G. W. R. Canham and A. B. P. Lever, Inorg. Nucl. Chem. Lett., 9, 513 (1974).

(m). S. J. Ebbs and L. T. Taylor, Inorg. Nucl. Chem. Lett., 10, 1137 (1974).

(n). L. J. Boucher and C. G. Coe, Inorg. Chem., 14, 1289 (1975).

(o). W. M. Coleman and L. T. Taylor, Inorg. Chem., 16, 1114 (1977).

59 (a). B. Gonzalez, J. Kouba, S. Yee, C. A. Reed, J. F. Kirner, and W. R. Scheidt, J. Amer. Chem. Soc., 97, 3247 (1975).

59 (b). C. J. Weschler, B. M. Hoffman, and F. Basolo, J. Amer. Chem. Soc., 97, 5278 (1975).

(c). B. M. Hoffman, C. J. Weschler, and F. Basolo, J. Amer. Chem. Soc., 98, 5473 (1976).

60. R. D. Jones, D. A. Summerville, and F. Basolo, J. Amer. Chem. Soc., 100, 4416 (1978).

61 (a). K. Uchida, S. Naito, M. Soma, T. Onishi, and K. Tamaru, J. Chem. Soc. Chem. Comm., 217 (1978).

(b). A. B. P. Lever, J. P. Wilshire, and S. K. Quan, J. Amer. Chem. Soc., 101, 3974 (1979).

62 (a). J. M. Latour, J. C. Marchon, and M. Nakajima, J. Amer. Chem. Soc., 101, (1979).

(b). J. C. Marchon, J. M. Latour, and C. J. Boreham, J. Mol. Catal., 7, 51 (1980).

63. B. R. Guilard, J. M. Latour, C. Lecomte, J. C. Marchon, J. Protas, D. Ripoll, Inorg. Chem., 17, 1228 (1978).

64. N. Farrell, D. H. Dolphin, and B. R. James, J. Amer. Chem. Soc., 100, 324 (1978).

65. B. R. James, A. W. Addison, M. Cairns, D. H. Dolphin, N. P. Farrell, D. R. Paulson, and S. Walker, Fundamental Res. Homogeneous Catal., 3, 751 (1979).

66. B. R. James and D. V. Stynes, J. Amer. Chem. Soc., 94, 6225 (1972).

67. B. B. Wayland and A. R. Newman, J. Amer. Chem. Soc., 101, 6472 (1979).

68 (a). C. Floriani and F. Calderazzo, J. Chem. Soc. A, 946 (1969).

(b). B. M. Hoffman, D. L. Diemente, and F. Basolo, J. Amer. Chem. Soc., 92, 61 (1970).

(c). E. I. Ochiai, J. Inorg. Nucl. Chem., 35, 1727 (1973).

68 (d). K. S. Murray, and R. M. Sheahan, J. Chem. Soc. Chem. Comm., 475 (1975).

(e). B. R. McGarvey, Can. J. Chem., 53, 2498 (1975).

(f). M. M. Rohmer, A. Dedieu, and A. Veillard, Theor. Chim. Acta., 39, 189 (1975).

(g). D. Getz, E. Melemud, B. L. Silver, and Z. Dori, J. Amer. Chem. Soc., 97, 3846 (1975).

(h). A. Dedieu, M. M. Rohmer, and A. Veillard, J. Amer. Chem. Soc., 98, 5789 (1976).

(i). R. Lancashire, T. D. Smith, and J. R. Pilbrow, J. Chem. Soc. Dalton, 66 (1979).

69 (a). L. Pauling, in "Haemoglobin," F. J. W. Roughton and J. C. Kendrew, Eds., Butterworth, London, 1949, p.57.

(b). L. Pauling, Nature (London), 203, 182 (1964).

70 (a). B. S. Tovrog and R. S. Drago, J. Amer. Chem. Soc., 96, 6765 (1974).

(b). B. S. Tovrog, D. J. Kitko, and R. S. Drago, J. Amer. Chem. Soc., 98 5144 (1976).

(c). R. S. Drago, Inorg. Chem., 18, 1408 (1979).

71 (a). J. S. Griffith, Proc. Roy. Soc. Ser. A, Math. Phys. Sci., 235, 23 (1956).

(b). H. B. Gray, Adv. Chem. Ser., 100, 365 (1971).

72 (a). E. Antonini, J. Wyman, M. Brunori, C. Fronticelli, E. Bucci, and A. Rossi-Fanelli, J. Biol. Chem., 240, 1096 (1965).

(b). C. A. Spilburg, B. M. Hoffman, and D. H. Petering, J. Biol. Chem., 247, 4219 (1972).

73. M. E. Fremy, Ann. Chim. Phys. Ser. 3, 35, 257 (1852).

74. A. Werner and A. Mylius, Z. Anorg. Chem., 16, 245 (1898).

75. P. Pfeiffer, E. Brieth, E. Lubbe, and T. Tsumaki, Just. Lieb. Ann. Chem., 503, 84 (1933).

76. T. Tsumaki, Bull. Chem. Soc. Jpn., 13, 252 (1938).

77 (a). A. E. Martell and M. Calvin, "Chemistry of the Metal Chelate Coumpounds," Prentice Hall, New York, N.Y., 1952, pp. 337-357.

(b). O. L. Harle and M. Calvin, J. Amer. Chem. Soc., 68, 2612 (1946).

(c). M. Calvin, R. H. Bailes, and W. K. Wilmarth, J. Amer. Chem. Soc., 68, 2254 (1946).

(d). G. H. Barkelew and M. Calvin, J. Amer. Chem. Soc., 68, 2257 (1946).

(e). W. K. Wilmarth, S. Aranoff, and M. Calvin, J. Amer. Chem. Soc., 68, 2263 (1946).

(f). M. Calvin and G. H. Barkelew, J. Amer. Chem. Soc., 68, 2267 (1946).

(g). R. H. Bailes and M. Calvin, J. Amer. Chem. Soc., 69, 1886 (1947).

78 (a). H. Diehl, Iowa State Coll. J. Sci., 21, 271 (1947).

(b). H. Diehl, C. C. Hach, G. C. Harrison, L. M. Ligget, and T. S. Chow, Iowa State Coll. J. Sci., 21, 287 (1947).

(c). G. C. Harrison and H. Diehl, Iowa State Coll. J. Sci., 21, 311 (1947).

(d). C. C. Hach, L. M. Ligget, and H. Diehl, Iowa State Coll. J. Sci., 21, 316 (1947).

(e). H. Diehl and L. M. Liggett, Iowa State Coll. J. Sci., 21, 326 (1947).

(f). H. Diehl, R. J. Brouns, G. C. Harrison, and L. M. Liggett, Iowa State Coll. J. Sci., 21, 335 (1947).

(g). H. Diehl and T. S. Chow, Iowa State Coll. J. Sci., 22, 126 (1948).

(h). H. Diehl, R. J. Brouns, G. C. Harrison, and L. M. Liggett, Iowa State Coll. J. Sci., 22, 129 (1948).

78(i). H. Diehl, L. M. Liggett, G. C. Harrison, C. C. Hach, and R. Curtis, Iowa State Coll. J. Sci., 22, 91 (1948).

(j). H. Diehl, L. M. Liggett, C. C. Hach, G. C. Harrison, L. Henselmeier, R. W. Schwandt, and J. Matthews, Iowa State Coll. J. Sci., 22, 110 (1948).

(k). L. M. Liggett and H. Diehl, Iowa State Coll. J. Sci., 22, 141 (1948).

(l). H. Diehl, C. C. Hach, G. C. Harrison, L. M. Liggett, and R. J. Brouns, Iowa State Coll. J. Sci., 22, 150 (1948).

(m). C. C. Hach and H. Diehl, Iowa State Coll. J. Sci., 22, 165 (1948).

(n). H. Diehl and J. Henn, Iowa State Coll. J. Sci., 23, 273 (1949).

79. R. F. Stewart, P. A. Estep, and J. J. S. Sebastian, U.S. Bur. Mines Inform., Circ. No. 7906 (1959).

80. A. J. Aducci, CHEMTECH, 6, 575 (1976).

81 (a). F. Calderazzo, C. Floriani, and J. J. Salzman, Inorg. Nucl. Chem. Lett., 2, 379 (1966).

(b). A. L. Crumbliss and F. Basolo, Science, 164, 1168 (1969).

(c). A. L. Crumbliss and F. Basolo, J. Amer. Chem. Soc., 92 55 (1970).

82. M. J. Carter, D. P. Rillema, and F. Basolo, J. Amer. Chem. Soc., 96, 392 (1974).

83. (a). M. J. Carter, L. M. Engelhardt, D. P. Rillema, and F. Basolo, J. Chem. Soc. Chem. Comm., 810 (1973).

(b). G. Costa, G. Mestroni, A. Puxeddu, E. Reisenhofer, J. Chem. Soc. A, 2870 (1970).

(c). G. Costa, A. Puxeddu, and L. B. Slefani, Inorg. Nucl. Chem. Lett., 6, 191 (1970).

84 (a). K. S. Murray and R. M. Sheahan, J. Chem. Soc. Dalton, 1134 (1976).

(b). M. F. Corrigan, K. S. Murray, B. O. West, P. R. Hicks, and J. R. Pilbrow, J. Chem. Soc. Dalton, 1478 (1977).

(c). L. S. Chen, M. E. Koehler, B. C. Pestel, and S. C. Cummings, J. Amer. Chem. Soc., 100, 7243 (1978).

85. T. Szymanski, T. W. Cape, R. P. Van Duyne, and F. Basolo, J. Chem. Soc. Chem. Comm., 5 (1979).

86. J. H. Burness, J. G. Dillard, and L. T. Taylor, J. Amer. Chem. Soc., 97, 6080 (1975).

87 (a). M. Calligaris, G. Nardin, and L. Randaccio, J. Chem. Soc. Dalton, 419 (1973).

(b). G. A. Rodley and W. T. Robinson, Nature (London), 235, 438 (1972).

(c). R. S. Gall, J. F. Rogers, W. P. Schaeffer, and G. C. Christoph, J. Amer. Chem. Soc., 98, 5135 (1976).

(d). A. Avdeef and W. P. Schaeffer, J. Amer. Chem. Soc. , 98, 5153 (1976).

(e). R. S. Gall and W. P. Schaeffer, Inorg. Chem., 15, 2758 (1976).

(f). B. T. Huie, R. M. Leyden, and W. P. Schaeffer, Inorg. Chem., 18, 125 (1979).

88 (a). B. M. Hoffman and D. H. Petering, Proc. Natl. Acad. Sci. USA, 67, 637 (1970).

(b). B. M. Hoffman, C. A. Spilburg, and D. H. Petering, Cold Spring Harbor Symp. Quant. Biol., 36, 343 (1971).

(c). G. C. Hsu, C. A. Spilburg, C. Bull, and B. M. Hoffman, Proc. Natl. Acad. Sci. USA, 69, 2122 (1972).

(d). J. C. W. Chien and L. C. Dickinson, Proc. Natl. Acad. Sci. USA, 69, 2783 (1972).

(e). T. Yonetani, H. Yamamoto, F. Kayne, and G. Woodrow, Biochem. Soc. Trans., 1, 44 (1973).

(f). L. C. Dickinson and J. C. W. Chien, J. Biol. Chem., 248, 5005 (1973).

(g). Q. H. Gibson, B. M. Hoffman, R. H. Crepeau, S. J. Edelstein, and C. Bull, Biochem. Biophys. Res. Commun., 59, 146 (1974).

(h). I. Kiyohiro, T. Yonetani, and M. Ikeda-Saito, J. Mol. Biol., 109, 83 (1977).

(i). M. Ikeda-Saito, T. Iizuka, H. Yamamoto, F. J. Kayne, and T. Yonetani, J. Biol. Chem., 252, 4882 (1977).

(j). T. S. Srivastava, S. Tyagi, and A. Nath, Proc. Natl. Acad. Sci. USA, 74, 4996 (1977).

(k). M. Ikeda-Saito, M. Brunori, and T. Yonetani, Biochim. Biophys. Acta., 533, 173 (1978).

(l). F. W. Snyder, Jr. and J. C. W. Chien, Eur. J. Biochem., 91, 83 (1978).

(m). E. E. Di Iorio, E. Fioretti, I. Ariani, F. Ascoli, G. Rotilio, and M. Brunori, FEBS Lett., 105, 229 (1979).

(n). L. C. Dickinson and J. C. W. Chien, Proc. Natl. Acad. Sci. USA, 77, 1235 (1980).

89. D. V. Stynes, H. C. Stynes, B. R. James, and J. A. Ibers, J. Amer. Chem. Soc., 95, 1796 (1973).

90 (a). J. P. Collman, R. R. Gagne, J. Kouba, and H. Ljusberg-Wahren, J. Amer. Chem. Soc., 96, 6800 (1974).

(b). J. P. Collman, J. I. Brauman, K. M. Doxsee, T. R. Halbert, S. E. Hayes, and K. S. Suslick, J. Amer. Chem. Soc., 100, 2761 (1978).

91 (a). H. C. Stynes and J. A. Ibers, J. Amer. Chem. Soc., 94, 5125 (1972).

91 (b). T. J. Beugelsdijk and R. S. Drago, J. Amer. Chem. Soc., 97, 6466 (1975).

(c). H. Yamamoto, T. Takayanagi, T. Kwan, and T. Yonetani, Bioinorg. Chem., 7, 189 (1977).

92 (a). F. A. Walker, J. Amer. Chem. Soc., 95, 1150 (1973).

(b). F. A. Walker, J. Amer. Chem. Soc., 95, 1154 (1973).

93 T. Takayanagi, H. Yamamoto, and T. Kwan, Bull. Chem. Soc. Jpn., 48, 2618 (1975).

94. F. A. Walker, D. Beroiz, and K. M. Kadish, J. Amer. Chem. Soc., 98, 3484 (1976).

95. D. J. Kent, BSc. Thesis, UBC, Vancouver, B.C. (1973).

96 (a). D. H. Dolphin, J. R. Sams, T. B. Tsin, and K. L. Wong, J. Amer. Chem. Soc., 98, 6970 (1976).

(b). B. R. James, K. J. Reimer, and T. C. T. Wong, J. Amer. Chem. Soc., 99, 4815 (1977).

(c). B. R. James, J. R. Sams, T. B. Tsin, and K. J. Reimer, J. Chem. Soc. Chem. Comm., 746 (1978).

97 (a). D. Burk, J. Hearon, L. Caroline, and A. Schade, J. Biol. Chem., 165, 723 (1946).

(b). D. Burk, J. Hearon, H. Levy, and A. Schade, Fed. Proc., Fed. Amer. Soc. Exp. Biol., 6, 242 (1947).

(c). J. Hearon, Fed. Proc., Fed. Amer. Soc. Exp. Biol., 6, 259 (1947).

(d). J. Hearon, A. Schade, H. Levy, nad D. Burk, Cancer Res., 7, 713 (1947).

(e). J. Gilbert, M. Otey, and V. Price, J. Biol. Chem., 190, 377 (1951).

(f). C. Tanford, D. C. Kirk, and M. K. Chantooni, J. Amer. Chem. Soc., 76, 5325 (1954).

98 (a). G. F. Vansant and J. H. Lunsford, Adv. Chem. Ser., 121, 441 (1973).

(b). R. F. Howe and J. H. Lunsford, J. Amer. Chem. Soc., 97, 5156 (1975).

(c). R. F. Howe and J. N. Lunsford, J. Phys. Chem., 79, 1836 (1975).

99. L. D. Brown and K. N. Raymond, Inorg. Chem., 14, 2595 (1975).

100 (a). N. W. Terry (III), E. L. Amma, and L. Vaska, J. Amer. Chem. Soc., 94, 653 (1972).

(b). C. J. Willis, J. Chem. Soc. Chem. Comm., 117 (1974).

101 (a). T. Hara, Y. Ohkatsu, and T. Osa, Chem. Lett., 103 (1973).

(b). T. Hara, Y. Ohkatsu, and T. Osa, Chem. Lett., 953 (1973).

(c). T. Hara, Y. Ohkatsu, and T. Osa, Bull. Chem. Soc. Jpn., 48, 85 (1975).

102. Y. Ohkatsu, T. Hara, and T. Osa, Bull. Chem. Soc. Jpn., 50, 696 (1977).

103 (a). Y. Ohkatsu, T. Sekiguchi, and T. Osa, Bull. Chem. Soc. Jpn., 50, 701 (1977).

(b). Y. Ohkatsu and T. Osa, Bull. Chem. Soc. Jpn., 50, 2945 (1977).

104. M. Tezuka, O. Sekiguchi, Y. Ohkatsu, and T. Osa, Bull. Chem. Soc. Jpn., 49, 2765 (1976).

105. A. Nishinaga, Chem. Lett., 273 (1975).

106. M. N. Dufour-Ricroch and A. Gaudemer, Tet. Lett., 45, 4079 (1976).

107 (a). T. Tanaka and W. E. Knox, J. Biol. Chem., 234, 4079 (1976).

(b). H. Maeno and P. Feigelson, J. Biol. Chem., 242, 1162 (1959).

(c). Y. Ishimura, M. Nozaki, O. Hayaishi, T. Nakamura, M. Tamura, and I. Yamazaki, J. Biol. Chem., 245, 3593 (1970).

108 (a). E. W. Abel, J. M. Pratt, R. Whelan, and P. J. Wilkinson, J. Amer. Chem. Soc., 96, 7119 (1974).

108 (b). J. M. Pratt, "Inorganic Chemistry of Vitamin B_{12}," Academic Press, New York, N.Y., 1972, p.202.

(c). A. Nishinaga, T. Tojo, and T. Matsuura, J. Chem. Soc. Chem. Comm., 896 (1974).

109. M. Baccouche, J. Ernst, J. H. Fuhrhop, R. Schlozer, and H. Arzoumanian, J. Chem. Soc. Chem. Comm., 821 (1977).

110 (a). A. L. Crumbliss and F. Basolo, Inorg. Chem., 10, 1676 (1971).

(b). T. Takayangi, K. Yamamoto, and T. Kwan, Chem. Pharm. Bull., 20, 2721 (1972).

(c). B. B. Wayland and D. Mohajer, Inorg. Nucl. Chem. Lett., 9, 633 (1973).

111. D. A. Summerville, T. W. Cape, E. D. Johnson, and F. Basolo, Inorg. Chem., 17, 3297 (1978).

112. D. F. Shriver, "The Manipulation of Air Sensitive Compounds," McGraw-Hill, New York, N.Y., 1969.

113. A. D. Adler, F. R. Longo, F. Kampas, and J. Kim, J. Inorg. Nucl. Chem., 32, 2443 (1970).

114. D. H. Dolphin, J. R. Sams, T. B. Tsin, Inorganic Syntheses, in press.

115. H. Fletcher, Tetrahedron, 22, 2481 (1966).

116. K. J. Reimer and B. R. James, unpublished results.

117 (a). W. R. Scheidt, J. Amer. Chem. Soc., 96, 90 (1974).

(b). P. N. Dwyer, P. Madura, and W. R. Scheidt, J. Amer. Chem. Soc., 96, 4815 (1974).

(c). R. G. Little and J. A. Ibers, J. Amer. Chem. Soc., 96, 4452 (1974).

(d). W. R. Scheidt and J. Ramanuja, Inorg. Chem., 14, 2643 (1975).

118 (a). W. R. Scheidt, J. Amer. Chem. Soc., 96, 84 (1974).

(b). R. G. Little and J. A. Ibers, J. Amer. Chem. Soc., 96 4440 (1974).

119 (a). S. J. Cole, G. C. Curthoys, and E. A. Magnusson, J. Amer. Chem. Soc., 92, 2991 (1970).

(b). S. J. Cole, G. C. Curthoys, and E. A. Magnusson, J. Amer. Chem. Soc., 93, 2153 (1971).

(c). S. J. Cole, G. C. Curthoys, E. A. Magnusson, and J. N. Phillips, Inorg. Chem., 11, 1024 (1972).

120. F. A. Walker, J. Amer. Chem. Soc., 92, 4235 (1970).

121. W. A. G. Graham, Inorg. Chem., 7, 315 (1968).

122. L. M. Epstein, D. K. Straub, and C. Maricondi, Inorg. Chem., 6, 1720 (1967).

123. D. V. Stynes, H. C. Stynes, J. A. Ibers, and B. R. James, J. Amer. Chem. Soc., 95, 1142 (1973).

124 (a). G. Scatchard, Chem. Rev., 10, 229 (1932).

(b). T. R. Griffiths and D. C. Pugh, Coord. Chem. Rev., 29, 129 (1979).

125. M. R. J. Dack, in "Techniques of Chemistry," Vol. 8, Part II, A. Weissberger, Ed., J. Wiley & Sons, New York, N.Y., 1976, p. 95.

126 (a). Y. Tanaka and H. Takeuchi, Tetrahedron, 24, 6433 (1968).

(b). Y. Drougard and D. Decrooq, Bull. Soc. Chim. Fr., 2972 (1969).

127. E. S. Amis, "Solvent Effects on Reaction Rates and Mechanisms," Academic Press, New York, N.Y., 1966.

128 (a). E. S. Amis, J. Chem Educ., 29, 337 (1952).

(b). K. J. Laidler and P. A. Landskroener, Trans Faraday Soc., 52, 200 (1956).

129. J. G. Kirkwood, J. Chem. Phys., 2, 351 (1934).

130. E. Grunwald and S. Winstein, J. Amer. Chem. Soc., 70, 846 (1948).

131. J. E. Falk, J. N. Phillips, and E. A. Magnusson, Nature (London) 212, 1531 (1966).

132. W. S. Caughey, W. Y. Fujimoto, and B. P. Johnson, Biochemistry, 5, 3830 (1966).

133. H. H. Jaffe and M. Orchin, "Theory and Application of Ultraviolet Spectroscopy," Wiley, New York, N. Y., 1962.

134. T. Yonetoni, H. Yamamoto, and G. V. Woodrow, III., J. Biol. Chem., 249, 682 (1974).

135. J. A. A. Ketelaar, G. van de Stolpe, A. Goudsmit, and W. Dzcubas, Rec. Trav. Chim., 71, 1104 (1952).

136 (a). W. I. White, in "The Porphyrins," Vol.5, D. Dolphin, Ed., Academic Press, New York, N.Y., 1978, p. 303.

(b). K. M. Smith, Acc. Chem. Res., 12, 374 (1979).

(c). H. Scheer and J. J. Katz, in "Porphyrins and Metalloporphyrins," K. M. Smith, Ed., American Elsevier, New York, N.Y., 1975, p. 399.

137. A. E. Alexander, J. Chem. Soc., 1813 (1937).

138. R. F. Pasternack, P. R. Huber, P. Boyd, G. Engasser, L. Francesconi, E. Gibbs, P. Fasella, G. C. Venturo, and L. de C. Hinds, J. Amer. Chem. Soc., 94, 4511 (1972).

139. W. I. White and R. A. Plane, Bioinorg. Chem., 4, 21 (1974).

140. G. N. LaMar and D. B. Viscio, J. Amer. Chem. Soc., 96, 7354 (1974).

141(a). W. S. Caughey, H. Eberspaecher, W. H. Fuchsman, S. McCoy, and J. O. Alben, Ann. N.Y. Acad. Sci., 153, 722 (1969).

(b). M. Krishnamurthy, J. R. Sutter, and P. M. Hambright, J. Chem. Soc., Chem. Commun., 13 (1975).

142. R. F. Pasternack, L. Francesconi, D. Raff, and E. Spiro, Inorg. Chem., 12, 2606 (1973).

143. P. A. Loach and M. Calvin, Biochemistry, 2, 361 (1963).

144. H. A. O. Hill, P. J. Sadler, and R. J. P. Williams, J. Chem. Soc. Dalton, 1663 (1973).

145. R. J. Abraham, P. A. Burbidge, A. H. Jackson, and G. W. Kenner, Proc. Chem. Soc., London, 134 (1963).

146 (a). R. W. Cowgill and W. M. Clark, J. Biol. Chem., 198, 33 (1952).

(b). W. A. Gallagher and W. B. Elliott, Ann. N.Y, Acad. Sci., 206, 463 (1973).

147 (a). D. Mauzerall, Biochemistry, 4, 1801 (1965).

(b). J.-H. Fuhrhop., P. Wasser, D. Reisner, and D. Mauzerall, J. Amer. Chem. Soc., 94, 7996 (1972).

148. D. G. Davis and J, G, Montalvo, Anal. Chem., 41, 1195 (1969).

149. J. James and P. M. Hambright, J. Coord. Chem., 3 183 (1973).

150. K. J. Reimer, M. Reimer, and C. Spidle-Sprague, 62nd Canadian Chemical Conference, Vancouver, B.C. (1979), IN-45; aggregation is reported for non aqueous visible spectroscopic soloutions of ZnOMBP.

151. D. A. Doughty and C. W. Dwiggins, Jr., J. Phys. Chem., 73, 423 (1969).

152 (a). T. E. Phillips and B. M. Hoffman, J. Amer. Chem. Soc., 99, 7734 (1977).

(b). T. E. Phillips, R. P. Scaringe, B. M. Hoffman, and J. A. Ibers, J. Amer. Chem. Soc., 102, 3435 (1980).

153. W. C. Lin, in "The Porphyrins," Vol. 4, D. Dolphin, Ed., Academic Press, New York, N.Y., 1978, p. 355.

154. K. Hoffman, "Imidazole and its Derivatives," Part I, in "The Chemistry of Heterocyclic Compounds," Vol. 6, A. Weissberger, Ed., Interscience, New York, N.Y., 1953, p. 7.

155. J. A. Riddick and W. B. Bunger, in "Techniques of Chemistry," Vol. 2, A. Weissberger, Ed., J. Wiley & Sons, New York, N.Y., 1973, p.61

156. ε estimated for neat CH_3-Im based on data in mixed toluene-CH_3-Im systems.

157. A. Sen and J. Halpern, J. Amer. Chem. Soc., 99, 8337 (1977).

158 (a). M. M. L. Chu, C. E. Castro, and G. M. Hathaway, Biochemistry, 17, 481 (1978).

(b). D. R. Eaton and K. M. Wilson, J. Inorg. Biochem., 10, 195 (1979).

159 (a). R. Ugo, A. Fusi, G. M. Zanderighi, and L. Casella, J. Mol. Catal., 7, 51 (1980).

(b). R. Ugo, G. M. Zanderighi, A. Fusi, D. Carreri, J. Amer. Chem. Soc., 102, 3745 (1980).

160. R. E. Merrifield and W. D. Phillips, J. Amer. Chem. Soc., 80, 2778 (1958).

161 (a). A. Nishinaga and H. Tomita, J. Mol. Catal., 7, 179 (1980).

(b). M. N. Dufour, A. L. Crumbliss, G. Johnston, and A. Gaudemer, J. Mol. Catal., 7, 277 (1980).

APPENDIX

RAW DATA USED FOR DETERMINING THERMODYNAMIC AND KINETIC PARAMETERS REPORTED IN THIS THESIS.

APPENDIX I

RAW DATA USED FOR DETERMINING THE THERMODYNAMIC PARAMETERS OF REVERSIBLE LIGAND BINDING TO CoOMBP

APPENDIX Ia. $Im + CoOMBP \rightleftharpoons ImCoOMBP$

Temperature = 5°C

A (412 nm)	[Im]	$A_o - A$	$A - A_\infty$	$\log \frac{A_o - A}{A - A_\infty}$	log[Im]
1.187	0	0	0.620		
1.157	3.35×10^{-6}	0.030	0.590	-1.294	-5.475
1.114	1.01×10^{-5}	0.073	0.547	-0.874	-4.998
1.034	2.01×10^{-5}	0.153	0.467	-0.484	-4.697
0.959	4.01×10^{-5}	0.228	0.398	-0.242	-4.396
0.817	8.34×10^{-5}	0.370	0.250	0.170	-4.079
0.668	1.66×10^{-4}	0.519	0.101	0.711	-3.780
0.578	3.29×10^{-4}	0.609	0.011	1.743	-3.483
0.567	2.84×10^{-3}	0.620	0		-2.547

Temperature = 22°C

A (412 nm)	[Im]	$A_o - A$	$A - A_\infty$	$\log \frac{A_o - A}{A - A_\infty}$	log[Im]
1.195	0	0	0.592		
1.122	6.7×10^{-6}	0.073	0.519	-0.854	-5.174
1.106	1.67×10^{-5}	0.089	0.503	-0.757	-4.776
1.029	3.35×10^{-5}	0.166	0.426	-0.412	-4.475
0.943	6.68×10^{-5}	0.252	0.340	-0.134	-4.175
0.871	1.33×10^{-4}	0.324	0.268	0.078	-3.876
0.823	2.97×10^{-4}	0.372	0.230	0.222	-3.527
0.783	6.16×10^{-4}	0.412	0.180	0.352	-3.211
0.687	1.54×10^{-3}	0.508	0.084	0.766	-2.813
0.603	2.84×10^{-3}	0.592	0		-2.547

Temperature = 40°C

A (412 nm)	[Im]	$A_o - A$	$A - A_\infty$	$\log \frac{A_o - A}{A - A_\infty}$	log[Im]
1.200	0	0	0.600		
1.150	1.67×10^{-5}	0.050	0.550	-1.041	-4.776
1.105	3.35×10^{-5}	0.095	0.505	-0.726	-4.475
1.101	6.68×10^{-5}	0.099	0.501	-0.704	-4.175
1.009	1.66×10^{-4}	0.191	0.409	-0.331	-3.780
0.906	3.29×10^{-4}	0.294	0.306	-0.017	-3.482
0.819	6.47×10^{-4}	0.381	0.219	0.240	-3.189
0.760	1.54×10^{-3}	0.440	0.160	0.439	-2.813
0.673	2.84×10^{-3}	0.527	0.073	0.858	-2.547

A_∞ estimated to be .600 based on data of the lower temperatures.

A — Absorbance at a known ligand concentration recorded at a particular wavelength corrected for dilution resulting from addition of a 0.0184 M Im solution in toluene

$[Im]$ — Molar concentration of added free Im

$A_o - A$ — Difference between initial absorbance and the absorbance at a known ligand concentration

$A - A_\infty$ — Difference between the absorbance at a known ligand concentration and the final absorbance

$\log \frac{A_o - A}{A - A_\infty}$ In the text this term is referred to as $\log \frac{A - A_o}{A_\infty - A}$. In the appendices $\log \frac{A_o - A}{A - A_\infty}$ is used when the absorbance at a monitored wavelength decreases and $\log \frac{A - A_o}{A_\infty - A}$ is used when the monitored absorbance increases during an experiment.

APPENDIX Ib. $CH_3\text{-Im} + CoOMBP \rightleftharpoons CH_3\text{-ImCoOMBP}$

Temperature = $-23^{\circ}C$

A (450 nm)	$[CH_3\text{-Im}]$	$A - A_o$	$A_\infty - A$	$\log \frac{A - A_o}{A_\infty - A}$	$\log[CH_3\text{-Im}]$
0.459	0	0	0.161		
0.463	2.0×10^{-7}	0.004	0.157	-1.594	-6.699
0.477	3.2×10^{-7}	0.018	0.143	-0.900	-6.495
0.509	5.2×10^{-7}	0.050	0.111	-0.364	-6.284
0.534	1.26×10^{-6}	0.075	0.086	-0.006	-5.900
0.572	2.68×10^{-6}	0.113	0.048	0.372	-5.572
0.579	4.63×10^{-6}	0.120	0.041	0.466	-5.334
0.609	8.4×10^{-6}	0.150	0.011	1.135	-5.076
0.620	1.62×10^{-5}	0.161	0		-4.790

Temperature = $0^{\circ}C$

A (450 nm)	$[CH_3\text{-Im}]$	$A - A_o$	$A_\infty - A$	$\log \frac{A - A_o}{A_\infty - A}$	$\log[CH_3\text{-Im}]$
0.405	0	0	0.230		
0.459	1.26×10^{-6}	0.044	0.186	-0.626	-5.901
0.497	2.51×10^{-6}	0.092	0.138	-0.176	-5.600
0.537	5.02×10^{-6}	0.132	0.098	0.129	-5.299
0.594	1.00×10^{-5}	0.189	0.041	0.664	-4.998
0.621	2.01×10^{-5}	0.216	0.014	1.188	-4.698
0.635	4.51×10^{-5}	0.230	0		-4.346

Temperature = $23^{\circ}C$ *

A (450 nm)	$[CH_3\text{-Im}]$	$A - A_o$	$A_\infty - A$	$\log \frac{A - A_o}{A_\infty - A}$	$\log[CH_3\text{-Im}]$
0.518	0	0	0.346		
0.564	2.87×10^{-6}	0.046	0.300	-0.814	-5.542
0.641	9.10×10^{-6}	0.123	0.223	-0.258	-5.041
0.711	1.81×10^{-5}	0.193	0.153	0.100	-4.742
0.743	3.61×10^{-5}	0.225	0.121	0.269	-4.442
0.781	7.22×10^{-5}	0.263	0.083	0.501	-4.141
0.864	4.15×10^{-4}	0.346	0		-3.382

* Data used for Figure III.1

Additions were made with a 0.0126 M solution of CH_3-Im in toluene.

APPENDIX Ic. $Pip + CoOMBP \rightleftharpoons PipCoOMBP$

Temperature = $-23^{\circ}C$

A (618 nm)	[Pip]	$A_o - A$	$A - A_\infty$	$\log \frac{A_o - A}{A - A_\infty}$	log[Pip]
0.737	0	0	0.125	———	———
0.720	1.0×10^{-7}	0.017	0.108	-0.803	-7.000
0.703	3.8×10^{-7}	0.034	0.091	-0.428	-6.420
0.668	1.10×10^{-6}	0.069	0.056	0.091	-5.959
0.639	2.6×10^{-6}	0.098	0.027	0.560	-5.585
0.623	5.8×10^{-6}	0.114	0.011	1.016	-5.231
0.612	1.38×10^{-5}	0.125	0	———	-4.860

Temperature = $0^{\circ}C$

A (618 nm)	[Pip]	$A_o - A$	$A - A_\infty$	$\log \frac{A_o - A}{A - A_\infty}$	log[Pip]
0.981	0	0	0.286	———	———
0.952	3.3×10^{-7}	0.029	0.257	-0.948	-6.481
0.918	8.6×10^{-7}	0.063	0.223	-0.549	-6.065
0.873	1.8×10^{-6}	0.108	0.178	-0.217	-5.745
0.817	3.5×10^{-6}	0.164	0.122	0.128	-5.456
0.767	6.8×10^{-6}	0.214	0.072	0.473	-5.167
0.734	1.25×10^{-5}	0.247	0.039	0.801	-4.903
0.711	3.2×10^{-5}	0.270	0.016	1.227	-4.494
0.695	1.3×10^{-4}	0.286	0	———	-3.886

Temperature = $26^{\circ}C$

A (618 nm)	[Pip]	$A_o - A$	$A - A_\infty$	$\log \frac{A_o - A}{A - A_\infty}$	log[Pip]
0.932	0	0	0.294	———	———
0.882	1.8×10^{-6}	0.050	0.244	-0.688	-5.737
0.852	3.7×10^{-6}	0.080	0.214	-0.427	-5.437
0.833	5.5×10^{-6}	0.099	0.195	-0.294	-5.262
0.801	9.1×10^{-6}	0.132	0.162	-0.089	-5.041
0.760	1.8×10^{-5}	0.172	0.122	0.149	-4.745
0.704	3.8×10^{-5}	0.228	0.066	0.538	-4.423
0.690	5.7×10^{-5}	0.242	0.052	0.668	-4.241
0.670	1.2×10^{-4}	0.262	0.032	0.913	-3.936
0.647	2.2×10^{-4}	0.285	0.009	1.500	-3.652
o.638	4.1×10^{-4}	0.294	0	———	-3.383

Additions were made with a 0.0101 M solution of Pip in toluene.

APPENDIX Id. $Py + CoOMBP \rightleftharpoons PyCoOMBP$

Temperature = $-23^{\circ}C$

A (618 nm)	[Py]	$A_o - A$	$A - A_\infty$	$\log \frac{A_o - A}{A - A_\infty}$	log[Py]
0.815	0	0	0.167	———	———
0.786	3.6×10^{-7}	0.029	0.138	-0.677	-6.444
0.742	1.45×10^{-6}	0.073	0.094	-0.110	-5.839
0.705	3.55×10^{-6}	0.110	0.057	-0.286	-5.450
0.668	7.8×10^{-6}	0.147	0.030	-0.690	-5.108
0.652	1.86×10^{-5}	0.163	0.004	-1.610	-4.730
0.648	4.25×10^{-5}	0.167	0	———	-4.372

Temperature = $0^{\circ}C$

A (618 nm)	[Py]	$A_o - A$	$A - A_\infty$	$\log \frac{A_o - A}{A - A_\infty}$	log[Py]
0.848	0	0	0.218	———	———
0.826	1.22×10^{-6}	0.022	0.196	-0.950	-5.915
0.783	3.44×10^{-6}	0.065	0.153	-0.372	-5.463
0.735	7.87×10^{-6}	0.113	0.105	0.032	-5.104
0.711	1.23×10^{-5}	0.137	0.081	0.228	-4.912
0.682	2.27×10^{-5}	0.166	0.052	0.504	-4.656
0.652	4.61×10^{-5}	0.196	0.022	0.950	-4.337
0.642	9.37×10^{-5}	0.206	0.012	1.234	-4.028
0.630	2.11×10^{-4}	0.218	0	———	-3.675

Temperature = $27^{\circ}C$

A (618 nm)	[Py]	$A_o - A$	$A - A_\infty$	$\log \frac{A_o - A}{A - A_\infty}$	log[Py]
1.092	0	0	0.294	———	———
1.069	2.25×10^{-6}	0.023	0.271	-1.071	-5.648
1.045	6.72×10^{-6}	0.047	0.247	-0.721	-5.172
0.982	1.78×10^{-5}	0.110	0.184	-0.223	-4.751
0.925	4.21×10^{-5}	0.167	0.127	0.119	-4.376
0.886	6.63×10^{-5}	0.206	0.088	0.369	-4.178
0.853	1.14×10^{-4}	0.239	0.055	0.638	-3.942
0.824	2.33×10^{-4}	0.268	0.026	1.013	-3.632
0.819	4.70×10^{-4}	0.273	0.021	1.114	-3.328
0.798	1.41×10^{-4}	0.294	0	———	-2.852

Additions were made with a 0.0124 M solution of Py in toluene.

APPENDIX Ie. $Et_3N + CoOMBP \rightleftharpoons Et_3NCoOMBP$

Temperature = 5°C

A (618 nm)	$[Et_3N]$	$A_o - A$	$A - A_\infty$	$\log \frac{A_o - A}{A - A_\infty}$	$\log [Et_3N]$
1.240	0	0	0.234	———	———
1.225	0.00261	0.015	0.219	-1.164	-2.584
1.210	0.00651	0.030	0.204	-0.833	-2.186
1.197	0.0130	0.043	0.191	-0.648	-1.886
1.180	0.0260	0.060	0.174	-0.462	-1.585
1.150	0.0518	0.090	0.144	-0.204	-1.286
1.105	0.103	0.135	0.099	0.135	-0.988
1.065	0.227	0.175	0.059	0.472	-0.644
1.041	0.463	0.199	0.035	0.755	-0.334
1.015	0.891	0.225	0.009	1.398	-0.050
1.006	1.753	0.234	0	———	0.244

Temperature = 22°C

A (618 nm)	$[Et_3N]$	$A_o - A$	$A - A_\infty$	$\log \frac{A_o - A}{A - A_\infty}$	$\log [Et_3N]$
1.207	0	0	0.185	———	———
1.202	0.00651	0.005	0.180	-1.556	-2.186
1.193	0.0130	0.014	0.171	-1.087	-1.886
1.170	0.0260	0.037	0.148	-0.602	-1.585
1.166	0.0518	0.041	0.144	-0.546	-1.286
1.138	0.103	0.069	0.116	-0.226	-0.988
1.110	0.227	0.097	0.088	0.042	-0.644
1.073	0.463	0.134	0.051	0.420	-0.344
1.056	0.891	0.151	0.034	0.647	-0.050
1.032	1.753	0.175	0.010	1.243	0.244
1.022	3.674	0.185	0	———	0.565

Temperature = 40°C

A (618 nm)	$[Et_3N]$	$A_o - A$	$A - A_\infty$	$\log \frac{A_o - A}{A - A_\infty}$	$\log [Et_3N]$
1.327	0	0	0.242	———	———
1.312	0.0130	0.015	0.227	-1.180	-1.886
1.304	0.0260	0.023	0.219	-0.979	-1.585
1.288	0.0518	0.039	0.203	-0.716	-1.286
1.257	0.103	0.070	0.172	-0.390	-0.988
1.230	0.227	0.097	0.145	-0.175	-0.644
1.168	0.463	0.159	0.083	0.282	-0.334
1.148	0.891	0.179	0.063	0.454	-0.050
1.122	1.153	0.205	0.037	0.744	0.244
1.085	2.920	0.242	0	———	0.465

Additions were made with neat Et_3N.

APPENDIX If. DMF + CoOMBP $\rightleftharpoons$ DMFCoOMBP

Temperature = 5°C

A (450 nm)	[DMF]	$A - A_o$	$A_\infty - A$	$\log \frac{A - A_o}{A_\infty - A}$	log[DMF]
0.787	0	0	0.500	———	———
0.814	0.0130	0.027	0.473	-1.243	-1.887
0.872	0.0388	0.085	0.415	-0.689	-1.411
0.926	0.0774	0.139	0.361	-0.414	-1.111
0.960	0.129	0.173	0.327	-0.277	-0.891
1.040	0.254	0.253	0.247	0.010	-0.594
1.092	0.499	0.305	0.195	0.194	-0.302
1.148	0.961	0.361	0.139	0.414	-0.017
1.192	1.980	0.405	0.095	0.630	0.297
1.287	4.765	0.500	0	———	0.698

Temperature = 22°C

A (450 nm)	[DMF]	$A - A_o$	$A_\infty - A$	$\log \frac{A - A_o}{A_\infty - A}$	log[DMF]
0.950	0	0	0.500	———	———
0.972	0.0259	0.022	0.478	-1.337	-1.587
1.014	0.0517	0.064	0.436	-0.837	-1.286
1.086	0.129	0.136	0.364	-0.426	-0.891
1.180	0.254	0.230	0.270	-0.070	-0.594
1.238	0.499	0.288	0.212	0.133	-0.302
1.309	1.180	0.359	0.141	0.406	-0.072
1.344	2.163	0.394	0.106	0.570	0.335
1.361	3.709	0.411	0.089	0.664	0.569
1.450	6.490	0.500	0	———	0.812

Temperature = 40°C

A (450 nm)	[DMF]	$A - A_o$	$A_\infty - A$	$\log \frac{A - A_o}{A_\infty - A}$	log[DMF]
0.922	0	0	0.506	———	———
0.954	0.0517	0.034	0.472	-1.137	-1.286
1.035	0.129	0.113	0.393	-0.535	-0.891
1.099	0.254	0.177	0.329	-0.261	-0.594
1.172	0.499	0.250	0.256	-0.010	-0.302
1.240	1.180	0.318	0.188	0.242	0.072
1.272	2.163	0.350	0.156	0.368	0.335
1.428	6.490	0.506	0	———	0.812

Additions were made with neat DMF.

APPENDIX Ig. THF + CoOMBP $\rightleftharpoons$ THFCoOMBP

Temperature = -23°C

A (417 nm)	[THF]	$A - A_o$	$A_\infty - A$	$\log \frac{A - A_o}{A_\infty - A}$	log [THF]
0.374	0	0	0.564	———	———
0.405	0.00248	0.031	0.533	-1.235	-2.606
0.464	0.0135	0.090	0.474	-0.722	-1.870
0.559	0.0378	0.185	0.379	-0.311	-1.423
0.617	0.0860	0.243	0.321	-0.121	-1.066
0.689	0.181	0.315	0.249	0.102	-0.742
0.795	0.413	0.421	0.143	0.468	-0.384
0.938	1.452	0.564	0	———	0.162

Temperature = 5°C

A (417 nm)	[THF]	$A - A_o$	$A_\infty - A$	$\log \frac{A - A_o}{A_\infty - A}$	log [THF]
0.904	0	0	0.621	———	———
0.960	0.0174	0.056	0.565	-1.004	-1.759
1.008	0.0358	0.104	0.517	-0.696	-1.446
1.065	0.0725	0.161	0.460	-0.456	-1.140
1.142	0.144	0.237	0.384	-0.210	-0.842
1.220	0.322	0.316	0.305	-0.015	-0.492
1.367	0.772	0.463	0.158	0.467	-0.112
1.438	1.763	0.534	0.087	0.788	0.246
1.525	4.930	0.621	0	———	0.693

Temperature = 22°C

A (417 nm)	[THF]	$A - A_o$	$A_\infty - A$	$\log \frac{A - A_o}{A_\infty - A}$	log [THF]
1.095	0	0	0.971	———	———
1.150	0.0066	0.055	0.916	-1.222	-2.180
1.225	0.0311	0.130	0.841	-0.811	-1.507
1.290	0.0677	0.195	0.776	-0.600	-1.169
1.357	0.128	0.262	0.709	-0.472	-0.894
1.488	0.364	0.393	0.578	-0.168	-0.439
1.900	3.526	0.805	0.166	0.686	0.547
2.066	5.842	0.971	0	———	0.767

Temperature = 40°C

A (417 nm)	[THF]	$A - A_o$	$A_\infty - A$	$\log \frac{A - A_o}{A_\infty - A}$	log [THF]
0.631	0	0	0.459	———	———
0.683	0.0419	0.052	0.407	-0.894	-1.392
0.723	0.103	0.092	0.367	-0.601	-0.987
0.785	0.223	0.154	0.305	-0.302	-0.652
0.824	0.456	0.193	0.266	-0.109	-0.342
0.879	0.821	0.248	0.211	-0.070	-0.086
0.960	1.964	0.324	0.130	0.403	0.293
1.090	5.031	0.459	0	———	0.702

Additions were made with neat THF.

APPENDIX Ih. $PPh_3 + CoOMBP \rightleftharpoons PPh_3CoOMBP$

Temperature = 5°C

A (460 nm)	$[PPh_3]$	$A - A_o$	$A_\infty - A$	$\log \frac{A - A_o}{A_\infty - A}$	$\log [PPh_3]$
0.610	0	0	0.422	———	———
0.616	1.19×10^{-4}	0.006	0.416	-1.870	-3.924
0.634	3.97×10^{-4}	0.024	0.398	-1.228	-3.402
0.715	1.19×10^{-3}	0.103	0.319	-0.490	-2.925
0.788	2.38×10^{-3}	0.178	0.244	-0.135	-2.626
0.850	4.76×10^{-3}	0.240	0.182	0.121	-2.323
0.912	8.54×10^{-3}	0.302	0.120	0.400	-2.068
0.945	1.60×10^{-2}	0.335	0.087	0.730	-1.796
0.990	3.61×10^{-2}	0.380	0.042	0.962	-1.443
1.032	1.32×10^{-1}	0.422	0	———	-0.878

Temperature = 22°C

A (460 nm)	$[PPh_3]$	$A - A_o$	$A_\infty - A$	$\log \frac{A - A_o}{A_\infty - A}$	$\log [PPh_3]$
0.800	0	0	0.643	———	———
0.817	3.97×10^{-4}	0.017	0.626	-1.564	-3.402
0.863	9.90×10^{-4}	0.063	0.580	-0.967	-3.004
0.920	1.98×10^{-3}	0.120	0.523	-0.638	-2.704
1.009	3.93×10^{-3}	0.209	0.434	-0.318	-2.406
1.107	7.78×10^{-3}	0.307	0.336	-0.038	-2.109
1.198	1.53×10^{-2}	0.398	0.245	0.212	-1.816
1.275	2.94×10^{-2}	0.475	0.168	0.453	-1.532
1.323	5.47×10^{-2}	0.523	0.120	0.642	-1.262
1.443	1.43×10^{-1}	0.643	0	———	-0.846

Temperature = 40°C

A (460 nm)	$[PPh_3]$	$A - A_o$	$A_\infty - A$	$\log \frac{A - A_o}{A_\infty - A}$	$\log [PPh_3]$
0.740	0	0	0.601	———	———
0.754	7.92×10^{-4}	0.014	0.587	-1.633	-3.101
0.775	1.58×10^{-3}	0.035	0.566	-1.215	-2.801
0.814	3.15×10^{-3}	0.074	0.527	-0.853	-2.502
0.877	6.34×10^{-3}	0.137	0.464	-0.531	-2.198
0.979	1.23×10^{-2}	0.239	0.362	-0.181	-1.910
1.057	1.89×10^{-2}	0.317	0.284	0.046	-1.723
1.128	2.77×10^{-2}	0.375	0.226	0.221	-1.558
1.205	5.18×10^{-2}	0.465	0.136	0.535	-1.286
1.341	1.41×10^{-1}	0.601	0	———	-0.851

Additions were made with a 0.397 M solution of PPh_3 in toluene.

APPENDIX Ii. $PBu_3 + CoOMBP \rightleftharpoons PBu_3CoOMBP$

Temperature = 5°C

A (618 nm)	$[PBu_3]$	$A_o - A$	$A - A_\infty$	$\log \frac{A_o - A}{A - A_\infty}$	$\log [PBu_3]$
1.058	0	0	0.564	———	———
1.042	1.21×10^{-6}	0.016	0.548	-1.534	-5.916
0.998	4.05×10^{-6}	0.060	0.504	-0.928	-5.393
0.953	8.08×10^{-6}	0.106	0.458	-0.636	-5.092
0.877	1.41×10^{-5}	0.181	0.383	-0.327	-4.850
0.833	2.01×10^{-5}	0.225	0.339	-0.180	-4.696
0.761	3.01×10^{-5}	0.297	0.267	0.046	-4.521

A_∞ estimated to be 0.494.

Temperature = 22°C *

A (618 nm)	$[PBu_3]$	$A_o - A$	$A - A_\infty$	$\log \frac{A_o - A}{A - A_\infty}$	$\log [PBu_3]$
0.950	0	0	0.564	———	———
0.923	4.05×10^{-6}	0.027	0.479	-1.249	-5.393
0.884	8.08×10^{-6}	0.066	0.440	-0.824	-5.092
0.832	1.41×10^{-5}	0.118	0.388	-0.517	-4.850
0.793	2.01×10^{-5}	0.157	0.349	-0.347	-4.696
0.744	3.01×10^{-5}	0.206	0.300	-0.163	-4.521

A_∞ estimated to be 0.444.

* Data used for Figure III.2

Temperature = 40°C

A (412 nm)	$[PBu_3]$	$A_o - A$	$A - A_\infty$	$\log \frac{A_o - A}{A - A_\infty}$	$\log [PBu_3]$
1.238	0	0	0.475	———	———
1.223	4.05×10^{-6}	0.015	0.460	-1.487	-5.393
1.203	8.08×10^{-6}	0.035	0.440	-1.099	-5.092
1.184	1.41×10^{-5}	0.054	0.421	-0.892	-4.850
1.134	2.82×10^{-5}	0.104	0.371	-0.552	-4.550

A_∞ estimated to be 0.763.

Additions were made with a 4.05×10^{-3} M solution of PBu_3 in toluene.

APPENDIX Ij. CH_3-Im + CH_3-ImCoOMBP $\rightleftharpoons$ $(CH_3\text{-Im})_2$CoOMBP

Temperature = -23°C *

A (435 nm)	$[CH_3\text{-Im}]$	$A - A_o$	$A - A_\infty$	$\log \frac{A - A_o}{A_\infty - A}$	$\log [CH_3\text{-Im}]$
0.451	2.5×10^{-5}	0	0.649	———	-4.600
0.496	0.00228	0.045	0.604	-1.128	-2.642
0.576	0.00680	0.125	0.524	-0.622	-2.168
0.688	0.0180	0.237	0.412	-0.240	-1.746
0.800	0.0425	0.349	0.300	0.066	-1.371
0.897	0.0915	0.446	0.203	0.342	-1.039
0.975	0.196	0.526	0.125	0.622	-0.707
1.019	0.446	0.568	0.081	0.846	-0.350
1.081	0.890	0.630	0.019	1.521	-0.050
1.100	1.867	0.642	0	———	0.271

* Data used for Figure III.3

Temperature = 0°C

A (435 nm)	$[CH_3\text{-Im}]$	$A - A_o$	$A_\infty - A$	$\log \frac{A - A_o}{A_\infty - A}$	$\log [CH_3\text{-Im}]$
0.443	1.14×10^{-4}	0	0.608	———	-3.942
0.525	0.00668	0.082	0.526	-0.807	-2.175
0.606	0.01765	0.163	0.445	-0.436	-1.753
0.654	0.0418	0.211	0.397	-0.275	-1.378
0.708	0.0899	0.265	0.343	-0.112	-1.046
0.790	0.193	0.347	0.261	0.124	-0.714
0.865	0.439	0.422	0.186	0.356	-0.358
0.936	0.876	0.493	0.115	0.632	-0.058
1.009	1.839	0.566	0.042	1.164	0.261

A_∞ estimated to be 1.051.

Temperature = 25°C

A (435 nm)	$[CH_3\text{-Im}]$	$A - A_o$	$A_\infty - A$	$\log \frac{A - A_o}{A_\infty - A}$	$\log [CH_3\text{-Im}]$
0.391	0.00114	0	0.764	———	-2.942
0.417	0.0114	0.026	0.738	-1.453	-1.942
0.459	0.0342	0.068	0.696	-1.010	-1.466
0.526	0.0908	0.135	0.629	-0.668	-1.042
0.621	0.202	0.230	0.534	-0.366	-0.695
0.711	0.419	0.320	0.444	-0.142	-0.378
0.802	0.931	0.411	0.353	0.066	-0.031
0.872	1.84	0.481	0.283	0.230	0.264
0.963	3.28	0.572	0.192	0.474	0.516

A_∞ estimated to be 1.154.

Additions were made with neat CH_3-Im.

APPENDIX Ik. $\quad Pip + PipCoOMBP \rightleftharpoons (Pip)_2CoOMBP$

Temperature = $-23^{\circ}C$

A (430 nm)	[Pip]	$A - A_o$	$A_\infty - A$	$\log \frac{A - A_o}{A_\infty - A}$	log[Pip]
0.358	4.1×10^{-5}	0	1.078	———	-4.383
0.420	0.00116	0.062	1.016	-1.215	-2.936
0.476	0.00274	0.118	0.960	-0.910	-2.562
0.530	0.00432	0.172	0.906	-0.722	-2.364
0.581	0.00590	0.223	0.855	-0.583	-2.229
0.659	0.00903	0.301	0.777	-0.412	-2.044
0.724	0.0121	0.366	0.712	-0.289	-1.916
0.798	0.0155	0.440	0.638	-0.161	-1.810
0.889	0.0244	0.531	0.548	-0.014	-1.613
1.026	0.0413	0.668	0.410	0.212	-1.384
1.115	0.0583	0.757	0.321	0.373	-1.234
1.202	0.0917	0.844	0.234	0.557	-1.169
1.293	0.175	0.935	0.143	0.815	-0.758
1.436	1.07	1.078	0	———	0.032

Temperature = $0^{\circ}C$

A (430 nm)	[Pip]	$A - A_o$	$A_\infty - A$	$\log \frac{A - A_o}{A_\infty - A}$	log[Pip]
0.452	1.3×10^{-4}	0	1.299	———	-3.890
0.496	0.0033	0.044	1.255	-1.455	-2.475
0.542	0.0068	0.090	1.209	-1.128	-2.169
0.616	0.014	0.164	1.135	-0.840	-1.868
0.725	0.027	0.273	1.026	-0.575	-1.572
0.847	0.045	0.395	0.901	-0.358	-1.345
0.954	0.064	0.502	0.797	-0.201	-1.197
1.013	0.082	0.561	0.738	-0.119	-1.087
1.107	0.117	0.655	0.644	0.003	-0.931
1.196	0.153	0.744	0.555	0.127	-0.815
1.281	0.225	0.829	0.470	0.246	-0.647
1.386	0.399	0.934	0.365	0.408	-0.399
1.520	1.18	1.068	0.231	0.426	0.074

A_∞ estimated to be 1.751 (based on data of $-23^{\circ}C$).

Temperature = $27^{o}C$

A (430 nm)	[Pip]	$A - A_o$	$A_\infty - A$	$\log \frac{A - A_o}{A_\infty - A}$	log[Pip]
0.387	1.44×10^{-4}	0	1.165	———	-3.842
0.435	0.0069	0.048	1.117	-1.396	-2.158
0.473	0.015	0.086	1.079	-1.099	-1.815
0.536	0.034	0.149	1.016	-0.834	-1.471
0.591	0.052	0.204	0.961	-0.673	-1.282
0.632	0.071	0.245	0.920	-0.575	-1.151
0.707	0.107	0.320	0.845	-0.422	-0.970
0.799	0.162	0.412	0.753	-0.266	-0.790
0.914	0.250	0.527	0.638	-0.083	-0.601
0.984	0.338	0.597	0.568	0.022	-0.471
1.055	0.458	0.668	0.477	0.159	-0.339
1.110	0.624	0.723	0.422	0.214	-0.205
1.237	2.09	0.850	0.315	0.431	0.322

A_∞ estimated to be 1.552 (based on data of $-23^{o}C$).

Additions were made with neat Pip.

APPENDIX II. $Py + PyCoOMBP \rightleftharpoons (Py)_2CoOMBP$

Temperature = $-23^{\circ}C$

A (428 nm)	[Py]	$A - A_o$	$A_\infty - A$	$\log \frac{A - A_o}{A_\infty - A}$	log[Py]
0.440	4.31×10^{-5}	0	1.415	———	-4.365
0.493	0.00202	0.053	1.362	-1.409	-2.695
0.533	0.00414	0.093	1.322	-1.153	-2.383
0.601	0.00837	0.161	1.254	-0.891	-2.077
0.676	0.0157	0.236	1.179	-0.699	-1.834
0.769	0.0229	0.329	1.086	-0.519	-1.640
0.838	0.0311	0.398	1.017	-0.407	-1.508
0.935	0.0435	0.495	0.920	-0.269	-1.361
1.015	0.0548	0.575	0.840	-0.165	-1.261
1.193	0.0770	0.753	0.662	0.060	-1.113
1.335	0.108	0.895	0.520	0.236	-0.966
1.462	0.187	1.022	0.383	0.426	-0.728
1.553	0.252	1.113	0.302	0.566	-0.599
1.605	0.338	1.165	0.250	0.668	-0.472
1.673	0.464	1.233	0.182	0.831	-0.334
1.731	0.668	1.491	0.124	1.080	-0.175
1.791	1.06	1.551	0.064	1.384	0.024
1.855	1.93	1.615	0	———	0.284

Temperature = $0^{\circ}C$

A (428 nm)	[Py]	$A - A_o$	$A_\infty - A$	$\log \frac{A - A_o}{A_\infty - A}$	log[Py]
0.415	2.11×10^{-4}	0	1.299	———	-3.675
0.538	0.0333	0.123	1.176	-0.981	-1.478
0.601	0.0564	0.186	1.113	-0.777	-1.249
0.654	0.0795	0.239	1.060	-0.647	-1.010
0.742	0.125	0.327	0.972	-0.473	-0.902
0.781	0.171	0.366	0.933	-0.406	-0.767
0.872	0.238	0.457	0.842	-0.265	-0.623
0.943	0.368	0.528	0.771	-0.164	-0.433
1.009	0.459	0.594	0.705	-0.074	-0.339
1.080	0.671	0.665	0.634	0.021	-0.173
1.242	1.07	0.827	0.472	0.244	0.031
1.405	1.97	0.990	0.309	0.506	0.294

A_∞ estimated to be 1.714 (based on data of $-23^{\circ}C$).

Temperature = 27°C

A (428 nm)	[Py]	$A - A_o$	$A_\infty - A$	$\log \frac{A - A_o}{A_\infty - A}$	log [Py]
0.555	0.00356	0	1.744	———	-2.449
0.603	0.0355	0.048	1.696	-1.548	-1.450
0.674	0.0821	0.119	1.625	-1.135	-1.085
0.760	0.151	0.205	1.539	-0.875	-0.820
0.833	0.220	0.278	1.466	-0.722	-0.658
0.912	0.310	0.357	1.387	-0.589	-0.509
1.002	0.443	0.447	1.297	-0.463	-0.354
1.105	0.658	0.550	1.194	-0.337	-0.182
1.244	1.07	0.689	1.055	-0.185	0.031
1.389	1.97	0.834	0.910	-0.038	0.295

A_∞ estimated to be 2.299 (based on data of -23°C).

Additions were made with neat Py.

APPENDIX Im. $PBu_3 + PBu_3CoOMBP \rightleftharpoons (PBu_3)_2CoOMBP$

Temperature = 5°C

A (412 nm)	$[PBu_3]$	$A - A_o$	$A_\infty - A$	$\log \frac{A - A_o}{A_\infty - A}$	$\log[PBu_3]$
0.950	3.01×10^{-5}	0.250	0.500	-0.301	-4.521
1.015	5.00×10^{-5}	0.315	0.435	-0.140	-4.301
1.118	6.97×10^{-5}	0.418	0.332	0.100	-4.157
1.211	8.91×10^{-5}	0.511	0.239	0.330	-4.050
1.280	1.56×10^{-4}	0.588	0.162	0.560	-3.808
1.450	1.07×10^{-3}	0.750	0	———	-2.970

A_o estimated to be 0.700.

Temperature = 22°C*

A (412 nm)	PBu_3	$A - A_o$	$A_\infty - A$	$\log \frac{A - A_o}{A_\infty - A}$	$\log PBu_3$
0.858	3.01×10^{-5}	0.208	0.502	-0.383	-4.521
0.939	4.60×10^{-5}	0.289	0.421	-0.163	-4.337
1.025	5.79×10^{-5}	0.375	0.335	0.049	-4.237
1.092	8.91×10^{-5}	0.442	0.268	0.217	-4.050
1.157	1.56×10^{-4}	0.507	0.203	0.398	-3.808
1.269	2.29×10^{-4}	0.619	0.091	0.833	-3.640
1.322	5.57×10^{-4}	0.672	0.038	1.248	-3.253
1.360	1.07×10^{-3}	0.750	0	———	-2.970

A_o estimated to be 0.650.

* Data used for Figure III.4

Temperature = 40°C

A (412 nm)	$[PBu_3]$	$A - A_o$	$A_\infty - A$	$\log \frac{A - A_o}{A_\infty - A}$	$\log[PBu_3]$
1.239	1.06×10^{-4}	0.476	0.341	0.145	-3.972
1.262	2.18×10^{-4}	0.499	0.318	0.195	-3.840
1.359	3.58×10^{-4}	0.596	0.221	0.431	-3.661
1.423	6.67×10^{-4}	0.660	0.157	0.624	-3.446
1.580	4.15×10^{-3}	0.717	0	———	-2.382

A_o estimated to be 0.763

Additions were made with 4.05×10^{-3} M PBu_3 in toluene or with neat PBu_3.

APPENDIX In. CH_3-Im + CoOMBP $\rightleftharpoons$ CH_3-ImCoOMBP in 1,2-dichloroethane

Temperature = 5°C

A (618 nm)	$[CH_3\text{-Im}]$	$A_o - A$	$A - A_\infty$	$\log \frac{A_o - A}{A - A_\infty}$	$\log [CH_3\text{-Im}]$
0.800	0	0	0.270	———	———
0.750	2.51×10^{-6}	0.050	0.220	-0.643	-5.600
0.730	5.62×10^{-6}	0.070	0.200	-0.456	-5.250
0.705	1.25×10^{-5}	0.095	0.175	-0.265	-4.901
0.643	2.80×10^{-5}	0.157	0.113	0.143	-4.553
0.590	6.25×10^{-5}	0.210	0.060	0.544	-4.204
0.530	1.14×10^{-4}	0.270	0	———	-2.942

Temperature = 20°C

A (618 nm)	$[CH_3\text{-Im}]$	$A_o - A$	$A - A_\infty$	$\log \frac{A_o - A}{A - A_\infty}$	$\log [CH_3\text{-Im}]$
0.780	0	0	0.255	———	———
0.713	1.25×10^{-5}	0.067	0.188	-0.498	-4.901
0.668	2.51×10^{-5}	0.112	0.143	-0.106	-4.601
0.592	5.00×10^{-5}	0.188	0.087	0.335	-4.301
0.566	1.24×10^{-4}	0.214	0.041	0.718	-3.905
0.525	5.98×10^{-4}	0.255	0	———	-3.223

Temperature = 40°C

A (618 nm)	$[CH_3\text{-Im}]$	$A_o - A$	$A - A_\infty$	$\log \frac{A_o - A}{A - A_\infty}$	$\log [CH_3\text{-Im}]$
0.840	0	0	0.283	———	———
0.763	1.25×10^{-5}	0.077	0.214	-0.423	-4.901
0.724	2.51×10^{-5}	0.116	0.167	-0.158	-4.601
0.670	6.25×10^{-5}	0.170	0.113	0.177	-4.204
0.633	1.24×10^{-4}	0.217	0.076	0.435	-3.905
0.595	3.06×10^{-4}	0.245	0.038	0.809	-3.514
0.557	1.14×10^{-4}	0.283	0	———	-2.942

Additions were made with a 1.26×10^{-2} M CH_3-Im solution in toluene.

APPENDIX Io. Pip + CoOMBP $\rightleftharpoons$ PipCoOMBP in 1,2-dichloroethane

Temperature = 5°C

A (618 nm)	[Pip]	$A_o - A$	$A - A_\infty$	$\log \frac{A_o - A}{A - A_\infty}$	log[Pip]
0.776	0	0	0.231	———	———
0.747	2.02×10^{-6}	0.027	0.204	-0.878	-5.695
0.658	1.01×10^{-5}	0.112	0.119	-0.026	-4.996
0.580	5.02×10^{-5}	0.190	0.041	0.666	-4.299
0.559	1.98×10^{-4}	0.211	0.020	1.023	-3.703
0.539	9.18×10^{-4}	0.231	0	———	-3.037

Temperature = 20°C

A (618 nm)	[Pip]	$A_o - A$	$A - A_\infty$	$\log \frac{A_o - A}{A - A_\infty}$	log[Pip]
0.738	0	0	0.207	———	———
0.712	2.02×10^{-6}	0.026	0.181	-0.843	-5.695
0.679	5.05×10^{-6}	0.059	0.148	-0.399	-5.297
0.663	1.01×10^{-5}	0.075	0.132	-0.246	-4.996
0.639	2.52×10^{-5}	0.099	0.108	-0.038	-4.557
0.557	7.52×10^{-5}	0.181	0.026	0.843	-4.124
0.531	9.18×10^{-4}	0.207	0	———	-3.037

Temperature = 40°C

A (618 nm)	[Pip]	$A_o - A$	$A - A_\infty$	$\log \frac{A_o - A}{A - A_\infty}$	log[Pip]
0.723	0	0	0.228	———	———
0.703	2.02×10^{-6}	0.020	0.218	-1.017	-5.695
0.661	1.01×10^{-5}	0.062	0.166	-0.423	-4.996
0.573	5.02×10^{-5}	0.150	0.078	0.284	-4.299
0.513	1.98×10^{-4}	0.210	0.018	1.067	-3.703
0.495	9.18×10^{-4}	0.228	0	———	-3.037

Additions were made with a 1.01×10^{-2} M Pip solution in toluene.

APPENDIX Ip. Py + CoOMBP $\rightleftharpoons$ PyCoOMBP in 1,2-dichloroethane

Temperature = 5°C

A (618 nm)	[Py]	$A_o - A$	$A - A_\infty$	$\log \frac{A_o - A}{A - A_\infty}$	log[Py]
0.693	0	0	0.143	———	———
0.684	2.48×10^{-6}	0.009	0.134	-1.173	-5.606
0.652	1.24×10^{-5}	0.041	0.102	-0.396	-4.907
0.627	2.47×10^{-5}	0.066	0.077	-0.067	-4.608
0.596	6.17×10^{-5}	0.097	0.046	0.324	-4.210
0.573	2.43×10^{-4}	0.131	0.012	1.038	-3.614
0.550	1.13×10^{-3}	0.143	0	———	-2.948

Temperature = 20°C

A (618 nm)	[Py]	$A_o - A$	$A - A_\infty$	$\log \frac{A_o - A}{A - A_\infty}$	log[Py]
0.800	0	0	0.187	———	———
0.795	2.48×10^{-6}	0.005	0.182	-1.561	-5.606
0.774	1.24×10^{-5}	0.026	0.161	-0.792	-4.907
0.748	2.47×10^{-5}	0.052	0.135	-0.414	-4.608
0.715	6.17×10^{-5}	0.095	0.092	0.014	-4.210
0.671	1.23×10^{-4}	0.129	0.058	0.347	-3.912
0.642	2.43×10^{-4}	0.158	0.029	0.736	-3.614
0.613	1.13×10^{-3}	0.187	0	———	-2.948

Temperature = 40°C

A (618 nm)	[Py]	$A_o - A$	$A - A_\infty$	$\log \frac{A_o - A}{A - A_\infty}$	log[Py]
0.850	0	0	0.234	———	———
0.837	1.24×10^{-5}	0.013	0.221	-1.230	-4.907
0.821	2.47×10^{-5}	0.029	0.205	-0.849	-4.608
0.785	6.17×10^{-5}	0.065	0.169	-0.415	-4.210
0.740	1.23×10^{-4}	0.110	0.124	-0.052	-3.912
0.695	2.43×10^{-4}	0.155	0.079	0.293	-3.614
0.657	4.81×10^{-4}	0.193	0.041	0.673	-3.318
0.616	2.24×10^{-3}	0.234	0	———	-2.650

Additions were made with a 1.24×10^{-2} M Py solution in toluene.

APPENDIX Iq. THF + CoOMBP $\rightleftharpoons$ THFCoOMBP in 1,2-dichloroethane

Temperature = 5°C

A (417 nm)	[THF]	$A - A_o$	$A_\infty - A$	$\log \frac{A - A_o}{A_\infty - A}$	log [THF]
0.875	0	0	0.435	———	———
0.898	0.0369	0.023	0.412	-1.253	-1.433
0.933	0.117	0.058	0.377	-0.813	-0.933
0.981	0.182	0.106	0.329	-0.492	-0.739
1.030	0.360	0.155	0.280	-0.256	-0.444
1.074	0.699	0.199	0.236	-0.074	-0.155
1.140	1.51	0.265	0.170	0.194	0.179
1.222	3.13	0.347	0.088	0.595	0.496
1.310	5.63	0.435	0	———	0.751

Temperature = 20°C

A (417 nm)	[THF]	$A - A_o$	$A_\infty - A$	$\log \frac{A - A_o}{A_\infty - A}$	log [THF]
0.905	0	0	0.806	———	———
0.974	0.0529	0.069	0.737	-1.029	-1.277
1.061	0.126	0.156	0.650	-0.620	-0.900
1.136	0.246	0.181	0.625	-0.538	-0.610
1.204	0.478	0.299	0.507	-0.229	-0.321
1.293	0.917	0.388	0.418	-0.032	-0.038
1.404	1.70	0.499	0.307	0.211	0.231
1.534	3.27	0.629	0.177	0.551	0.514
1.711	5.63	0.806	0	———	0.714

Temperature = 40°C

A (417 nm)	[THF]	$A - A_o$	$A_\infty - A$	$\log \frac{A - A_o}{A_\infty - A}$	log [THF]
0.786	0	0	0.600	———	———
0.802	0.0369	0.016	0.584	-1.562	-1.433
0.856	0.117	0.070	0.530	-0.879	-0.933
0.883	0.163	0.097	0.503	-0.715	-0.789
0.937	0.358	0.151	0.449	-0.473	-0.445
1.004	0.699	0.218	0.382	-0.244	-0.155
1.051	1.22	0.265	0.335	-0.102	0.087
1.114	2.92	0.328	0.272	0.081	0.465
1.236	5.52	0.450	0.150	0.477	0.742

A_∞ estimated to be 1.386

Additions were made with neat THF.

APPENDIX II

RAW DATA USED FOR DETERMINING THE THERMODYNAMIC PARAMETERS OF REVERSIBLE DIOXYGEN BINDING TO L_nCoOMBP.

(n = 1 or 2)

APPENDIX IIa. CH_3-ImCoOMBP + $O_2 \rightleftharpoons CH_3$-ImCoOMBP($O_2$)

Temperature = -56.5°C*

A (408 nm)	P_{O_2}	$A_o - A$	$A - A_\infty$	$\log \frac{A_o - A}{A - A_\infty}$	$\log P_{O_2}$
1.500	0	0	0.770	———	———
1.480	0.23	0.020	0.750	-1.574	-0.637
1.464	1.1	0.036	0.734	-1.309	0.041
1.451	5.2	0.049	0.721	-1.168	0.716
1.377	14	0.123	0.647	-0.721	1.146
1.268	32	0.232	0.538	-0.365	1.505
1.115	60	0.385	0.385	0.000	1.778
1.013	100	0.487	0.283	0.236	2.000
0.947	178	0.553	0.217	0.406	2.250
0.850	306	0.650	0.120	0.733	2.486
0.775	498	0.725	0.045	1.207	2.697
0.730	825	0.770	0	———	2.916

* Data used for Figure IV.1

Temperature = -45°C

A (408 nm)	P_{O_2}	$A_o - A$	$A - A_\infty$	$\log \frac{A_o - A}{A - A_\infty}$	$\log P_{O_2}$
0.803	0	0	0.371	———	———
0.800	2.5	0.003	0.368	-2.089	0.405
0.798	6.2	0.005	0.366	-1.865	0.789
0.761	17.9	0.042	0.329	-0.894	1.253
0.688	46	0.115	0.256	-0.348	1.663
0.638	75	0.165	0.206	-0.096	1.875
0.585	124	0.218	0.153	0.154	2.093
0.545	222	0.258	0.113	0.359	2.346
0.500	336	0.303	0.068	0.649	2.526
0.465	578	0.338	0.030	1.052	2.762
0.432	815	0.371	0	———	2.911

Temperature = -31°C

A (408 nm)	P_{O_2}	$A_o - A$	$A - A_\infty$	$\log \frac{A_o - A}{A - A_\infty}$	$\log P_{O_2}$
0.916	0	0	0.466	———	———
0.889	20	0.027	0.439	-1.211	1.301
0.842	40	0.074	0.394	-0.726	1.602
0.774	80	0.142	0.324	-0.358	1.903
0.734	141	0.182	0.284	-0.194	2.149
0.660	236	0.256	0.210	0.087	2.379
0.603	430	0.313	0.153	0.311	2.633
0.546	825	0.370	0.096	0.584	2.916

A_∞ estimated to be 0.450 (based on data of -56.5°C.

P_{O_2} - pressure of O_2 in the system, measured in Torr.

APPENDIX IIb. PipCoOMBP + $O_2 \rightleftharpoons$ PipCoOMBP(O_2)

Temperature = -63.5°C

A (408 nm)	P_{O_2}	$A_o - A$	$A - A_\infty$	$\log \frac{A_o - A}{A - A_\infty}$	$\log P_{O_2}$
1.200	0	0	0.620	———	———
1.179	4.9	0.021	0.599	-1.455	0.690
1.143	13	0.057	0.563	-0.995	1.114
1.079	31	0.121	0.499	-0.615	1.491
0.956	71	0.244	0.376	-0.188	1.851
0.803	136	0.397	0.223	0.250	2.134
0.743	182	0.457	0.163	0.448	2.260
0.677	306	0.523	0.097	0.732	2.486
0.648	599	0.552	0.068	0.909	2.777
0.635	825	0.565	0.055	1.012	2.916

A_∞ estimated to be 0.580

Temperature = -56.5°C

A (408 nm)	P_{O_2}	$A_o - A$	$A - A_\infty$	$\log \frac{A_o - A}{A - A_\infty}$	$\log P_{O_2}$
1.500	0	0	0.600	———	———
1.482	4.7	0.018	0.582	-1.510	0.672
1.490	10.3	0.020	0.580	-1.462	1.013
1.445	24	0.055	0.545	-0.996	1.380
1.397	51	0.103	0.497	-0.684	1.708
1.290	100	0.210	0.390	-0.269	2.000
1.228	152	0.272	0.328	-0.081	2.182
1.155	225	0.345	0.255	0.131	2.352
1.090	340	0.410	0.190	0.334	2.531
1.033	573	0.467	0.137	0.545	2.758
0.945	843	0.555	0.045	1.082	2.926

A_∞ estimated to be 0.900

Temperature = -45°C

A (408 nm)	P_{O_2}	$A_o - A$	$A - A_\infty$	$\log \frac{A_o - A}{A - A_\infty}$	$\log P_{O_2}$
0.900	0	0	0.460	———	———
0.876	16	0.026	0.434	-1.233	1.204
0.829	38	0.071	0.389	-0.739	1.580
0.793	58	0.107	0.353	-0.518	1.763
0.774	73	0.126	0.334	-0.423	1.863
0.748	116	0.152	0.308	-0.307	2.064
0.722	163	0.178	0.282	-0.200	2.212
0.685	232	0.215	0.245	-0.057	2.365
0.650	325	0.250	0.210	0.076	2.512
0.610	840	0.290	0.170	0.232	2.924

A_∞ estimated to be 0.440

APPENDIX IIc. $PyCoOMBP + O_2 \rightleftharpoons PyCoOMBP(O_2)$

Temperature = -63.5°C

A (407 nm)	P_{O_2}	$A_o - A$	$A - A_\infty$	$\log \frac{A_o - A}{A - A_\infty}$	$\log P_{O_2}$
1.450	0	0	0.580	———	———
1.437	1.9	0.013	0.567	-1.640	0.279
1.424	3.9	0.026	0.544	-1.321	0.591
1.419	10	0.031	0.539	-1.240	1.000
1.414	19	0.036	0.534	-1.171	1.278
1.280	39	0.170	0.410	-0.382	1.591
1.221	60	0.229	0.351	-0.185	1.778
1.145	100	0.305	0.275	0.045	2.000
1.086	150	0.364	0.216	0.227	2.176
1.008	240	0.442	0.138	0.506	2.380
0.936	397	0.514	0.066	0.891	2.599
0.870	835	0.580	0	———	2.922

Temperature = -56.5°C

A (407 nm)	P_{O_2}	$A_o - A$	$A - A_\infty$	$\log \frac{A_o - A}{A - A_\infty}$	$\log P_{O_2}$
1.500	0	0	0.800	———	———
1.490	5.9	0.010	0.790	-1.898	0.777
1.478	13.5	0.022	0.778	-1.549	1.130
1.412	31	0.088	0.712	-0.908	1.492
1.299	61	0.201	0.599	-0.474	1.785
1.173	97	0.327	0.473	-0.160	1.987
1.073	128	0.427	0.373	0.059	2.107
1.007	188	0.493	0.307	0.205	2.274
0.926	298	0.574	0.226	0.405	2.474
0.854	504	0.646	0.154	0.623	2.702
0.759	844	0.741	0.059	1.099	2.926

A_∞ estimated to be 0.700

Temperature = -45°C

A (407 nm)	P_{O_2}	$A_o - A$	$A - A_\infty$	$\log \frac{A_o - A}{A - A_\infty}$	$\log P_{O_2}$
1.140	0	0	0.554	———	———
1.135	3.8	0.005	0.549	-2.041	0.580
1.125	10	0.015	0.539	-1.555	1.000
1.123	20	0.017	0.537	-1.500	1.301
1.085	40	0.055	0.499	-0.958	1.602
1.041	77	0.099	0.455	-0.662	1.886
0.958	148	0.181	0.373	-0.314	2.170
0.865	235	0.275	0.279	-0.006	2.371
0.750	393	0.390	0.164	0.376	2.594
0.647	840	0.493	0.061	0.908	2.924

A_∞ estimated to be 0.586

APPENDIX IId. $Et_3NCoOMBP + O_2 \rightleftharpoons Et_3NCoOMBP(O_2)$

Temperature = -78°C

A (407 nm)	P_{O_2}	$A_o - A$	$A - A_\infty$	$\log \frac{A_o - A}{A - A_\infty}$	$\log P_{O_2}$
1.203	0	0	0.643	———	———
1.096	22	0.107	0.536	-0.700	1.342
0.745	104	0.458	0.185	0.394	2.017
0.660	594	0.543	0.100	0.735	2.774
0.560	845	0.643	0	———	2.927

Temperature = -63.5°C

A (407 nm)	P_{O_2}	$A_o - A$	$A - A_\infty$	$\log \frac{A_o - A}{A - A_\infty}$	$\log P_{O_2}$
1.140	0	0	0.585	———	———
1.098	10	0.042	0.543	-1.112	1.000
1.028	50	0.112	0.473	-0.626	1.699
0.887	100	0.253	0.332	-0.118	2.000
0.817	150	0.323	0.262	0.091	2.176
0.752	225	0.388	0.197	0.294	2.352
0.703	350	0.437	0.148	0.467	2.544
0.555	845	0.585	0	———	2.927

Temperature = -56.5°C

A (407 nm)	P_{O_2}	$A_o - A$	$A - A_\infty$	$\log \frac{A_o - A}{A - A_\infty}$	$\log P_{O_2}$
1.229	0	0	0.649	———	———
1.149	40	0.080	0.569	-0.851	1.602
1.078	80	0.151	0.498	-0.517	1.903
0.969	120	0.260	0.389	-0.174	2.079
0.884	200	0.345	0.304	0.056	2.301
0.795	395	0.434	0.215	0.307	2.597
0.702	845	0.527	0.122	———	2.927

A_∞ estimated to be 0.580

Temperature = -45°C

A (407 nm)	P_{O_2}	$A_o - A$	$A - A_\infty$	$\log \frac{A_o - A}{A - A_\infty}$	$\log P_{O_2}$
0.828	0	0	0.438	———	———
0.790	50	0.038	0.400	-1.022	1.699
0.745	150	0.083	0.355	-0.639	2.176
0.668	298	0.160	0.278	-0.240	2.474
0.621	491	0.207	0.231	-0.048	2.691
0.584	845	0.244	0.194	0.100	———

A_∞ estimated to be 0.390

Temperature = -23°C

A (407nm)	P_{O_2}	$A_o - A$	$A - A_\infty$	$\log \frac{A_o - A}{A - A_\infty}$	$\log P_{O_2}$
1.333	0	0	0.693	———	———
1.298	103	0.035	0.658	-1.274	-2.013
1.269	194	0.064	0.629	-0.992	-2.288
1.203	392	0.130	0.563	-0.637	-2.593
1.126	855	0.207	0.486	-0.371	-2.932

A_∞ estimated to be 0.640

APPENDIX IIe. $DMFCoOMBP + O_2 \rightleftharpoons DMFCoOMBP(O_2)$

Temperature = -78°C

A (434 nm)	P_{O_2}	$A - A_o$	$A_\infty - A$	$\log \frac{A - A_o}{A_\infty - A}$	$\log P_{O_2}$
0.673	0	0	0.540	———	———
0.938	8	0.265	0.275	-0.016	0.903
0.990	18	0.317	0.223	0.153	1.255
1.098	38	0.425	0.115	0.568	1.580
1.160	100	0.487	0.053	0.963	2.000
1.208	287	0.535	0.005	2.029	2.458
1.213	865	0.540	0	———	2.937

Temperature = -63.5°C

A (434 nm)	P_{O_2}	$A - A_o$	$A_\infty - A$	$\log \frac{A - A_o}{A_\infty - A}$	$\log P_{O_2}$
0.670	0	0	0.543	———	———
0.700	9	0.030	0.513	-1.233	0.954
0.888	18	0.218	0.325	-0.173	1.255
0.996	39	0.326	0.217	0.176	1.591
1.096	74	0.426	0.117	0.561	1.869
1.140	148	0.470	0.073	0.809	2.170
1.173	290	0.503	0.040	1.100	2.462
1.217	865	0.543	0	———	2.937

Temperature = -56.5°C

A (434 nm)	P_{O_2}	$A - A_o$	$A_\infty - A$	$\log \frac{A - A_o}{A_\infty - A}$	$\log P_{O_2}$
0.830	0	0	0.620	———	———
0.845	11	0.015	0.605	-1.606	1.041
0.940	20	0.110	0.510	-0.666	1.301
1.027	39	0.197	0.427	-0.336	1.591
1.120	76	0.280	0.340	-0.084	1.881
1.257	152	0.427	0.193	0.345	2.182
1.315	288	0.485	0.135	0.555	2.459
1.395	860	0.565	0.055	1.012	2.984

A_∞ estimated to be 1.450

Temperature = -45°C

A (434 nm)	P_{O_2}	$A - A_o$	$A_\infty - A$	$\log \frac{A - A_o}{A_\infty - A}$	$\log P_{O_2}$
0.670	0	0	0.550	———	———
0.675	1.2	0.005	0.545	-2.037	0.079
0.683	6.2	0.013	0.537	-1.616	0.792
0.690	18	0.020	0.530	-1.423	1.255
0.712	38	0.042	0.508	-1.083	1.580
0.745	75	0.075	0.475	-0.802	1.875
0.825	150	0.155	0.395	-0.406	2.116
0.870	250	0.200	0.350	-0.243	2.380
0.920	450	0.250	0.300	-0.079	2.653
0.997	850	0.327	0.223	0.166	2.929

A_∞ estimated to be 1.220

Temperature = -23°C

A (434 nm)	P_{O_2}	$A - A_o$	$A_\infty - A$	$\log \frac{A - A_o}{A_\infty - A}$	$\log P_{O_2}$
0.900	0	0	0.650	———	———
0.910	17	0.010	0.640	-1.806	1.230
0.913	40	0.013	0.637	-1.690	1.602
0.945	94	0.045	0.605	-1.129	1.973
0.955	193	0.055	0.595	-1.034	2.286
0.990	402	0.090	0.560	-0.794	2.604
1.038	845	0.138	0.512	-0.569	2.926

A_∞ estimated to be 1.550

APPENDIX IIf. $PPh_3CoOMBP + O_2 \rightleftharpoons PPh_3CoOMBP(O_2)$

Temperature = -78°C

A (412 nm)	P_{O_2}	$A_o - A$	$A - A_\infty$	$\log \frac{A_o - A}{A - A_\infty}$	$\log P_{O_2}$
1.297	0	0	0.700	———	———
1.297	98	0	0.700	———	1.991
1.253	200	0.044	0.656	-1.176	2.301
1.197	385	0.100	0.600	-0.778	2.585
1.130	845	0.167	0.483	-0.461	2.927

A_∞ estimated to be 0.597

Temperature = -63.5°C

A (412 nm)	P_{O_2}	$A_o - A$	$A - A_\infty$	$\log \frac{A_o - A}{A - A_\infty}$	$\log P_{O_2}$
1.430	0	0	0.772	———	———
1.316	827	0.114	0.668	-0.761	2.918

A_∞ estimated to be 0.658

APPENDIX IIg. $PBu_3CoOMBP + O_2 \rightleftharpoons PBu_3CoOMBP(O_2)$

Temperature = -63.5°C

A (618 nm)	P_{O_2}	$A_o - A$	$A - A_\infty$	$\log \frac{A_o - A}{A - A_\infty}$	$\log P_{O_2}$
1.120	0	0	0.600	———	———
1.099	16	0.021	0.579	-1.410	1.204
0.887	82	0.233	0.367	-0.197	1.914
0.698	221	0.422	0.178	0.395	2.344
0.609	553	0.511	0.089	0.759	2.727
0.520	845	0.600	0	———	2.927

Temperature = -45°C

A (618 nm)	P_{O_2}	$A_o - A$	$A - A_\infty$	$\log \frac{A_o - A}{A - A_\infty}$	$\log P_{O_2}$
1.419	0	0	0.779	———	———
1.390	12	0.029	0.750	-1.413	1.079
1.361	25	0.058	0.721	-1.095	1.398
1.273	55	0.146	0.623	-0.633	1.740
1.163	100	0.266	0.513	-0.285	2.000
1.033	199	0.386	0.393	-0.008	2.299
0.832	385	0.537	0.242	0.346	2.585
0.780	820	0.639	0.140	0.659	2.914

A_∞ estimated to be 0.640

Temperature = -23°C

A (618 nm)	P_{O_2}	$A_o - A$	$A - A_\infty$	$\log \frac{A_o - A}{A - A_\infty}$	$\log P_{O_2}$
0.897	0	0	0.650	———	———
0.873	36	0.024	0.626	-1.450	1.556
0.842	67	0.055	0.595	-1.069	1.826
0.763	130	0.134	0.516	-0.626	2.114
0.637	249	0.260	0.440	-0.228	2.396
0.536	410	0.361	0.339	0.027	2.613
0.447	845	0.450	0.250	0.255	2.927

A_∞ estimated to be 0.247

APPENDIX IIh. $PBu_3CoOMBP + O_2 \rightleftharpoons PBu_3CoOMBP(O_2)$ as a function of $[PBu_3]$

$[PBu_3] = 1.01 \times 10^{-6}$ M

A (618 nm)	P_{O_2}	$A_o - A$	$A - A_\infty$	$\log \frac{A_o - A}{A - A_\infty}$	$\log P_{O_2}$
1.253	0	0	0.600	———	———
1.194	48	0.059	0.541	-0.962	1.681
1.105	190	0.148	0.452	-0.485	2.279
1.016	390	0.239	0.361	-0.179	2.591
0.924	845	0.329	0.271	·0.085	2.927

A_∞ estimated to be 0.653

$[PBu_3] = 4.04 \times 10^{-6}$ M

A (618 nm)	P_{O_2}	$A_o - A$	$A - A_\infty$	$\log \frac{A_o - A}{A - A_\infty}$	$\log P_{O_2}$
1.273	0	0	0.623	———	———
1.188	37	0.085	0.538	-0.801	1.568
1.093	78	0.180	0.443	-0.391	1.892
0.992	157	0.281	0.342	-0.085	2.196
0.868	317	0.405	0.218	0.269	2.501
0.745	828	0.528	0.095	0.745	2.918

A_∞ estimated to be 0.650

$[PBu_3] = 1.10 \times 10^{-5}$ M

A (618 nm)	P_{O_2}	$A_o - A$	$A - A_\infty$	$\log \frac{A_o - A}{A - A_\infty}$	$\log P_{O_2}$
1.120	0	0	0.600	———	———
1.099	16	0.021	0.579	-1.410	1.204
0.887	82	0.233	0.369	-1.197	1.914
0.698	221	0.422	0.178	0.935	2.344
0.609	553	0.511	0.089	0.759	2.727
0.520	845	0.600	0	———	2.927

A_∞ estimated to be 0.620

$[PBu_3] = 4.04 \times 10^{-5}$ M

A (618 nm)	P_{O_2}	$A_o - A$	$A - A_\infty$	$\log \frac{A_o - A}{A - A_\infty}$	$\log P_{O_2}$
1.327	0	0	0.717		
1.245	18	0.082	0.635	-0.899	1.255
1.154	38	0.173	0.544	-0.498	1.580
1.036	81	0.291	0.426	-0.166	1.908
0.878	173	0.449	0.268	0.224	2.238
0.775	350	0.552	0.165	0.524	2.544
0.675	845	0.652	0.065	1.001	2.927

A_∞ estimated to be 0.610

$[PBu_3] = 1.01 \times 10^{-4}$ M

A (618 nm)	P_{O_2}	$A_o - A$	$A - A_\infty$	$\log \frac{A_o - A}{A - A_\infty}$	$\log P_{O_2}$
1.184	0	0	0.624		
1.122	17	0.062	0.562	-0.957	1.230
1.034	39	0.150	0.474	-0.499	1.591
0.940	84	0.244	0.380	-0.192	1.924
0.789	182	0.395	0.229	0.237	2.260
0.703	378	0.481	0.143	0.527	2.577
0.620	845	0.564	0.060	0.973	2.927

A_∞ estimated to be 0.560

$[PBu_3] = 4.04 \times 10^{-4}$ M

A (618 nm)	P_{O_2}	$A_o - A$	$A - A_\infty$	$\log \frac{A_o - A}{A - A_\infty}$	$\log P_{O_2}$
1.147	0	0	0.607		
0.930	95	0.217	0.390	-0.255	1.978
0.807	195	0.340	0.267	0.105	2.290
0.699	390	0.448	0.159	0.450	2.591
0.617	845	0.530	0.077	0.838	2.927

A_∞ estimated to be 0.540

$[PBu_3] = 4.04 \times 10^{-3}$ M

A (618 nm)	P_{O_2}	$A_o - A$	$A - A_\infty$	$\log \frac{A_o - A}{A - A_\infty}$	$\log P_{O_2}$
1.287	0	0			
1.282	198	0.005			2.297
1.263	402	0.024			2.591
1.247	828	0.040			2.918

APPENDIX II i. $L_2CoOMBP + O_2 \rightleftharpoons LCoOMBP(O_2) + L$ @ -45°C

L = CH_3-Im*

A (457 nm)	P_{O_2}	$A_o - A$	$A - A_\infty$	$\log \frac{A_o - A}{A - A_\infty}$	$\log P_{O_2}$
0.845	0	0	0.545	———	———
0.828	41	0.017	0.528	-1.492	1.613
0.817	80	0.028	0.517	-1.266	1.903
0.778	140	0.067	0.478	-0.853	2.146
0.734	238	0.111	0.434	-0.581	2.377
0.681	447	0.164	0.381	-0.360	2.650
0.604	840	0.241	0.304	-0.101	2.924

A_∞ estimated to be 0.300, based on oxygenation data of CH_3-ImCoOMBP.

* Data used for Figure IV.3

L = Pip

A (430 nm)	P_{O_2}	$A_o - A$	$A - A_\infty$	$\log \frac{A_o - A}{A - A_\infty}$	$\log P_{O_2}$
1.130	0	0	0.160	———	———
1.119	99	0.011			1.996
1.112	397	0.018			2.599
1.108	820	0.022			2.914

A_∞ estimated to be 0.970, based on oxygenation data of PipCoOMBP.

Insufficient spectral changes to show that oxygenation occurs.

L = Py

A (428 nm)	A (458 nm)	P_{O_2}	$\log P_{O_2}$
1.440	0.259	0	———
1.425	0.263	98	1.991
1.423	0.269	206	2.314
1.415	0.280	402	2.604
1.415	0.287	842	2.925

Based on oxygenation data of CoOMBP, oxygenation appears to be 15% complete.

APPENDIX IIj. CH_3-ImCoOMBP + $O_2 \rightleftharpoons$ CH_3-ImCoOMBP(O_2) in a solvent system of 4:1 by volume toluene:1,2-dichloroethane.

Temperature = -56.5°C

A (408 nm)	P_{O_2}	$A_o - A$	$A - A_\infty$	$\log \frac{A_o - A}{A - A_\infty}$	$\log P_{O_2}$
1.100	0	0	0.650	———	———
1.082	1.6	0.018	0.632	-1.545	0.204
1.058	4.9	0.042	0.608	-1.161	0.690
0.991	9.6	0.109	0.541	-0.696	0.982
0.834	17	0.266	0.384	-0.159	1.230
0.722	28	0.378	0.272	0.143	1.447
0.640	42	0.460	0.190	0.384	1.623
0.579	76	0.521	0.129	0.606	1.881
0.512	164	0.588	0.062	0.977	2.215
0.474	346	0.626	0.024	1.416	2.539
0.450	825	0.650	0	———	2.915

Temperature = -45°C

A (408 nm)	P_{O_2}	$A_o - A$	$A - A_\infty$	$\log \frac{A_o - A}{A - A_\infty}$	$\log P_{O_2}$
1.250	0	0	0.750	———	———
1.244	0.4	0.006	0.744	-2.093	-0.420
1.233	0.9	0.017	0.733	-1.635	-0.060
1.199	1.9	0.051	0.699	-1.137	0.279
1.149	4.0	0.101	0.649	-0.808	0.602
1.100	7.8	0.150	0.600	-0.602	0.892
1.030	15.2	0.220	0.530	-0.382	1.182
0.927	26.2	0.323	0.427	-0.121	1.418
0.809	51	0.429	0.321	0.126	1.708
0.726	99	0.524	0.226	0.365	1.996
0.649	193	0.601	0.149	0.606	2.286
0.578	390	0.672	0.078	0.935	2.591
0.500	840	0.750	0	———	2.924

Temperature = $-31^{\circ}C$

A (408 nm)	P_{O_2}	$A_o - A$	$A - A_\infty$	$\log \frac{A_o - A}{A - A_\infty}$	$\log P_{O_2}$
1.030	0	0	0.620	———	———
1.003	1	0.027	0.593	-1.342	0.000
0.990	2	0.040	0.580	-1.161	0.301
0.977	4	0.053	0.567	-1.029	0.602
0.941	8	0.089	0.531	-0.776	0.903
0.880	16	0.150	0.470	-0.496	1.206
0.820	33	0.210	0.410	-0.291	1.519
0.748	67	0.282	0.338	-0.079	1.826
0.653	132	0.377	0.243	0.190	2.121
0.561	267	0.469	0.151	0.492	2.427
0.510	563	0.520	0.100	0.716	2.751
0.480	843	0.550	0.070	0.895	2.927

A_∞ estimated to be 0.410

APPENDIX IIk. $L_2CoOMBP + O_2 \rightleftharpoons LCoOMBP(O_2) + L$ @ -45°C.

In a solvent system of 4:1 toluene:1,2-dichloroethane.

L = CH_3-Im

A (457 nm)	P_{O_2}	$A_o - A$	$A - A_\infty$	$\log \frac{A_o - A}{A - A_\infty}$	$\log P_{O_2}$
0.790	0	0	0.210	———	———
0.775	52	0.015	0.195	-1.114	1.716
0.770	79	0.020	0.190	-0.973	1.898
0.754	159	0.036	0.176	-0.689	2.201
0.720	320	0.070	0.140	-0.301	2.505
0.620	823	0.170	0.040	0.628	2.915

A_∞ estimated to be 0.580

L = Pip

A (466 nm)	P_{O_2}	$A_o - A$	$A - A_\infty$	$\log \frac{A_o - A}{A - A_\infty}$	$\log P_{O_2}$
0.538	0	0	———	———	———
0.548	20	0.010			1.301
0.549	162	0.011			2.210
0.552	320	0.014			2.505
0.552	820	0.014			2.914

Insufficient spectral changes to show that oxygenation occurs

L = Py

A (452 nm)	P_{O_2}	$A_o - A$	$A - A_\infty$	$\log \frac{A_o - A}{A - A_\infty}$	$\log P_{O_2}$
0.342	0	0	———	———	———
0.369	49	0.027			1.690
0.378	198	0.036			2.297
0.411	810	0.063			2.908

APPENDIX II.1. CH_3-ImCoOMBP + O_2 $\rightleftharpoons$ CH_3-ImCoOMBP

In a solvent system of 1:1 by volume toluene:DMF.

Temperature = -56.5°C

A (408 nm)	P_{O_2}	$A_o - A$	$A - A_\infty$	$\log \frac{A_o - A}{A - A_\infty}$	$\log P_{O_2}$
0.732	0	0	0.387	———	———
0.697	1.9	0.035	0.352	-1.002	0.283
0.613	3.7	0.119	0.268	-0.352	0.568
0.535	7.9	0.197	0.190	0.016	0.898
0.487	14.8	0.245	0.142	0.237	1.170
0.397	31	0.335	0.052	0.809	1.491
0.360	76	0.372	0.015	1.395	1.881
0.345	830	0.387	0 0	———	2.919

Temperature = -45°C

A (408 nm)	P_{O_2}	$A_o - A$	$A - A_\infty$	$\log \frac{A_o - A}{A - A_\infty}$	$\log P_{O_2}$
0.650	0	0	0.350	———	———
0.632	1.3	0.018	0.332	-1.266	0.114
0.620	2.9	0.030	0.320	-1.028	0.462
0.583	5.6	0.067	0.283	-0.628	0.748
0.505	11	0.145	0.205	-0.150	1.041
0.403	21	0.247	0.103	0.380	1.322
0.355	40	0.295	0.055	0.729	1.602
0.315	78	0.335	0.015	1.348	1.892
0.300	195	0.350	0	———	2.290
0.300	825	0.350	0	———	2.916

Temperature = -31°C

A (408 nm)	P_{O_2}	$A_o - A$	$A - A_\infty$	$\log \frac{A_o - A}{A - A_\infty}$	$\log P_{O_2}$
0.732	0	0	0.332	———	———
0.677	12	0.055	0.312	-0.702	1.079
0.627	24	0.105	0.227	-0.335	1.380
0.553	47	0.180	0.152	0.073	1.672
0.480	100	0.252	0.080	0.498	2.000
0.425	195	0.307	0.025	1.089	2.290
0.415	395	0.317	0.015	1.325	2.597
0.400	830	0.332	0	———	2.919

Temperature = $-23^{o}C$

A (408 nm)	P_{O_2}	$A_o - A$	$A - A_\infty$	$\log \frac{A_o - A}{A - A_\infty}$	$\log P_{O_2}$
0.760	0	0	0.345	———	———
0.747	3.5	0.013	0.332	-1.394	0.544
0.742	7.2	0.018	0.327	-1.259	0.857
0.690	15.5	0.070	0.275	-0.594	1.190
0.620	38	0.140	0.205	-0.165	1.580
0.567	69	0.193	0.152	0.104	1.839
0.505	119	0.255	0.080	0.503	2.076
0.467	214	0.293	0.052	0.750	2.330
0.435	395	0.335	0.020	1.224	2.597
0.415	815	0.355	0	———	2.911

APPENDIX IIm. $PipCoOMBP + O_2 \rightleftharpoons PipCoOMBP(O_2)$

In a solvent system of 1:1 by volume toluene:DMF

Temperature = -56.5°C

A (408 nm)	P_{O_2}	$A_o - A$	$A - A_\infty$	$\log \frac{A_o - A}{A - A_\infty}$	$\log P_{O_2}$
0.803	0	0	0.410	———	———
0.713	6.2	0.120	0.290	-0.383	0.792
0.657	12.3	0.166	0.244	-0.167	1.090
0.563	23.6	0.240	0.170	0.150	1.373
0.495	45	0.308	0.102	0.480	1.653
0.448	80	0.355	0.055	0.810	1.903
0.421	160	0.382	0.028	1.135	2.204
0.408	312	0.395	0.015	1.421	2.494
0.393	815	0.410	0	———	2.911

Temperature = -45°C

A (408 nm)	P_{O_2}	$A_o - A$	$A - A_\infty$	$\log \frac{A_o - A}{A - A_\infty}$	$\log P_{O_2}$
0.950	0	0	0.520	———	———
0.930	1.7	0.020	0.500	-1.398	0.228
0.900	3.3	0.050	0.470	-0.973	0.519
0.870	6.9	0.080	0.440	-0.740	0.839
0.800	13.8	0.150	0.370	-0.392	1.140
0.730	25	0.220	0.300	-0.135	1.398
0.610	48	0.340	0.180	0.276	1.681
0.557	100	0.393	0.127	0.491	2.000
0.500	200	0.450	0.070	0.808	2.301
0.460	390	0.495	0.025	1.297	2.926

Temperature = -31°C

A (408 nm)	P_{O_2}	$A_o - A$	$A - A_\infty$	$\log \frac{A_o - A}{A - A_\infty}$	$\log P_{O_2}$
1.100	0	0	0.590	———	———
1.020	7.9	0.080	0.510	-0.804	0.897
0.988	15.1	0.112	0.478	-0.630	1.179
0.950	30.2	0.150	0.440	-0.467	1.480
0.870	60	0.230	0.360	-0.195	1.778
0.790	118	0.310	0.280	0.042	2.072
0.695	235	0.405	0.185	0.340	2.371
0.610	820	0.490	0.100	0.690	2.914

A_∞ estimated to be 0.510

Temperature = $-23^{\circ}C$

A (408 nm)	P_{O_2}	$A_o - A$	$A - A_\infty$	$\log \frac{A_o - A}{A - A_\infty}$	$\log P_{O_2}$
1.029	0	0	0.569	———	———
0.992	12	0.037	0.522	-1.149	1.079
0.910	31	0.119	0.450	-0.578	1.491
0.887	39	0.122	0.447	-0.564	1.591
0.843	60	0.166	0.403	-0.385	1.778
0.783	126	0.266	0.303	-0.057	2.100
0.673	197	0.356	0.213	0.223	2.297
0.627	348	0.402	0.167	0.382	2.542
0.586	845	0.443	0.126	0.546	2.927

A_∞ estimated to be 0.460

APPENDIX IIn. $PyCoOMBP + O_2 \rightleftharpoons PyCoOMBP(O_2)$

In a solvent system of 1:1 by volume toluene:DMF

Temperature = -56.5°C

A (407 nm)	P_{O_2}	$A_o - A$	$A - A_\infty$	$\log \frac{A_o - A}{A - A_\infty}$	$\log P_{O_2}$
0.780	0	0	0.470	———	———
0.757	1.8	0.023	0.447	-1.289	0.248
0.735	7.7	0.045	0.425	-0.975	0.886
0.662	16.0	0.118	0.352	-0.474	1.204
0.587	30.4	0.193	0.277	-0.157	1.483
0.463	60	0.317	0.253	0.098	1.775
0.407	98	0.353	0.117	0.480	1.991
0.390	280	0.390	0.080	0.687	2.447
0.320	845	0.470	0	———	2.927

Temperature = -45°C

A (407 nm)	P_{O_2}	$A_o - A$	$A - A_\infty$	$\log \frac{A_o - A}{A - A_\infty}$	$\log P_{O_2}$
0.820	0	0	0.480	———	———
0.808	1.5	0.012	0.468	-1.591	0.187
0.795	3.1	0.025	0.455	-1.260	0.491
0.750	10	0.070	0.410	-0.768	1.000
0.737	15	0.083	0.397	-0.680	1.175
0.672	33	0.148	0.332	-0.351	1.519
0.617	50	0.203	0.277	-0.135	1.699
0.537	98	0.283	0.197	0.157	1.991
0.463	200	0.357	0.123	0.463	2.301
0.413	450	0.407	0.083	0.691	2.602
0.380	840	0.440	0.040	1.041	2.927

A_∞ estimated to be 0.340

Temperature = -31°C

A (407 nm)	P_{O_2}	$A_o - A$	$A - A_\infty$	$\log \frac{A_o - A}{A - A_\infty}$	$\log P_{O_2}$
0.700	0	0	0.370	———	———
0.667	10	0.033	0.337	-1.009	1.000
0.647	25	0.053	0.317	-0.777	1.398
0.610	50	0.090	0.280	-0.493	1.694
0.560	100	0.140	0.230	-0.216	2.000
0.520	140	0.180	0.190	-0.023	2.146
0.500	180	0.200	0.170	0.071	2.255
0.460	280	0.240	0.130	0.266	2.447
0.390	845	0.310	0.060	0.713	2.927

A_∞ estimated to be 0.330

Temperature = $-23^{o}C$

A (407 nm)	P_{O_2}	$A_o - A$	$A - A_\infty$	$\log \frac{A_o - A}{A - A_\infty}$	$\log P_{O_2}$
0.710	0	0	0.380	———	———
0.698	20	0.012	0.368	-1.487	1.301
0.667	50	0.043	0.337	-0.894	1.699
0.637	100	0.073	0.317	-0.637	2.000
0.607	148	0.103	0.277	-0.430	2.170
0.580	245	0.130	0.250	-0.283	2.386
0.523	450	0.187	0.193	-0.014	2.653
0.468	840	0.242	0.138	0.244	2.927

A_∞ estimated to be 0.330

APPENDIX IIo. PipCoOMBP + $O_2 \rightleftharpoons$ PipCoOMBP(O_2) @ -56.5°C

With varying amounts of DMF in the solvent system.

[DMF] = 0, ϵ = 2.38

A (408 nm)	P_{O_2}	$A_o - A$	$A - A_\infty$	$\log \frac{A_o - A}{A - A_\infty}$	$\log P_{O_2}$
1.500	0	0	0.600	———	———
1.482	4.7	0.018	0.582	-1.510	0.672
1.480	10.3	0.020	0.580	-1.462	1.013
1.445	24	0.055	0.545	-0.996	1.380
1.397	51	0.103	0.497	-0.684	1.708
1.290	100	0.210	0.390	-0.269	2.000
1.228	152	0.272	0.328	-0.081	2.182
1.155	225	0.345	0.255	0.131	2.352
1.090	340	0.410	0.190	0.334	2.531
1.033	573	0.467	0.137	0.545	2.758
0.945	843	0.555	0.045	1.082	2.926

A_∞ estimated to be 0.900

[DMF] = 0.649 M, ϵ = 3.63

A (408 nm)	P_{O_2}	$A_o - A$	$A - A_\infty$	$\log \frac{A_o - A}{A - A_\infty}$	$\log P_{O_2}$
1.100	0	0	0.635	———	———
1.063	10	0.037	0.598	-1.205	1.000
1.028	20	0.072	0.563	-0.893	1.301
1.000	32	0.100	0.535	-0.728	1.505
0.877	100	0.223	0.412	-0.266	2.000
0.717	245	0.383	0.252	0.182	2.389
0.635	450	0.465	0.170	0.437	2.653
0.550	845	0.550	0.085	0.810	2.927

A_∞ estimated to be 0.465

[DMF] = 1.298 M, ϵ = 4.92

A (408 nm)	P_{O_2}	$A_o - A$	$A - A_\infty$	$\log \frac{A_o - A}{A - A_\infty}$	$\log P_{O_2}$
1.400	0	0	0.635	———	———
1.369	11.4	0.031	0.604	-1.290	1.056
1.317	34.9	0.103	0.532	-0.713	1.542
1.121	79	0.279	0.356	-0.106	1.897
0.970	148	0.430	0.205	0.322	2.170
0.882	250	0.518	0.117	0.646	2.398
0.815	440	0.585	0.050	1.068	2.643
0.765	840	0.635	0	———	2.924

[DMF] = 2.596 M, ϵ = 7.80

A (408 nm)	P_{O_2}	$A_o - A$	$A - A_\infty$	$\log \frac{A_o - A}{A - A_\infty}$	$\log P_{O_2}$
1.000	0	0	0.433	———	———
0.947	15	0.053	0.380	-0.856	1.176
0.858	31	0.142	0.291	-0.312	1.488
0.765	59	0.235	0.198	0.074	1.770
0.667	120	0.333	0.100	0.522	2.079
0.623	235	0.377	0.056	0.828	2.371
0.567	845	0.433	0	———	2.927

[DMF] = 4.327 M, ϵ = 11.2

A (408 nm)	P_{O_2}	$A_o - A$	$A - A_\infty$	$\log \frac{A_o - A}{A - A_\infty}$	$\log P_{O_2}$
0.863	0	0	0.418	———	———
0.810	1.8	0.053	0.365	-0.838	0.266
0.805	4.0	0.058	0.360	-0.793	0.602
0.787	7.7	0.076	0.342	-0.653	0.886
0.670	15.4	0.193	0.225	-0.067	1.187
0.600	30	0.263	0.155	0.230	1.477
0.536	50	0.327	0.091	0.556	1.699
0.490	98	0.373	0.045	0.918	1.991
0.454	195	0.409	0.009	1.657	2.290
0.445	390	0	0.418	———	2.591
0.445	840	0	0.418	———	2.911

[DMF] = 6.489 M, $\epsilon \sim$ 18

A (408 nm)	P_{O_2}	$A_o - A$	$A - A_\infty$	$\log \frac{A_o - A}{A - A_\infty}$	$\log P_{O_2}$
0.803	0	0	0.410	———	———
0.683	6.2	0.120	0.290	-0.383	0.792
0.637	12.3	0.166	0.244	-0.167	1.096
0.563	23.6	0.240	0.170	0.150	1.373
0.495	45	0.308	0.102	0.480	1.653
0.448	80	0.355	0.055	0.816	1.903
0.421	160	0.382	0.028	1.135	2.204
0.408	312	0.395	0.015	1.421	2.494
0.393	845	0.410	0	———	2.911

APPENDIX III

RAW DATA USED FOR DETERMINING THE THERMODYNAMIC PARAMETERS OF REVERSIBLE LIGAND BINDING TO CoDADIXDME AND CoDBrDIXDME

APPENDIX IIIa. CH_3-Im + CoDADIXDME $\rightleftharpoons$ CH_3-ImCoDADIXDME

Temperature = 5°C

A (550 nm)	$[CH_3\text{-Im}]$	$A - A_o$	$A_\infty - A$	$\log \frac{A - A_o}{A_\infty - A}$	$\log[CH_3\text{-Im}]$
0.833	0	0	0.203	———	———
0.843	2.22×10^{-6}	0.010	0.193	-1.286	-5.653
0.861	8.03×10^{-6}	0.028	0.175	-0.794	-5.095
0.897	2.11×10^{-5}	0.064	0.139	-0.337	-4.675
0.953	5.56×10^{-5}	0.120	0.083	0.160	-4.225
1.002	1.46×10^{-4}	0.169	0.034	0.696	-3.835
1.025	3.88×10^{-4}	0.192	0.011	1.245	-3.420
1.033	9.98×10^{-4}	0.200	0.003	1.806	-3.001
1.036	3.18×10^{-3}	0.203	0	———	-2.498

Temperature = 22°C*

A (550 nm)	$[CH_3\text{-Im}]$	$A - A_o$	$A_\infty - A$	$\log \frac{A - A_o}{A_\infty - A}$	$\log[CH_3\text{-Im}]$
0.933	0	0	0.234	———	———
0.953	1.25×10^{-5}	0.020	0.214	-1.030	-4.901
0.981	2.51×10^{-5}	0.048	0.186	-0.588	-4.601
1.022	5.00×10^{-5}	0.091	0.143	-0.196	-4.301
1.077	9.97×10^{-5}	0.144	0.090	0.204	-4.001
1.107	1.98×10^{-4}	0.174	0.059	0.470	-3.704
1.133	3.89×10^{-4}	0.200	0.034	0.770	-3.410
1.155	8.44×10^{-4}	0.222	0.012	1.267	-3.074
1.167	5.53×10^{-3}	0.234	0	———	-2.257

* Data ysed for Figure V.1

Temperature = 40°C

A (550 nm)	$[CH_3\text{-Im}]$	$A - A_o$	$A_\infty - A$	$\log \frac{A - A_o}{A_\infty - A}$	$\log[CH_3\text{-Im}]$
0.810	0	0	0.180	———	———
0.840	2.51×10^{-5}	0.030	0.150	-0.699	-4.601
0.853	5.00×10^{-5}	0.043	0.137	-0.503	-4.301
0.880	9.97×10^{-5}	0.070	0.110	-0.196	-4.001
0.913	1.98×10^{-4}	0.103	0.077	0.126	-3.704
0.935	3.89×10^{-4}	0.125	0.055	0.357	-3.410
0.965	8.44×10^{-4}	0.155	0.025	0.792	-3.074
0.973	1.66×10^{-3}	0.163	0.017	0.982	-2.781
0.980	6.02×10^{-3}	0.170	0.010	1.230	-2.220
0.990	2.78×10^{-2}	0.180	0	———	-1.556

APPENDIX IIIb. Pip + CoDADIXDME $\rightleftharpoons$ PipCoDADIXDME

Temperature = 5°C

A (550 nm)	[Pip]	$A - A_o$	$A_\infty - A$	$\log \frac{A - A_o}{A_\infty - A}$	log[Pip]
0.817	0	0	0.281	———	———
0.827	4.04×10^{-6}	0.010	0.271	-1.433	-5.394
0.844	1.01×10^{-5}	0.027	0.254	-0.973	-4.996
0.877	2.02×10^{-5}	0.060	0.221	-0.566	-4.696
0.913	4.02×10^{-5}	0.096	0.185	-0.285	-4.395
0.988	8.02×10^{-5}	0.171	0.110	0.192	-4.096
1.032	1.59×10^{-4}	0.215	0.215	0.513	-3.798
1.057	3.13×10^{-4}	0.240	0.041	0.767	-3.504
1.083	6.78×10^{-4}	0.265	0.015	1.249	-3.169
1.092	1.33×10^{-3}	0.275	0.006	1.661	-2.875
1.090	4.84×10^{-3}	0.273	0.008	1.533	-2.315
1.098	2.23×10^{-2}	0.281	0	———	-1.652

Temperature = 22°C

A (550 nm)	[Pip]	$A - A_o$	$A_\infty - A$	$\log \frac{A - A_o}{A_\infty - A}$	log[Pip]
0.947	0	0	0.270	———	———
0.967	1.01×10^{-5}	0.020	0.250	-1.097	-4.996
0.994	2.02×10^{-5}	0.047	0.223	-0.676	-4.686
1.015	4.02×10^{-5}	0.068	0.202	-0.494	-4.395
1.072	8.02×10^{-5}	0.125	0.145	-0.064	-4.096
1.119	1.59×10^{-4}	0.172	0.098	0.244	-3.798
1.193	3.13×10^{-4}	0.246	0.034	0.859	-3.504
1.192	6.78×10^{-4}	0.245	0.035	0.845	-3.169
1.204	1.33×10^{-3}	0.257	0.013	1.289	-2.875
1.217	4.83×10^{-3}	0.270	0	———	-2.315
1.217	2.33×10^{-2}	0.270	0	———	-1.652

Temperature = 40°C

A (550 nm)	[Pip]	$A - A_o$	$A_\infty - A$	$\log \frac{A - A_o}{A_\infty - A}$	log[Pip]
0.927	0	0	0.234	———	———
0.942	2.02×10^{-5}	0.015	0.219	-1.184	-4.696
0.960	4.02×10^{-5}	0.033	0.201	-0.785	-4.395
0.986	8.02×10^{-5}	0.059	0.175	-0.472	-4.096
1.032	1.59×10^{-4}	0.105	0.129	-0.089	-3.798
1.080	3.13×10^{-4}	0.153	0.081	0.276	-3.504
1.097	6.78×10^{-4}	0.170	0.064	0.424	-3.169
1.131	1.33×10^{-3}	0.204	0.030	0.833	-2.875
1.161	4.83×10^{-3}	0.234	0	———	-2.315

APPENDIX IIIc. Py + CoDADIXDME $\rightleftharpoons$ PyCoDADIXDME

Temperature = 5°C

A (550 nm)	[Py]	$A - A_o$	$A_\infty - A$	$\log \frac{A - A_o}{A_\infty - A}$	log[Py]
0.685	0	0	0.149	———	———
0.691	4.13×10^{-6}	0.006	0.143	-1.377	-5.385
0.705	2.06×10^{-5}	0.020	0.129	-0.872	-4.685
0.730	4.11×10^{-5}	0.045	0.104	-0.364	-4.385
0.749	8.21×10^{-4}	0.064	0.085	-0.123	-4.086
0.781	1.63×10^{-4}	0.096	0.053	0.258	-3.787
0.804	3.22×10^{-4}	0.119	0.030	0.598	-3.492
0.821	6.28×10^{-4}	0.136	0.013	1.020	-3.202
0.824	1.20×10^{-3}	0.149	0	———	-2.903

Temperature = 22°C

A (550 nm)	[Py]	$A - A_o$	$A_\infty - A$	$\log \frac{A - A_o}{A_\infty - A}$	log[Py]
0.852	0	0	0.172	———	———
0.862	2.06×10^{-5}	0.010	0.162	-1.210	-4.685
0.881	4.11×10^{-5}	0.029	0.143	-0.693	-4.385
0.897	8.21×10^{-5}	0.045	0.127	-0.451	-4.086
0.926	1.63×10^{-4}	0.074	0.098	-0.122	-3.787
0.957	3.22×10^{-4}	0.105	0.067	0.195	-3.492
0.985	6.28×10^{-4}	0.133	0.039	0.533	-3.202
1.005	1.20×10^{-3}	0.153	0.019	0.906	-2.923
1.015	2.18×10^{-3}	0.163	0.009	1.258	-2.661
1.024	2.26×10^{-2}	0.172	0	———	-1.690

Temperature = 40°C

A (550 nm)	[Py]	$A - A_o$	$A_\infty - A$	$\log \frac{A - A_o}{A_\infty - A}$	log[Py]
0.833	0	0	0.155	———	———
0.837	4.11×10^{-5}	0.004	0.151	-1.547	-4.385
0.859	1.23×10^{-4}	0.026	0.129	-0.696	-3.911
0.883	2.43×10^{-4}	0.050	0.105	-0.322	-3.614
0.909	4.77×10^{-4}	0.076	0.079	-0.017	-3.322
0.935	9.19×10^{-4}	0.102	0.053	0.284	-3.037
0.948	1.71×10^{-3}	0.115	0.040	0.459	-2.767
0.962	3.85×10^{-3}	0.129	0.026	0.696	-2.414
0.977	8.13×10^{-2}	0.144	0.011	1.117	-2.193
0.988	3.57×10^{-2}	0.155	0	———	-1.447

APPENDIX IIId. DMF + CODADIXDME $\rightleftharpoons$ DMFCoDADIXDME

Temperature = 5°C

A (574 nm)	[DMF]	$A_o - A$	$A - A_\infty$	$\log \frac{A_o - A}{A - A_\infty}$	$\log$[DMF]
1.061	0	0	0.350	———	———
1.059	0.0216	0.002	0.348	-2.241	-1.666
1.057	0.0538	0.004	0.346	-1.937	-1.269
1.043	0.160	0.018	0.332	-1.266	-0.795
1.022	0.316	0.039	0.311	-0.902	-0.500
0.990	0.618	0.071	0.279	-0.594	-0.209
0.978	1.18	0.083	0.267	-0.507	-0.072
0.912	2.74	0.149	0.201	-0.130	0.438
0.818	5.90	0.243	0.107	0.107	0.771

A_∞ estimated to be 0.711

Temperature = 22°C

A (574 nm)	[DMF]	$A_o - A$	$A - A_\infty$	$\log \frac{A_o - A}{A - A_\infty}$	$\log$[DMF]
1.393	0	0	0.520	———	———
1.378	0.107	0.015	0.505	-1.527	-0.970
1.368	0.213	0.025	0.495	-1.297	-0.672
1.330	0.419	0.063	0.457	-0.861	-0.378
1.276	0.998	0.117	0.403	-0.537	-0.001
1.237	1.85	0.146	0.374	-0.409	0.268
1.191	3.24	0.202	0.318	-0.197	0.511
1.063	5.90	0.330	0.190	0.238	0.771

A_∞ estimated to be 0.869

Temperature = 40°C

A (574 nm)	[DMF]	$A_o - A$	$A - A_\infty$	$\log \frac{A_o - A}{A - A_\infty}$	$\log$[DMF]
1.097	0	0	0.370	———	———
1.076	0.213	0.021	0.349	-1.221	-0.672
1.067	0.419	0.029	0.341	-1.076	-0.378
1.047	0.998	0.050	0.320	-0.806	-0.001
1.000	1.85	0.097	0.273	-0.449	0.268
0.924	3.24	0.140	0.230	-0.056	0.611
0.854	5.90	0.210	0.160	0.118	0.711

A_∞ estimated to be 0.722

APPENDIX IIIe. CH_3-Im + CoDBrDIXDME $\rightleftharpoons$ CH_3-ImCoDBrDIXDME

Temperature = 5°C

A (555 nm)	$[CH_3\text{-Im}]$	$A_o - A$	$A - A_\infty$	$\log \frac{A_o - A}{A - A_\infty}$	$\log[CH_3\text{-Im}]$
0.672	0	0	0.125	———	———
0.635	2.5×10^{-5}	0.037	0.088	-0.376	-4.601
0.598	5.0×10^{-5}	0.074	0.051	0.162	-4.301
0.576	1.24×10^{-4}	0.096	0.029	0.520	-3.905
0.561	3.06×10^{-4}	0.111	0.014	0.899	-3.514
0.547	2.0×10^{-3}	0.125	0	———	-2.698

Temperature = 22°C*

A (555 nm)	$[CH_3\text{-Im}]$	$A_o - A$	$A - A_\infty$	$\log \frac{A_o - A}{A - A_\infty}$	$\log[CH_3\text{-Im}]$
1.408	0	0	0.507	———	———
1.341	5.0×10^{-6}	0.067	0.440	-0.817	-5.299
1.335	2.5×10^{-5}	0.073	0.434	-0.774	-4.601
1.253	5.0×10^{-5}	0.155	0.352	-0.356	-4.301
1.179	9.97×10^{-5}	0.229	0.278	-0.084	-4.001
1.085	1.98×10^{-4}	0.323	0.184	0.244	-3.704
1.004	3.89×10^{-4}	0.404	0.103	0.594	-3.410
0.954	7.55×10^{-4}	0.454	0.053	0.933	-3.122
0.924	1.43×10^{-3}	0.484	0.023	1.323	-2.846
0.901	2.8×10^{-2}	0.507	0	———	-1.553

* Data used for Figure V.2

Temperature = 40°C

A (555 nm)	$[CH_3\text{-Im}]$	$A_o - A$	$A - A_\infty$	$\log \frac{A_o - A}{A - A_\infty}$	$\log[CH_3\text{-Im}]$
1.313	0	0	0.274	———	———
1.261	3.76×10^{-5}	0.052	0.222	-0.636	-4.425
1.208	8.73×10^{-5}	0.105	0.169	-0.203	-4.059
1.168	1.86×10^{-4}	0.145	0.129	0.051	-3.731
1.084	7.34×10^{-4}	0.229	0.049	0.670	-3.134
1.039	2.8×10^{-2}	0.274	0	———	-1.553

APPENDIX IIIf. Pip + CoDBrDIXDME $\rightleftharpoons$ PipCoDBrDIXDME

Temperature = 5°C

A (555 - 530 nm)	[Pip]	$A_o - A$	$A - A_\infty$	$\log \frac{A_o - A}{A - A_\infty}$	log[Pip]
0.839	0	0	0.534	———	———
0.816	2.02×10^{-6}	0.023	0.511	-1.347	-5.695
0.795	6.05×10^{-6}	0.044	0.490	-1.047	-5.218
0.738	2.02×10^{-5}	0.101	0.433	-0.632	-4.696
0.691	4.02×10^{-5}	0.147	0.387	-0.420	-4.395
0.531	8.01×10^{-5}	0.308	0.227	0.134	-4.096
0.471	1.20×10^{-4}	0.368	0.166	0.346	-3.922
0.387	1.79×10^{-4}	0.452	0.082	0.741	-3.748
0.324	2.94×10^{-4}	0.515	0.019	1.433	-3.532
0.305	1.85×10^{-2}	0.534	0	———	-1.733

NOTE: As the baseline was difficult to determine, the difference between the absorbance at 555 and 530 nm was recorded so that any baseline fluctuations would be cancelled.

Temperature = 22°C

A (555 nm)	[Pip]	$A_o - A$	$A - A_\infty$	$\log \frac{A_o - A}{A - A_\infty}$	log[Pip]
1.331	0	0	0.225	———	———
1.327	4.04×10^{-6}	0.004	0.221	-1.742	-5.394
1.313	1.01×10^{-5}	0.018	0.207	-1.061	-4.996
1.308	2.02×10^{-5}	0.023	0.202	-0.944	-4.696
1.305	4.02×10^{-5}	0.026	0.199	-0.884	-4.395
1.244	6.02×10^{-4}	0.087	0.138	-0.323	-4.220
1.234	1.00×10^{-4}	0.097	0.128	-0.120	-4.000
1.206	1.98×10^{-4}	0.125	0.100	0.097	-3.703
1.167	3.88×10^{-4}	0.164	0.061	0.430	-3.411
1.133	9.18×10^{-4}	0.198	0.027	0.865	-3.037
1.106	2.18×10^{-2}	0.225	0	———	-1.662

Temperature = 40°C

A (555 nm)	[Pip]	$A_o - A$	$A - A_\infty$	$\log \frac{A_o - A}{A - A_\infty}$	log[Pip]
1.440	0	0	0.232	———	———
1.426	2.02×10^{-5}	0.014	0.218	-1.192	-4.395
1.385	4.02×10^{-5}	0.055	0.177	-0.508	-4.096
1.353	8.01×10^{-5}	0.087	0.145	-0.222	-3.790
1.298	1.59×10^{-4}	0.142	0.090	0.198	-3.504
1.253	3.13×10^{-4}	0.177	0.055	0.508	-3.217
1.213	6.07×10^{-4}	0.227	0.005	1.657	-2.914
1.208	2.19×10^{-2}	0.232	0	———	-1.660

APPENDIX IIIg. Py + CoDBrDIXDME $\rightleftharpoons$ PyCoDBrDIXDME

Temperature = 5°C

A (555 - 530 nm)	[Py]	$A_o - A$	$A - A_\infty$	$\log \frac{A_o - A}{A - A_\infty}$	log[Py]
0.695	0	0	0.406	———	———
0.676	1.24×10^{-5}	0.019	0.387	-1.309	-4.907
0.646	4.94×10^{-5}	0.049	0.357	-0.862	-4.606
0.587	9.84×10^{-5}	0.108	0.298	-0.441	-4.306
0.539	1.95×10^{-4}	0.156	0.250	-0.205	-4.007
0.461	3.85×10^{-4}	0.234	0.172	0.134	-3.709
0.400	7.46×10^{-4}	0.295	0.111	0.424	-3.415
0.335	1.41×10^{-3}	0.360	0.046	0.894	-3.127
0.301	2.53×10^{-3}	0.378	0.028	1.130	-2.852
0.289	2.62×10^{-2}	0.406	0	———	-1.582

NOTE: As the baseline was difficult to determine, the difference between the absorbance at 555 and 530 nm was recorded so that any baseline fluctuations would be cancelled.

Temperature = 22°C

A (555 nm)	[Py]	$A_o - A$	$A - A_\infty$	$\log \frac{A_o - A}{A - A_\infty}$	log[Py]
1.172	0	0	0.220	———	———
1.147	2.48×10^{-5}	0.025	0.195	-0.892	-4.606
1.130	4.94×10^{-5}	0.042	0.178	-0.692	-4.306
1.097	9.84×10^{-5}	0.075	0.145	-0.286	-4.007
1.087	1.95×10^{-4}	0.085	0.135	-0.201	-3.709
1.071	3.85×10^{-4}	0.101	0.119	-0.071	-3.415
1.026	7.46×10^{-4}	0.146	0.074	0.295	-3.127
1.001	1.41×10^{-3}	0.171	0.049	0.542	-2.852
0.977	2.53×10^{-3}	0.195	0.025	0.892	-2.597
0.952	2.62×10^{-2}	0.220	0	———	———

Temperature = 40°C

A (555 nm)	[Py]	$A_o - A$	$A - A_\infty$	$\log \frac{A_o - A}{A - A_\infty}$	log[Py]
1.185	0	0	0.249	———	———
1.175	4.94×10^{-5}	0.010	0.239	-1.378	-4.306
1.164	9.84×10^{-5}	0.021	0.228	-1.036	-4.007
1.138	1.95×10^{-4}	0.037	0.212	-0.759	-3.709
1.068	3.85×10^{-4}	0.099	0.150	-0.180	-3.415
1.047	7.46×10^{-4}	0.138	0.111	0.095	-3.127
1.003	1.41×10^{-3}	0.183	0.066	0.442	-2.852
0.941	2.53×10^{-3}	0.244	0.005	1.689	-2.597
0.936	2.62×10^{-2}	0.249	0	———	———

APPENDIX IIIh. DMF + CoDBrDIXDME $\rightleftharpoons$ DMFCoDBrDIXDME

Temperature = 5°C

A (535 nm)	[DMF]	$A - A_o$	$A_\infty - A$	$\log \frac{A - A_o}{A_\infty - A}$	log[DMF]
0.677	0	0	0.386	———	———
0.697	0.00259	0.020	0.366	-1.262	-2.587
0.700	0.00778	0.023	0.363	-1.198	-2.109
0.719	0.0258	0.042	0.344	-0.913	-1.589
0.740	0.0518	0.063	0.323	-0.709	-1.286
0.760	0.129	0.083	0.303	-0.562	-0.891
0.782	0.255	0.105	0.281	-0.428	-0.594
0.838	0.499	0.161	0.225	-0.145	-0.302
0.923	1.18	0.246	0.140	0.245	0.072
0.963	2.16	0.286	0.100	0.456	0.335
1.044	6.49	0.367	0.019	1.286	0.812

A_∞ estimated to be 1.063

Temperature = 22°C

A (535 nm)	[DMF]	$A - A_o$	$A_\infty - A$	$\log \frac{A - A_o}{A_\infty - A}$	log[DMF]
0.580	0	0	0.278	———	———
0.590	0.0258	0.010	0.268	-1.428	-1.589
0.593	0.0518	0.013	0.265	-1.325	-1.286
0.605	0.129	0.025	0.253	-1.005	-0.891
0.630	0.259	0.050	0.228	-0.659	-0.594
0.670	0.499	0.090	0.188	-0.320	-0.302
0.733	1.18	0.153	0.125	0.088	0.072
0.770	2.16	0.190	0.088	0.334	0.335
0.803	3.71	0.223	0.055	0.608	0.569
0.828	6.49	0.248	0.030	0.917	0.812

A_∞ estimated to be 0.858

Temperature = 40°C

A (535 nm)	[DMF]	$A - A_o$	$A_\infty - A$	$\log \frac{A - A_o}{A_\infty - A}$	log[DMF]
0.827	0	0	0.450	———	———
0.837	0.0518	0.010	0.440	-1.643	-1.286
0.852	0.129	0.025	0.425	-1.230	-0.891
0.877	0.259	0.050	0.400	-0.903	-0.594
0.911	0.499	0.084	0.366	-0.639	-0.302
0.972	1.18	0.145	0.305	-0.323	0.072
1.016	2.16	0.189	0.261	-0.140	0.335
1.077	3.71	0.250	0.200	0.097	0.569
1.127	6.49	0.300	0.150	0.301	0.812

A_∞ estimated to be 1.277

APPENDIX IV

RAW DATA USED FOR DETERMINING THE THERMODYNAMIC PARAMETERS OF REVERSIBLE DIOXYGEN BINDING TO LCoDADIXDME AND LCoDBrDIXDME

APPENDIX IVa. CH_3-ImCoDADIXDME + $O_2 \rightleftharpoons$ CH_3-ImCoDADIXDME(O_2)

Temperature = -63.5°C

A (591 nm)	P_{O_2}	$A - A_o$	$A_\infty - A$	$\log \frac{A - A_o}{A_\infty - A}$	$\log P_{O_2}$
0.760	0	0	0.448	———	———
0.850	8	0.070	0.378	-0.732	0.903
0.890	20	0.130	0.318	-0.388	1.301
1.005	55	0.245	0.213	0.081	1.740
1.085	95	0.325	0.123	0.422	1.978
1.143	150	0.383	0.065	0.770	2.176
1.178	247	0.418	0.030	1.144	2.392
1.208	833	0.448	0	———	

Temperature = -56.5°C *

A (591 nm)	P_{O_2}	$A - A_o$	$A_\infty - A$	$\log \frac{A - A_o}{A_\infty - A}$	$\log P_{O_2}$
0.670	0	0	0.410	———	———
0.710	12	0.040	0.370	-0.966	1.079
0.770	26	0.100	0.310	-0.491	1.415
0.831	50	0.161	0.249	-0.189	1.699
0.904	100	0.234	0.176	0.124	2.000
0.964	190	0.297	0.113	0.420	2.279
1.018	388	0.348	0.062	0.749	2.589
1.080	845	0.410	0	———	2.927

* Data used for Figure VI.1

Temperature = -45°C

A (591 nm)	P_{O_2}	$A - A_o$	$A_\infty - A$	$\log \frac{A - A_o}{A_\infty - A}$	$\log P_{O_2}$
0.543	0	0	0.394	———	———
0.559	10	0.016	0.370	-1.373	1.000
0.580	28	0.046	0.348	-0.879	1.447
0.656	60	0.093	0.301	-0.510	1.778
0.697	99	0.134	0.260	-0.208	1.996
0.738	149	0.175	0.219	-0.097	2.173
0.775	228	0.212	0.182	0.066	2.358
0.846	350	0.283	0.111	0.406	2.544
0.878	513	0.315	0.079	0.601	2.710
0.957	825	0.394	0	———	2.916

Temperature = $-23^{o}C$

A (591 nm)	P_{O_2}	$A - A_o$	$A_\infty - A$	$\log \frac{A - A_o}{A_\infty - A}$	$\log P_{O_2}$
0.560	0	0	0.390	———	———
0.565	19	0.005	0.385	-1.886	1.279
0.591	50	0.031	0.359	-1.064	1.699
0.599	100	0.039	0.351	-0.954	2.000
0.665	201	0.105	0.285	-0.434	2.303
0.721	300	0.161	0.229	-0.153	2.477
0.782	448	0.222	0.168	0.121	2.651
0.821	828	0.261	0.129	0.306	2.918

A_∞ estimated to be 0.950

APPENDIX IVb. PipCoDADIXDME + $O_2 \rightleftharpoons$ PipCoDADIXDME(O_2)

Temperature = -63.5°C

A (589 nm)	P_{O_2}	$A - A_o$	$A_\infty - A$	$\log \frac{A - A_o}{A_\infty - A}$	$\log P_{O_2}$
0.450	0	0	0.423	———	———
0.463	10	0.013	0.410	-1.499	1.000
0.479	20	0.029	0.394	-1.133	1.301
0.512	40	0.062	0.361	-0.765	1.602
0.588	80	0.134	0.289	-0.334	1.903
0.669	142	0.219	0.204	0.034	2.152
0.747	262	0.297	0.126	0.372	2.418
0.848	451	0.398	0.025	1.202	2.654
0.873	843	0.423	0	———	2.926

Temperature = -56.5°C

A (589 nm)	P_{O_2}	$A - A_o$	$A_\infty - A$	$\log \frac{A - A_o}{A_\infty - A}$	$\log P_{O_2}$
0.470	0	0	0.405	———	———
0.489	12	0.019	0.386	-1.308	1.079
0.494	26	0.024	0.381	-1.201	1.415
0.519	50	0.049	0.356	-0.861	1.716
0.560	100	0.090	0.315	-0.544	1.991
0.641	190	0.171	0.234	-0.136	2.290
0.767	388	0.297	0.108	0.439	2.592
0.827	845	0.357	0.048	0.871	2.927

A estimated to be 0.875

Temperature = -45°C

A (589 nm)	P_{O_2}	$A - A_o$	$A_\infty - A$	$\log \frac{A - A_o}{A_\infty - A}$	$\log P_{O_2}$
0.520	0	0	0.455	———	———
0.520	20	0	0.455	———	1.301
0.522	40	0.002	0.453	-2.355	1.602
0.559	80	0.039	0.416	-1.028	1.902
0.615	155	0.095	0.360	-0.579	2.190
0.691	295	0.171	0.284	-0.220	2.470
0.737	485	0.217	0.238	-0.040	2.668
0.860	847	0.340	0.115	0.471	2.928

A_∞ estimated to be 0.975

Temperature = $-23^{\circ}C$

A (589 nm)	P_{O_2}	$A - A_o$	$A_\infty - A$	$\log \frac{A - A_o}{A_\infty - A}$	$\log P_{O_2}$
0.540	0	0	0.460	———	———
0.560	39	0.020	0.440	-1.342	1.591
0.560	105	0.020	0.440	-1.342	2.021
0.571	201	0.031	0.429	-1.146	2.312
0.600	398	0.060	0.400	-0.824	2.600
0.717	843	0.177	0.283	-0.204	2.926

A_∞ estimated to be 1.000

APPENDIX IVc. PyCoDADIXDME + $O_2 \rightleftharpoons$ PyCoDADIXDME(O_2)

Temperature = -78°C

A (590 nm)	P_{O_2}	$A - A_o$	$A_\infty - A$	$\log \frac{A - A_o}{A_\infty - A}$	$\log P_{O_2}$
0.655	0	0	0.465	———	———
0.735	20	0.080	0.385	-0.682	1.301
0.773	44	0.118	0.347	-0.468	1.643
0.806	84	0.151	0.314	-0.318	1.924
0.960	160	0.305	0.160	0.280	2.204
1.081	316	0.426	0.039	1.038	2.500
1.120	840	0.465	0	———	———

Temperature = -63.5°C

A (590 nm)	P_{O_2}	$A - A_o$	$A_\infty - A$	$\log \frac{A - A_o}{A_\infty - A}$	$\log P_{O_2}$
0.800	0	0	0.440	———	———
0.800	17	0	0.440	———	1.230
0.839	51	0.039	0.401	-1.012	1.708
0.877	105	0.077	0.363	-0.673	2.021
0.943	198	0.143	0.297	-0.317	2.297
1.024	400	0.224	0.216	0.016	2.602
1.120	845	0.320	0.120	0.437	2.927

A_∞ estimated to be 1.240

Temperature = -56.5°C

A (590 nm)	P_{O_2}	$A - A_o$	$A_\infty - A$	$\log \frac{A - A_o}{A_\infty - A}$	$\log P_{O_2}$
0.500	0	0	0.430	———	———
0.500	25	0	0.430	———	1.398
0.512	50	0.012	0.418	-1.542	1.699
0.558	103	0.058	0.372	-0.807	2.013
0.612	195	0.112	0.318	-0.453	2.290
0.684	397	0.184	0.246	-0.126	2.599
0.775	845	0.275	0.155	0.249	2.927

A_∞ estimated to be 0.930

Temperature = $-45^{\circ}C$

A (590 nm)	P_{O_2}	$A - A_o$	$A_\infty - A$	$\log \frac{A - A_o}{A_\infty - A}$	$\log P_{O_2}$
0.620	0	0	0.420	———	———
0.626	55	0.006	0.414	-1.839	1.740
0.650	100	0.030	0.390	-1.114	2.000
0.681	197	0.061	0.359	-0.770	2.294
0.631	390	0.111	0.309	-0.445	2.591
0.815	845	0.195	0.215	-0.042	2.921

A_∞ estimated to be 1.040

APPENDIX IVd. DMFCoDADIXDME + $O_2 \rightleftharpoons$ DMFCoDADIXDME(O_2)

Temperature = -78°C

A (588 nm)	P_{O_2}	$A - A_o$	$A_\infty - A$	$\log \frac{A - A_o}{A_\infty - A}$	$\log P_{O_2}$
0.580	0	0	0.212	———	———
0.623	6	0.043	0.169	-0.594	0.778
0.690	16	0.110	0.102	0.033	1.204
0.747	50	0.167	0.055	0.482	1.699
0.777	118	0.197	0.015	1.118	2.072
0.792	338	0.212	0	———	2.529
0.792	855	0.212	0	———	2.932

Temperature = -63.5°C

A (588 nm)	P_{O_2}	$A - A_o$	$A_\infty - A$	$\log \frac{A - A_o}{A_\infty - A}$	$\log P_{O_2}$
0.630	0	0	0.330	———	———
0.695	12	0.065	0.265	-0.610	1.079
0.778	40	0.148	0.188	-0.104	1.602
0.873	96	0.243	0.087	0.446	1.982
0.943	220	0.313	0.017	1.265	2.342
0.960	860	0.330	0	———	2.934

Temperature = -45°C

A (588 nm)	P_{O_2}	$A - A_o$	$A_\infty - A$	$\log \frac{A - A_o}{A_\infty - A}$	$\log P_{O_2}$
0.610	0	0	0.287	———	———
0.640	26	0.030	0.257	-0.933	1.415
0.705	64	0.095	0.192	-0.305	1.806
0.797	163	0.187	0.100	0.272	2.212
0.843	365	0.233	0.054	0.635	2.562
0.897	850	0.287	0	———	2.929

APPENDIX IVe. CH_3-ImDBrDIXDME + $O_2 \rightleftharpoons$ CH_3-ImDBrDIXDME(O_2)

Temperature = -78°C

A (569 nm)	P_{O_2}	$A - A_o$	$A_\infty - A$	$\log \frac{A - A_o}{A_\infty - A}$	$\log P_{O_2}$
0.590	0	0	0.635	———	———
0.909	10	0.319	0.316	0.004	1.000
0.974	17	0.384	0.251	0.185	1.230
1.133	50	0.543	0.092	0.771	1.699
1.170	100	0.580	0.055	1.023	2.000
1.225	845	0.635	0	———	2.927

Temeperature = -63.5°C

A (569 nm)	P_{O_2}	$A - A_o$	$A_\infty - A$	$\log \frac{A - A_o}{A_\infty - A}$	$\log P_{O_2}$
0.425	0	0	0.525	———	———
0.450	5.3	0.025	0.500	-1.301	0.724
0.521	16.5	0.096	0.429	-0.650	1.217
0.676	50	0.251	0.274	-0.038	1.699
0.796	125	0.371	0.154	0.382	2.097
0.919	390	0.494	0.031	1.202	2.591
0.950	845	0.525	0	———	2.927

Temperature = 56.5°C*

A (569 nm)	P_{O_2}	$A - A_o$	$A_\infty - A$	$\log \frac{A - A_o}{A_\infty - A}$	$\log P_{O_2}$
0.710	0	0	0.555	———	———
0.789	18	0.079	0.476	-0.780	1.255
0.807	25	0.097	0.458	-0.674	1.398
0.895	44	0.185	0.370	-0.301	1.643
1.040	106	0.330	0.225	0.166	2.025
1.156	259	0.446	0.109	0.612	2.413
1.215	637	0.505	0.050	1.004	2.804
1.243	845	0.533	0.022	1.384	2.927

A_∞ estimated to be 1.265

* Data used for Figure VI.2.

Temperature = $-45^{\circ}C$

A (569 nm)	P_{O_2}	$A - A_o$	$A_\infty - A$	$\log \frac{A - A_o}{A_\infty - A}$	$\log P_{O_2}$
0.300	0	0	0.545	———	———
0.323	20	0.023	0.522	-1.356	1.301
0.438	50	0.138	0.407	-0.470	1.699
0.530	98	0.230	0.315	-0.137	1.991
0.641	195	0.341	0.204	0.223	2.290
0.728	387	0.428	0.117	0.563	2.588
0.800	845	0.500	0.045	1.046	2.927

A_∞ estimated to be 0.845

Temperature = $-23^{\circ}C$

A (569 nm)	P_{O_2}	$A - A_o$	$A_\infty - A$	$\log \frac{A - A_o}{A_\infty - A}$	$\log P_{O_2}$
0.395	0	0	0.435	———	———
0.410	48	0.015	0.420	-1.447	1.681
0.455	107	0.060	0.365	-0.717	2.029
0.517	195	0.122	0.313	-0.409	2.290
0.570	386	0.175	0.260	-0.172	2.587
0.660	855	0.265	0.170	0.193	2.932

A_∞ estimated to be 0.830

APPENDIX IVf. PipCoDBrDIXDME + $O_2 \rightleftharpoons$ PipCoDBrDIXDME(O_2)

Temperature = -78°C

A (568 nm)	P_{O_2}	$A - A_o$	$A_\infty - A$	$\log \frac{A - A_o}{A_\infty - A}$	$\log P_{O_2}$
0.445	0	0	0.527	———	———
0.423	3.3	0.022	0.505	-1.361	0.519
0.501	10	0.056	0.471	-0.925	1.000
0.601	30	0.156	0.371	-0.376	1.477
0.767	96	0.322	0.205	0.196	1.968
0.894	267	0.449	0.078	0.760	2.427
0.952	501	0.507	0.020	1.404	2.700
0.972	845	0.527	0	———	2.927

Temperature = -63.5°C

A (568 nm)	P_{O_2}	$A - A_o$	$A_\infty - A$	$\log \frac{A - A_o}{A_\infty - A}$	$\log P_{O_2}$
0.368	0	0	0.577	———	———
0.368	11	0	0.577	———	1.041
0.423	37	0.055	0.522	-0.977	1.568
0.468	87	0.100	0.477	-0.679	1.940
0.633	194	0.265	0.312	-0.071	2.288
0.771	454	0.403	0.174	0.365	2.657
0.847	845	0.479	0.098	0.689	2.927

A_∞ estimated to be 0.945

Temperature = -56.5°C

A (568 nm)	P_{O_2}	$A - A_o$	$A_\infty - A$	$\log \frac{A - A_o}{A_\infty - A}$	$\log P_{O_2}$
0.470	0	0	0.530	———	———
0.494	12	0.024	0.506	-1.324	1.079
0.501	26	0.031	0.499	-1.207	1.415
0.534	52	0.064	0.466	-0.862	1.716
0.588	98	0.118	0.412	-0.542	1.991
0.650	195	0.180	0.350	-0.289	2.290
0.767	391	0.297	0.233	0.105	2.592
0.859	845	0.389	0.141	0.441	2.927

A_∞ estimated to be 1.000

Temperature = -45°C

A (568 nm)	P_{O_2}	$A - A_o$	$A_\infty - A$	$\log \frac{A - A_o}{A_\infty - A}$	$\log P_{O_2}$
0.400	0	0	0.580	———	———
0.400	47	0	0.580	———	1.672
0.437	100	0.037	0.543	-1.163	2.090
0.455	168	0.055	0.525	-0.980	2.225
0.556	286	0.156	0.424	-0.434	2.456
0.700	849	0.300	0.280	0.030	2.929

A_∞ estimated to be 0.980

Temperature =-23°C

A (568 nm)	P_{O_2}	$A - A_o$	$A_\infty - A$	$\log \frac{A - A_o}{A_\infty - A}$	$\log P_{O_2}$
0.345	0	0	0.500	———	———
0.345	96	0	0.500	———	1.982
0.363	195	0.017	0.483	-1.453	2.290
0.399	394	0.054	0.446	-0.917	2.595
0.455	845	0.110	0.390	-0.550	2.927

A_∞ estimated to be 0.845

APPENDIX IVg. $PyCoDBrDIXDME + O_2 \rightleftharpoons PyCoDBrDIXDME(O_2)$

Temperature = -78°C

A (569 nm)	P_{O_2}	$A - A_o$	$A_\infty - A$	$\log \frac{A - A_o}{A_\infty - A}$	$\log P_{O_2}$
0.660	0	0	0.627	———	———
0.728	20	0.068	0.559	-0.915	1.301
0.832	51	0.172	0.455	-0.424	1.708
0.899	98	0.239	0.388	-0.210	1.991
1.023	198	0.363	0.264	0.138	2.297
1.119	410	0.459	0.168	0.437	2.613
1.287	845	0.627	0	———	2.927

Temperature = -63.5°C

A (569 nm)	P_{O_2}	$A - A_o$	$A_\infty - A$	$\log \frac{A - A_o}{A_\infty - A}$	$\log P_{O_2}$
0.755	0	0	0.695	———	———
0.831	46	0.076	0.619	-0.911	1.663
0.910	102	0.155	0.540	-0.543	2.009
1.005	198	0.250	0.445	-0.250	2.297
1.188	396	0.433	0.262	0.218	2.598
1.450	845	0.695	0	———	2.927

Temperature = -56.5°C

A (569 nm)	P_{O_2}	$A - A_o$	$A_\infty - A$	$\log \frac{A - A_o}{A_\infty - A}$	$\log P_{O_2}$
0.613	0	0	0.587	———	———
0.656	73	0.043	0.544	-1.102	1.857
0.743	164	0.130	0.457	-0.546	2.215
0.867	382	0.254	0.333	-0.118	2.582
0.998	845	0.385	0.202	0.280	2.927

A_∞ estimated to be 1.200

Temperature = -45°C

A (569 nm)	P_{O_2}	$A - A_o$	$A_\infty - A$	$\log \frac{A - A_o}{A_\infty - A}$	$\log P_{O_2}$
0.470	0	0	0.430	———	———
0.475	10	0.005	0.425	-1.929	1.000
0.488	45	0.018	0.412	-1.360	1.653
0.536	185	0.066	0.364	-0.742	2.267
0.686	845	0.216	0.214	0.004	2.927

A_∞ estimated to be 0.900

APPENDIX IVh. DMFCoDBrDIXDME + $O_2 \rightleftharpoons$ DMFCoDBrDIXDME(O_2)

Temperature = -78°C

A (571 nm)	P_{O_2}	$A - A_o$	$A_\infty - A$	$\log \frac{A - A_o}{A_\infty - A}$	$\log P_{O_2}$
0.278	0	0	0.274	———	———
0.320	11	0.042	0.232	-0.742	1.041
0.356	20	0.078	0.196	-0.400	1.301
0.400	40	0.122	0.154	-0.101	1.602
0.452	80	0.174	0.100	0.241	1.903
0.508	152	0.230	0.044	0.718	2.182
0.530	325	0.252	0.022	1.059	2.512
0.552	860	0.274	0	———	2.934

Temperature = -63.5°C

A (571 nm)	P_{O_2}	$A - A_o$	$A_\infty - A$	$\log \frac{A - A_o}{A_\infty - A}$	$\log P_{O_2}$
0.170	0	0	0.835	———	———
0.220	10	0.050	0.785	-1.196	1.000
0.335	24	0.165	0.670	-0.609	1.380
0.525	61	0.355	0.480	-0.131	1.785
0.710	118	0.540	0.295	0.263	2.072
0.860	243	0.690	0.145	0.677	2.387
0.947	528	0.777	0.058	1.127	2.723
1.005	845	0.835	0	———	2.927

NOTE: A reference screen (A = 0.29) was used during this run.

Temperature = -45°C

A (571 nm)	P_{O_2}	$A - A_o$	$A_\infty - A$	$\log \frac{A - A_o}{A_\infty - A}$	$\log P_{O_2}$
0.427	0	0	0.617	———	———
0.440	7	0.013	0.604	-1.667	0.845
0.497	20	0.070	0.547	-0.893	1.301
0.605	55	0.128	0.489	-0.582	1.740
0.810	170	0.383	0.234	0.214	2.230
0.934	537	0.507	0.110	0.664	2.730
1.044	860	0.617	0	———	2.934

APPENDIX V

RAW DATA USED FOR DETERMINING THE KINETICS OF OXIDATION OF COBALT PORPHYRIN COMPLEXES

Note: Final data points were sometimes not considered in determining rate constants if the experimental error for those points was judged to be high.

APPENDIX Va. CoOMBP Aggrregation Data with Toluene as a Solvent

CoOMBP

$[Co_T]$, M	ε	$\frac{\varepsilon_o - \varepsilon}{\varepsilon_o - \varepsilon_\infty}$	$\frac{\varepsilon - \varepsilon_\infty}{\varepsilon_o - \varepsilon_\infty}$	[CoP]	$[nCoP_n]$	log [CoP]	log n + log $[CoP_n]$
5.7×10^{-6}	5.53×10^{4}	0.176	0.824	4.70×10^{-6}	1.00×10^{-6}	-5.33	-6.00
1.19×10^{-5}	5.28×10^{4}	0.242	0.758	9.02×10^{-6}	2.88×10^{-6}	-5.04	-5.54
1.77×10^{-5}	5.04×10^{4}	0.306	0.694	1.23×10^{-5}	5.72×10^{-6}	-4.91	-5.27
2.9×10^{-5}	5.00×10^{4}	0.316	0.684	1.98×10^{-5}	9.16×10^{-6}	-4.70	-5.04
4.6×10^{-5}	4.56×10^{4}	0.432	0.568	2.61×10^{-5}	1.99×10^{-5}	-4.58	-4.70
8.9×10^{-5}	4.14×10^{4}	0.542	0.458	4.08×10^{-5}	4.82×10^{-5}	-4.39	-4.32
1.67×10^{-4}	3.71×10^{4}	0.655	0.345	5.76×10^{-5}	1.09×10^{-4}	-4.24	-3.96
2.9×10^{-4}	3.38×10^{4}	0.742	0.258	7.48×10^{-5}	2.16×10^{-4}	-4.13	-3.67
4.5×10^{-4}	3.21×10^{4}	0.787	0.213	9.59×10^{-5}	3.54×10^{-4}	-4.02	-3.45

Data used in Figure VII.6; trace with $\varepsilon = 5.00 \times 10^{4}$ $M^{-1}cm^{-1}$ not ijcluded in Figure VII.6 as it is so similar to trace with $\varepsilon = 5.04 \times 10^{4}$ $M^{-1}cm^{-1}$.

CH_3-ImCoOMBP

$[CH_3\text{-ImCoOMBP}]$, M	log $[CH_3\text{-ImCoOMBP}]$	$\varepsilon_{408\ nm}$	$\varepsilon_{618\ nm}$
5.7×10^{-6}	-5.24	4.79×10^4	3.64×10^4
1.19×10^{-5}	-4.92	4.62×10^4	3.70×10^4
2.35×10^{-5}	-4.63	4.69×10^4	3.64×10^4
4.06×10^{-5}	-4.39	4.69×10^4	3.73×10^4
4.6×10^{-5}	-4.34	4.90×10^4	3.48×10^4
8.9×10^{-5}	-4.05	4.81×10^4	3.54×10^4
1.67×10^{-4}	-3.77	4.88×10^4	3.49×10^4
3.84×10^{-4}	-3.42	4.65×10^4	3.33×10^4

Data used in Figure VII.8

$(CH_3\text{-Im})_2$CoOMBP

$[(CH_3\text{-Im})_2\text{CoOMBP}]$, M	log $[(CH_3\text{-Im})_2\text{CoOMBP}]$	$\varepsilon_{437\ nm}$	$\varepsilon_{456\ nm}$	$\varepsilon_{619\ nm}$
6.0×10^{-6}	-5.22	7.57×10^4	4.89×10^4	3.43×10^4
1.19×10^{-5}	-4.93	8.18×10^4	4.34×10^4	3.44×10^4
2.35×10^{-5}	-4.63	6.91×10^4	4.73×10^4	3.28×10^4
4.6×10^{-5}	-4.34	———	———	3.30×10^4
4.8×10^{-5}	-4.32	7.30×10^4	4.87×10^4	3.46×10^4
9.6×10^{-5}	-4.02	6.72×10^4	4.61×10^4	3.21×10^4
1.92×10^{-4}	-3.72	6.91×10^4	4.87×10^4	3.22×10^4
3.8×10^{-4}	-3.42	———	4.74×10^4	3.22×10^4

Data used Figure VII.9

ε measured in $M^{-1}cm^{-1}$

APPENDIX Vb. CoOMBP Aggregation Data with DCE as a Solvent

CoOMBP

Co_T , M	ε	$\frac{\varepsilon_o - \varepsilon}{\varepsilon_o - \varepsilon_\infty}$	$\frac{\varepsilon - \varepsilon_\infty}{\varepsilon_o - \varepsilon_\infty}$	CoP	$nCoP_n$	log CoP	log n + log CoP_n
1.19×10^{-5}	5.01×10^{4}	0.316	0.684	8.14×10^{-6}	3.76×10^{-6}	-5.09	-5.43
2.35×10^{-5}	4.62×10^{4}	0.421	0.579	1.36×10^{-5}	9.88×10^{-6}	-4.87	-5.01
4.62×10^{-5}	4.03×10^{4}	0.571	0.429	1.98×10^{-5}	2.64×10^{-5}	-4.70	-4.58
1.09×10^{-4}	4.23×10^{4}	0.518	0.482	5.25×10^{-5}	5.64×10^{-5}	-4.28	-4.25
2.0×10^{-4}	3.94×10^{4}	0.594	0.406	8.12×10^{-5}	1.19×10^{-4}	-4.08	-3.92
3.43×10^{-4}	3.66×10^{4}	0.673	0.327	1.12×10^{-4}	2.30×10^{-4}	-3.95	-3.64

CH_3-ImCoOMBP

[CH_3-ImCoOMBP] , M	log[CH_3-ImCoOMBP]	$\varepsilon_{408\ nm}$	$\varepsilon_{618\ nm}$
1.19×10^{-5}	-4.92	5.01×10^4	4.24×10^4
2.35×10^{-5}	-4.63	4.62×10^4	3.97×10^4
4.62×10^{-5}	-4.34	4.33×10^4	3.73×10^4
1.09×10^{-4}	-3.96	4.53×10^4	3.63×10^4
2.0×10^{-4}	-3.70	4.44×10^4	3.57×10^4
3.43×10^{-4}	-3.46	4.26×10^4	3.47×10^4

Py_2CoOMBP

[Py_2CoOMBP] , M	log[Py_2CoOMBP]	$\varepsilon_{427\ nm}$	$\varepsilon_{617\ nm}$
1.20×10^{-5}	-4.92	7.65×10^4	3.69×10^4
2.40×10^{-5}	-4.62	7.50×10^4	3.63×10^4
4.80×10^{-5}	-4.32	7.91×10^4	3.65×10^4
9.59×10^{-5}	-4.02	7.77×10^4	3.65×10^4
1.92×10^{-4}	-3.72	7.67×10^4	3.62×10^4
3.84×10^{-4}	-3.42	7.38×10^4	3.56×10^4

ε measured in $M^{-1}cm^{-1}$

APPENDIX V c $\quad ImCoOMBP + O_2 \longrightarrow ImCoOMBP(O_2)CoOMBP \cdot Im$

As a function of oxygen pressure.

$[Co] = 1.9 \times 10^{-5}$ M; $[Im] = 1.46 \times 10^{-3}$ M; $T = 22^{\circ}C$; $P_{O_2} = 54$ Torr

A (408 nm)	t (sec)	$A_o - A$	$A - A_\infty$	$\ln A - A_\infty$
0.963	0	0	0.750	-0.288
0.777	45	0.186	0.564	-0.573
0.717	100	0.246	0.504	-0.685
0.647	174	0.316	0.434	-0.835
0.583	258	0.380	0.370	-0.994
0.539	346	0.414	0.336	-1.091
0.473	484	0.490	0.260	-1.347
0.413	670	0.550	0.200	-1.609
0.360	918	0.603	0.147	-1.917
0.323	1175	0.640	0.110	-2.207
0.290	1523	0.673	0.077	-2.564
0.250	3005	0.713	0.037	-3.297

A_∞ estimated to be 0.213

$[Co] = 1.8 \times 10^{-5}$ M; $[Im] = 1.46 \times 10^{-3}$ M; $T = 22^{\circ}C$; $P_{O_2} = 97$ Torr

A (408 nm)	t (sec)	$A_o - A$	$A - A_\infty$	$\ln A - A_\infty$
0.908	0	0	0.700	-0.357
0.638	61	0.270	0.430	-0.844
0.560	112	0.348	0.352	-1.044
0.483	192	0.425	0.275	-1.291
0.410	287	0.498	0.202	-1.599
0.370	362	0.528	0.172	-1.760
0.327	494	0.571	0.129	-2.048
0.287	629	0.621	0.079	-2.538
0.260	773	0.648	0.052	-2.957
0.240	1003	0.668	0.032	-3.442
0.225	1512	0.683	0.017	-4.075

A_∞ estimated to be 0.208

$[Co] = 1.8 \times 10^{-5}$ M; $[Im] = 1.46 \times 10^{-3}$ M; $T = 22^{o}C$; P_{O_2} = 147 Torr

A (408 nm)	t (sec)	$A_o - A$	$A - A_\infty$	ln $A - A_\infty$
0.913	0	0	0.700	-0.357
0.630	47	0.283	0.417	-0.875
0.569	85	0.344	0.356	-1.033
0.507	132	0.406	0.294	-1.224
0.465	171	0.448	0.252	-1.378
0.412	232	0.501	0.199	-1.614
0.354	319	0.559	0.141	-1.959
0.303	429	0.610	0.090	-2.408
0.280	552	0.633	0.067	-2.703
0.250	727	0.663	0.037	-3.297
0.225	1074	0.688	0.012	-4.423

A_∞ estimated to be 0.713

$[Co] = 1.7 \times 10^{-5}$ M $[Im] = 1.46 \times 10^{-3}$ M; $T = 22^{o}C$; P_{O_2} = 190 Torr

A (408 nm)	t (sec)	$A_o - A$	$A - A_\infty$	ln $A - A_\infty$
0.830	0	0	0.600	-0.511
0.650	39	0.180	0.420	-0.868
0.573	76	0.257	0.347	-1.058
0.533	110	0.297	0.307	-1.181
0.450	175	0.380	0.220	-1.514
0.405	248	0.425	0.175	-1.743
0.350	350	0.480	0.120	-2.120
0.295	478	0.535	0.065	-2.733
0.275	625	0.555	0.045	-3.101
0.235	915	0.595	0.005	-5.298

A_∞ estimated to be 0.230

$[Co] = 1.8 \times 10^{-5}$ M $[Im] = 1.46 \times 10^{-3}$ M; $T = 22^{o}C$; P_{O_2} = 278 Torr

A (408 nm)	t (sec)	$A_o - A$	$A - A_\infty$	ln $A - A_\infty$
0.900	0	0	0.650	-0.431
0.608	46	0.292	0.358	-1.027
0.525	82	0.375	0.275	-1.291
0.462	117	0.438	0.212	-1.551
0.395	172	0.505	0.145	-1.931
0.347	235	0.553	0.097	-2.333
0.310	327	0.590	0.060	-2.813
0.270	455	0.630	0.020	-3.912
0.255	947	0.645	0.005	-5.298

A_∞ estimarted to be 0.250

APPENDIX Vd. $ImCoOMBP + O_2 \longrightarrow ImCoOMBP(O_2)CoOMBP \cdot Im$

As a function of ligand concentration.

$[Co] = 1.6 \times 10^{-5}$ M; $[Im] = 2.2 \times 10^{-4}$ M; $T = 22^{\circ}C$; $P_{O_2} = 95$ Torr

A (408 nm)	t (sec)	$A_o - A$	$A - A_\infty$	$\ln A - A_\infty$
0.765	0	0	0.550	-0.598
0.689	56	0.076	0.474	-0.747
0.657	132	0.108	0.442	-0.816
0.607	263	0.158	0.392	-0.936
0.562	416	0.203	0.347	-1.058
0.518	619	0.247	0.303	-1.194
0.463	913	0.302	0.248	-1.394
0.388	1462	0.377	0.173	-1.754
0.325	2436	0.440	0.110	-2.207
0.280	4431	0.485	0.065	-2.733
0.240	8423	0.525	0.025	-3.689

A_∞ estimated to be 0.215

$[Co] = 1.7 \times 10^{-5}$ M; $[Im] = 4.4 \times 0^{-4}$M; $T = 22^{\circ}C$; $P_{O_2} = 95$ Torr

A (408 nm)	t (sec)	$A_o - A$	$A - A_\infty$	$\ln A - A_\infty$
0.830	0	0	0.585	-0.536
0.732	55	0.098	0.487	-0.719
0.699	101	0.131	0.454	-0.790
0.647	187	0.183	0.402	-0.911
0.580	298	0.250	0.335	-1.094
0.520	410	0.310	0.275	-1.291
0.498	534	0.332	0.253	-1.374
0.425	747	0.405	0.180	-1.715
0.380	1030	0.450	0.135	-2.002
0.317	1645	0.513	0.072	-2.631
0.268	2762	0.562	0.023	-3.772
0.245	5129	0.585	0	

[Co] = 1.8×10^{-5} M; [Im] = 7.3×10^{-4} M; T = 22°C; P_{O_2} = 96 Torr

A (408 nm)	t (sec)	$A_o - A$	$A - A_\infty$	ln $A - A_\infty$
0.880	0	0	0.650	-0.431
0.697	52	0.183	0.467	-0.761
0.640	99	0.240	0.410	-0.892
0.592	150	0.288	0.362	-1.016
0.542	221	0.338	0.312	-1.165
0.487	312	0.393	0.257	-1.359
0.428	428	0.452	0.198	-1.619
0.379	570	0.501	0.149	-1.904
0.342	767	0.538	0.112	-2.189
0.300	1031	0.580	0.070	-2.659
0.273	1503	0.607	0.043	-3.147
0.245	3149	0.635	0.015	-4.200

A_∞ estimated to be 0.230

[Co] = 1.7×10^{-5} M; [Im] = 9.2×10^{-4} M; T = 22°C; P_{O_2} = 95 Torr

A (408 nm)	t (sec)	$A_o - A$	$A - A_\infty$	ln $A - A_\infty$
0.837	0	0	0.587	-0.533
0.635	63	0.202	0.385	-0.955
0.570	158	0.267	0.320	-1.139
0.505	253	0.332	0.255	-1.366
0.450	358	0.387	0.200	-1.609
0.403	474	0.434	0.153	-1.877
0.370	607	0.467	0.120	-2.120
0.340	744	0.497	0.090	-2.408
0.315	930	0.522	0.065	-2.733
0.284	1318	0.553	0.034	-3.381
0.270	2116	0.567	0.020	-3.912
0.250	3535	0.587	0	———

[Co] = 1.8×10^{-5} M; [Im] 14.6 $\times 10^{-4}$ M; T = 22°C; P_{O_2} = 97 Torr

A (408 nm)	t (sec)	$A_o - A$	$A - A_\infty$	ln $A - A_\infty$
0.908	0	0	0.700	-0.357
0.638	61	0.270	0.430	-0.844
0.560	112	0.348	0.352	-1.044
0.483	192	0.425	0.275	-1.291
0.410	287	0.498	0.202	-1.599
0.370	362	0.528	0.172	-1.760
0.327	494	0.571	0.129	-2.048
0.287	629	0.621	0.079	-2.538
0.260	773	0.648	0.052	-2.957
0.240	1003	0.668	0.032	-3.442
0.225	1512	0.683	0.017	-4.075

A_∞ estimated to be 0.208

$[Co] = 1.6 \times 10^{-5}$ M; $[Im] = 18.4 \times 10^{-4}$ M; $T = 22^{o}C$; P_{O_2} 95 = Torr

A (408 nm)	t (sec)	$A_o - A$	$A - A_\infty$	$\ln A - A_\infty$
0.752	0	0	0.532	-0.631
0.465	54	0.287	0.245	-1.406
0.420	96	0.332	0.200	-1.580
0.392	146	0.360	0.172	-1.760
0.345	228	0.407	0.125	-2.079
0.299	359	0.453	0.079	-2.538
0.250	598	0.502	0.030	-3.507
0.233	885	0.519	0.013	-4.343
0.220	1503	0.532	0	———

$[Co] = 1.7 \times 10^{-5}$ M; $[Im] = 29.2 \times 10^{-4}$ M; $T = 22^{o}C$; P_{O_2} = 95 Torr

A (408 nm)	t (sec)	$A_o - A$	$A - A_\infty$	$\ln A - A_\infty$
0.830	0	0	0.650	-0.431
0.523	52	0.307	0.347	-1.058
0.462	90	0.368	0.282	-1.266
0.397	146	0.437	0.213	-1.546
0.343	215	0.487	0.163	-1.814
0.280	311	0.550	0.100	-2.303
0.230	503	0.600	0.050	-2.996
0.190	960	0.640	0.010	-4.605

A_∞ estimated to be 0.180

APPENDIX V e. $ImCoOMBP + O_2 \longrightarrow ImCoOMBP(O_2)CoOMBP \cdot Im$

As a function of ligand concentration.

$[Co] = 2.0 \times 10^{-5}$ M; $[Im] = 0.55 \times 10^{-4}$ M; $T = 22^{\circ}C$; P_{O_2} = 395 Torr

A (408 nm)	t (sec)	$A_o - A$	$A - A_\infty$	$\ln A - A_\infty$
1.001	0	0	0.681	-0.384
0.813	49	0.188	0.493	-0.707
0.788	103	0.213	0.468	-0.759
0.760	170	0.241	0.440	-0.821
0.700	319	0.301	0.380	-0.968
0.648	530	0.353	0.328	-1.115
0.590	804	0.411	0.270	-1.309
0.527	1312	0.474	0.207	-1.575
0.477	1999	0.524	0.157	-1.852
0.412	3004	0.589	0.092	-2.386
0.372	5007	0.629	0.052	-2.957
0.355	9150	0.646	0.035	-3.352
0.320	24445	0.681	0	

$[Co] = 1.7 \times 10^{-5}$ M; $[Im] = 1.1 \times 10^{-4}$ M; $T = 22^{\circ}C$; P_{O_2} = 406 Torr

A (408 nm)	t (sec)	$A_o - A$	$A - A_\infty$	$\ln A - A_\infty$
0.859	0	0	0.600	-0.511
0.702	50	0.157	0.443	-0.814
0.677	96	0.182	0.418	-0.872
0.620	184	0.239	0.361	-1.019
0.572	315	0.287	0.313	-1.162
0.478	606	0.381	0.219	-1.519
0.407	1009	0.452	0.148	-1.911
0.380	1435	0.479	0.121	-2.112
0.338	2099	0.514	0.086	-2.453
0.320	3596	0.529	0.071	-2.645
0.305	7003	0.554	0.046	-3.079

A_∞ estimated to be 0.259

[Co] = 1.9×10^{-5} M; [Im] = 2.2×10^{-4} M; T = 22°C; P_{O_2} = 395 Torr

A (408 nm)	t (sec)	$A_o - A$	$A - A_\infty$	$\ln A - A_\infty$
0.941	0	0	0.650	-0.431
0.717	61	0.224	0.426	-0.853
0.669	103	0.272	0.378	-0.973
0.615	166	0.326	0.324	-1.127
0.555	249	0.386	0.264	-1.332
0.483	376	0.458	0.192	-1.650
0.417	505	0.524	0.126	-2.071
0.389	634	0.552	0.098	-2.323
0.350	897	0.591	0.059	-2.830
0.320	1502	0.621	0.029	-3.540
0.310	3010	0.631	0.019	-3.963

A_∞ estimated to be 0.291

[Co] = 1.7×10^{-5} M; [Im] = 4.4×10^{-4} M; T = 22°C; P_{O_2} = 397 Torr

A (408 nm)	t (sec)	$A_o - A$	$A - A_\infty$	$\ln A - A_\infty$
0.852	0	0	0.599	-0.512
0.632	74	0.220	0.379	-0.970
0.581	114	0.271	0.328	-1.115
0.513	184	0.339	0.260	-1.347
0.432	295	0.420	0.179	-1.720
0.363	422	0.489	0.110	-2.207
0.313	553	0.539	0.060	-2.813
0.292	702	0.560	0.039	-3.244
0.266	1007	0.586	0.013	-4.343
0.253	1603	0.599	0	

APPENDIX V f. $ImCoOMBP + O_2 \longrightarrow ImCoOMBP(O_2)CoOMBP \cdot Im$

As a function of ligand concentration

$[Co] = 1.8 \times 10^{-5}$ M; $[Im] = 0.15 \times 10^{-4}$ M; $T = 22^{\circ}C$; $P_{O_2} = 825$ Torr

A (410 nm)	t (sec)	$A_o - A$	$A - A_\infty$	$\ln A - A_\infty$
0.905	0	0	0.600	-0.511
0.830	59	0.075	0.525	-0.644
0.818	111	0.087	0.513	-0.667
0.800	239	0.105	0.495	-0.703
0.760	731	0.145	0.455	-0.787
0.738	1999	0.167	0.433	-0.837
0.672	4004	0.233	0.367	-1.002
0.620	7788	0.285	0.315	-1.155

A_∞ estimated to be 0.305

$[Co] = 1.9 \times 10^{-5}$ M; $[Im] = 0.23 \times 10^{-4}$ M; $T = 22^{\circ}C$; $P_{O_2} = 825$ Torr

A (410 nm)	t (sec)	$A_o - A$	$A - A_\infty$	$\ln A - A_\infty$
0.987	0	0	0.650	-0.431
0.873	54	0.114	0.536	-0.624
0.842	148	0.145	0.505	-0.683
0.803	351	0.184	0.466	-0.764
0.772	640	0.215	0.435	-0.832
0.720	1298	0.267	0.383	-0.960
0.657	2502	0.330	0.320	-1.134
0.578	5106	0.409	0.241	-1.423

A_∞ estimated to be 0.332

$[Co] = 1.7 \times 10^{-5}$ M; $[Im] = 0.3 \times 10^{-4}$ M; $T = 22^{\circ}C$; $P_{O_2} = 825$ Torr

A (410 nm)	t (sec)	$A_o - A$	$A - A_\infty$	$\ln A - A_\infty$
0.847	0	0	0.517	-0.660
0.680	82	0.167	0.350	-1.050
0.650	137	0.197	0.320	-1.139
0.587	266	0.260	0.257	-1.359
0.557	501	0.290	0.227	-1.483
0.523	1005	0.324	0.193	-1.645
0.507	2005	0.340	0.177	-1.716
0.475	4050	0.372	0.145	-1.931

A_∞ estimated to be 0.330

$[Co] = 1.6 \times 10^{-5}$ M; $[Im] = 0.6 \times 10^{-4}$ M; $T = 22^{\circ}C$; P_{O_2} = 825 Torr

A (410 nm)	t (sec)	$A_o - A$	$A - A_\infty$	$\ln A - A_\infty$
0.725	0	0	0.480	-0.734
0.594	60	0.131	0.349	-1.053
0.552	144	0.173	0.307	-1.181
0.495	257	0.230	0.250	-1.386
0.445	417	0.280	0.200	-1.609
0.396	623	0.329	0.151	-1.890
0.353	1022	0.372	0.108	-2.226
0.325	1824	0.400	0.080	-2.526
0.295	3443	0.430	0.050	-2.996

A_∞ estimated to be 0.245

$[Co] = 1.7 \times 10^{-5}$ M; $[Im] = 1.2 \times 10^{-4}$ M; $T = 22^{\circ}C$; P_{O_2} = 825 Torr

A (410 nm)	t (sec)	$A_o - A$	$A - A_\infty$	$\ln A - A_\infty$
0.820	0	0	0.520	-0.654
0.597	83	0.227	0.293	-1.228
0.557	146	0.267	0.253	-1.374
0.520	216	0.300	0.220	-1.514
0.485	302	0.335	0.185	-1.687
0.447	427	0.373	0.147	-1.917
0.392	598	0.428	0.092	-2.386
0.338	997	0.482	0.038	-3.270
0.308	1810	0.512	0.008	-4.828
0.301	3401	0.519	0.001	-6.908

A_∞ estimated to be 0.300

APPENDIX Vq. $ImCoOMBP + O_2 \longrightarrow ImCoOMBP(O_2)CoOMBP \cdot Im$

As a function of cobalt concentration

$[Co] = 0.06 \times 10^{-5}$ M; $[Im] = 18.4 \times 10^{-4}$ M; T = 22°C; P_{O_2} = 160 Torr

A (408 nm)	t (sec)	$A_o - A$	$A - A_\infty$	ln $A - A_\infty$	ln $[Co_T]$
0.370	0	0	0.182	-1.704	-14.326
0.340	35	0.030	0.152	-1.884	-14.506
0.292	108	0.078	0.104	-2.263	-14.885
0.238	251	0.132	0.050	-2.996	-15.618
0.198	559	0.172	0.010	-4.605	-17.227
0.188	1263	0.182	0		

$[Co] = 0.1 \times 10^{-5}$ M; $[Im] = 18.4 \times 10^{-4}$ M; T = 22°C; P_{O_2} = 160 Torr

A (408 nm)	t (sec)	$A_o - A$	$A - A_\infty$	ln $A - A_\infty$	ln $[Co_T]$
0.570	0	0	0.380	-0.968	-13.816
0.460	38	0.110	0.270	-1.309	-14.157
0.425	78	0.145	0.235	-1.448	-14.296
0.367	140	0.203	0.177	-1.732	-14.570
0.292	265	0.278	0.102	-2.283	-15.131
0.235	444	0.335	0.045	-3.101	-15.949
0.190	944	0.380	0		

$[Co] = 0.2 \times 10^{-5}$ M; $[Im] = 18.4 \times 10^{-4}$ M; T = 22°C; P_{O_2} = 160 Torr

A (408 nm)	t (sec)	$A_o - A$	$A - A_\infty$	ln $A - A_\infty$	ln $[Co_T]$
1.045	0	0	0.630	-0.462	-13.122
0.925	47	0.120	0.510	-0.673	-13.333
0.827	94	0.218	0.412	-0.887	-13.547
0.767	143	0.278	0.352	-1.044	-13.704
0.687	201	0.358	0.272	-1.302	-13.942
0.618	270	0.315	0.203	-1.595	-14.235
0.563	344	0.482	0.148	-1.911	-14.551
0.515	440	0.530	0.100	-2.303	-14.943
0.460	565	0.585	0.045	-3.101	-15.741
0.442	715	0.603	0.027	-3.612	-16.252
0.415	953	0.630	0		

$[Co] = 0.8 \times 10^{-5}$ M; $[Im] = 18.4 \times 10^{-4}$ M; T = 22°C; P_{O_2} = 100 Torr

A (408 nm)	t (sec)	$A_o - A$	$A - A_\infty$	ln $A - A_\infty$	ln $[Co_T]$
0.389	0	0	0.278	-1.280	-11.736
0.303	46	0.086	0.192	-1.650	-12.106
0.286	87	0.103	0.175	-1.742	-12.198
0.247	185	0.142	0.136	-1.995	-12.401
0.199	383	0.190	0.088	-2.430	-12.836
0.135	785	0.254	0.024	-3.730	-14.136
0.111	1586	0.278	0		

$[Co] = 1.6 \times 10^{-5}$ M; $[Im] = 18.4 \times 10^{-4}$ M; T = 22°C; P_{O_2} = 95 Torr

A (408 nm)	t (sec)	$A_o - A$	$A - A_\infty$	ln $A - A_\infty$	ln $[Co_T]$
0.752	0	0	0.532	-0.631	-11.043
0.465	54	0.287	0.245	-1.406	-11.818
0.420	96	0.332	0.200	-1.580	-11.992
0.392	146	0.360	0.172	-1.760	-12.172
0.345	228	0.407	0.125	-2.079	-12.491
0.299	359	0.453	0.079	-2.538	-12.950
0.250	598	0.502	0.030	-3.507	-13.919
0.233	885	0.519	0.013	-4.343	-14.755
0.220	1503	0.532	0		

$[Co] = 2.4 \times 10^{-5}$ M; $[Im] = 18.4 \times 10^{-4}$ M; T = 22°C; P_{O_2} = 100 Torr

A (408 nm)	t (sec)	$A_o - A$	$A - A_\infty$	ln $A - A_\infty$	ln $[Co_T]$
1.183	0	0	0.868	-0.142	-10.637
0.870	60	0.313	0.555	-0.589	-11.084
0.795	102	0.388	0.480	-0.734	-11.229
0.729	149	0.454	0.414	-0.882	-11.377
0.663	196	0.520	0.348	-1.056	-11.551
0.600	254	0.583	0.285	-1.255	-11.750
0.537	322	0.646	0.222	-1.505	-12.000
0.483	401	0.700	0.168	-1.784	-12.279
0.432	510	0.751	0.117	-2.146	-12.641
0.383	658	0.800	0.068	-2.688	-13.183
0.338	974	0.845	0.023	-3.772	-14.267
0.315	1620	0.868	0		

$[Co] = 4.5 \times 10^{-5}$ M; $[Im] = 18.4 \times 10^{-4}$ M; $T = 22^{\circ}C$; P_{O_2} = 100 Torr

A (408 nm)	t (sec)	$A_o - A$	$A - A_\infty$	$\ln A - A_\infty$	$\ln [Co_T]$
0.487	0	0	0.350	-1.050	-10.009
0.328	58	0.159	0.191	-1.655	-10.614
0.262	104	0.225	0.125	-2.079	-11.038
0.242	158	0.245	0.105	-2.254	-11.213
0.198	267	0.289	0.061	-2.797	-11.756
0.153	499	0.334	0.016	-4.135	-13.094
0.142	1007	0.345	0.005	-5.298	-14.257
0.137	2005	0.350	0		

$[Co] = 7 \times 10^{-5}$ M; $[Im] = 18.4 \times 10^{-4}$ M; $T = 22^{\circ}C$; P_{O_2} = 100 Torr

A (408 nm)	t (sec)	$A_o - A$	$A - A_\infty$	$\ln A - A_\infty$	$\ln [Co_T]$
0.682	0	0	0.479	-0.736	-9.567
0.430	66	0.262	0.227	-1.483	-10.314
0.370	110	0.312	0.167	-1.790	-10.621
0.317	167	0.365	0.114	-2.174	-11.005
0.278	243	0.404	0.075	-2.590	-11.421
0.242	403	0.440	0.039	-3.244	-12.075
0.227	708	0.455	0.024	-3.730	-13.561
0.203	1538	0.479	0		

$[Co] = 8.0 \times 10^{-5}$ M; $[Im] = 18.4 \times 10^{-4}$ M; $T = 22^{\circ}C$; P_{O_2} = 100 Torr

A (408 nm)	t (sec)	$A_o - A$	$A - A_\infty$	$\ln A - A_\infty$	$\ln [Co_T]$
0.842	0	0	0.604	-0.504	-9.433
0.570	51	0.272	0.332	-1.103	-10.032
0.480	91	0.362	0.242	-1.419	-10.348
0.412	144	0.430	0.174	-1.749	-10.678
0.362	205	0.480	0.124	-2.087	-11.016
0.304	314	0.538	0.066	-2.718	-11.647
0.282	500	0.560	0.044	-3.124	-12.053
0.248	1008	0.594	0.010	-4.605	-13.534
0.238	2001	0.604	0		

APPENDIX V h. $ImCoOMBP + O_2 \longrightarrow ImCoOMBP(O_2)CoOMBP \cdot Im$

As a function of cobalt concentration

$[Co] = 1.8 \times 10^{-5}$ M; $[Im] = 14.6 \times 10^{-4}$ M; $T = 22^{\circ}C$; $P_{O_2} = 97$ Torr

A (408 nm)	t (sec)	$A_o - A$	$A - A_\infty$	$\ln A - A_\infty$	$\ln [Co_T]$
0.908	0	0	0.700	-0.357	-10.925
0.638	61	0.270	0.430	-0.844	-11.412
0.560	112	0.348	0.352	-1.044	-11.612
0.483	192	0.425	0.275	-1.291	-11.859
0.410	287	0.498	0.202	-1.599	-12.167
0.370	362	0.528	0.172	-1.760	-12.328
0.327	494	0.571	0.129	-2.048	-12.616
0.287	629	0.621	0.079	-2.538	-13.106
0.260	773	0.648	0.052	-2.957	-13.525
0.240	1003	0.668	0.032	-3.442	-14.010

A_∞ estimated to be 0.208

$[Co] = 13 \times 10^{-5}$ M; $[Im] = 14.6 \times 10^{-4}$ M; $T = 22^{\circ}C$; $P_{O_2} = 100$ Torr

A (408 nm)	t (sec)	$A_o - A$	$A - A_\infty$	$\ln A - A_\infty$	$\ln [Co_T]$
1.315	0	0	1.100	0.095	-8.948
0.633	47	0.682	0.418	-0.872	-9.655
0.530	85	0.785	0.315	-1.155	-9.938
0.457	123	0.858	0.242	-1.419	-10.202
0.395	178	0.920	0.180	-1.715	-10.498
0.340	270	0.975	0.125	-2.079	-10.862
0.313	388	1.002	0.098	-2.323	-11.106
0.285	585	1.030	0.070	-2.659	-11.442
0.265	1181	1.050	0.050	-2.996	-11.779

A_∞ estimated to be 0.215

$[Co] = 24 \times 10^{-5}$ M; $[Im] = 14.6 \times 10^{-4}$ M; $T = 22^{\circ}C$ $P_{O_2} = 95$ Torr

A (408 nm)	t (sec)	$A_o - A$	$A - A_\infty$	$\ln A - A_\infty$	$\ln [Co_T]$
1.209	0	0	0.950	0.051	-8.335
0.517	59	0.692	0.258	-1.355	-9.741
0.421	104	0.788	0.162	-1.820	-10.206
0.377	145	0.832	0.118	-2.137	-10.523
0.340	207	0.869	0.081	-2.513	-10.899
0.312	299	0.897	0.053	-2.937	-11.323
0.285	701	0.924	0.026	-3.650	-12.036

A_∞ estimated to be 0.259

APPENDIX Vi. $ImCoOMBP + O_2 \longrightarrow ImCooMBP(O_2)CoOMBP \cdot Im$

As a function of temperature

$[Co] = 2.3 \times 10^{-5}$ M; $[Im] = 14.6 \times 10^{-4}$ M; $T = 10^{\circ}C$; $P_{O_2} = 97$ Torr

A (408 nm)	t (sec)	$A_o - A$	$A - A_\infty$	$\ln A - A_\infty$
1.150	0	0	0.900	-0.105
0.920	45	0.230	0.670	-0.400
0.818	82	0.332	0.568	-0.566
0.733	121	0.417	0.483	-0.728
0.643	167	0.507	0.393	-0.934
0.580	213	0.570	0.330	-1.109
0.533	260	0.617	0.283	-1.262
0.482	326	0.668	0.232	-1.461
0.405	423	0.745	0.155	-1.864
0.360	531	0.790	0.110	-2.207
0.315	669	0.835	0.065	-2.733
0.298	998	0.852	0.048	-3.037
0.270	2007	0.880	0.020	-3.912

A_∞ estimated to be 0.250

$[Co] = 1.8 \times 10^{-5}$ M; $[Im] = 14.6 \times 10^{-4}$ M; $T = 22^{\circ}C$; $P_{O_2} = 97$ Torr

A (408 nm)	t (sec)	$A_o - A$	$A - A_\infty$	$\ln A - A_\infty$
0.908	0	0	0.700	-0.357
0.638	61	0.270	0.430	-0.844
0.560	112	0.348	0.352	-1.044
0.483	192	0.425	0.275	-1.291
0.410	287	0.498	0.202	-1.599
0.370	362	0.528	0.172	-1.760
0.327	494	0.571	0.129	-2.048
0.287	629	0.621	0.079	-2.538
0.260	773	0.648	0.052	-2.957
0.240	1003	0.668	0.032	-3.442
0.225	1512	0.683	0.017	-4.075

A_∞ estimated to be 0.208

$[Co] = 2.6 \times 10^{-5}$ M; $[Im] = 14.6 \times 10^{-4}$ M; $T = 30^{\circ}C$; P_{O_2} = 98 Torr

A (408 nm)	t (sec)	$A_o - A$	$A - A_\infty$	$\ln A - A_\infty$
1.373	0	0	1.300	0.262
1.017	47	0.356	0.944	-0.058
0.855	93	0.518	0.782	-0.246
0.760	131	0.613	0.687	-0.375
0.673	176	0.700	0.600	-0.511
0.590	225	0.783	0.517	-0.660
0.525	288	0.848	0.452	-0.794
0.427	385	0.946	0.354	-1.038
0.357	487	1.016	0.284	-1.259
0.283	621	1.090	0.210	-1.561
0.213	800	1.160	0.140	-1.966
0.135	1134	1.238	0.062	-2.781
0.090	1603	1.283	0.017	-4.075

A_∞ estimated to be 0.073

$[Co] = 1.6 \times 10^{-5}$ M; $[Im] = 14.6 \times 10^{-4}$ M; $T = 35^{\circ}C$; P_{O_2} = 100 Torr

A (408 nm)	t (sec)	$A_o - A$	$A - A_\infty$	$\ln A - A_\infty$
0.750	0	0	0.600	-0.511
0.593	56	0.157	0.443	-0.814
0.560	94	0.190	0.410	-0.892
0.503	163	0.247	0.353	-1.041
0.420	295	0.330	0.270	-1.309
0.353	426	0.397	0.203	-1.595
0.325	573	0.425	0.175	-1.743
0.275	792	0.475	0.125	-2.079
0.215	1235	0.535	0.065	-2.733

A_∞ estimated to be 0.150

APPENDIX Vj. CH_3-ImCoOMBP + O_2 ⟶ CH_3-ImCoOMBP(O_2)CoOMBP·CH_3-Im

As a function of cobalt concentration

[Co] = 3×10^{-6} M; [CH_3-Im] = 8.2×10^{-4} M; T = 20°C; P_{O_2} = 800 Torr

A (408 nm)	t (sec)	$A_o - A$	$\frac{A_o - A}{A_o - A_\infty}$	$\frac{A - A_\infty}{A_o - A_\infty}$	$\ln \frac{A - A_\infty}{A_o - A_\infty}$
1.275	0	0	0	1.000	0
1.197	129	0.078	0.103	0.897	-0.109
1.098	319	0.177	0.233	0.767	-0.265
1.000	511	0.275	0.362	0.638	-0.449
0.874	835	0.401	0.528	0.472	-0.751
0.803	1087	0.472	0.621	0.379	-0.970
0.730	1408	0.545	0.717	0.283	-1.262
0.658	2037	0.617	0.812	0.188	-1.671
0.605	3074	0.670	0.882	0.118	-2.137
0.563	4276	0.712	0.937	0.063	-2.765
0.515	10229	0.760	1.000	0	———
0.515	25793	0.760	1.000	0	———

[Co] = 8×10^{-6} M; [CH_3-Im] = 8.2×10^{-6} M; T = 20°C; P_{O_2} = 800 Torr

A (408 nm)	t (sec)	$A_o - A$	$\frac{A_o - A}{A_o - A_\infty}$	$\frac{A - A_\infty}{A_o - A_\infty}$	$\ln \frac{A - A_\infty}{A_o - A_\infty}$
0.523	0	0	0	1.000	0
0.500	53	0.023	0.079	0.921	-0.082
0.486	193	0.039	0.138	0.852	-0.149
0.464	531	0.059	0.209	0.793	-0.232
0.432	1215	0.091	0.317	0.683	-0.381
0.392	2476	0.131	0.459	0.541	-0.633
0.333	4124	0.190	0.666	0.334	-1.097
0.316	4973	0.207	0.724	0.276	-1.287
0.278	8423	0.245	0.855	0.145	-1.931
0.272	14918	0.251	0.879	0.121	-2.112
0.257	~175000	0.266	0.931	0.069	-2.674
0.237	~250000	0.286	1.000	0	———
0.237	~475000	0.286	1.000	0	———

$[Co] = 1.8 \times 10^{-5}$ M; $[CH_3\text{-Im}] = 8.2 \times 10^{-4}$ M; T = 20°C; P_{O_2} = 800 Torr

A (408 nm)	t (sec)	$A_o - A$	$\frac{A_o - A}{A_o - A_\infty}$	$\frac{A - A_\infty}{A_o - A_\infty}$	$\ln \frac{A - A_\infty}{A_o - A_\infty}$
0.918	0	0	0	1.000	0
0.862	53	0.058	0.104	0.896	-0.110
0.855	194	0.063	0.113	0.887	-0.120
0.825	522	0.093	0.167	0.833	-0.183
0.780	1234	0.138	0.247	0.753	-0.284
0.732	2443	0.186	0.333	0.667	-0.405
0.674	4161	0.244	0.437	0.563	-0.574
0.658	4989	0.260	0.466	0.534	-0.627
0.609	8455	0.309	0.554	0.446	-0.807
0.591	14979	0.327	0.586	0.416	-0.877
0.440	~175000	0.478	0.856	0.144	-1.938
0.360	~250000	0.558	1.000	0	———
0.360	~425000	0.558	1.000	0	———

$[Co] = 8.2 \times 10^{-5}$ M; $[CH_3\text{-Im}] = 8.2 \times 10^{-4}$ M; T = 20°C; P_{O_2} = 800 Torr

A (408 nm)	t (sec)	$A_o - A$	$\frac{A_o - A}{A_o - A_\infty}$	$\frac{A - A_\infty}{A_o - A_\infty}$	$\ln \frac{A - A_\infty}{A_o - A_\infty}$
0.953	0	0	0	1.000	0
0.899	57	0.054	0.092	0.908	-0.097
0.891	223	0.062	0.107	0.893	-0.113
0.881	437	0.072	0.124	0.876	-0.132
0.856	856	0.097	0.166	0.834	-0.182
0.848	1478	0.105	0.180	0.820	-0.198
0.821	2657	0.132	0.227	0.773	-0.257
0.784	3816	0.169	0.290	0.710	-0.343
0.755	5784	0.198	0.341	0.659	-0.417
0.732	8637	0.221	0.380	0.620	-0.478
0.681	12097	0.272	0.467	0.533	-0.629
0.634	17523	0.319	0.548	0.452	-0.793
0.608	22631	0.345	0.592	0.408	-0.897
0.504	~185000	0.449	0.771	0.229	-1.473
0.371	~650000	0.582	1.000	0	———

$[Co] = 2.1 \times 10^{-4}$ M; $[CH_3\text{-Im}] = 8.2 \times 10^{-4}$ M; $T = 20^{\circ}C$; P_{O_2} = 800 Torr

A (408 nm)	t (sec)	$A_o - A$	$\frac{A_o - A}{A_o - A_\infty}$	$\frac{A - A_\infty}{A_o - A_\infty}$	$\ln \frac{A - A_\infty}{A_o - A_\infty}$
0.960	0	0	0	1.000	0
0.891	69	0.069	0.120	0.880	-0.128
0.890	249	0.070	0.122	0.878	-0.130
0.887	637	0.077	0.134	0.866	-0.144
0.878	2274	0.082	0.143	0.857	-0.154
0.865	6203	0.095	0.166	0.834	-0.182
0.830	15512	0.130	0.227	0.773	-0.257
0.785	26260	0.175	0.305	0.695	-0.364
0.777	35095	0.183	0.319	0.601	-0.509
0.672	~182000	0.288	0.503	0.497	-0.699
0.387	~1000000	0.573	1.000	0	———

APPENDIX Vk. CH_3-ImCoOMBP + O_2 ⟶ CH_3-ImCoOMBP(O_2)CoOMBP·CH_3-Im

As a function of CH_3-Im concentration

$[Co] = 1.8 \times 10^{-5}$ M; $[CH_3\text{-Im}] = 2.8 \times 10^{-4}$ M; T = 20°C; P_{O_2} = 800 Torr

A (408 nm)	t (sec)	$A_o - A$	$\frac{A_o - A}{A_o - A_\infty}$	$\frac{A - A_\infty}{A_o - A_\infty}$	$\ln \frac{A - A_\infty}{A_o - A_\infty}$
0.947	0	0	0	1.000	0
0.893	51	0.054	0.094	0.906	-0.099
0.868	196	0.059	0.103	0.897	-0.109
0.852	518	0.095	0.166	0.834	-0.182
0.815	1222	0.132	0.231	0.769	-0.263
0.769	2501	0.178	0.311	0.689	-0.373
0.715	4198	0.232	0.406	0.594	-0.521
0.690	5031	0.257	0.449	0.551	-0.596
0.644	8503	0.303	0.530	0.470	-0.755
0.622	15004	0.325	0.568	0.432	-0.839
0.490	175000	0.457	0.799	0.201	-1.604
0.375	250000	0.572	1.000	0	———
0.375	425000	0.572	1.000	0	———

$[Co] = 1.8 \times 10^{-5}$ M; $[CH_3\text{-Im}] = 8.2 \times 10^{-4}$ M; T = 20°C; P_{O_2} = 800 Torr

A (408 nm)	t (sec)	$A_o - A$	$\frac{A_o - A}{A_o - A_\infty}$	$\frac{A - A_\infty}{A_o - A_\infty}$	$\ln \frac{A - A_\infty}{A_o - A_\infty}$
0.918	0	0	0	1.000	0
0.860	53	0.058	0.104	0.896	-0.110
0.855	194	0.063	0.113	0.887	-0.120
0.825	522	0.098	0.167	0.833	-0.183
0.780	1234	0.138	0.247	0.753	-0.284
0.732	2443	0.186	0.333	0.667	-0.405
0.674	4161	0.244	0.437	0.563	-0.574
0.658	4989	0.260	0.466	0.534	-0.627
0.609	8455	0.309	0.554	0.446	-0.807
0.591	14979	0.327	0.586	0.416	-0.877
0.440	~175000	0.478	0.856	0.144	-1.938
0.360	~250000	0.558	1.000	0	———
0.360	~425000	0.558	1.000	0	———

$[Co] = 1.8 \times 10^{-5}$ M; $[CH_3\text{-Im}] = 2.4 \times 10^{-3}$ M; $T = 20^{o}C$; $P_{O_2} = 800$ Torr

A (408 nm)	t (sec)	$A_o - A$	$\frac{A_o - A}{A_o - A_\infty}$	$\frac{A - A_\infty}{A_o - A_\infty}$	$\ln \frac{A - A_\infty}{A_o - A_\infty}$
0.932	0	0	0	1.000	0
0.877	57	0.055	0.098	0.902	-0.103
0.870	201	0.062	0.110	0.890	-0.114
0.837	518	0.095	0.168	0.832	-0.184
0.790	1217	0.142	0.252	0.748	-0.290
0.742	2496	0.190	0.337	0.663	-0.411
0.680	4201	0.252	0.447	0.553	-0.592
0.658	5002	0.274	0.486	0.514	-0.666
0.611	8507	0.321	0.569	0.431	-0.842
0.591	15021	0.341	0.605	0.395	-0.929
0.433	~175000	0.499	0.885	0.115	-2.163
0.368	~250000	0.564	1.000	0	———
0.368	~425000	0.564	1.000	0	———

APPENDIX VI. CH_3-ImCoOMBP + O_2 ⟶ CH_3-ImCoOMBP(O_2)CoOMBP·CH_3-Im

As a function of Oxygen Pressure

$[Co] = 1.8 \times 10^{-5}$ M; $[CH_3\text{-Im}] = 8.2 \times 10^{-4}$ M; T = 20°C; P_{O_2} = 800 Torr

A (408 nm)	t (sec)	$A_o - A$	$\frac{A_o - A}{A_o - A_\infty}$	$\frac{A - A_\infty}{A_o - A_\infty}$	$\ln \frac{A - A_\infty}{A_o - A_\infty}$
0.918	0	0	0	1.000	0
0.860	53	0.058	0.104	0.896	-0.110
0.855	194	0.063	0.113	0.887	-0.120
0.825	522	0.098	0.167	0.833	-0.183
0.780	1234	0.138	0.247	0.753	-0.284
0.732	2443	0.186	0.333	0.667	-0.405
0.674	4161	0.244	0.437	0.563	-0.574
0.658	4989	0.260	0.466	0.534	-0.627
0.609	8455	0.309	0.554	0.446	-0.807
0.591	14979	0.327	0.586	0.416	-0.877
0.440	~175000	0.478	0.856	0.144	-1.938
0.360	~250000	0.558	1.000	0	———
0.360	~425000	0.558	1.000	0	———

$[Co] = 1.8 \times 10^{-5}$ M; $[CH_3\text{-Im}] = 8.2 \times 10^{-4}$ M; T = 20°C; P_{O_2} = 400 Torr

A (408 nm)	t (sec)	$A_o - A$	$\frac{A_o - A}{A_o - A_\infty}$	$\frac{A - A_\infty}{A_o - A_\infty}$	$\ln \frac{A - A_\infty}{A_o - A_\infty}$
0.928	0	0	0	1.000	0
0.900	65	0.028	0.048	0.952	-0.049
0.895	211	0.033	0.057	0.943	-0.059
0.882	456	0.046	0.079	0.921	-0.082
0.862	910	0.066	0.113	0.887	-0.120
0.841	1748	0.087	0.149	0.851	-0.161
0.808	3048	0.120	0.206	0.794	-0.231
0.777	4537	0.151	0.259	0.741	-0.300
0.703	7982	0.225	0.386	0.614	-0.488
0.642	11668	0.286	0.491	0.509	-0.675
0.590	15925	0.338	0.580	0.420	-0.868
0.534	20479	0.396	0.679	0.321	-1.136
0.442	43135	0.484	0.830	0.170	-1.772
0.370	81700	0.558	0.957	0.043	-3.147
0.345	~625000	0.583	1.000	0	———

$[Co] = 1.8 \times 10^{-5}$ M; $[CH_3\text{-Im}] = 8.2 \times 10^{-4}$ M; T = 20°C; P_{O_2} = 200 Torr

A (408 nm)	t (sec)	$A_o - A$	$\frac{A_o - A}{A_o - A_\infty}$	$\frac{A - A_\infty}{A_o - A_\infty}$	$\ln \frac{A - A_\infty}{A_o - A_\infty}$
0.936	0	0	0	1.000	0
0.920	72	0.016	0.027	0.973	-0.027
0.918	250	0.018	0.031	0.969	-0.032
0.914	525	0.022	0.038	0.962	-0.039
0.904	978	0.032	0.055	0.945	-0.057
0.888	1802	0.048	0.081	0.919	-0.084
0.867	3003	0.069	0.118	0.882	-0.125
0.847	4526	0.089	0.152	0.848	-0.165
0.805	8014	0.131	0.224	0.776	-0.253
0.764	11802	0.172	0.293	0.707	-0.347
0.706	16012	0.230	0.392	0.608	-0.497
0.649	20534	0.287	0.489	0.511	-0.672
0.540	42679	0.396	0.675	0.325	-1.124
0.398	82859	0.538	0.916	0.084	-2.472
0.349	~500000	0.587	1.000	0	———

APPENDIX Vm. $PipCoOMBP + O_2 \longrightarrow PipCoOMBP(O_2)CoOMBP \cdot Pip$

$[Co] = 3 \times 10^{-6}$ M; $[Pip] = 7.6 \times 10^{-4}$; $T = 20^{\circ}C$; $P_{O_2} = 800$ Torr

A (408 nm)	t (sec)	$A_o - A$	$\frac{A_o - A}{A_o - A_\infty}$	$\frac{A - A_\infty}{A_o - A_\infty}$	$\ln \frac{A - A_\infty}{A_o - A_\infty}$
1.262	0	0	0	1.000	0
1.212	67	0.051	0.068	0.932	-0.070
1.193	198	0.070	0.093	0.907	-0.098
1.102	516	0.161	0.213	0.787	-0.240
1.057	1167	0.206	0.277	0.723	-0.325
1.042	2374	0.221	0.293	0.703	-0.352
1.000	3996	0.263	0.349	0.651	-0.429
0.956	8247	0.307	0.407	0.593	-0.523
0.894	15027	0.369	0.489	0.511	-0.672
0.697	~165000	0.566	0.763	0.237	-1.439
0.550	~450000	0.713	0.944	0.056	-2.887

A_∞ estimated to be 0.508 based on data when DCE is solvent

$[Co] = 1.8 \times 10^{-5}$ M; $[Pip] = 7.6 \times 10^{-4}$; $T = 20^{\circ}C$; $P_{O_2} = 800$ Torr

A (408 nm)	t (sec)	$A_o - A$	$\frac{A_o - A}{A_o - A_\infty}$	$\frac{A - A_\infty}{A_o - A_\infty}$	$\ln \frac{A - A_\infty}{A_o - A_\infty}$
1.077	0	0	0	1.000	0
1.033	79	0.044	0.063	0.937	-0.065
1.027	222	0.050	0.072	0.928	-0.075
0.993	726	0.084	0.120	0.880	-0.128
0.975	1525	0.102	0.146	0.854	-0.158
0.970	3241	0.107	0.153	0.847	-0.166
0.953	12048	0.124	0.177	0.823	-0.195
0.833	61992	0.244	0.349	0.651	-0.429
0.780	~150000	0.297	0.425	0.575	-0.553
0.765	~450000	0.312	0.446	0.554	-0.591

A_∞ estimated to be 0.378 based on data when DCE is solvent

APPENDIX Vn. PyCoOMBP + O_2 ⟶ PyCoOMBP(O_2)CoOMBP·Py

[Co] = 3 x 10^{-6} M; [Py] = 8.0 x 10^{-4} M; T = 20°C; P_{O_2} = 800 Torr

A (408 nm)	t (sec)	$A_o - A$	$\frac{A_o - A}{A_o - A_\infty}$	$\frac{A - A_\infty}{A_o - A_\infty}$	$\ln \frac{A - A_\infty}{A_o - A_\infty}$
1.275	0	0	0	1.000	0
1.210	57	0.049	0.065	0.935	-0.067
1.135	195	0.106	0.140	0.860	-0.151
1.106	523	0.128	0.169	0.831	-0.185
1.072	1198	0.154	0.203	0.797	-0.227
1.026	2396	0.189	0.249	0.751	-0.287
0.973	3396	0.229	0.302	0.698	-0.386
0.813	8012	0.350	0.462	0.538	-0.620
0.758	15872	0.392	0.517	0.483	-0.727
0.550	~185000	0.725	0.956	0.044	-3.119
0.517	~450000	0.758	1.000	0	

[Co] = 1.6 x 10^{-5} M; [Py] = 8.0 x 10^{-4} M; T = 20°C; P_{O_2} = 800 Torr

A (408 nm)	t (sec)	$A_o - A$	$\frac{A_o - A}{A_o - A_\infty}$	$\frac{A - A_\infty}{A_o - A_\infty}$	$\ln \frac{A - A_\infty}{A_o - A_\infty}$
0.843	0	0	0	1.000	0
0.811	41	0.032	0.060	0.940	-0.062
0.799	204	0.044	0.082	0.912	-0.092
0.790	614	0.053	0.099	0.901	-0.104
0.780	1638	0.063	0.118	0.882	-0.126
0.757	3578	0.086	0.161	0.839	-0.176
0.710	12506	0.133	0.249	0.751	-0.286
0.670	35784	0.173	0.323	0.677	-0.390
0.598	83846	0.245	0.456	0.544	-0.609
0.573	~125000	0.270	0.505	0.495	-0.703
0.477	~170000	0.366	0.684	0.316	-1.152

A_∞ estimated to be 0.308 based on above data

APPENDIX Vo. CH_3-ImCoOMBP + O_2 ⟶ CH_3-ImCoOMBP(O_2)CoOMBP·CH_3-Im

As a function of solvent

$[Co] = 2 \times 10^{-5}$ M; $[CH_3\text{-Im}] = 8 \times 10^{-4}$ M; T = 20°C; P_{O_2} = 800 T; in toluene

A (408 nm)	t (sec)	$A_o - A$	$\frac{A_o - A}{A_o - A_\infty}$	$\frac{A - A_\infty}{A_o - A_\infty}$	$\ln \frac{A - A_\infty}{A_o - A_\infty}$
0.918	0	0	0	1.000	0
0.860	53	0.058	0.104	0.896	-0.110
0.855	194	0.063	0.113	0.887	-0.120
0.780	522	0.093	0.167	0.833	-0.183
0.732	1234	0.138	0.247	0.753	-0.284
0.674	2443	0.186	0.333	0.667	-0.405
0.658	4161	0.244	0.437	0.563	-0.574
0.609	4989	0.260	0.466	0.534	-0.627
0.591	8455	0.309	0.554	0.446	-0.807
0.440	14979	0.478	0.856	0.144	-1.938
0.360	~175000	0.558	1.000	0	———
0.360	~425000	0.558	1.000	0	———

$[Co] = 2 \times 10^{-5}$ M; $[CH_3\text{-Im}] = 8 \times 10^{-4}$ M; T = 20°C; P_{O_2} = 800 T; in 5:1 tol:DCE

A (440 nm)	t (sec)	$A_o - A$	$\frac{A_o - A}{A_o - A_\infty}$	$\frac{A - A_\infty}{A_o - A_\infty}$	$\ln \frac{A - A_\infty}{A_o - A_\infty}$
0.440	0	0	0	1.000	0
0.472	71	0.062	0.115	0.885	-0.122
0.496	209	0.086	0.160	0.840	-0.174
0.527	477	0.117	0.218	0.782	-0.246
0.557	984	0.147	0.274	0.726	-0.320
0.610	2109	0.200	0.372	0.628	-0.465
0.652	3608	0.242	0.451	0.549	-0.600
0.683	6925	0.273	0.508	0.492	-0.709
0.907	42357	0.497	0.926	0.076	-2.577
0.947	73565	0.537	1.000	0	———
0.947	~140000	0.537	1.000	0	———

[Co] = 2 x 10^{-5} M; [CH_3-Im] = 8 x 10^{-4} M; T = 20°C; P_{O_2} = 800 T; in 4:1 tol:DCE

A (408 nm)	t (sec)	$A_o - A$	$\frac{A_o - A}{A_o - A_\infty}$	$\frac{A - A_\infty}{A_o - A_\infty}$	$\ln \frac{A - A_\infty}{A_o - A_\infty}$
1.320	0	0	0	1.000	0
1.168	56	0.152	0.202	0.798	-0.226
1.112	134	0.208	0.276	0.724	-0.323
1.057	272	0.263	0.349	0.651	-0.429
0.982	583	0.338	0.449	0.551	-0.596
0.897	1135	0.423	0.562	0.438	-0.826
0.797	2098	0.523	0.695	0.305	-1.187
0.737	3173	0.583	0.774	0.226	-1.487
0.687	5023	0.633	0.841	0.159	-1.839
0.630	8041	0.690	0.916	0.084	-2.477
0.567	43502	0.753	1.000	0	———

[Co] = 2 x 10^{-5} M; [CH_3-Im] = 8 x 10^{-4} M; T = 20°C; P_{O_2} = 800 T; in 1:1 tol:DCE

A (440 nm)	t (sec)	$A_o - A$	$\frac{A_o - A}{A_o - A}$	$\frac{A - A_\infty}{A_o - A_\infty}$	$\ln \frac{A - A_\infty}{A_o - A_\infty}$
0.298	0	0	0	1.000	0
0.368	80	0.078	0.307	0.693	-0.367
0.468	253	0.178	0.701	0.299	-1.207
0.512	402	0.222	0.874	0.126	-2.071
0.544	790	0.544	1.000	0	———
0.544	1640	0.544	1.000	0	———

$[Co] = 2 \times 10^{-5}$ M; $[CH_3\text{-Im}] = 8 \times 10^{-4}$ M; T = 20°C; P_{O_2} = 800 T; Chlorobenzene

A (408 nm)	t (sec)	$A_o - A$	$\frac{A_o - A}{A_o - A_\infty}$	$\frac{A - A_\infty}{A_o - A_\infty}$	$\ln \frac{A - A_\infty}{A_o - A_\infty}$
0.730	0	0	0	1.000	0
0.658	60	0.072	0.167	0.833	-0.183
0.645	266	0.085	0.198	0.802	-0.221
0.629	541	0.101	0.235	0.765	-0.268
0.613	974	0.117	0.272	0.728	-0.317
0.592	1919	0.138	0.321	0.679	-0.387
0.553	3398	0.177	0.412	0.588	-0.531
0.523	5220	0.207	0.481	0.519	-0.654
0.482	11061	0.248	0.577	0.423	-0.860
0.467	20087	0.263	0.612	0.388	-0.947
0.413	60326	0.317	0.737	0.263	-1.336
0.391	90735	0.339	0.788	0.212	-1.551
0.315	171686	0.415	0.965	0.035	-3.352
0.300	~280000	0.430	1.000	0	

$[Co] = 2 \times 10^{-5}$ M; $[CH_3\text{-Im}] = 8 \times 10^{-4}$ M; T = 20°C; P_{O_2} = 800 T; Chlorobutane

A (408 nm)	t (sec)	$A_o - A$	$\frac{A_o - A}{A_o - A_\infty}$	$\frac{A - A_\infty}{A_o - A_\infty}$	$\ln \frac{A - A_\infty}{A_o - A_\infty}$
0.747	0	0	0	1.000	0
0.718	69	0.029	0.070	0.930	-0.073
0.703	228	0.044	0.107	0.893	-0.113
0.690	465	0.057	0.138	0.862	-0.149
0.672	994	0.075	0.182	0.818	-0.201
0.646	2052	0.101	0.245	0.755	-0.281
0.607	4196	0.140	0.340	0.660	-0.416
0.567	8346	0.180	0.437	0.563	-0.574
0.335	~175000	0.412	1.000	0	
0.335	~260000	0.412	1.000	0	

$[Co] = 2 \times 10^{-5}$ M; $[CH_3\text{-Im}] = 8 \times 10^{-4}$ M; T = 20°C; P_{O_2} = 800 T; in DCM

A (408 nm)	t (sec)	$A_o - A$	$\frac{A_o - A}{A_o - A_\infty}$	$\frac{A - A_\infty}{A_o - A_\infty}$	$\ln \frac{A - A_\infty}{A_o - A_\infty}$
1.107	0	0	0	1.000	0
0.820	68	0.287	0.434	0.566	-0.569
0.728	209	0.379	0.573	0.427	-0.851
0.652	382	0.455	0.687	0.313	-1.162
0.610	517	0.497	0.751	0.249	-1.390
0.567	727	0.540	0.816	0.184	-1.693
0.537	957	0.570	0.861	0.139	-1.973
0.519	1212	0.588	0.888	0.112	-2.189
0.482	1893	0.625	0.944	0.056	-2.882
0.453	3088	0.654	0.988	0.012	-4.423
0.445	5054	0.662	1.000	0	———

$[Co] = 2 \times 10^{-5}$ M; $[CH_3\text{-Im}] = 8 \times 10^{-4}$ M; T = 20°C; P_{O_2} = 800 T; in DCE

A (408 nm)	t (sec)	$A_o - A$	$\frac{A_o - A}{A_o - A_\infty}$	$\frac{A - A_\infty}{A_o - A_\infty}$	$\ln \frac{A - A_\infty}{A_o - A_\infty}$
0.757	0	0	0	1.000	0
0.580	45	0.177	0.392	0.608	-0.498
0.501	109	0.256	0.568	0.432	-0.839
0.334	244	0.423	0.926	0.074	-2.604
0.300	381	0.457	1.000	0	———
0.300	1220	0.457	1.000	0	———
0.300	2463	0.457	1.000		———

APPENDIX Vp. CH_3-ImCoOMBP + O_2 ⟶ CH_3-ImCoOMBP(O_2)CoOMBP·CH_3-Im in DCE

$[Co] = 1.7 \times 10^{-5}$ M; $[CH_3\text{-Im}] = 8.2 \times 10^{-4}$ M; $T = 20^{\circ}C$; P_{O_2} = 800 Torr

A (408 nm)	t (sec)	$A_o - A$	$\frac{A_o - A}{A_o - A_\infty}$	$\frac{A - A_\infty}{A_o - A_\infty}$	$\ln \frac{A - A_\infty}{A_o - A_\infty}$
0.757	0	0	0	1.000	0
0.580	45	0.177	0.392	0.608	-0.498
0.501	109	0.256	0.568	0.432	-0.839
0.334	244	0.426	0.926	0.074	-2.604
0.300	381	0.457	1.000	0	———
0.300	1220	0.457	1.000	0	———
0.300	2463	0.457	1.000	0	———

$[Co] = 1.8 \times 10^{-5}$ M; $[CH_3\text{-Im}] = 8.2 \times 10^{-4}$ M; $T = 20^{\circ}C$; P_{O_2} = 200 Torr

A (408 nm)	t (sec)	$A_o - A$	$\frac{A_o - A}{A_o - A_\infty}$	$\frac{A - A_\infty}{A_o - A_\infty}$	$\ln \frac{A - A_\infty}{A_o - A_\infty}$
0.828	0	0	0	1.000	0
0.675	54	0.153	0.320	0.680	-0.385
0.485	181	0.343	0.718	0.282	-1.266
0.386	308	0.432	0.904	0.196	-1.630
0.345	458	0.473	0.990	0.010	-4.605
0.340	659	0.478	1.000	0	———
0.340	1400	0.478	1.000	0	———

$[Co] = 1.4 \times 10^{-4}$ M; $[CH_3\text{-Im}] = 8.2 \times 10^{-4}$ M; $T = 20^{\circ}C$; P_{O_2} = 800 Torr

A (408 nm)	t (sec)	$A_o - A$	$\frac{A_o - A}{A_o - A_\infty}$	$\frac{A - A_\infty}{A_o - A_\infty}$	$\ln \frac{A - A_\infty}{A_o - A_\infty}$
0.722	0	0	0	1.000	0
0.490	67	0.232	0.640	0.360	-1.022
0.364	221	0.358	0.989	0.011	-4.509
0.360	358	0.362	1.000	0	———
0.360	700	0.362	1.000	0	———

$[Co] = 1.6 \times 10^{-6}$ M; $[CH_3\text{-Im}] = 8.2 \times 10^{-4}$ M; T = 20°C P_{O_2} = 800 Torr

A (408 nm)	t (sec)	$A_o - A$	$\frac{A_o - A}{A_o - A_\infty}$	$\frac{A - A_\infty}{A_o - A_\infty}$	$\ln \frac{A - A_\infty}{A_o - A_\infty}$
0.592	0	0	0	1.000	0
0.442	41	0.150	0.661	0.339	-1.082
0.403	217	0.189	0.833	0.167	-1.790
0.376	361	0.216	0.952	0.048	-3.037
0.370	523	0.222	0.978	0.028	-3.817
0.365	845	0.227	1.000	0	———

APPENDIX Vq. PyCoOMBP + O_2 ⟶ PyCoOMBP(O_2)CoOMBP·Py in DCE

$[Co] = 1.6 \times 10^{-4}$ M; $[Py] = 8.0 \times 10^{-4}$ M; T = 20°C; P_{O_2} = 800 Torr

A (408 nm)	t (sec)	$A_o - A$	$\frac{A_o - A}{A_o - A_\infty}$	$\frac{A - A_\infty}{A_o - A_\infty}$	$\ln \frac{A - A_\infty}{A_o - A_\infty}$
0.677	0	0	0	1.000	0
0.643	64	0.034	0.076	0.924	-0.079
0.618	202	0.059	0.132	0.868	-0.142
0.600	347	0.077	0.172	0.828	-0.189
0.570	548	0.107	0.239	0.761	-0.273
0.568	837	0.109	0.244	0.756	-0.280
0.567	1331	0.110	0.246	0.754	-0.282
0.513	2321	0.164	0.367	0.633	-0.457
0.440	4343	0.237	0.530	0.470	-0.755
0.378	8363	0.299	0.669	0.331	-1.106
0.287	20857	0.390	0.872	0.128	-2.056
0.230	~180000	0.447	1.000	0	

$[Co] = 1.8 \times 10^{-5}$ M; $[Py] = 8.0 \times 10^{-4}$ M; T = 20°C; P_{O_2} = 800 Torr

A (408 nm)	t (sec)	$A_o - A$	$\frac{A_o - A}{A_o - A_\infty}$	$\frac{A - A_\infty}{A_o - A_\infty}$	$\ln \frac{A - A_\infty}{A_o - A_\infty}$
0.883	0	0	0	1.000	0
0.817	55	0.066	0.113	0.887	-0.120
0.762	187	0.121	0.208	0.792	-0.233
0.712	321	0.171	0.293	0.707	-0.347
0.672	481	0.211	0.362	0.638	-0.449
0.623	648	0.260	0.446	0.554	-0.591
0.600	845	0.283	0.485	0.515	-0.664
0.567	1132	0.316	0.542	0.458	-0.781
0.530	1629	0.353	0.605	0.395	-0.929
0.473	2780	0.410	0.703	0.297	-1.214
0.425	4623	0.458	0.786	0.214	-1.542
0.330	8393	0.553	0.949	0.051	-2.976
0.315	18323	0.568	0.974	0.026	-3.650
0.300	72831	0.583	1.000	0	

$[Co] = 1.7 \times 10^{-5}$ M; $[Py] = 8.0 \times 10^{-4}$ M; T = 30°C; P_{O_2} = 800 Torr

A (408 nm)	t (sec)	$A_o - A$	$\frac{A_o - A}{A_o - A_\infty}$	$\frac{A - A_\infty}{A_o - A_\infty}$	$\ln \frac{A - A_\infty}{A_o - A_\infty}$
0.783	0	0	0	1.000	0
0.767	58	0.016	0.033	0.967	-0.034
0.702	205	0.081	0.166	0.834	-0.182
0.657	339	0.126	0.258	0.742	-0.298
0.617	486	0.166	0.340	0.660	-0.416
0.587	622	0.196	0.402	0.598	-0.514
0.548	844	0.235	0.482	0.518	-0.657
0.522	1111	0.261	0.535	0.465	-0.766
0.473	1629	0.310	0.635	0.365	-1.008
0.418	2634	0.365	0.748	0.252	-1.378
0.353	4638	0.430	0.881	0.119	-2.129
0.318	8629	0.465	0.953	0.047	-3.058
0.313	16643	0.470	0.963	0.037	-3.297
0.308	41004	0.475	0.973	0.027	-3.612
0.295	73254	0.488	1.000	0	———

$[Co] = 1.7 \times 10^{-5}$ M; $[Py] = 8.0 \times 10^{-4}$ M; T = 40°C; P_{O_2} = 800 Torr

A (408 nm)	t (sec)	$A_o - A$	$\frac{A_o - A}{A_o - A_\infty}$	$\frac{A - A_\infty}{A_o - A_\infty}$	$\ln \frac{A - A_\infty}{A_o - A_\infty}$
0.758	0	0	0	1.000	0
0.657	57	0.101	0.193	0.807	-0.214
0.596	189	0.162	0.310	0.690	-0.371
0.547	329	0.211	0.403	0.597	-0.516
0.513	461	0.245	0.468	0.532	-0.631
0.493	623	0.265	0.507	0.493	-0.707
0.449	824	0.309	0.591	0.409	-0.894
0.397	1193	0.361	0.690	0.310	-1.171
0.360	1657	0.398	0.761	0.239	-1.431
0.314	2641	0.444	0.849	0.151	-1.890
0.240	4642	0.518	0.990	0.010	-4.605
0 235	8619	0.523	1.000	0	———
0.235	16614	0.523	1.000	0	———
0.235	82568	0.523	1.000	0	———

APPENDIX Vr. PipCoOMBP + O_2 ⟶ PipCoOMBP(O_2)CoOMBP·Pip in DCE

$[Co] = 1.9 \times 10^{-5}$ M; $[Pip] = 7.6 \times 10^{-4}$ M; T = 20°C; P_{O_2} = 800 Torr

A (408 nm)	t (sec)	$A_o - A$	$\frac{A_o - A}{A_o - A_\infty}$	$\frac{A - A_\infty}{A_o - A_\infty}$	$\ln \frac{A - A_\infty}{A_o - A_\infty}$
0.895	0	0	0	1.000	0
0.810	50	0.085	0.145	0.855	-0.157
0.740	173	0.155	0.265	0.735	-0.308
0.671	308	0.224	0.383	0.617	-0.483
0.600	478	0.295	0.504	0.496	-0.701
0.563	617	0.332	0.568	0.432	-0.839
0.533	741	0.362	0.619	0.389	-0.944
0.500	890	0.395	0.675	0.325	-1.124
0.463	1070	0.432	0.738	0.262	-1.339
0.417	1267	0.478	0.817	0.183	-1.698
0.416	1507	0.479	0.819	0.181	-1.709
0.383	2011	0.512	0.875	0.125	-2.079
0.337	2997	0.558	0.954	0.046	-3.079
0.317	5002	0.578	0.988	0.012	-4.423
0.310	9007	0.585	1.000	0	———

$[Co] = 1.9 \times 10^{-5}$ M; $[Pip] = 7.6 \times 10^{-4}$ M; T = 30°C; P_{O_2} = 800 Torr*

A (408 nm)	t (sec)	$A_o - A$	$\frac{A_o - A}{A_o - A_\infty}$	$\frac{A - A_\infty}{A_o - A_\infty}$	$\ln \frac{A - A_\infty}{A_o - A_\infty}$
0.962	0	0	0	1.000	0
0.829	64	0.133	0.209	0.791	-0.234
0.723	192	0.239	0.375	0.625	-0.470
0.608	331	0.354	0.558	0.442	-0.816
0.549	455	0.413	0.648	0.352	-1.044
0.500	568	0.462	0.725	0.275	-1.291
0.464	701	0.498	0.782	0.218	-1.523
0.427	833	0.535	0.840	0.160	-1.833
0.403	1004	0.559	0.878	0.128	-2.056
0.373	1498	0.589	0.925	0.075	-2.596
0.325	2502	0.637	1.000	0	———
0.325	4502	0.637	1.000	0	———
0.325	8910	0.637	1.000	0	———

*Data used in Figure VII.1; final trace not shown as it dupilcates the previous one.

$[Co] = 1.9 \times 10^{-5}$ M; $[Pip] = 7.6 \times 10^{-4}$ M; T = 40°C; P_{O_2} = 800 Torr

A (408 nm)	t (sec)	$A_o - A$	$\frac{A_o - A}{A_o - A_\infty}$	$\frac{A - A_\infty}{A_o - A_\infty}$	$\ln \frac{A - A_\infty}{A_o - A_\infty}$
0.949	0	0	0	1.000	0
0.815	59	0.134	0.221	0.779	-0.250
0.663	182	0.286	0.472	0.528	-0.639
0.555	303	0.394	0.650	0.350	-1.050
0.477	432	0.472	0.779	0.221	-1.510
0.424	552	0.525	0.866	0.134	-2.010
0.387	695	0.562	0.927	0.073	-2.617
0.368	813	0.581	0.959	0.041	-3.194
0.357	1047	0.592	0.977	0.023	-3.772
0.350	1552	0.599	0.988	0.012	-4.423
0.350	2549	0.599	0.988	0.012	-4.423
0.343	4639	0.606	1.000	0	———
0.343	8550	0.606	1.000	0	———

$[Co] = 1.9 \times 10^{-4}$ M; $[Pip] = 7.6 \times 10^{-4}$ M; T = 40°C; P_{O_2} = 800 Torr

A (408 nm)	t (sec)	$A_o - A$	$\frac{A_o - A}{A_o - A_\infty}$	$\frac{A - A_\infty}{A_o - A_\infty}$	$\ln \frac{A - A_\infty}{A_o - A_\infty}$
0.917	0	0	0	1.000	0
0.690	90	0.227	0.413	0.587	-0.533
0.577	222	0.340	0.619	0.381	-0.965
0.516	352	0.401	0.730	0.270	-1.309
0.475	474	0.442	0.805	0.195	-1.635
0.445	615	0.472	0.860	0.140	-1.966
0.408	805	0.509	0.927	0.073	-2.617
0.407	1199	0.510	0.929	0.071	-2.645
0.392	2013	0.525	0.956	0.044	-3.124
0.387	4635	0.530	0.965	0.035	-3.352
0.368	8098	0.549	1.000	0	———

APPENDIX Vs. $(CH_3\text{-Im})_2CoOMBP + O_2 \longrightarrow CH_3\text{-ImCoOMBP}(O_2)CoOMBP\cdot CH_3\text{-Im}$

As a function of oxygen pressure

$[Co] = 2 \times 10^{-5}$ M; $[CH_3\text{-Im}] = 6.28$ M; $T = 20^{o}C$; $P_{O_2} = 400$ Torr

V	t (sec)	$V_o - V$	$\frac{V_o - V}{V_o - V_\infty}$	$\frac{V - V_\infty}{V_o - V_\infty}$	$\ln \frac{V - V_\infty}{V_o - V_\infty}$
5.7	0	0	0	1.000	0
5.3	5	0.4	0.073	0.927	-0.076
5.1	10	0.6	0.109	0.891	-0.115
4.9	15	0.8	0.145	0.855	-0.157
4.7	20	1.0	0.182	0.818	-0.201
4.4	25	1.3	0.236	0.744	-0.296
4.2	30	1.5	0.276	0.727	-0.319
4.1	35	1.6	0.291	0.709	-0.344
3.9	40	1.8	0.327	0.673	-0.396
3.7	45	2.0	0.364	0.636	-0.453
3.5	50	2.2	0.400	0.600	-0.511
3.3	60	2.4	0.436	0.564	-0.573
3.0	70	2.7	0.491	0.509	-0.675
2.7	80	3.0	0.545	0.455	-0.787
2.5	90	3.2	0.582	0.418	-0.872
2.2	100	3.5	0.636	0.364	-1.011
1.8	120	3.9	0.709	0.291	-1.234
1.5	140	4.2	0.764	0.236	-1.444
1.3	160	4.4	0.800	0.200	-1.609

$V_\infty = 0.2$

V - reading on the vertical scale of the stopped-flow oscilloscope
1 vertical scale division set at 0.2 V

1 horizontal scale division set at 5 sec

$[Co] = 2 \times 10^{-5}$ M; $[CH_3\text{-Im}] = 6.28$ M; $T = 20^{\circ}C$; $P_{O_2} = 300$ Torr

V	t (sec)	$V_o - V$	$\frac{V_o - V}{V_o - V_\infty}$	$\frac{V - V_\infty}{V_o - V_\infty}$	$\ln \frac{V - V_\infty}{V_o - V_\infty}$
7.1	0	0	0	1.000	0
6.9	5	0.2	0.025	0.975	-0.025
6.6	10	0.5	0.062	0.938	-0.064
6.4	15	0.7	0.086	0.914	-0.090
6.2	20	0.9	0.111	0.889	-0.118
6.0	25	1.1	0.136	0.864	-0.146
5.8	30	1.3	0.160	0.840	-0.174
5.6	35	1.5	0.185	0.815	-0.205
5.4	40	1.7	0.210	0.790	-0.236
5.3	45	1.8	0.222	0.778	-0.251
5.1	50	2.0	0.247	0.753	-0.284
4.6	60	2.5	0.309	0.691	-0.370
4.3	70	2.8	0.346	0.654	-0.425
3.9	80	3.2	0.396	0.604	-0.504
3.6	90	3.5	0.432	0.568	-0.566
3.3	100	3.8	0.469	0.531	-0.633
2.7	120	4.4	0.543	0.457	-0.783
2.2	140	4.9	0.605	0.395	-0.929
1.7	160	5.4	0.667	0.333	-1.100

$V_\infty = -1.0$

$[Co] = 2 \times 10^{-5}$ M; $[CH_3\text{-Im}] = 6.28$ M; $T = 20^{\circ}C$; $P_{O_2} = 200$ Torr

V	t (sec)	$V_o - V$	$\frac{V_o - V}{V_o - V}$	$\frac{V - V_\infty}{V_o - V_\infty}$	$\ln \frac{V - V_\infty}{V_o - V_\infty}$
7.0	0	0	0	1.000	0
6.9	5	0.1	0.026	0.974	-0.026
6.8	10	0.2	0.053	0.947	-0.054
6.6	15	0.4	0.105	0.895	-0.111
6.5	20	0.5	0.132	0.868	-0.142
6.4	25	0.6	0.158	0.842	-0.172
6.4	30	0.6	0.158	0.842	-0.172
6.3	35	0.7	0.184	0.816	-0.203
6.3	40	0.7	0.184	0.816	-0.203
6.2	45	0.8	0.210	0.790	-0.236
6.2	50	0.8	0.210	0.790	-0.236
6.2	60	0.8	0.210	0.790	-0.236
6.1	70	0.9	0.237	0.763	-0.270
5.9	80	1.1	0.289	0.711	-0.341
5.9	90	1.1	0.289	0.711	-0.341
5.8	100	1.2	0.316	0.684	-0.380
5.5	120	1.5	0.395	0.605	-0.503
5.4	140	1.6	0.421	0.579	-0.546
5.3	160	1.7	0.447	0.553	-0.592

$V_\infty = 3.2$

$[Co] = 2 \times 10^{-5}$ M; $[CH_3\text{-Im}] = 6.28$ M; $T = 20^{\circ}C$; $P_{O_2} = 100$ Torr

V	t (sec)	$V_o - V$	$\frac{V_o - V}{V_o - V_\infty}$	$\frac{V - V_\infty}{V_o - V_\infty}$	$\ln \frac{V - V_\infty}{V_o - V_\infty}$
6.0	0	0	0	1.000	0
5.9	5	0.1	0.029	0.971	-0.029
5.8	10	0.2	0.057	0.943	-0.059
5.8	15	0.2	0.057	0.943	-0.059
5.7	20	0.3	0.086	0.914	-0.090
5.7	25	0.3	0.086	0.914	-0.090
5.7	30	0.3	0.086	0.914	-0.090
5.6	35	0.4	0.114	0.886	-0.121
5.6	40	0.4	0.114	0.886	-0.090
5.6	45	0.4	0.114	0.886	-0.090
5.6	50	0.4	0.114	0.886	-0.090
5.2	105	0.8	0.229	0.771	-0.090

$V_\infty = 2.5$

APPENDIX Vt. $(CH_3\text{-Im})_2CoOMBP + O_2 \longrightarrow CH_3\text{-ImCoOMBP}(O_2)CoOMBP\cdot CH_3\text{-Im}$

As a function of temperature

$[Co] = 2 \times 10^{-5}$ M; $[CH_3\text{-Im}] = 6.28$ M; $T = 10^{\circ}C$; $P_{O_2} = 400$ Torr

V	t (sec)	$V_o - V$	$\frac{V_o - V}{V_o - V_\infty}$	$\frac{V - V_\infty}{V_o - V_\infty}$	$\ln \frac{V - V_\infty}{V_o - V_\infty}$
8.0	0	0	0	1.000	0
7.8	5	0.2	0.025	0.975	-0.025
7.5	10	0.5	0.063	0.937	-0.065
7.4	15	0.6	0.076	0.924	-0.079
7.2	20	0.8	0.101	0.899	-0.106
7.0	25	1.0	0.127	0.873	-0.136
6.7	30	1.3	0.165	0.835	-0.180
6.6	35	1.4	0.177	0.823	-0.195
6.4	40	1.6	0.203	0.797	-0.227
6.2	45	1.8	0.228	0.772	-0.259
6.0	50	2.0	0.253	0.747	-0.292
5.6	60	2.4	0.304	0.696	-0.362
5.3	70	2.7	0.342	0.658	-0.419
5.0	80	3.0	0.380	0.620	-0.478
4.7	90	3.3	0.418	0.582	-0.541
4.4	100	3.6	0.456	0.544	-0.609
3.9	120	4.1	0.519	0.481	-0.732
3.6	140	4.4	0.557	0.443	-0.814
3.2	160	4.8	0.608	0.392	-0.956

$V_\infty = 0.1$

$[Co] = 2 \times 10^{-5}$ M; $[CH_3\text{-Im}] = 6.28$ M; $T = 20^{\circ}C$; $P_{O_2} = 400$ Torr

V	t (sec)	$V_o - V$	$\frac{V_o - V}{V_o - V_\infty}$	$\frac{V - V_\infty}{V_o - V_\infty}$	$\ln \frac{V - V_\infty}{V_o - V_\infty}$
5.7	0	0	0	1.000	0
5.3	5	0.4	0.073	0.927	-0.076
5.1	10	0.6	0.109	0.891	-0.115
4.9	15	0.8	0.145	0.855	-0.157
4.7	20	1.0	0.182	0.818	-0.201
4.4	25	1.3	0.236	0.744	-0.296
4.2	30	1.5	0.273	0.727	-0.319
4.1	35	1.6	0.291	0.709	-0.344
3.9	40	1.8	0.327	0.673	-0.396
3.7	45	2.0	0.364	0.636	-0.453
3.5	50	2.2	0.400	0.600	-0.511
3.3	60	2.4	0.436	0.564	-0.573
3.0	70	2.7	0.491	0.509	-0.675
2.7	80	3.0	0.545	0.455	-0.787
2.5	90	3.2	0.582	0.418	-0.872
2.2	100	3.5	0.636	0.364	-1.011
1.8	120	3.9	0.709	0.291	-1.234
1.5	140	4.2	0.764	0.236	-1.444
1.3	160	4.4	0.800	0.200	-1.609

$V_\infty = 0.2$

$[Co]$ 2 x 10^{-5} M; $[CH_3\text{-Im}]$ = 6.28 M; T = 30°C; P_{O_2} = 400 Torr

V	t (sec)	$V_o - V$	$\frac{V_o - V}{V_o - V_\infty}$	$\frac{V - V_\infty}{V_o - V_\infty}$	$\ln \frac{V - V_\infty}{V_o - V_\infty}$
6.4	0	0	0	1.000	0
5.9	5	0.5	0.091	0.909	-0.095
5.5	10	0.9	0.164	0.856	-0.155
5.0	15	1.4	0.255	0.745	-0.294
4.6	20	1.8	0.327	0.673	-0.396
4.2	25	2.2	0.400	0.600	-0.511
3.8	30	2.6	0.473	0.527	-0.641
3.5	35	2.9	0.527	0.473	-0.749
3.3	40	3.1	0.564	0.436	-0.830
3.1	45	3.3	0.600	0.400	-0.916
2.9	50	3.5	0.636	0.364	-1.011
2.7	55	3.7	0.673	0.327	-1.118
2.6	60	3.8	0.691	0.309	-1.174
2.3	65	4.1	0.745	0.255	-1.366
2.2	70	4.2	0.764	0.236	-1.444
2.0	75	4.4	0.800	0.200	-1.609
1.9	80	4.5	0.818	0.182	-1.704
1.8	85	4.6	0.836	0.164	-1.808
1.7	90	4.7	0.855	0.145	-1.931
1.6	95	4.8	0.873	0.127	-2.063
1.6	100	4.8	0.873	0.127	-2.063
1.5	105	4.9	0.891	0.109	-2.216

V_∞ = 0.9

APPENDIX Vu. $Py_2CoOMBP + O_2 \longrightarrow PyCoOMBP(O_2)CoOMBP \cdot Py$

In 1:1 v/v toluene:Py; T = 18°C; [Co] = 2.2 x 10^{-5}M

A (430 nm)	t (sec)	$A_o - A$	$\frac{A_o - A}{A_o - A_\infty}$	$\frac{A - A_\infty}{A_o - A_\infty}$	$\ln \frac{A - A_\infty}{A_o - A_\infty}$
1.458	0	0	0	1.000	0
1.393	62	0.065	0.072	0.928	-0.075
1.378	204	0.080	0.089	0.911	-0.093
1.358	668	0.100	0.111	0.889	-0.118
1.303	2775	0.155	0.173	0.827	-0.190
1.228	7890	0.230	0.256	0.744	-0.296
1.092	31569	0.366	0.408	0.592	-0.524
0.975	44769	0.483	0.538	0.462	-0.772
0.922	79227	0.536	0.597	0.403	-0.909
0.803	~120000	0.655	0.729	0.271	-1.306
0.738	~160000	0.720	0.802	0.198	-1.619
0.670	~250000	0.788	0.878	0.122	-2.104

A_∞ estimated to be 0.560.

APPENDIX Vv. $Py_2CoOMBP + O_2 \longrightarrow PyCoOMBP(O_2)CoOMBP \cdot Py$

In neat Py as a function of temperature.

$[Co] = 2.1 \times 10^{-5}$ M; $T = 15^{\circ}C$; $P_{O_2} = 800$ Torr

A (430 nm)	t (sec)	$A_o - A$	$\frac{A_o - A}{A_o - A_\infty}$	$\frac{A - A_\infty}{A_o - A_\infty}$	$\ln \frac{A - A_\infty}{A_o - A_\infty}$
1.375	0	0	0	1.000	0
1.370	97	0.005	0.007	0.993	-0.007
1.363	237	0.012	0.017	0.983	-0.017
1.363	514	0.012	0.017	0.993	-0.017
1.361	1157	0.014	0.020	0.980	-0.020
1.358	2429	0.018	0.025	0.975	-0.025
1.332	5008	0.043	0.060	0.940	-0.062
1.308	7548	0.067	0.094	0.906	-0.099
1.263	12508	0.112	0.157	0.843	-0.171
1.217	17561	0.158	0.221	0.779	-0.250
1.197	25499	0.178	0.249	0.751	-0.286
1.108	50636	0.267	0.373	0.627	-0.467
1.053	82267	0.322	0.450	0.550	-0.598

A_∞ estimated to be 0.660

$[Co] = 1.8 \times 10^{-5}$ M; $T = 20^{\circ}C$; $P_{O_2} = 800$ Torr

A (430 nm)	t (sec)	$A_o - A$	$\frac{A_o - A}{A_o - A_\infty}$	$\frac{A - A_\infty}{A_o - A_\infty}$	$\ln \frac{A - A_\infty}{A_o - A_\infty}$
1.159	0	0	0	1.000	0
1.094	61	0.048	0.063	0.937	-0.065
1.092	157	0.050	0.066	0.934	-0.068
1.088	455	0.064	0.084	0.916	-0.088
1.053	1659	0.099	0.130	0.870	-0.139
0.992	4123	0.160	0.210	0.790	-0.236
0.967	7138	0.185	0.243	0.757	-0.278
0.893	13423	0.259	0.340	0.660	-0.416
0.781	32680	0.371	0.487	0.513	-0.667
0.721*	59618	0.431	0.566	0.434	-0.835
0.405*	80000	0.747	0.980	0.020	-3.912
0.390	150000	0.762	1.000	0	———

* Sample exposed to light between runs.

$[Co] = 1.9 \times 10^{-5}$ M; $T = 30^{o}C$; P_{O_2} = 800 Torr

A (430 nm)	t (sec)	$A_o - A$	$\frac{A_o - A}{A_o - A_\infty}$	$\frac{A - A_\infty}{A_o - A_\infty}$	$\ln \frac{A - A_\infty}{A_o - A_\infty}$
1.212	0	0	0	1.000	0
1.207	92	0.005	0.007	0.993	-0.007
1.200	212	0.012	0.017	0.983	-0.017
1.187	514	0.025	0.035	0.965	-0.036
1.178	1114	0.034	0.047	0.953	-0.048
1.158	2320	0.054	0.075	0.925	-0.078
1.120	5153	0.092	0.127	0.873	-0.136
1.073	9840	0.139	0.193	0.807	-0.214
1.009	19035	0.203	0.281	0.719	-0.330
0.913*	39587	0.299	0.414	0.586	-0.534
0.570*	~125000	0.642	0.889	0.111	-2.198
0.490*	~250000	0.722	1.000	0	———

* Sample exposed to light between runs.

$[Co] = 1.9 \times 10^{-5}$ M; $T = 40^{o}C$; P_{O_2} = 800 Torr

A (430 nm)	t (sec)	$A_o - A$	$\frac{A_o - A_\infty}{A_o - A_\infty}$	$\frac{A - A_\infty}{A_o - A_\infty}$	$\ln \frac{A - A_\infty}{A_o - A_\infty}$
1.286	0	0	0	1.000	0
1.262	76	0.024	0.033	0.967	-0.034
1.212	208	0.074	0.101	0.899	-0.106
1.207	337	0.079	0.107	0.893	-0.113
1.203	646	0.083	0.113	0.887	-0.120
1.188	1399	0.098	0.133	0.867	-0.143
1.165	2918	0.121	0.164	0.836	-0.179
1.130	5321	0.156	0.212	0.788	-0.238
1.100	9881	0.186	0.253	0.744	-0.292
1.019	26651	0.267	0.363	0.637	-0.451
0.963	40140	0.323	0.439	0.561	-0.578
0.895	76500	0.391	0.531	0.469	-0.757

A_∞ estimated to be 0.550.

APPEDIX Vw. $Py_2CoOMBP + O_2 \longrightarrow PyCoOMBP(O_2)CoOMBP \cdot Py$

In neat Py as a function of cobalt concentration.

$[Co] = 1.8 \times 10^{-5}$ M; T = 20°C; P_{O_2} = 800 Torr

A (430 nm)	t (sec)	$A_o - A$	$\frac{A_o - A}{A_o - A_\infty}$	$\frac{A - A_\infty}{A_o - A_\infty}$	$\ln \frac{A - A_\infty}{A_o - A_\infty}$
1.159	0	0	0	1.000	0
1.094	61	0.048	0.063	0.937	-0.065
1.092	157	0.050	0.064	0.934	-0.068
1.088	455	0.064	0.084	0.916	-0.088
1.053	1659	0.099	0.130	0.870	-0.139
0.992	4123	0.160	0.210	0.790	-0.236
0.967	7138	0.185	0.243	0.757	-0.278
0.893	13423	0.259	0.340	0.660	-0.416
0.781	32680	0.371	0.487	0.513	-0.667
0.721*	59618	0.431	0.566	0.434	-0.835
0.405*	80000	0.747	0.980	0.020	-3.912
0.390	150000	0.762	1.000	0	

* Sample exposed to light between runs.

$[Co] = 1.2 \times 10^{-4}$ M; T = 20°C; P_{O_2} = 800 Torr

A (430 nm)	t (sec)	$A_o - A$	$\frac{A_o - A}{A_o - A_\infty}$	$\frac{A - A_\infty}{A_o - A_\infty}$	$\ln \frac{A - A_\infty}{A_o - A_\infty}$
0.756	0	0	0	1.000	0
0.756	88	0	0	1.000	0
0.753	225	0.003	0.008	0.992	-0.008
0.750	464	0.006	0.016	0.984	-0.016
0.734	977	0.022	0.059	0.941	-0.061
0.707	2026	0.049	0.132	0.868	-0.142
0.683	4194	0.073	0.197	0.803	-0.219
0.653	8008	0.103	0.278	0.722	-0.326
0.603	16042	0.153	0.412	0.588	-0.531
0.545	31123	0.211	0.569	0.431	-0.842
0.508	53428	0.248	0.668	0.332	-1.103
0.448	114085	0.308	0.830	0.170	-1.772

A_∞ estimated to be 0.385.

APPENDIX Vx. $(CH_3\text{-Im})_2CoOMBP + O_2 \longrightarrow CH_3\text{-ImCoOMBP}(O_2)CoOMBP\cdot CH_3\text{-Im}$

As a function of solvent

$[Co] = 2 \times 10^{-5}$ M; T = 20°C; P_{O_2} = 400 Torr; Solvent: 1:1 v/v toluene:CH_3-Im

V	t (sec)	$V_o - V$	$\frac{V_o - V}{V_o - V_\infty}$	$\frac{V - V_\infty}{V_o - V_\infty}$	$\ln \frac{V - V_\infty}{V_o - V_\infty}$
5.7	0	0	0	1.000	0
5.3	5	0.4	0.073	0.927	-0.076
5.1	10	0.6	0.109	0.891	-0.115
4.9	15	0.8	0.145	0.855	-0.157
4.7	20	1.0	0.182	0.818	-0.201
4.4	25	1.3	0.236	0.744	-0.296
4.2	30	1.5	0.276	0.727	-0.319
4.1	35	1.6	0.291	0.709	-0.344
3.9	40	1.8	0.327	0.673	-0.396
3.7	45	2.0	0.364	0.636	-0.453
3.5	50	2.2	0.400	0.600	-0.511
3.3	60	2.4	0.436	0.564	-0.573
3.0	70	2.7	0.491	0.509	-0.675
2.7	80	3.0	0.545	0.455	-0.787
2.5	90	3.2	0.582	0.418	-0.872
2.2	100	3.5	0.636	0.364	-1.011
1.8	120	3.9	0.709	0.291	-1.234
1.5	140	4.2	0.764	0.236	-1.444
1.3	160	4.4	0.800	0.200	-1.609

$V_\infty = 0.2$

V - reading on vertical scale of the stopped-flow ocsilloscope
1 vertical scale division set at 0.2 V

1 horizontal scale division set at 5 sec

[Co] = 2×10^{-5} M; T = 20°C; P_{O_2} = 400 Torr; Solvent: Neat CH_3-Im

V	t (sec)	$V_o - V$	$\frac{V_o - V}{V_o - V_\infty}$	$\frac{V - V_\infty}{V_o - V_\infty}$	$\ln \frac{V - V_\infty}{V_o - V_\infty}$
6.0	0	0	0	1.000	0
5.6	5	0.4	0.067	0.933	-0.069
5.2	10	0.8	0.133	0.867	-0.143
4.7	15	1.3	0.217	0.783	-0.245
4.3	20	1.7	0.283	0.717	-0.333
3.8	25	2.2	0.367	0.633	-0.457
3.4	30	2.6	0.433	0.567	-0.567
3.2	35	2.8	0.467	0.533	-0.629
2.9	40	3.1	0.517	0.483	-0.728
2.6	45	3.4	0.567	0.433	-0.837
2.4	50	3.6	0.600	0.400	-0.916

V_∞ = 0.0

[Co] = 2×10^{-5} M; T = 30°C; P_{O_2} = 400 Torr; Solvent: 1:1 v/v toluene:CH_3-Im

V	t (sec)	$V_o - V$	$\frac{V_o - V}{V_o - V}$	$\frac{V - V_\infty}{V_o - V_\infty}$	$\ln \frac{V - V_\infty}{V_o - V_\infty}$
6.4	0	0	0	1.000	0
5.9	5	0.5	0.091	0.909	-0.095
5.5	10	0.9	0.164	0.856	-0.155
5.0	15	1.4	0.255	0.745	-0.294
4.6	20	1.8	0.327	0.673	-0.396
4.2	25	2.2	0.400	0.600	-0.511
3.8	30	2.6	0.473	0.527	-0.641
3.5	35	2.9	0.527	0.473	-0.749
3.3	40	3.1	0.564	0.436	-0.830
3.1	45	3.3	0.600	0.400	-0.916
2.9	50	3.5	0.636	0.364	-1.011
2.7	55	3.7	0.673	0.327	-1.118
2.6	60	3.8	0.691	0.309	-1.174
2.3	65	4.1	0.745	0.255	-1.366
2.2	70	4.2	0.764	0.236	-1.444
2.0	75	4.4	0.800	0.200	-1.609
1.9	80	4.5	0.818	0.182	-1.704
1.8	85	4.6	0.836	0.164	-1.808
1.7	90	4.7	0.855	0.145	-1.931
1.6	95	4.8	0.873	0.127	-2.063
1.6	100	4.8	0.873	0.127	-2.063
1.5	105	4.9	0.891	0.109	-2.216

V_∞ = 0.9

$[Co] = 2 \times 10^{-5}$ M; T = 30°C; P_{O_2} = 400 Torr; Solvent: 1:1 v/v DCE:CH_3-Im

V	t (sec)	$V_o - V$	$\frac{V_o - V}{V_o - V_\infty}$	$\frac{V - V_\infty}{V_o - V_\infty}$	$\ln \frac{V - V_\infty}{V_o - V_\infty}$
5.6	0	0	0	1.000	0
5.2	1	0.4	0.154	0.846	-0.167
4.6	2	1.0	0.385	0.615	-0.486
4.2	3	1.4	0.538	0.462	-0.772
3.9	4	1.7	0.653	0.347	-1.058
3.7	5	1.9	0.731	0.269	-1.313
3.6	6	2.0	0.769	0.231	-1.465
3.5	7	2.1	0.808	0.192	-1.650
3.4	8	2.2	0.846	0.154	-1.871
3.3	9	2.3	0.885	0.115	-2.163
3.2	10	2.4	0.923	0.077	-2.564

V_∞ = 3.0

1 horizontal scale division set at 1 sec

APPENDIX Vy. $Py_2CoOMBP + O_2 \longrightarrow PyCoOMBP(O_2)CoOMBP \cdot Py$

In 1:1 v/v DCE:Py as a function of temperature

$[Co] = 1.8 \times 10^{-5}$ M; T = 20°C; P_{O_2} = 800 Torr

A (445 nm)	t (sec)	$A - A_o$	$\frac{A - A_o}{A_\infty - A_o}$	$\frac{A_\infty - A}{A_\infty - A_o}$	$\ln \frac{A_\infty - A}{A_\infty - A_o}$
0.530	0	0	0	1.000	0
0.560	72	0.030	0.039	0.961	-0.040
0.580	199	0.050	0.065	0.935	-0.067
0.595	332	0.065	0.085	0.915	-0.089
0.625	513	0.095	0.124	0.876	-0.132
0.693	1131	0.163	0.213	0.787	-0.240
0.800	2346	0.270	0.353	0.647	-0.435
0.880	3342	0.350	0.458	0.542	-0.612
0.940	4838	0.410	0.536	0.464	-0.768
1.025	6837	0.495	0.647	0.353	-1.041
1.105	9334	0.575	0.752	0.248	-1.394
1.165	12333	0.635	0.830	0.170	-1.772
1.210	16537	0.680	0.889	0.111	-2.198
1.270	26870	0.740	0.967	0.037	-3.474
1.295	74544	0.765	1.000	0	

$[Co] = 1.8 \times 10^{-5}$ M; T = 30°C; P_{O_2} = 800 Torr

A (445 nm)	t (sec)	$A - A_o$	$\frac{A - A_o}{A_\infty - A_o}$	$\frac{A_\infty - A}{A_\infty - A_o}$	$\ln \frac{A_\infty - A}{A_\infty - A_o}$
0.550	0	0	0	1.000	0
0.585	78	0.035	0.046	0.954	-0.047
0.610	213	0.060	0.079	0.921	-0.082
0.635	363	0.085	0.112	0.888	-0.119
0.670	583	0.120	0.158	0.842	-0.172
0.730	985	0.180	0.237	0.763	-0.270
0.803	1582	0.253	0.333	0.667	-0.405
0.880	2535	0.330	0.434	0.566	-0.569
0.940	3541	0.390	0.513	0.487	-0.719
0.997	4543	0.447	0.588	0.412	-0.887
1.060	6008	0.510	0.671	0.329	-1.112
1.123	7829	0.573	0.754	0.246	-1.402
1.188	10424	0.638	0.839	0.161	-1.826
1.280	20047	0.730	0.960	0.040	-3.079
1.310	76522	0.760	1.000	0	

$[Co] = 1.9 \times 10^{-5}$ M; $T = 40^{\circ}C$; $P_{O_2} = 800$ Torr

A (445 nm)	t (sec)	$A - A_o$	$\frac{A - A_o}{A_\infty - A_o}$	$\frac{A_\infty - A}{A_\infty - A_o}$	$\ln \frac{A_\infty - A}{A_\infty - A_o}$
0.580	0	0	0	1.000	0
0.645	138	0.065	0.075	0.925	-0.078
0.675	274	0.095	0.110	0.890	-0.117
0.720	430	0.140	0.162	0.838	-0.177
0.770	629	0.190	0.220	0.780	-0.248
0.840	923	0.260	0.301	0.699	-0.358
0.910	1323	0.330	0.382	0.618	-0.481
0.950	1828	0.370	0.428	0.572	-0.559
1.053	2529	0.473	0.547	0.453	-0.792
1.130	3531	0.550	0.636	0.364	-1.011
1.207	5087	0.627	0.725	0.275	-1.291
1.290	7007	0.710	0.821	0.179	-1.720
1.360	10014	0.780	0.902	0.098	-2.323
1.420	15016	0.840	0.971	0.029	-3.540
1.430	25082	0.850	0.983	0.017	-4.075
1.445	75000	0.865	1.000	0	———

APPENDIX Vz. $Py_2CoOMBP + O_2 \longrightarrow PyCoOMBP(O_2)CoOMBP \cdot Py$

In 1:1 v/v DCE:Py as a function of cobalt concentration

$[Co] = 2 \times 10^{-6}$ M; $T = 20^{\circ}C$; $P_{O_2} = 800$ Torr

A (445 nm)	t (sec)	$A - A_o$	$\frac{A - A_o}{A_\infty - A_o}$	$\frac{A_\infty - A}{A_\infty - A_o}$	$\ln \frac{A_\infty - A}{A_\infty - A_o}$
0.652	0	0	0	1.000	0
0.701	147	0.049	0.063	0.937	-0.065
0.722	252	0.070	0.091	0.909	-0.095
0.755	505	0.103	0.133	0.867	-0.143
0.806	1012	0.154	0.199	0.801	-0.222
0.850	1502	0.198	0.256	0.744	-0.296
0.929	2467	0.277	0.358	0.642	-0.443
1.052	4271	0.400	0.517	0.487	-0.719
1.139	6032	0.487	0.630	0.370	-0.994
1.253	9276	0.601	0.777	0.223	-1.501
1.361	15573	0.709	0.917	0.083	-2.489
1.411	24738	0.759	0.982	0.018	-4.017

$[Co] = 1.8 \times 10^{-5}$ M; $T = 20^{\circ}C$; $P_{O_2} = 800$ Torr

A (445 nm)	t (sec)	$A - A_o$	$\frac{A - A_o}{A - A_o}$	$\frac{A_\infty - A}{A_\infty - A_o}$	$\ln \frac{A_\infty - A}{A_\infty - A_o}$
0.530	0	0	0	1.000	0
0.560	72	0.030	0.039	0.961	-0.040
0.580	199	0.050	0.050	0.935	-0.067
0.595	332	0.065	0.085	0.915	-0.089
0.625	513	0.095	0.124	0.876	-0.132
0.693	1131	0.163	0.213	0.787	-0.240
0.800	2346	0.270	0.353	0.647	-0.435
0.880	3342	0.350	0.458	0.542	-0.612
0.940	4838	0.410	0.536	0.464	-0.768
1.025	6837	0.495	0.647	0.353	-1.041
1.105	9334	0.575	0.752	0.248	-1.394
1.165	12333	0.635	0.830	0.170	-1.772
1.210	16537	0.680	0.889	0.111	-2.198
1.270	26870	0.740	0.967	0.037	-3.474
1.295	74544	0.765	1.000	0	

$[Co] = 1.9 \times 10^{-4}$ M; $T = 20^{\circ}C$; $P_{O_2} = 800$ Torr

A (445 nm)	t (sec)	$A - A_o$	$\frac{A - A_o}{A_\infty - A_o}$	$\frac{A_\infty - A}{A_\infty - A_o}$	$\ln \frac{A_\infty - A}{A_\infty - A_o}$
0.600	0	0	0	1.000	0
0.630	125	0.030	0.041	0.959	-0.042
0.640	263	0.040	0.055	0.945	-0.057
0.650	503	0.050	0.068	0.932	-0.070
0.697	996	0.097	0.132	0.868	-0.142
0.741	1504	0.141	0.192	0.808	-0.213
0.830	2516	0.230	0.314	0.686	-0.377
0.883	3516	0.283	0.386	0.614	-0.488
0.967	4506	0.367	0.501	0.499	-0.695
1.042	5509	0.442	0.603	0.397	-0.924
1.082	6499	0.489	0.667	0.333	-1.100
1.173	8516	0.573	0.782	0.218	-1.523
1.218	10502	0.618	0.843	0.157	-1.852
1.278	15529	0.678	0.925	0.075	-2.590
1.300	25495	0.700	0.955	0.045	-3.101
1.330	78640	0.730	1.000	0	———

APPENDIX Vaa. $PipCoOMBP + O_2 \longrightarrow PipCoOMBP(O_2)CoOMBP \cdot Pip$

In 1:1 v/v DCE:Pip

$[Co] = 2.0 \times 10^{-5}$ M; $T = 20^{\circ}C$; P_{O_2} = 800 Torr

A (432 nm)	t (sec)	$A_o - A$	$\frac{A_o - A}{A_o - A_\infty}$	$\frac{A - A_\infty}{A_o - A_\infty}$	$\ln \frac{A - A_\infty}{A_o - A_\infty}$
1.301	0	0	0	1.000	0
1.072	87	0.229	0.313	0.687	-0.375
1.063	229	0.238	0.326	0.674	-0.395
1.048	461	0.253	0.346	0.654	-0.425
1.015	971	0.286	0.391	0.609	-0.496
0.950	2294	0.351	0.480	0.520	-0.654

A_∞ estimated to be 0.570 based on Py data

$[Co] = 2.1 \times 10^{-4}$ M; $T = 20^{\circ}C$; P_{O_2} = 800 Torr

A (432 nm)	t (sec)	$A_o - A$	$\frac{A_o - A}{A_o - A_\infty}$	$\frac{A - A_\infty}{A_o - A_\infty}$	$\ln \frac{A - A_\infty}{A_o - A_\infty}$
1.460	0	0	0	1.000	0
1.435	46	0.025	0.030	0.970	-0.030
1.430	160	0.030	0.036	0.964	-0.037
1.428	419	0.032	0.039	0.961	-0.040
1.403	1000	0.051	0.069	0.931	-0.071
1.356	2034	0.104	0.125	0.875	-0.134
1.356	3042	0.104	0.125	0.875	-0.134
1.355	5037	0.105	0.127	0.873	-0.136
1.345	9046	0.115	0.139	0.861	-0.150
1.250	50173	0.210	0.253	0.747	-0.292

A_∞ estimated to be 0.670 based on Py data

APPENDIX Vbb. CH_3-ImCoTPP + O_2 ⟶ CH_3-ImCoTPP(O_2)CoTPP·CH_3-Im

[Co] = 5.1×10^{-5} M; [CH_3-Im] = 0.0625 M; T = 20°C; P_{O_2} = 800 Torr

Solvent = Toluene

A (412 nm)	t (sec)	$A_o - A$	$\frac{A_o - A}{A_o - A}$	$\frac{A - A_\infty}{A_o - A_\infty}$	$\ln \frac{A - A_\infty}{A_o - A_\infty}$
1.268	0	0	0	1.000	0
1.232	83	0.036	0.034	0.966	-0.035
1.220	212	0.048	0.048	0.955	-0.046
1.210	528	0.058	0.055	0.945	-0.057
1.199	1234	0.071	0.067	0.933	-0.069
1.190	3038	0.078	0.074	0.926	-0.077
1.140	8021	0.128	0.128	0.878	-0.130
1.109	13019	0.159	0.151	0.849	-0.164
1.097	18589	0.171	0.162	0.838	-0.177
1.070	34881	0.198	0.188	0.812	-0.208
1.000	70058	0.268	0.255	0.745	-0.294

[Co] = 3.6×10^{-6} M; [CH_3-Im] = 0.0625 M; T = 20°C; P_{O_2} = 800 Torr

Solvent = Toluene

A (412 nm)	t (sec)	$A_o - A$	$\frac{A_o - A}{A_o - A_\infty}$	$\frac{A - A_\infty}{A_o - A_\infty}$	$\ln \frac{A - A_\infty}{A_o - A_\infty}$
0.957	0	0	0	1.000	0
0.918	68	0.039	0.051	0.949	-0.052
0.903	199	0.054	0.071	0.929	-0.074
0.872	579	0.085	0.112	0.888	-0.119
0.858	1455	0.099	0.130	0.870	-0.139
0.823	3840	0.134	0.176	0.824	-0.194
0.762	10262	0.195	0.256	0.744	-0.296

A_∞ estimated to be 0.215 for [Co] = 5.1×10^{-5} M, 0.195 for [Co] = 3.8×10^{-6} M; based on data in DCE.

APPENDIX Vcc. CH_3-ImCoTPP + O_2 ⟶ CH_3-ImCoTPP(O_2)CoTPP·CH_3-Im

In DCE as a function of cobalt concentration.

[Co] = 4.0×10^{-6} M; [CH_3-Im] = 0.0625 M; T = 20°C; P_{O_2} = 800 Torr

A (412 nm)	t (sec)	$A_o - A$	$\frac{A_o - A}{A_o - A_\infty}$	$\frac{A - A_\infty}{A_o - A_\infty}$	$\ln \frac{A - A_\infty}{A_o - A_\infty}$
0.982	0	0	0	1.000	0
0.807	150	0.175	0.223	0.777	-0.252
0.778	237	0.204	0.260	0.740	-0.301
0.712	498	0.270	0.344	0.656	-0.422
0.453	1798	0.529	0.675	0.325	-1.124
0.308	2813	0.674	0.860	0.140	-1.966
0.198	6383	0.784	1.000	0	———

[Co] = 5.2×10^{-5} M; [CH_3-Im] = 0.0625 M; T = 20°C; P_{O_2} = 800 Torr

A (540 nm)	t (sec)	$A_o - A$	$\frac{A_o - A}{A_o - A_\infty}$	$\frac{A - A_\infty}{A_o - A_\infty}$	$\ln \frac{A - A_\infty}{A_o - A_\infty}$
0.608	0	0	0	1.000	0
0.578	77	0.030	0.190	0.810	-0.211
0.568	180	0.040	0.253	0.747	-0.292
0.554	425	0.054	0.342	0.658	-0.419
0.523	1016	0.085	0.538	0.462	-0.772
0.490	1789	0.118	0.747	0.253	-1.374
0.460	3002	0.148	0.937	0.063	-2.765
0.450	4322	0.158	1.000	0	———
0.450	5920	0.158	1.000	0	———

[Co] = 7.6×10^{-4} M; [CH_3-Im] = 0.0625 M; T = 20°C; P_{O_2} = 800 Torr*

A (540 nm)	t (sec)	$A_o - A$	$\frac{A_o - A}{A_o - A_\infty}$	$\frac{A - A_\infty}{A_o - A_\infty}$	$\ln \frac{A - A_\infty}{A_o - A_\infty}$
0.850	0	0	0	1.000	0
0.815	73	0.035	0.123	0.877	-0.131
0.807	142	0.043	0.151	0.849	-0.164
0.792	287	0.058	0.204	0.796	-0.228
0.780	344	0.070	0.246	0.754	-0.282
0.740	606	0.110	0.386	0.614	-0.488
0.690	1111	0.160	0.561	0.439	-0.823
0.685	1197	0.165	0.579	0.421	-0.865
0.675	1283	0.175	0.614	0.386	-0.952
0.620	2253	0.230	0.807	0.193	-1.645
0.565	16983	0.285	1.000	0	———

* Data used in Figure VII.4

APPENDIX Vdd. CH_3-ImEpI + O_2 ⟶ CH_3-ImCoEpI(O_2)CoEpI·CH_3-Im

In DCE as a function of cobalt concentration

$[Co] = 6.0 \times 10^{-6}$ M; $[CH_3\text{-Im}] = 0.0625$ M; T = 30°C; P_{O_2} = 800 Torr

A (395 nm)	t (sec)	$A_o - A$	$\frac{A_o - A}{A_o - A_\infty}$	$\frac{A - A_\infty}{A_o - A_\infty}$	$\ln \frac{A - A_\infty}{A_o - A_\infty}$
0.620	0	0	0	1.000	0
0.418	53	0.202	0.495	0.505	-0.683
0.390	152	0.230	0.564	0.436	-0.830
0.334	396	0.286	0.701	0.299	-1.207
0.280	656	0.340	0.833	0.167	-1.790
0.235	1325	0.385	0.944	0.056	-2.882
0.212	3728	0.408	1.000	0	

$[Co] = 1.1 \times 10^{-5}$ M; $[CH_3\text{-Im}] = 0.0625$ M; T = 30°C; P_{O_2} = 800 Torr

A (395 nm)	t (sec)	$A_o - A$	$\frac{A_o - A}{A_o - A_\infty}$	$\frac{A - A_\infty}{A_o - A_\infty}$	$\ln \frac{A - A_\infty}{A_o - A_\infty}$
1.073	0	0	0	1.000	0
0.679	90	0.396	0.580	0.420	-0.868
0.650	172	0.423	0.619	0.381	-0.965
0.610	254	0.463	0.678	0.322	-1.133
0.586	355	0.487	0.713	0.287	-1.248
0.556	484	0.517	0.757	0.243	-1.415
0.519	615	0.554	0.811	0.189	-1.666
0.484	775	0.589	0.862	0.138	-1.981
0.446	1181	0.627	0.918	0.082	-2.501
0.420	1630	0.653	0.956	0.044	-3.124
0.395	2476	0.678	0.993	0.007	-4.962
0.390	3921	0.683	1.000	0	

$[Co] = 5.2 \times 10^{-5}$ M; $[CH_3\text{-Im}] = 0.0625$ M; $T = 30^{\circ}C$; $P_{O_2} = 800$ Torr

A (548 nm)	t (sec)	$A_o - A$	$\frac{A_o - A}{A_o - A_\infty}$	$\frac{A - A_\infty}{A_o - A_\infty}$	$\ln \frac{A - A_\infty}{A_o - A_\infty}$
0.793	0	0	0	1.000	0
0.585	95	0.208	0.520	0.480	-0.734
0.580	139	0.213	0.533	0.467	-0.761
0.540	295	0.253	0.633	0.367	-1.002
0.505	480	0.288	0.720	0.280	-1.273
0.450	898	0.343	0.858	0.142	-1.952
0.395	2121	0.398	0.995	0.005	-5.298
0.393	4058	0.400	1.000	0	

$[Co] = 4.7 \times 10^{-4}$ M; $[CH_3\text{-Im}] = 0.0625$ M; $T = 30^{\circ}C$; $P_{O_2} = 800$ Torr

A (548 nm)	t (sec)	$A_o - A$	$\frac{A_o - A}{A_o - A_\infty}$	$\frac{A - A_\infty}{A_o - A_\infty}$	$\ln \frac{A - A_\infty}{A_o - A_\infty}$
0.758	0	0	0	1.000	0
0.610	77	0.148	0.381	0.619	-0.480
0.600	149	0.158	0.407	0.593	-0.523
0.595	175	0.163	0.420	0.580	-0.545
0.557	289	0.201	0.518	0.482	-0.730
0.512	459	0.246	0.634	0.366	-1.005
0.468	693	0.290	0.747	0.253	-1.374
0.427	1032	0.331	0.853	0.147	-1.917
0.383	1890	0.375	0.966	0.034	-3.381
-.370	5737	0.388	1.000	0	

$[Co] = 2 \times 10^{-3}$ M; $[CH_3\text{-Im}] = 0.0625$ M; $T = 22^{\circ}C$; $P_{O_2} = 800^{*}$

I	t (sec)	$I_o - I$	$\frac{I_o - I}{I_o - I_\infty}$	$\frac{I - I_\infty}{I_o - I_\infty}$	$\ln \frac{I - I_\infty}{I_o - I_\infty}$
1.8	0	———	———	———	———
53.5	210	0	0	1.000	0
48.2	470	5.3	0.102	0.898	-0.108
43.0	730	10.5	0.202	0.798	-0.226
39.5	990	14.0	0.269	0.731	-0.313
35.5	1250	18.0	0.346	0.654	-0.425
33.0	1670	20.5	0.394	0.606	-0.501
28.0	2587	25.5	0.490	0.510	-0.673
22.6	3750	30.9	0.594	0.406	-0.901
16.1	5215	37.4	0.719	0.281	-1.269
11.0	6992	42.5	0.817	0.187	-1.677
5.3	8425	48.2	0.927	0.073	-2.617
1.5	12240	52.0	1.000	0	———

This run monitored by ESR; I represents signal intensity in arbitrary units.

* Data used in Figure VII.5

APPENDIX Vee. CH_3-ImEpI + O_2 ⟶ CH_3-ImCoEpI(O_2)CoEpI·CH_3-Im

In DCE as a function of temperature

$[Co] = 1.2 \times 10^{-5}$ M; $[CH_3\text{-Im}] = 0.0625$ M; T = 10°C; P_{O_2} = 800 Torr

A (418 nm)	t (sec)	$A - A_o$	$\frac{A - A_o}{A_\infty - A_o}$	$\frac{A_\infty - A}{A_\infty - A_o}$	$\ln \frac{A_\infty - A}{A_\infty - A_o}$
0.580	0	0	0	1.000	0
1.000	65	0.420	0.481	0.519	-0.656
1.045	194	0.465	0.532	0.468	-0.759
1.055	330	0.475	0.543	0.457	-0.783
1.085	653	0.505	0.578	0.422	-0.863
1.145	1218	0.565	0.646	0.354	-1.038
1.225	2107	0.645	0.738	0.262	-1.339
1.290	3014	0.710	0.812	0.188	-1.671
1.347	4098	0.767	0.878	0.122	-2.104
1.397	5789	0.817	0.935	0.065	-2.733
1.440	7568	0.860	0.984	0.016	-4.135
1.454	13864	0.874	1.000	0	———

$[Co] = 1.2 \times 10^{-5}$ M; $[CH_3\text{-Im}] = 0.0625$ M; T = 20°C; P_{O_2} = 800 Torr

A (418 nm)	t (sec)	$A - A_o$	$\frac{A - A_o}{A_\infty - A_o}$	$\frac{A_\infty - A}{A_\infty - A_o}$	$\ln \frac{A_\infty - A}{A_\infty - A_o}$
0.443	0	0	0	1.000	0
0.920	43	0.477	0.453	0.547	-0.603
0.935	173	0.492	0.468	0.532	-0.631
0.978	304	0.535	0.509	0.491	-0.713
1.023	441	0.580	0.551	0.449	-0.801
1.064	574	0.621	0.590	0.410	-0.892
1.133	794	0.690	0.656	0.344	-1.067
1.183	993	0.740	0.703	0.297	-1.214
1.243	1231	0.800	0.760	0.240	-1.427
1.313	1530	0.870	0.827	0.173	-1.754
1.358	1830	0.915	0.870	0.130	-2.040
1.435	2474	0.992	0.943	0.057	-2.865
1.495	8400	1.052	1.000	0	———

Data used in Figure VII.2

$[Co] = 1.1 \times 10^{-5}$ M; $[CH_3\text{-Im}] = 0.0625$ M; T = 30°C; P_{O_2} = 800 Torr

A (395 nm)	t (sec)	$A_o - A$	$\frac{A_o - A}{A_o - A_\infty}$	$\frac{A - A_\infty}{A_o - A_\infty}$	$\ln \frac{A - A_\infty}{A_o - A_\infty}$
1.073	0	0	0	1.000	0
0.679	90	0.396	0.580	0.420	-0.868
0.650	172	0.423	0.619	0.381	-0.965
0.610	254	0.463	0.678	0.322	-1.133
0.586	355	0.487	0.713	0.287	-1.248
0.556	484	0.517	0.757	0.243	-1.415
0.519	615	0.554	0.811	0.189	-1.666
0.484	775	0.589	0.862	0.138	-1.981
0.446	1181	0.627	0.918	0.082	-2.501
0.420	1630	0.653	0.956	0.044	-3.124
0.395	2476	0.678	0.993	0.007	-4.962
0.390	3921	0.683	1.000	0	———

APPENDIX V ff. CH_3-ImCoOEP + O_2 ⟶ CH_3-ImCoOEP(O_2)CoOEP·CH_3-Im

In DCE as a function of cobalt concentration

$[Co] = 7.5 \times 10^{-6}$ M; $[CH_3\text{-Im}] = 0.0625$ M; T = 30°C; P_{O_2} = 800 Torr

A (395 nm)	t (sec)	$A_o - A$	$\frac{A_o - A}{A_o - A_\infty}$	$\frac{A - A_\infty}{A_o - A_\infty}$	$\ln \frac{A - A_\infty}{A_o - A_\infty}$
0.705	0	0	0	1.000	0
0.535	134	0.221	0.345	0.655	-0.423
0.520	236	0.236	0.369	0.631	-0.460
0.489	333	0.281	0.439	0.561	-0.578
0.464	447	0.336	0.525	0.475	-0.744
0.420	592	0.376	0.588	0.412	-0.887
0.397	748	0.422	0.659	0.341	-1.076
0.366	924	0.461	0.720	0.280	-1.273
0.334	1268	0.522	0.816	0.184	-1.693
0.297	1723	0.586	0.916	0.084	-2.477
0.295	2605	0.640	1.000	0	

$[Co] = 3.1 \times 10^{-5}$ M; $[CH_3\text{-Im}] = 0.0625$ M; T = 30°C; P_{O_2} = 800 Torr

A (418 nm)	t (sec)	$A - A_o$	$\frac{A - A_o}{A_\infty - A_o}$	$\frac{A_\infty - A}{A_\infty - A_o}$	$\ln \frac{A_\infty - A}{A_\infty - A_o}$
0.129	0	0	0	1.000	0
0.330	194	0.207	0.349	0.651	-0.429
0.353	284	0.224	0.389	0.621	-0.476
0.421	383	0.292	0.507	0.493	-0.707
0.477	507	0.348	0.604	0.396	-0.926
0.517	635	0.388	0.674	0.324	-1.127
0.556	862	0.437	0.759	0.241	-1.423
0.606	1083	0.477	0.828	0.178	-1.726
0.652	1453	0.523	0.908	0.092	-2.386
0.674	1823	0.545	0.946	0.054	-2.919
0.676	2603	0.547	0.950	0.050	-2.996
0.705	8527	0.576	1.000	0	

$[Co] = 7.9 \times 10^{-5}$ M; $[CH_3\text{-Im}] = 0.0625$ M; T = 30°C; P_{O_2} = 800 Torr*

A (548 nm)	t (sec)	$A_o - A$	$\frac{A_o - A}{A_o - A_\infty}$	$\frac{A - A_\infty}{A_o - A_\infty}$	$\ln \frac{A - A_\infty}{A_o - A_\infty}$
1.383	0	0	0	1.000	0
1.059	152	0.324	0.445	0.555	-0.589
1.018	275	0.365	0.501	0.499	-0.695
0.993	343	0.390	0.536	0.464	-0.768
0.943	445	0.440	0.604	0.396	-0.926
0.902	550	0.481	0.661	0.349	-1.053
0.855	668	0.528	0.725	0.275	-1.291
0.809	820	0.574	0.788	0.212	-1.551
0.768	1018	0.615	0.845	0.155	-1.864
0.714	1412	0.669	0.919	0.081	-2.513
0.683	1870	0.700	0.962	0.038	-3.270
0.658	2599	0.725	0.996	0.004	-5.521
0.655	4083	0.728	1.000	0	

* Data used for Figure VII.3

$[Co] = 6.6 \times 10^{-4}$ M; $[CH_3\text{-Im}] = 0.0625$ M; T = 30°C; P_{O_2} = 800 Torr

A (548 nm)	t (sec)	$A_o - A$	$\frac{A_o - A}{A_o - A_\infty}$	$\frac{A - A_\infty}{A_o - A_\infty}$	$\ln \frac{A - A_\infty}{A_o - A_\infty}$
1.315	0	0	0	1.000	0
0.990	155	0.325	0.448	0.552	-0.594
0.945	256	0.370	0.510	0.490	-0.713
0.905	367	0.410	0.566	0.434	-0.835
0.855	503	0.460	0.634	0.366	-1.005
0.806	631	0.509	0.702	0.298	-1.211
0.773	787	0.542	0.748	0.252	-1.378
0.745	945	0.570	0.786	0.214	-1.542
0.715	1243	0.600	0.828	0.172	-1.760
0.683	1621	0.632	0.872	0.128	-2.056
0.663	2095	0.652	0.899	0.101	-2.293
0.633	3375	0.682	0.941	0.059	-2.830
0.613	5074	0.702	0.968	0.032	-3.442
0.595	7587	0.720	0.993	0.007	-4.962
0.590	10132	0.725	1.000	0	

$[Co] = 2.x\ 10^{-3}$ M; $[CH_3\text{-Im}] = 0.0625$ M; T = 23°C; P_{O_2} = 800 Torr

I	t (sec)	$I_o - I$	$\frac{I_o - I}{I_o - I_\infty}$	$\frac{I - I_\infty}{I_o - I_\infty}$	$\ln \frac{I - I_\infty}{I_o - I_\infty}$
1.4	0	———	———	———	———
44.2	263	0	0	1.000	0
39.0	526	4.8	0.109	0.981	-0.115
36.4	787	7.8	0.177	0.823	-0.195
33.5	1138	10.7	0.243	0.757	-0.278
30.2	1618	14.0	0.317	0.683	-0.381
27.0	2112	17.2	0.390	0.610	-0.494
22.6	2985	21.6	0.490	0.510	-0.673
18.4	3871	25.8	0.585	0.415	-0.879
14.8	5073	29.4	0.667	0.333	-1.100
9.8	6850	34.4	0.780	0.220	-1.514
4.3	9480	39.9	0.905	0.095	-2.354
0.1	15575	44.1	1.000	0	———

APPENDIX Vgg. CH_3-ImCoOEP + O_2 ⟶ CH_3-ImCoOEP(O_2)CoOEP·CH_3-Im

In DCE as a function of temperature

$[Co] = 7.0 \times 10^{-5}$ M; $[CH_3\text{-Im}] = 0.0625$ M; T = 10°C P_{O_2} = 800 Torr

A (548 nm)	t (sec)	$A_o - A$	$\frac{A_o - A}{A_o - A_\infty}$	$\frac{A - A_\infty}{A_o - A_\infty}$	$\ln \frac{A - A_\infty}{A_o - A_\infty}$
1.150	0	0	0	1.000	0
0.794	64	0.356	0.556	0.444	-0.812
0.770	184	0.380	0.594	0.406	-0.901
0.760	328	0.390	0.609	0.391	-0.939
0.755	454	0.395	0.617	0.383	-0.960
0.740	765	0.410	0.641	0.359	-1.024
0.717	1287	0.433	0.677	0.323	-1.130
0.686	2239	0.464	0.725	0.275	-1.291
0.641	3827	0.509	0.795	0.205	-1.585
0.580	6583	0.570	0.891	0.109	-2.216
0.510	23958	0.640	1.000	0	

$[Co] = 7.9 \times 10^{-5}$ M; $[CH_3\text{-Im}] = 0.0625$ M; T = 20°C; P_{O_2} = 800 Torr

A (548 nm)	t (sec)	$A_o - A$	$\frac{A_o - A}{A_o - A_\infty}$	$\frac{A - A_\infty}{A_o - A_\infty}$	$\ln \frac{A - A_\infty}{A_o - A_\infty}$
1.386	0	0	0	1.000	0
0.990	87	0.396	0.527	0.473	-0.749
0.979	158	0.407	0.541	0.459	-0.779
0.965	250	0.421	0.560	0.440	-0.821
0.936	366	0.450	0.598	0.402	-0.911
0.920	472	0.466	0.620	0.380	-0.968
0.887	659	0.499	0.664	0.336	-1.091
0.840	971	0.546	0.726	0.274	-1.295
0.790	1415	0.596	0.793	0.207	-1.575
0.737	1969	0.649	0.863	0.137	-1.988
0.693	2872	0.693	0.922	0.078	-2.551
0.653	4387	0.733	0.975	0.025	-3.689
0.627	5947	0.749	0.996	0.004	-5.521
0.623	9986	0.752	1.000	0	

$[Co] = 7.9 \times 10^{-5}$ M; $[CH_3\text{-Im}] = 0.0625$ M; T = 30°C; P_{O_2} = 800 Torr

A (548 nm)	t (sec)	$A_o - A$	$\frac{A_o - A}{A_o - A_\infty}$	$\frac{A - A_\infty}{A_o - A_\infty}$	$\ln \frac{A - A_\infty}{A_o - A_\infty}$
1.383	0	0	0	1.000	0
1.059	152	0.324	0.445	0.555	-0.589
1.018	275	0.365	0.501	0.499	-0.695
0.993	343	0.390	0.536	0.464	-0.768
0.943	445	0.440	0.604	0.396	-0.926
0.902	550	0.481	0.661	0.349	-1.053
0.855	668	0.528	0.725	0.275	-1.291
0.809	820	0.574	0.788	0.212	-1.551
0.768	1018	0.615	0.845	0.155	-1.864
0.714	1412	0.669	0.919	0.081	-2.513
0.683	1870	0.700	0.962	0.038	-3.270
0.658	2599	0.725	0.996	0.004	-5.521
0.655	4083	0.728	1.000	0	———

APPENDIX V hh. CH_3-ImCoOEP + O_2 ⟶ CH_3-ImCoOEP(O_2)CoOEP·CH_3-Im

In DCE as a function of oxygen pressure

$[Co] = 6.7 \times 10^{-5}$ M; $[CH_3\text{-Im}] = 0.0625$ M; T = 30°C; P_{O_2} = 100 Torr

A (548 nm)	t (sec)	$A_o - A$	$\frac{A_o - A}{A_o - A_\infty}$	$\frac{A - A_\infty}{A_o - A_\infty}$	$\ln \frac{A - A_\infty}{A_o - A_\infty}$
1.210	0	0	0	1.000	0
1.170	93	0.038	0.059	0.941	-0.061
1.163	253	0.047	0.073	0.927	-0.076
1.133	411	0.077	0.119	0.881	-0.127
1.127	580	0.083	0.128	0.872	-0.137
1.076	922	0.134	0.207	0.793	-0.232
1.037	1277	0.173	0.267	0.733	-0.311
0.995	1641	0.225	0.348	0.652	-0.428
0.945	2017	0.275	0.425	0.575	-0.553
0.904	2378	0.306	0.473	0.527	-0.641
0.855	2765	0.355	0.549	0.451	-0.796
0.810	3186	0.400	0.618	0.382	-0.962
0.754	3667	0.456	0.705	0.295	-1.221
0.692	4144	0.518	0.801	0.199	-1.614
0.647	4622	0.503	0.870	0.130	-2.040
0.587	4888	0.623	0.963	0.037	-3.297
0.563	5861	0.647	1.000	0	———
0.563	12009	0.647	1.000	0	———

$[Co] = 7.9 \times 10^{-5}$ M; $[CH_3\text{-Im}] = 0.0625$ M; T = 30°C P_{O_2} = 150 Torr

A (548 nm)	t (sec)	$A_o - A$	$\frac{A_o - A}{A_o - A_\infty}$	$\frac{A - A_\infty}{A_o - A_\infty}$	$\ln \frac{A - A_\infty}{A_o - A_\infty}$
1.353	0	0	0	1.000	0
1.258	78	0.095	0.127	0.873	-0.136
1.252	140	0.101	0.135	0.865	-0.145
1.227	260	0.126	0.169	0.831	-0.185
1.181	422	0.172	0.230	0.770	-0.261
1.127	672	0.226	0.303	0.697	-0.361
1.081	923	0.272	0.364	0.636	-0.453
1.028	1273	0.325	0.435	0.565	-0.571
0.994	1524	0.359	0.481	0.519	-0.656
0.945	1805	0.408	0.546	0.454	-0.790
0.897	2302	0.456	0.610	0.390	-0.942
0.850	2857	0.503	0.673	0.327	-1.118
0.801	3406	0.552	0.739	0.261	-1.343
0.747	4744	0.606	0.811	0.189	-1.666
0.706	5477	0.647	0.866	0.134	-2.010
0.654	7172	0.699	0.936	0.064	-2.749
0.617	12476	0.739	0.989	0.011	-4.510
0.606	21782	0.747	1.000	0	———

$[Co] = 7.2 \times 10^{-5}$ M; $[CH_3\text{-Im}] = 0.0625$ M; T = 30°C; P_{O_2} = 200 Torr

A (548 nm)	t (sec)	$A_o - A$	$\frac{A_o - A}{A_o - A_\infty}$	$\frac{A - A_\infty}{A_o - A_\infty}$	$\ln \frac{A - A_\infty}{A_o - A_\infty}$
1.222	0	0	0	1.000	0
1.110	80	0.112	0.170	0.830	-0.186
1.093	147	0.129	0.196	0.804	-0.218
1.073	216	0.149	0.227	0.773	-0.257
1.057	284	0.165	0.251	0.749	-0.289
1.040	337	0.182	0.277	0.723	-0.324
0.993	515	0.229	0.349	0.651	-0.429
0.958	694	0.264	0.402	0.598	-0.514
0.912	927	0.310	0.472	0.528	-0.639
0.868	1198	0.354	0.539	0.461	-0.774
0.830	1399	0.392	0.597	0.403	-0.909
0.777	1842	0.446	0.679	0.321	-1.136
0.733	2202	0.489	0.744	0.256	-1.356
0.690	2878	0.532	0.810	0.190	-1.661
0.660	3226	0.562	0.855	0.145	-1.931
0.614	4243	0.608	0.925	0.075	-2.590
0.592	5298	0.630	0.959	0.041	-3.194
0.568	7568	0.654	0.995	0.005	-5.298
0.565	10078	0.657	1.000	0	———
0.565	15472	0.657	1.000	0	———

$[Co] = 8.2 \times 10^{-5}$ M; $[CH_3\text{-Im}] = 0.0625$ M; T = 30°C; P_{O_2} = 300 Torr

A (458 nm)	t (sec)	$A_o - A$	$\frac{A_o - A}{A_o - A_\infty}$	$\frac{A - A_\infty}{A_o - A_\infty}$	$\ln \frac{A - A_\infty}{A_o - A_\infty}$
1.449	0	0	0	1.000	0
1.269	79	0.182	0.228	0.772	-0.259
1.258	138	0.192	0.241	0.759	-0.276
1.233	187	0.216	0.271	0.729	-0.316
1.200	275	0.249	0.312	0.688	-0.374
1.143	405	0.306	0.384	0.616	-0.485
1.103	568	0.348	0.437	0.563	-0.574
1.040	705	0.409	0.513	0.487	-0.719
0.995	847	0.454	0.570	0.430	-0.844
0.957	1038	0.492	0.617	0.387	-0.949
0.906	1306	0.543	0.681	0.319	-1.143
0.867	1515	0.582	0.730	0.270	-1.309
0.809	1945	0.640	0.803	0.197	-1.625
0.765	2405	0.684	0.858	0.142	-1.952
0.728	2927	0.721	0.905	0.095	-2.354
0.690	3657	0.759	0.952	0.048	-3.037
0.667	5002	0.782	0.981	0.019	-3.963
0.653	7532	0.796	0.999	0.001	-6.908
0.652	11273	0.797	1.000	0	———

$[Co] = 7.9 \times 10^{-5}$ M; $[CH_3\text{-Im}] = 0.0625$ M; $T = 30^{\circ}C$; $P_{O_2} = 400$ Torr

A (548 nm)	t (sec)	$A_o - A$	$\frac{A_o - A_\infty}{A_o - A_\infty}$	$\frac{A - A_\infty}{A_o - A_\infty}$	$\ln \frac{A - A_\infty}{A_o - A_\infty}$
1.329	0	0	0	1.000	0
1.177	77	0.149	0.205	0.795	-0.229
1.128	142	0.198	0.272	0.728	-0.317
1.072	207	0.254	0.349	0.651	-0.429
1.010	345	0.316	0.435	0.565	-0.571
0.955	497	0.371	0.510	0.490	-0.713
0.909	622	0.417	0.574	0.426	-0.853
0.858	785	0.468	0.644	0.356	-1.033
0.809	987	0.517	0.711	0.289	-1.241
0.770	1192	0.556	0.765	0.235	-1.448
0.730	1405	0.596	0.820	0.180	-1.715
0.700	1689	0.626	0.861	0.139	-1.973
0.658	2205	0.668	0.919	0.081	-2.513
0.607	3874	0.719	0.989	0.011	-4.510
0.599	6024	0.727	1.000	0	———
0.599	10037	0.727	1.000	0	———

$[Co] = 7.5 \times 10^{-5}$ M; $[CH_3\text{-Im}] = 0.0625$ M; $T = 30^{\circ}C$; $P_{O_2} = 530$ Torr

A (548 nm)	t (sec)	$A_o - A$	$\frac{A_o - A}{A_o - A_\infty}$	$\frac{A - A_\infty}{A_o - A_\infty}$	$\ln \frac{A - A_\infty}{A_o - A_\infty}$
1.316	0	0	0	1.000	0
1.062	86	0.254	0.356	0.644	-0.440
1.034	225	0.282	0.396	0.604	-0.504
1.004	276	0.312	0.438	0.562	-0.576
0.957	382	0.359	0.504	0.496	-0.701
0.932	425	0.384	0.539	0.461	-0.774
0.898	517	0.418	0.587	0.413	-0.884
0.847	680	0.469	0.659	0.341	-1.076
0.795	862	0.521	0.732	0.268	-1.317
0.752	1045	0.564	0.792	0.208	-1.570
0.718	1295	0.598	0.840	0.160	-1.833
0.686	1505	0.630	0.885	0.115	-2.163
0.655	1857	0.661	0.928	0.072	-2.631
0.624	2567	0.692	0.972	0.028	-3.576
0.604	3537	0.712	1.000	0	———
0.604	4889	0.712	1.000	0	———
0.604	6027	0.712	1.000	0	———

$[Co] = 6.5 \times 10^{-5}$ M; $[CH_3\text{-Im}] = 0.0625$ M; T = 30°C; P_{O_2} = 670 Torr

A (548 nm)	t (sec)	$A_o - A$	$\frac{A_o - A}{A_o - A_\infty}$	$\frac{A - A_\infty}{A_o - A_\infty}$	$\ln \frac{A - A_\infty}{A_o - A_\infty}$
1.103	0	0	0	1.000	0
0.958	77	0.145	0.245	0.742	-0.298
0.938	142	0.165	0.293	0.707	-0.347
0.864	237	0.239	0.423	0.577	-0.550
0.796	397	0.307	0.545	0.455	-0.787
0.742	543	0.361	0.641	0.359	-1.024
0.703	707	0.400	0.710	0.290	-1.238
0.663	909	0.440	0.782	0.218	-1.523
0.618	1202	0.485	0.861	0.139	-1.973
0.583	1605	0.520	0.924	0.076	-2.577
0.560	2402	0.543	0.964	0.036	-3.324
0.560	3618	0.543	0.964	0.036	-3.324
0.540	6024	0.563	1.000	0	

$[Co] = 7.9 \times 10^{-5}$ M; $[CH_3\text{-Im}] = 0.0625$ M; T = 30°C; P_{O_2} = 800 Torr

A (548 nm)	t (sec)	$A_o - A$	$\frac{A_o - A}{A_o - A_\infty}$	$\frac{A - A_\infty}{A_o - A_\infty}$	$\ln \frac{A - A_\infty}{A_o - A_\infty}$
1.383	0	0	0	1.000	0
1.059	152	0.324	0.445	0.555	-0.589
1.018	275	0.365	0.501	0.499	-0.695
0.993	343	0.390	0.536	0.464	-0.768
0.943	445	0.440	0.604	0.396	-0.926
0.902	550	0.481	0.661	0.349	-1.053
0.855	668	0.528	0.725	0.275	-1.291
0.809	820	0.574	0.788	0.212	-1.551
0.768	1018	0.615	0.845	0.155	-1.864
0.714	1412	0.669	0.919	0.081	-2.513
0.683	1870	0.700	0.962	0.038	-3.270
0.658	2599	0.725	0.996	0.004	-5.521
0.655	4083	0.728	1.000	0	

APPENDIX Vii. CH_3-ImCoOEP + O_2 ⟶ CH_3-ImCoOEP(O_2)CoOEP·CH_3-Im

As a function of solvent

$[Co] = 6.6 \times 10^{-4}$ M; $[CH_3\text{-Im}] = 0.0625$ M; $T = 30^{\circ}C$; $P_{O_2} = 800$ Torr

Solvent = DCE

A (548 nm)	t (sec)	$A_o - A$	$\frac{A_o - A}{A_o - A_\infty}$	$\frac{A - A_\infty}{A_o - A_\infty}$	$\ln \frac{A - A_\infty}{A_o - A_\infty}$
1.315	0	0	0	1.000	0
0.990	155	0.325	0.448	0.552	-0.594
0.945	256	0.370	0.510	0.490	-0.713
0.905	367	0.410	0.566	0.434	-0.835
0.855	503	0.460	0.634	0.366	-1.005
0.806	631	0.509	0.702	0.298	-1.211
0.773	787	0.542	0.748	0.252	-1.378
0.745	945	0.570	0.786	0.214	-1.542
0.715	1243	0.600	0.828	0.172	-1.760
0.683	1621	0.632	0.872	0.128	-2.056
0.663	2095	0.652	0.899	0.101	-2.293
0.633	3375	0.682	0.941	0.059	-2.830
0.613	5074	0.702	0.968	0.032	-3.442
0.595	7587	0.720	0.993	0.007	-4.962
0.590	10132	0.725	1.000	0	

$[Co] = 6 \times 10^{-4}$ M; $[CH_3\text{-Im}] = 0.122$ M; $T = 30^{\circ}C$; $P_{O_2} = 800$ Torr

Solvent = DMA

A (548 nm)	t (sec)	$A_o - A$	$\frac{A_o - A}{A_o - A_\infty}$	$\frac{A - A_\infty}{A_o - A_\infty}$	$\ln \frac{A - A_\infty}{A_o - A_\infty}$
1.071	0	0	0	1.000	0
0.857	76	0.214	0.355	0.645	-0.439
0.857	169	0.214	0.355	0.645	-0.439
0.855	205	0.216	0.358	0.642	-0.443
0.817	1134	0.254	0.421	0.579	-0.567
0.810	1221	0.261	0.433	0.567	-0.567
0.740	3236	0.334	0.549	0.451	-0.796
0.647	7013	0.424	0.703	0.297	-1.214
0.587	10647	0.484	0.803	0.197	-1.624
0.539	17651	0.532	0.882	0.112	-2.189
0.468	~100000	0.603	1.000	0	

$[Co] = 6 \times 10^{-4}$ M; $[CH_3\text{-Im}] = 12.57$ M; $T = 30^{\circ}C$; $P_{O_2} = 800$ Torr

Solvent = CH_3-Im

A (548 nm)	t (sec)	$A_o - A$	$\frac{A_o - A}{A_o - A_\infty}$	$\frac{A - A_\infty}{A_o - A_\infty}$	$\ln \frac{A - A_\infty}{A_o - A_\infty}$
1.101	0	0	0	1.000	0
0.667	81	0.434	0.714	0.286	-1.252
0.635	265	0.466	0.766	0.234	-1.452
0.615	414	0.486	0.799	0.201	-1.604
0.590	614	0.511	0.840	0.160	-1.833
0.557	1000	0.544	0.895	0.105	-2.254
0.525	1554	0.576	0.947	0.053	-2.937
0.503	3644	0.598	0.984	0.016	-4.135
0.493	9748	0.608	1.000	0	———

APPENDIX Vjj. CH_3-ImCoPpIXDME + O_2 ⟶ CH_3-ImCoPpIXDME(O_2)CoPpIXDME·CH_3-Im

As a function of cobalt concentration

[Co] = 7×10^{-6} M; [CH_3-Im] = 0.0625 M; T = 20°C; P_{O_2} = 800 Torr

A (405 nm)	t (sec)	$A_o - A$	$\frac{A_o - A}{A_o - A_\infty}$	$\frac{A - A_\infty}{A_o - A_\infty}$	$\ln \frac{A - A_\infty}{A_o - A_\infty}$
1.156	0	0	0	1.000	0
0.875	50	0.281	0.470	0.530	-0.635
0.870	109	0.286	0.478	0.528	-0.639
0.840	240	0.316	0.528	0.472	-0.751
0.805	374	0.351	0.587	0.413	-0.884
0.765	633	0.391	0.654	0.346	-1.061
0.665	1234	0.491	0.821	0.179	-1.720
0.568	3680	0.598	1.000	0	———
0.568	7255	0.598	1.000	0	———

[Co] = 6×10^{-5} M; [CH_3-Im] = 0.0625 M; T = 20°C; P_{O_2} = 800 Torr

A (558 nm)	t (sec)	$A_o - A$	$\frac{A_o - A}{A_o - A_\infty}$	$\frac{A - A_\infty}{A_o - A_\infty}$	$\ln \frac{A - A_\infty}{A_o - A_\infty}$
0.954	0	0	0	1.000	0
0.776	70	0.178	0.388	0.612	-0.491
0.749	161	0.205	0.447	0.553	-0.592
0.715	350	0.239	0.521	0.479	-0.736
0.688	596	0.266	0.580	0.420	-0.868
0.638	1105	0.316	0.688	0.312	-1.165
0.582	1813	0.372	0.810	0.190	-1.661
0.518	3088	0.436	0.950	0.050	-2.996
0.508	4860	0.456	0.993	0.007	-4.962
0.505	8404	0.459	1.000	0	———

$[Co] = 7.9 \times 10^{-4} M$; $[CH_3\text{-Im}] = 0.0625$ M; $T = 20^{\circ}C$; $P_{O_2} = 800$ Torr

A (558 nm)	t (sec)	$A_o - A$	$\frac{A_o - A}{A_o - A_\infty}$	$\frac{A - A_\infty}{A_o - A_\infty}$	$\ln \frac{A - A_\infty}{A_o - A_\infty}$
1.173	0	0	0	1.000	0
0.915	80	0.258	0.445	0.555	-0.589
0.900	187	0.273	0.471	0.529	-0.637
0.866	320	0.307	0.529	0.471	-0.753
0.817	626	0.356	0.614	0.386	-0.952
0.780	1097	0.393	0.678	0.322	-1.133
0.735	1853	0.438	0.755	0.245	-1.407
0.682	3196	0.491	0.847	0.153	-1.877
0.635	5144	0.538	0.928	0.072	-2.631
0.593	9629	0.560	1.000	0	———

APPENDIX Vkk. CH_3-ImCoOEP + O_2 ⟶ CH_3-ImCoOEP(O_2)CoOEP·CH_3-Im

In DCE as a function of CH_3-Im concentration

[Co] = 7.8×10^{-5} M; [CH_3-Im] = 0.0251 M; T = 24°C; P_{O_2} = 800 Torr

A (548 nm)	t (sec)	$A_o - A$	$\frac{A_o - A}{A_o - A_\infty}$	$\frac{A - A_\infty}{A_o - A_\infty}$	$\ln \frac{A - A_\infty}{A_o - A_\infty}$
1.356	0	0	0	1.000	0
1.117	91	0.239	0.337	0.663	-0.411
1.043	238	0.313	0.441	0.559	-0.582
0.998	403	0.358	0.504	0.496	-0.701
0.961	534	0.395	0.556	0.444	-0.812
0.902	678	0.454	0.639	0.361	-1.019
0.866	837	0.490	0.690	0.310	-1.171
0.803	1062	0.553	0.779	0.221	-1.510
0.766	1297	0.590	0.831	0.169	-1.778
0.739	1605	0.617	0.869	0.131	-2.032
0.712	1807	0.644	0.907	0.093	-2.375
0.691	2247	0.665	0.937	0.063	-2.765
0.646	5287	0.710	1.000	0	———

[Co] = 8.2×10^{-5} M; [CH_3-Im] = 0.087 M; T = 24°C; P_{O_2} = 800 Torr

A (548 nm)	t (sec)	$A_o - A$	$\frac{A_o - A}{A_o - A_\infty}$	$\frac{A - A_\infty}{A_o - A_\infty}$	$\ln \frac{A - A_\infty}{A_o - A_\infty}$
1.427	0	0	0	1.000	0
1.126	78	0.301	0.400	0.600	-0.511
1.070	237	0.357	0.475	0.525	-0.644
0.968	422	0.459	0.610	0.390	-0.941
0.901	682	0.526	0.699	0.301	-1.202
0.844	878	0.583	0.775	0.225	-1.492
0.816	1062	0.611	0.813	0.187	-1.677
0.775	1347	0.652	0.867	0.133	-2.017
0.736	1657	0.691	0.919	0.081	-2.513
0.715	2203	0.712	0.947	0.053	-2.937
0.675	4973	0.752	1.000	0	———

$[Co] = 7.6 \times 10^{-5}$ M; $[CH_3\text{-Im}] = 0.248$ M; $T = 24^{\circ}C$; $P_{O_2} = 800$ Torr

A (548 nm)	t(sec)	$A_o - A$	$\frac{A_o - A}{A_o - A_\infty}$	$\frac{A - A_\infty}{A_o - A_\infty}$	$\ln \frac{A - A_\infty}{A_o - A_\infty}$
1.367	0	0	0	1.000	0
1.184	57	0.183	0.261	0.739	-0.302
1.135	197	0.232	0.330	0.670	-0.400
1.002	359	0.365	0.520	0.480	-0.734
0.903	603	0.464	0.661	0.339	-1.082
0.829	797	0.538	0.766	0.234	-1.452
0.786	1042	0.581	0.828	0.172	-1.760
0.737	1337	0.630	0.897	0.103	-2.273
0.699	1677	0.668	0.952	0.048	-3.037
0.665	3598	0.702	1.000	0	———

APPENDIX VI

RAW DATA FOR DETERMINING THE THERMODYNAMIC AND KINETIC PARAMETERS OF LIGAND BINDING AND OXYGENATION OF Co(SALEN) COMPLEXES

APPENDIX VIa. $CH_3\text{-Im} + Co(salen) \rightleftharpoons CH_3\text{-ImCo(salen)}$

In dichloromethane

Temperature = 3°C

A (410 nm)	$[CH_3\text{-Im}]$	$A_o - A$	$A - A_\infty$	$\log \frac{A_o - A}{A - A_\infty}$	$\log [CH_3\text{-Im}]$
1.310	0	0	0.812	———	———
1.230	0.001257	0.080	0.732	-0.961	-2.901
1.190	0.002514	0.120	0.692	-0.761	-2.600
1.150	0.003751	0.160	0.652	-0.610	-2.424
1.063	0.006284	0.247	0.565	-0.359	-2.202
0.951	0.009424	0.359	0.453	-0.101	-2.026
0.870	0.01256	0.440	0.372	0.073	-1.903
0.769	0.01883	0.541	0.271	0.300	-1.725
0.670	0.02510	0.640	0.172	0.571	-1.600
0.621	0.03136	0.689	0.123	0.748	-1.504
0.565	0.04386	0.745	0.067	1.046	-1.358
0.558	0.06256	0.752	0.060	1.098	-1.204
0.535	0.09361	0.775	0.037	1.412	-1.029
0.515	0.1245	0.795	0.017	1.670	-0.905
0.516	0.1858	0.794	0.018	1.645	-0.731
0.498	0.2466	0.812	0	———	-0.608

Temperature = 15°C

A (410 nm)	$[CH_3\text{-Im}]$	$A_o - A$	$A - A_\infty$	$\log \frac{A_o - A}{A - A_\infty}$	$\log [CH_3\text{-Im}]$
1.218	0	0	0.748	———	———
1.092	0.003143	0.126	0.622	-0.693	-2.503
1.014	0.006284	0.204	0.544	-0.426	-2.202
0.851	0.01256	0.367	0.381	-0.016	-1.901
0.788	0.01883	0.430	0.318	0.131	-1.725
0.713	0.02510	0.505	0.243	0.318	-1.600
0.624	0.03761	0.594	0.154	0.586	-1.425
0.555	0.06256	0.663	0.085	0.892	-1.204
0.506	0.09361	0.712	0.036	1.292	-1.029
0.490	0.1245	0.728	0.020	1.561	-0.905
0.478	0.1859	0.740	0.008	1.966	-0.731
0.470	0.2466	0.748	0	———	-0.608

Temperature = 25°C

A (410 nm)	$[CH_3\text{-Im}]$	$A_o - A$	$A - A_\infty$	$\log \frac{A_o - A}{A - A_\infty}$	$\log [CH_3\text{-Im}]$
1.380	0	0	0.653	———	———
1.362	0.001886	0.018	0.635	-1.548	-2.724
1.329	0.003771	0.051	0.602	-1.072	-2.424
1.300	0.006284	0.080	0.573	-0.855	-2.202
1.255	0.008796	0.125	0.528	-0.626	-2.056
1.210	0.01131	0.170	0.483	-0.453	-1.947
1.154	0.01507	0.226	0.429	-0.278	-1.822
1.088	0.01883	0.292	0.361	-0.092	-1.725
0.991	0.03136	0.389	0.264	0.168	-1.504
0.842	0.06256	0.538	0.115	0.670	-1.204
0.795	0.09361	0.585	0.068	0.935	-1.029
0.748	0.1245	0.632	0.021	1.478	-0.905
0.729	0.1552	0.651	0.002	2.513	-0.809
0.727	0.1848	0.653	0	———	-0.733

Temperature = 35°C

A (410 nm)	$[CH_3\text{-Im}]$	$A_o - A$	$A - A_\infty$	$\log \frac{A_o - A}{A - A_\infty}$	$\log [CH_3\text{-Im}]$
1.258	0	0	0.767	———	———
1.181	0.006284	0.077	0.690	-0.952	-2.202
1.155	0.008796	0.103	0.664	-0.809	-2.056
1.081	0.01507	0.177	0.590	-0.523	-1.822
1.034	0.01883	0.224	0.543	-0.385	-1.725
0.981	0.02510	0.277	0.490	-0.248	-1.600
0.931	0.03761	0.327	0.440	-0.129	-1.425
0.884	0.06266	0.374	0.393	-0.022	-1.204
0.708	0.1245	0.550	0.217	0.404	-0.905
0.695	0.1552	0.563	0.204	0.441	-0.809
0.491	0.4837	0.767	0	———	———

Additions made with neat CH_3-Im

APPENDIX VIb. Pip + Co(salen) $\rightleftharpoons$ PipCo(salen)

In dichloromethane

Temperature = 3°C

A (410 nm)	[Pip]	$A_o - A$	$A - A_\infty$	$\log \frac{A_o - A}{A - A_\infty}$	log[Pip]
1.195	0	0	0.567	———	———
1.102	0.002526	0.093	0.474	-0.707	-2.598
0.998	0.005060	0.123	0.444	-0.557	-2.296
0.901	0.01010	0.197	0.370	-0.274	-1.996
0.815	0.01514	0.294	0.273	0.032	-1.820
0.741	0.02017	0.380	0.187	0.308	-1.695
0.714	0.02519	0.454	0.113	0.604	-1.599
0.677	0.03021	0.481	0.086	0.748	-1.520
0.665	0.04024	0.518	0.049	1.024	-1.395
0.628	0.05028	0.530	0.037	1.156	-1.299
0.628	0.07521	0.567	0	———	-1.124

Temperature = 15°C

A (410 nm)	[Pip]	$A_o - A$	$A - A_\infty$	$\log \frac{A_o - A}{A - A_\infty}$	log[Pip]
1.093	0	0	0.519	———	———
0.993	0.005060	0.100	0.419	-0.622	-2.296
0.889	0.01010	0.204	0.315	-0.189	-1.996
0.804	0.01574	0.289	0.230	-0.099	-1.820
0.734	0.02017	0.359	0.160	0.351	-1.695
0.683	0.02519	0.410	0.109	0.575	-1.599
0.622	0.03760	0.471	0.042	1.050	-1.425
0.599	0.05028	0.494	0.025	1.296	-1.299
0.574	0.1001	0.519	0	———	-1.000

Temperature = 25°C

A (410 nm)	[Pip]	$A_o - A$	$A - A_\infty$	$\log \frac{A_o - A}{A - A_\infty}$	log[Pip]
1.370	0	0	0.503	———	———
1.289	0.005060	0.081	0.422	-0.717	-2.296
1.202	0.01010	0.168	0.335	-0.300	-1.996
1.141	0.01514	0.229	0.274	-0.078	-1.820
1.083	0.02017	0.287	0.216	0.123	-1.695
1.030	0.02519	0.340	0.163	0.319	-1.599
0.967	0.03760	0.403	0.100	0.605	-1.425
0.920	0.05028	0.450	0.053	0.929	-1.299
0.867	0.1001	0.503	0	———	-1.000

Temperature = 35°C

A (410 nm)	[Pip]	$A_o - A$	$A - A_\infty$	$\log \frac{A_o - A}{A - A_\infty}$	log[Pip]
1.362	0	0	0.353	———	———
1.342	0.002531	0.020	0.333	-1.221	-2.597
1.337	0.005060	0.025	0.328	-1.118	-2.296
1.302	0.007588	0.060	0.293	-0.689	-2.120
1.254	0.01010	0.108	0.245	-0.356	-1.996
1.243	0.01264	0.119	0.234	-0.294	-1.898
1.202	0.01514	0.162	0.191	-0.072	-1.818
1.178	0.01768	0.184	0.169	0.037	-1.753
1.095	0.02520	0.267	0.086	0.492	-1.599
1.030	0.05028	0.332	0.021	1.199	-1.299
1.001	0.1001	0.342	0.011	1.493	-1.000
1.009	0.1496	0.353	0	———	-0.825

Additions made with neat Pip

APPENDIX VIc. Py + Co(salen) $\rightleftharpoons$ PyCo(salen)

In dichloromethane

Temperature = 3°C

A (410 nm)	[Py]	$A_o - A$	$A - A_\infty$	$\log \frac{A_o - A}{A - A_\infty}$	log[Py]
1.080	0	0	0.623	———	———
1.013	0.006204	0.067	0.556	-0.919	-2.207
0.884	0.01855	0.196	0.427	-0.338	-1.732
0.782	0.03713	0.298	0.325	-0.038	-1.430
0.679	0.06176	0.401	0.222	0.257	-1.209
0.622	0.09241	0.458	0.165	0.443	-1.034
0.585	0.1275	0.495	0.128	0.587	-0.894
0.497	0.3028	0.583	0.040	1.164	-0.519
0.464	0.5911	0.616	0.007	1.944	-0.228
0.457	1.128	0.623	0	———	0.052
0.466	1.619	0.614	0	———	0.209

Temperature = 15°C

A (410 nm)	[Py]	$A_o - A$	$A - A_\infty$	$\log \frac{A_o - A}{A - A_\infty}$	log[Py]
1.260	0	0	0.710	———	———
1.211	0.006204	0.049	0.661	-1.130	-2.207
1.078	0.03056	0.182	0.528	-0.463	-1.515
0.939	0.06176	0.321	0.389	-0.083	-1.209
0.916	0.09241	0.344	0.366	-0.027	-1.034
0.810	0.1229	0.450	0.260	0.238	-0.910
0.653	0.3028	0.607	0.103	0.770	-0.519
0.599	0.5511	0.661	0.049	1.130	-0.259
0.561	1.128	0.699	0.019	1.566	0.052
0.555	1.619	0.705	0.005	2.149	0.209
0.550	2.483	0.710	0	———	0.395
0.563	3.218	———	———	———	0.508

Temperature = 25°C

A (410 nm)	[Py]	$A_o - A$	$A - A_\infty$	$\log \frac{A_o - A}{A - A_\infty}$	log[Py]
1.428	0	0	0.711	———	———
1.401	0.006204	0.027	0.684	-1.404	-2.207
1.280	0.03713	0.148	0.563	-0.580	-1.430
1.112	0.09241	0.316	0.395	-0.097	-1.034
0.976	0.157	0.452	0.259	0.242	-0.803
0.774	0.551	0.654	0.057	1.060	-0.259
0.731	2.483	0.697	0.014	1.697	0.395
0.717	3.218	0.711	0	———	0.508

Temperature = 35°C

A (410 nm)	[Py]	$A_o - A$	$A - A_\infty$	$\log \frac{A_o - A}{A - A_\infty}$	log[Py]
1.422	0	0	0.692	———	———
1.349	0.01239	0.073	0.619	-0.928	-1.907
1.328	0.03056	0.094	0.598	-0.804	-1.515
1.240	0.06176	0.182	0.510	-0.438	-1.209
1.186	0.1832	0.236	0.440	-0.242	-0.737
1.020	0.3028	0.402	0.290	0.170	-0.519
0.850	0.7031	0.572	0.120	0.697	-0.153
0.758	1.849	0.664	0.028	1.375	0.267
0.733	2.673	0.689	0.003	2.361	0.427
0.731	3.767	0.691	0.001	2.840	0.576
0.730	4.873	0.692	0	———	0.688

Additions made with neat Py, 35°C data from D. Hegedic, B. R. James, unpublished results.

APPENDIX VId. CH_3-ImCo(salen) + $O_2 \rightleftharpoons$ CH_3-ImCo(salen)(O_2)

In dichloromethane.

Temperature = -78°C

A (400 nm)	P_{O_2}	$A - A_o$	$A - A_\infty$	$\log \frac{A - A_o}{A_\infty - A}$	$\log P_{O_2}$
0.737	0	0	0.361	———	———
0.810	0.42	0.073	0.288	-0.596	-0.375
0.898	1.21	0.161	0.200	-0.094	0.082
0.995	1.69	0.258	0.103	0.398	0.228
1.043	2.47	0.306	0.055	0.745	0.392
1.070	11.2	0.333	0.028	1.070	1.049
1.089	20.2	0.352	0.003	2.060	1.305
1.098	102	0.361	0	———	2.009
1.098	782	0.361	0	———	2.893

Temperature = -63.5°C

A (400 nm)	P_{O_2}	$A - A_o$	$A_\infty - A$	$\log \frac{A - A_o}{A_\infty - A}$	$\log P_{O_2}$
0.930	0	0	0.492	———	———
0.980	0.19	0.050	0.442	-0.946	-0.727
1.040	0.36	0.110	0.382	-0.540	-0.447
1.124	1.10	0.194	0.298	-0.186	0.043
1.186	2.37	0.256	0.236	0.035	0.375
1.255	3.37	0.325	0.167	0.289	0.527
1.360	12.1	0.430	0.062	0.841	1.083
1.380	24.9	0.450	0.042	1.030	1.397
1.402	109	0.472	0.020	1.370	2.037
1.422	765	0.492	0	———	2.884

Temperature = -45°C

A (400 nm)	P_{O_2}	$A - A_o$	$A_\infty - A$	$\log \frac{A - A_o}{A_\infty - A}$	$\log P_{O_2}$
0.714	0	0	0.141	———	———
0.742	1	0.028	0.113	-0.701	0
0.754	4	0.040	0.101	-0.402	0.602
0.794	9	0.078	0.063	0.093	0.954
0.836	19	0.122	0.019	0.223	1.270
0.850	39	0.136	0.005	1.430	1.591
0.853	81	0.139	0.002	1.842	1.908
0.855	767	0.141	0	———	2.885

Temperature = $-31^{\circ}C$

A (400 nm)	P_{O_2}	$A - A_o$	$A_\infty - A$	$\log \frac{A - A_o}{A_\infty - A}$	$\log P_{O_2}$
0.803	0	0	0.402	———	———
0.831	2	0.028	0.374	-1.112	0.301
0.892	8	0.089	0.313	-0.546	0.903
0.980	20	0.177	0.225	-0.104	1.301
1.043	39	0.240	0.162	0.171	1.591
1.112	82	0.309	0.093	0.521	1.914
1.159	175	0.356	0.056	0.803	2.243
1.205	772	0.402	0	———	2.888

Temperature = $-23^{\circ}C$

A (400 nm)	P_{O_2}	$A - A_o$	$A_\infty - A$	$\log \frac{A - A_o}{A_\infty - A}$	$\log P_{O_2}$
0.852	0	0	0.447	———	———
0.891	4	0.039	0.408	-1.020	0.602
0.960	14	0.108	0.339	-0.497	1.142
1.051	35	0.199	0.248	-0.096	1.544
1.129	72	0.277	0.170	0.212	1.857
1.199	157	0.347	0.100	0.540	2.196
1.240	302	0.388	0.059	0.818	2.480
1.299	772	0.447	0	———	2.888

APPENDIX VIe. $PipCo(salen) + O_2 \rightleftharpoons PipCo(salen)(O_2)$

In dichloromethane

Temperature = -78°C

A (400 nm)	P_{O_2}	$A - A_o$	$A_\infty - A$	$\log \frac{A - A_o}{A_\infty - A}$	$\log P_{O_2}$
1.000	0	0	0.180	———	———
1.072	0.55	0.072	0 108	-0.176	-0.262
1.106	1.60	0.106	0.074	0.156	0.203
1.130	3.56	0.130	0.050	0.415	0.552
1.147	5.07	0.147	0.033	0.649	0.705
1.160	8.71	0.160	0.020	0.903	0.940
1.168	18.6	0.168	0.012	1.146	1.270
1.180	57	0.180	0	———	1.756
1.180	778	0.180	0	———	2.891

Temperature = -63.5°C

A (400 nm)	P_{O_2}	$A - A_o$	$A_\infty - A$	$\log \frac{A - A_o}{A_\infty - A}$	$\log P_{O_2}$
0.971	0	0	0.209	———	———
0.990	0.20	0.019	0.190	-1.000	-0.702
1.011	0.45	0.040	0.169	-0.651	-0.345
1.042	1.00	0.071	0.138	-0.289	0.000
1.085	2.25	0.114	0.095	0.079	0.352
1.123	4.25	0.152	0.057	0.426	0.628
1.147	8.36	0.176	0.033	0.727	0.922
1.169	81	0.198	0.011	1.255	1.908
1.180	775	0.209	0	———	2.889

Temperature = -45°C

A (400 nm)	P_{O_2}	$A - A_o$	$A_\infty - A$	$\log \frac{A - A_o}{A_\infty - A}$	$\log P_{O_2}$
1.018	0	0	0.225	———	———
1.032	0.38	0.014	0.211	-1.206	-0.420
1.049	0.92	0.031	0.194	-0.796	-0.036
1.075	2.0	0.057	0.168	-0.469	0.301
1.111	4	0.093	0.132	-0.152	0.602
1.147	7	0.129	0.096	0.128	0.845
1.183	13	0.165	0.060	0.439	1.114
1.226	57	0.208	0.017	1.088	1.756
1.247	762	0.225	0	———	2.882

APPENDIX VIf. $PyCo(salen) + O_2 \rightleftharpoons PyCo(salen)(O_2)$

In dichloromethane

Temperature = -78°C

A (390 nm)	P_{O_2}	$A - A_o$	$A - A_\infty$	$\log \frac{A - A_o}{A_\infty - A}$	$\log P_{O_2}$
0.950	0	0	0.380	———	———
1.012	0.38	0.062	0.318	-0.710	-0.416
1.037	0.61	0.087	0.293	-0.527	-0.215
1.062	0.91	0.112	0.268	-0.379	-0.039
1.110	1.61	0.160	0.220	-0.138	0.207
1.172	2.15	0.222	0.158	0.147	0.332
1.191	3.22	0.247	0.133	0.269	0.508
1.230	5.98	0.280	0.100	0.447	0.777
1.262	9.74	0.312	0.068	0.662	0.989
1.273	16.5	0.323	0.057	0.753	1.217
1.290	34.5	0.340	0.040	0.929	1.538
1.330	760	0.380	0	———	2.881

Temperature = -63.5°C

A (470 nm)	P_{O_2}	$A_o - A$	$A - A_\infty$	$\log \frac{A_o - A}{A - A_\infty}$	$\log P_{O_2}$
0.355	0	0	0.357	———	———
0.330	0.38	0.025	0.332	-1.120	-0.416
0.320	0.53	0.035	0.322	-0.964	-0.276
0.310	0.65	0.045	0.312	-0.840	-0.185
0.300	0.87	0.055	0.302	-0.740	-0.059
0.268	1.24	0.087	0.270	-0.492	0.092
0.218	2.73	0.137	0.220	-0.205	0.436
0.184	3.91	0.171	0.186	-0.037	0.592
0.153	5.45	0.202	0.155	0.115	0.736
0.121	9.73	0.234	0.123	0.279	0.988
0.080	15.6	0.275	0.082	0.526	1.192
0.050	25.5	0.305	0.052	0.768	1.406
0.012	142	0.343	0.014	1.390	2.152
0.005	291	0.350	0.007	1.690	2.464
-0.002	810	0.357	0	———	2.908

Temperature = -45°C

A (360 nm)	P_{O_2}	$A_o - A$	$A - A_\infty$	$\log \frac{A_o - A}{A - A_\infty}$	$\log P_{O_2}$
1.440	0	0	0.435	———	———
1.325	6	0.115	0.320	-0.444	0.778
1.211	14	0.229	0.206	0.046	1.146
1.140	26	0.300	0.135	0.347	1.415
1.098	38	0.342	0.093	0.566	1.580
1.095	51	0.345	0.090	0.584	1.708
1.050	95	0.390	0.045	0.938	1.978
1.035	152	0.405	0.030	1.130	2.182
1.005	772	0.435	0	———	2.888

Temperature = -31°C

A (360 nm)	P_{O_2}	$A_o - A$	$A - A_\infty$	$\log \frac{A_o - A}{A - A_\infty}$	$\log P_{O_2}$
1.370	0	0	0.240	———	———
1.328	8	0.042	0.198	-0.673	0.903
1.286	22	0.084	0.156	-0.269	1.342
1.260	27	0.110	0.130	-0.073	1.431
1.195	62	0.175	0.065	0.430	1.792
1.172	105	0.198	0.042	0.673	2.021
1.130	762	0.240	0	———	2.882

Temperature = -23°C

A (360 nm)	P_{O_2}	$A_o - A$	$A - A_\infty$	$\log \frac{A_o - A}{A - A_\infty}$	$\log P_{O_2}$
1.665	0	0	0.215	———	———
1.630	12	0.035	0.180	-0.711	1.079
1.625	20	0.040	0.175	-0.641	1.301
1.570	42	0.095	0.120	-0.101	1.623
1.535	68	0.130	0.085	0.185	1.833
1.525	108	0.140	0.075	0.271	2.033
1.450	409	0.215	0	———	2.612

Data from -23°C from D. Hegedic, B. R. James, unpublished results.

APPENDIX VIg. $Co(salen) + O_2 \rightleftharpoons Co(salen)(O_2)$

In dichloromethane

Temperature = -83°C

A (410 nm)	P_{O_2}	$A_o - A$	$A - A_\infty$	$\log \frac{A_o - A}{A - A_\infty}$	$\log P_{O_2}$
1.475	0	0	0.675	———	———
1.435	8	0.040	0.635	-1.201	0.903
1.190	26	0.285	0.390	-0.136	1.415
1.062	50	0.413	0.262	0.198	1.699
0.910	125	0.565	0.110	0.711	2.097
0.880	201	0.595	0.080	0.871	2.303
0.835	387	0.640	0.035	1.262	2.588
0.800	742	0.675	0	———	2.870

Temperature = -78°C

A (410 nm)	P_{O_2}	$A_o - A$	$A - A_\infty$	$\log \frac{A_o - A}{A - A_\infty}$	$\log P_{O_2}$
1.267	0	0	0.197	———	———
1.243	10	0.024	0.173	-0.858	1.000
1.232	20	0.035	0.162	-0.665	1.301
1.200	53	0.067	0.130	-0.311	1.724
1.146	100	0.121	0.076	0.202	2.000
1.109	200	0.158	0.039	0.610	2.301
1.100	390	0.167	0.030	0.745	2.591
1.070	780	0.197	0	———	2.892

Temperature = -63.5°C

A (410 nm)	P_{O_2}	$A_o - A$	$A - A_\infty$	$\log \frac{A_o - A}{A - A_\infty}$	$\log P_{O_2}$
1.072	0	0	0.192	———	———
1.061	15	0.011	0.181	-1.220	1.176
1.045	30	0.027	0.165	-0.786	1.477
1.011	60	0.061	0.131	-0.332	1.778
0.979	120	0.093	0.099	-0.027	2.079
0.958	340	0.114	0.078	0.165	2.531
0.934	790	0.138	0.054	0.407	2.898

A_∞ estimated to be 0.880

$P_{\frac{1}{2}O_2}$ @ -45°C estimated to be ~1900 Torr based on data from kinetic run.

APPPENDIX VIh. $Co(salen) + O_2 \rightleftharpoons Co(salen)(O_2)$

Kinetics in dichloromethane as a function of oxygen pressure @ -83.5°C

P_{O_2} = 205 Torr*

A (410 nm)	t (sec)	$A_o - A$	$\frac{A_o - A}{A_o - A_\infty}$	$\frac{A - A_\infty}{A_o - A_\infty}$	$\ln \frac{A - A_\infty}{A_o - A_\infty}$
1.233	0	0	0	1.000	0
1.127	184	0.106	0.212	0.788	-0.238
1.038	455	0.195	0.390	0.610	-0.494
0.990	757	0.243	0.486	0.514	-0.666
0.928	1130	0.305	0.609	0.391	-0.939
0.882	1357	0.351	0.701	0.299	-1.207
0.840	1565	0.393	0.784	0.216	-1.532
0.823	1987	0.410	0.818	0.182	-1.704
0.798	2247	0.435	0.868	0.132	-2.025
0.763	3289	0.470	0.938	0.062	-2.781
0.743	4321	0.490	0.978	0.022	-3.817
0.732	5671	0.501	1.000	0	———
0.732	7044	0.501	1.000	0	———
0.732	8672	0.501	1.000	0	———

* Data used for Figure VIII.3

P_{O_2} = 415 (Torr)

A (410 nm)	t (sec)	$A_o - A$	$\frac{A_o - A}{A_o - A_\infty}$	$\frac{A - A_\infty}{A_o - A_\infty}$	$\ln \frac{A - A_\infty}{A_o - A_\infty}$
1.020	0	0	0	1.000	0
1.010	179	0.010	0.033	0.967	-0.034
1.004	246	0.016	0.053	0.947	-0.054
0.983	390	0.037	0.123	0.877	-0.131
0.924	573	0.096	0.320	0.680	-0.386
0.890	691	0.130	0.433	0.567	-0.567
0.808	920	0.212	0.707	0.293	-1.227
0.795	1039	0.225	0.750	0.250	-1.386
0.788	1183	0.232	0.773	0.227	-1.483
0.769	1435	0.251	0.837	0.163	-1.814
0.768	1690	0.252	0.840	0.160	-1.833
0.739	1986	0.261	0.870	0.130	-2.040
0.732	2227	0.288	0.960	0.040	-2.219
0.720	2584	0.300	1.000	0	———
0.720	2883	0.300	1.000	0	———

P_{O_2} = 795 Torr

A (410 nm)	t (sec)	$A_o - A$	$\frac{A_o - A}{A_o - A_\infty}$	$\frac{A - A_\infty}{A_o - A_\infty}$	$\ln \frac{A - A_\infty}{A_o - A_\infty}$
1.102	0	0	0	1.000	0
0.978	68	0.124	0.365	0.635	-0.454
0.947	127	0.155	0.456	0.544	-0.609
0.920	183	0.182	0.535	0.465	-0.766
0.880	258	0.222	0.653	0.347	-1.058
0.849	351	0.255	0.750	0.250	-1.386
0.823	444	0.279	0.821	0.179	-1.720
0.803	552	0.299	0.879	0.121	-2.112
0.793	687	0.309	0.909	0.091	-2.397
0.783	820	0.319	0.938	0.062	-2.781
0.775	951	0.327	0.962	0.038	-3.270
0.762	1586	0.340	1.000	0	———

APPENDIX VIi. $Co(salen) + O_2 \rightleftharpoons Co(salen)(O_2)$

Kinetics of dichloromethane as a function of oxygen pressure @ -78°C

P_{O_2} = 197 Torr

A (410 nm)	t (sec)	$A_o - A$	$\frac{A_o - A}{A_o - A_\infty}$	$\frac{A - A_\infty}{A_o - A_\infty}$	$\ln \frac{A - A_\infty}{A_o - A_\infty}$
1.304	0	0	0	1.000	0
1.203	163	0.101	0.218	0.782	-0.246
1.180	322	0.124	0.267	0.733	-0.311
1.149	520	0.155	0.334	0.666	-0.406
1.111	723	0.197	0.425	0.575	-0.664
1.072	950	0.232	0.500	0.500	-0.693
1.048	1170	0.256	0.552	0.448	-0.803
1.014	1385	0.290	0.625	0.375	-0.983
0.984	1740	0.320	0.690	0.310	-1.171
0.950	2093	0.354	0.763	0.237	-1.440
0.940	2397	0.364	0.784	0.216	-1.532
0.928	2777	0.376	0.810	0.190	-1.661
0.840	5023	0.464	1.000	0	———

P_{O_2} = 407 Torr

A (410 nm)	t (sec)	$A_o - A$	$\frac{A_o - A}{A_o - A}$	$\frac{A - A_\infty}{A_o - A_\infty}$	$\ln \frac{A - A_\infty}{A_o - A_\infty}$
1.497	0	0	0	1.000	0
1.412	135	0.085	0.120	0.880	-0.128
1.385	194	0.152	0.215	0.785	-0.242
1.317	288	0.180	0.255	0.745	-0.294
1.218	479	0.279	0.395	0.605	-0.503
1.133	722	0.364	0.515	0.485	-0.724
1.037	985	0.460	0.650	0.350	-1.050
0.988	1212	0.509	0.720	0.280	-1.273
0.937	1573	0.560	0.792	0.208	-1.570
0.905	1963	0.592	0.837	0.163	-1.814
0.875	2324	0.622	0.880	0.120	-2.120
0.825	2890	0.672	0.950	0.050	-2.996
0.790	3633	0.707	1.000	0	———

P_{O_2} = 790 Torr

A (410 nm)	A (375 nm)	t (sec)	$\Delta A_o - \Delta A$	$\frac{A_o - A}{A_o - A_\infty}$	$\frac{A - A_\infty}{A_o - A_\infty}$	$\ln \frac{A - A_\infty}{A_o - A_\infty}$
1.338	0.862	0	0	0	1.000	0
1.198	0.982	120	0.260	0.457	0.543	-0.611
1.105	0.930	161	0.301	0.523	0.477	-0.740
1.058	0.898	200	0.316	0.555	0.445	-0.810
1.020	0.882	260	0.334	0.587	0.413	-0.884
0.992	0.882	330	0.366	0.643	0.357	-1.030
0.947	0.885	433	0.414	0.728	0.272	-1.302
0.918	0.893	586	0.451	0.793	0.207	-1.575
0.902	0.898	701	0.472	0.830	0.170	-1.772
0.895	0.902	834	0.483	0.849	0.151	-1.890
0.872	0.912	1266	0.516	0.907	0.093	-2.375
0.862	0.930	1686	0.544	0.956	0.044	-3.124
0.845	0.938	2115	0.569	1.000	0	———
0.840	0.933	2652	0.569	1.000	0	———

As the baseline fluctuated somewhat in this experiment, kinetic data were based on the absorbance differences between 410 and 375 nm.

APPENDIX VIj. $Co(salen) + O_2 \rightleftharpoons Co(salen)(O_2)$

Kinetics in dichloromethane as a function of temperature

Temperature = -83.5°C; P_{O_2} = 795 Torr

A (410 nm)	t (sec)	$A_o - A$	$\frac{A_o - A}{A_o - A_\infty}$	$\frac{A - A_\infty}{A_o - A_\infty}$	$\ln \frac{A - A_\infty}{A_o - A_\infty}$
1.102	0	0	0	1.000	0
0.978	68	0.124	0.365	0.635	-0.454
0.947	127	0.155	0.456	0.544	-0.609
0.920	183	0.182	0.535	0.465	-0.766
0.880	258	0.222	0.653	0.347	-1.058
0.849	351	0.255	0.750	0.250	-1.386
0.823	444	0.279	0.821	0.179	-1.720
0.803	552	0.299	0.879	0.121	-2.112
0.793	687	0.309	0.909	0.091	-2.397
0.783	820	0.319	0.938	0.062	-2.781
0.775	951	0.327	0.962	0.038	-3.270
0.762	1586	0.340	1.000	0	———

Temperature = -78°C; P_{O_2} = 790 Torr

A (410 nm)	A (375 nm)	t (sec)	$A_o - A$	$\frac{A_o - A}{A_o - A_\infty}$	$\frac{A - A}{A_o - A_\infty}$	$\ln \frac{A - A}{A_o - A_\infty}$
1.338	0.862	0	0	0	1.000	0
1.198	0.982	120	0.260	0.457	0.543	-0.611
1.105	0.930	161	0.301	0.523	0.477	-0.740
1.058	0.898	200	0.316	0.555	0.445	-0.810
1.020	0.882	260	0.334	0.587	0.413	-0.884
0.992	0.882	330	0.366	0.643	0.357	-1.030
0.947	0.885	433	0.414	0.728	0.272	-1.302
0.918	0.893	586	0.451	0.793	0.207	-1.575
0.902	0.898	701	0.472	0.830	0.170	-1.772
0.895	0.902	834	0.483	0.849	0.151	-1.890
0.872	0.912	1266	0.516	0.907	0.093	-2.375
0.862	0.930	1686	0.544	0.956	0.044	-3.124
0.845	0.938	2115	0.569	1.000	0	———
0.840	0.933	2652	0.569	1.000	0	———

Temperature = -63.5°C; P_{O_2} = 743 Torr

A (410 nm)	t (sec)	$A_o - A$	$\frac{A_o - A}{A_o - A_\infty}$	$\frac{A - A_\infty}{A_o - A_\infty}$	$\ln \frac{A - A_\infty}{A_o - A_\infty}$
1.312	0	0	0	1.000	0
1.250	65	0.062	0.189	0.819	-0.200
1.226	132	0.086	0.262	0.738	-0.304
1.195	237	0.117	0.357	0.647	-0.435
1.162	365	0.150	0.457	0.547	-0.603
1.130	507	0.182	0.555	0.445	-0.810
1.100	668	0.212	0.646	0.354	-1.038
1.080	844	0.232	0.707	0.293	-1.228
1.052	1081	0.260	0.793	0.207	-1.575
1.033	1344	0.279	0.851	0.149	-1.904
1.015	1542	0.297	0.905	0.095	-2.354
0.992	1796	0.320	0.976	0.026	-3.650
0.984	2033	0.328	1.000	0	

Temerature = -45°C; P_{O_2} = 750 Torr

A (410 nm)	t (sec)	$A_o - A$	$\frac{A_o - A}{A_o - A_\infty}$	$\frac{A - A_\infty}{A_o - A_\infty}$	$\ln \frac{A - A_\infty}{A_o - A_\infty}$
1.478	0	0	0	0	0
1.470	32	0.008	0.046	0.954	-0.057
1.444	69	0.034	0.194	0.806	-0.216
1.428	148	0.050	0.286	0.714	-0.337
1.403	239	0.075	0.429	0.571	-0.560
1.388	328	0.090	0.514	0.486	-0.722
1.380	421	0.098	0.560	0.440	-0.821
1.367	534	0.111	0.634	0.366	-1.005
1.340	851	0.138	0.789	0.211	-1.556
1.340	965	0.138	0.789	0.211	-1.556
1.303	2177	0.175	1.000	0	

APPENDIX VIk. CH_3-Im + Co(salen) $\rightleftharpoons$ CH_3-ImCo(salen)

In DMF

Temperature = 5°C

A (408 nm)	$[CH_3\text{-Im}]$	$A_o - A$	$A - A_\infty$	$\log \frac{A_o - A}{A - A_\infty}$	$\log [CH_3\text{-Im}]$
1.426	0	0	0.813	———	———
1.318	0.00299	0.108	0.705	-0.814	-2.525
1.249	0.00597	0.177	0.636	-0.555	-2.224
1.194	0.00894	0.232	0.581	-0.399	-2.049
1.101	0.0149	0.325	0.488	-0.177	-1.826
1.039	0.0201	0.387	0.426	-0.042	-1.697
0.963	0.0299	0.463	0.350	0.122	-1.525
0.871	0.0447	0.555	0.258	0.333	-1.350
0.793	0.0744	0.633	0.180	0.546	-1.128
0.657	0.296	0.769	0.044	1.242	-0.529
0.613	2.712	0.813	0	———	0.433

Temperature = 15°C

A (408 nm)	$[CH_3\text{-Im}]$	$A_o - A$	$A - A_\infty$	$\log \frac{A_o - A}{A - A_\infty}$	$\log [CH_3\text{-Im}]$
1.400	0	0	0.852	———	———
1.355	0.00299	0.045	0.807	-1.254	-2.525
1.260	0.00894	0.140	0.712	-0.706	-2.049
1.176	0.0149	0.224	0.628	-0.448	-1.827
1.101	0.0209	0.299	0.553	-0.267	-1.681
1.038	0.0269	0.362	0.490	-0.131	-1.571
0.978	0.0357	0.422	0.430	-0.008	-1.447
0.904	0.0506	0.496	0.356	0.144	-1.296
0.825	0.0744	0.575	0.287	0.302	-1.128
0.758	0.104	0.642	0.210	0.485	-0.982
0.709	0.147	0.691	0.161	0.633	-0.832
0.612	0.296	0.788	0.064	1.090	-0.529
0.548	2.712	0.852	0	———	0.433

Temperature = 25°C

A (408 nm)	$[CH_3\text{-Im}]$	$A_o - A$	$A - A_\infty$	$\log \frac{A_o - A}{A - A_\infty}$	$\log [CH_3\text{-Im}]$
1.285	0	0	0.686	———	———
1.192	0.00597	0.093	0.593	-0.804	-2.224
1.120	0.0119	0.165	0.521	-0.499	-1.923
1.056	0.0179	0.229	0.457	-0.300	-1.748
0.956	0.0299	0.329	0.357	-0.035	-1.525
0.890	0.0417	0.395	0.291	0.133	-1.380
0.837	0.0593	0.448	0.238	0.275	-1.227
0.759	0.0893	0.526	0.160	0.517	-1.049
0.718	0.119	0.567	0.119	0.678	-0.925
0.674	0.179	0.611	0.075	0.911	-0.748
0.599	0.585	0.686	0	———	-0.233
0.600	3.314	0.685	———	———	0.520

Temperature = 35°C

A (408 nm)	$[CH_3\text{-Im}]$	$A_o - A$	$A - A_\infty$	$\log \frac{A_o - A}{A - A_\infty}$	$\log [CH_3\text{-Im}]$
1.313	0	0	0.743	———	———
1.225	0.00597	0.088	0.655	-0.872	-2.224
1.155	0.0119	0.158	0.585	-0.568	-1.923
1.091	0.0179	0.222	0.521	-0.370	-1.748
1.011	0.0299	0.302	0.441	-0.164	-1.525
0.947	0.0417	0.366	0.377	-0.013	-1.380
0.877	0.0593	0.436	0.307	0.152	-1.227
0.804	0.0893	0.509	0.234	0.338	-1.049
0.760	0.119	0.553	0.190	0.464	-0.925
0.707	0.179	0.606	0.137	0.646	-0.748
0.592	0.585	0.721	0.022	1.516	-0.233
0.570	3.314	0.743	0	———	0.520

Temperature = 45°C

A (408 nm)	$[CH_3\text{-Im}]$	$A_o - A$	$A - A_\infty$	$\log \frac{A_o - A}{A - A_\infty}$	$\log [CH_3\text{-Im}]$
1.340	0	0	0.715	———	———
1.255	0.00597	0.085	0.630	-0.870	-2.224
1.177	0.0119	0.163	0.552	-0.530	-1.923
1.124	0.0179	0.218	0.497	-0.358	-1.748
1.051	0.0299	0.289	0.426	-0.169	-1.525
1.003	0.0417	0.337	0.378	-0.050	-1.380
0.932	0.0593	0.408	0.307	0.123	-1.227
0.863	0.0893	0.477	0.238	0.302	-1.049
0.764	0.119	0.576	0.139	0.617	-0.925
0.721	0.179	0.619	0.096	0.809	-0.748
0.638	0.585	0.702	0.013	1.132	-0.233
0.625	3.314	0.715	0	———	0.520

APPENDIX VII. Pip + Co(salen) $\rightleftharpoons$ PipCo(salen)

In DMF

Temperature = 5°C

A (408 nm)	[Pip]	$A_o - A$	$A - A_\infty$	$\log \frac{A_o - A}{A - A_\infty}$	log[Pip]
1.300	0	0	0.695	———	———
1.170	0.00303	0.130	0.565	-0.638	-2.518
1.097	0.00505	0.203	0.492	-0.384	-2.297
1.014	0.00808	0.286	0.409	-0.155	-2.093
0.941	0.0111	0.359	0.336	0.029	-1.954
0.891	0.0151	0.409	0.286	0.155	-1.820
0.844	0.0202	0.456	0.239	0.280	-1.695
0.784	0.0302	0.586	0.179	0.460	-1.519
0.653	0.100	0.647	0.048	1.130	-1.000
0.605	0.919	0.695	0	———	-0.037

Temperature = 25°C

A (408 nm)	[Pip]	$A_o - A$	$A - A_\infty$	$\log \frac{A_o - A}{A - A_\infty}$	log[Pip]
1.310	0	0	0.592	———	———
1.278	0.00202	0.032	0.560	-1.243	-2.694
1.216	0.00505	0.094	0.498	-0.724	-2.297
1.138	0.0101	0.172	0.420	-0.388	-1.996
1.080	0.0151	0.230	0.362	-0.197	-1.820
0.999	0.0252	0.311	0.281	0.044	-1.598
0.931	0.0353	0.379	0.213	0.250	-1.453
0.887	0.0453	0.423	0.169	0.398	-1.344
0.805	0.0603	0.505	0.087	0.764	-1.220
0.779	0.0752	0.531	0.061	0.940	-1.124
0.739	0.149	0.571	0.021	1.434	-0.826
0.718	0.919	0.592	0	———	-0.037

Temperature = 35°C

A (408 nm)	[Pip]	$A_o - A$	$A - A_\infty$	$\log \frac{A_o - A}{A - A_\infty}$	log [Pip]
1.362	0	0	0.725	———	———
1.304	0.00303	0.058	0.667	-1.061	-2.518
1.231	0.00707	0.131	0.594	-0.657	-2.151
1.158	0.0121	0.204	0.521	-0.407	-1.917
1.078	0.0182	0.284	0.439	-0.181	-1.741
1.006	0.0252	0.356	0.369	-0.016	-1.598
0.920	0.0353	0.442	0.283	0.194	-1.453
0.860	0.0453	0.502	0.223	0.352	-1.344
0.771	0.0752	0.591	0.134	0.644	-1.124
0.686	0.149	0.676	0.049	1.140	-0.826
0.657	0.249	0.705	0.020	1.547	-0.531
0.637	0.919	0.725	0	———	-0.037
0.640	2.332	———	———	———	0.367

Temperature = 55°C

A (408 nm)	[Pip]	$A_o - A$	$A - A_\infty$	$\log \frac{A_o - A}{A - A_\infty}$	log [Pip]
1.213	0	0	0.542	———	———
1.194	0.00505	0.019	0.523	-1.440	-2.297
1.096	0.0151	0.117	0.425	-0.560	-1.820
1.033	0.0252	0.180	0.362	-0.303	-1.598
0.954	0.0403	0.259	0.283	-0.038	-1.395
0.895	0.0603	0.318	0.224	0.152	-1.220
0.807	0.0902	0.406	0.136	0.475	-1.045
0.761	0.149	0.452	0.090	0.701	-0.826
0.704	0.294	0.509	0.033	1.188	-0.531
0.671	0.919	0.542	0	———	-0.037
0.690	2.888	———	———	———	0.461

APPENDIX VIm. Py + Co(salen) $\rightleftharpoons$ PyCo(salen)

In DMF

Temperature = 5°C

A (408 nm)	[Py]	$A_o - A$	$A - A_\infty$	$\log \frac{A_o - A}{A - A_\infty}$	log[Py]
1.296	0	0	0.633	———	———
1.161	0.0124	0.135	0.498	-0.567	-1.907
1.072	0.0248	0.224	0.409	-0.261	-1.606
1.010	0.0371	0.286	0.347	-0.084	-1.430
0.925	0.0618	0.371	0.262	0.151	-1.209
0.860	0.0863	0.436	0.197	0.345	-1.064
0.811	0.123	0.485	0.148	0.515	-0.910
0.770	0.183	0.526	0.107	0.692	-0.736
0.724	0.303	0.572	0.061	0.972	-0.519
0.693	0.591	0.603	0.030	1.303	-0.228
0.666	2.096	0.633	0	———	0.316

Temperature = 15°C

A (408 nm)	[Py]	$A_o - A$	$A - A_\infty$	$\log \frac{A_o - A}{A - A_\infty}$	log[Py]
1.168	0	0	0.596	———	———
1.051	0.0124	0.117	0.479	-0.612	-1.907
1.005	0.0248	0.163	0.433	-0.424	-1.606
0.921	0.0495	0.247	0.349	-0.150	-1.306
0.865	0.0741	0.303	0.293	0.015	-1.130
0.807	0.111	0.361	0.235	0.186	-0.956
0.762	0.159	0.406	0.190	0.330	-0.798
0.726	0.232	0.442	0.154	0.458	-0.635
0.677	0.350	0.491	0.105	0.670	-0.456
0.626	0.580	0.542	0.054	1.002	-0.236
0.572	1.610	0.596	0	———	0.207

Temperature = 25°C

A (408 nm)	[Py]	$A_o - A$	$A - A_\infty$	$\log \frac{A_o - A}{A - A_\infty}$	log[Py]
1.080	0	0	0.561	———	———
1.049	0.0124	0.031	0.530	-1.233	-1.907
0.997	0.0248	0.083	0.478	-0.760	-1.606
0.937	0.0495	0.143	0.418	-0.466	-1.306
0.872	0.0863	0.208	0.353	-0.230	-1.064
0.821	0.123	0.259	0.302	-0.067	-0.910
0.753	0.183	0.327	0.234	0.145	-0.736
0.707	0.244	0.373	0.188	0.298	-0.613
0.644	0.362	0.436	0.125	0.543	-0.442
0.617	0.477	0.463	0.098	0.674	-0.321
0.569	0.703	0.511	0.050	1.009	-0.153
0.534	1.128	0.546	0.015	1.561	0.052
0.519	3.549	0.561	0	———	0.550

Temperature = 35°C

A (408 nm)	[Py]	$A_o - A$	$A - A_\infty$	$\log \frac{A_o - A}{A - A_\infty}$	log[Py]
1.220	0	0	0.647	———	———
1.149	0.0124	0.071	0.576	-0.964	-1.907
1.125	0.0248	0.095	0.552	-0.764	-1.606
1.068	0.0495	0.152	0.495	-0.513	-1.306
1.014	0.0863	0.206	0.441	-0.331	-1.064
0.965	0.123	0.255	0.392	-0.187	-0.910
0.901	0.183	0.319	0.328	-0.012	-0.736
0.839	0.243	0.381	0.266	0.156	-0.614
0.780	0.362	0.440	0.207	0.327	-0.442
0.737	0.477	0.483	0.164	0.469	-0.321
0.668	0.702	0.552	0.095	0.764	-0.153
0.608	1.128	0.612	0.035	1.243	0.052
0.573	2.484	0.647	0	———	0.395

Temperature = 65°C

A (408 nm)	[Py]	$A_o - A$	$A - A_\infty$	$\log \frac{A_o - A}{A - A_\infty}$	log[Py]
0.913	0	0	0.513	———	———
0.908	0.0124	0.005	0.508	-2.007	-1.907
0.854	0.0621	0.059	0.454	-0.886	-1.207
0.788	0.123	0.125	0.388	-0.492	-0.910
0.704	0.244	0.209	0.304	-0.163	-0.613
0.664	0.362	0.249	0.264	-0.025	-0.442
0.616	0.591	0.297	0.216	0.138	-0.228
0.521	1.62	0.392	0.121	0.511	0.210

A_∞ estimated to be 0.400, based on lower temperature data.

APPENDIX VIn. CH_3-Im + Co(salen) $\rightleftharpoons$ CH_3-ImCo(salen)

In toluene

Temperature = 5°C

A (418 nm)	$[CH_3\text{-Im}]$	$A_o - A$	$A - A_\infty$	$\log \frac{A_o - A}{A - A_\infty}$	$\log [CH_3\text{-Im}]$
1.388	0	0	0.700	———	———
1.060	0.00305	0.328	0.372	-0.054	-2.516
0.900	0.00672	0.488	0.212	0.362	-2.173
0.825	0.0109	0.563	0.137	0.613	-1.961
0.784	0.0150	0.604	0.096	0.798	-1.823
0.744	0.0251	0.644	0.056	1.061	-1.601
0.717	0.0438	0.671	0.029	1.364	-1.359
0.701	0.107	0.687	0.013	1.723	-0.973
0.694	0.723	0.694	0.006	2.063	-0.139
0.688	3.314	0.700	0	———	0.520

Temperature = 15°C

A (418 nm)	$[CH_3\text{-Im}]$	$A_o - A$	$A - A_\infty$	$\log \frac{A_o - A}{A - A_\infty}$	$\log [CH_3\text{-Im}]$
1.197	0	0	0.564	———	———
0.983	0.00278	0.214	0.350	-0.213	-2.556
0.836	0.00639	0.361	0.203	0.250	-2.194
0.777	0.0104	0.420	0.144	0.464	-1.983
0.706	0.0192	0.491	0.073	0.828	-1.717
0.679	0.0336	0.518	0.046	1.052	-1.474
0.671	0.0717	0.526	0.038	1.141	-1.144
0.666	0.302	0.531	0.033	1.207	-0.520
0.633	3.314	0.564	0	———	0.520

Temperature = 25°C

A (418 nm)	$[CH_3\text{-Im}]$	$A_o - A$	$A - A_\infty$	$\log \frac{A_o - A}{A - A_\infty}$	$\log [CH_3\text{-Im}]$
1.003	0	0	0.516	———	———
0.868	0.00261	0.135	0.381	-0.451	-2.583
0.743	0.00597	0.260	0.256	0.007	-2.224
0.642	0.00998	0.361	0.155	0.367	-2.001
0.574	0.0130	0.429	0.087	0.693	-1.885
0.548	0.0180	0.455	0.061	0.873	-1.745
0.514	0.0413	0.489	0.027	1.258	-1.385
0.499	0.0945	0.504	0.015	1.526	-1.025
0.487	0.725	0.516	0	———	-0.140
0.488	3.314	0.515	0	———	0.520

Temperature = 35°C

A (418 nm)	$[CH_3\text{-Im}]$	$A_o - A$	$A - A_\infty$	$\log \frac{A_o - A}{A - A_\infty}$	$\log [CH_3\text{-Im}]$
1.254	0	0	0.678	———	———
1.120	0.00246	0.134	0.544	-0.608	-2.609
0.988	0.00561	0.266	0.412	-0.190	-2.251
0.864	0.00923	0.390	0.288	0.132	-2.035
0.789	0.0126	0.466	0.212	0.342	-1.898
0.728	0.0170	0.526	0.152	0.539	-1.770
0.685	0.0255	0.549	0.129	0.629	-1.593
0.651	0.0392	0.603	0.075	0.905	-1.407
0.549	0.0897	0.655	0.023	1.455	-1.048
0.580	0.614	0.674	0.004	2.227	-0.212
0.576	1.808	0.678	0	———	0.257
0.581	3.314	———	———	———	0.520

Temperature = 45°C

A (418 nm)	$[CH_3\text{-Im}]$	$A_o - A$	$A - A_\infty$	$\log \frac{A_o - A}{A - A_\infty}$	$\log [CH_3\text{-Im}]$
1.037	0	0	0.539	———	———
0.952	0.00233	0.085	0.454	-0.728	-2.634
0.875	0.00534	0.162	0.377	-0.369	-2.272
0.790	0.00872	0.247	0.292	-0.073	-2.060
0.726	0.0119	0.307	0.232	0.122	-1.924
0.683	0.0161	0.354	0.185	0.282	-1.795
0.646	0.0240	0.391	0.148	0.422	-1.618
0.597	0.0369	0.440	0.099	0.648	-1.433
0.567	0.0600	0.470	0.069	0.833	-1.222
0.524	0.201	0.513	0.026	1.295	-0.696
0.510	1.808	0.527	0.012	1.643	0.257
0.498	3.314	0.539	0	———	0.520

Temperature = 55°C

A (418 nm)	$[CH_3\text{-Im}]$	$A_o - A$	$A - A_\infty$	$\log \frac{A_o - A}{A - A_\infty}$	$\log [CH_3\text{-Im}]$
1.353	0	0	0.669	———	———
1.250	0.00228	0.103	0.566	-0.740	-2.642
1.176	0.00398	0.177	0.492	-0.444	-2.401
1.057	0.00854	0.296	0.373	-0.100	-2.069
0.994	0.0117	0.359	0.310	0.064	-1.932
0.910	0.0158	0.443	0.226	0.292	-1.801
0.878	0.0195	0.475	0.194	0.389	-1.710
0.823	0.0276	0.530	0.139	0.581	-1.560
0.801	0.0362	0.552	0.117	0.674	-1.441
0.757	0.0588	0.596	0.073	0.912	-1.231
0.737	0.108	0.616	0.053	1.065	-0.966
0.713	0.567	0.640	0.029	1.344	-0.256
0.690	1.808	0.663	0.006	2.043	0.257
0.684	3.314	0.669	0	———	0.520

Temperature = 65°C

A (418 nm)	$[CH_3\text{-Im}]$	$A_o - A$	$A - A_\infty$	$\log \frac{A_o - A}{A - A_\infty}$	$\log [CH_3\text{-Im}]$
1.140	0	0	0	———	———
1.045	0.00366	0.095	0.537	-0.752	-2.436
0.988	0.00677	0.152	0.480	-0.499	-2.169
0.905	0.0100	0.235	0.397	-0.228	-2.000
0.823	0.0149	0.317	0.315	0.003	-1.827
0.763	0.0191	0.377	0.255	0.170	-1.718
0.713	0.0240	0.427	0.205	0.319	-1.419
0.691	0.0345	0.449	0.183	0.390	-1.462
0.599	0.0753	0.541	0.091	0.774	-1.123
0.545	0.161	0.595	0.037	1.206	-0.793
0.536	1.808	0.604	0.028	1.334	0.257
0.508	3.314	0.632	0	———	0.520

APPENDIX VIo. Pip + Co(salen) $\rightleftharpoons$ PipCo(salen)

In toluene

Temperature = 5°C

A (418 nm)	[Pip]	$A_o - A$	$A - A_\infty$	$\log \frac{A_o - A}{A - A_\infty}$	log[Pip]
1.152	0	0	0.633	———	———
0.932	0.00101	0.220	0.413	-0.274	-2.996
0.820	0.00202	0.332	0.301	0.043	-2.694
0.751	0.00303	0.401	0.232	0.238	-2.518
0.702	0.00505	0.450	0.183	0.391	-2.297
0.616	0.0101	0.536	0.097	0.742	-1.996
0.568	0.0202	0.584	0.049	1.076	-1.695
0.528	0.100	0.624	0.009	1.874	-1.000
0.519	0.919	0.633	0	———	-0.037

Temperature = 15°C

A (418 nm)	[Pip]	$A_o - A$	$A - A_\infty$	$\log \frac{A_o - A}{A - A_\infty}$	log[Pip]
1.227	0	0	0.633	———	———
1.083	0.00101	0.144	0.527	-0.563	-2.996
1.000	0.00202	0.227	0.444	-0.291	-2.694
0.973	0.00303	0.314	0.357	-0.056	-2.518
0.860	0.00404	0.367	0.304	0.078	-2.393
0.815	0.00505	0.412	0.259	0.202	-2.297
0.751	0.00707	0.475	0.196	0.384	-2.151
0.708	0.0101	0.518	0.153	0.530	-1.996
0.665	0.0151	0.561	0.110	0.708	-1.820
0.614	0.0252	0.611	0.060	1.008	-1.598
0.550	0.100	0.671	0	———	-1.000
0.515	0.919	———	———	———	———

Temperature = 25°C

A (418 nm)	[Pip]	$A_o - A$	$A - A_\infty$	$\log \frac{A_o - A}{A - A_\infty}$	log[Pip]
1.183	0	0	0.637	———	———
1.137	0.00101	0.046	0.591	-1.109	-2.996
1.103	0.00202	0.080	0.557	-0.842	-2.694
1.048	0.00404	0.135	0.502	-0.570	-2.393
0.969	0.00707	0.214	0.423	-0.296	-2.151
0.911	0.0101	0.272	0.365	-0.128	-1.996
0.830	0.0151	0.353	0.284	0.094	-1.820
0.782	0.0202	0.401	0.236	0.230	-1.695
0.735	0.0302	0.448	0.189	0.375	-1.519
0.601	0.100	0.582	0.055	1.025	-1.000
0.546	0.919	0.637	0	———	-0.037
0.546	1.685	0.637	0	———	0.227

APPENDIX VIp. Py + Co(salen) $\rightleftharpoons$ PyCo(salen)

In toluene

Temperature = 5°C

A (418 nm)	[Py]	$A_o - A$	$A - A_\infty$	$\log \frac{A_o - A}{A - A_\infty}$	log[Py]
1.208	0	0	0.531	———	———
1.090	0.00621	0.118	0.413	-0.544	
1.009	0.0124	0.199	0.319	-0.205	-2.207
0.939	0.0186	0.269	0.262	0.011	-1.907
0.891	0.0248	0.317	0.214	0.171	-1.730
0.820	0.0371	0.388	0.143	0.433	-1.606
0.793	0.0495	0.415	0.116	0.554	-1.430
0.747	0.0741	0.461	0.070	0.819	-1.306
0.690	0.184	0.518	0.013	1.600	-0.736
0.677	0.303	0.531	0	———	-0.519
0.677	1.13	0.531	0	———	0.053

Temperature = 15°C

A (418 nm)	[Py]	$A_o - A$	$A - A_\infty$	$\log \frac{A_o - A}{A - A_\infty}$	log[Py]
1.000	0	0	0.511	———	———
0.943	0.00621	0.057	0.454	-0.901	-2.207
0.898	0.0124	0.102	0.409	-0.603	-1.907
0.824	0.0248	0.176	0.335	-0.280	-1.606
0.759	0.0371	0.241	0.270	-0.049	-1.430
0.725	0.0495	0.275	0.236	0.066	-1.306
0.651	0.0741	0.349	0.162	0.333	-1.130
0.602	0.0986	0.398	0.103	0.587	-1.006
0.586	0.123	0.416	0.095	0.641	-0.910
0.533	0.244	0.467	0.044	1.029	-0.613
0.499	0.591	0.501	0.010	1.699	-0.228
0.489	1.128	0.511	0	———	0.052

Temperature = 35°C

A (418 nm)	[Pip]	$A_o - A$	$A - A_\infty$	$\log \frac{A_o - A}{A - A_\infty}$	log [Pip]
1.200	0	0	0.588	———	———
1.168	0.00202	0.032	0.556	-1.240	-2.694
1.108	0.00505	0.092	0.496	-0.732	-2.297
1.034	0.0101	0.166	0.422	-0.405	-1.996
0.961	0.0151	0.239	0.349	-0.164	-1.820
0.899	0.0202	0.301	0.287	0.021	-1.695
0.846	0.0252	0.354	0.234	0.180	-1.598
0.800	0.0353	0.400	0.188	0.328	-1.453
0.767	0.0503	0.437	0.151	0.462	-1.299
0.702	0.100	0.498	0.090	0.743	-1.000
0.686	0.198	0.516	0.072	0.855	-0.703
0.612	0.919	0.588	0	———	-0.037
0.612	1.685	0.588	0	———	-0.227

Temperature = 45°C

A (418 nm)	[Pip]	$A_o - A$	$A - A_\infty$	$\log \frac{A_o - A}{A - A_\infty}$	log [Pip]
1.009	0	0	0.489	———	———
0.990	0.00202	0.019	0.470	-1.393	-2.694
0.947	0.00505	0.062	0.427	-0.838	-2.297
0.890	0.0101	0.119	0.370	-0.493	-1.996
0.802	0.0202	0.207	0.282	-0.134	-1.695
0.737	0.0303	0.272	0.217	0.098	-1.519
0.690	0.0403	0.319	0.170	0.273	-1.395
0.650	0.0603	0.359	0.130	0.441	-1.220
0.604	0.100	0.405	0.084	0.683	-1.000
0.520	0.919	0.489	0	———	-0.037
0.528	1.685	———	———	———	0.227

Trmperature = 65°C

A (418 nm)	[Pip]	$A_o - A$	$A - A_\infty$	$\log \frac{A_o - A}{A - A_\infty}$	log [Pip]
1.077	0	0	0.570	———	———
1.034	0.00505	0.043	0.527	-1.088	-2.297
0.968	0.0151	0.109	0.461	-0.626	-1.820
0.915	0.0252	0.172	0.398	-0.364	-1.598
0.824	0.0503	0.253	0.317	-0.098	-1.299
0.727	0.100	0.350	0.220	0.202	-1.000
0.644	0.198	0.433	0.137	0.137	-0.703
0.534	0.919	0.543	0.027	0.027	-0.037
0.507	1.685	0.570	0	———	0.227

Temperature = 25°C

A (418 nm)	[Py]	$A_o - A$	$A - A_\infty$	$\log \frac{A_o - A}{A - A_\infty}$	log[Py]
1.233	0	0	0.609	———	———
1.180	0.00372	0.053	0.556	-1.021	-2.429
1.158	0.00745	0.075	0.534	-0.852	-2.128
1.135	0.0124	0.098	0.511	-0.717	-1.907
1.080	0.0186	0.153	0.456	-0.472	-1.730
1.045	0.0248	0.188	0.421	-0.350	-1.606
0.983	0.0371	0.250	0.359	-0.157	-1.430
0.951	0.0495	0.282	0.327	-0.064	-1.306
0.854	0.0741	0.380	0.229	0.220	-1.130
0.780	0.0986	0.419	0.190	0.343	-1.006
0.750	0.123	0.453	0.156	0.463	-0.910
0.721	0.159	0.483	0.126	0.584	-0.798
0.698	0.220	0.512	0.097	0.722	-0.658
0.654	0.303	0.535	0.074	0.859	-0.519
0.649	0.539	0.584	0.030	1.286	-0.272
0.649	1.128	0.584	0.025	1.368	0.052
0.624	2.068	0.609	0	———	0.316

Temperature = 35°C

A (418 nm)	[Py]	$A_o - A$	$A - A_\infty$	$\log \frac{A_o - A}{A - A_\infty}$	log[Py]
1.397	0	0	0.732	———	———
1.368	0.00621	0.029	0.703	-1.385	-2.207
1.331	0.0124	0.066	0.666	-1.004	-1.907
1.239	0.0248	0.158	0.574	-0.560	-1.606
1.182	0.0371	0.217	0.515	-0.370	-1.430
1.118	0.0556	0.279	0.453	-0.210	-1.255
1.020	0.0863	0.377	0.355	0.026	-1.064
0.954	0.123	0.443	0.289	0.186	-0.910
0.871	0.184	0.526	0.206	0.407	-0.734
0.826	0.244	0.571	0.161	0.550	-0.613
0.759	0.362	0.618	0.114	0.734	-0.442
0.730	0.591	0.667	0.065	1.011	-0.228
0.684	1.128	0.713	0.019	1.574	0.052
0.670	2.069	0.727	0.005	2.163	0.316
0.665	3.549	0.732	0	———	0.550

Temperature = 45°C

A (418 nm)	[Py]	$A_o - A$	$A - A_\infty$	$\log \frac{A_o - A}{A - A_\infty}$	log [Py]
1.108	0	0	0.477	———	———
1.079	0.00621	0.029	0.448	-1.189	-2.207
1.055	0.0186	0.053	0.424	-0.903	-1.730
1.013	0.0371	0.095	0.382	-0.604	-1.430
0.956	0.0741	0.156	0.321	-0.313	-1.130
0.886	0.123	0.222	0.255	-0.060	-0.910
0.822	0.184	0.286	0.191	0.175	-0.736
0.792	0.244	0.316	0.161	0.293	-0.613
0.744	0.362	0.364	0.113	0.508	-0.442
0.717	0.539	0.391	0.086	0.658	-0.272
0.681	0.813	0.427	0.050	0.931	-0.090
0.647	1.128	0.461	0.016	1.385	-0.052
0.630	2.069	0.477	0	———	0.316
0.641	3.549	———	———	———	0.550

APPENDIX VIq. CH_3-ImCo(salen) + $O_2 \rightleftharpoons$ CH_3-ImCo(salen)(O_2)

In DMF

Temperature = -45°C

A (400 nm)	P_{O_2}	$A - A_o$	$A_\infty - A$	$\log \frac{A - A_o}{A_\infty - A}$	$\log P_{O_2}$
0.823	0	0	0.510	———	———
0.844	0.08	0.021	0.489	-1.367	-1.097
0.907	0.23	0.084	0.426	-0.705	-0.637
0.967	0.46	0.144	0.366	-0.405	-0.336
1.015	0.69	0.197	0.313	-0.201	-0.160
1.058	1.15	0.235	0.275	-0.068	0.061
1.150	1.92	0.327	0.183	0.252	0.284
1.207	2.85	0.384	0.126	0.484	0.454
1.285	8	0.462	0.048	0.983	0.903
1.325	13	0.502	0.008	1.798	1.114
1.333	98	0.510	0	———	1.991
1.333	767	0.510	0	———	2.885

Temperature = -23°C

A (400 nm)	P_{O_2}	$A - A_o$	$A_\infty - A$	$\log \frac{A - A_o}{A_\infty - A}$	$\log P_{O_2}$
0.867	0	0	0.413	———	———
0.917	0.69	0.050	0.363	-0.861	-0.160
0.967	1.23	0.100	0.313	-0.496	0.090
1.020	2.23	0.153	0.260	-0.230	0.348
1.095	3.46	0.228	0.185	0.098	0.539
1.170	7	0.303	0.110	0.440	0.845
1.246	15	0.379	0.034	1.047	1.176
1.247	32	0.380	0.033	1.061	1.505
1.280	103	0.413	0	———	2.013
1.280	762	0.413	0	———	2.882

Temperature = 0°C

A (400 nm)	P_{O_2}	$A - A_o$	$A_\infty - A$	$\log \frac{A - A_o}{A_\infty - A}$	$\log P_{O_2}$
0.740	0	0	0.438	———	———
0.740	0.77	0	0.438	———	-0.114
0.770	1.54	0.030	0.408	-1.134	0.187
0.790	2.85	0.050	0.388	-0.890	0.454
0.856	6.23	0.116	0.322	-0.443	0.795
1.000	11.54	0.260	0.178	0.165	1.062
1.105	19.64	0.365	0.073	0.699	1.294
1.140	30.8	0.400	0.038	1.022	1.488
1.178	53	0.438	0	———	1.724
1.178	615	0.438	0	———	2.789

Irreversible oxidation appears to be occurring in this run.

APPENDIX VIr. $PipCo(salen) + O_2 \rightleftharpoons PipCo(salen)(O_2)$

In DMF

Temperature = -45°C

A (400 nm)	P_{O_2}	$A - A_o$	$A_\infty - A$	$\log \frac{A - A_o}{A_\infty - A}$	$\log P_{O_2}$
0.920	0	0	0.424	———	———
0.943	0.31	0.023	0.401	-1.241	-0.511
1.007	0.69	0.087	0.337	-0.588	-0.160
1.067	1.46	0.147	0.277	-0.275	0.165
1.143	2.69	0.223	0.201	0.045	0.430
1.226	4.54	0.306	0.118	0.414	0.657
1.323	10	0.403	0.021	1.283	1.000
1.344	20	0.424	0	———	1.301
1.344	62	0.424	0	———	1.792
1.344	154	0.424	0	———	2.188
1.388	762	0.424	0	———	2.882

Temperature = -23°C

A (400 nm)	P_{O_2}	$A - A_o$	$A_\infty - A$	$\log \frac{A - A_o}{A_\infty - A}$	$\log P_{O_2}$
0.623	0	0	0.277	———	———
0.630	0.23	0.007	0.270	-1.586	-0.637
0.647	0.62	0.024	0.253	-1.023	-0.211
0.668	1.15	0.045	0.232	-0.712	0.062
0.707	2.38	0.084	0.193	-0.361	0.377
0.740	4.08	0.117	0.160	-0.135	0.611
0.774	6.46	0.151	0.126	0.079	0.810
0.774	10	0.151	0.126	0.079	1.000
0.800	22	0.177	0.100	0.248	1.342
0.765	83	0.142	0.135	0.022	1.919
0.762	765	0.139	0.138	0.003	2.884

A_∞ estimated to be 0.900; oxidation appears to be a problem.

APPENDIX VIs. $PyCo(salen) + O_2 \rightleftharpoons PyCo(salen)(O_2)$

In DMF

Temperature = -45°C

A (400 nm)	P_{O_2}	$A - A_o$	$A_\infty - A$	$\log \frac{A - A_o}{A_\infty - A}$	$\log P_{O_2}$
0.770	0	0	0.347	———	———
0.800	0.77	0.030	0.317	-1.063	-0.114
0.860	1.62	0.090	0.257	-0.456	0.208
0.910	3.23	0.140	0.207	-0.170	0.509
1.010	5.69	0.190	0.157	0.083	0.755
1.067	9.00	0.297	0.050	0.774	0.954
1.100	11.6	0.330	0.017	1.288	1.065
1.115	20.4	0.345	0.002	2.538	1.309
1.115	30.4	0.345	0.002	2.538	1.483
1.117	60	0.347	0	———	1.778

Temperature = -23°C

A (400 nm)	P_{O_2}	$A - A_o$	$A_\infty - A$	$\log \frac{A - A_o}{A_\infty - A}$	$\log P_{O_2}$
0.865	0	0	0.505	———	———
0.878	0.38	0.013	0.492	-1.578	-0.415
0.893	0.92	0.028	0.477	-1.231	-0.035
0.928	1.31	0.063	0.442	-0.846	0.117
0.970	2.31	0.105	0.400	-0.581	0.363
1.040	4.00	0.175	0.300	-0.275	0.602
1.080	6.00	0.215	0.290	-0.130	0.778
1.165	9.85	0.300	0.205	0.165	0.993
1.230	14.0	0.371	0.134	0.442	1.145
1.270	19.4	0.405	0.100	0.607	1.287
1.305	30.2	0.440	0.065	0.831	1.480
1.327	47.2	0.462	0.043	1.031	1.674
1.341	63	0.476	0.031	1.186	1.799
1.350	156	0.485	0.020	1.385	2.193
1.360	400	0.495	0.010	1.695	2.602
1.370	800	0.505	0	———	2.903

Temperature = 0°C

A (400 nm)	P_{O_2}	$A - A_o$	$A - A_\infty$	$\log \frac{A - A_o}{A_\infty - A}$	$\log P_{O_2}$
0.647	0	0	0.540	———	———
0.678	2.00	0.031	0.509	-1.215	0.301
0.690	2.77	0.043	0.497	-1.063	0.442
0.705	4.54	0.058	0.482	-0.920	0.657
0.728	6.77	0.081	0.459	-0.753	0.831
0.785	11.7	0.138	0.402	-0.464	1.068
0.865	19.3	0.218	0.322	-0.169	1.286
0.930	30.2	0.283	0.257	0.042	1.480
1.003	45.8	0.356	0.184	0.287	1.661
1.090	61	0.443	0.097	0.660	1.785
1.130	102	0.483	0.057	0.928	2.005
1.150	200	0.503	0.037	1.133	2.301
1.174	404	0.527	0.013	1.608	2.606
1.187	816	0.540	0	———	2.912

APPENDIX VIt. CH_3-ImCo(salen) + O_2 $\rightleftharpoons$ CH_3-ImCo(salen)(O_2)

In toluene

Temperature = -45°C

A (400 nm)	P_{O_2}	$A - A_o$	$A_\infty - A$	$\log \frac{A - A_o}{A_\infty - A}$	$\log P_{O_2}$
0.836	0	0	0.157	———	———
0.850	2.00	0.014	0.143	-1.009	0.301
0.862	3.15	0.026	0.131	-0.720	0.498
0.875	5.38	0.039	0.118	-0.481	0.731
0.892	8.92	0.056	0.101	-0.256	0.951
0.905	17.8	0.069	0.088	-0.106	1.251
0.933	38.1	0.097	0.060	0.209	1.581
0.952	80	0.116	0.041	0.452	1.903
0.976	200	0.140	0.017	0.915	2.301
0.989	400	0.153	0.004	1.583	2.602
0.993	800	0.157	0	———	2.903

Temperature = -45°C

A (400 nm)	P_{O_2}	$A - A_o$	$A_\infty - A$	$\log \frac{A - A_o}{A_\infty - A}$	$\log P_{O_2}$
1.033	0	0	0.187	———	———
1.033	1.00	0	0.187	———	0.000
1.055	3.31	0.022	0.165	-0.875	0.520
1.080	9.15	0.047	0.140	-0.474	0.961
1.110	21.15	0.077	0.110	-0.155	1.325
1.126	30	0.093	0.094	-0.005	1.475
1.137	40	0.104	0.083	0.098	1.602
1.163	80	0.130	0.057	0.358	1.903
1.190	200	0.157	0.030	0.718	2.301
1.220	800	0.187	0	———	2.903

APPENDIX VIu. PipCo(salen) + O_2 $\rightleftharpoons$ PipCo(salen)(O_2)

In toluene

Temperature = -78°C

A (400 nm)	P_{O_2}	$A - A_o$	$A_\infty - A$	$\log \frac{A - A_o}{A_\infty - A}$	$\log P_{O_2}$
0.760	0	0	0.150	———	———
0.760	4	0	0.150	———	0.602
0.796	23	0.036	0.114	-0.501	1.362
0.815	38	0.055	0.095	-0.237	1.580
0.815	56	0.055	0.095	-0.237	1.748
0.815	75	0.055	0.095	-0.237	1.875
0.827	113	0.067	0.080	-0.098	2.053
0.840	170	0.080	0.070	-0.058	2.230
0.860	800	0.100	0.050	0.301	2.903

A_∞ estimated to be 0.910.

APPENDIX VIv. $PyCo(salen) + O_2 \rightleftharpoons PyCo(salen)(O_2)$

In toluene

Temperature = -45°C

A (400 nm)	P_{O_2}	$A - A_o$	$A_\infty - A$	$\log \frac{A - A_o}{A_\infty - A}$	$\log P_{O_2}$
1.061	0	0	0.260	———	———
1.078	2	0.017	0.243	-1.153	0.303
1.090	12	0.029	0.231	-0.901	1.079
1.103	25	0.042	0.218	-0.715	1.397
1.147	58	0.086	0.174	-0.306	1.763
1.172	120	0.110	0.150	-0.135	2.079
1.212	250	0.151	0.109	0.142	2.398
1.258	540	0.197	0.063	0.495	2.732

A_∞ estimated to be 1.321

APPENDIX VII

RAW DATA FOR DETERMINING THE THERMODYNAMIC AND KINETIC PARAMETERS OF REACTING OLEFINIC SUBSTRATES WITH COBALT MACROCYCLIC SYSTEMS.

APPENDIX VIIa. $MA + CoOMBP \rightleftharpoons MACoOMBP$

In toluene

Temperature = 5°C

A (412 nm)	[MA]	$A_o - A$	$A - A_\infty$	$\log \frac{A_o - A}{A - A_\infty}$	log[MA]
1.033	0	0	0.785	———	———
0.951	9.44×10^{-4}	0.082	0.703	-0.933	-3.026
0.912	1.88×10^{-3}	0.121	0.664	-0.739	-2.725
0.870	3.76×10^{-3}	0.163	0.622	-0.582	-2.425
0.806	4.73×10^{-3}	0.227	0.558	-0.391	-2.325
0.733	7.49×10^{-2}	0.300	0.485	-0.209	-2.126
0.607	1.49×10^{-2}	0.426	0.359	0.074	-1.828
0.455	5.70×10^{-2}	0.578	0.207	0.446	-1.244
0.345	0.108	0.687	0.098	0.846	-0.966
0.308	0.196	0.725	0.060	1.082	-0.708
0.248	0.494	0.785	0	———	-0.306

Temperature = 22°C

A (412 nm)	[MA]	$A_o - A$	$A - A_\infty$	$\log \frac{A_o - A}{A - A_\infty}$	log[MA]
1.253	0	0	0.974	———	———
1.219	9.44×10^{-4}	0.034	0.940	-1.442	-3.026
1.210	1.88×10^{-3}	0.043	0.931	-1.335	-2.725
1.187	3.76×10^{-3}	0.066	0.908	-1.139	-2.425
1.156	4.73×10^{-3}	0.097	0.877	-0.956	-2.325
1.116	7.49×10^{-3}	0.137	0.837	-0.786	-2.126
1.089	1.49×10^{-2}	0.164	0.810	-0.694	-1.828
0.945	2.26×10^{-2}	0.308	0.666	-0.335	-1.645
0.709	0.108	0.544	0.420	0.112	-0.966
0.408	0.196	0.845	0.129	0.816	-0.708
0.279	0.494	0.974	0	———	-0.306

Temperature = 40°C

A (412 nm)	[MA]	$A_o - A$	$A - A_\infty$	$\log \frac{A_o - A}{A - A_\infty}$	log[MA]
1.100	0	0	0.845	———	———
1.079	3.76×10^{-3}	0.021	0.824	-1.594	-2.425
1.075	4.51×10^{-3}	0.025	0.820	-1.516	-2.326
1.046	1.17×10^{-2}	0.054	0.791	-1.166	-1.932
0.971	3.64×10^{-2}	0.129	0.716	-0.744	-1.439
0.762	0.111	0.338	0.507	-0.176	-0.753
0.479	0.318	0.621	0.224	0.443	-0.597
0.432	0.439	0.668	0.177	0.577	-0.358

A_∞ estimated to be 0.255 based on lower temperature data.

Additions made with 1.037 M MA solution in toluene.

APPENDIX VIIb. MA + CoOMBP $\rightleftharpoons$ MACoOMBP

In DCE

Temperature = 20°C

A (412 nm)	[MA]	$A_o - A$	$A - A_\infty$	$\log \frac{A_o - A}{A - A_\infty}$	log[MA]
1.033	0	0	0.773	———	———
1.033	1.95×10^{-4}	0	0.773	———	-3.701
1.026	9.94×10^{-4}	0.007	0.766	-2.069	-3.026
1.019	3.76×10^{-3}	0.014	0.759	-1.734	-2.425
0.989	1.86×10^{-2}	0.044	0.729	-1.219	-1.730
0.916	3.64×10^{-2}	0.117	0.656	-0.749	-1.439
0.843	7.03×10^{-2}	0.190	0.583	-0.487	-1.153
0.718	0.108	0.315	0.458	-0.163	-0.967
0.561	0.196	0.472	0.301	0.195	-0.707
0.260	0.494	0.565	0.208	0.434	-0.306

APPENDIX VIIc. MA + PipCoOMBP $\rightleftharpoons$ Pip + MACoOMBP

[Pip] = 2×10^{-3} M; Temperature = 20°C

A (450 nm)	A (618 nm)	[MA]	A_o - A (450 nm)	A_o - A (618 nm)
0.568	1.056	0	0	0
0.581	1.071	9.94×10^{-4}	-0.013	-0.015
0.501	1.288	3.76×10^{-3}	0.067	-0.227
0.473	1.267	5.63×10^{-3}	0.095	-0.211
0.528	1.211	9.26×10^{-2}	0.040	-0.155
0.463	1.090	1.85×10^{-2}	0.118	-0.034
0.355	0.729	3.64×10^{-2}	0.213	0.327
0.334	0.392	7.03×10^{-2}	0.234	0.664
0.375	0.197	0.131	0.193	0.859
0.391	0.196	0.277	0.177	0.860
0.362	0.200	0.494	0.206	0.856

MA + PipCoOMBP $\rightleftharpoons$ PipCoOMBP(MA)

[Pip] = 4×10^{-2} M; Temperature = 20°C

A (440 nm)	A (618 nm)	[MA]	A_o - A (440 nm)	A_o - A (618 nm)
1.130	1.218	0	0	0
0.852	1.223	1.88×10^{-3}	0.278	-0.005
0.833	1.222	3.76×10^{-3}	0.297	-0.004
0.809	1.227	7.49×10^{-3}	0.321	-0.009
0.751	1.214	1.49×10^{-2}	0.379	0.004
0.794	1.312	2.93×10^{-2}	0.336	-0.094
0.889	1.254	5.70×10^{-2}	0.241	-0.036
1.105	1.105	0.108	0.025	0.113
1.466	0.790	0.196	-0.336	0.428
1.642	0.439	0.494	-0.512	0.779

$$PipCoOMBP(MA) \longrightarrow PipCoOMBP + MA$$

Pip = 5×10^{-3} M; MA = 0.0528 M; Temperature = $20^{o}C$

A (440 nm)	t	$A_o - A$	$A - A_{eq}$	$\ln A - A_{eq}$
0.963	0	0	0.363	-1.013
0.885	177	0.078	0.285	-1.255
0.769	383	0.194	0.169	-1.778
0.670	1282	0.293	0.070	-2.659
0.627	2297	0.336	0.027	-3.612

A_{eq} estimated to be 0.600

APPENDIX VIId. MA + DMFCoOMBP $\rightleftharpoons$ DMFCoOMBP(MA)

In DMF

Temperature = 5°C

A (418 nm)	[MA]	$A_o - A$	$A - A_\infty$	$\log \frac{A_o - A}{A - A_\infty}$	log[MA]
1.130	0	0	0.588	———	———
1.115	2.17×10^{-4}	0.015	0.573	-1.582	-3.664
1.105	4.34×10^{-4}	0.025	0.563	-1.353	-3.363
1.091	1.08×10^{-3}	0.039	0.549	-1.149	-2.965
1.065	2.17×10^{-3}	0.065	0.523	-0.906	-2.664
1.046	4.32×10^{-3}	0.084	0.504	-0.778	-2.364
0.905	1.71×10^{-2}	0.180	0.408	-0.355	-1.767
0.913	2.75×10^{-2}	0.217	0.371	-0.233	-1.561
0.805	4.40×10^{-2}	0.325	0.263	0.092	-1.357
0.679	9.86×10^{-2}	0.451	0.137	0.517	-1.006
0.550	0.181	0.580	0.008	1.860	-0.743
0.542	0.310	0.588	0	———	-0.507

Temperature = 22°C

A (418 nm)	[MA]	$A_o - A$	$A - A_\infty$	$\log \frac{A_o - A}{A - A_\infty}$	log[MA]
1.200	0	0	0.650	———	———
1.175	4.34×10^{-4}	0.025	0.625	-1.398	-3.363
1.174	1.08×10^{-3}	0.026	0.624	-1.380	-2.965
1.169	2.17×10^{-3}	0.031	0.619	-1.300	-2.664
1.147	4.32×10^{-3}	0.053	0.597	-1.052	-2.364
1.111	8.61×10^{-3}	0.089	0.561	-0.800	-2.065
1.085	1.71×10^{-2}	0.115	0.535	-0.668	-1.767
1.019	3.36×10^{-2}	0.181	0.469	-0.413	-1.473
0.891	6.53×10^{-2}	0.309	0.341	-0.043	-1.185
0.569	0.123	0.639	0.011	1.743	-0.910
0.550	0.221	0.650	0	———	-0.635
0.550	0.340	0.650	0	———	-0.469

Temperature = $40^{o}C$

A (418 nm)	[MA]	$A_o - A$	$A - A_\infty$	$\log \frac{A_o - A}{A - A_\infty}$	log[MA]
1.120	0	0	0.575	———	———
1.119	1.08×10^{-3}	0.001	0.574	-2.759	-2.965
1.111	3.25×10^{-3}	0.009	0.566	-1.799	-2.485
1.095	6.47×10^{-3}	0.025	0.550	-1.342	-2.189
1.078	1.29×10^{-2}	0.042	0.533	-1.103	-1.891
1.046	2.54×10^{-2}	0.074	0.501	-0.831	-1.596
1.014	5.02×10^{-2}	0.106	0.469	-0.646	-1.299
0.930	9.93×10^{-2}	0.190	0.385	-0.307	-1.003
0.882	0.197	0.238	0.337	-0.152	-0.706
0.804	0.395	0.316	0.259	0.086	-0.403
0.782	0.700	0.338	0.237	0.154	-0.155

A_∞ estimated to be 0.545 based on lower temperature data.

APPENDIX VIIe. MACoOMBP + Pip ⟶ PipCoOMBP(MA)

In 0.518 M MA in toluene.

Temperature = 22°C

A (630 nm)	[Pip]	t (sec)	$A - A_o$	$A - A_\infty$	$\ln A - A_\infty$
0.110	1.01×10^{-3}	0	0	———	———
0.130	1.01×10^{-3}	50	0.020	———	———
0.130	1.01×10^{-3}	170	0.020	———	———
0.200	5.05×10^{-3}	50	0	———	———
0.212	5.05×10^{-3}	193	0.012	———	———
0.442	2.02×10^{-2}	73	0	0.388	-0.947
0.465	2.02×10^{-2}	202	0.023	0.365	-1.002
0.465	2.02×10^{-2}	339	0.023	0.365	-1.002
0.500	2.02×10^{-2}	725	0.058	0.330	-1.109
0.540	2.02×10^{-2}	1553	0.098	0.290	-1.238
0.620	2.02×10^{-2}	2398	0.178	0.210	-1.561
0.695	2.02×10^{-2}	3438	0.253	0.135	-2.002
0.783	2.02×10^{-2}	5717	0.341	0.047	-3.058
0.830	2.02×10^{-2}	18411	0.388	0	———

t and $A - A_o$ refer to from when the particular additions of Pip are made.

MA + CoOMBP ⟶ MACoOMBP

In 0.518 M MA in toluene

Temperature = 20°C

A (412 nm)	t (sec)	$A_o - A$	$A - A_\infty$	$\ln A - A_\infty$	$\frac{1}{A - A_\infty}$
0.503	53	0	0.153	-1.877	6.536
0.427	186	0.076	0.077	-2.564	12.997
0.410	322	0.097	0.097	-2.882	17.857
0.389	660	0.114	0.039	-3.244	25.641
0.377	1243	0.126	0.027	-3.612	37.037

By the time the MA has been mixed with the CoOMBP solution, the reaction had proceeded too far to be properly analyzed.

APPPENDIX VIIf. $PipCoOMBP + C_2H_4 \longrightarrow PipCoOMBP(C_2H_4)$

In DCE

Temperature = 20°C; $P_{C_2H_4}$ = 780 Torr

A (442 nm)	t (sec)	$A - A_o$	$A_\infty - A$	$\ln A_\infty - A$
0.330	0	0	0.587	-0.533
0.477	99	0.147	0.440	-0.821
0.502	309	0.172	0.415	-0.879
0.542	622	0.212	0.375	-0.981
0.597	1038	0.267	0.320	-1.139
0.723	2132	0.393	0.294	-1.224
0.905	4128	0.575	0.012	-4.423
0.917	10987	0.587	0	

$PipCoOMBP(C_2H_4) \longrightarrow PipCoOMBP + C_2H_4$

In DCE

Temperature = 20°C

A (442 nm)	t (sec)	$A - A_o$	$A_\infty - A$	$\ln A_\infty - A$
0.912	0	0		
0.987	after pumping off C_2H_4, consistent with solvent loss.			
0.397	10856 - partial reversal, further reversal may not be observed because of oxygen entering the system.			

$PipCoOMBP + C_2H_2 \longrightarrow PipCoOMBP(C_2H_2)$

In DCE

Temperature = 20°C; $P_{C_2H_2}$ = 780 Torr

A (440 nm)	t (sec)	$A - A_o$	$A_\infty - A$	$\ln A_\infty - A$
0.231	0	0	0.499	-0.695
0.362	71	0.131	0.368	-1.000
0.378	181	0.147	0.352	-1.044
0.397	314	0.166	0.333	-1.100
0.430	590	0.199	0.300	-1.204
0.478	911	0.247	0.252	-1.378
0.523	1316	0.292	0.207	-1.575
0.560	1744	0.329	0.170	-1.772
0.610	2272	0.369	0.130	-2.040
0.653	2837	0.432	0.067	-2.703
0.690	3483	0.469	0.030	-3.507
0.713	4228	0.482	0.017	-4.075
0.730	5162	0.499	0	

$$PipCoOMBP(C_2H_2) \longrightarrow PipCoOMBP + C_2H_2$$

In DCE

Tmeperature = $20^{o}C$

A (440 nm)	t (sec)	$A_o - A$	$A - A_\infty$	$\ln A - A_\infty$
0.733	0	———	———	———
0.757	60	0	0.500	-0.693
0.697	777	0.060	0.440	-0.821
0.677	1528	0.080	0.420	-0.868
0.641	2515	0.116	0.384	-0.957
0.631	3619	0.126	0.374	-0.983
0.608	5272	0.149	0.351	-1.041
0.582	7238	0.175	0.325	-1.124

A_∞ estimated to be 0.257 based on the forward reaction; reaction cannot analyzed for first order; oxygen entering the system appears to be a problem as the reaction does not completely reverse and spectrum resembling oxidation product is observed after being left overnight.

APPENDIX VIIg. Olefins Reacting with Co(salen) Complexes

CH_3-ImCo(salen) + $C_2H_4 \rightleftharpoons$ CH_3-ImCo(salen)C_2H_4

A (410 nm)	Conditions
0.830	Under 1 atm of Ar
0.870	Under 1 atm of C_2H_4 @ -63.5°C
0.860	Under vacuum

CH_3-ImCo(salen) + $C_2H_2 \rightleftharpoons$ CH_3-ImCo(salen)C_2H_2

A (410 nm)	Conditions
0.530	Under 1 atm of Ar
0.562	Under 1 atm of C_2H_2
0.557	Under vacuum

Co(salen) + 1-hexene + O_2

A (410 nm)	time	Conditions	Conclusion
1.217	0	Under vacuum	
1.219	63	Under 800 Torr O_2	
1.213	1237	" " " "	
1.198	3478	" " " "	
1.192	10562	" " " "	No apparent reaction

Co(salen) + cyclooctene + O_2

A (410 nm)	time	Conditions	Conclusion
1.082	0	Under vacuum	
1.097	72	Under 800 Torr O_2	
1.090	1177	" " " "	
1.065	36562	" " " "	No apparent reaction

Co(salen) + styrene + O_2

A (410 nm)	time	Conditions	Conclusion
1.147	0	Under vacuum	
1.132	51	Under 800 Torr O_2	
0.670	52973	" " " "	Possible reaction
0.690	193	System evacuated	
1.005	40 hr	" "	Reaction reversed

Co(salen) + 3,4-dichlorobutene + O_2

A (410 nm)	time	Conditions	Conclusion
1.155	0	Under vacuum	
1.130	137	Under 800 Torr O_2	
0.840	50261	" " " "	Possible reaction
0.850	73	System evacuated	
0.897	1 hr	" "	
0.957	10 hr	" "	
1.037	42 hr	" "	Reaction reversed

Co(salen) + diethylfumarate + O_2

A (410 nm)	time	Conditions	Conclusion
1.300	0	Under vacuum	
1.205	205	Under 800 Torr O_2	
1.165	641	" " " "	
1.078	2047	" " " "	
0.681	21285	" " " "	
0.693	58	System evacuated	Possible presence
0.697	14 hr	" "	of peroxides

APPENDIX VIII

DATA USED IN DETERMINING DIELECTRIC CONSTANTS

MATERIAL	USE	CAPACITANCE (pf)*	DIELECTRIC CONSTANT
air	standard	62.2	1.0006
hexane	standard	109.9	1.890
benzene	standard	131.8	2.284
toluene	standard	137.7	2.38
ethyl ether	standard	238.8	4.335
chlorobenzene	standard	316.4	5.708
1-chlorobutane	standard	399.2	7.39
1,2-dichloro-ethane	standard	584.3	10.65
1-butanol	standard	994.5	17.8
acetone	standard	1155.5	20.7
acetyl-acetone	standard	1488.4	25.7
1:1 v/v toluene:Pip	solvent	181.7	3.22
1:1 v/v toluene:Py	solvent	400.8	7.37
1:1 v/v toluene:CH_3-Im	solvent	1013.0	18.45
1:1 v/v DCE:Pip	solvent	~402	~7.4
1:1 v/v DCE:Py	solvent	~700	~12.7
1:1 v/v DCE:CH_3-Im	solvent	——	——
1:1 v/v toluene:DCE	solvent	297.1	5.32
4:1 v/v toluene:DCE	solvent	190.3	3.43
5:1 v/v toluene:DCE	solvent	181.1	3.22
10:1 v/v toluene:DCE	solvent	281.1	5.06

MATERIAL	USE	CAPACITANCE (pf)*	DIELECTRIC CONSTANT
CH_3-Im	solvent	———	———
5% DMF in toluene	solvent	202.1	3.63
10% DMF in toluene	solvent	270.8	4.92
20% DMF in toluene	solvent	430.8	7.80
33% DMF in toluene	solvent	613.7	11.23
50% DMF in toluene	solvent	~1000	~18

*pf - picofarad

Approximate values due to excessive conductance through the solvent; if conductance is very great than capacitance cannot be measured.

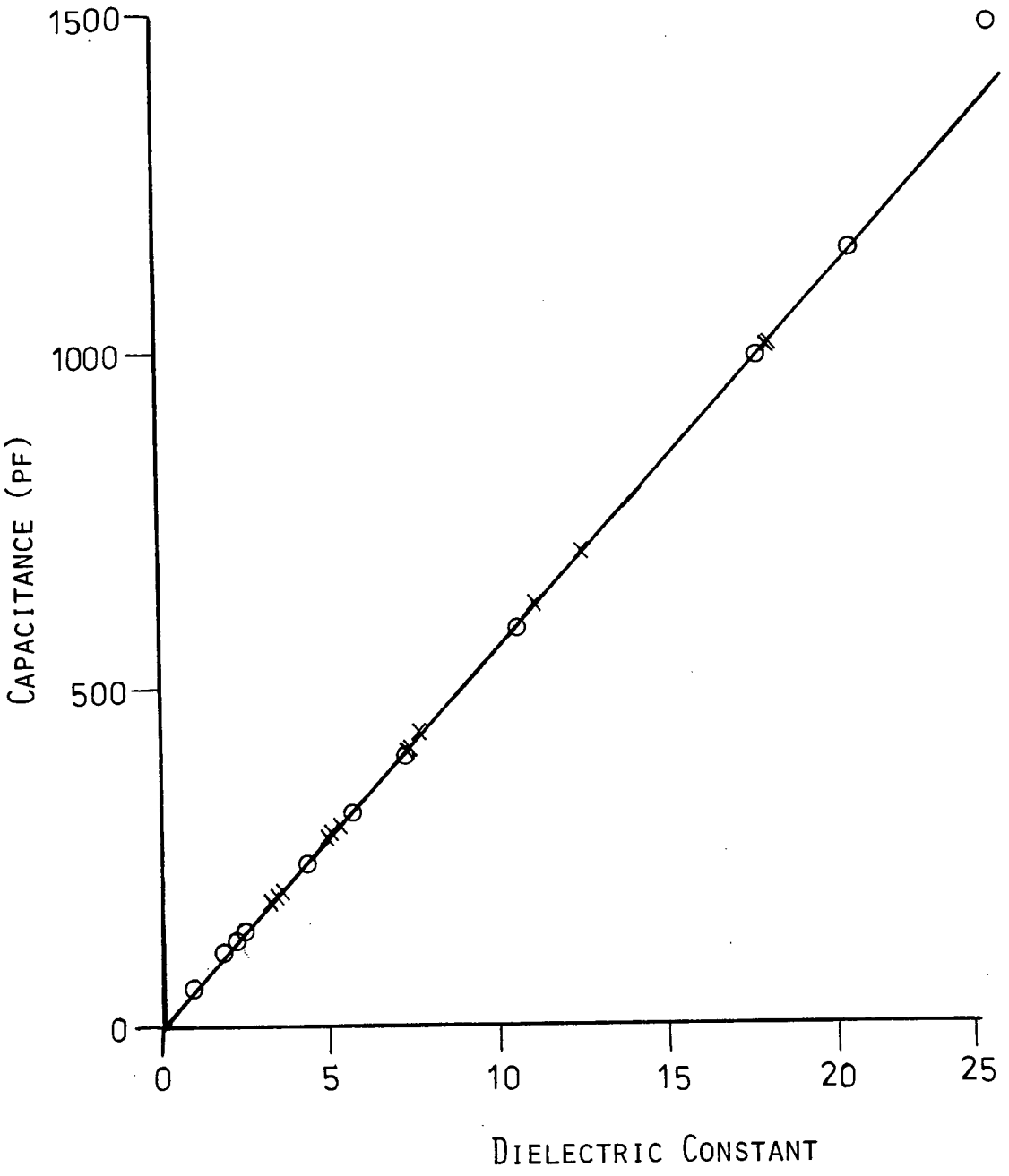

Calibration curve for determining dielectric constants

O Standard

X Experimental Solvent

APPENDIX IX

ESR PARAMETERS DETERMINED IN THIS THESIS

Note: ESR parameters were determined by comparisons with previously reported signals and so are not thoroughly discussed.

COMPLEX	g_x	g_y	g_z	g_{iso}	A_x	A_y	A_z	A_{iso}	A_N
CH_3-ImCo(salen)	2.390	2.183	2.021		~18	~14	87.5		15.1
PipCo(salen)	2.36	2.16	2.02				80.7		15.1
Py_2Co(salen)	2.350	2.27	2.031				75.1		11.4
sty-Co(salen)				~1.88					
DCB-Co(salen)				~1.88					
Co(salen)(O_2)	1.997	1.997	2.076		~12	~12	15.6		
CH_3-ImCo(salen)(O_2)	1.996	1.996	2.077		11.0	11.0	15.6		
PipCo(salen)(O_2)	1.996	1.996	2.076		11.4	11.4	15.6		
PyCo(salen)(O_2)	1.997	1.997	2.074		12.5	12.5	15.6		
styCo(salen)(O_2)	1.988	1.988	2.090		15.6	15.6	23.5		
DCBCo(salen)(O_2)	1.986	1.986	2.095		12.4	12.4	23.6		
CH_3-ImCoPpIX	2.31	2.31	2.034				75		
CoPpIX(O_2)	1.98	1.98	2.07		18.1	18.1	~21		
CH_3-ImCoPpIX(O_2)	1.99	1.99	2.07				15.8		
CoOMBP(O_2)	1.975	1.975	2.06	2.028			13.2		9.7
CH_3-ImCoOMBP(O_2)	1.985	1.985	2.07	2.031			15.5		9.7
CH_3-ImCoOEP(O_2)				1.946					
CH_3-ImCoEpI(O_2)				1.946					
PipCoPpIX(O_2)	1.99	1.99	2.07				15.5		
PyCoPpIX(O_2)	1.999	1.999	2.079				14.5		